

NAT'L INST. OF STAND & TECH



A11106 222333

**UBE '01**

NIST  
PUBLICATIONS

# 12TH INTERNATIONAL CONFERENCE ON AUTOMATIC FIRE DETECTION



## PROCEEDINGS

March 26 - 28, 2001  
Gaithersburg, Maryland, USA

QC  
100  
.U57  
NO.965  
2001  
C.2



**NIST**  
National Institute of  
Standards and Technology  
Technology Administration  
U.S. Department of Commerce







# AUBE '01

## 12TH INTERNATIONAL CONFERENCE ON AUTOMATIC FIRE DETECTION

March 25 - 28, 2001

National Institute Of Standards and Technology  
Gaithersburg, Maryland U.S.A.

## PROCEEDINGS

Editors: Kellie Beall, William Grosshandler and Heinz Luck



**NIST**  
National Institute of Standards and Technology  
Technology Administration, U.S. Department of Commerce

## ACKNOWLEDGEMENT

The 12th International Conference on Automatic Fire Detection was organized through the cooperative effort of an international steering committee co-chaired by Prof. Dr.-Ing. H. Luck of Gerhard-Mercator-Universität, Duisburg, Germany, and Dr. William Grosshandler of the National Institute of Standards and Technology (NIST), Gaithersburg, USA. The co-chairs wish to acknowledge the assistance provided by the steering committee members and their institutions: Mr. Richard Bukowski, NIST Gaithersburg; Prof. Dr. Ingolf Willms, Gerhard-Mercator-Universität, Duisburg; Dr. Markus Loepfe, Siemens Building Technologies AG, Cerberus Division, Männedorf, Switzerland; Prof. Hiromitsu Ishii, Department of Electrical Engineering, Nihon University, Tokyo, Japan; and Dr. Yoshiyuki Matsubara, National Research Institute of Fire and Disaster, Tokyo, Japan. The co-chairs especially wish to acknowledge the organizational skills and numerous editing tasks performed by Ms. Kellie Beall of NIST, Gaithersburg.

The endorsement of AUBE '01 by the European Society for Automatic Alarm Systems (EUSAS), Zurich, Switzerland, is acknowledged. Partial support for the conference came from

- National Electrical Manufacturers Association (NEMA), USA
- Hughes Associates, Incorporated, Baltimore, MD, USA
- FM Global, Norwood, MA, USA

The financial contributions of these organizations to the success of the conference are gratefully acknowledged.



## Table of Contents

<i>A History of NBS/NIST Research on Fire Detectors</i> , Richard Bukowski .....	1
NIST, Gaithersburg USA	

<i>European Standards and Certification Procedure</i> .....	13
Reinhard Conrads, VdS, Cologne GERMANY	

### SMOKE CHARACTERIZATION

<i>An Apparatus for Light Scattering Studies of Smoke Particles</i> .....	31
Darryl Weinert, George Mulholland, NIST, Gaithersburg USA	

<i>Calibration of Fire Sensors in the Sub Micron Range</i> .....	43
A. Trampe, H. Fissan, Gerhard-Mercator-Universität, Duisburg GERMANY	

<i>Size Distribution and Light Scattering Properties of Test Smokes</i> .....	58
Darryl Weinert, Thomas Cleary, George Mulholland, NIST, Gaithersburg USA	

### DETECTION BY RADIATED EMISSION

<i>Smoldering Fire Detection by Image Processing</i> .....	71
Daisuke Kozeki, National Research Institute of Fire and Disaster, Tokyo JAPAN	

<i>Smoke Detection in Tunnels Using Video Images</i> .....	79
Dieter Wieser, Thomas Brupbacher, Siemens Building Technologies, Männedorf SWITZERLAND	

<i>Characterization of Spectral Radiation Intensities from Standard Test Fires for Fire Detection</i> .....	91
Woo Kim, Yudaya Sivathanu, Jay P. Gore, Purdue University, West LaFayette USA	

<i>Is Microwave Radiation Useful for Fire Detection?</i> .....	107
Thomas Kaiser, Thorsten Kempka, Gerhard-Mercator-Universität, Duisburg GERMANY	

### DETECTION SYSTEMS AND ALGORITHMS

<i>An Energy Model in Fire Detection and Integrated Analysis on False Alarms</i> .....	122
Shu Yan, Shu Wang, Zheng Dou, Huazhong University of Science and Technology, Wuhan PRC	

<i>A New Approach to Fire Detection Algorithms Based on the Hidden Markov Model</i> .....	129
Hans-Christian Müller, Gerhard-Mercator-Universität, Duisburg GERMANY	

<i>Distributed Sensor Fire Detection</i> .....	139
Thomas Cleary, Kathy Notarrianni, NIST, Gaithersburg USA	

<i>Spot and Aspirated Laser Smoke Detection in Telecommunications Facilities</i> .....	151
Daniel Gottuk, Lawrence McKenna, Jr., Hughes Associates, Inc., Baltimore USA	



<i>Strategies for the Development of Detection Algorithms .....</i>	63
Rainer Siebel, Gerhard-Mercator-Universität, Duisburg GERMANY	
<i>Real-Time Probabilistic Neural Network Performance and Optimization for Fire Detection and Nuisance Alarm Rejection .....</i>	70
Susan Rose-Pehrsson, Sean Hart, Thomas Street, Patricia Tatem, Frederick Williams, Naval Research Laboratory, Washington DC USA; Mark Hammond, NOVA Research, Alexandria USA; Daniel Gottuk, Mark Wright, Jennifer Wong, Hughes Associates, Baltimore USA	
<i>A New Type of Neural Fuzzy System and its Application in Automatic Fire Detection .....</i>	9
ShuWang, Shu Yan, Zheng Dou, Huazhong University of Science and Technology of China, Wuhan PRC	
<i>A New Algorithm for Adaptive Alarm Threshold in Fire Detection System .....</i>	0
Milan Blagojevich, Dejan Petkovich, Djordje Simich, Faculty of Occupational Safety, Nish YUGOSLAVIA	

## WIRELESS SYSTEMS & ELECTROMAGNETIC COMPATIBILITY

<i>Electromagnetic Compatibility and Radio-linked Systems.....</i>	10
Pascal Dubois, CNPP, Saint Marcel FRANCE	
<i>Radio Module Characteristics and Their Relevance to Fire Detection Systems.....</i>	2
Karlheinz Schreyer, Siemens Gebäudesicherheit, Munich, GERMANY	
<i>Internet Technology: New Perspectives for Alarm Systems .....</i>	
George Schmitz, Peter Witschital, Siemens, Gebäudesicherheit, Munich, GERMANY	
<i>Technical State of 868-870 MHz Radio Modules in the SRD Band.....</i>	12
Bjoern Silberberg, Siemens Gebäudesicherheit, Munich GERMANY	

## TEST METHODS AND INSTRUMENTATION

<i>Testing Methods for Gas Sensor Based Fire Detectors.....</i>	5
Oliver Linden, Hans H Iemann, University of Wuppertal GERMANY	
<i>A Modular Data Acquisition System for the Measurement of Fire Characteristics.....</i>	
Wolfgang Krüll, Gerhard-Mercator-Universität, Duisburg GERMANY	
<i>Response-Time Comparisons of Ionization and Photoelectric/Heat Detectors.....</i>	3
J.R. Qualey, III, L. Desmarais, J. Pratt, Simplex Time Recorder, Co., Westminster USA	
<i>The Performance of Mains-Powered Residential Smoke Alarms with a Backup Energy Source.....</i>	
J. N. Smithies, FRS Building Research Establishment Ltd. Watford, UK; M. J. Spearpoint, University of Canterbury, Christchurch NEW ZEALAND	
<i>The Fire Emulator/Detector Evaluator: Design, Operation, and Performance.....</i>	
Thomas Cleary, Michelle Donnelly, William L. Grosshandler, NIST, Gaithersburg USA	
<i>Fire Protection Systems for Traffic Tunnels Under Test .....</i>	
Rudolf, Mägerle, Siemens Building Technologies, Männedorf SWITZERLAND	



<i>Concepts for the Test of Volumetric Fire Detectors</i> .....	338
Ingolf Willms, Gerhard-Mercator-Universität Duisburg GERMANY	

## GAS & MULTI-ELEMENT DETECTION

<i>Enhanced Residential Fire Detection by Combining Smoke and Carbon Monoxide Sensors</i> .....	346
Thomas Cleary, NIST, Gaithersburg USA; Takashi Ono, Nihon University, Tokyo JAPAN	
<i>A Diode Laser Multigas Analyzer for Advanced Detection of Fires</i> .....	358
David Bomse, Southwest Sciences, Inc., Santa Fe USA	
<i>Requirements to Gas Sensors in Fire Alarms for Residential Use</i> .....	370
A. Pfefferseder, Bosch Telecom, Ottobrunn GERMANY	
<i>A Rugged Led-Based Sensor for Fire Detection</i> .....	378
Jeffrey Goldmeer, Southwest Sciences, Inc., Santa Fe USA	
<i>Measuring Results of a Combined Optical, Thermal and CO Detector in Real Sites and Classifying the Signals</i> .....	390
U. Oppelt, Bosch Telecom, Ottobrunn GERMANY	
<i>Measurements for Fire Detection by Means of Gas Sensors in an Insulation Material Factory</i> .....	403
J. Großer, C. Kubon, O. Linden, H. H. Temann, University of Wuppertal, GERMANY	
<i>Early Detection and Distinction of Fire Gases with a Gas Sensor Microarray</i> .....	416
M. Harms, J. Goschnick, Forschungszentrum, Karlsruhe GERMANY	
<i>Fire Location Estimation Using Temperature Sensor Arrays</i> .....	432
Martin Berentsen, Thomas Kaiser, Gerhard-Mercator-Universität, Duisburg GERMANY	

## MODELING AND COMPUTER SIMULATION

<i>Field Modeling of an Initial Stage of Fire in a Compartment: Comparison with a Fire Experiment Measured in an Enclosure</i> .....	444
N. Miyamoto, T. Someya, T. Omori, Tokyo Gas Co., Ltd., Tokyo, JAPAN	
<i>Fire Detector Performance Predictions in a Simulated Multi-Room Configuration</i> .....	455
Thomas Cleary, Michelle Donnelly, George Mulholland, NIST, Gaithersburg USA; Bakhtier Farouk, Drexel University, Philadelphia USA	
<i>Fire Sensor Modelling and Simulation</i> .....	470
Frank Gockel, Gerhard-Mercator-Universität, Duisburg GERMANY	
<i>Simulation of Smoke Transport and Coagulation for a Standard Test Fire</i> .....	482
B. Farouk, Drexel University, Philadelphia USA; G. W. Mulholland, K. B. McGrattan, NIST, Gaithersburg USA	
<i>A Sensor-Driven Fire Model</i> .....	494
William Davis, Glenn Forney, NIST, Gaithersburg USA	



<i>Revisiting Modelling of Fluid Penetration into Smoke Detectors Revisited for Low Speed Ceiling Jets</i> .....	506
O. Keski-Rahkonen, VTT Building and Transport, Espoo FINLAND	
<i>A General Approach for Simulating Signals of Scattered Light Detectors</i> .....	517
Claudia Rexfort, Thomas Kaiser, Gerhard-Mercator-Universität Duisburg GERMANY	
<i>Fire Detection Modeling -- The Research-Application Gap</i> .....	529
Robert Schifiliti, R. P. Schifiliti Associates, Inc. Reading USA	

## INTEGRATED FIRE DETECTION/BUILDING CONTROL SYSTEM

<i>Development of Fire Detection Systems in the Intelligent Building</i> .....	561
Z. Liu, J. Makar, A. K. Kim, Institute for Research in Construction, Ottawa CANADA	
<i>Using High Reliability Detection for Fire Service Response in Buildings</i> .....	574
Walter Jones, Richard Bukowski, NIST, Gaithersburg USA	
<i>An Open Distributed Fire Detection System</i> .....	592
Xiangyang Li, Weihau Liu, Aizhong Wang, Jing Su, Gulf Security Tech. Co., Qinhuangdao PRC	
<i>Analysis on Data Stream Model of Network Image Fire Detection System</i> .....	602
Tao Chen, Longbiao Wu, Weicheng Fan, Weiguo Song, University of Science and Technology of China, Hefei PRC	

## FIRE DETECTION IN AIRCRAFT, TRANSPORT SYSTEMS AND SPECIAL HAZARDS

<i>Initial Development of Improved Aircraft Cargo Compartment Fire Detection Certification Criteria</i> .....	615
David Blake, FAA Technical Center, Atlantic City USA; Stefan Domino, Walt Gill, Louis Gritz, Jill Williams, Sandia National Laboratories, Albuquerque USA	
<i>Aircraft Fire Detection: Requirements, Qualification, and Certification Aspects</i> .....	630
Klaus Schmoetzer, EADS Airbus GmbH, Bremen GERMANY	
<i>New Approaches to Aircraft Fire Protection</i> .....	641
A. Freiling, EADS Airbus GmbH, Bremen GERMANY	
<i>Fire Detection for Aircraft Cargo Compartments, Reduction of False Alarms</i> .....	653
Phillipe Mangon, Cerberus S. A., Buc FRANCE	
<i>The Cargo Fire Monitoring System (CFMS) for the Visualisation of Fire Events in Aircraft Cargo Holds</i> .....	665
T. Wittkopp, C. Hecker, D. Opitz, VIDAIR-AG, Mönchengladbach GERMANY	
<i>Two Dimentional Multi Detection Fire Sensor, System Architecture and Performances</i> .....	677
G. Boucourt, Latecoere, Toulouse FRANCE	
<i>Aircraft Cargo Compartment Fire and Nuisance Source Test in the FE/DE</i> .....	689
Thomas Cleary, Michelle Donnelly, NIST Gaithersburg USA	



Richard W. Bukowski

National Institute of Standards and Technology, Gaithersburg, MD 20899 USA

## **A History of NBS/NIST Research on Fire Detectors**

### **Early History of Fire Research at NBS**

The celebration of the National Bureau of Standards/National Institute of Standards and Technology's (NBS/NIST) centennial year has led to many looks back over a century of research activities. The fire research program at NBS began shortly after the agency's founding in 1901 with the initial funded studies focused on fire resistance and flammability properties of materials beginning with the hiring of Simon Ingberg in 1914. In those days the primary objective of fire research was to prevent fires from burning down large sections of cities. A summary of the early work at NBS was prepared by Dan Gross for the third International Association of Fire Safety Science (IAFSS) Conference in 1991<sup>1</sup>.

The earliest studies at NBS of the performance of detectors were conducted in the 1920's and 30's. In the 1950's pioneering work was conducted by McCamy on flame detectors for aircraft engine nacelles<sup>2</sup> in which he published data on both ultraviolet (UV) and infrared (IR) signatures and proposed coupling IR sensors with flame flicker circuits to discriminate hot objects from actual flame.

### **Operation Breakthrough**

In the late 1960's the US Department of Housing and Urban Development (HUD) instituted a major, innovative housing demonstration project called "Operation Breakthrough<sup>3</sup>." Intended to facilitate the development of novel approaches to design, materials, and construction techniques of use in addressing low income housing issues, the program included not only the submission of concepts but also the actual construction of a home using the proposed techniques. Recognizing that traditional, prescriptive building codes could not deal effectively with these innovative methods



and materials NBS developed one of the earliest performance-based code approaches not too dissimilar from those now being promulgated globally.

At the time of Breakthrough, fire alarm systems in homes were rare, and where installed used commercial detectors and panels designed by the rules applied to commercial properties. Here heat detectors were used in most occupiable spaces. In commercial installations smoke detectors were usually only used to protect high value items, so they were rare in home systems. The typical residential system cost as much (in 1968 dollars) as residential sprinkler systems cost today. The (single-station) smoke alarm had been developed in 1965 but sales were low and availability poor for the few models being marketed.

One of NBS's fire protection engineers, Mr. Richard (Dick) Bright, had been impressed with an article published by Canada's National Research Council in 1962. John McGuire and Brian Ruscoe<sup>4</sup> studied 342 residential fire deaths in Ontario from 1956-1960 and judged the life saving potential of a heat detector in every room or a single, smoke detector outside the bedrooms and at the head of the basement stairs (if the home had a basement). Their judgement was that the heat detectors would have reduced the fatalities by 8% and the smoke detectors by 41%.

NBS included in its Breakthrough criteria<sup>5</sup> (essentially the building code applied to the demonstration houses) a requirement for smoke detectors located in accordance with the McGuire and Ruscoe guidelines. Since only one of each of the selected homes were built and none were ever occupied, no fire experience with these detectors was ever gained.

### **Hurricane Agnes**

In 1971 Hurricane Agnes followed a track up the Chesapeake bay destroying many homes in central Pennsylvania and lower New York. HUD mounted a federal disaster relief effort (this was long before FEMA) including the provision of temporary housing for many poor residents of the region. HUD purchased 17,000 mobile homes (later



called manufactured homes) and asked NBS to apply some of the lessons of Breakthrough to the purchase specification. NBS included a requirement for a (single-station) smoke detector outside the bedrooms of each unit. The order for 17,000 smoke detectors had to be split among five manufacturers because at the time no single company had the production capacity to fill the order. Today, one manufacturer could do so with two days' production.

The 17,000 homes were delivered to several sites and were used by families until they could rebuild or find alternative accommodations. Most lived in the homes for a year but some were still occupied three years later. The fire safety statistics were surprising. While there were nearly the statistically expected number of fires, there were no fire deaths and few injuries. The smoke detectors were credited with getting occupants out before they became trapped – just as McGuire and Ruscoe surmised.

This was the first, large installation of residential smoke detectors and the results convinced the manufactured housing industry to adopt the first smoke detector “ordinance.” In 1975 it became the policy of the Mobile Home Manufacturing Association (the predecessor of today's Manufactured Housing Institute) that one smoke detector located outside the bedrooms be provided in every manufactured home produced by a member company.

## **Developing Standards**

### **UL 217**

The large procurement of smoke detectors for the Agnes homes piqued Dick Bright's curiosity about just how well these devices performed in detecting fires. He modified a spare prototype of the NBS Smoke Chamber (that later became ASTM D662) to generate smoke from a small source and circulate it with a small bar heater. Hanging production smoke detectors in the box he was appalled to see the “power on” light on many disappear in the smoke without a sound from the detector.



Further tests revealed a problem with smoke entry into the outer housing at low convective flow rates. The smoke box test used by Underwriters Laboratories (UL) at the time had two large fans pointed directly at the detector forcing the smoke in – a not so realistic condition. This experience led Bright and his supervisor Irwin Benjamin to conclude that the potential of residential smoke detectors would not be realized unless there were effective product approval standards that assured their proper performance and reliability.

Bright and Benjamin approached UL about participation in a cooperative project under NBS' Industry Research Associate program where UL would assign an employee to work at NBS for a year to develop the basis for such a standard that UL would then promulgate. I was selected by UL for the one-year assignment, beginning in the Fall of 1973.

One of the unique aspects of this project was that it was conducted in close cooperation with the residential smoke detector industry, who themselves were working with an immature technology. Companies provided samples of current product and were very grateful for constructive criticism. Company engineers began to visit with prototypes of models under development that were jointly evaluated and improved. This cooperative environment led to rapid improvements in the performance of detectors that benefitted the public and the industry.

The work that year covered a number of issues identified as problems (or potential problems) that were corrected by the industry and incorporated in the suggested standard that was presented to UL and formed the basis for the first edition of their Safety Standard for Single- and Multiple-Station Smoke Detectors, UL217. These included:

- Identification and quantification of low velocity smoke entry problems into detector housings or sensor assemblies and the associated Variable Velocity and Directionality tests in the new Standard.



- Design of a new smoke box for sensitivity testing with improvements to the flow characteristics and instrumentation that is now used for all smoke detectors.
- Effects of the condensation of moisture on sensor or circuit boards that could cause false alarms or non-operation and the Humidity Plunge test placed in the Standard to address this issue.
- Development of an electrical transients test to improve reliability by reducing the susceptibility of detectors to damage from transients.
- The application of the “full-scale fire tests” to all smoke detectors where they had previously been used only for ionization type.
- Agreement on the policies of minimum one-year battery life, including the battery with the detector at purchase, the use of commonly available batteries, functional testing features, and others.

In the Fall of 1974 I returned to UL and completed the development and adoption of UL217. Dick Bright had been appointed Chair of the National Fire Protection Association (NFPA) Committee on Household Fire Warning Equipment that developed the NFPA 74 Standard on the Installation, Maintenance, and Use of Household Fire Warning equipment. First published in 1967 as a guide for homeowners this document reflected the philosophy of the times that homes should be protected in the same way as commercial businesses – with a heat detector in every room wired to a fire alarm panel and alarm bells. The cost of such a residential fire alarm system for an average home was about \$1500 so they were rare.

#### NFPA 74

Since the installation of residential fire alarm equipment was voluntary (and no one thought that requiring fire safety equipment in homes would ever happen), Bright felt that homeowners should be given the opportunity to choose a minimum system that



provided some protection at low cost, like that suggested by McGuire and Ruscoe. The committee proposed a system of four “Levels of Protection” in the 1974 edition of NFPA 74. These were:

- Level 4 was a smoke detector outside the bedrooms and at the head of any basement stairs from McGuire and Ruscoe.
- Level 3 added heat or smoke detectors in living or family rooms which had the highest statistical likelihood of residential fire initiation.
- Level 2 added heat or smoke detectors in the bedrooms that were next on the list of fire initiation.
- Level 1 was the full system of a heat or smoke detector in every room.

This unique concept was presented to the NFPA Membership for adoption at the May 1974 meeting in Miami Beach and it was strongly opposed by the fire service (the Fire Marshals and Fire Chiefs). Their concern was that they saw no evidence that anything less than “complete protection” (Level 1) was adequate. They were correct – the levels were solely based on the judgement of the committee and that of McGuire and Ruscoe.

### **Full-scale tests of Smoke Detector Performance**

#### **The Indiana Dunes Tests<sup>6</sup>**

While the Levels of Protection concept was adopted at that meeting the concern expressed by the fire service were not taken lightly. Bright proposed that NBS fund a research project to assess the effectiveness of the Levels of Protection and this contract was awarded to IIT Research Institute and UL. The Principle Investigators were Tom Waterman of IITRI, and William Christian and myself from UL.

The idea was to take detectors currently available on the market and install them in actual homes that were to be demolished. Fires involving actual residential contents would be used and instruments would monitor conditions within the homes to judge



when unassisted escape out doors (but not jumping out windows) would no longer be practical.

The research involved 76 experiments conducted over two years in three homes scheduled for demolition as part of an expansion of the Indiana Dunes National Lakeshore Park. The data showed that in fact, the optimum performance was obtained with a smoke detector on every floor level of the home, mostly because smoke flow up stairs could be impeded by flows induced by HVAC systems, especially air conditioning. A closed door at the top of the basement stairs could create a dead air space that delayed response. The home was better protected from fires starting in the basement by a smoke detector on the basement ceiling near the stairway.

The report presented results in a unique way, in terms of the escape time (time between detector alarm and reaching one of the tenability limits defined by the study) provided by the detectors. These escape times were used to produce a probability plot of the percent of experiments in which a given amount of escape time was provided. Thus the reader could select a time needed and determine the percent of cases in which that (or more) time was available.

In an independent analysis of the first year results, a fire safety panel advising the governor of Massachusetts on a statewide detector law an arbitrary 3 minute escape time assumption was applied. This resulted in the observation that a smoke detector on every level would provide the required 3 minutes in 89% of the cases and a smoke detector in every room would only increase that to 93%.

### **Manufactured Homes**

In 1978 the US Department of Housing and Urban Development (HUD) commissioned a study similar to the Indiana Dunes Tests to be conducted in a manufactured home<sup>7</sup>. HUD was preparing to promulgate their federal Manufactured Home Construction and Safety Standards (49CFR3280) and this work provided the basis for the smoke detector requirements therein.



## **Smoke Detector Regulations**

The Indiana Dunes tests had a strong and immediate impact and soon various jurisdictions began to adopt laws requiring the provision of every level smoke detectors in new residential housing. More surprising to many was the adoption by some of regulations requiring the installation of smoke alarms in existing residences. This ran counter to the U.S. tradition of “a man’s home is his castle” and most opposition was not to the smoke detectors but to the change in this tradition. Montgomery County Maryland was one of the first to adopt such an ordinance in 1975, effective in 1978. Even more startling later was the immediate impact of the law. As implementation began the residential fire death rate that had been steady for some years around 32 per year began to drop precipitously. After the law was effective fatalities hit zero in compliant homes and stayed there for several years, convincing others to adopt similar laws.

Successes like Montgomery County led to the rapid adoption of mandatory smoke detectors in most state or provincial building codes in the U.S. and Canada. Codes at the city or county level often went further to require the installation of smoke detectors in existing residential properties. Coupled with effective marketing campaigns by major appliance manufacturers such as GE and Gillette, and retailers like Sears, compliance with these regulations was unusually high – typically above 90 %. The result was a decline in U.S. fire deaths by 50 % between 1975 and 1998 that has been largely attributed to the smoke detector.

## **Quantifying Escape Time Needs**

The “Indiana Dunes Tests” and other similar studies conducted in the 1970's and 80's clearly demonstrated that the occupants of most homes with every level smoke detectors could expect 3 to 5 minutes of escape time for most fires. However there were several human factors questions such as how effective smoke detectors were at awakening



sleeping people and how much time was needed for a family, especially with young children, to escape.

To address these issues NBS awarded a grant to Prof. E. Harris Nober at the University of Massachusetts at Amherst to conduct a study. Prof. Nober had a sleep lab on campus and experience in this field although like most sleep researchers had focused on insomnia as opposed to awakening.

Prof. Nober's work<sup>8</sup> began in the laboratory but soon moved into homes in order to provide more realism and to address the questions of families. They developed a protocol in which they installed a smoke detector in a test home that could be activated with a radio transmitter from the street. Waiting several weeks to avoid biasing the trial the researchers showed up in the middle of the night and activated the alarm. The subjects were instructed to turn on a bedroom light immediately on awakening (this gave a measure of awakening time) and then place a call to the Amherst Fire Department (who were part of the study and provided a time for the call). Then the family all evacuated outside to a pre-arranged meeting place in front of the house. Through these experiments it was determined that the three minutes assumed almost a decade prior was a typical value for families.

### **Detection for Special Applications**

In the early 1980's NBS decided that the residential smoke detector issues had largely been addressed and the technology matured. Product approval standards (UL217) and installation standards (NFPA74) were in place and the combination of regulatory and voluntary installations were at a pace that soon nearly every home would be equipped. Thus NBS decided to apply its limited resources in other areas.

The result was limited studies mostly aimed at improving detector performance in special applications. The applications addressed included health care facilities<sup>9,10</sup> (especially reducing the incidence of nuisance alarms that were affecting system credibility), fire protection for atria<sup>11</sup> (these had become a common architectural

feature), and even spacecraft<sup>12</sup>. NASA had begun advanced planning for their 21<sup>st</sup> Century projects including Space Station and wanted to explore innovative techniques for fire detection.

### **Computational Studies**

In the 1990's NIST (formerly NBS) pioneered the use of computational experiments to study the performance of, and to develop guidelines for the installation of smoke detectors. In a project funded through a public/private consortium through the (National) Fire Protection Research Foundation, NIST researchers evaluated the effects of both geometry and physical barriers, and the interaction with mechanical ventilation systems on smoke and heat detector activation times. While others have used computational techniques to design specific installations, this was the first time anyone performed parametric calculations designed like a series of experiments to provide systematic information on a hypothesis.

The results of the study were revealing; confirming some common practice and indicating that some assumptions may be wrong. The results had a direct and significant effect on the code requirements.<sup>13·14·15·16</sup>

### **Current and Future Activities**

NIST is still involved in detector research. One project involves the development of an apparatus for evaluating the performance of multi-sensor devices. Called the Fire Emulator/Detector Evaluator (or FE/DE), the apparatus shows real promise for international standardization<sup>17</sup>.

With links to the Indiana Dunes Tests, NIST is conducting a new evaluation of residential smoke detectors (now commonly referred to as smoke alarms). This work intends to re-examine the installation and siting rules, the efficacy of current sensor technologies, examine nuisance alarm sources, and develop data with which alarm algorithms might be developed for multi-sensor devices.



Finally, NIST is using its experience in computational fire models to develop a "sensor-driven" or "inverse" model<sup>18</sup>. Where traditional fire models start with the heat release rate of the fire and predict the fire's impact on the building this model takes the analog signal from fire sensors and predicts the heat release rate of the fire most likely to be producing those signals. This model holds promise in allowing fire alarm systems to produce real time data of significant use to the fire service in making tactical decisions, as well as evaluating detector signals for consistency with fire chemistry and physics and determining the level of threat to people and property.

Fire detectors and the systems to which they connect play a significant role in the reduction of fire losses. Thus the NIST fire program will continue to conduct research on detection as a means to achieve its goals of reducing the burden of fire.

## References

- 
- <sup>1</sup> Gross, D., Fire Research at NBS: The First 75 Years, Fire Safety Science - Proc of the Third International Symposium, Elsevier Applied Science, London, pp 119-133, 1991.
  - <sup>2</sup> McCamy, C.S., A Five-Band Recording Spectroradiometer, NBS J. Res., 56, 5, 293, 1956.
  - <sup>3</sup> Feedback. Operation Breakthrough. Phase 1. Design and Development of Housing Systems. Department of Housing and Urban Development, Washington, DC, HUD-RT-28; 261 p. 1973.
  - <sup>4</sup> McGuire, J.H. and Ruscoe, B.E., The Value of a Fire Detector in the Home, National Research Council of Canada, Fire Study No. 9 of the Division of Building Research, Ottawa, Canada, 1962.
  - <sup>5</sup> Benjamin, I. A., Criteria for Fire Safety in Operation Breakthrough, National Bureau of Standards, Washington, DC, Building Standards, Vol. 40, No. 6, 33-36, November/December 1971.
  - <sup>6</sup> Bukowski, R.W., Field Investigation of Residential Smoke Detectors, NBSIR 76-1126, 1976; and *Fire Journal*, 71, No. 2, pp 18-41, 1977.
  - <sup>7</sup> Bukowski, R. W., Investigation of the Effects of Heating and Air Conditioning on the Performance of Smoke Detectors in Mobile Homes, NBSIR 79-1915, 1979.
  - <sup>8</sup> Nober, E. H.; Peirce, H.; Well, A. D., Waking Effectiveness of Household Smoke and Fire Detection Devices. Final Report. Massachusetts Univ., Amherst, National Bureau of Standards, Gaithersburg, MD, Available

---

from National Technical Information Service NBS GCR 83-439; 92 p. July 1983.

<sup>9</sup> Bukowski, R. W., Tests on the Performance of Automatic Fire Detectors in Health Care Occupancies - A Preliminary Report, NBSIR 79-1739, 1979.

<sup>10</sup> Bukowski, R. W. and Istvan, S. M., A Survey of Field Experience with Smoke Detectors in Health Care Facilities, NBSIR 80-2130, 1980.

<sup>11</sup> Bukowski, R. W., Smoke Detectors, Alarms, and Controls, NFPA Round table on Fire Safety in Atriums - Are the Codes Meeting the Challenge?, December 15-16, 1988, pp 1-19, 1988.

<sup>12</sup> Bukowski, R. W., Techniques for Fire Detection, *Proceedings of the NASA Workshop on Spacecraft Fire Safety*, Nat. Aeronautics and Space Admin. (US) pp 9-29, 1987.

<sup>13</sup> Forney, G. P., Bukowski, R. W., and Davis, W. D., Fire Modeling: Effects of Flat Beamed Ceilings on Detector and Sprinkler Response. International Fire Detection Research Project. Technical Report. Year 1. 59p., 1993.

<sup>14</sup> Davis, W. D., Forney, G. P., and Bukowski, R. W., Field Modeling: Simulating the Effect of Sloped, Beamed Ceilings on Detector and Sprinkler Response, International Fire Detection Research Project. Technical Report. Year 2. 34p., 1994.

<sup>15</sup> Klote, J.H., Forney, G.P., Davis, W.D., and Bukowski, R.W., Field Modeling: Simulating the Effects of HVAC Induced Air Flow from Slot Diffusers on Detector Response, Year 3 Technical Report, National Fire Protection Research Foundation, Quincy, MA 02269, 1996.

<sup>16</sup> Klote, J.H., Davis, W.D., Forney, G.P., and Bukowski, R.W., Field Modeling: Simulating the Effects of HVAC Induced Airflow From Various Diffusers and Returns on Detector Response, Technical Report, Year 4, National Fire Protection Research Foundation, Quincy, MA 02269, 1998.

<sup>17</sup> Grosshandler, W. L., Towards the Development of a Universal Fire Emulator-Detector Evaluator. National Institute of Standards and Technology, Gaithersburg, MD . Fire Safety Journal, Vol. 29, 113-127, 1997. University of Duisburg. International Conference on Automatic Fire Detection "AUBE '95", 10th. April 4-6, 1995, Duisburg, Germany, Luck, H., Editor, 368-380 pp, 1995.

<sup>18</sup> Davis, W. D.; Forney, G. P. Sensor-Driven Inverse Zone Fire Model. National Institute of Standards and Technology, Gaithersburg, MD Research and Practice: Bridging the Gap. Fire Suppression and Detection Research Application Symposium. Proceedings. Fire Protection Research Foundation. February 23-25, 2000, Orlando, FL, 204-211 pp, 2000.



Reinhard Conrads, Head of the Certification Department (VdS Cert)  
VdS Schadenverhütung Köln (VdS Loss Prevention Cologne – Germany)

## **European Standards and Certification Procedure**

### **1 Introduction**

The protection of life and real values is too important to leave it to the free interplay of forces of economy. In a world getting more complex every day the people, authorities, trade and industry and insurers expect a proved and confirmed function and reliability when thinking about useful protection measures against fire, explosion, intrusion, hold-up and other hazards. The introduction of a test and certification scheme for products and services in the field of fire protection and security technology [1] was the consequence of this request in most of the European countries.

The following article will describe this system of testing and certification of products and crosses questions regarding the co-operation of different test houses and certification bodies within Europe which is becoming more and more one unit in some sectors.

### **2 Importance of testing and certification**

One of the characteristics of all security and protection measures against fire, intrusion and hold-up in practical use is the fact that normal users unfortunately are not able to verify the functionality and reliability of such systems. Users also cannot differ between useful systems of high quality and systems which are to the benefit of the salesman only.

Another important aspect is the fact that faulty functions of protection measures may cause losses in another area or at least big trouble with people, neighbours etc. The unintentional flooding of an area which is

protected by an automatic sprinkler system is one example, the need for evacuation of an area flooded by mistake with CO<sub>2</sub>-gas by an automatic CO<sub>2</sub>-extinguishing system another one. But also the faulty function of a detection system like an automatic fire detection system may cause serious problems if you think about the jeopardising which is caused by the vehicles of the fire brigade which are driving very fast through the night. Additionally the confidence in protection measures giving false alarms is sinking rapidly. Which policeman is reacting to an alarm of an intruder alarm system when he has made the experience that this is typically a false alarm?

It is one of the greatest challenges for the technical development departments in the industry that safety installations on the one hand in the case of an actual hazard have perfectly to work mostly in short times; on the other hand these installations have to survive huge periods in a “stand-by” mode under most different environmental conditions, probably with changing modes for use for the protected premises, other operators etc.

Therefore it is a good and long tradition in Europe that products in the fire protection and security technology market are tested by independent Test Laboratories (Test Labs) and certified by independent Certification Bodies (CB). The initiative for these activities mainly came from the insurers. Already at the end of the 19<sup>th</sup> century they knew that the assurance in much cases is more reasonable than just to insure. First emphasis was given on products for fire prevention. Later on also the field of protection against intrusion and hold-up was considered. In Germany for example the insurers against losses who gathered in associations founded a department of loss prevention in 1906. Same activities started in countries like France or Great Britain even before this date.

The assessment of products first was made on-side during installation. Later – e. g. in Germany – universities made this assessment on the basis of



product samples. There one concentrated first on the key functions of a product, e. g. is the sprinkler system extinguishing fire and then on the options against false function. In the 60ies this activity was no more of interest for the universities because their work is not focused on type-testing. The insurers – in front of the decision to give up the item prevention - decided to found own laboratories which took over this activity in 1967. In other European organisations the development was similar.

A further aspect should be raised here: the installation of specified and qualified protection measures as e. g. a certified automatic sprinkler system may lead to enormous reductions in insurance rates. So the loss prevention is not only useful but also cost reducing.

Finally the advantage for users when changing to another insurer cannot be denied because everyone knows what measures are existent when standardised and certified products are used and a new assessment of the measures on side is not necessary.

### **3 Activities of the insurers and other organisations**

As mentioned above testing in the past was first concentrated on the key functions of a product, later in addition on the key options against false function of that product. Beginning with the 70ies the idea of "type testing" was initiated; this meant that samples of the products were sent to the laboratories for testing. The insurers' laboratories together with their associations and in co-operation with universities – as an example in Germany the University of Aachen and later Duisburg, developed test schedules for the different products. A lot of these test schedules were the predecessors of national and international standards (example: the insurers' test schedules for heat and smoke detectors are now a part of the European standard EN54) [2].

Products which have passed the testing with success got a "letter of conformity " with the remark that this product has been approved by the insurance association. Restrictions in function or time limitation of this "approval" were unknown in the first years, neither terms like complete test report nor quality assurance. In the 70ies the test schedules got more complete, also the problems of avoiding faulty function were more and more tackled and solved. What was furthermore found out was the fact that testing on samples of products or even only one specimen handed in by the manufacturer is not sufficient as a sample test for all products.

Given this idea further requirements as the testing of several samples, the visit of the manufacturers' plant, single re-tests of approved products and a kind of product surveillance of the installed systems which also have been assessed by the staff of the insurers' department of loss prevention were described. The rules and standards of the insurers changed in the same way; those, often versions lying in the office tables of the laboratories in the 80ies, became specifications equivalent to "regular" standards.

In the meantime the information on the approval was given not only by letter but the laboratories also issued approval certificates which were limited timely and which constrained both parties to re-check – normally after 4 years – if the characteristics of the product are still actual. Furthermore the tested and approved products were listed accordingly.

The described procedure had a great advantage; solutions for problems which were detected during visits on site – or in struggles with the failure of protection systems – or the bypassing of intrusion prevention measures by more skilled intruders – could directly be introduced in the testing schemes; not in every case to the pleasure of the manufacturers. At the end



of the 80ies - at least in Germany - a satisfying level of the tools for loss prevention against fire and intrusion was reached.

The industry was not sleeping that time. Especially those companies who wanted to stand out from the majority and wanted to have confirmed the quality of their products made big efforts towards a standardization of performance and quality characteristics for fire prevention and security technology. First traces of this standardisation can be found e. g. in Germany in the year 1913 [3]. In other countries there were similar developments and in the 70ies and 80ies all major countries in Europe had own national standards in the field of fire prevention and security. This trend was continued by the European standardisation bodies CEN (European Committee for Standardization) and CENELEC (European Committee for Electrotechnical Standardization).

#### **4 Certification and accreditation against European standards EN 45 000 ff.**

A decisive turning point in the activities of loss prevention was introduced by the activities of the European Community (EC) regarding a combined European market. These activities started in the middle of the 80ies. The aim of the harmonisation of the European market, anchored in the foundation act of the EEC already in the middle of the 50ies (so-called Treaties of Rome), was blocked at that time by a series of trade restrictions between the member states. These restrictions were mainly given by:

- different interstate legal and administrative regulations
- different or missing technical standards
- different test, certification and surveillance procedures

The commission of the EC decided that all these trade restrictions should be cleared up, and as a consequence the standardisation bodies in Europe

should begin to transform national standards and specifications into European standards. The different test, certification and surveillance procedures were to be standardised. Today, in the year 2001, we can notice that we are still far away from reaching this aim, e.g. in the area of intruder alarm systems. It has, however, to be considered that it is not possible to equalise very strong habits which have grown in long decades and even centuries just "by order". The different languages represent further difficulties. Insider only know the difficulties of a group of people discussing about complex items when everyone of them is talking in another language. Also the actual use of standards is different: in some countries standards are used seriously like laws, in others they are more or less advices.

As far as the different test procedures, certification and surveillance procedures are taken into account it was easier to come to an agreement. For testing and certification one has to distinguish between the so-called legally controlled area, e.g. where safety in electrical installations or safety of machines is required (see also clause 7) and the voluntary area to which at the moment all in clause 1 mentioned products count. In order to create the conditions for a trustful co-operation the **European Organisation for Testing and Certification – EOTC** - [4] was founded in April 1990 by the European Commission, the European Free Trade Association (EFTA) and the European Standards bodies. The EOTC was charged with the elaboration of transparent and trustworthy accreditation and certification models for Europe in order to reach the aim of one-stop-testing.

In order that all institutions like laboratories, certification bodies and institutions for product surveillance are working according to the same rules, a European standard series was elaborated valid for all these institutions [5] [6] [7]. Furthermore accreditation systems in the member states of the EU were established with the aim to check on side if all participating institutions are working according to the same rules. The so-



called sectorial committees within the national accreditation bodies elaborated product-by-product specific standards, against which laboratories, certification bodies were assessed.

In this connection also the requirement to give proof of a certified quality management system (QMS) according to the ISO 9000 series of standards came up [8] [9]. These requirements represented also a reaction on the activities of the Japanese in the 80ies regarding a higher quality of products compared with the rest of the world.

The realisation of the requirements of the accreditation bodies was not very easy; a lot of ingrained structures had to be adopted to the requirements of the standards; standards existing only on the paper had to be brought to applied standards and specifications; testing procedures had to be described in detail. Now there is more exactness but in a lot of cases the spontaneity was lost, as e. g. the change of standards regarding requirements which have become outdated.

A major problem was created by the requirement for a certified quality management system for smaller companies – especially in Germany where traditionally personnel enjoys a long-lasting training (e. g. 3 to 4 years for a junior handicraftsman), before beginning to work without steady observation. This is in contradiction to the philosophy in other countries where staff is employed without training and is then working according to detailed and unambiguous instructions. But it was mentioned already that the European unification is not a very easy task.

Taken all these arguments into consideration the constraint for accreditation of institutions which deal seriously with testing and certification of products in the fields of fire protection and security technology has lead to an amelioration of results in many areas [10]. The whole procedure has become more formulised, there are real test reports

and real documented certificates now. Also the items testing (that means the measurement of facts) and certification (that means the confirmation of conformity with a technical specification) were divided into two independent procedures to allow a qualified verification and evaluation of the test results which have been ascertained in the laboratories.

Lists of all certified products had to be published regularly, the rules of the insurers became quasi-standards. Also requirements as e. g. certified quality management system, regular product surveillance lead to the fact that not only the few tested and certified products (the test samples) were good but - what can be assumed by the additional measures - all certified products which are leaving the factory.

In principle the certification – or approval – now is based on three equal pillars:

- Successful testing of test specimen
- Operation of a certified quality management system according to ISO 9000 by the manufacturer
- Regular product surveillance and – if necessary - re-testing of samples.

But now each member state of the European Union (EU) felt forced to found laboratories and certification bodies for the field of fire protection and security technology - a disadvantage as suddenly for those economically small areas more laboratories and certification bodies than manufacturers were existing. And due to the different mentalities and the legal administrations in Europe the organisations of accreditation bodies had different characteristics. Some of them worked thoroughly and tested each step of the certification bodies and laboratory, others concentrated on formal items. So, for the time being the Europeans cannot be satisfied with what has been reached until now. There is still a lot of work to do.



## **5 Active certification bodies in Europe**

Due to the variety of the languages in Europe it is not easy to get an overview of the nowadays existing test and certification schemes for products and services in the field of fire protection and security technology and their efficiency in the market. According to the knowledge of the author – which may possibly not be complete - the situation for this field of activity in the most important countries of the European Economic Area represents as follows:

Italy: Certification of intruder and automatic fire alarm systems, safes and strongrooms

France: Certification of gas and water extinguishing systems, safes and strongrooms, intruder and automatic fire alarm systems, access control systems

Belgium: Certification of intruder alarm systems and automatic fire detection systems

Germany: Certification of intruder and automatic fire alarm systems, access control systems, gas and water extinguishing systems, safes and strongrooms, physical security equipment and locks, portable fire extinguishers

Great Britain: Certification of intruder and automatic fire alarm systems, gas and water extinguishing systems, safes and strongrooms, physical security equipment, portable fire extinguishers

Denmark: Certification of automatic fire alarm systems

Sweden: Certification of safes and strongrooms, physical security and locks

Switzerland: Certification of intruder and automatic fire alarm systems

Austria: Certification of intruder alarm systems and safes and strongrooms

The meaning of the different certification marks in the market seems to be very different; in some countries there is already no chance to get an

allowance to use a building by the authorities without the use of certified products in the area of fire protection, in other countries the insurers are very strict: that means no underwriting in specific risks without sufficient certified protection against intrusion. But certification marks also may only be an item “nice to have” or a marketing instrument of the sales department.

## **6 Testing and Certification in a united Europe**

The great differences of the certification systems and test specifications in Europe are causing series of trade restrictions between the individual states in Europe. This may lead to the fact that a system which is seen positively and in accordance with the standards in one country may not be applied in another country – and in the worst case – has to be changed and re-tested and re-certified. In the legally controlled area these differences will be abandoned by the introduction of the CE-marking (see clause 7). However, the CE-marking represents the smallest common factor for requirements of a product. In case trade restrictions are not based on liabilities as we know it in the legally controlled area but on the free interplay of forces, the governmental authorities cannot take direct nor indirect influence. This situation can be avoided by two measures: on the one hand the technical specifications which are included in the national certification schemes have to be harmonised. On the other hand agreements between the certification bodies should be made in order to ensure the mutual acceptance of test results and the additional requirements like a certified quality management system in accordance with ISO 9000, regular product surveillance, sampling and re-testing of products.

Agreements between certification bodies, however, are only possible if impartial fundamentals for a trustful co-operation between the certification



bodies do exist. This ideal situation is not yet completely achieved in the higher sophisticated European unification procedure.

Therefore the „European Fire and Security Group“ (EFSG) was founded in 1991 [11] with the aim to avoid unnecessary duplication of testing, assessment and certification work – but to keep this work on the proven high level. EFSG started with the three members: APSAD (Assemblée Plénière des Sociétés d'Assurances Dommage – today Centre National de Prévention et de Protection (CNPP) in France, Loss Prevention Council (LPC) – today BRE Certification Ltd. in Great Britain, and Verband der Sachversicherer e.V. – today VdS Schadenverhütung (VdS) in Germany. Today EFSG has 8 members in 6 European countries [12] and some other organisations are waiting to get accepted as members

A former aim of EFSG was the introduction of a harmonised European certification mark (EFS Mark). But it has been abandoned because the mark was not requested from the market nor was it possible to remedy the almost insuperable obstacles caused by the missing of harmonised standards and specifications. Furthermore there were and are reservations of the national certification bodies regarding the loss of their independence. Another important issue is the fact that Certification Bodies carry the full responsibility for the decision of a certification. From the legal point of view the certification body may get great problems in case of damages caused by a product tested and/or certified by another organisation.

In order to come closer to a mutual recognition of test results without jeopardising the autonomy of the certification bodies the basic philosophy of EFSG has been renewed in the year 2000:

Now the testing and certification procedures are left to the relevant national certification bodies or associated laboratories. The certification bodies stay

autonomous in future and will not be forced to issue certificates on base of a test result without any further condition. Agreements on a product-by-product basis are made between the single certification bodies on base of which certifications may be performed. These agreements may be bilateral or even multilateral agreements and may cover a complete test and certification scheme for a specific product or parts of it only.

These agreements may be similar to the Memorandum of Understanding (MoU) which exists already between BRE and VdS and works satisfactory since August 1997. Under this MoU test results in the area of automatic fire detection systems have been exchanged between BRE and VdS without problems. Personal of the laboratories work close together e. g. in standardisation groups and regulary exchange information important for the daily work. An extention of the MoU to other areas is planned.

Members of EFSG – the certification bodies – have to fulfil the requirements specified in the Terms of Reference (a kind of statutes of EFSG), as e. g. the accreditation according to EN 45011, qualified personell, regular training of the staff, round-robin tests. These are some of the requirements for a trustful co-operation between the EFSG members. Same severe requirements are to be fulfilled by the associated laboratories. A Certification Body may nominate one or more laboratories as associated, which then acts as subcontractors to perform the tests necessary for the certification. The fulfilment of these requirements for certification bodies and associated laboratories is checked in form of audits by EFSG.

Finally it must be stated that EFSG now is associated member of the European Fire and Advisory Council (EFSAC) [13], an umbrella organisation of the manufacturers in the field of intrusion and fire protection. Membership within EFSAC brings together European industrial



associations, the Confederation of Fire Protection Associations (CFPA) and the European Insurance Committee (CEA) [14].

## **7 CE-marking versus testing and certification**

As already mentioned in clause 6 the commission of the European Union (EU) [15] tries to harmonise the technical specifications and test/certification systems in areas which match health and safety with legal influence to level out trade restrictions between the single states in Europe. Now the main set of products used in the field of fire prevention will become part of the „Construction Product Directive“ (CPD) and are therefore part of the legally controlled area which requires CE-marking in the future.

As soon as the so-called harmonised standards for these products are available – and after a transition period of 1 – 2 years – all these products have to be CE-marked by the manufacturer and in addition show a „Certificate of Conformity“ issued by a „Notified Body“. Notified Bodies have to be listed in Brussels (at EU level) for the field of activities testing, certification and surveillance.

From the point of view of the insurers the oncoming CE-marking does not guarantee in every case the same level of product quality as known today; the CE-mark is more or less not more than a „passport“ allowing products to cross borders and to demonstrate that the products are conform with European laws. Very often „CE“ represents the smallest common factor for requirements of a product. Also a „system“, that means the combined function of different products (e.g. the chain: fire detectors - fire alarm control and indicating equipment – alarm transmission equipment), will not be tested for CE-marking. But the main concern is the fact that Notified Bodies will come into the market which are not active in the field of testing

and certification of products in the area of fire protection until today. This may cause great differences in quality of the products marked with "CE".

The established certification bodies working together in EFSG will continue to work on a level of quality of testing and certification as known today. Therefore the mentioned „Certificate of Conformity“ for CE-marking will be a subset of the certificate which is issued today. The certification marks of today (e.g. CNPP, LPCB, VdS) will continue to guarantee a high level of product quality above the level of the CE-marking.

## **8 Conclusion**

The third party testing and certification of products and services of the fire protection and security technology has been applied in Europe since decades with success. Only the impartial judgement assures that user, insurer and authorities can trust on the functionality and reliability of these services and products.

All certification bodies which are united in the „European Fire and Security Group“ (EFSG) work in order to reduce the expenses for testing, quality assurance and product surveillance on the base of European standards and specifications – but to keep the quality of the certified products on a high level. Also they would like to stay independent certification bodies with their own independent decision and their own certification marks.

Basis of these activities on one hand is a trustful co-operation between the certification bodies on the base of equal conditions – on the other hand the availability of harmonised and comparable requirements and test methods. Here big deficits still exist, especially in the area of security. Automatic fire detection technology is in a slightly better situation.



But the oncoming CE-marking in the field of fire prevention will not supersede marks of qualified certification bodies because of lack of quality in technical specifications and in the confidence of the issuing bodies.

## References

[1] Fire protection: e.g. automatic fire alarm systems, water extinguishing systems (sprinkler systems), gas extinguishing systems (CO<sub>2</sub>), smoke and heat exhausting and ventilation systems (SHEVS), portable fire extinguishers

Security technology: e.g. intruder alarm systems, hold-up alarm systems, access control systems, safes and strongrooms, high security locks, physical security equipment, locks

[2] EN 54 series of Standards of Fire Detection and Fire Alarm Systems

[3] E. g. German standard DIN 14 675 Feuermelde- und Alarmanlagen (Fire signalling and alarm systems), VDE 0800 Bestimmungen für Fernmeldeanlagen (Regulations for communication systems), first edition published 1913)

[4] EOTC – European Organisation for Conformity Assessment

Rue d'Egmont 15, B-1000 Brussels Web: <http://www.eotc.be>

[5] EN 45 001 General criteria for the operation of testing laboratories

[6] EN 45 011 General requirements for bodies operating product certification systems

[7] EN 45 012 General requirements for certification bodies operating Quality System certification

[8] EN ISO 9001 Quality systems – model for quality assurance in design/development, production, installation and servicing

[9] EN ISO 9002 Quality systems – model for quality assurance in production, installation and servicing

[10] The laboratories and certification bodies of most of the members of EFSG were accredited at beginning of the 90ties; e. g. VdS Schadenverhütung was accredited for testing and certification of products in the area of fire protection and security technology in 1992.

[11] „European Fire and Security Group“ (EFSG)

The secretary:

European Fire and Security Group

Amsterdamer Str. 172- 174

D-50735 Köln Germany

Telephone: +49-221-7766-375

Telefax: +49-221-7766-377

Email: [gspaeth@efsg.org](mailto:gspaeth@efsg.org)

Internet: <http://www.efsg.org>

[12] „European Fire and Security Group“ (EFSG) – members December 2000

- BRE Certification Ltd. – Great Britain

Building 3, Bucknalls Lane, Garston, Watford, Hertfordshire GB-WD25 9XX

e-Mail-Adresse: [FieldP@bre.co.uk](mailto:FieldP@bre.co.uk)

- Centre National de Prévention et de Protection (CNPP) – France

BP 2265, F-27950 St. Marcel

e-Mail-Adresse: [Isabelle.Glasner@cnpp.com](mailto:Isabelle.Glasner@cnpp.com)

- Forschungs- und Prüfungsgemeinschaft Geldschränke und Tresoranlagen (FuP) - Germany

Lyoner Str. 18, D-60528 Frankfurt

e-Mail-Adresse: [fup@vdma.org](mailto:fup@vdma.org)



- Svensk Brand- och Säkerhetscertifiering AB (SBSC) – Sweden  
Tegeluddsvägen 100, S-11587 Stockholm  
e-Mail-Adresse: [kjell.nordahl@sbsc.se](mailto:kjell.nordahl@sbsc.se)
- Istituto di Certificazione Industriale per la Meccanica (ICIM) - Italy  
Piazza Diaz 2, I-20123 Milano  
e-Mail-Adresse: [icimorg@tin.it](mailto:icimorg@tin.it)
- Istituto Italiano del Marchio di qualita (IMQ) - Italy  
Via Quintiliano 43, I-20138 Milano  
e-Mail-Adresse: [baggio@imq.it](mailto:baggio@imq.it)
- VdS Schadenverhütung GmbH – Germany  
Amsterdamer Str. 172- 174, D-50735 Köln  
e-Mail-Adresse: [hschuengel@vds.de](mailto:hschuengel@vds.de)
- Schweizerisches Institut zur Förderung der Sicherheit (SI) –  
Switzerland  
Nüscherstrasse 45, CH-8001 Zürich  
e-Mail-Adresse: [safety@swissi.ch](mailto:safety@swissi.ch)

[13] „European Fire and Security Advisory Council“ (EFSAC)

The secretary:

c/o Hans Schüngel

Amsterdamer Str. 172

D-50735 Köln Germany

Telephone: +49-221-7766-185

Telefax: +49-221-7766-150

Email: [info@efsac.org](mailto:info@efsac.org)

Internet: <http://www.efsac.org>

[14] „European Fire and Security Advisory Council“ (EFSAC) – members

January 2001-01

- European Federation of Associations of Lock and Builders Hardware  
Manufacturers – ARGE , Postbus 190, NL-2700 AD Zoetermeer

- Comité Européen des Assurances – CEA  
3 Bis, rue de la Chaussée d'Antin, F-75009 Paris
- Confederation of fire protection associations – CFPA  
Nüscherstrasse 45, CH-8001 Zürich
- European Association of Manufacturers of Fire and Intruder Alarm Systems – Euralarm  
Hofmannstraße 51, D-81379 München
- European Committee of the Manufacturers of Fire Protection Equipment and Fire Fighting Vehicles – Eurofeu  
c/o Minimax GmbH, Industriestraße 10 – 12, , D-20840 Bad Oldesloe
- European Committee of Safe Manufacturers Association – Eurosafe  
Merwedestraat 48, NL-3300 AB Dordrecht
- European Doors and Shutters Federation – EDSF  
c/o Verband Tore-Türen-Zargen, Hochstraße 113, D-58095 Hagen

[15] The „European Union” (EU) is the successor of the „European Community” (EC), which was founded 1957 in Rome as „European Economic Community” (EEC) by France, Italy, Germany, Netherlands, Belgium and Luxemburg in order to push the economical and political integration of Europe.



Building and Fire Research Laboratory, National Institute of Standards and Technology,  
Gaithersburg, MD 20899, USA

\*Guest Researcher on leave from the Center for Environmental Safety and Risk  
Engineering, Victoria University, Melbourne, PO Box 14428, VIC 8001, AUSTRALIA

### **An apparatus for light scattering studies of smoke particles**

#### **1. Introduction**

There is great interest in being able to distinguish between flaming, non-flaming and nuisance alarm aerosols using light scattering methods. Commercially available light scattering smoke detectors are not able to make such distinctions. Past studies have examined various aspects of light scattering from smoke and nuisance aerosols. Two such studies [1] have examined the light scattering from smoke generated by flaming and non-flaming fuels using fixed position detectors. Loepfe et al. [2] made use of polystyrene spheres for calibration of their instrument and both studies had the instruments installed in a fire test room. Meacham and Motevaili [1] examined the detector response signals at individual angles, while Loepfe et al. [2] discriminated between smokes using the degree of linear polarization as a function of angle. We have developed a facility for measuring the light scattered by smokes as a function of the scattering angle and linear polarization. By using monosize polystyrene calibration particles and filter collection for gravimetric measurement, we were able to measure for the first time the differential (angular distribution) scattering cross section per mass of a smoke aerosol. This differential mass scattering cross section is a measure of the light scattering strength of a particle in units of area per mass.

In this paper we focus on the optical design of the light scattering facility, the calibration method and results for acetylene soot. This method is applied to two non-flame generated smokes and three flame generated smokes and presented in another paper [3].

## 2. Apparatus

This study was carried out by adapting the existing large agglomerate optical facility (LAOF) developed at the National Institute of Standards and Technology (NIST), MD, USA. The LAOF was originally [4] used to measure the mass specific extinction coefficient for flame generated smoke and the total scattering coefficient using a reciprocal nephelometer [5], which has a cosine sensor/photomultiplier tube set at the center of the upper cell in Figure 1. For the differential light scattering experiments the long upper glass section with the tapered inlet was replaced with a short column. This column has opposing inlets on either side of the column to promote mixing of the aerosol when it

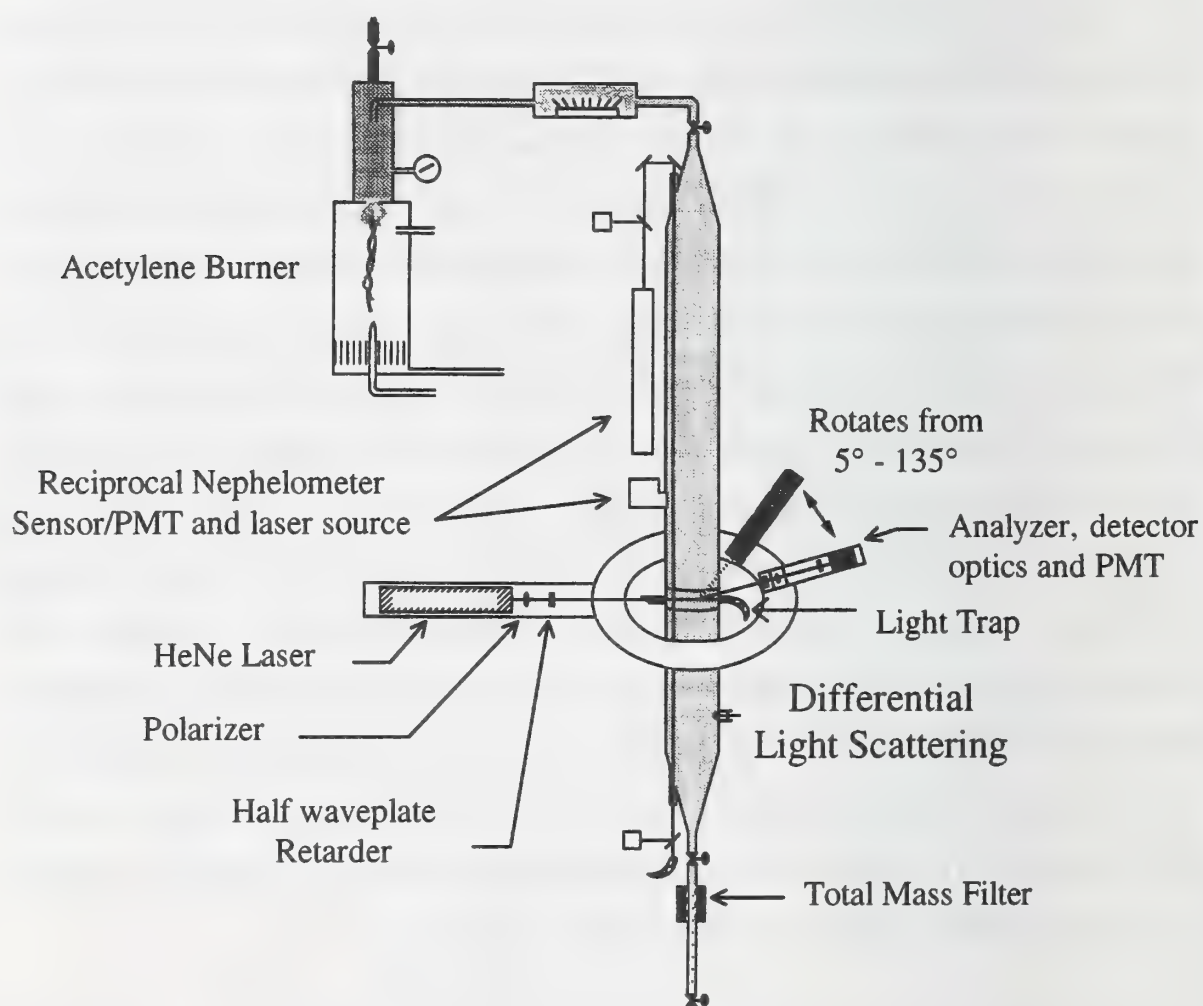


**Figure 1:** A schematic of the basic LAOF set up.

enters the LAOF. The particles are carried by the air flow to the scattering cell in the midsection of the column where the light scattering occurs. The particles then flow to the bottom of the LAOF where they are collected on a 47 mm filter at a known



volumetric flow rate. The mass concentration of the aerosol is determined from the mass of particles on the filter and the volume flow rate. A constant flow rate of  $10 \text{ L min}^{-1}$  is maintained with a mass flow controller followed by a vacuum pump.

### **3. Generation of Calibration and Smoke Aerosol**

Nebulizing a suspension of monosize (nominally) 496 nm diameter PS spheres in water produces a monosize polystyrene latex (PS) aerosol which was used as the calibration aerosol. This size was chosen for its similarity to non-flaming smoke particle sizes and its Mie scattering pattern, which is free of high frequency variation. The suspension is prepared by adding about 2 ml of the concentrated (0.01 volume fraction) suspension to 50 ml of particle free water. Nebulized droplets containing a single sphere evaporate as they flow through a diffusion drier, resulting in a PS aerosol. The drier consists of a 500 mm long, 70 mm ID tube with a 10 mm diameter screen tubing surrounded by silica gel. A majority of the particles are singlets but there is a small fraction of doublets resulting from the drying of a droplet containing two spheres. Once the spheres have exited the diffusion drier some dilution air is added to the flow at a rate of about  $5 \text{ L min}^{-1}$  and this aerosol stream is passed into a 3 L volume for final mixing. The flow is then introduced into the LAOF. A by-pass exists between the mixing volume and the LAOF to maintain nearly atmospheric pressure in the LAOF. A filter is connected to the by-pass line to prevent PS spheres from escaping into the atmosphere if the flow rate of PS aerosol should be greater than the vacuum flow rate. Also the by-pass filter will prevent ambient particles from entering the system if the PS aerosol flow rate is less than the vacuum flow rate.

The acetylene smoke used in this study was produced in a steady-state and repeatable manner by a co-flow laminar diffusion burner [6]. The smoke concentration was adjusted to the required range by adding dilution air to the small amount of soot that is sampled from the burner before it enters the scattering cell.

### **4. Optical System**

The light scattering cell is located in the midsection of the LAOF and fabricated from

10 cm inner diameter glass tubing ending in ground glass flanges. The flanges allow connection to the upper and lower neighbors, which are also fabricated from glass. The scattering cell has an entrance window for the incident light beam and a light trap directly opposite. The scattering plane is defined to be the plane in which the incident and scattered beams lie; for our experiments this is the horizontal plane. The scattering angle,  $\theta$ , is given by the angle measured from the direction of propagation, so that  $\theta = 0^\circ$  is the forward direction of the incident beam. The incident beam originates from a HeNe laser (wavelength  $\lambda = 632.8$  nm) in continuous wave (CW) mode which has a 500:1 linear polarization ratio. The CW beam is immediately passed through a rotating chopper ( $f = 80$  Hz) to reduce background noise when measuring low signals. The incident beam then passes through an optical train of polarizing elements that prepare the optical properties of the beam. This optical train consists of a linear Glan-Taylor type generating polarizer orientated with its optical axis at an angle  $\phi_p = 0^\circ$ , where  $\phi_p$  is the angle of the optical axis of the polarizer from the scattering plane. A subscript H then is then used to denote this polarization as the horizontal polarization. This generated polarization essentially eliminates the residual perpendicular or vertical (subscript V) polarization of the laser. The next optical element is a quartz zero-order half-waveplate retarder. This is the key element in the incident optical train as a  $45^\circ$  rotation of its fast axis from the scattering plane induces a rotation of the beam from horizontal to vertically polarized light. In this way an incident polarization of either horizontal or vertical orientation can be chosen. The next optical element before the scattering volume is the entrance window, which is set at a slight angle to avoid the multiple reflection of the incident beam. This angle does have an effect of reducing the intensity of the incident beam, as do all the other elements of the incident light optical train. After passing through the window, the laser beam passes through a 10 cm pathlength of uniformly distributed smoke or calibration aerosol. The light scattering is apparent as a red line of light with a few bright spots arising from large agglomerate particles in the case of the acetylene smoke.

The scattered light first passed through the wall of the LAOF's scattering cell with a slight loss of light due to reflection. The opposite side of the scattering cell to the



detectors view was coated in a base layer of matte black paint and then a layer of carbon paint was added onto this. Reducing reflection of scattered light entering the detector field of view. This was particularly important near the entrance window and the light trap as reflections and stray light were appreciable in these areas. The entrance window itself had to be kept to a small diameter, so that plasma light from the laser and beam dispersion did not create a large area of reflection bigger than the entrance of the light trap, which was 5 mm. The effect of this stray light at the entrance window and near the light trap entrance would otherwise add significantly to the scattered light signal in the forward and  $135^\circ$  directions respectively.

To align the polarizers optical axes correctly, the first generating polarizer is set in a precision mount and reference to a polarizing beam splitter. A null or crossed polarizer approach is then used to determine the positions for the half waveplate and the analyzer, so that horizontal incident and horizontal scattered polarized light (HH) can be produced and similarly, vertical-vertical polarization (VV). The analyzer is a linear polarizer used to measure the vertical or horizontal scattered light incident on the detector. The generating polarizer was set at either  $\phi_p = 90^\circ$  or  $\phi_p = 0$  to cross the analyzer during alignment, but was not changed from the  $\phi_p = 0^\circ$  position during an experiment. Once the polarizer and analyzer were aligned, the half waveplate retarder was placed in the optical train and aligned. The analyzer,  $\phi_A$ , and retarder,  $\phi_R$ , angles are changed manually as required when conducting an experiment. These changes were found to cause a standard uncertainty of about 3 % (1 std. deviation) in the measured signal. In this paper the standard uncertainty refers to one standard deviation about the mean value of a series of measurements. The combined uncertainty refers to the combined standard uncertainties of the variables using a root-sum-of-squares method. All uncertainties are expressed as a percentage of the mean value.

The scattered light was detected by a series of optical elements mounted on a rotation stage with stepper motor drive and encoder feedback. PC control of the rotation stage was accomplished by a computer program and interfaced through an indexer-board in the PC. This program also monitored the detector signal via an analogue-to-digital

converter board. The rotation stage would move the detector and its optical elements in  $\Delta\theta = 5^\circ$  steps in the scattering plane from  $5^\circ$  to  $135^\circ$  to measure the scattered light. Essentially any angle in the range could be chosen for a measurement; for example, an extra measurement is usually made at  $\theta = 8^\circ$ . Alignment of the detector zero position was also automated but required the placement of neutral density filters in the incident beam and removal of the light trap. The rotation stage was then positioned manually until the detector indicated a peak intensity was found. The computer program then made the rotation stage scan a range of  $\pm 2.5^\circ$  about this peak position in  $0.25^\circ$  steps. The peak signal detected was then redefined as zero and another fine step scan was conducted from  $\pm 1^\circ$  of this position in  $0.1^\circ$  steps; again the peak position was redefined if necessary and this became the  $\theta = 0^\circ$  position. The detector would then move out of the beam to the  $4^\circ$  resting position to await the beginning of an experimental scan.

The first optical element carried by the detector rotation stage was the analyzing polarizer, a Glan-Taylor prism, which was aligned to analyze either the horizontal,  $\phi_A = 0^\circ$ , or vertical polarization,  $\phi_A = 90^\circ$  component of the scattered light for a given scan. Following the analyzer was a 5 mm entrance aperture of the detector housing. The detector housing is a sealed tube containing (in order) a laser line filter, an achromatic lens, a 1 mm diameter aperture stop, a diffuser and finally the side mounted photomultiplier tube. The filter reduces the background by allowing only the laser wavelength to pass. The achromatic lens with the aperture at the focal point of the lens is positioned to limit the scattered light to  $\pm 0.3^\circ$  of the scattering angle. This small acceptance angle is important for minimizing the forward scattering bias at small angles. A large area diffuser is positioned between the aperture stop and PMT to spread the initially focused beam over the active area of the PMT and reduce the effects of PMT polarization dependence.

The signal from the PMT was taken through a variable resistor to a lock-in amplifier unit. The lock-in used a chopper to provide the lock-in frequency and the sensitivity of the amplifier was chosen manually when required as the detector is moved to a new position. The output signal from the lock-in was then passed through a voltage divider



to the analogue-to-digital converter in the controlling PC. In a series of calibration and smoke experiments the sensitivity of the amplifier is the only parameter in the detection circuit that is changed.

As the detector scans through the scattering angles, the scattering volume changes in proportion to  $1/\sin(\theta)$ . This angular dependence results in more than a factor of 10 change in the detector's view of the scattering volume as the scattering angle increases from  $5^\circ$  to  $90^\circ$ . To correct for the effects of angular dependence of the scattering volume geometry as well as signal scaling, a calibration needs to be performed.

## 5. Calibration

By scattering light from the PS calibration aerosol and then normalizing the detected signal by the theoretical signal for these spheres we can determine a calibration function,  $K(\theta)$ . This calibration function corrects for the scattering volume, detector effects, and the small error effects of the optical train. In this study the calibration function also includes the scaling due to the incident beam irradiance, as we have assumed that it is constant during the experiments. The object of these calibrations is to determine the differential (angular distribution) mass scattering cross section,  $\sigma(\theta)$ , of the smoke particles to be examined.

From Debey-Mie theory [7] the differential scattering cross section,  $C_{th}(\theta)$ , for a single 496 nm polystyrene sphere is calculated. This is then converted to a theoretical differential scattering cross section per mass,

$$\sigma_{th}(\theta) = C_{th}(\theta)/V_p \rho_p, \quad (1)$$

by dividing by the particles mass; here the values  $V_p$  and  $\rho_p$  are the particle volume and density ( $1.05 \text{ g cm}^{-3}$  for PS spheres) respectively. The calibration experiment is conducted by introducing the PS spheres into the scattering volume and making detector signal measurements,  $U_p(\theta)$ , for a given polarization. The detector signal,  $U_p(\theta)$ , has a dependence on the scattering volume that varies as  $1/\sin(\theta)$  to the first order, this can be corrected by calculating  $u_p(\theta) = U_p(\theta) \sin(\theta)$ . The mass concentration,  $M_p$ , of

calibration particles is determined from the filter mass. The theoretical value,  $\sigma_{th}(\theta)$ , is used to normalize the detector signal to determine the calibration function,  $K(\theta)$ , such that

$$K(\theta) = \frac{u_p(\theta)}{M_p \sigma_{th}(\theta)} \quad (2)$$

where  $p$  is the subscript for the calibration particle values. The calibration function is

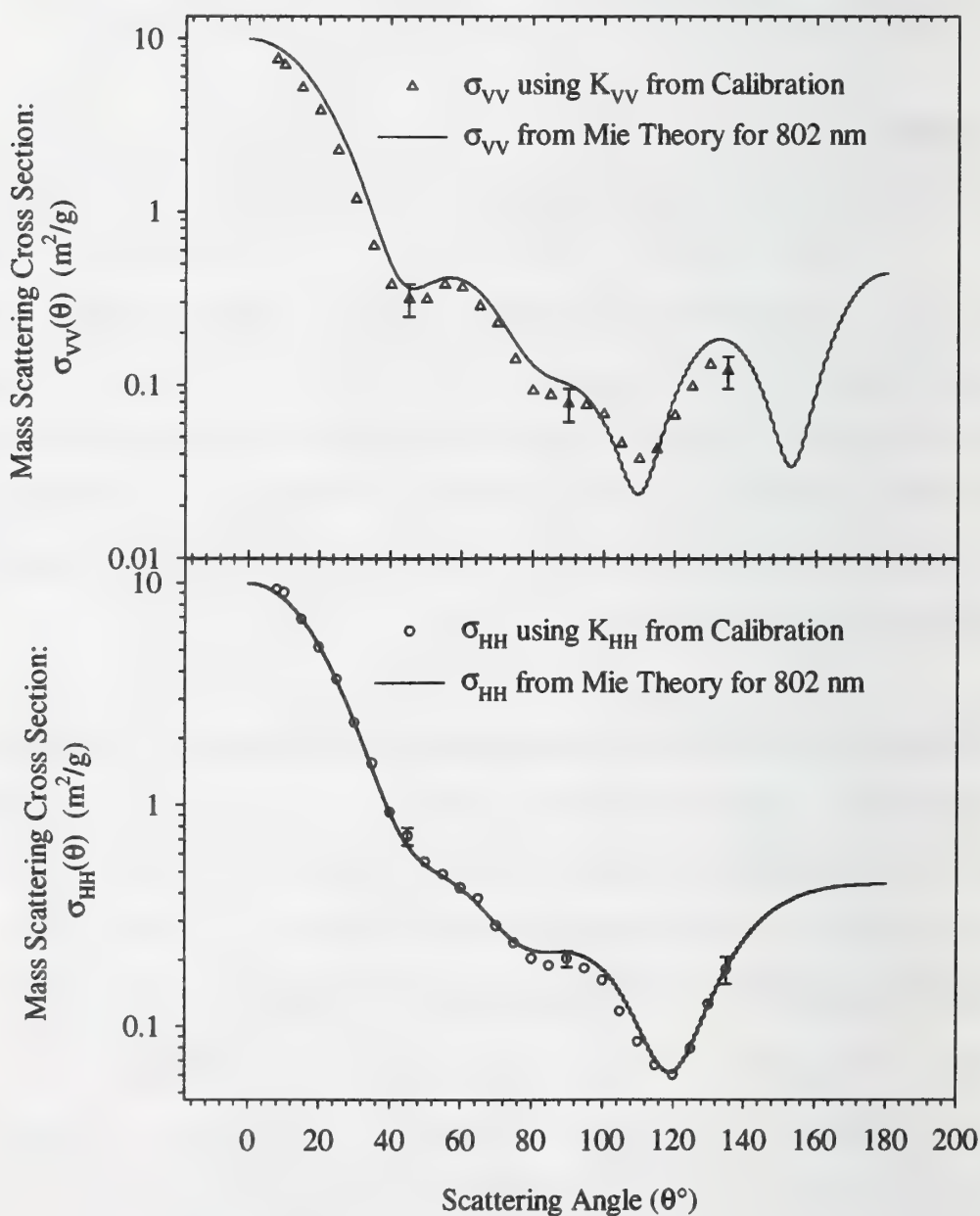




**Figure 2:** Light scattering results, VV and HH polarization, for nominally 802 nm diameter PS spheres.

determined from Eq. (2), for each angle of measurement and for two different polarization states: incident and detected vertical,  $K_{VV}(\theta)$ , and incident and detected horizontal polarization,  $K_{HH}(\theta)$ . The angular average,  $K_{VV}$  and  $K_{HH}$ , of the calibration function is then determined and referred to as the calibration factor. Averaging reduced overcompensation caused by using the respective calibration functions, which weighted minima in the calibration particles scattering cross section too strongly. When an experiment with an aerosol is conducted both the volume corrected detector signal,  $u(\theta)$ , and the mass concentration of particles,  $M$ , are determined to then give the particles mass scattering cross section for a given polarization (polarization notation suppressed),

$$\sigma(\theta) = \frac{u(\theta)}{M K}. \quad (3)$$

The calibration factor would be determined from calibration experiments directly preceding an aerosol experiment.

In Figure 2 the application of an average calibration factor to the scattering signal from 802 nm nominal diameter PS spheres has been shown. The difference between experiment and theory is about 20 % of the Mie theory for  $\sigma_{VV}(\theta)$  and less than about 10 % for  $\sigma_{HH}(\theta)$ . The larger deviation in  $\sigma_{VV}(\theta)$  is due to a miss alignment of the optical elements in this case, but the agreement between the data sets is still quite clear. Error bars are shown for sample points only, and indicate combined uncertainty of a measurement when considering the variables of Eq. 2 and 3. The largest component of this combined uncertainty is due to the use of the angular average of the calibration function, which have standard uncertainty typically about 10 % in the HH polarization and 15 % in the VV polarization. The standard uncertainty of a detector signal measurement, of which 10 are made at given angle in an experiment, varies between 2 % and 6 %, approaching the higher value for smaller scattering signals. Specific effects due to doublets of polystyrene sphere are unknown for our experiments.

6. Smoke Results

Before each set of VV and HH measurement of the light scattered from smoke particles, a set of calibration experiments would be completed. The calibration factor from these experiments would then be applied to the detector signal for the smoke particle experiments that followed. A second set of calibration experiments was completed after the smoke to ensure that no change in system calibration had occurred. Figure 3 shows the first measurement of the mass scattering cross section for acetylene from a laminar co-flow diffusion burner, the general shape of the data curve is consistent with that reported by others [8]. However, our results go beyond previous studies by including the cross section per mass concentration. Such information is important in comparing measurement and theory. The repeatability of the measurements is demonstrated by the presence of a second experiment's results. The minima at  $\sigma_{HH}(90)$  is a result of Rayleigh-like scattering of the small primary particles that make up the agglomerate.

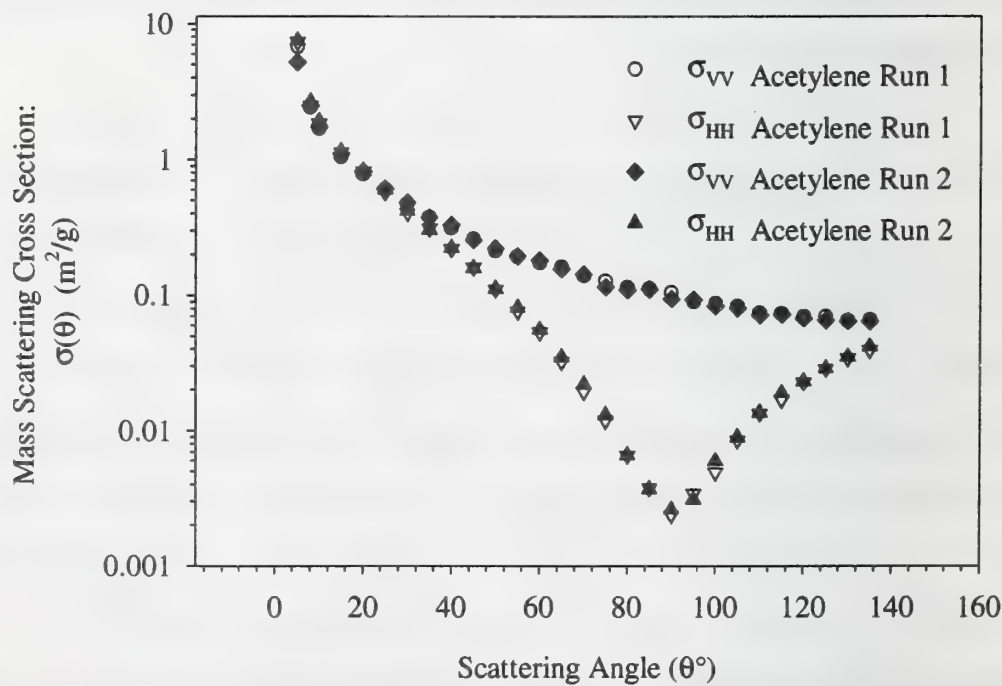


Figure 3: Differential mass scattering cross section results for acetylene soot.

The influence of the far field interference between the light scattered by individual



primary particles in the soot agglomerate is apparent at the forward scattering angles, and the 2 to 4 order of magnitude changes in the scattering cross sections over the angular range. The light scattered by the soot agglomerate is related to the morphology of the soot agglomerate and thus its fractal geometry [6].

With the differential mass scattering cross section determined it is then possible to determine the truncated (5° to 135°) total mass scattering cross section,  $C_{msca}$ , of the particles, which is given by:

$$C_{msca} = 2\pi \int_5^{135} \frac{(\sigma_{VV}(\theta) + \sigma_{HH}(\theta))}{2} \sin(\theta) d\theta . \tag{4}$$

The integration was performed numerically and calculated cross sections are shown in Table 1. The results are also compared to Debye-Mie theory and results from other studies.

Particles	Total Mass Scattering Cross Section (m <sup>2</sup> /g)	Uncertainty (m <sup>2</sup> /g)
Mie Theory for 802 nm diameter	7.49	
802 nm diameter PS Spheres	6.3, 6.1	±1.6
Acetylene Soot*	1.95	±0.08
Acetylene Soot	1.8, 2.0	±0.5

**Table 2:** Truncated total mass scattering cross sections for the particles investigated in this study. The results for our multiple experiments (Runs 1 & 2) are shown. \*This result is a measured total quantity, not truncated [4].

### 7. Conclusion

This study has demonstrated the application of polystyrene spheres suspended in air as a calibration technique for measurements of the differential scattering cross section per mass,  $\sigma(\theta)$ . Introduced for the first time was the quantification of aerosol particle scattering in terms of the differential scattering cross section per mass, which is made possible by gravimetric measurement of the particle mass concentration. This will allow

direct comparison between measurements and light scattering theory. The light scattering apparatus used in these measurements has provided repeatable results over a dynamic signal range of 3 to 4 orders of magnitude. Uncertainties lie in the range of 10 % to 20 % and are mainly due to the uncertainties in the calibration factor. The method was then applied to acetylene smoke, which was produced in a consistent and reproducible manner by a co-flow laminar diffusion burner, facilitating the experimental measurements.

#### Reference List

- [1] Meacham BJ, Motevalli V: Characterization of smoke from smoldering combustion for the evaluation of light scattering type smoke detector response. *Journal of Fire Protection Engineering* 1992; 4:17-28
- [2] Loepfe M, Ryser P, Tomkin C, Wieser D: Optical properties of fires and non-fire aerosols. *Fire Safety Journal* 1997; 29:185-194
- [3] Weinert DW, Cleary T, Mulholland GW: Size distribution and light scattering properties of test smokes. *Submitted: AUBE 2001*
- [4] Mulholland, G. W. and Choi, M. Y. Measurement of the mass specific extinction coefficient for acetylene and ethylene smoke using the large agglomerate optics facility. The Combustion Institute. Twenty-Seventh Symposium (international) on Combustion. 1515-1522. 1998. Pittsburgh, The Combustion Institute.
- [5] Mulholland GW, Bryner NP: Radiometric model of the transmission cell-reciprocal nephelometer. *Atmospheric Environment* 1994; 28:873-887
- [6] Samson RJ, Mulholland GW, Gentry JW: Structural analysis of soot agglomerates. *Langmuir* 1987; 3:272-281
- [7] Bohren CF, Huffman DR: *Absorption and scattering of light by small particles* New York, John Wiley & Sons, 1983
- [8] Koylu UO, Faeth GM: Optical properties of overfine soot in buoyant turbulent diffusion flames at long residence times. *Journal of Heat Transfer* 1994; 116:152-159



## **Kalibrierung von Brandmeldern im Sub – Mikron Bereich**

### **1 Einleitung**

Zur Detektion von Bränden werden unterschiedliche Melder eingesetzt, die auf Zustandsänderungen im Raum reagieren. Mehrere Melderarten reagieren auf die beim Brand sich ändernden Partikelanzahlkonzentrationen, gewichtet mit unterschiedlichen Partikel – Durchmesserfunktionen. Ausgangspunkt zur Beschreibung der Reaktion eines Melders ist zunächst die Partikelanzahlkonzentration in Abhängigkeit vom Partikeldurchmesser. Bei einem beginnenden Brand wird das bereits im Raum vorliegende Hintergrundaerosol durch das Brandaerosol überlagert, das aus der Dampfphase gebildet wird und deswegen zunächst aus kleinsten Partikeln (Nanopartikel) besteht, die aufgrund nachfolgend wirkender aerosoldynamischer Prozesse vergrößert werden. Da die Nanopartikel bei einem beginnenden Brand das erste Brandsignal darstellen, ist ihre Erfassung bei der Charakterisierung von Brandaerosolen von besonderer Bedeutung. Die bisher eingesetzten Verfahren sind aber in ihrer unteren Nachweisgrenze in Hinblick auf die Partikelgröße begrenzt. Im Rahmen dieses Beitrages wird eine Weiterentwicklung des Differentiellen Mobilitätsanalysators (DMPS), der die Erfassung der Größenverteilung bis in den Nanometerbereich mit hoher Auflösung erlaubt, vorgestellt. Eine hohe Integration der Gerätekomponenten erhöht die Feldtauglichkeit dieses Gerätes.

Auch die eingesetzten Brandmelder haben eine untere Nachweisgrenze im Hinblick auf die Partikelgröße, die für die Reaktionszeit eines Melders auf einen beginnenden Brand maßgeblich ist. Zur Verbesserung der Beurteilung des Reaktionsverhaltens eines Melders ist die Bestimmung dieser unteren Nachweisgrenze von zentraler Bedeutung. Sie kann mit Hilfe wohl definierter, monodisperser Aerosole, insbesondere im Nanometerbereich, bestimmt werden. Eine Methode zur Bestimmung der unteren Nachweisgrenze wird hier vorgestellt.

## 2 Aerosoldynamik

Brandmelder, die auf Partikel reagieren, können als Partikelsensoren betrachtet werden, deren Ausgangssignal von der Partikelanzahlkonzentration, von der Partikelgrößenverteilung und der Partikelart abhängt. Solange kein Brand vorliegt, wird von dem Sensor die am Ort der Probennahme vorliegende natürliche Hintergrundbelastung an Partikeln gemessen. Das sich ergebende Signal liegt unterhalb des Schwellwertes für einen Brand. Werden von mehreren Stellen mit Hilfe eines Leitungssystems Proben zum Sensor geführt, so entsteht ein Gemisch der Aerosole der einzelnen Probenahmestellen. In der Abbildung 1 ist die Anzahlgrößenverteilung für eine saubere ländliche sowie für eine durchschnittliche städtische Umgebung gezeigt.

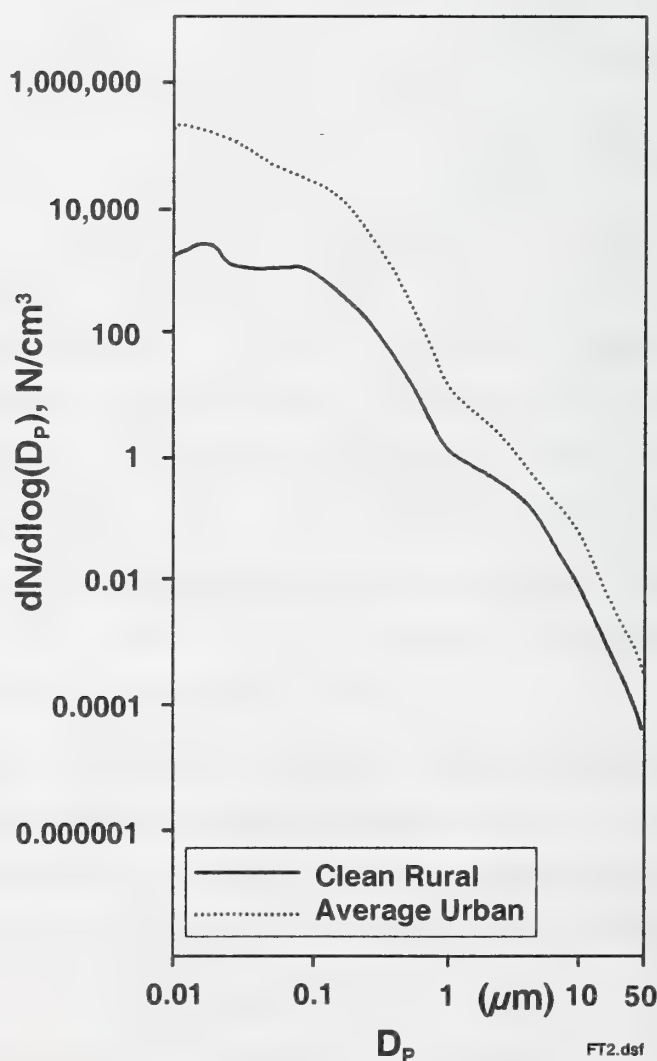


Abbildung 1: Partikelgrößenverteilung als Hintergrundbelastung für Brandsensoren



Der natürliche Größenbereich der Partikeldurchmesser erstreckt sich von wenigen Nanometern bis ca. 100  $\mu\text{m}$ . Ohne äußeren Einfluss bzw. ohne besondere Ereignisse stellt sich in der Raumluft eine relativ stabile Größenverteilung ein. Änderungen vollziehen sich eher langsam. Trotzdem enthält jedes Aerosol eine gewisse Dynamik. Diese Dynamik führt zu Veränderungen in den so genannten Nukelations- und Akkumulationsmoden. Diese Moden in der Partikelgrößenverteilung erkennt man erst, wenn aus der Anzahlverteilung unter Annahme kugelförmiger Partikel die Volumenverteilung berechnet wird. Abbildung 2 zeigt quantitativ eine typische Volumenverteilung.

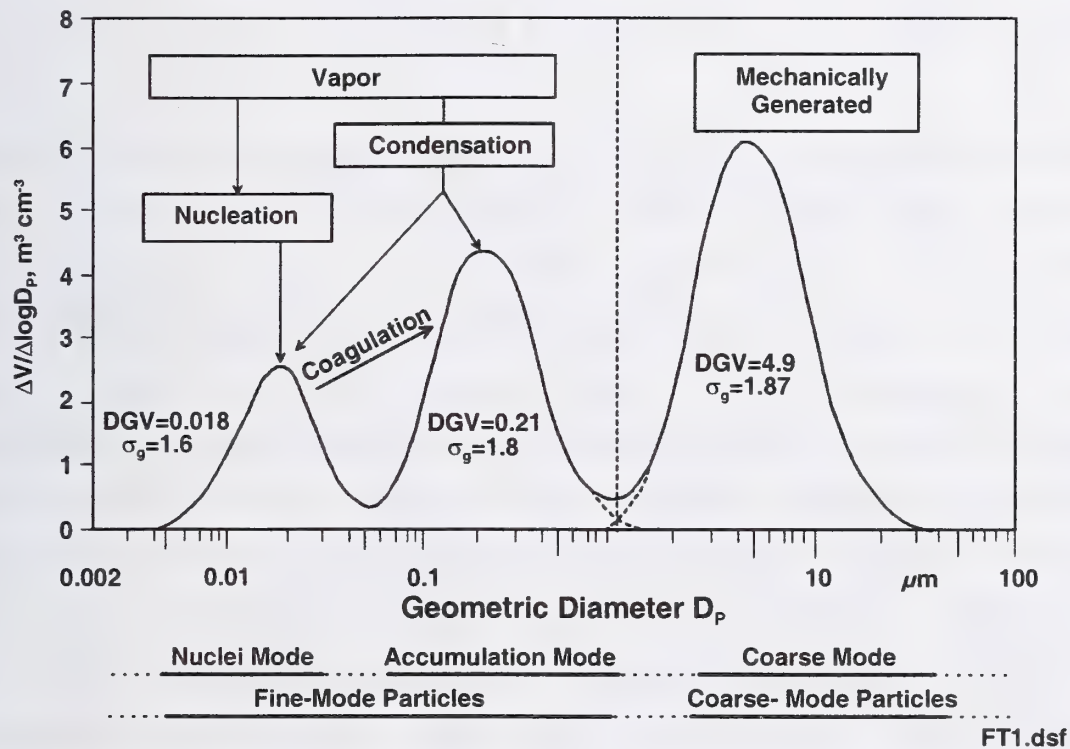


Abbildung 2 Typische Volumenverteilung

Der mechanische Mode bleibt stabil. Es kommt zu keinem Austausch von Partikeln mit den beiden Moden im submikronen Bereich. Die beiden unteren Moden hingegen unterliegen ständigen Veränderungen insbesondere bei Bränden aufgrund Partikelbildung aus der Dampfphase (Nukleation und Kondensation) bzw. Partikelkoagulation bei hohen Anzahlkonzentrationen. Die Partikel des Nukleationsmode wachsen praktisch in den Akkumulationsmode hinein. Diese Vorgänge sind in der Abbildung 3 bildlich verdeutlicht.

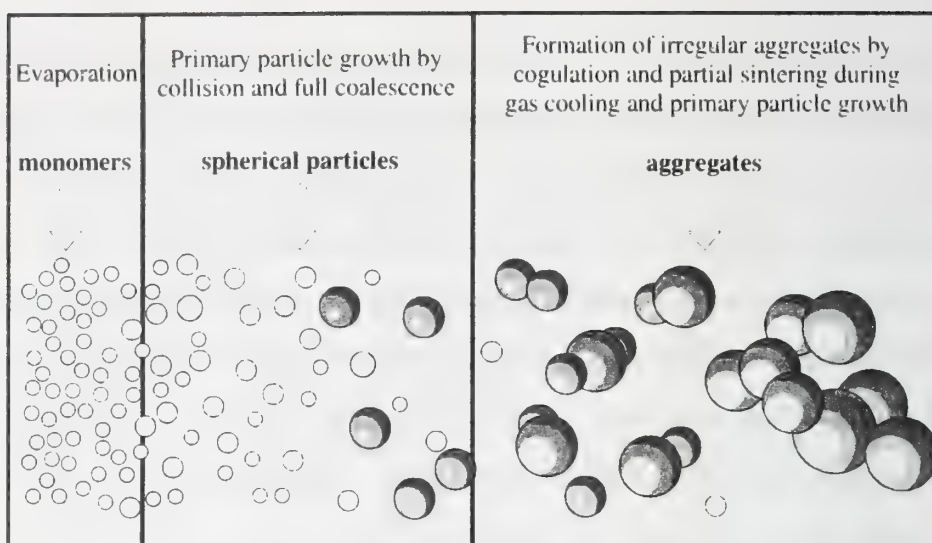


Abbildung 3 Partikelbildung durch Nukleation, Kondensation und Koagulation

Aus der Dampfphase entstehen Keime in sehr hohen Anzahlkonzentration, die durch Kollisionen untereinander und durch Dampfkondensation weiter wachsen. Die Anzahlkonzentration in dieser Phase ist immer noch so hoch, so dass die Partikel aufgrund ihrer Bewegung im Gas häufig kollidieren. Die Partikel bleiben nach der Kollision aneinander haften und wachsen dadurch sehr schnell weiter an. Die Anzahlkonzentration im Aerosol nimmt während der Koagulation stetig ab, wenn keine neuen Partikel zugeführt werden. Dieser Vorgang setzt sich fort, bis die Wahrscheinlichkeit einer Kollision aufgrund der niedrigeren Anzahlkonzentration sehr klein geworden ist. Das Aerosol ist dann relativ stabil. Die Koagulation kann sich über einen Zeitraum von Bruchteilen einer Sekunde bis zu Minuten erstrecken.

Ähnliche Vorgänge spielen sich bei Beginn eines Brandes ab. Es entstehen in unmittelbarer Nähe des Brandes sehr viele Partikel im Nanometerbereich. Mit zunehmendem Alter des Aerosols verschiebt sich die Größenverteilung zu größeren Partikeln. In der Abbildung 4 sind die Größenverteilungen für verschiedene Testbrandaerosole [1] zu verschiedenen Zeiten nach Beginn des Brandes gezeigt.



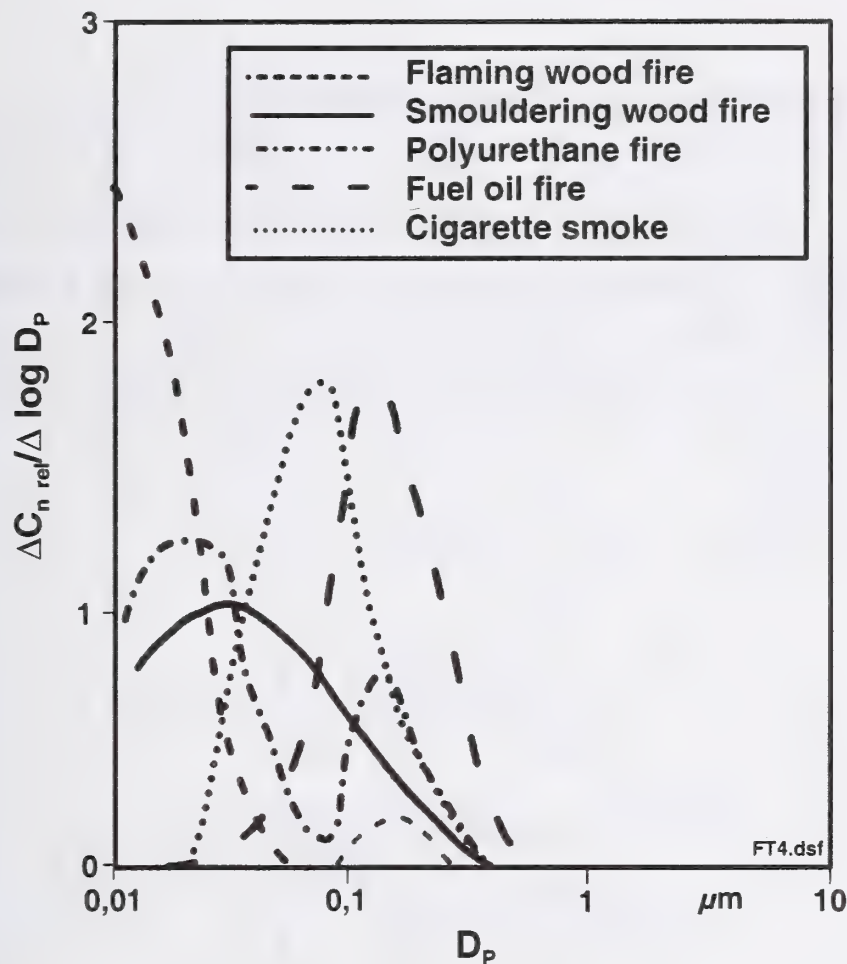


Abbildung 4 Größenverteilungen von Testbrandaerosolen

Bei offenem Holzbrand erkennt man den Nukleationsmode, dessen Maximum vom Messsystem nicht vollständig erfasst werden konnte. Die untere Nachweisgrenze des verwendeten DMPS reichte dazu nicht aus. Das Aerosol des Holzbrandes bildet ab 100 nm einen zweiten Mode, hier noch mit einer geringen Anzahlkonzentration. Der Kunststoffbrand zeigt schon deutlicher den Akkumulationsmode. Für die Beurteilung des Brandfortschrittes bzw. für die frühzeitige Erkennung eines entstehenden Brandes ist es also besonders wichtig, die Größenverteilung, beginnend mit Partikeln im Nanometerbereich, in ihrem zeitlichen Verlauf zu messen. Die oben gezeigten Messungen wurden mit einem DMPS aufgenommen. Das System kann Partikel in einem Bereich von 20 nm bis ca. 1  $\mu\text{m}$  mit einer nichtausreichenden Zeitauflösung von 20 Minuten messen. Ab einem Partikeldurchmessern von 100 nm bis zur unteren Nachweisgrenze von 20 nm zeigen sich aber schon größere Fehler in der Messung. Diese Fehler sind u. a. auf Verluste im Messgerät und auf die mit abnehmender Partikelgröße abnehmende Größenauflösung zurückzuführen.

### 3. Entwicklung eines DMPS mit erweitertem Messbereich

Die geschilderten Unzulänglichkeiten führten zur Entwicklung eines verbesserten Gerätes [2]. Ziel der Neuentwicklung war in erster Linie eine Erweiterung des Messbereichs bis zur kleinsten Partikelgröße von 3 nm und eine Minimierung der Partikelverluste im Gerät. Die wesentlichen Komponenten des Messsystems sind in der Abbildung 5 gezeigt.

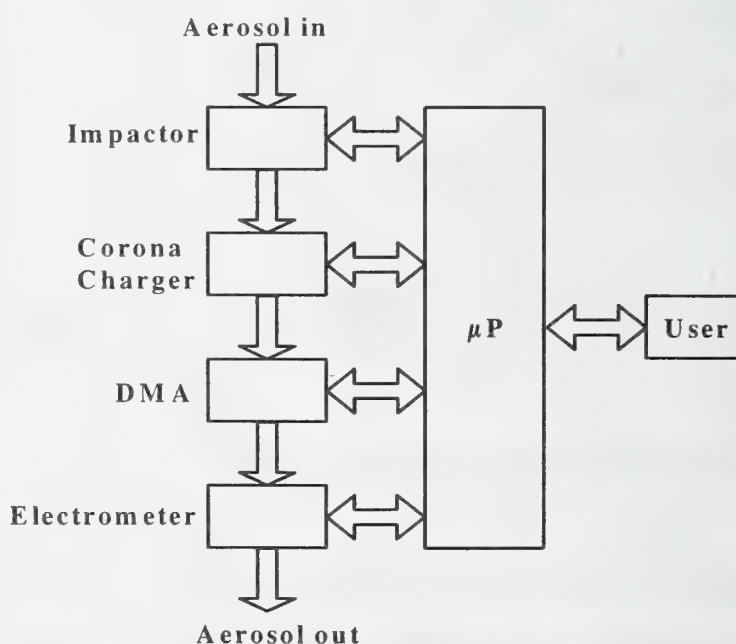


Abbildung 5 Prinzipdarstellung des Wide Range DMPS

Das zu untersuchende Aerosol wird durch einen Impaktor in seinem Größenbereich oberhalb  $1\text{ }\mu\text{m}$  quasi abgeschnitten und anschließend durch einen Auflader in einen definierten elektrischen Ladungszustand gebracht. Die elektrisch geladenen Partikel werden dann anschließend in dem elektrischen Feld einer Kondensatoranordnung (DMA) fraktioniert. Die Partikel bewegen sich dabei senkrecht zu dem elektrischen Feld in der Anordnung. Die Kraftwirkung des elektrischen Feldes führt zu Bahnkurven, auf der die Partikel sich in Richtung einer Elektrode bewegen. Nur Partikel einer bestimmten elektrischen Mobilität bewegen sich auf einer Bahnkurve, die zum Auslass führt. Die Partikel, die diesen Auslass erreichen, werden gezählt. Somit ist die Anzahl der Partikel im Aerosol mit einer bestimmten Mobilität bekannt. Aus der Mobilität lässt sich auf den Partikeldurchmesser schließen [3]. Durch Variation der elektrischen



Feldstärke im DMA wird die Mobilität der Partikel geändert, die zum Auslass und damit zum Partikelzähler gelangen. Damit wird erreicht, dass der gesamte Mobilitäts- bzw. Partikelgrößenbereich erfasst wird.

Um die Anforderungen an das verbesserte Gerät zu erfüllen, wurden maßgeblich zwei Lösungsansätze umgesetzt:

- Integration aller Komponenten zu einem Gerät. Dies minimiert die Verluste und verbessert die Feldtauglichkeit.
- Verwendung einer radialen DMA-Anordnung mit zwei Einlassschlitzen und unterschiedlichen Volumenstromverhältnissen, um den gesamten Größenbereich abdecken zu können.

In der Abbildung 6 ist das entwickelte Konzept dargestellt.

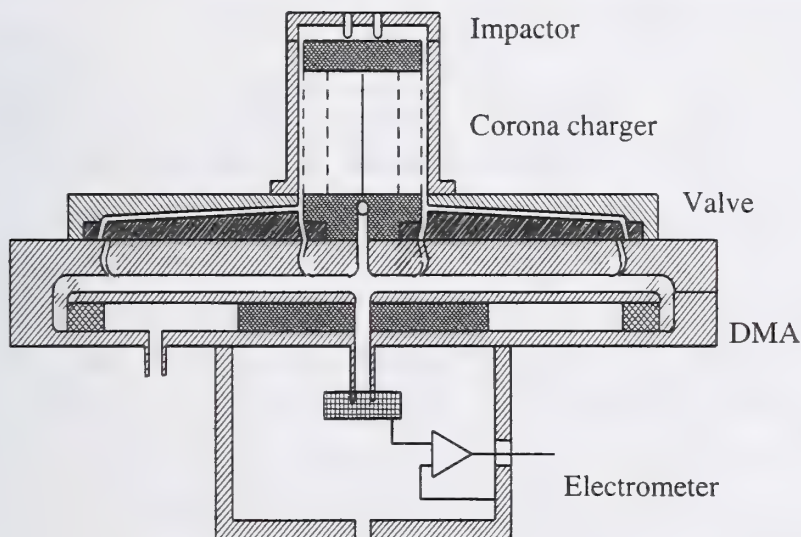


Abbildung 6 Konzept des neuen DMPS für submikrone Aerosole

Aus der Querschnittsdarstellung ist direkt zu erkennen, dass alle Komponenten zu einer sehr kompakten Gesamteinheit integriert wurden. Die besondere Strömungsführung mit minimalen Querschnitts- und Richtungsänderungen sorgt für minimale Verluste durch Abscheidung. Die einzelnen Komponenten sind in der Reihenfolge der Durchströmung erklärt.

Der Impaktor gewährleistet, dass keine Partikel in das System gelangen, deren Größe oberhalb der oberen Messbereichsgrenze liegen. Die auf diese Weise erfolgte Festlegung der oberen Nachweisgrenze des Gerätes erlaubt die Korrektur des Fehlers

verursacht durch mehrfach geladene Partikel. Der Impaktor besitzt zwei Abscheidestufen. Die erste Stufe ist ein Vorabscheider, der die nachfolgenden Stufen vor einer möglichen Verstopfung schützt, indem Partikel größer  $5\text{ }\mu\text{m}$  schon abgeschieden werden. Bei der nachfolgenden Stufe lässt sich die Abscheidegrenze wahlweise zwischen  $1,4\text{ }\mu\text{m}$  und  $0,4\text{ }\mu\text{m}$  umschalten. Die Notwendigkeit ergibt sich aus den Messbereichsgrenzen des weiter unten erläuterten DMA's.

Zur Aufladung der Partikel wurde ein elektrischer Auflader gewählt. Der Auflader ist leicht steuerbar und benötigt keine radioaktiven Quellen. Das Prinzip basiert auf der Koronaentladung zur Erzeugung freier Ladungsträger. Die im elektrischen Feld der koaxialen Elektroden emittierten Elektronen werden in den Aerosolstrom geleitet. In dieser Aufladungszone kollidieren die Partikel mit den Elektronen. Durch eine gezielte Steuerung der Anzahlkonzentration der Elektronen und der Verweildauer der Partikel in der Aufladungszone lässt sich die Ladungsverteilung des Aerosols in weiten Grenzen einstellen. Für dieses Gerät wurde das Prinzip nach [4] optimiert.

Die Fraktionierung der geladenen Partikel erfolgt im differentiellen Mobilitätsanalysator (DMA), wie oben beschrieben. Der Messbereich eines DMA's wird durch zwei Effekte begrenzt. Für die Fraktionierung großer Partikel werden hohe Feldstärken benötigt, die begrenzt werden durch die Durchschlagsfeldstärken der Trärgase. Aus diesem Grund benötigt man DMA Anordnungen mit langen Bahnkurven, damit die großen und somit trägeren Partikel noch bei realisierbaren Feldstärken fraktioniert werden können. Bei kleinen Partikeldurchmessern und langen Bahnkurven - und damit langen Verweilzeiten im DMA - erhöht sich der Einfluss der Diffusion. Die Bahnkurven einer bestimmten Mobilität enden nicht immer am Auslass, sondern verteilen sich um den Auslass. Die Auflösung, also die Fähigkeit eines DMA's unterschiedliche Partikelmobilitäten zu fraktionieren, wird somit für kleinere Partikel immer schlechter. Die Verweilzeit im DMA muss daher für kleine Partikel so kurz wie möglich sein. Diese beiden konträren Anforderungen für kleine, bzw. große Partikel, lassen sich nur durch die Integration zweier DMA's in einer Konstruktion befriedigen. In der Abbildung 7 ist das Prinzip eines solchen DMA's gezeigt.



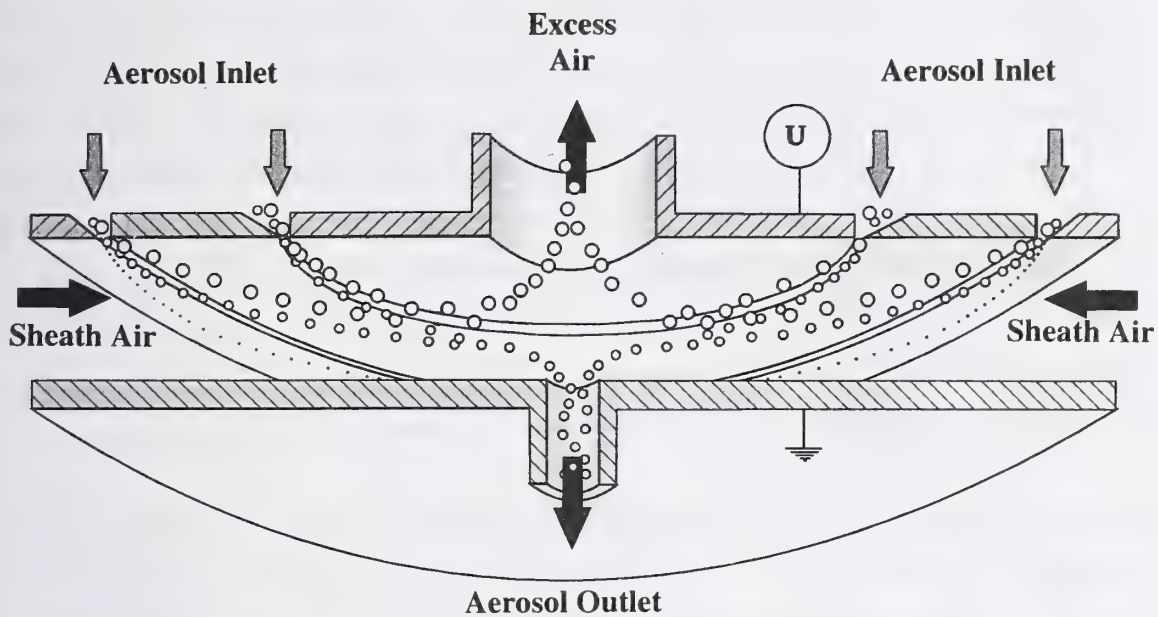


Abbildung 7 Prinzipdarstellung eines radialen DMA's mit zwei Einlässen

Der neue DMA ist als so genannter radialer DMA ausgeführt. Er besitzt zwei parallele kreisrunde Elektroden, zwischen denen ein homogenes, elektrisches Feld besteht. In radialer Richtung strömt das Aerosol durch einen schmalen Ringspalt in den DMA hinein und durch eine zentrale Öffnung heraus. Damit der große geforderte Messbereich realisiert werden kann, wurden hier erstmalig zwei Einlassspalte mit unterschiedlichen Durchmessern realisiert. Der innere Spalt führt zu kurzen Verweilzeiten des Aerosols im DMA und damit zu einer hohen Auflösung bis zu 3 nm Partikeldurchmesser. Strömt das Aerosol durch den äußeren Spalt, ist die Verweilzeit länger, und bei gleicher maximaler Feldstärke können Partikel bis 1000 nm fraktioniert werden. Eine spezielle Ventilscheibe gibt alternativ einen der beiden Einlassspalte frei.

Bei der Konstruktion wurde erreicht, dass die Strömung des Aerosols völlig frei von einer tangentialen Komponente ist. Nur so bilden sich rein zentrisch gerichtete Bahnkurven aus. Dies ist eine Voraussetzung für die Berechnung der Partikelgrößen.

Die Strömungsverhältnisse an den kritischen Einlassspalten wurden mit Hilfe dreidimensionaler Modelle simuliert. Es zeigten sich bei der optimierten Strömungsführung keine Turbulenzen, welche die Bahnkurven stören könnten. Die Auflösung des neuen Gerätes ist im Nanometer-Bereich besser als alle zur Zeit verfügbaren DMA's.

Als Partikelzähler ist ein Elektrometer entwickelt worden. Gegenüber den häufig verwendeten Kondensationskernzählern besitzt das Elektrometer die Vorteile der weitgehenden Unabhängigkeit von dem thermodynamischen Zustand der Aerosole und

dem Fehlen von Betriebsflüssigkeiten wie Butanol o. ä.. Damit ist das System überhaupt erst feldtauglich. Die fraktionierten Partikel werden auf einem Filter in einem Faradayschen Käfig abgeschieden. Dieser muss von seinem Prinzip her feldfrei sein. Damit dies erfüllt ist, fließt ein dem Partikelstrom entsprechender Ausgleichs- bzw. Verschiebestrom. Dieser sehr kleine elektrische Strom wird gemessen und daraus die Anzahl der abgeschiedenen Partikel pro Zeiteinheit berechnet. Diese Anzahl der Partikel muss mit der bekannten Ladungsverteilung gewichtet werden. Der kleinste, messbare, elektrische Strom entspricht einer Konzentration von 25 einfach geladenen Partikeln pro  $\text{cm}^3$  bei einem Volumenstrom von 1,5 l/min.

Das Messsystem benötigt einige periphere Komponenten, die die Gasflüsse realisieren und regeln, Temperatur, Druck und Feuchtigkeit erfassen und wandeln und die diversen elektrischen Spannungen bereitstellen. Die Steuerung und Erfassung aller Daten des Gerätes werden zentral durch einen PC durchgeführt.

Mit diesem Gerät ist es möglich, Brandaerosole in dem interessierenden Größenbereich von 3 nm bis 1  $\mu\text{m}$  schnell zu messen, insbesondere bei Verwendung einer noch zu modifizierenden Software, wie sie im SMPS eingesetzt wird.

#### **4 Kalibrierung von Brandmeldern**

Aus den oben stehenden Ausführungen wird klar, dass für die Entscheidung, ob ein Brand vorliegt oder nicht, die entstehenden Partikel im Nanometerbereich eine besondere Bedeutung haben. Bedingt durch die Grenzen der Technik besitzt jeder Brandmelder eine untere Nachweisgrenze bezüglich der Partikelgröße. Diese Grenze muss bekannt sein, damit beurteilt werden kann, inwieweit der Sensor überhaupt einen Brand in der Entstehung detektieren kann oder nicht.

Die Kennlinie optischer Brandsensoren kann mit Hilfe der Mie Theorie oder weiterführenden numerischen Ansätzen berechnet werden. Für einen Ionisationsmelder kann man in erster Näherung einen linearen Zusammenhang zwischen dem Ausgangssignal und der Partikelgröße sowie der Partikelanzahlkonzentration ableiten. In der Abbildung 8 sind die Kennlinien für beide Melderarten qualitativ dargestellt.



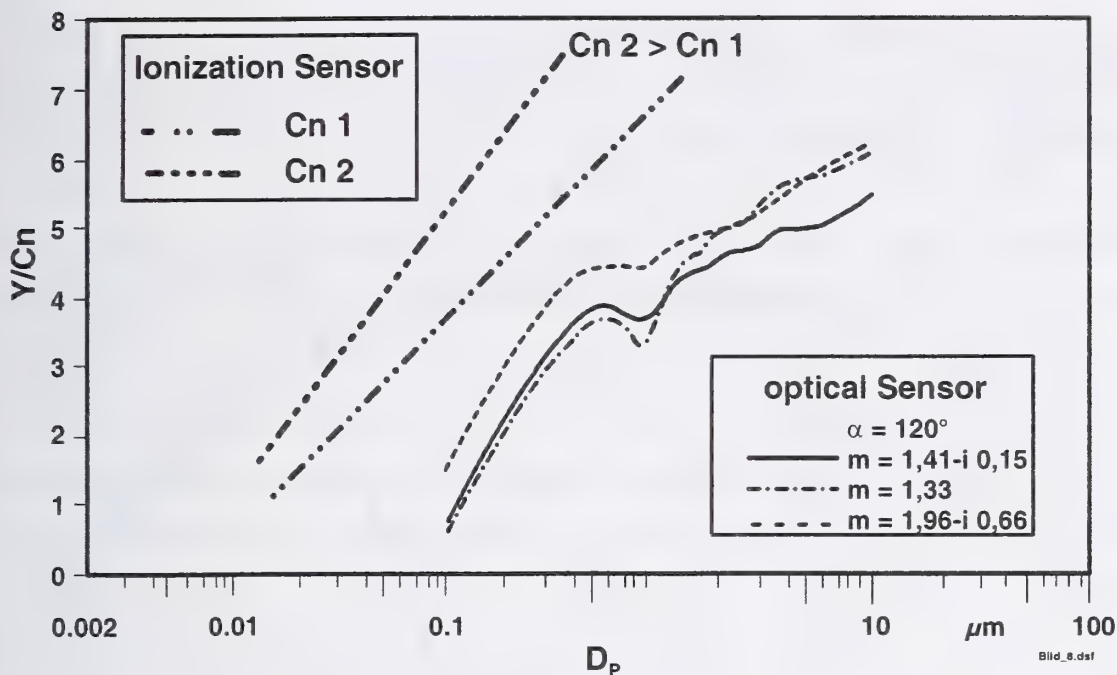


Abbildung 8 Kennlinien optischer Brandsensoren normiert auf die Partikelanzahlkonzentration

Für jeden individuellen Sensor können die Kennlinien auf der Abszisse verschoben sein. Bei den Ionisationsmeldern kann je nach Typ des Melders die Steigung der Geraden variieren. Bei den optischen Sensoren ist es wesentlich komplexer, da der Verlauf der Kennlinie nicht nur von der Geometrie des Sensors und seinen Komponenten abhängt, sondern auch von der Partikelform und dem Partikelmaterial.

Der Bereich der Kennlinien im Hinblick auf den erfassten Partikelgrößenbereich wird durch die obere und untere Nachweisgrenze des Sensors im Hinblick auf die Partikelgröße festgelegt. Die obere Nachweisgrenze ist hier nicht von Bedeutung, weil ein beginnender Brand kaum die Größenverteilung des Aerosols im Bereich großer Partikel verändert. Das Gegenteil trifft für die untere Nachweisgrenze zu. Zur Festlegung der unteren Nachweisgrenze verwendet man den sog. Zählwirkungsgrad, der angibt, welcher Anteil der Partikel gezählt wird. Der Verlauf des Zählwirkungsgrades wird maßgeblich durch das Rauschen in den Komponenten des Sensors geprägt. Weiterhin wird der Zählwirkungsgrad des Brandmelders im gesamten Messbereich durch die Verluste bei der Probenahme beeinflusst. Die Verluste in Rohrleitungssystemen sind in [5] betrachtet worden. Man kann den Zählwirkungsgrad

mit dem Wirkungsgrad des Probenahmesystems gewichten und erhält dann den Wirkungsgrad des Gesamtsystems. In der Abbildung 9 sind die verschiedenen Wirkungsgrade qualitativ dargestellt.

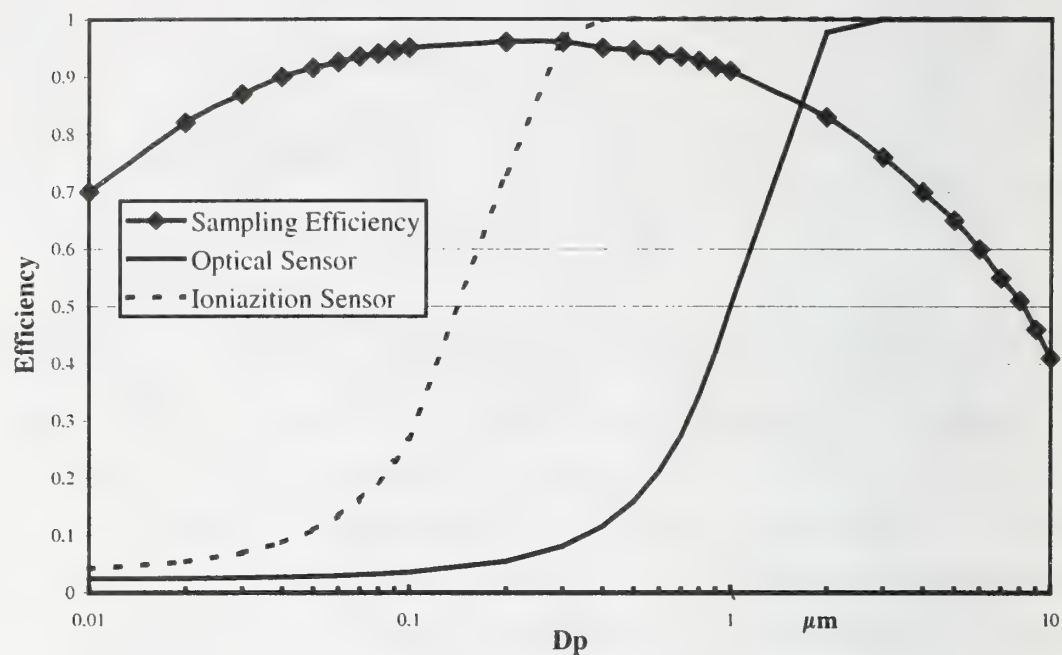


Abbildung 9 Zählwirkungsgrad für optische Brandsensoren und Ionisationsmelder

Zur Bestimmung der unteren Nachweisgrenze muss ein monodisperses Aerosol genügend hoher Konzentration bereitgestellt werden. Der typische Aufbau zur Erzeugung der Aerosole ist in der Abbildung 10 gezeigt.

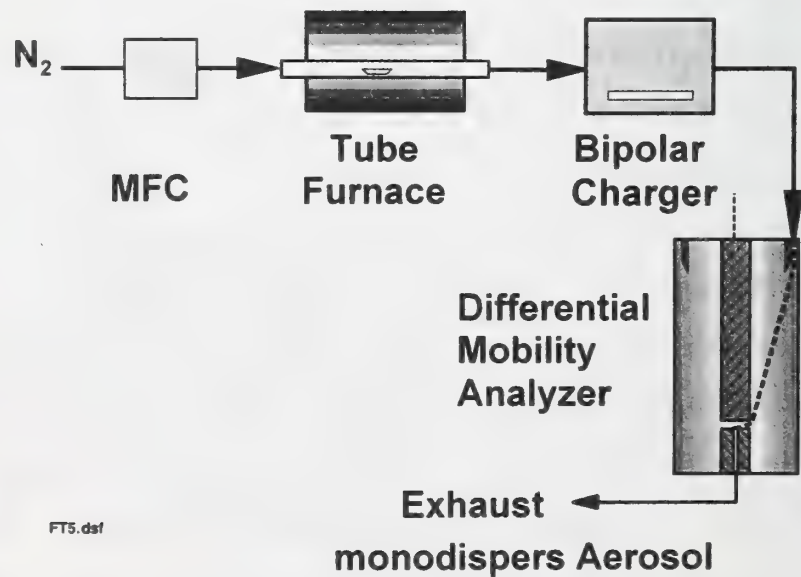


Abbildung 10 Aufbau zur Erzeugung von monodispersen Testaerosolen

Das Partikelmaterial wird in einem Rohrofen verdampft und durch die Gasströmung aus dem Ofen transportiert. Hinter dem Ofen kondensiert das Material aus der Dampfphase. Die Größe der Partikel lässt sich durch die gezielte Abkühlung z. B. durch Beimischung von kaltem Gas beeinflussen. Es entsteht ein stabiles aber polydisperses Feststoffaerosol. Analog zur Klassierung der Partikel bei der Messung der Brandaerosole wird auch hier durch definierte Aufladung und Fraktionierung im elektrischen Feld (DMA) ein monodisperses Aerosol erzeugt. Durch die Variation der Spannung am DMA lässt sich die Partikelgröße des monodispersen Aerosols einstellen. Mit diesen Testaerosolen werden dann die Sensoren beaufschlagt und ihre Signale gemessen. Bei Meldern, die Einzelpartikel zählen, wird die Partikelanzahlkonzentration mit einem unabhängigen Partikelzähler ermittelt, dessen Zählwirkungsgrad in dem betrachteten Partikelgrößenbereich nachweislich 100 % beträgt. Das Verhältnis der gemessenen Konzentrationen gibt den Wirkungsgrad an. In der Abbildung 11 werden die Kurven des Zählwirkungsgrades für einen optischen Sensor gezeigt.

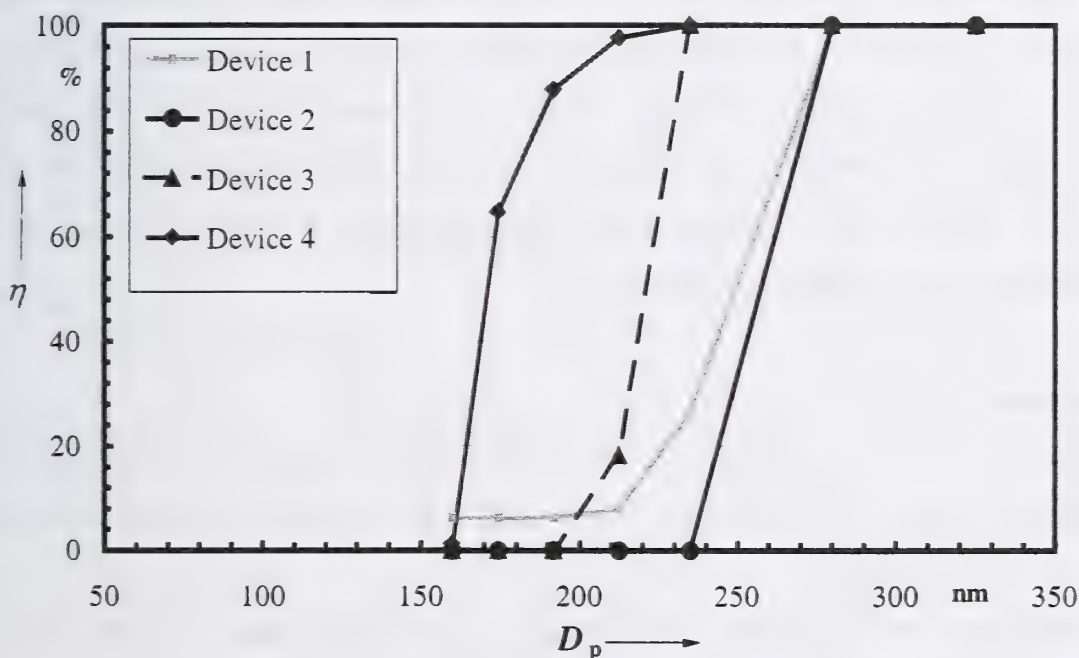


Abbildung 11 Experimentell ermittelte Kurven des Zählwirkungsgrades für optische Sensoren

Die Ergebnisse sind mit einem optischen Sensor, der Einzelpartikel bis zu Konzentrationen von  $10^5 \text{ cm}^{-3}$  zählt ermittelt worden. Die unterschiedlichen Verläufe des Zählwirkungsgrades beruhen auf der Anwendung verschiedener Algorithmen zur



Signalauswertung. Es ist deutlich zu erkennen, dass mit Hilfe der Signalauswertung die untere Nachweisgrenze zu kleineren Partikeln verschoben werden kann [6].

Für Brandmelder, die das Partikelkollektiv messen, muss ein validiertes Modell herangezogen werden, um das zu erwartende Signal für die gegebene Partikelanzahlkonzentration zu berechnen. Der Wirkungsgrad ergibt sich dann aus dem Verhältnis des gemessenen Signals zum berechneten Signal.

## **5. Zusammenfassung**

Mit Hilfe der hier vorgestellten Technik lassen sich Brandaerosole im Bereich von 3 nm bis 1  $\mu\text{m}$  schnell und mit hoher Auflösung messen. Das ermöglicht die Bestimmung charakteristischer Merkmale von Brandaerosolen, auch in ihrem zeitlichen Verlauf. Mit diesen Kenntnissen können Kriterien zur Alarmauslösung weiter verbessert werden.

Sollen Brandmelder diese Merkmale sicher messen können, muss im Rahmen einer Kalibrierung sichergestellt werden, dass der Melder diese Brandaerosole auch vor dem Hintergrund der natürlichen Aerosolbelastung messen kann. Dazu muss die untere Nachweisgrenze der Brandmelder bestimmt werden. Für diese Aufgabe ist das dargestellte System zur Erzeugung von monodispersen Testaerosolen in dem Größenbereich von 3 nm bis 100 nm geeignet.

## **6 References**

- [1] Fissan, H.; Helsper, C.; Franzen, H. Particle Size Distribution of Combustion Aerosols Atmospheric Pollution. M. M. Benarie (Ed.), Studies in Environmental Science 1987, 1: 263-266
- [2] Müschenborn, P.; Otten, F.; Trampe, A.; Luo, J.; Neumann, S.; Fissan, H. Development of a new wide-range Differential Mobility Particle Sizer. 3.ETH-Workshop „Nanoparticle-Measurement“; ETH, Zürich, Swiss, Aug 1999
- [3] Hinds W. C. Aerosol Technology. Wiley-Interscience Publication, New York 1982, 288

- [4] Büscher, P.; Schmidt-Ott, A.; Wiedensohler, A. Performance of a Unipolar "Square Wave" Diffusion Charger with Variable  $nt$ -Product. J. Aerosol Sci. 1994, 25: 651-663
- [5] Fissan, H.; Otto, E.; Dixkens, J. Particle Transport in Sampling Lines used in Fire Detection Systems. Fire Safety Journal 1997, 29; 205-215
- [6] Borggräfe, P. Erweiterung des Messbereiches von optischen Partikelzählern durch gezielte Reduzierung der Störquellen und mit digitalen Signalverarbeitungsmethoden. Dissertation, Gerhard-Mercator-Universität Duisburg, 1999

National Institute of Standards and Technology, Gaithersburg, MD, U.S.A.

\*Guest Researcher on leave from the Center for Environmental Safety and Risk Engineering, Victoria University, Melbourne, PO Box 14428, VIC 8001, AUSTRALIA

## **Size Distribution and Light Scattering Properties of Test Smokes**

### **1. Introduction**

It is well documented that the response of a detector to smoke depends on the detector design and the particular smoke that it is exposed to. Detailed measurements of smoke particle size distributions and optical properties from fires could yield a better understanding of existing detector designs and facilitate design improvements; NIST is making such measurements now on smokes produced in the fire emulator/detector evaluator (FE/DE) [1,2]. One flaming (propylene) and two non-flaming tests smokes (cotton smolder and wood pyrolysis) are studied in this paper. The smokes produced by the non-flaming fuels are similar to two of the smokes produced by the EN54 test fires. The work presented here complement previous measurements of test smoke size distributions and various moments of the distributions [3,4], as well as light scattering studies [5,6]. Our results provide the size distribution using a cascade impactor and an optical particle counter. Our light scattering measurements provide the first differential cross sections for these three smokes on a per mass basis. In addition light scattering data for ethylene and acetylene smoke are expressed in terms of the scattering parameter  $q$  to assess the generality of the fractal description of such smokes. An approach based on the scattering parameter for discrimination between smoke particles from flaming and non-flaming fires is discussed.

### **2. Smoke Generation and Sampling**

The smokes are generated in the FE/DE and extracted for size distribution and light scattering analysis. A detailed description of the FE/DE and its operation is presented in another paper at this conference [2]. The flaming test smoke is soot from a propylene



diffusion flame burner attached to the FE/DE duct. Due to the high soot yield from propylene diffusion flames, the burner can output a large amount of soot at moderate fuel flow. Varying the burner fuel flow and the amount of smoke directed to the duct controls smoke concentration in the FE/DE. The smoke concentration is constant over the aerosol extraction time. A staged-wick-ignition-smolder device inside the FE/DE generates one of the non-flaming fuel smokes, cotton wicks used in EN54 (part 9, test fire 3). Wicks are smoldered and smoke was collected when the light extinction measurement indicated a steady smoke concentration in the duct. The wood pyrolysis smoke is generated by heating wood blocks identical to those specified in EN54 (part 9, test fire 2) on an electrically heated hot plate. The rate of smoke evolution from the wood is characterized by a gradually increasing concentration as the wood block heats up followed by a period of quasi-steady-state smoke production.

For size distribution measurements of the smokes two instruments were used; an optical particle counter (OPC) and a cascade impactor. The smoke produced in the FE/DE is sampled directly into a MOUDI cascade impactor [7] at  $30 \text{ L min}^{-1}$  for determining the mass distribution, while for the other measurements the smokes were collected in a particle-free drum ( $0.24 \text{ m}^3$ ) by drawing smoke from the test section of the FE/DE into the drum. For the OPC about 20 L of smoke was drawn in to the drum at a nominal rate of  $10 \text{ L min}^{-1}$  and in the case of the scattering cross section, about 120 L of smoke was sampled into the drum at a rate of  $20 \text{ L min}^{-1}$ . The smoke filled drum was then transported to the laboratory where the light scattering instruments used in the smoke characterization were situated. These instruments were an OPC used to measure the number distribution and the large agglomerate optical facility (LAOF) developed at NIST [8] for measuring differential scattering cross sections of smoke particles. During the 10 to 30 minutes for obtaining the light scattering data there was little change in the differential scattering cross section.

### **3. Size Distribution Measurements**

The optical particle counter (OPC) utilizes an active cavity laser scattering cell and focused jet of particles to determine the particle's number size distribution from the

scattered light signal of individual particles. The instrument is calibrated with monodisperse polystyrene spheres to relate the detector output to the particle size. An additional dilution by about a factor of 50 was required to dilute the smoke concentration below the  $10^4$  particles  $\text{cm}^{-3}$  operating threshold; above this level there would be more than one particle in the scattering volume causing coincidence errors. The cascade impactor makes use of an airborne particle's inertia to impact large particles in preference to small particles as they pass through the impactor. Each stage of the impactor collects the particles of a given range of aerodynamic diameter, which is the diameter of a sphere of unit density having the same settling velocity as the particle. The impactor stages are covered by aluminum foil, which is weighed before being placed on the stage. After the smoke is sampled through the impactor the foils are removed and their weight measured again. The weight of the collected particles is divided by  $\Delta \log D$  of the two adjacent 50 % cut points, then plotted against the stages mid-range diameter to give the mass distribution as a function of aerodynamic diameter. Figure 1 shows the mass distribution results from the impactor and the calculation of the volume distribution from the number distribution data of the OPC. The large spikes in the OPC volume distribution are a result of changes in the width of the size channel from as small as  $0.005 \mu\text{m}$  for  $0.07 \mu\text{m}$  particles to  $0.1 \mu\text{m}$  width for  $0.7 \mu\text{m}$  particles.

Almost half, 48 %, of the total mass of the cotton wick smoke was found to be below the last stage of the impactor, i.e. less than  $0.056 \mu\text{m}$  in aerodynamic diameter, implying that the cotton lamp wick smoke is bimodal. The volume distribution OPC data and impactor mass distribution, both shown in Figure 1, agree well for cotton wick smoke for particle sizes larger than  $0.07 \mu\text{m}$ . In the case of the wood smoke, the comparison is incomplete because of the lack of the OPC data above  $1 \mu\text{m}$ . The fact that only 2.2 % of the total wood smoke mass was found below  $0.056 \mu\text{m}$  indicates that the mass size distribution is unimodal.

The wood smoke examined in these experiments were found to have a mass mean aerodynamic diameter (MMAD) of about  $1.6 \mu\text{m}$  and a geometric standard deviation (GSD) of about 2. If the mode of the distribution of the cotton wick smoke is treated as

a single log-normal distribution then it has a MMAD of about 0.3  $\mu\text{m}$  and a GSD of about 1.9. The GSD values are typical of polydisperse aerosol systems. The cotton wick smoke has a substantially smaller mean aerodynamic diameter compared to the wood smoke when considering the single mode of cotton wick smoke measured. The number

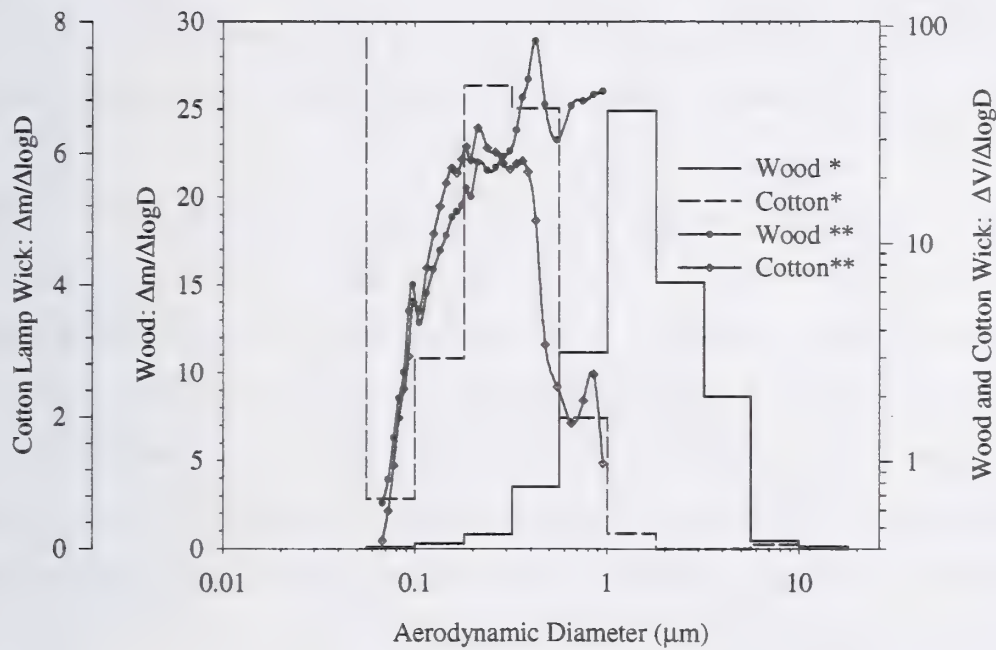


**Figure 1:** Mass distribution from impactor data (\*- outlined bar graph, separate scales on left) and Volume distribution calculated from OPC data (\*\* - line connects data points, scale on right) for non-flaming wood and cotton lamp wick smokes.

distribution from the OPC (not shown) gives a mean number diameter for wood and cotton wick smokes as 0.14  $\mu\text{m}$ . Helsper et al. [3] used a bimodal log-normal distribution to describe the size distribution of smoke from EN 54 test fuels. Our results are close to the median size of the second (i.e. highest) mode of the distribution of [3], 0.14  $\mu\text{m}$  and 0.13  $\mu\text{m}$  for smoldering wood and smoldered cotton wick respectively. Our cascade impactor data is consistent with [3] for the cotton wick as it indicates a second peak below 0.056  $\mu\text{m}$ , but is inconclusive when considering a second peak below 0.056  $\mu\text{m}$  for the wood smoke.



The cotton wick smoke particles less than  $0.056\ \mu\text{m}$  will contribute very little to light extinction or light scattering signals; however, these small particles are expected to contribute significantly to an ionization smoke detector signal, which is proportional to the product of the number concentration and mean diameter. This was verified in the FE/DE by measuring the response of a measuring ionisation chamber (MIC) to both smokes along with light extinction measurements [2]. It was found that the ionization response was about 3.4 times greater for cotton wick smoke compared to smoke from pyrolysed wood for the average extinction coefficient over the time of smoke collection.

In Figure 2 transmission electron micrographs of smoke particles from flaming acetylene and ethylene can be seen [9]. These are chain like structures, called agglomerates as they are made up of an agglomeration of small primary particles, typically 20 nm to 80 nm in diameter depending on fuel and combustion conditions. It is also apparent from the TEM images, which have the same magnification, that the primary spheres for the acetylene smoke are larger (about 30 %) than the ethylene primary spheres. The size distribution of the acetylene agglomerates ranged from about  $0.04\ \mu\text{m}$  to  $20\ \mu\text{m}$  [9].

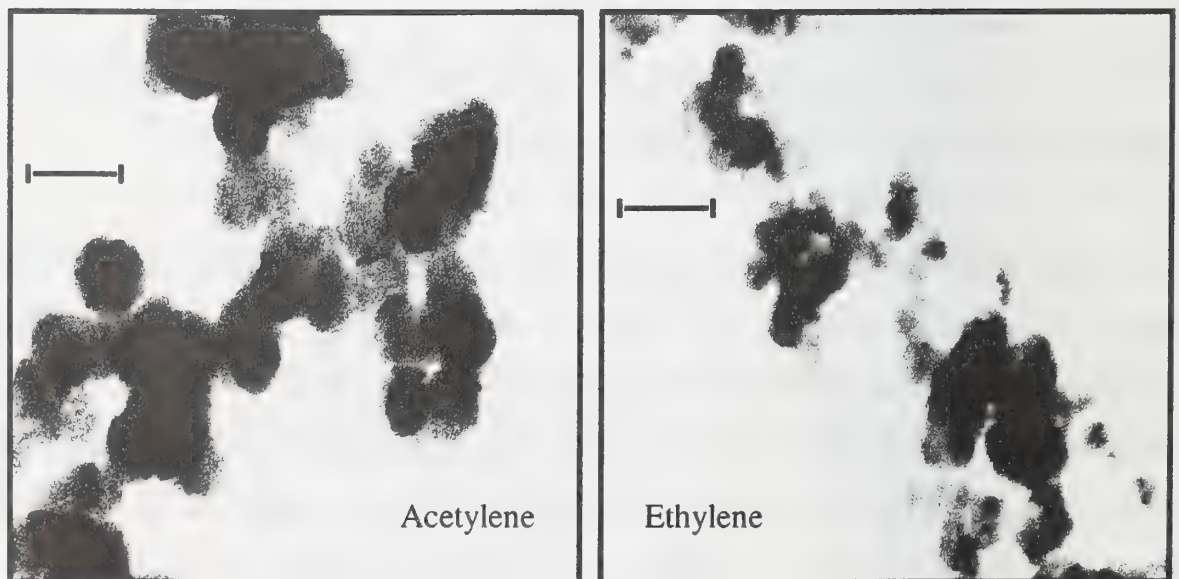


**Figure 2:** Transmission Electron Microscope image of acetylene and ethylene [10], both images are at the same magnification, 50,000x. The scale bar represents  $0.1\ \mu\text{m}$ .

4. Light Scattering Measurements

The light scattering properties of the smoke particles were examined using the LAOF's differential scattering system and methodology described elsewhere [8]. The differential (angular distribution) scattering study presented here has examined the

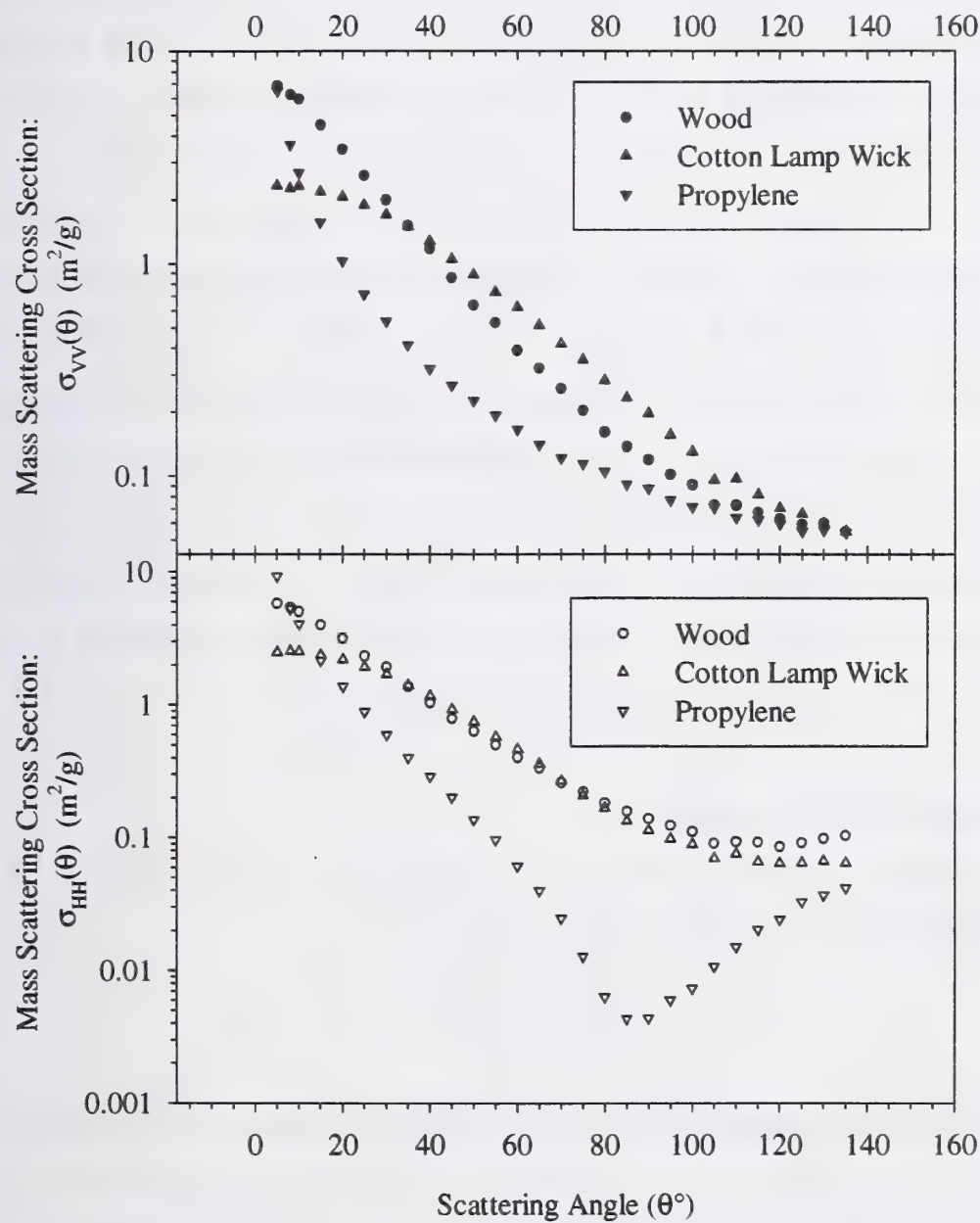


**Figure 3:** Differential mass scattering cross section for wood, cotton lamp wick and propylene smoke particles generated in the Fire Emulator/ Detector Evaluator at NIST.

scattering of linearly polarized light for the scattering angles between  $5^\circ$  and  $135^\circ$ , and determined the smoke particle's differential mass scattering cross sections,  $\sigma_{VV}(\theta)$  and  $\sigma_{HH}(\theta)$ , for different polarizations. The first subscript denotes the incident polarization and the second denotes scattered polarization measured: V for vertical and H for horizontal to the scattering plane. The differential mass scattering cross section is determined in units of area ( $\text{m}^2$ ) per particle mass (g) at a given scattering angle,  $\theta$ . Figure 3 shows the differential mass scattering cross section for the three smokes produced in the FE/DE at NIST. The fractional combined uncertainty (based on one standard deviation) of the differential mass scattering cross sections varies but is typically in the range of 10 % to 20 % due mainly to the calibration with monosize polystyrene spheres [8]. The effect of larger mean size of the wood smoke particles on the scattering cross section,  $\sigma_{VV}(\theta)$ , can be seen in the steeper slope in the forward direction as opposed to the less steep slope for the cotton wick results. The comparison of the two non-flaming fuel smokes for HH polarization shows that their values are similar at most angles except the at forward angles and near  $135^\circ$ . The smooth curves for the non-flaming fuel smoke particles seen in Figure 3 are a result of the polydisperse nature of these smoke aerosols. Scattering from polydisperse ensembles of particles averages out the detail seen in single particle scattering data.

## 5. Treatment of Polarization

The information in Figure 3 can be rearranged to give the degree of linear polarization,  $P(\theta)$ , (with angular notation suppressed)

$$P = \frac{\sigma_{VV} - \sigma_{HH}}{\sigma_{HH} + \sigma_{VV}}. \quad (1)$$

The quantity  $P(\theta)$  has previously been measured for the EN54 test smokes over an angular range of  $5^\circ$  to  $165^\circ$  [6]. The degree of polarization for the FE/DE generated smokes is shown in Figure 4, along with the theoretical curve expected from Rayleigh scattering. The deviation from  $P(0) = 0$  in Figure 4 is due to polarization dependent errors in the optical system, particularly for the propylene. The other results are mainly influenced by the uncertainty in the calibration [8]. The results in Figure 4 compare well



with [6] as they found the highest degree of polarization corresponded to the soot particles, a medium value existed for the cotton wick smoke, and that the lowest values were found for the pyrolyzed wood smoke.

Another widely used and related measure is the polarization ratio, defined as

$$\rho(\theta) = \frac{\sigma_{HH}(\theta)}{\sigma_{VV}(\theta)} \tag{2}$$

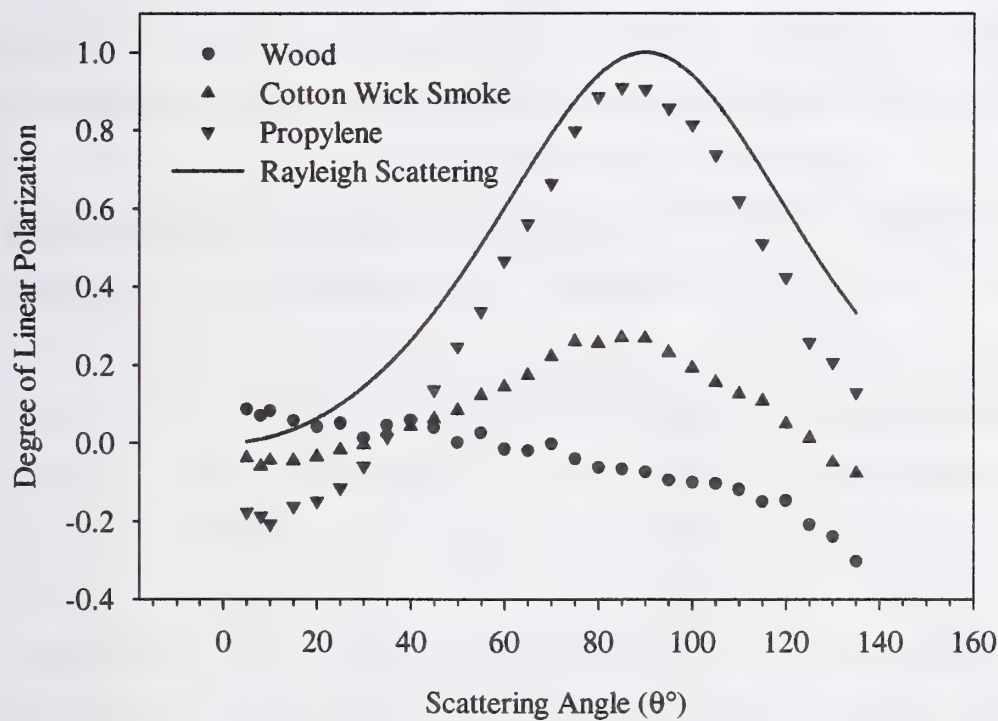


**Figure 4:** Degree of linear polarization,  $P(\theta)$ , for the FE/DE produced smoke particles.

Table 1 includes the polarization ratio at 90° for the FE/DE smokes and two other soots, acetylene and ethylene, generated using a laminar co-flow diffusion burner [8]. The degree of polarization or the polarization ratio in Table 1 indicates that two detectors positioned perpendicular to each other, with incident linear polarized light, could distinguish between smoke from flaming or non-flaming fires. The greatest difference

in  $P(\theta)$  or  $\rho(\theta)$  for the flame generated smoke versus non-flaming occurs at  $\theta = 90^\circ$ . The ratio of polarization is also sensitive to the fuel for flame generated smoke particles (see Table 1), which is related to the soot agglomerates different primary particle diameters. Previous measurement [9] indicate that the fuel type affects the primary sphere size, and this may account for the fuel dependence of  $\rho(\theta)$ .

## 6 Fractal Analysis of Scattered Light

It has been stated that the high values of the degree of polarization (i.e. near  $\theta = 90^\circ$ ,  $P(\theta) \rightarrow 1$ ) for flame generated smokes is due to their particle size being small compared to the wavelength of the incident beam [6]. This is misleading in that it implies the soot particles scatter light according to Rayleigh theory. The scattering from agglomerates with sizes up to  $20 \mu\text{m}$  [9] is more complex than Rayleigh theory.

Fuel	Degree of Polarization $P(90/120)$	Polarization $P(90/120)^*$	Polarization Ratio $\rho(90^\circ)$
Wood (flaming)	--	0.94 / 0.5	--
Wood (pyrolysed)	-0.07 / -0.15	-0.12 / -0.25	1.16
Cotton wick	0.27 / 0.05	0.3 / 0.13	0.58
Propylene	0.90 / 0.43	--	0.05
Acetylene	0.96 / 0.53	--	0.023
Ethylene	0.97 / 0.51	--	0.013

**Table 1:** Ratio of linear polarization at  $\theta = 90^\circ$ , for various smoke particles: wood, cotton wick and propylene generated in the FE/DE ; while acetylene and ethylene were generated in a co-flow laminar diffusion burner [11]. \* Data has been taken from [6].

The total scattering from soot agglomerates can be represented as (angular notation suppressed)

$$\sigma_{XX} = (S_{ag} \cdot S_r)_{XX} \text{ but } (S_{ag})_{VV} \approx (S_{ag})_{HH} \quad (3)$$

where  $S_r$  is the Rayleigh-like scattering component and X denotes a given polarization. The term  $S_{ag}$  arises from the interference in the far field of the Rayleigh scattering by

the individual primary particles making up the agglomerate. The term,  $S_{ag}$ , can vary by three orders of magnitude (Figure 3) while for Rayleigh scattering,  $(S_r)_{VV}$ , is independent of angle. Since  $S_{ag}$  is independent of the polarization direction it is effectively reduced in the polarization ratio,  $\rho(\theta)$ , which then reflects the Rayleigh-like scattering from the primary spheres.

The general formalism of agglomerate light scattering [12] can be expressed in terms of the scattering parameter,  $q$ , which follows a power law relation that reduces to  $\sigma_{VV}(\theta) \propto q^{-D}$  for  $q > R^{-1}$ : where  $R$  is the agglomerate characteristic radius;  $q = 4\pi\lambda^{-1} \sin(\theta/2)$  is the elastic scattering wavevector magnitude or scattering parameter; and  $D$  is the fractal dimension characterizing the agglomerate. Various studies for in-flame and post-flame soot have reported fractal dimensions to be about 1.7 to 1.85 using laser scattering techniques [13]. This general behavior is related to the fact that all soot shares the same fundamental mechanisms of agglomeration growth [14].

Fuel	Fractal Dimension, $D$	
Acetylene	1.6	1.85*
Ethylene	1.7	1.84*
polypropylene	1.8	1.83*

**Table 2:** Fractal dimensions determined from Figure 5, for  $q \geq 5.1 \mu\text{m}^{-1}$  and (\*) results reported by [15].

Figure 5 shows the log-log plot for mass scattering cross section (vertical-vertical polarization) as a function of the scattering parameter,  $q$ , for the three soots, ethylene, acetylene and propylene, as well as the smoke from wood and cotton wick. The slopes for the soots at  $q \geq 5.1 \mu\text{m}^{-1}$  are tabulated in Table 2 and compared with another study [15]. The low value for acetylene might be due to the presence of super-agglomerates ( $>> 50 \mu\text{m}$ ).



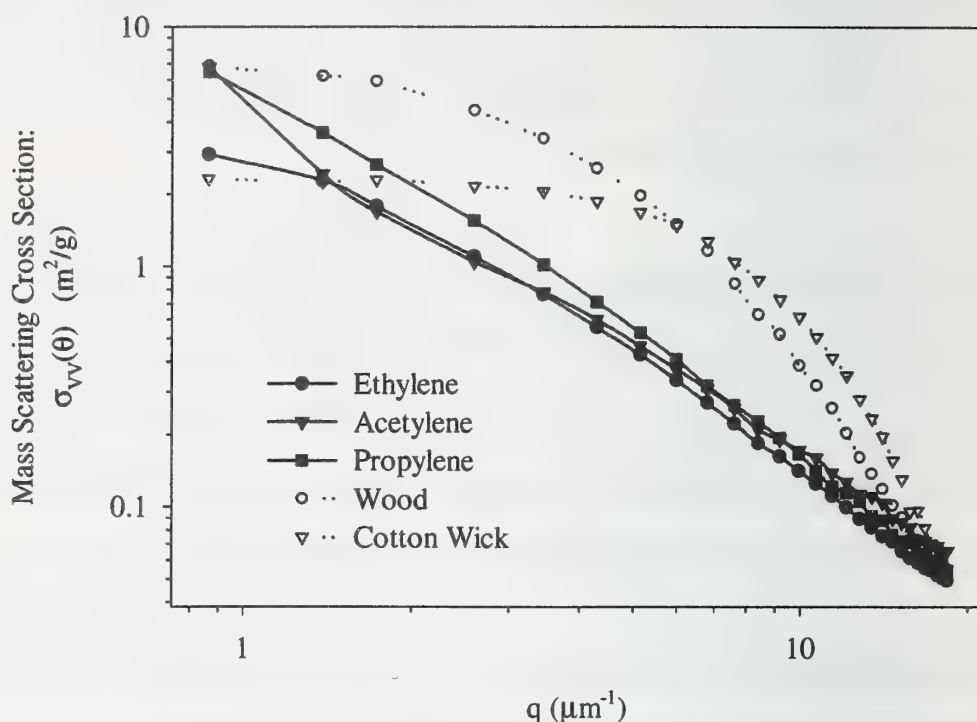


**Figure 5:** Mass scattering cross section (VV) as plotted against the scattering wavevector,  $q$ .

We also observe in Figure 5 that there is a qualitative difference between the  $q$  dependence for soot compared to non-flaming smoke particles. The higher forward scattering for the wood smoke is apparent and the slope for scattering angles corresponding to  $q \geq 12 \mu\text{m}^{-1}$  ( $\theta \geq 75^\circ$ ) yield slopes of about 3 and 4.6 for wood and cotton wick smoke respectively. The exact relationship in the context of Mie theory between these qualitative differences and the morphology, size and refractive index of a scattering particle is only recently being considered [11]. A detector with a diode array in the back scattering angles could be used to compare the slope of the signal when treated as a function of  $q$ . Large integer values of the slope,  $\geq 3$ , would indicate compact scattering particles while small values,  $\leq 2$ , would indicate open agglomerates. There is a need to obtain data for a wide range of non-flaming smokes as well as nuisance aerosol results to assess the utility of this approach.

## 6 Conclusion

This study presents results for the first time of the mass scattering cross section ( $\text{m}^2 \text{g}^{-1}$ ) of smokes similar to those used in smoke detector standards EN54 and UL 217. Smokes were generated in the fire emulator/detector evaluator (FE/DE) at NIST and characterized in terms of their size and optical properties. The size characterization shows that the smoke from pyrolysed wood blocks is a unimodal distribution with a MMAD of  $1.6 \mu\text{m}$ , while the smoldered cotton lamp wick fuel has a bimodal distribution with a MMAD of  $0.3 \mu\text{m}$  for its measurable mode. It was found that 48 % of the mass of the cotton wick smoke was below  $0.056 \mu\text{m}$ . The difference in mass/aerodynamic diameter is also observed in the differential mass scattering cross sections for near forward scattering angles, where the wood smoke scatters light more strongly than cotton wick smoke particles due to its larger mean size.

The ratio of polarization and the degree of linear polarization have been demonstrated as a means of distinguishing between soot from flaming fires and smoke particles from non-flaming fires. The ratio of polarization is shown to be more sensitive than the degree of polarization to soots from different flaming fuels, probably due to the different primary particle size. All three flame generated smokes are shown to have similar “ $q$ ” plots, which are easily distinguished from the two “ $q$ ” plots for the non-flaming fuels smokes.

## Reference List

- [1] Grosshandler WL: Towards the development of a universal fire emulator-detector evaluator. *Fire Safety Journal* 1997; 29:113-127
- [2] Cleary, T., Donnelly, M., and Grosshandler, W. The Fire Emulator/Detector Evaluator: Design, Operation and Performance. 12th International Conference on Automatic Fire Detection. AUBE, 2001
- [3] Helsper C, Fissan HJ, Muggli J, Scheidweiler A: Particle number distributions of aerosols from test fires. *Journal of Aerosol Science* 1980; 11:439-446
- [4] Tamm E, Mirme A, Sievert U, Franken D: Aerosol particle concentration and

- size distribution measurements of test-fires as a background for fire detector modeling. *Internationale Konferenz über Automatische Brandentdeckung, AUBE '99* 1999;150-159
- [5] Meacham BJ, Motevalli V: Characterization of smoke from smoldering combustion for the evaluation of light scattering type smoke detector response. *Journal of Fire Protection Engineering* 1992; 4:17-28
- [6] Loepfe M, Ryser P, Tomkin C, Wieser D: Optical properties of fires and non-fire aerosols. *Fire Safety Journal* 1997; 29:185-194
- [7] Marple VA, Rubow KL, Behm SM: A Microorifice Uniform Deposit Impactor (MOUDI): Description, calibration and use. *Aerosol Science and Technology* 1991; 14:434-446
- [8] Weinert, D. and Mulholland, G. W. An apparatus for light scattering studies of smoke particles. 12th International Conference of Automatic Fire Detection AUBE, 2001.
- [9] Mulholland, G. W. and Choi, M. Y. Measurement of the mass specific extinction coefficient for acetylene and ethylene smoke using the large agglomerate optics facility. The Combustion Institute. Twenty-Seventh Symposium (international) on Combustion. 1515-1522. 98. Pittsburgh, The Combustion Institute.
- [10] Zhu J and Choi MY, University of Illinois, Personal Correspondence, 2000
- [11] Sorensen CM, Fischbach DJ: Patterns in Mie Scattering. *Optics Communications* 2000; 173:145-153
- [12] Sorensen CM: Light Scattering from Fractal Aggregates. *To be submitted for publication*
- [13] Sorensen CM, Feke GD: The morphology of macroscopic soot. *Aerosol Science and Technology* 1996; 25:328-337
- [14] Mountain RD, Mulholland GW: Light scattering from simulated smoke agglomerated. *Langmuir* 1988; 4:1321-1326
- [15] Koylu UO, Faeth GM, Farias TL, Carvalho MG: Fractal and projected structure properties of soot agglomerates. *Combustion and Flame* 1995; 100:621-633



D. Kozeki

National Research Institute of Fire and Disaster, Tokyo, Japan

### **Smoldering Fire Detection by Image-processing**

#### **Abstract**

Since fire detectors are not installed in all buildings, too many victims and property damages are caused in building fires every year in the world. One reason of non-installation is the fire detectors currently on sale are not always reliable mainly due to the so-called false alarms. Therefore the author has been examining many possibilities of new reliable fire detection system, including a possibility of multi-element fire sensor. At the AUBE'99 in Duisburg, the author reported another newly developing fire detection system using a thermal video camera system, related to the heat image due to fires, where the author proposed a method to eliminate non fire sources. In this report, the author has further advanced the image processing method to detect smoldering fires, together with the verification of software by experiments. And it has been indicated that this system is very effective in detecting smoldering fires very early and reliably.

#### **1. Introduction**

Too many victims and property damage are caused in building fires every year in the world. It is well known that fire detectors can reduce building fires, but unfortunately fire detectors are not always widely installed in buildings. One reason is the problem of price of fire detectors and installation. Another reason is the fire detectors currently on sale are not always reliable mainly due to the so-called false alarms, since most current fire detectors are based on a too primitive sensing element and logic. The author has longly studied the method of how to reduce the false alarms of fire detectors. One possibility developed by the author is to use the newly developed three sensing element fire detector (including new CO sensor) and artificial intelligence logic to judge between a real fire and a false fire[1]. It has been found that this new fire detector is very effective to reduce false alarms, therefore increasing the reliability of fire detection. The new three-element fire detector has, however, still a problem of price

to manufacture particularly on CO sensing element at present. Therefore, the author has been examining other possibilities of new reliable fire detection systems also.

At the AUBE'99 in Duisburg, the author reported another newly developed fire detection system using a thermal video camera system, which is related to the analysis of heat images[2]. This newly developed fire detection system is particularly effective in detecting smoldering fires. As well known, it is comparatively easy to detect flaming fires by infrared or ultraviolet sensors or CCD cameras[3], particularly in the air conditioned rooms. On the other hand it is not always easy to detect smoldering fires, since there is no ways to detect smoldering fires by remote sensors at present. Although there have already been some studies to detect forest fires using infrared cameras[4], those methods are not always in common. Thus there is a possibility that the detection of a smoldering fire is delayed. Keeping this in mind, studies to develop a method to detect smoldering fires has been made, by introducing a thermal video camera. Thermal images are resistive against the influence by the airflow from the air conditioners or high-temperature layer in the room. To improve the disadvantage of current smoke detectors in smoldering fire, the author has been developing a new fire detection system using thermal images. In this report, the author deals with image processing software for smoldering fire detection, together with the verification by experiments.

## **2. Algorithm of Image Processing to Detect Smoldering Fires**

### **2.1 Preprocessing of thermal images to eliminate noises**

In order to detect fires correctly, it is important to eliminate false signals by preprocessing of thermal images. Generally video signals often import unwanted noises due to miscellaneous sources, including electric ones and thermal ones. There are many sources, which emit thermal radiation, for example by thermal reflection or something warm. Therefore, those noises should be removed. The procedure employed here to eliminate noises is as shown in Fig.1. Details are as follows.

- (1) An infrared thermo-graphic camera (picture (a) in Fig.1), with semiconductor imaging cell consisting of 256 x 256 resolution, imports 30 images per second.
- (2) With 30 pictures per second, six imported thermal images per minute are stored into a computer memory as 8-bit data (picture (b) (a part of picture (c)) and picture (c) in Fig. 1). Figs. 1(b) ,(c),(d),(f),(g) are related to electric radiant heater as an example.
- (3) By comparing a preset threshold value, 8-bit data are transformed into binary data

(picture (d) in Fig.1). A threshold is placed between high and low temperatures. Many threshold values were tested. It was found that the thermal value of 200°C was best. And then all thermal data are transformed into binary. If a pixel value is larger than a preset value, the pixel changed into “1” and if smaller, changed into “0”. However original 8-bit data are also kept for another purpose, to be explained later.

- (4) High temperature pixels surrounded by low temperature pixels are defined as “high temperature cluster”. Fig. 1(e) shows how to define the high temperature cluster. Number of pixels and centroid of each high temperature cluster within the thermal image are measured, by judging the connection way between the neighboring pixels. High temperature clusters are extracted from the binary image using the well known “eight-neighborhood connected component processing method”[5]. After that, the identification number is labeled to each high temperature cluster. Then calculated is the number of pixels and centroid as shown in Fig. 1(f).
- (5) Next processed is the removal of thermal noises by the way that smaller clusters are ignored. Thermal noises are eliminated in the pixel domain, by counting the number of pixels consisting of a cluster and comparing the preset value. Here a cluster consisting of 10 pixels is eliminated (pictures (g) in Fig.1).

## 2.2 Image processing to eliminate non-fire cluster

- (1) Follow up of increase and decrease of high temperature clusters

Here, non-fire clusters are defined as the tools such as cooking stove, room heater and smoothing iron, which remain at almost the same size with time. Other sources can not be considered, since the temperature of 200 °C is too high in normal conditions. Therefore each cluster size is followed up on the basis of discriminating separation or fusion of high temperature cluster from time series images, and the time varying size and location are calculated. Detailed following up procedure is as follows, needed is the information, such as identification number of each cluster, number of pixels, centroid and intensity (namely 8-bit image data as mentioned above) of all pixel obtained from extraction process mentioned in section 2.1-(4) for each image. This information is named “Cluster ID Information”. In the smoldering fires, time dependent shift of the centroid is very small. It is easy to identify the moved clusters using the Cluster ID Information between two deferent images.



## (2) Discriminate separation or fusion of high temperature cluster

In this method, the discrimination between the real smoldering fire and the non-fire is based on the time-dependent variation of the centroid and size of the high temperature cluster. Differently from non-fires, the centroid and size of the high temperature cluster are highly time dependent. If two separate clusters reach close to each other and merge in one cluster, the centroid location and cluster size will suddenly be changed. Similarly to this, if one cluster separates into multiple clusters, the same situation will happen. In Fig. 2, one example of fusion of 6 clusters in Fig.2(b) into 3 clusters in Fig.2(d) is shown, namely clusters C and D in Fig.2(b) fused into the cluster H in Fig.2(d). Details are shown in Table 1.

Here many trials were made to identify which clusters fuse into one cluster and employed method is a simulation to search most appropriate combinations on the centroid shift and pixel numbers. In the case of clusters C and D in Fig.2-(b) fused into the cluster H in Fig.2-(d), the centroid location of cluster H is 355 in X direction and 228 in Y direction while the average centroid location of cluster C and D is 354 in X direction and 228 in Y direction, as shown in Table 1. Both are very close and it was judged that clusters C and D fused into cluster H. Based on the procedure mentioned above, a software to detect smoldering fires and to eliminate non-fires is developed using C language.

## 3. Verification of the Software by Detection Tests of smoldering fire

Using the newly developed software, based on the procedure mentioned in section 2, experimental verification tests were repeatedly made. Here particularly focused in the tests are the elimination of the heat from cooking instruments or room heater, and also the accurate detection of the smoldering fires. It was found that heat from cooking instruments or room heater could easily be discriminated by the calculation of centroid coordinates and the size of high temperature cluster. The threshold value was varied from 100 °C to 300 °C. If the threshold value is too low, too many clusters appeared. And if it is too high, the cluster size differs only a little with time. Then the value employed here was 200 °C as most appropriate value.

Fig. 3 shows the changing high temperature cluster of electric radiant heater as a non-fire test material. In this case, the centroid and the size were almost the same for more than 5 minutes after the initial one minute rapid increase as shown in Figs.3 and 4,

where the pixel number was fixed at about 7500 after one minute and at the same time the centroid did not shift. Next examined was a smoldering fire using silk cotton cushion. Fig. 5 shows the changing high temperature cluster of smoldering silk cotton cushion. Fig. 6 shows the time dependent pixel number of smoldering cushion. As shown in Figs.5 and 6 the heated area, namely number of pixels, is rapidly increasing, differently from the case of electric radiant heater. Additional verification tests using other smoldering ropes were made. It has been found that the developed software is very useful to detect smoldering fires and to eliminate non-fires. The detection of flaming fires is comparatively easy, as mentioned earlier. The threshold value of 200 °C employed here is not always fixed, but can be flexible depending on the circumstances of rooms, using artificial intelligent processing.

#### 4. Conclusions

In this study an image processing algorism has been proposed to detect smoldering fires and to eliminate non-fires. It is verified that the image processing software works correctly for smoldering stage of silk cotton cushion and experiments using an electric radiant heater.

#### References

- [1] Satoh, K., Takemoto, A., Kozeki, D. Intelligent Fire Detection System using Multi-sensor Fire Detector (including CO sensor) and Fuzzy Expert System. Technical Report of Fire Research Institute of Japan No.26 (1991).
- [2] Kozeki, D. : Observation of Early Stage Fires by a Multi Spectrum Camera. Proceedings of AUBE'99 1999: 180-186.
- [3] Chen, X., Wu, J., Yuan, X., Zhou, H. Principles for a Video Fire Detection System. University of Science and Technology of China, People's Republic of China, Fire Safety Journal, July 1999: Vol. 33, No. 1, 57-69, .
- [4] MURILLO, J J., OLLERO, A., et al. A hybrid infrared/visual system for improving reliability of fire detection systems. Univ. Sevilla, Sevilla, ESP., IFAC Symposium on Fault Detection, Supervision and Safety for echnical Processes, Fault Detect Superv Saf. Tech. Process 1997 Vol 2
- [5] Hasegawa, J., Koshimizu, H., Yamanaka, A., Yokoi, S. Image Processing on Personal Computer. Gijyutsu-Hyoron Co., Ltd.

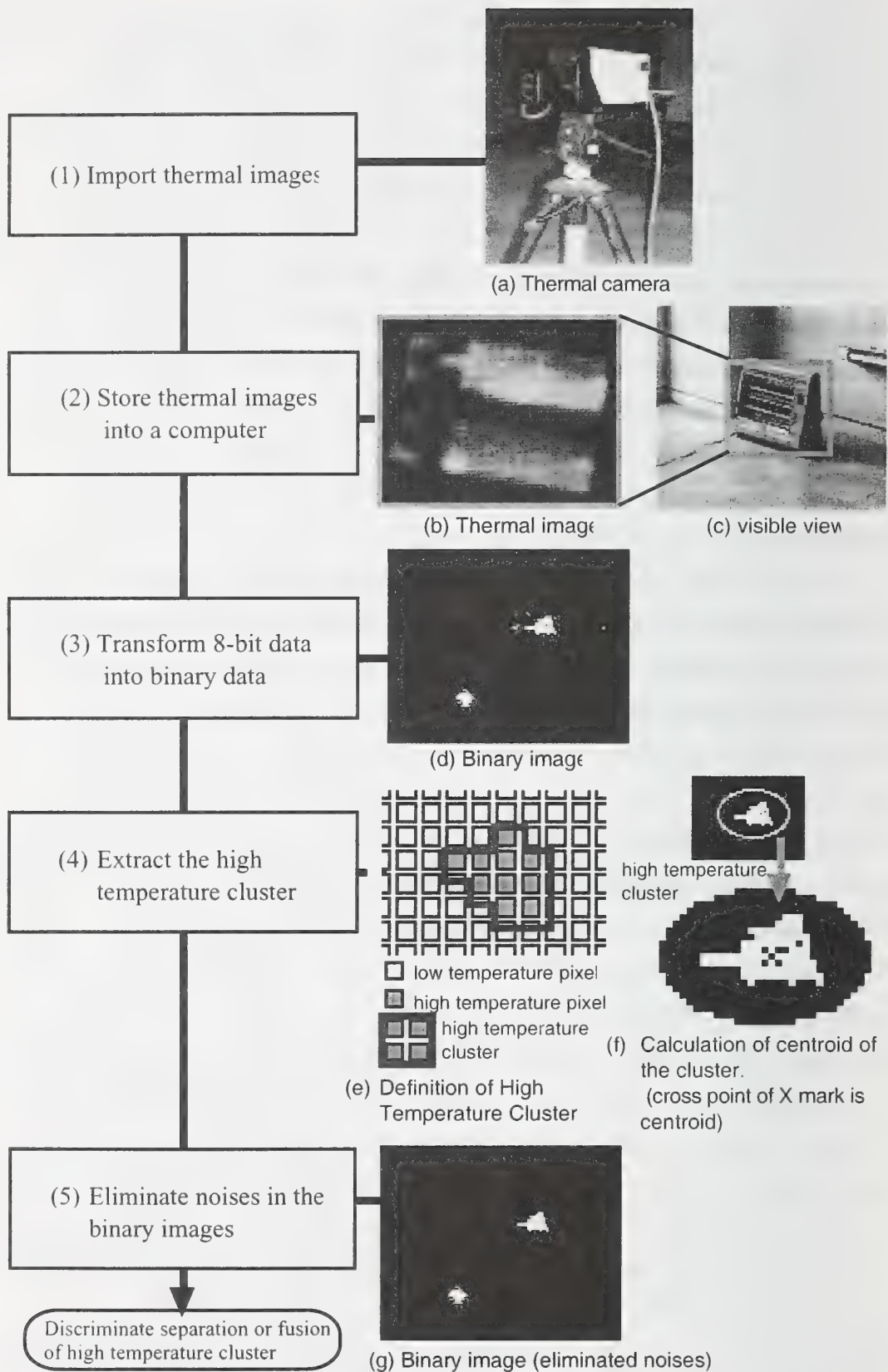


Fig. 1 Algorithm of Image Processing to Detect Smoldering Fires



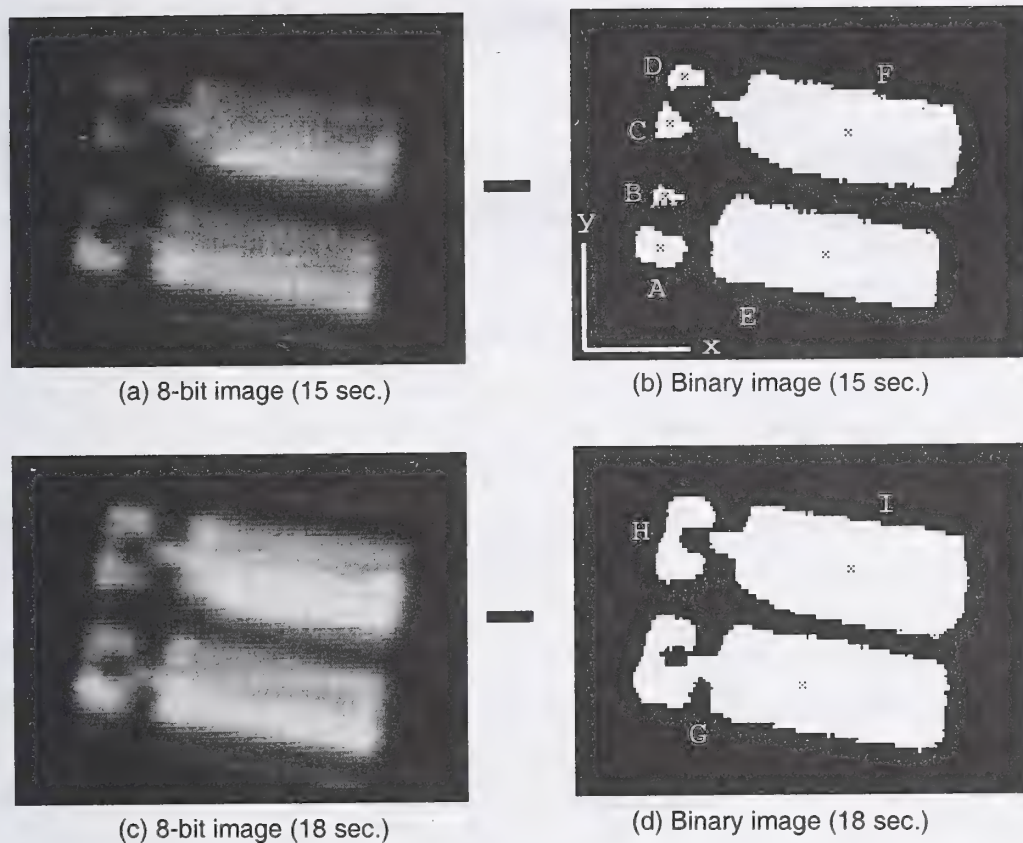


Fig. 2 Discriminate separation or fusion of high temperature cluster  
(Number of second is elapsed time from turn on the heater)

Table 1 Centroid and pixel number of clusters  
in Fig.2 (b) and (d)

Cluster ID	Centroid		Pixel number
	X	Y	
A	347	172	225
B	349	192	55
C	351	220	117
D	357	238	97
E	411	169	2650
F	420	216	2847
G	401	171	3836
A+B+E	405	170	2930
H	355	228	456
C+D	354	228	214
I	420	216	3465
F	420	216	2847



(a) 10 sec. (b) 60 sec. (c) 180 sec.  
 Fig.3 Growth of high temperature cluster of electric radiant heater  
 (Number of second is elapsed time from turn on the heater)

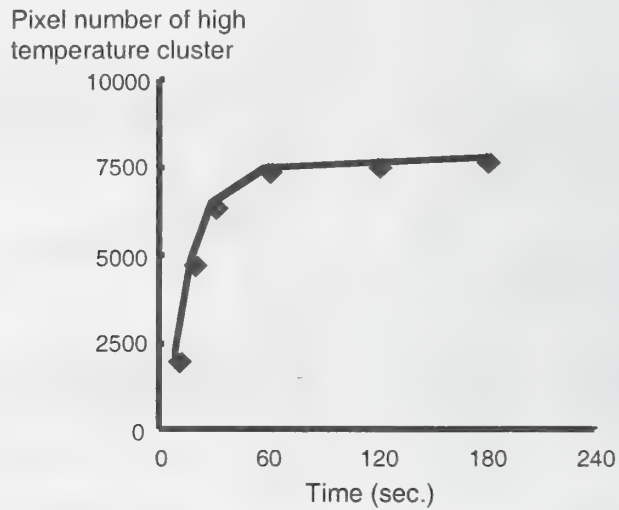


Fig. 4 The time dependent pixel number of electric radiant heater



(a) 10 sec. (b) 60 sec. (c) 120 sec. (d) 180 sec. (e) 240 sec. (f) 360 sec.  
 Fig.5 Growth of high temperature cluster of smoldering cushion  
 (Number of second is elapsed time from ignition)

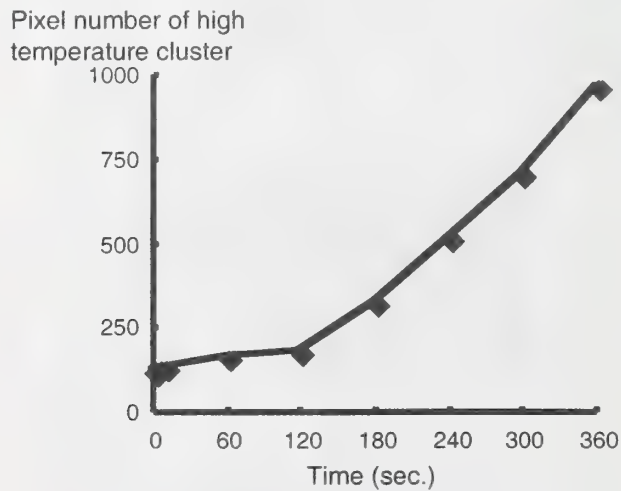


Fig. 6 The time dependent pixel number of smoldering cushion

Dieter Wieser<sup>1</sup> and Thomas Brupbacher  
Siemens Building Technologies AG, Cerberus Products/Alarmcom Division  
8708 Männedorf, Switzerland  
dieter.wieser@cerberus.ch

## Smoke detection in tunnels using video images

### Abstract

In the aftermath of the two disastrous fires in the Mont Blanc and the Hohentauern road tunnels, there is a strong trend in Europe to require additional safety installations in tunnels for the detection of fires. Smoke detection based on processing of video images promises fast detection of fires and can complement more traditional techniques such as temperature sensing. Because it uses already required installations (the video system), this video smoke detection system can be deployed at a reasonable cost and, furthermore, it can be retrofitted into already existing installations.

In this paper a new video smoke detection system is described and a report on full scale fire tests in tunnels is given. Furthermore, it is demonstrated that the video smoke detection system correctly processes video sequences prone to give false alarms; no false alarms were given.

### 1. Introduction

There is a fast-growing infrastructure of video surveillance and monitoring equipment in European tunnels. A standard technique is to connect cameras to a video multiplexing device and to have a human operator judge selected images at a time. This approach has several deficiencies; two of them being the fact that it is inefficient because only a small number of images are observed at a given point in time, and that it is expensive because attentive watching of video images is tiring work and requires the operator to be changed frequently. More and more traffic control systems based on automatic video processing are, therefore, being installed to detect automatically critical conditions and to display to the operator only images of

---

<sup>1</sup>corresponding author



those situations which must be assessed quickly; it is then up to the operator to take appropriate measures. There are now several products available to automatically measure traffic flow, detect traffic jams, detect wrong-way drivers, etc.

As consequence of several disastrous fires in road tunnels (and in other tunnels, e.g. the Kaprun funicular catastrophe), public tenders in Europe for automatic video surveillance of road tunnels now often also require automatic video smoke detection even though there are other, more traditional techniques, such as the very reliable temperature sensor cables (e.g. the Siemens Cerberus system FibroLaser II), to detect fires in tunnels. This is because video smoke detection promises to alert operators very quickly and display to them images of endangered tunnel sections. Using both systems would, therefore, allow one to combine a very fast but more false alarm prone technique for smoke detection with a slower but more reliable technique that could even be used to control extinguishing.

Previous efforts ([1, 2, 3, 4, 5, 6]) in video smoke detection concentrate on three main techniques:

*Histogram based techniques:* These approaches calculate the histogram of an acquired image and then use the information in the histogram to detect the presence of smoke/fire. Some approaches in this category compare the computed histogram with pre-computed histograms of typical smoke/fire scenes to make the decision. Other approaches use statistical measures such as the mean and standard deviation to determine the likelihood of the existence of a fire in the scene.

*Temporal based techniques:* Approaches in this category use the difference(s) between frames to generate growth patterns that could be smoke/fire objects. The number of frames used in calculating the difference image varies depending on the approach.

Once the difference frames are calculated, different techniques are used to segment and identify smoke objects. In some approaches, a number of statistical metrics are calculated from the difference images, then that information is used to infer the presence of smoke/fire. Other approaches use the colour information in the generated patterns to classify and identify smoke objects in the image. Techniques such as color matching filtering are used.

*Rule based techniques:* A third category of video smoke detection uses domain spe-

cific information coded as rules to infer the presence of fire from a sequence of images. Approaches in this category are in some cases combined with approaches in the first two categories to help during the recognition phase.

In road tunnels, smoke detection algorithms must be able to overcome several difficulties. Moving objects (the vehicles) which may stand for a while (traffic jam) can fill most of the image, making definitions of stable references difficult. In addition, car lights may induce dramatic changes in lighting conditions, especially with on-coming traffic, and near the openings of the tunnel water spray from cars passing by may make detection even more difficult.

Our system analyzes the contrast in the image and uses special procedures to overcome the above difficulties. The aim of this paper is not to explain the algorithm being used (the system will soon be commercialized), but to illustrate for an audience more oriented towards indoor fire detection the possibilities of and difficulties in this tunnel application.

## 2. Estimation of the loss of contrast

As mentioned above, our approach to the detection of smoke in a tunnel is based on a loss of contrast in the image caused by the presence of smoke. For simplicity, we consider only the luminance contrast. The contrast  $C$  of an isolated object viewed against a uniform, extended background is defined by [7]

$$C = (L_o - L_b)/L_b \quad (1)$$

$L_o$  and  $L_b$ , respectively, are the luminance of the object and of the background. If a light extinguishing medium, such as smoke, is present, then the contrast after passing for a distance  $R$  through the medium is reduced to

$$C_R = C \exp(-K R) \quad (2)$$

The extinction of light caused by smoke can be expressed through the particle concentration in the smoke as

$$K = 2.3 D = 2.3 D_m \frac{\Delta M}{V_c} \quad (3)$$

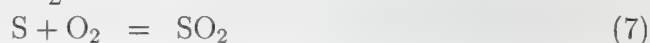
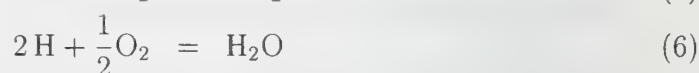
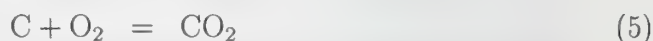
with  $D$  being the optical density per metre,  $D_m$  the mass optical density,  $\Delta M$  the mass loss of the burning sample, and  $V_c$  the volume of the chamber containing the

fire. Values for  $D_m$  are tabulated and can be found e.g. in Mulholland [7]. In tunnels, Equation (3) has to be modified to account for the wind

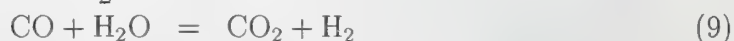
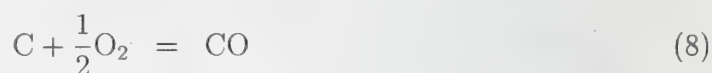
$$K = 2.3 D_m \frac{\dot{M}}{\dot{V}} \quad (4)$$

For an estimate of  $\dot{V}$ , the volume flow of air in the tunnel, both the effects of the fire and of the forced air flow (natural and forced convection) have to be taken into account. By looking at the relevant combustion reactions, the volume of exhaust gases can be put into relation with the mass loss in the fire.

In the early stage of a typical fire in a tunnel, e.g. a burning car, mostly organic matter (in the chemical sense) is decomposing. This means that we can restrict the discussion to the most common elements occurring in organic substances, namely carbon (chemical symbol C), hydrogen (H), and oxygen (O), and to sulphur (S), which is often contained in fossile fuels as an impurity. Because of the superposition principle for chemical reactions, it also suffices to look at the combustion reactions of the elements.



In the case of oxygen deficiency, carbon monoxide, CO, is additionally formed and at the same time the reaction of CO with water has to be taken into account:



This last reaction, the reduction of water to hydrogen, is endothermic and is thus strongly dependent on the temperature in the reaction zone. If the substances involved in the fire also contain halogens (fluorine F, chlorine Cl, bromine Br, iodine I), these react preferentially with hydrogen to form acids. Halogens are largely being replaced in todays materials (e.g. PVC is being replaced by other compounds) and are, therefore, neglected in the following discussion.

Assuming the above stoichiometric reactions (5 – 9), the mass of oxygen,  $m_{\text{O}}$ , needed for complete combustion of 1 kg of burning material can be calculated from

$$m_{\text{O}} = 2.664 w_{\text{C}} + 7.937 w_{\text{H}} + 0.998 w_{\text{S}} - w_{\text{O}} \quad (10)$$



Where  $w_X$  denote the mass fraction of the elements in the burning substance. Using the ideal gas equation, this mass can be transferred into an equivalent volume at any given pressure, temperature, and composition of the burning material.

A common and time-proven estimate of the development of a fire with time is given by

$$\frac{d}{dt}q = \dot{q} = A b t^2, \quad (11)$$

with  $\frac{d}{dt}q$  being the rate of heat release,  $A$  the area of the fire,  $b$  a constant, and  $t$  the time since ignition. The rate of heat release increases until it reaches a maximum  $\dot{q}_{\max}$  that is dependent on the geometry of the fire and on the nature of the combustant. With the reaction enthalpies of the chemical reactions ((5 – 9), the rate of heat release  $\dot{q}$  can be linked to the rate of mass loss of the combustant  $\dot{M}$ . The combustion enthalpy can be calculated as

$$h = (338 \times 10^5 w_C + 1004 \times 10^5 w_H + 95 \times 10^5 w_S - w_O) \frac{\text{J}}{\text{kg}}, \quad (12)$$

using reaction enthalpies from [8]. Using  $\dot{q} = h\dot{M}$ , the rate of mass loss in the combustant can be calculated to

$$\dot{M} = \frac{A b t^2}{h}. \quad (13)$$

As an example, consider the scenario of a simple model calculation for a burning car in a tunnel with a cross-section  $A_{\text{tunnel}} = 60 \text{ m}^2$ : The combustible mass is assumed to have a composition of  $w_C = 0.78$ ,  $w_H = 0.12$ , and  $w_O = 0.1$ , typical for plastics and hydrocarbons. Using equation (10), the mass of oxygen needed to combust 1 kg of substance equals to 0.852 kg, corresponding to approximately 26.7 mol of atomic oxygen, or a volume  $V = 0.33 \text{ m}^3$  at standard conditions. The relative composition of oxygen in air is 21 volume percent, thus this corresponds to roughly  $1.5 \text{ m}^3$  air. This is a relatively small volume compared to a convection of  $120 \text{ m}^3/\text{s}$  at a wind speed of 2 m/s; it becomes clear that, at least in the early stages of the fire, convection a) can feed the fire with enough oxygen, and b) dominates the mass flow. It is, therefore, justified to set  $\dot{V}$  to the wind speed times the tunnel cross-section area. From this simplification, the time needed to raise an alarm can be now estimated: Using equations (4) and (13), the extinction factor can be calculated to

$$K = 2.3 D_m \frac{A b t^2}{h \dot{V}}. \quad (14)$$

After ignition of the fire, there will be a certain time delay until the smoke enters the detection zone over which the extinction  $KL$  will be integrated. During this

time nothing is detected. Then the extinction  $KL$  will increase until it reaches a maximum.

*Example:* Assume the geometry of the tunnel as above, a distance between the camera and the fire of 150 m, and a distance  $L$  over which we integrate of 10 m. The fire is given by  $\dot{q}_{\max} = 5$  MW,  $A = 2$  m<sup>2</sup>,  $b = 30$  W/m<sup>2</sup>/s<sup>2</sup>, a composition as above and thus  $h = 12$  MJ/kg, and  $D_m = 0.5$  m<sup>2</sup>/g. The smoke of the fire enters the detection path 70 s after ignition of the fire; at this point in time  $K$  approximately equals 23%/m. So already a short optical path length suffices to detect the smoke.

### **3. Test results**

#### **3.1. Fires in the fire test laboratory**

The development of the video smoke detection method was based on experiences with test-fires, done according to the European norm EN-54, performed in the fire test laboratory at Siemens Cerberus. The dynamic contrast analysis algorithm was developed so far that smoke is detected within seconds in normal office rooms. Long term tests in hallways were also performed; these showed that the system gave no to false alarms when running for weeks at a time.

#### **3.2. Tests at the test tunnel Hagerbach**

Siemens Cerberus have a tunnel fire laboratory installed in the ventilation section of the "Versuchsstollen Hagerbach" near Sargans (Switzerland) and have been performing weekly tests with fires for the last two years. Figure 1 shows a schematic of the setup. In collaboration with "Vereinigung deutscher Schadensversicherer" (VdS) in Köln, a simulation program to describe tunnel fires is developed to allow for a scaling up or scaling down of arbitrary fires in tunnels. Test fires with heat releases of up to 5 MW can be produced under controlled conditions using different combustants; the wind speed can be varied between 0.5 and 5 m/s. All fires are monitored using several video cameras.

One insight gained from the experiments in the Hagerbach tunnel is that the wind speed is critical to the contrast observed in the video image; reliable detection at wind speeds above 2.5 m/s, where the smoke is turbulently mixed with air and

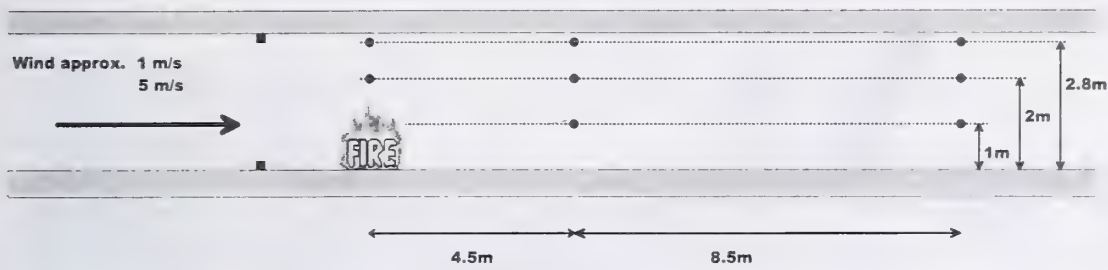


Figure 1: Schematic setup in the Hagerbach tunnel

diluted by the tunnel wind, is very important.

### 3.3. Calibration in a smoke box

Based on the results and experience gained from the Hagerbach experiments, realistic smoke densities were able to be reproduced in a “smoke box” sized  $1\text{m} \times 1\text{m} \times 1\text{m}$ . Figure 2 shows this box equipped with an aerosolgenerator (PALAS AGF2.0), ventilator (generates the turbulence), extinction measurement device (MIREX, according to EN54), video camera, and several light sources.

A fire with hydro carbons (gasoline, diesel, plastic) generates aerosols and soot particles with diameters of less than 1000 nm. For the simulation of smoke, aerosols with a Sauter-diameter of 500–1000 nm were produced from Di(2-ethylhexyl)-Seabacte (Merck 1263). Using the above mentioned experimental setup, the contrast-algorithm was calibrated to raise an alarm at a total extinction  $KL = 12\%$  over a path-length  $L$ .

### 3.4. Alarm tests with large scale tunnel fires

Tests with open gasoline fires conducted on the 22<sup>nd</sup> September 1999 in the road tunnel “Schönberg” near Salzburg were recorded using standard video cameras. These recordings were afterwards used to test the calibrated smoke detection algorithm. The series of images in figure 3 illustrate this test; the image labelled with “!!!Fire!!!” is taken as a screen shot from a computer running the video smoke detection algorithm.

Considering the transfer time needed for the smoke to reach the position of the



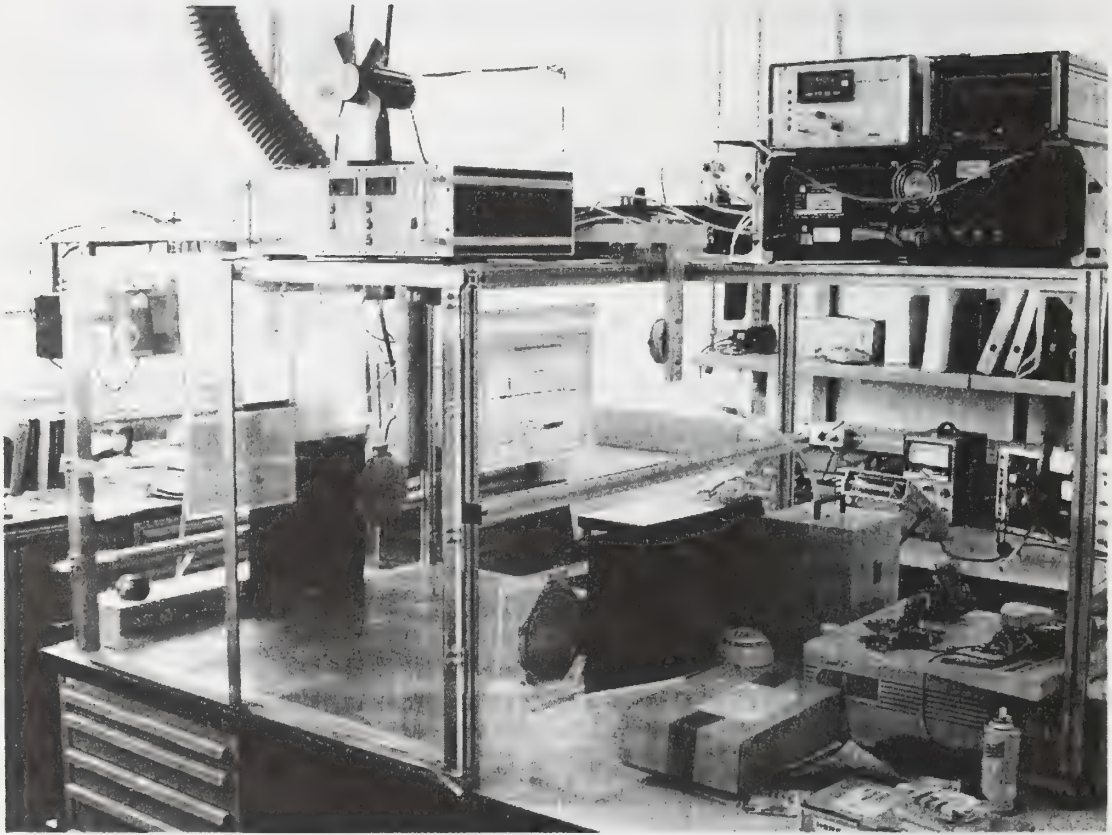


Figure 2: The smoke box used to develop and calibrate the algorithm.

camera (60 m distance, wind speed of 1 m/s), the algorithm triggered an alarm four seconds after the smoke could have reached the position of the camera. The smoke density at the position of the camera was at this point in time far below that found in the case of a fully developed fire. The calibration to  $KL = 12\%$  set from measurements in the laboratory was adequate to trigger the alarm in the early stages of a real, fullscale fire. It should be noted that the visibility decreases rapidly with time after the alarm was given and quickly approaches 0 m. At this point, it is impossible to monitor the fire with the camera raising the alarm.

### 3.5. Long term tests

To test the long term stability of the contrast algorithm under realistic conditions, several cameras in the Gubrist tunnel in the greater Zürich area were monitored. This allowed for a test of the algorithm under difficult conditions, such as traffic line ups, accidents and ensuing line ups, switching of the lights from day to night mode,



Figure 3: Screen shots of the large scale test in the Schönberg tunnel near Salzburg. Width of tunnel = 10 m, height = 6 m. Wind speed 1.0 – 1.2 m/s. Area of fire 1 m<sup>2</sup>, 20 L gasoline with 5 L diesel added. Distance between camera and fire 60 m

and combinations of the above. Figure 4 shows a schematic of the system setup.

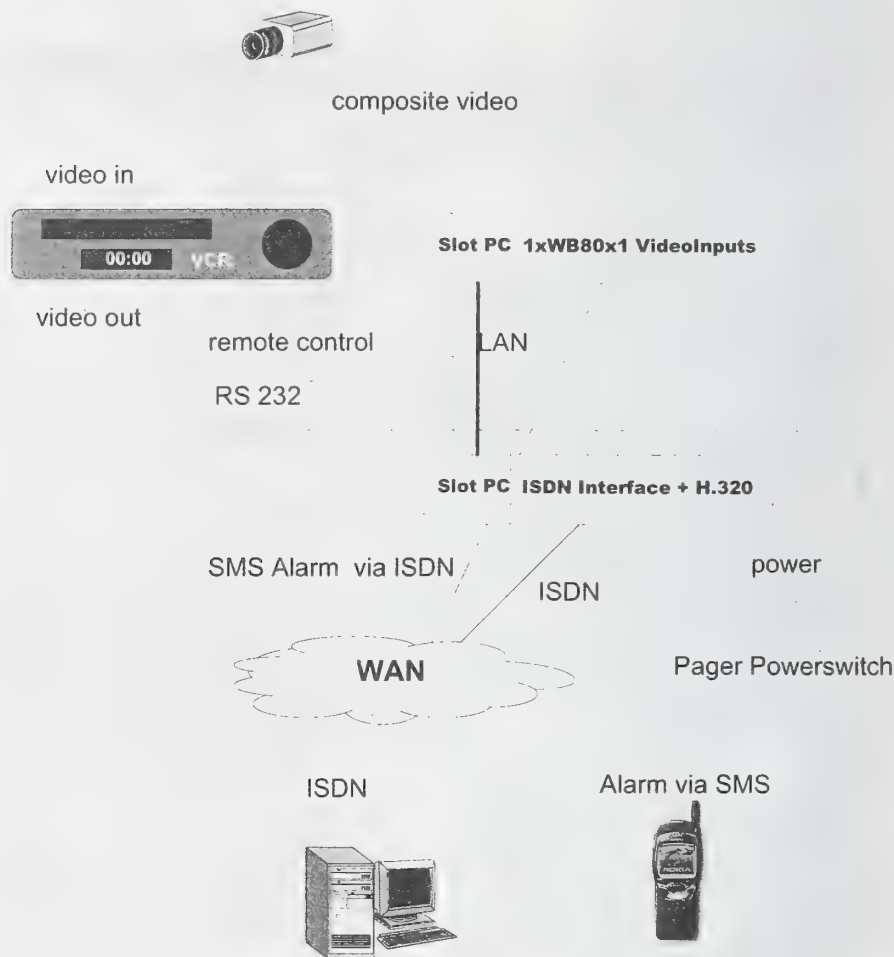


Figure 4: Schematic of the setup for the long term tests in the Gubrist tunnel.

Four cameras were installed at the side-wall of the tunnel, and four cameras were installed in the centre of the ceiling in the tunnel. Cameras on the side were installed at a height of 2.75 m, ceiling cameras at 4.3 m. The video smoke detection algorithm was run on a computer, and video recorders were installed that would be controlled by a second computer. The whole system can be controlled through an ISDN link so as to allow for critical sequences to be recorded.

Sequences of three hours duration each were recorded and especially critical situations were analysed. These sequences are now being used to test modifications of the video smoke detection algorithm for false-alarm proofness. So far, situations with solid line-ups, beginning line-ups, changing lighting conditions at the entrance of the tunnel, and of changing lighting due to the changes between night and day in the tunnel have been analysed. The algorithm has not produced a false alarm and



because there was no fire during the test period, also no fire was detected.

#### 4. Conclusions

Results from a contrast-analysing video smoke detection algorithm have been given. Experience so far indicates that the algorithm is quick to detect smoke in video sequences and at the same time immune to false alarms. In the near future, the system will be installed in several road tunnels to gain experience with non-stop operation.

To judge a video smoke detection system, one has not only to consider response times, but also how the system deals with effects which could induce false alarms such as car lights, motion, blooming, reflexes and other disturbing effects. Unfortunately customers are often not aware of the importance of the above effects. In order to establish video smoke detection as a new technique, system providers should, therefore, define a standard test procedure which takes into account the above mentioned effects as well as real fire situations. At Siemens Cerberus we are working towards such a standard.

#### References

- [1] B. Aird and A. Brown, "Detection and Alarming of the Early Appearance of Fire Using CCTV Cameras", Nuclear Engineering International Fire & Safety conference, London, 24-26 Feb. 1997.
- [2] T. Oikawa, M. Tomizawa and S. Degawa, "New Monitoring System for Thermal Power Plants Using Digital Image Processing and Sound Analysis", pp. 221-224, IFAC Control of Power Plants and Power Systems, Cancun, Mexico, 1995.
- [3] V. Cappellini, L. Mattii and A. Mecocci, "An Intelligent System for Automatic Fire Detection in Forests", University of Florence, Italy.
- [4] S. Noda and K. Ueda, "Fire Detection in Tunnels Using an Image Processing Method", Vehicle Navigation & Information Systems Conference Proceedings, pp. 57-62, Yokohama, Japan, 1994.

- [5] G. Healy, D. Slater, T. Lin, D. Drda and D. Goedeke, "A system for Real-Time Fire detection", IEEE computer Vision and Pattern Recognition, pp. 605–606, New York, N.Y., 1993.
- [6] S. Y. Foo, "A Rule-based machine vision for fire detection in aircraft dry bays and engine compartments", Knowledge-Based Systems, Vol. 9, No. 8, pp. 531–540, 1996
- [7] George W. Mulholland, "Smoke Production and properties" in DiNenno et al. SFPE Handbook of Fire Protection Engineering, 2<sup>nd</sup> Edition, Chapter 15, Section 2, pp 217–227
- [8] H. D. Baehr, Thermodynamik, Springer, 1973.

Woo C. Kim, Yudaya R. Sivathanu, and Jay P. Gore  
Mid Infrared Sensing Diagnostics and Control Consortium  
School of Mechanical Engineering  
Purdue University, West Lafayette, IN 47907-1003

**Characterization of Spectral Radiation Intensities  
from Standard Test Fires for Fire Detection**

**Abstract**

Spectral radiation intensities at 160 mid infrared wavelengths leaving six standard test fires specified in the guidelines of the European Committee for Standardization (ECN Fires) were measured. A recently developed Fast Infrared Array Spectrometer (FIAS) was utilized to acquire spectral radiation intensities in the 1.8 – 4.9  $\mu\text{m}$  wavelength range from the transient as well as the steady burning fires. The mean and root mean square, the Probability Density Function (PDF), the Cumulative Probability Density Function (CPDF), and the Power Spectral Density (PSD) of the spectral radiation intensities were studied to characterize the fires. The spectral radiation intensity in the 4.3  $\mu\text{m}$  micron carbon dioxide band is larger than that at other wavelengths for the open fires. The continuum radiation from soot particles dominates gas band radiation for the smoldering fires. The statistical characteristics of the fires depend on the fuel type, time after ignition and measurement wavelength and can be used in fire detection algorithms.

**1. Introduction**

Current residential fire detectors include optical smoke sensors, ionization smoke sensors, and temperature (heat) detectors [1]. These detectors have response times of the order of 2 to 20 minutes depending on the location of



the fire relative to the detector because combustion products must travel to the detector location for the operation.

More recently, there has been increased interest in the use of radiation emission sensors (flame detectors) for faster fire detection compared to smoke and heat sensors [2]. A combination of detectors may be necessary to detect fires that do not have significant radiation signatures. Single or multiple radiation-based fire detectors with ultraviolet, near infrared and mid infrared filters have been used under various conditions to allow detection with minimal false alarms. Ultraviolet signals are emitted by indoor radiation sources such as incandescent lights, arc welding processes, etc. Therefore, ultraviolet sensors are limited to outdoor usage where interfering solar radiation is absorbed by the earth's atmosphere. Another disadvantage of ultraviolet flame detectors is that any contamination of the optical windows causes a significant loss of sensitivity. Sivathanu and Tseng [3] showed that a two-wavelength near infrared fire detector is capable of detecting fires from a wide variety of materials with low false alarm rates and fast response time. However, the near infrared fire detector can barely detect an indirect smoldering fire since the signals from these fires are very low in the near infrared. In addition, non-luminous fires [4], such as those burning alcohol were not detected.

Radiation emitted by a fire has two primary components: continuum radiation from glowing soot particles in the flame and various emission bands such as at  $2.7\ \mu\text{m}$  and  $4.3\ \mu\text{m}$  originating from carbon dioxide molecules and at  $2.7$  and  $6.3\ \mu\text{m}$  originating from the water vapor in the combustion products. The characteristic temperatures of most accidental fires are such that the continuum radiation peaks in the mid infrared region of the spectrum. These unique characteristics may allow development of multi-wavelength fire detectors that recognize the spectral characteristics to avoid false alarms.

Past studies of spectral radiation properties of flames have involved luminous and non-luminous laboratory flames. These have included turbulent jet diffusion flames and pool fires. Two-wavelength pyrometric measurements conducted by Sivathanu and Faeth [5], Sivathanu et. al. [6], and Sivathanu and Gore [7] in luminous pool and jet fires indicate that the peak temperatures within these fires are in the range  $1400 \pm 300$  K. Other radiation properties of the fires include the Probability Density Functions (PDFs) and the Power Spectral Densities (PSDs) of the turbulent fluctuations.

These characteristics can be used to design fire detectors that can avoid false alarms. However, other than the pool fires, which can occur in fire accidents, the fire spectral radiation intensities have not been studied in the literature. Based on the background information provided above, measurements of the spectral radiation intensities in the mid infrared part of the spectrum leaving standard test fires conforming to the European Committee for Standardization - CEN-54 (ECN) [8] were measured. These data can contribute to advanced fire detection algorithm.

## **2. Experimental apparatus and method**

To obtain measurements of spectral radiation intensities from fires for fast and reliable fire detection, the use of fast spectrometer is required, because the instantaneous intensities at different wavelengths should be used to analyze the frequency contents of six standard ECN fires. In particular, emissions of radiation from soot fluctuate at a higher frequency and have larger fluctuation intensity than the emission of gas band radiation. Hence, measurements were made using Fast Infrared Array Spectrometer (FIAS) to acquire spectral radiation intensities at 160 pixels in the  $1.8 - 4.9 \mu\text{m}$  wavelength ranges and this unit is able to capture instantaneous spectra from the fires at a rate of 390 Hz. Findings by Ji, et al. [9] show that the

agreement between the FIAS measurements and the previous data is very good.

FIAS was aimed at different angles and positions depending on whether the test fire is developing with time or not, assuming that all test fires are axisymmetric. For the transient test fire, – open cellulosic fire (TF1), smoldering pyrolysis fire (TF2), glowing smoldering fire (TF3), and open plastics fire (TF4) - the FIAS view angle is set at 45 degrees from the gravitational direction, where the angle is defined as shown in Figure 1., and a different radius from the flame axis, and time dependent data are acquired in a fixed position. For the TF1, TF2, and TF3, the FIAS is located at 300 mm in radial direction and 500 mm for TF4.

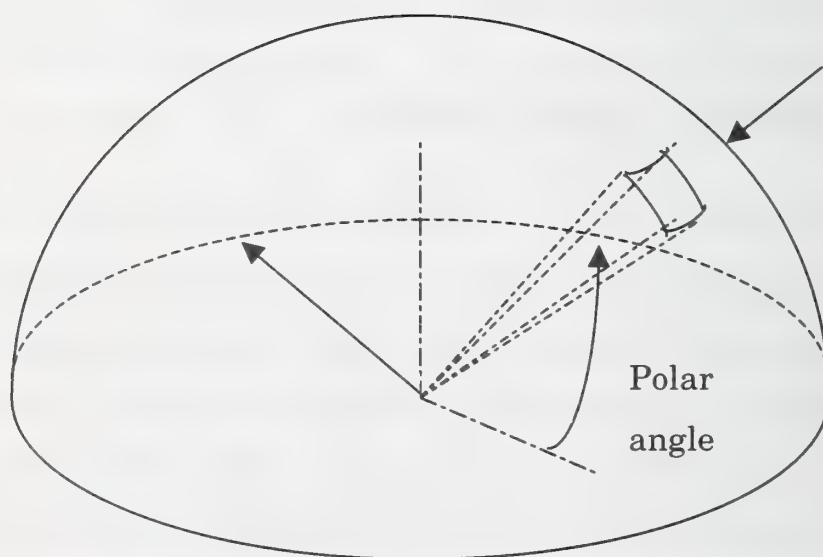


Figure 1. Schematic of defining the direction viewed by the FIAS for the TF1, TF2, TF3, and TF4



The present work involves utilization of fire radiation for detection and generally the need for early fire detection suggests that the fire is smaller than the size of the enclosure at the time of detection. Therefore, in the case of the steady state test fires – liquid fire (n-heptane, TF5), and liquid fire (ethanol, TF2) -, intensities leaving the fire at four different heights were collected as representative values of fire development, and schematic diagram for experimental facility is shown in Figure 2.

Detailed descriptions of ECN fires are provided in Ref. [8]. The dimensions of TF1 were scaled down to one half so as to be able to accommodate our laboratories. The liquid fires stabilized on a water-cooled 15 cm diameter stainless steel burner. The height of the burner is 10 cm and the flame was stabilized with a lip height (depth of liquid surface below the pool edge) of 10 mm. The pool fires reached a steady state operating condition in approximately 3 to 4 minutes.

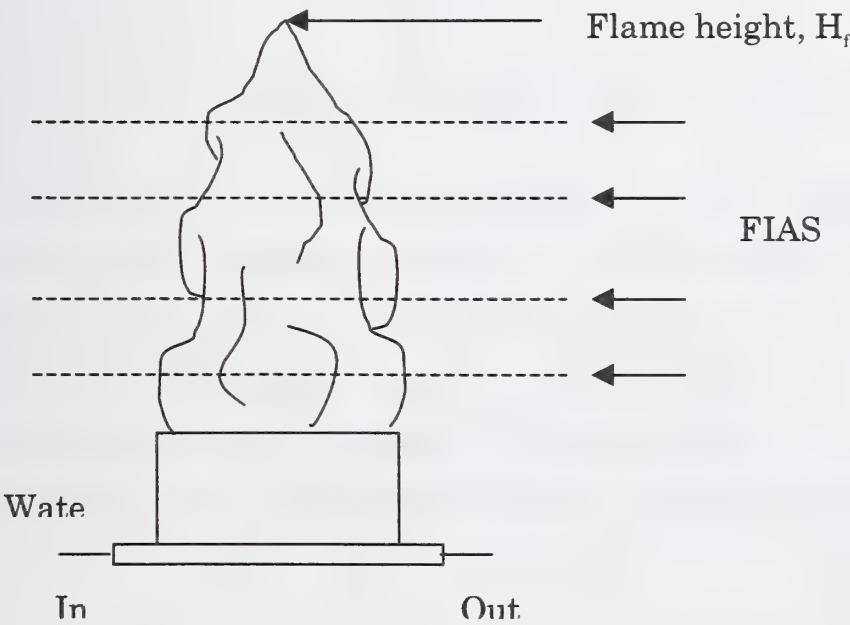


Figure 2. Schematic of defining the direction viewed by the FIAS for TF5 and TF6

### 3. Results and Discussion

#### 3.1. General descriptions about standard test fires

The TF1 lasted around 13 minutes before going out automatically. During the first 5 minutes, the infrared signature from the methylated spirit dominated the spectral radiation intensities from the wooden crib, however in 5 minutes, the instantaneous spectral radiation intensities from both gas band and in-flame soot resulting from the fire grew and reached peak values around 9 minutes after ignition.

The TF2 began smoldering in 5mins and flame was made automatically in 9mins. Because the FIAS was aimed at the beechwood sticks, the infrared signatures from the TF2 were low compared with other standard test fires.

For the TF3, the igniter flames were immediately put out after ignition, and the cotton wicks continued to glow for the duration of the test.

The TF4 lasted around 7 mins and reached its peak intensities in 4mins.

TF5 is luminous and emit radiation from both soot and combustion products. The radiation heat flux directly contributes to the hazard posed by the flame and the spread rate of the fire. Fuels of similar composition, such as fuels classified as paraffin or alcohols generally have comparable flame shapes. The alcohol fuels, TF6, generally necked in just above the burner lip and the paraffin (n-heptane) fuels had a larger distance before necking begins.

#### 3.2. Mean Values of Spectral Radiation Intensities during 12.8sec

Figure 3 represents the mean spectral radiation intensities during 12.8 sec for all six standard test fires. Care should be taken for the scales of

ordinate, because the radiation signature from TF2 was too small to keep the same scale with the other fires. One more thing to keep in mind is that the positions of FIAS are different between the transient TFs and steady state ones as we discussed earlier.

The TF1 and TF4 are very luminous and both gas band radiation and continuous soot radiation are evident. The radiation intensity from carbon dioxide and soot at  $4.3 \mu\text{m}$  is more than two orders higher than that from soot, water, and carbon dioxide at  $2.7 \mu\text{m}$ , which is similar to the spectral distributions observed in the open pool fires (TF5 and TF6).

For the two smoldering fires, TF2 and TF3, the continuous radiation from the smoldering surface is evident and the gas band radiation is hardly found, furthermore, the absorption in the carbon dioxide band in the room air at  $4.3 \mu\text{m}$  is seen. Using Wien's displacement law to estimate temperature of the TF3, the temperature of inflame soot is 1024 K.



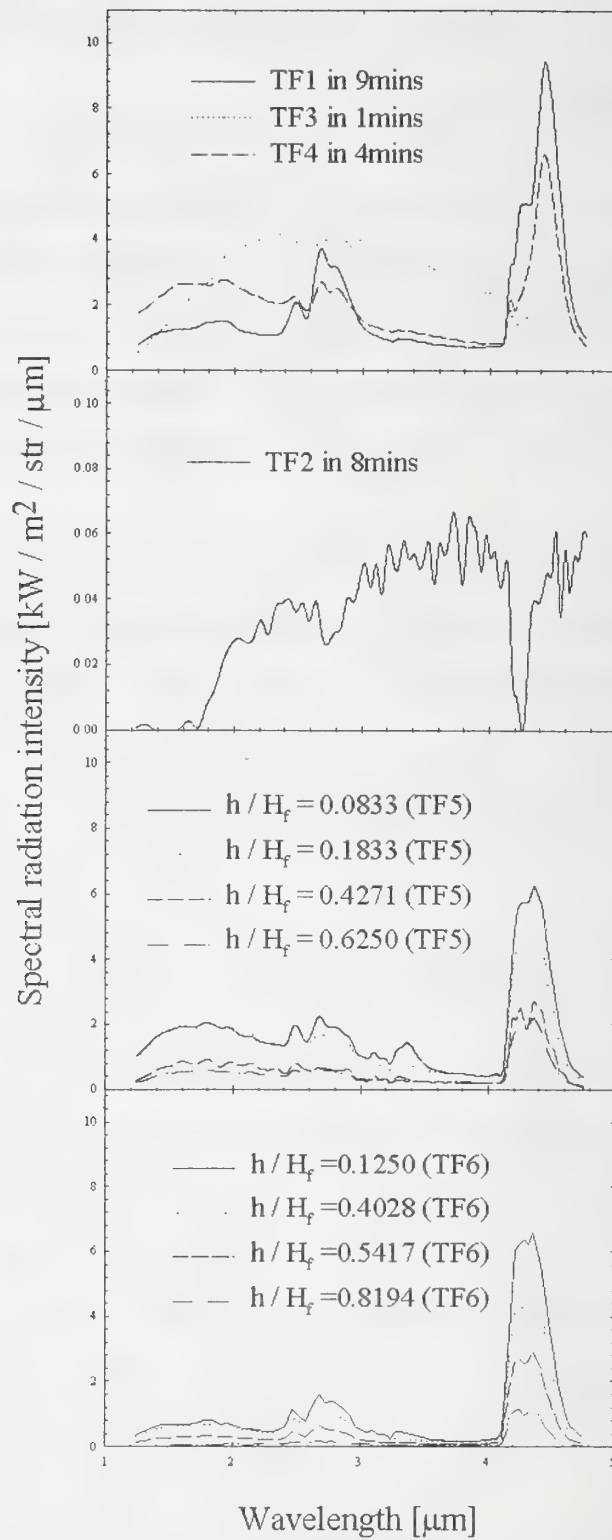


Figure 3. Spectral radiation intensities in TFs during 12.8 sec

The flame height of the TF5 and TF6 is 480 mm, 360 mm respectively, measured by visual inspection and four different dimensionless flame

heights from the lip of the flame are shown. Radiation from the  $\text{CO}_2$  band and the  $\text{H}_2\text{O}$  band are evident in the spectra. However, the TF6 contains less soot than the TF5, and hence the radiation spectra are less dominated by soot. Radiation from  $\text{H}_2\text{O}$  becomes less intense as the dimensionless flame height increase. The continuum radiation for soot particles is also evident. As the dimensionless height increases, the spectral radiation intensities decrease. If we use Wien's displacement law to estimate the flame temperature associated with the maximum intensity of the soot radiation, a temperature of approximately 1630 K for the TF5 and 1476 K for the TF6 respectively, is obtained.

### *3.3. PDFs and CPDFs of spectral radiation intensities*

The time series of normalized measured radiation intensities from inflame soot and the gas band at  $1.45 \mu\text{m}$ ,  $2.47 \mu\text{m}$ ,  $2.68 \mu\text{m}$ , and  $4.35 \mu\text{m}$  obtained from the test fires were analyzed to evaluate their Probability Density Function (PDF). The four wavelengths are selected to study the effects of soot radiation separately from those of soot+ $\text{CO}_2$ + $\text{H}_2\text{O}$  radiation and soot+ $\text{CO}_2$  radiation, and, to study the differences between the open fire, and smoldering fire, the PDFs of TF5 at  $h/H_f = 0.0833$  and TF3 were chosen and shown in Figure 4.

Figure 4 illustrates that the PDFs are clipped Gaussian in shape, especially for the carbon dioxide and soot band at  $4.3 \mu\text{m}$ , where carbon dioxide radiation is dominant, is almost symmetric around the mean intensity value, however the PDF at  $1.45 \mu\text{m}$  for TF5, where in-flame soot dominates the spectral radiation intensity, is not symmetric in shape, and shows a lognormal behavior. Because of the large fluctuations in soot radiation, the overall ranges are broad.

Comparing the PDFs in TF3 with TF5, we can conclude that the PDFs are still Gaussian in shape, although there is some noise. However the TF3

continued to glow for the duration of the test and the fluctuation in radiation is not so high compared with TF6, the range of spectral radiation intensities is not so broad.

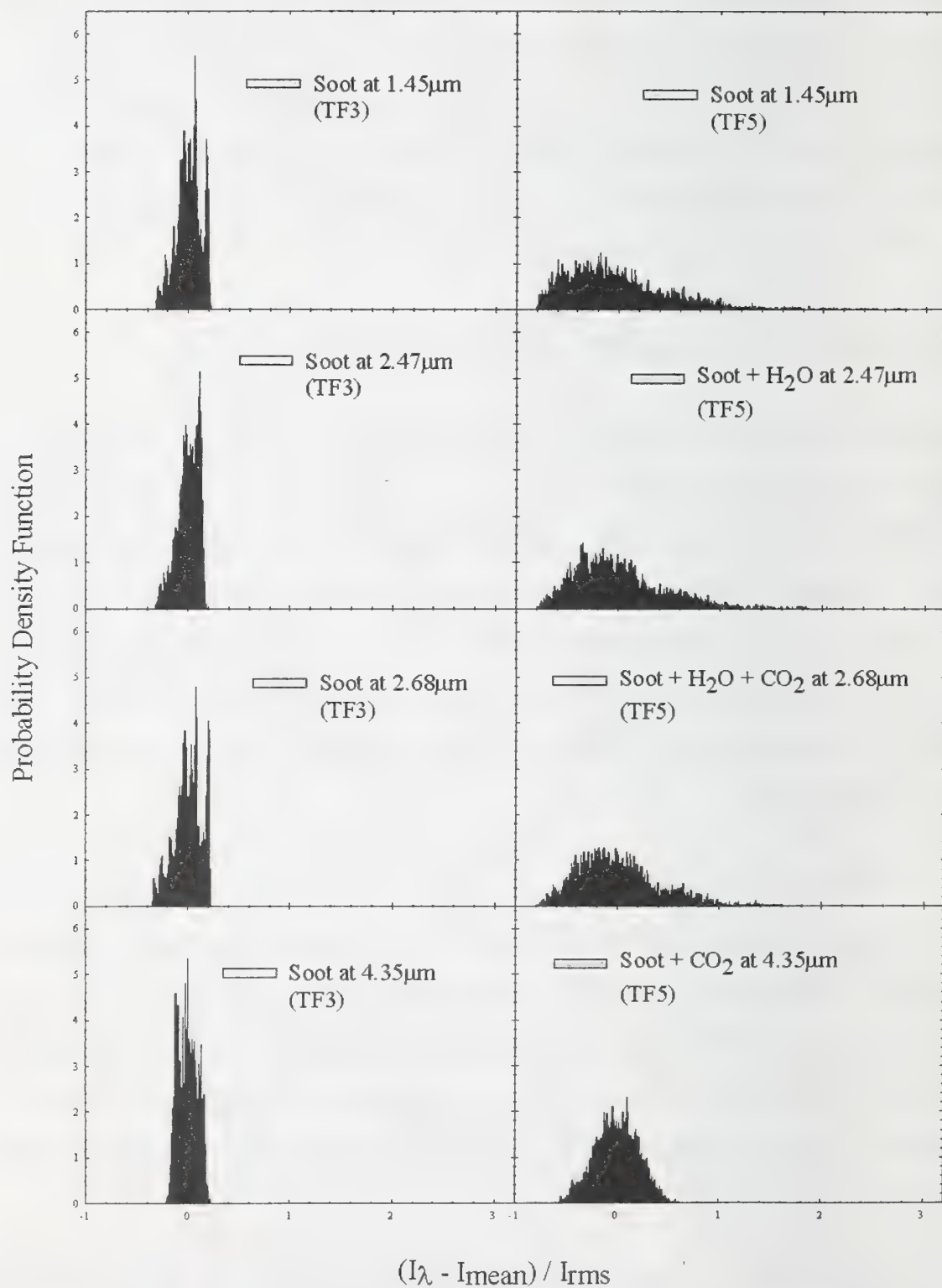


Figure 4. PDFs of spectral radiation intensities of TF3 and TF5 at  $h/H_f = 0.0833$



The differences in the statistical behavior of intensities at different wavelengths can be examined in even greater detail by studying the Cumulative Probability Density Function (CPDF) shown in Figure. 5, which shows CPDFs of TF3 and TF6 at  $h/H_f = 0.1250$ . The CPDF is an integral of the PDF and therefore less noisy. The information it presents consists of the intensity values at which the probability of occurrence of intensities below that value builds rapidly.

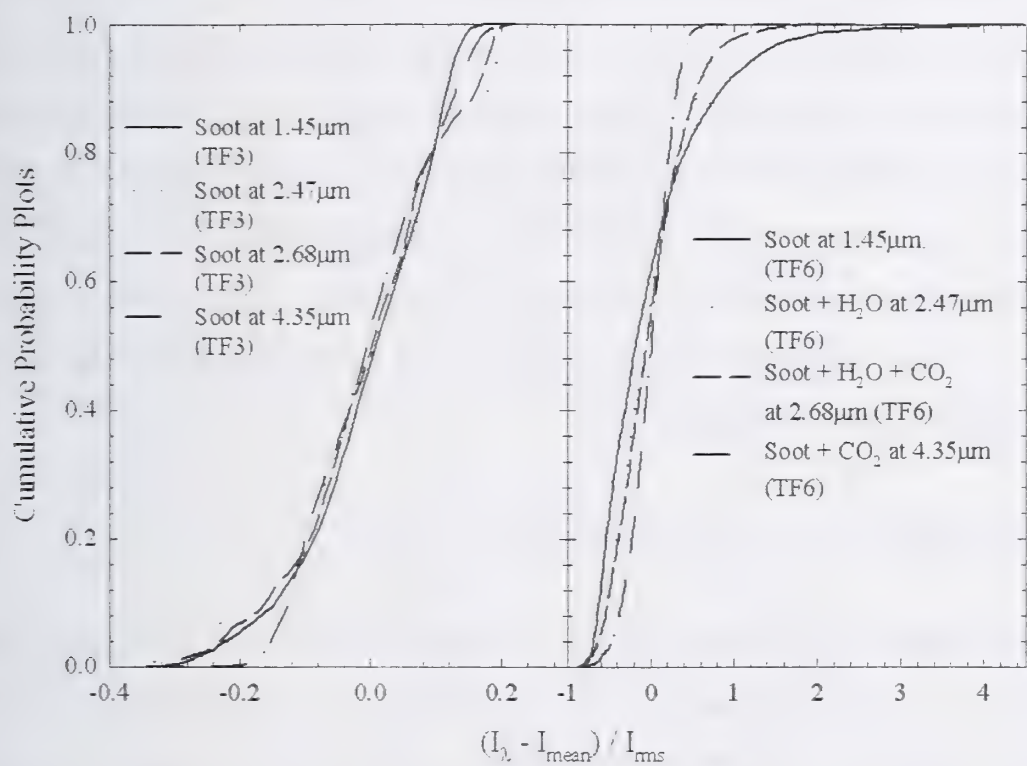


Figure 5. CPDFs of spectral radiation intensities of TF3 and TF6 at  $h/H_f = 0.1250$

Figure 5 shows that the CPDF for intensities originating from the gaseous molecules rise very rapidly near a well-defined most probable value. In addition, the rise is the sharpest for the  $\text{CO}_2$  band at  $4.35 \mu\text{m}$ . The gas band CPDFs are steep because the concentration fluctuations are strongly related to the level of mixing through the state relationships. The soot CPDF is flatter because various amounts of soot can exist at different levels of mixing depending on chemical kinetic and differential diffusion effects.

Independent of the reasons for this, the characteristic that a flatter CPDF exists at soot wavelengths and a steeper CPDF exists at the gas band wavelengths can be used as an effective discrimination method in the sensor logic.

All the CPDFs of TF3 exhibit similar trend in slope because of the continuum emission from the same surface.

For the case of TF6, the PDFs of the soot+CO<sub>2</sub> and H<sub>2</sub>O intensities at 2.47  $\mu$ m and 2.68  $\mu$ m respectively show a smaller weight in intensity near zero compared to the PDF of soot+CO<sub>2</sub> at 4.35  $\mu$ m. This may be related to the self-absorption by cold CO<sub>2</sub> in the outer reaches of the flame at many instances. In addition, the soot+ CO<sub>2</sub> emission at 4.35  $\mu$ m shows a clip at the highest intensity values. These results suggest caution regarding the use of this wavelength for fire detection. In addition, the result is also of relevance to the fundamentals of participating media heat transfer in fire and combustion environments.

### *3.4. PSDs of spectral radiation intensities*

The Power Spectral Densities (PSDs) of spectral radiation intensities from the soot, CO<sub>2</sub> and H<sub>2</sub>O bands for TF3 and TF4 were analyzed to obtain their frequency content as shown in Figure 6. The PSD at the respective wavelengths were normalized by the mean-square fluctuations to compare with one another; hence the total area under each PSD is unity. The PSD is characterized by the flicker frequency and is determined by the size of the fire, the gravitational constant, and the turbulent flow established within the fire. The area under the PSD curve for any frequency range is proportional to the energy of the instantaneous fluctuations of the apparent source temperatures from the mean value. Although there is some noise around the Nyquist frequency of 195 Hz, this could be ignored considering the SN ratio.

It is important to note that the integrated infrared intensities do not show characteristic pulsation frequencies observed in planar imaging studies. There are commercial detectors that rely on pulsation frequencies and the present results do not support their sensor logic.

For the case of open fire, TF4, the PSD at the wavelengths (all wavelengths other than the  $4.35\text{ }\mu\text{m}$ ) dominated by soot radiation show higher energy content at higher frequencies compared to those dominated by the gas radiation ( $4.35\text{ }\mu\text{m}$ ). This characteristic of the sooty fires can also be utilized as a discriminator in fire sensor logic. Most of the energy of the fluctuations of the spectral radiation intensities is below 10-20 Hz and shows a decline to noise levels that are approximately five to six orders of magnitude lower for frequencies higher than 20 Hz.

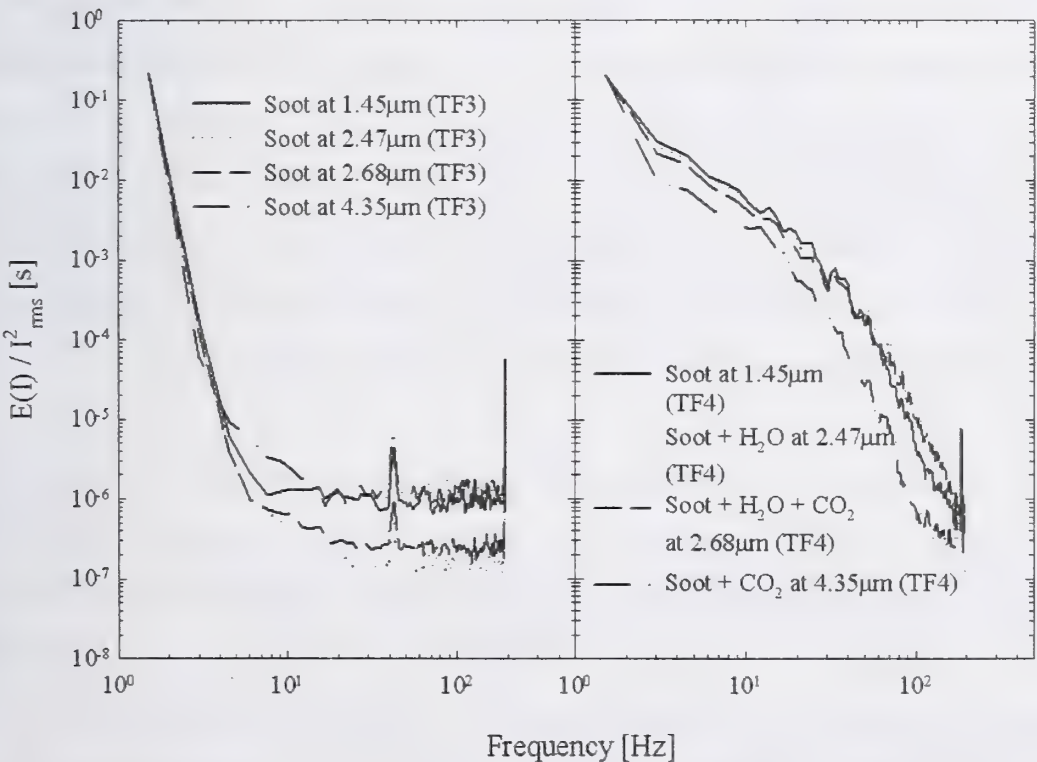


Figure 6. PSDs of spectral radiation intensities of TF3 and TF4



An interesting and most distinguishable feature of smoldering fire could be deduced from the left panel of Figure 6. Most of the energy of the fluctuations of the spectral radiation intensities is below 2 or 3 Hz and declines very rapidly to the noise levels that are approximately five to six orders of magnitude lower after 3 Hz. However, flicker frequency of the open fires is around 10 – 20Hz and declines relatively smoothly to the noise level. The fact that the radiation from a smoldering fire has characteristics similar to those of a hot surface poses special challenges to the detection of such fires especially in environments where hot surfaces are to be expected. However, since smoldering fires are likely to be away from kitchens and utility rooms, a fire detector could still be devised but caution will be needed in addressing the false alarm issues.

#### **4. Conclusions**

(1). The open test fires are very luminous and both gas band radiation and continuous soot radiation are evident. The radiation intensity from carbon dioxide and soot at  $4.3 \mu\text{m}$  is more than two orders higher than that from soot, water, and carbon dioxide at  $2.7 \mu\text{m}$ . For the two smoldering fires, TF2 and TF3, the continuous radiation from the smoldering surface is evident and the gas band radiation is hardly found, furthermore, the absorption in the carbon dioxide band in the room air at  $4.3 \mu\text{m}$  is seen.

(2). The PDFs are clipped Gaussian in shape, especially for the carbon dioxide and soot band at  $4.3 \mu\text{m}$ , where carbon dioxide radiation is dominant, is almost symmetric around the mean intensity value, however, in the case of open test fires, the PDF at  $1.45 \mu\text{m}$ , where in-flame soot dominates the spectral radiation intensity, is not symmetric in shape, and shows a lognormal behavior. Because of the large fluctuations in soot radiation, the overall ranges are broad, which is not applied to the case of smoldering fires.

(3). The gas band CPDFs are steep because of the concentration fluctuations are strongly related to the level of mixing through the state relationships. On the other hand, the soot CPDF is flatter because various amounts of soot can exist at different levels of mixing depending on chemical kinetic and differential diffusion effects.

(4). Most of the energy of the fluctuations of the spectral radiation intensities in smoldering fires is below 2 or 3 Hz and declines very rapidly to the noise levels. However, flicker frequency of the open fires is around 10 – 20Hz and declines relatively smoothly to the noise level.

(5). TF3 was used as to study the mid infrared characteristics of smoldering fire, because, although it has same characteristics with TF2, the IR signature from TF2 is not so high, and as a result of this, there are some noises in PDFs, CPDFs, and PSDs of TF2.

## **5. Acknowledgement**

This work was performed under the sponsorship of the U. S. Department of Commerce, National Institute of Standards and Technology under Grant No. 60NANB5D0113 with Dr. William Grosshandler and Dr. George Mullholand serving as the federal Program Officer.

## **References**

- [1] Grosshandler, W. L., An Assessment of Technologies for Advanced Fire Detection. Heat and Mass Transfer in Fire and Combustion Systems, HTD vol 223, ASME, New York, 1992:1-9.
- [2] Middleton, J. F. Flame Detectors. Ninth International Conference on Automatic Fire Detection, AUBE 89, Duinsburg, Germany, 1989:143-154.
- [3] Sivathanu, Y. R., and Tseng, L. K, Characterization of Radiation Properties of Fires Using Multi-Wavelength Measurements, Thirtieth

section anniversary technical meeting, Central states section, The combustion institute, 1996:304-309.

[4] Lloyd, A. C., Development and Evaluation of Fire Detection Algorithm with Source Temperature Discrimination and Frequency Content, MSME Thesis, Purdue University, West Lafayette, IN, 1997.

[5] Sivathanu, Y. R. and Faeth, G. M., Temperature / Soot Volume Fraction Correlations in the Fuel-Rich Region of Buoyant Turbulent Diffusion Flames, Combustion and Flame, 1990;81:150-165.

[6] Sivathanu, Y. R., Gore, J. P., and Dolinar, J., Transient Scalar Properties of Strongly Radiating Jet Flames, Combustion Science and Technology, 1991;76:45-66.

[7] Sivathanu, Y. R., and Gore, J. P., Simultaneous Multiline Emission Absorption Measurements in Optically Thick Turbulent Flames, Combustion Science and Technology, 1991;80:1-21.

[8] CEN, Components of Automatic Fire Detection Systems: Fire Sensitivity Test, Part 9, European Committee for Standardization, Brussels, 1982.

[9] Ji, J., Gore, J. P., Sivathanu, Y. R., and Lim, J., Fast Infrared Array Spectrometer Used for Radiation Measurements of Lean Premixed Flames, 34<sup>th</sup> National Heat Transfer Conference, Pittsburgh, Pennsylvania, 2000:1-6.



## Is microwave radiation useful for fire detection ?

### Abstract

This paper deals with the question of whether microwaves might be useful for fire detection. PLANCK's law shows us that a black body emits electromagnetic radiation also in the micro- or millimeterwave region. Since such waves exhibit a different attenuation behaviour than infrared radiation an investigation of this phenomenon is interesting for a fire researcher. In this paper we will present the physical basics, explain how to measure and to use such radiation for estimation of the fire location and give some preliminary results obtained by first experiments.

## 1 Introduction

There are already high-tech products available on the market to locate the fire origin, or may be also persons in danger, through the smoke. Such image processing devices are based on the *infrared radiation* (IR) of a hot spot. In general, such devices are called *radiometers* since they simply measure the intensity of radiation. In the following we will distinguish between IR-radiometers and MW-radiometers where MW stands for microwaves or also for millimeter-waves. Radiometers are most commonly used for remote sensing of the earth from satellites and airplanes, but that topic is beyond the scope of this paper. In the industry, radiometers can be used for remote measurement of temperatures in ovens, converters, kilns, and other places where the use of conventional contacting temperature sensors or IR-radiometers is impossible because of high temperatures, smoke, or water vapour. However, MW-radiometers can often not compete with IR-radiometers or conventional sensors since the latter are usually cheaper and simpler to build. The main advantages of MW-radiometers for the use in fire detection are fourfold:

1. The possibility to measure through *optically thick smoke and vapor*.
2. The insensitivity of MW-radiometers to environmental conditions, such as water vapor and dust (contrary to infrared methods), and high temperatures (contrary to semiconductor sensors).

3. The fact that thermal microwave noise radiation comes from a *thicker surface layer* than the IR radiation does.
4. The fact that MW penetrates all materials except of metals.

In contrast, their main disadvantages concerning fire detection are:

1. The higher the center frequency, the more expensive are the electronic components.
2. Because of the relatively long wavelengths compared to IR, the achievable spatial resolution might be limited.

Hence, the only thing which is almost sure is that much efforts are needed to investigate whether MW-radiation can be useful for fire detection. Exactly this problem is the central topic of this paper. In the following we will present the physical basics prepared for the non-physicist, explain how to measure and to use such radiation for estimation of the fire location and give some preliminary results obtained by first experiments.

## 2 The physical basics

To investigate whether MW-radiation can be useful for fire detection we can split this problem into three separate questions:

1. How much MW-power  $P_E$  emits a fire ?
2. How much MW-power  $P_R$  receives an antenna ?
3. How much MW-power  $P_D$  is available for detection at the antenna output ?

Before we start to answer these three questions let us shortly comment them. Of course, a theoretical analysis to predict the expected power at the antenna output is essential to judge the use of MW-radiation in fire detection. For this reason we have first to find a formula for the emitted MW-power of a fire. Obviously, since we usually not know the burned material we cannot expect to find a general formula being independent of the material properties. Fortunately, we cannot only find an upper bound but also a rough idea how much the deviation of the upper bound is. This will be explained by answering the first question. Then we consider the case of ideal transmission where we have no attenuation on the propagation of the electromagnetic radiation through the air. Later on we will discuss the influence of smoke or water vapor or solid materials. So we obtain an estimation of the received power. By answering the third question we demonstrate that an antenna is definitely not an ideal measurement device. We have to include its own

temperature and its directivity pattern to calculate the output power. This output power is the most interesting quantity, since we have to process the antenna output signal to detect a fire. Moreover, by use of an antenna array instead of a single antenna we are able to scan the whole scenario and, therefore, we are also able to locate the fire origin within a certain resolution. To illustrate the whole problem – separated into three different questions – consider Fig. 1.

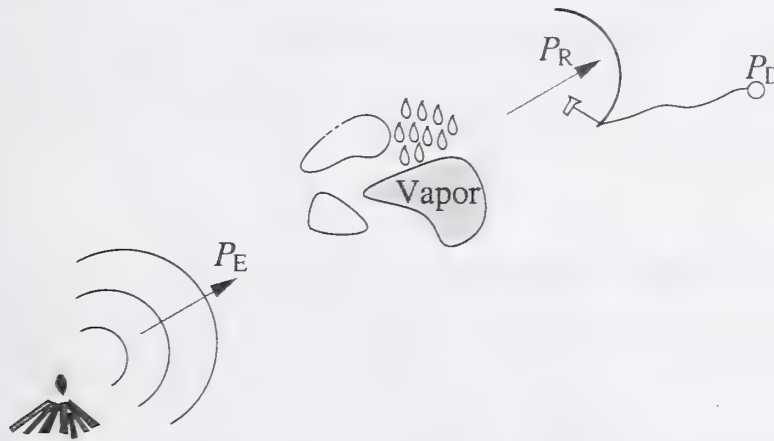


Figure 1: The emitted power  $P_E$ , the received power  $P_R$ , and the detected power  $P_D$

## 2.1 How much MW-power $P_E$ emits a fire ?

Consider an electromagnetic wave of frequency  $f$  which hits an arbitrary body with temperature  $T$ . The *power of the incident wave* is denoted as  $P_I(f)$ , whereas  $P_{\text{Ref}}(f, T)$  is the

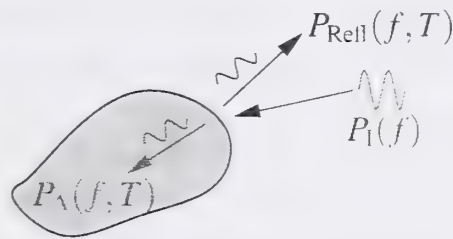


Figure 2: The incident power  $P_I(f)$ , the reflected power  $P_{\text{Ref}}(f, T)$ , and the absorbed power  $P_A(f, T)$

*reflected power*, and  $P_A(f, T)$  is the *absorbed power*. Note that the reflected as well as the absorbed power do not only depend on the frequency  $f$  of the incident wave but also on the temperature  $T$ . In general, they are also dependent on the direction of the incident radiation related to the surface of the body – the so-called *direction of arrival* – as well as to the polarization of the electromagnetic wave. Since here the latter two parameters are



more of random nature and thus we consider them as uniform distributed, we omit them as independent variables.

Let us now define the *degree of absorption* (or *absorptivity* for short) as

$$a(f, T) = \frac{\text{absorbed power}}{\text{incident power}} = \frac{P_A(f, T)}{P_I(f)}. \quad (1)$$

Obviously, the range of the absorptivity is between zero and one ( $0 \leq a(f, T) \leq 1$ ). An interesting body is such a one which absorbs all incident power irrespective of the frequency  $f$  and the temperature  $T$ . Such a body is called *black body* (remember how a *black hole* works) and is fully described by

$$a_{BB}(f, T) \stackrel{!}{=} 1, \quad \forall f, T,$$

where the index BB denotes the black body.

Let us leave the area of absorption and consider now the area of *emission*. If a body has a temperature greater than  $T > 0\text{K}$ , it will emit radiation caused e.g. by a jump of an electron to a state of lower energy. In case of such a jump an electromagnetic wave occurs with energy  $hf$ , where  $h = 6.626 \cdot 10^{-34} \text{Ws}^2$  is PLANCK's constant. Consequently, each body with  $T > 0\text{K}$  radiates electromagnetic waves. Suppose that an arbitrary body emits the power  $P_E(f, T)$  then the *degree of emission* (or *emissivity* for short) is defined as

$$e(f, T) = \frac{\text{emitted power}}{\text{emitted power of a black body}} = \frac{P_E(f, T)}{P_{E, BB}(f, T)}. \quad (2)$$

In contrast to the absorption we do not have an incident wave. Thus we need a reference quantity, where the black body emission  $P_{E, BB}(f, T)$  is a natural choice. Note that the emissivity of a black body is obviously equal to one. Note also that at this point we cannot state that the emissivity does not exceed the value 1. This will be shown later. In the following we try to find a relation between the emissivity  $e(f, T)$  and the absorptivity  $a(f, T)$  of an arbitrary body. For this reason consider Fig. 3. Suppose that the

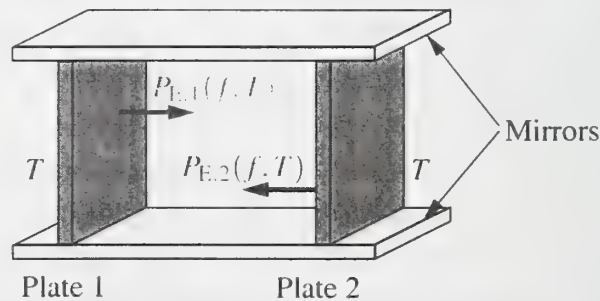


Figure 3: An experiment to find a relation between  $e(f, T)$  and  $a(f, T)$ .

two plates are on the same temperature  $T$ . Each of them emit the power  $P_{E,1}(f, T)$  or

$P_{E,2}(f, T)$ . The plates are surrounded by two mirrors, so that no emitted radiation can be lost. Consequently,  $P_{E,2}(f, T)$  is the incident power for the left plate whereas  $P_{E,1}(f, T)$  is the incident power for the right plate. In other words,  $a_1(f, T)P_{E,2}(f, T)$  is the absorbed power of plate 1 and  $a_2(f, T)P_{E,1}(f, T)$  of plate 2, where  $a_1(f, T)$  and  $a_2(f, T)$  are the absorptivity of plate 1 and plate 2, respectively. Since we assume a thermal equilibrium – both plates have the same temperature  $T$  – both absorbed powers must be the same for each frequency and for each temperature

$$a_1(f, T)P_{E,2}(f, T) \stackrel{!}{=} a_2(f, T)P_{E,1}(f, T).$$

By use of eq. (2) we immediately obtain

$$\frac{a_1(f, T)}{e_1(f, T)} \stackrel{!}{=} \frac{a_2(f, T)}{e_2(f, T)}$$

where  $e_1(f, T)$  and  $e_2(f, T)$  are the emissivity of plate 1 and plate 2, respectively. Suppose that plate 2 is a black body then we get

$$\frac{a_1(f, T)}{e_1(f, T)} \stackrel{!}{=} 1$$

since for a black body the absorptivity and the emissivity are per definition equal to one. It follows for an *arbitrary* body – here represented by plate 1 –

$$a(f, T) \stackrel{!}{=} e(f, T) \quad \forall f, T. \quad (3)$$

This rule is called KIRCHHOFF's law and it means that an arbitrary body that absorbs much power also emits much power in the *same* band of frequencies. Of course, it can be a good absorber/emitter in one frequency band but a bad one in another.

We are now able to write the emitted power of an arbitrary body as

$$P_E(f, T) \stackrel{!}{=} a(f, T) P_{E,BB}(f, T). \quad (4)$$

Since the absorptivity has a range  $0 \leq a(f, T) \leq 1$  we are now able to say that the emitted power of an arbitrary body is always *equal to* or *less than* the emitted power of a black body. Thus, if we know  $P_{E,BB}(f, T)$  we can use it as an *upper* bound for  $P_E(f, T)$ . Note that such a result is not clear by only use of the definition (2) for the emissivity. At that point we are not able to say that the emissivity is always less or equal to one.

The radiation  $P_{E,BB}(f, T)$  of a black body was first derived by PLANCK, the founder of the *quantum theory*. Since the derivation is complicated we will here only give the final result, widely known as PLANCK's law

$$\frac{dP_{E,BB}(f, T)}{df} = \frac{4\pi Ahf^3}{c^2} \frac{1}{e^{\frac{hf}{kT}} - 1}, \quad (5)$$

where  $A$  is the bodies surface,  $c = 3 \cdot 10^8 \text{m/s}$  is the velocity of light,  $k = 1.38 \cdot 10^{-23} \text{Ws/K}$  is the BOLTZMANN-constant, and an emission in a half sphere is assumed (this means a solid angle of  $\Omega = 2\pi$ ). Observe that the unit of  $dP_{\text{E,BB}}(f, T)/df$  is  $\text{W/Hz}$ , so that it can be interpreted as the distribution of the power versus frequency. The following Fig. 4 shows this quantity as a function of the frequency for different temperatures and a body surface  $A = 1 \text{m}^2$ . It can be clearly seen that on the considered range of micro- and millimeter-

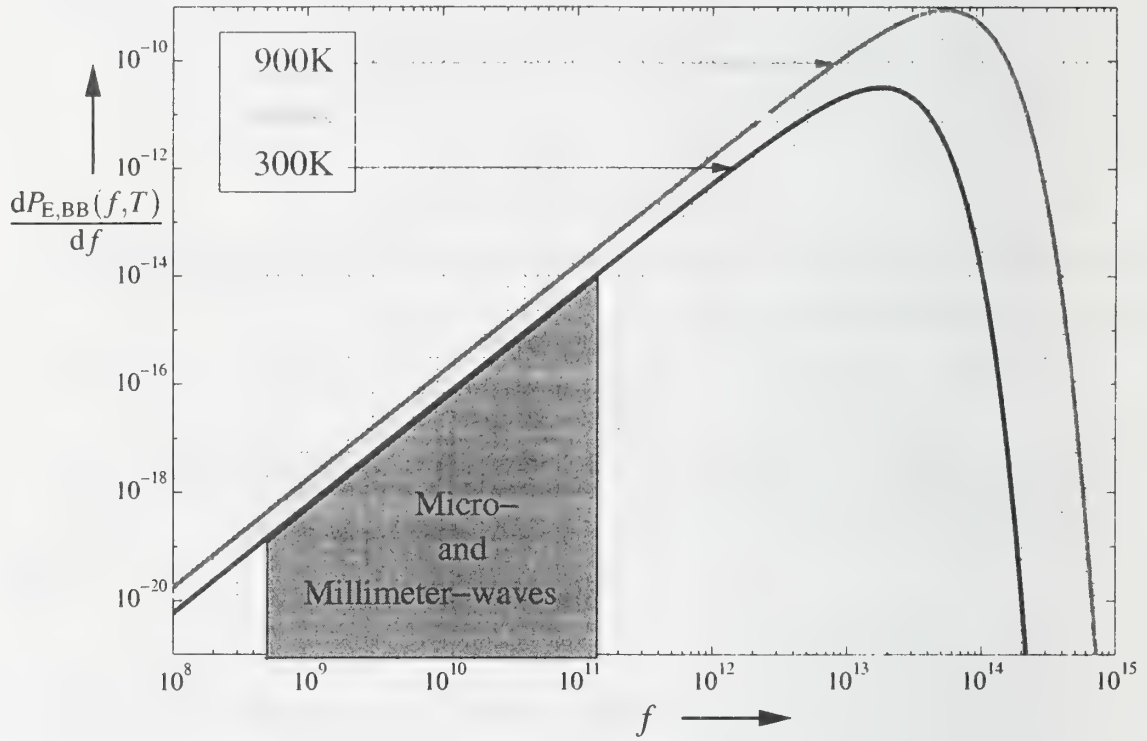


Figure 4: PLANCK's Law for  $A = 1 \text{m}^2$

waves PLANCK's law can be approximated by a linear function in a logarithmic scale. The mathematical reason is that for such small frequencies the power series for the exponential function

$$e^{\frac{hf}{kT}} = \sum_{n=0}^{\infty} \frac{1}{n!} \left( \frac{hf}{kT} \right)^n$$

can be broken off after the second term

$$e^{\frac{hf}{kT}} \approx 1 + \frac{hf}{kT} \quad \text{for } hf \ll kT$$

We obtain

$$\frac{dP_{\text{E,BB}}(f, T)}{df} \approx \frac{4\pi A f^2 kT}{c^2}, \quad (6)$$



which is a linear function in a logarithmic scale. This result is known as the law of RAYLEIGH-JEANS. The advantage of eq. (6) is the possibility for an integration in a closed form. Denoting  $f_c$  as a *center frequency* and  $\Delta f$  as the considered *bandwidth* the total emitted power can be calculated as

$$\begin{aligned} P_{E,BB}(f_c, \Delta f, T) &\approx \int_{f_c - \Delta f/2}^{f_c + \Delta f/2} \frac{4\pi A f^2 kT}{c^2} df \\ &= \frac{4\pi A kT}{3c^2} (3f_c^2 \Delta f - 2(\Delta f/2)^3) \end{aligned} \quad (7)$$

$$\stackrel{f_c \gg \frac{\Delta f}{\sqrt{12}}}{=} \frac{4\pi A kT}{c^2} f_c^2 \Delta f \quad (8)$$

We have now obtained an equation for the transmitted power of a black body depending on the user-chooseable center frequency  $f_c$ , the user-chooseable bandwidth  $\Delta f$ , the surface  $A$  and the temperature  $T$  of the black body. To get a feeling about the range of this power consider a practical scenario. Suppose a surface of  $A = 0.5\text{m}^2$ ,  $T = 1000\text{K}$ ,  $f_c = 11\text{GHz}$ ,  $\Delta f = 1\text{GHz}$ , then the emitted power is equal to  $P_{E,BB}(11\text{GHz}, 1\text{GHz}, 1000\text{K}) = 116.24\text{nW}$  which is easy to detect with conventional antennas. Of course, here we have not only omitted the absorptivity  $a(f, T)$  but also the distance  $r$  between the antenna and the fire. Before we explain how to include  $r$  we will finish the first question by a short discussion about  $a(f, T)$ .

From PLANCK's law it can be seen *that only the surface  $A$  of the black body influences the emitted power*. It is also known that microwaves or also millimeter-waves can travel through solid material with sometimes only a small attenuation. This is in contrast to IR-radiation which is clearly attenuated by solid materials. Thus, we might expect that in case of MW-radiation not only the surface but also the inner of a real body (e.g. the fire) will contribute to the emitted power. Since the black body radiation does only depend on  $A$  the absorptivity  $a(f, T)$  must exhibit a corresponding behaviour. In other words we have to expect – as a tendency – that  $a(f, T)$  must be higher for MW-frequencies than for IR-frequencies. Moreover, this tendency must be valid for all temperatures. Therefore, it might be very interesting to measure the absorptivity  $a(f, T)$  of typical fire materials (e.g. wood). This is planned for a future research project. To get a feeling about the quantity of absorptivity and equivalently of the emissivity, consider the following tabular (see [1]). Although these are *not* materials typically occurring in fire detection it shows that the values for the absorptivity and emissivity are not very small. Of course, one exception is *metal* which totally attenuates electromagnetic radiation due to the huge number of free electrons. So, the emissivity as well as the absorptivity are nearly zero for metal.

After we have answered the question *How much MW-power  $P_E$  emits a fire ?* we can say that a detection of a fire by measurement of MW-radiation seems to be possible if all radiation near  $f_c$  can be collected. However, this would mean that around the fire an

Material	$e(30 - 90\text{GHz}, 280\text{K})$	Material	$e(30 - 90\text{GHz}, 280\text{K})$
Sand	0.90	Smooth rock	0.75
Asphalt	0.83	Concrete	0.76
Coarse gravel	0.84	Heavy vegetation	0.93

Table 1: Typical emissivity for normal incidence and 280K

half sphere have to be constructed which fully works as an antenna. Since this is a very unpractical approach we have to ask the second question:

### 2.2 How much MW-power $P_R$ receives an antenna ?

To explain the principal problem consider Fig. 5. We assume that a fire *omnidirectionally*

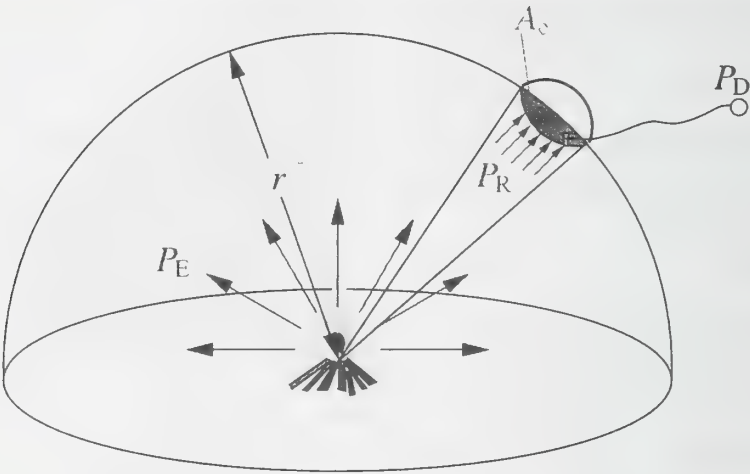


Figure 5: A practical setup

emits its radiation in a half sphere so that each point on the half sphere receives the same amount of radiation power. Since a half sphere has a surface of  $2\pi r^2$  we immediately obtain for the received power

$$P_R(f, T) = \frac{A_e}{2\pi r^2} P_E(f, T), \tag{9}$$

where  $A_e$  is the so-called *effective area* indicated in Fig. 5 directly beneath the antenna as a patterned region. We will not discuss the details of the idea of the *effective area*. For a short explanation consider an antenna of reasonable size and regular shape, e.g. a satellite dish. Then the effective area is nearly equivalent to the geometrical surface of the parabolic mirror. It should be pointed out that the effective area does only depend on the antennas shape and *not* on the received radiation. We emphasize this fact because in the

literature the relation  $A_e = \lambda_c^2 G_e / (4\pi)$  can often be found. Here  $\lambda_c = c_0 / f_c$  is the *center wavelength* and  $G_e$  is the so-called *antenna gain*. Since the antenna gain is often given as a number (e.g. for a  $\lambda_c/2$ -dipole  $G_e = 1.64$ ), we might assume that the *effective area* becomes quadratically dependent on the carrier frequency. This might cancel the increase of  $P_{E,BB}(f_c, \Delta f, T)$  on  $f_c^2$  in eq. (8) so that the received power  $P_R(f, T)$  would not longer depend on the center frequency. This is not true, since the antenna gain *is* frequency dependent and the effective area *is not*.

Thus, it follows from eq. (9) that the received power decreases inversely proportional to the square  $r^2$  of the distance  $r$  and increases linearly with the antennas effective area. Suppose that a measurement of picowatts is possible with a satellite dish. Assume that the parabolic mirror has a diameter of 80cm. Then we obtain for the maximum distance between the antenna and the fire in our practical example

$$r_{\max} = \sqrt{\frac{\pi(0.4\text{m})^2 P_E(11\text{GHz}, 1\text{GHz}, 1000\text{K})}{2\pi 10^{-12} \text{ W}}} = 96.43\text{m}.$$

Such a maximum distance might be sufficient in numerous applications. However, note that the maximum distance is linearly depending on the center frequency  $f_c$  so that it can be increased if needed.

Up to now we do not have considered a possible attenuation during the propagation of the electromagnetic wave from the fire to the antenna. In other words we have assumed a free space between fire and antenna. So, let us fill this free space with some material, e.g. air, fog, smoke or a solid. Of course, we will have some additional attenuation which depends on the emitted frequency  $f$  as well as the temperature  $T$  and may be also on other parameters, e.g. the humidity of the material. Hence, we have to extend eq. (9) as follows

$$P_R(f, T) = |H(f, r)|^2 \frac{A_e}{2\pi r^2} P_E(f, T), \quad (10)$$

where  $H(f, r)$  is the transfer function from the fire to the antenna (or vice versa) for a given frequency  $f$  and distance  $r$ . In general, suppose that a source emits a signal  $s_e \sin(2\pi ft)$  with a constant amplitude  $s_e$ . This signal propagates through the considered material, e.g. air, fog or smoke, over a distance  $r$  and a sink receives the signal  $s_r(f, r) \sin(2\pi ft + \phi(f))$  with a frequency dependent amplitude  $s_r(f)$  and an arbitrary phase  $\phi(f)$ . Then the transfer function is simply given by

$$H(f, r) = \frac{s_r(f)}{s_e} e^{-\alpha r} e^{j\phi(f)}$$

where  $\alpha \in \mathbb{R}$  includes the properties (particle size distribution, optical index of refraction) of the considered material and the received amplitude  $s_r(f, r)$  can be separated as

$$s_r(f, r) = s_r(f) e^{-\alpha r}.$$



The next figure shows the attenuation  $10 \log |H(f, 1\text{m})|^2$  in dB/m in case of air and fog. It can be seen that the attenuation in case of air is strongly fluctuating. This is due to the

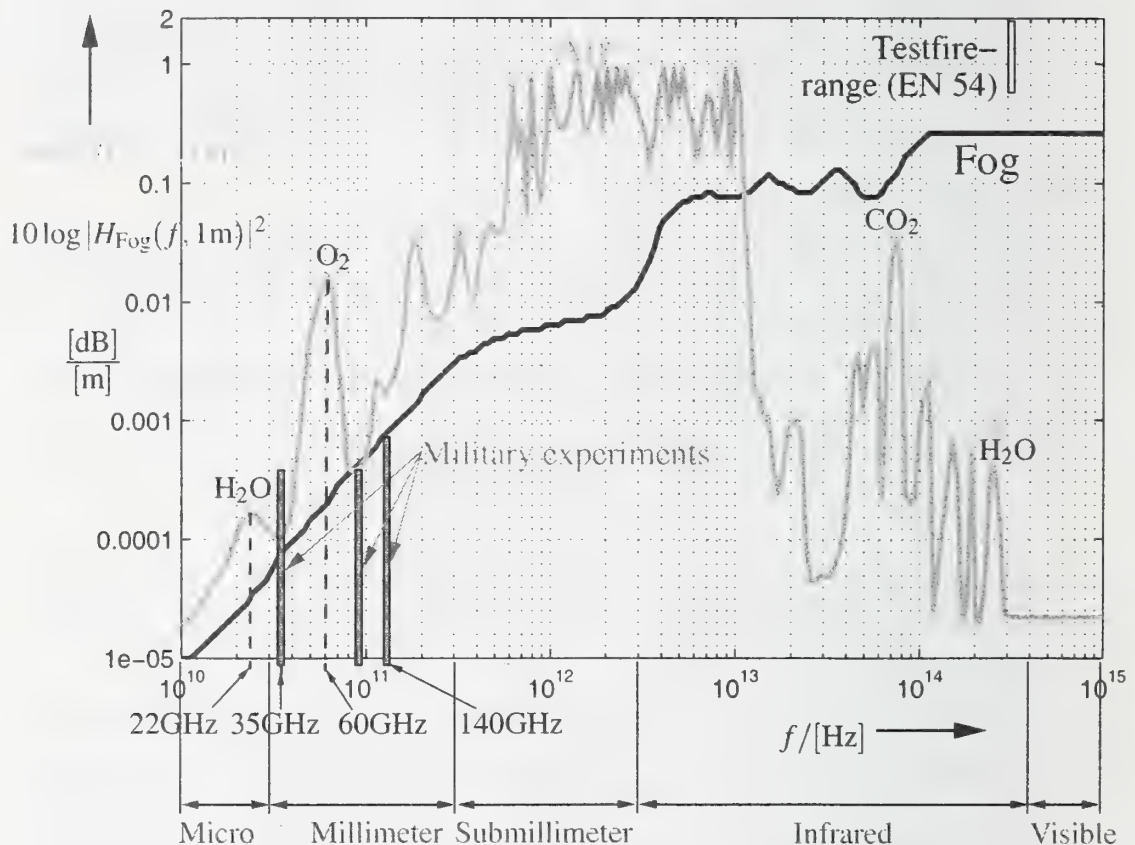


Figure 6: Attenuation of Air and Fog

molecules in the air, like e.g.  $\text{O}_2$  or  $\text{H}_2\text{O}$ , which absorb energy in certain frequency bands leading to a high attenuation. This must not be necessarily a disadvantage. For example in future generations of wireless communication a carrier frequency of 60GHz might be chosen to achieve small communication cells.

Comparing the MW- to the IR-region it can be also seen that the IR-region exhibits numerous window frequencies whereas the MW-region shows a principal increasing behaviour with increasing frequency. This means that for MW the considered center frequency  $f_c$  should not be too high which is in contradiction to the result we found in eq. (7) or (8), where the center frequency should be as high as possible to increase the emitted power. In other words, here a compromise has to be found in future.

The other curve – fog – shows not only a more smooth behaviour, but, much more interesting, it demonstrates that IR-radiation is *clearly attenuated* whereas the attenuation of MW-radiation nearly *remains unchanged*. Therefore, the MW-radiation power of a real body might become to a similar order of magnitude as the IR-radiation power for fog or,

more interesting, *smoke*. Although this result is surprising, it is further confirmed by the former discussion that for MW-radiation not only the surface of the burning material but also the deeper layers are contributing to the total emitted power. Moreover, it can be seen in Fig. 6 that according to the EN 54 (European Standard) all of the smoke generating test fires are leading to an attenuation *greater* than fog in the IR-domain around 300THz (corresponding to a wavelength of approximately 900nm). We have indicated well-known typical values of 0.6dB/m (open wood fire) to 2dB/m (smouldering woodfire (pyrolysis), glowing smouldering fire (cotton)) for these test fires. To our best knowledge only a few things are known on the attenuation of MW-radiation in case of smoke (see [2]). The experiments were done by the military (fog oil, dust dispersed by detonating high explosives, white and red phosphorous packages). For the window frequencies 35GHz and 94GHz only the dust experiments – not the smoke experiments – have shown an attenuation of 0dB/m to 0.000375dB/m. At 35GHz the maximum attenuation is a little bit increased to 0.0005dB/m. These results are also shown in Fig. 6. as three filled bars. Thus, in case of a smoke caused by a fire we expect only a very small attenuation so that the MW-radiation approach might be preferred in comparison with existing IR-Radiation based techniques. In conclusion we can state that more research is needed about the attenuation of MW-radiation for fire detection.

After answering the second question we ask the last question:

### 2.3 How much MW-power $P_D$ detects an antenna ?

The remaining task is now to construct an almost ideal antenna which converts the received electromagnetic radiation  $P_R$  in an electric power  $P_D$  as optimal as possible. Here we are faced with two principal problems:

1. The antenna will also receive other radiation not caused by the fire.
2. The antenna itself introduces additional noise due to their imperfectness.

Concerning the first problem, it is clear to suppress as much as possible of the undesired radiation. This leads to the question – What is the cause of undesired radiation ? Of course, each antenna has a directivity pattern which shows to which extent an incident wave under angle  $\phi$  is amplified. For example, a satellite dish exhibits a high directivity in one direction – the so-called *main lobe* – whereas other directions (side lobes) are mainly suppressed. However, if a small fire is propagating and even if the main lobe is directed to the fire, then the antenna will also receive additional radiation caused by other heat sources. These other sources are simply some material, e.g. the wall of the closed room, for which the temperature is higher than 0K. Thus, in practice we have to expect a lot of

distortions. For this reason it is very important to develop an antenna with a very narrow beam and very low side lobes. We will not further discuss this task since this is outside the scope of this paper. However, even if we have developed such an antenna, how can we achieve that its main beam is always pointed directly to the fire ? This problem can be solved by the so-called *smart antennas* known from wireless communications or radar processing. Smart antennas are usually consisting of an *array* of antennas where all the antenna outputs are processed together to steer the main beam of the whole antenna array in a certain direction. In other words, the antenna array is able to *scan* the environment. Of course, this scanning leads to a *picture* which shows the temperature profile of the environment. This picture could be for example displayed on a screen so that a fireman entering a smoked room could be able to locate the fire. Moreover, since the antenna array scans the whole environment, the resulting temperature profile might show – beside the fire location – also people in danger. The following figure shows the principal setup for a non-mobile situation.

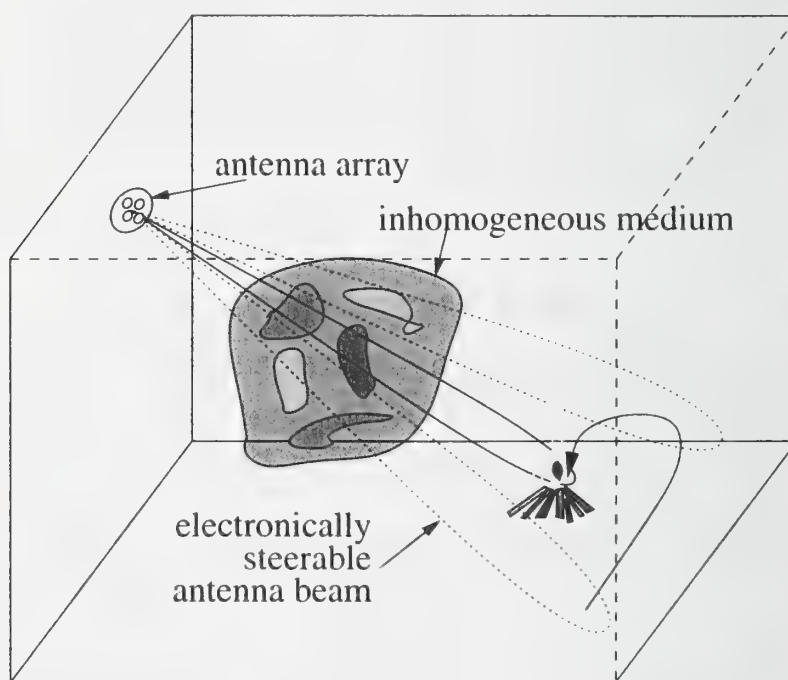


Figure 7: An antenna array to estimate the location of the fire origin.

Now let us consider the second problem. Since the antenna will also exhibit a temperature of higher than 0K, it will introduce some additional thermal noise in our measurement. In addition, all successive amplifiers will decrease the precision of our measurement due to additional thermal noise. Fortunately, a very clever approach is known to suppress at least the noise caused by the amplifiers. This principle is called *DICKE-radiometer* and it works as follows. The antenna output signal and a signal of a reference object of *variable*



temperature  $T_r$  are the inputs of a switch – called the DICKE-switch. The output of the switch is connected with an amplifier circuit so that the output of this circuit is used to measure the incident radiation power. The switch will be periodically switched, e.g. with a frequency of 1kHz. During the measurement the temperature of the reference object will be varied until the output power of the whole amplifier circuit remains constant. So the output power will be independent of the switching cycles. In this case we can determine the temperature of the received radiation – it is simply equal to  $T_r$  in this case – and due to PLANCK's law also proportional to the power of the received radiation. Consequently, the thermal noise of the amplifiers will not affect our measurement if we successfully apply the DICKE-approach.

In this subsection we discussed the main problems and gave an approach how it could be possible to solve them. Of course, much work is still needed to find an optimal antenna configuration for the desired purpose. In the last section we will show the first results obtained by some experiments in the fire detection laboratory of GERHARD-MERCATOR-University Duisburg, Germany.

### 3 Some first experiments

The first experiments for fire detection in garbage bunkers with microwaves were done by DASA (DaimlerChrysler Aerospace AG). Their results have motivated us to investigate this idea more detailed. In contrast to IR-radiation the MW-radiation seems not only to be technically unused in fire detection but also it seems not to be measured for standardized test fires (TFs). For this reason some first experiments were done at the fire detection laboratory of GERHARD-MERCATOR-University Duisburg.

We have used a commercial satellite dish and a low noise converter (LNC). The dish was adjustable in space so that either the MW-radiation of the room walls or of the fire was measured. The center frequency was  $f_c = 11$  GHz and the chosen bandwidth was  $\Delta f = 1$  MHz.

In the first experiment charcoal of an area of  $0.15 \text{ m}^2$  was ignited with a distance to the antenna of  $r = 4$  m. The measured power difference was fluctuating between 0.4 – 0.6 dBm. To study the principal effect of smoke we have blown some water vapor between the antenna and the fire. The maximum loss in power was 0.05 dBm compared to the smokeless situation. To get a more detailed picture we have carried out most of all test fires according to the European standard (EN 54), where now the distance between the antenna and the fire origin was increased to nearly the maximum possible of  $r = 7$  m. We have obtained the following results.

All fires containing some glowing material (TF1, TF2, TF4) can be easily detected. In

Test fire	typical behaviour	power gain	remarks
TF 1 - open wood fire	flames and later glowing wood	0.6 dBm	embers were measureable, flames were not measureable
TF 2 pyrolysis	much smoke and later glowing wood	0.15 dBm	smoke has no influence, embers were measureable
TF 4 - open polyurethan fire	smoke, flames and embers	0.15 dBm	increased power level probably due to embers
TF 5 - liquid n-Heptan fire	flames and high temperature	0 dBm	no change
TF 6 - liquid spirit fire	flames	0 dBm	no change
TF 7 - dekalin fire	flames, dark smoke, low temperature	0 dBm 0 dBm	neon tube behind the fire can be easily detected

Table 2: Results of the test fires

contrast, fires only consisting of flames (TF 5, TF 6, TF7) cannot be seen. This is not surprising since a flame has spectral components mainly in the IR- or visible light-region. However, flames are not in our focus since sophisticated flame detectors are already developed to reliably solve this detection problem [3]. To get a first impression of the influence of smoke we have arranged behind the test fire TF 7 a neon tube. Despite the optical dark smoke the neon tube can be easily detected by its MW-radiation. As a consequence, the assumption that smoke only slightly attenuate the MW-radiation is confirmed by this example.

## 4 Conclusions

In this paper we presented the fundamentals of microwave radiation for fire detection. MW-radiation offers some distinct advantages in comparison with conventional IR-radiation. For example, MW-radiation penetrates also optical thick smoke and vapor with only a slight attenuation and it penetrates principally all materials except metals. Moreover, MW-radiometers are very insensitive to environmental conditions, such as water vapor and dust (contrary to infrared methods) and high temperatures (contrary to semiconductor sensors). Last but not least, thermal microwave noise radiation comes from a *thicker surface layer* than does IR radiation. In contrast, two main disadvantages concerning fire detection can be given, first, with increased center frequency the costs are clearly increased, and second, because of the relatively long wavelengths compared to IR, the

achievable spatial resolution might be limited.

We have also derived a closed formula for the received antenna power. This formula shows the influence of chosen parameters, like the antenna bandwidth, the antenna effective area and the antenna center frequency and of non-chooseable parameters, like the temperature of the fire, the distance between fire and antenna, and the surface of the fire. By some first experiments we have demonstrated that with a very simple setup – a commercial satellite dish – fires can be easily detected if the burning material is glowing. In our opinion much research is needed on this area, since many applications can be imagined where microwaves are very useful for fire detection.

## References

- [1] H. Hellsten, J. Kjellgren, G. Stenström, and A. Sume, "A Scanning Airborne Radiometer for 30GHz and 90GHz", *Infrared and Millimeter Waves*, Vol. 15, Academic Press 1986
- [2] L. A. Klein, "Millimeter-Wave and Infrared Multisensor Design and Signal Processing", Artech House, Inc., Boston, London 1998
- [3] R. Siebel: "Ein LOW-COST Flammenmelder mit guten Alarm- und Falschalarmeigenschaften" (in German), *Proceedings AUBE '99 zur 11. Internationalen Konferenz über Automatische Brandentdeckung*, 16.-18.3.1999 in Duisburg, Heinz Luck (Ed.), Agst Verlag, Moers 1999, ISBN 3 926875 31 3



Shu Yan, Shu Wang, Zheng Dou

Huazhong University of Science & Technology, Wuhan, China

Henry Systems Technology, Nanjing, China

## **An Energy Model in Fire Detection and Integrated Analysis on False Alarms**

### **Abstract**

Fires in a closed space are theoretically considered as a thermodynamic system in this paper. Genuine fires and fire like factors cause entropy increment, which demonstrates the release of kinds of energy including heat, light radiation and material loss. Genuine fires release much more energy than deceptive fire like factors.

An energy model was constructed and applied to smoke detection. Theoretical analysis and test result showed that this model and the algorithm of energy release prediction were suitable to fire detection study, and multi-sensor technique and adaptive alarm threshold method are effective way to reduce the rate of false alarm and the rate of failure to alert.

### **1. Introduction**

The causes of false alarm are very complicated in automatic fire detection. Major aspects are:

- a) Non-fire aerosols like cooking fumes, steam, dust, insecticide and cigarette smoking,
- b) Environmental factors including electromagnetic interferences, airflow and rapid change of environmental temperature caused by air-conditioning,
- c) Aging of components,
- d) Poor quality in product design and production, and
- e) Poor engineering design including wrong selection of the model and location of detectors, and poor quality in installation, commissioning and maintenance.

This paper only focuses attention to the false alarm problems that are related to signal of sensors and signal processing. In order to quantitatively analyze the false alarm, an energy model in fire detection was constructed. Theoretical relations of the rate of false alarm and the rate of failure to alert were deduced from this model. Application of this

model in smoke detection showed evidence that this energy model was an effective method to reduce false alarm related to signal of sensors and signal processing <sup>[1]</sup>.

## 2. The energy model

Fires in a closed space are theoretically considered as a thermodynamic system in this paper. Genuine fire and deceptive fire like phenomena in this system cause the increments of entropy, which demonstrates the release of kinds of energy such as heat, light radiation and material losses (smoke and gasses etc.). The increments of entropy are different for genuine fires and for deceptive fire like phenomena. When a genuine fire happens, the system releases energy for a fairly long time, and total energy released reaches a higher scale. When a deceptive phenomenon happens, the system releases energy only for a short time, and not so much energy are released<sup>[2]</sup>.

In the real world, theoretically closed space does not exist. All systems are affected by environmental factors. We may possibly find the system's entropy increase or decrease. This means that there are energy flows outside the system caused by environmental factors and it should be considered in fire detection. In fact, some fire detectors have a variable steady value tracing environmental changes. In most cases genuine fires and deceptive fire like phenomena do not last very long, the system's steady values do not change too much. Therefore the system can be considered as a closed thermodynamic system during observation period. The energy release will depend on the system itself rather than outside world (see figure 1).

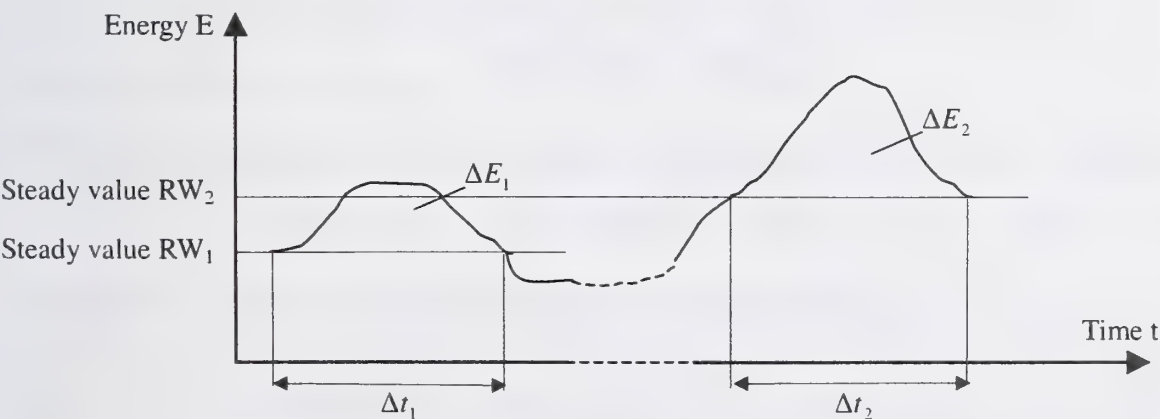


Fig. 1 Energy release of a closed system

The energy releases  $\Delta E$  for a closed thermodynamic system are kind of random variable having statistical feature.

Suppose the functions of probability density of the energy release  $\Delta E$  under non-fire and fire are respectively  $P(\Delta E, x=0)$  and  $P(\Delta E, x=1)$ , where  $x$  are Boolean values that stand for non-fire and fire. For a given alarm threshold  $\Delta E_T$  (see figure 2), the rate of false alarm is

$$P_{fa} = \int_{\Delta E_T}^{+\infty} P(\Delta E, x=0) d\Delta E, \quad (1)$$

while the detectivity rate of fire alarm is

$$P_d = \int_{\Delta E_T}^{+\infty} P(\Delta E, x=1) d\Delta E. \quad (2)$$

The rate of failure to alert is  $P_E = 1 - P_d$ . Since  $\int_{-\infty}^{+\infty} P(\Delta E, x=1) d\Delta E = 1$ , we get

$$P_E = \int_{-\infty}^{\Delta E_T} P(\Delta E, x=1) d\Delta E. \quad (3)$$

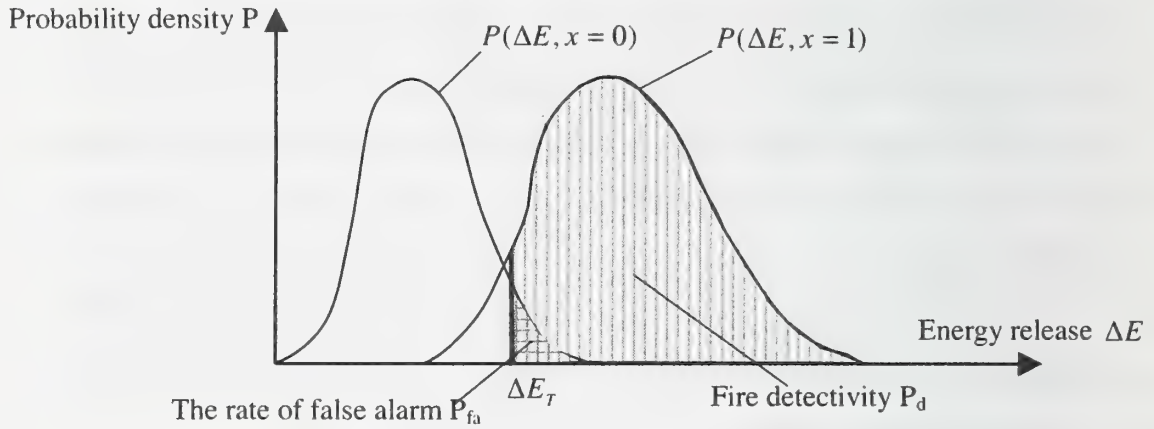


Fig. 2 Probability distribution of the energy released in a closed thermodynamic system

For a system with adaptive threshold values, the function of probability density of a threshold  $\Delta \hat{E}_T$  is  $P(\Delta \hat{E}_T)$ . Then the instantaneous rate of false alarm is

$\hat{P}_{fa} = \int_{\Delta \hat{E}_T}^{+\infty} P(\Delta E, x=0) d\Delta E$ , and the general rate of false alarm is

$$P_{fa} = E[\hat{P}_{fa}] = \int_{-\infty}^{+\infty} P(\Delta \hat{E}_T) \int_{\Delta \hat{E}_T}^{+\infty} P(\Delta E, x=0) d\Delta E d\Delta \hat{E}_T. \quad (4)$$

In the same way, the general detectivity is

$$P_d = E[\hat{P}_d] = \int_{-\infty}^{+\infty} P(\Delta \hat{E}_T) \int_{\Delta \hat{E}_T}^{+\infty} P(\Delta E, x=1) d\Delta E d\Delta \hat{E}_T, \quad (5)$$

and the general rate of failure to alert is



$$P_E = 1 - P_d = \int_{-\infty}^{+\infty} P(\Delta \hat{E}_T) \int_{-\infty}^{\Delta \hat{E}_T} P(\Delta E, x=1) d\Delta E d\Delta \hat{E}_T. \quad (6)$$

It is clear, from above equations, that by using an adaptive alarm threshold  $\Delta \hat{E}_T$  the rate of false alarm can be considerably reduced while the detectivity keeps at a given value, or the detectivity can be considerably improved while the rate of false alarm keeps at a given value.

With the method of constant rate of false alarm used in the signal processing in radar, we can reduce the rate of false alarm to a given value provided that the function of probability density and statistical feature of energy release  $\Delta E$  are available.

According to the equations of thermodynamics, temperature rise is proportional to energy release. Smoke and gas release are mass losses in a closed thermodynamic system. From the mass-energy relation  $E = mc^2$ , mass loss is proportional to energy release too. The total energy release of a system is the sum of heat energy release, mass loss (such as smoke, gas and so on) and other energy release (such as light etc.). Existent fire detectors, such as heat detectors, smoke detectors, gas detectors and light detectors, all take indirect measurement of energy release.

For different type of fire, the percentages of each part of energy release are different. That is the reason why the fire detectors with single sensor cannot respond to all type fires. The success of multi-sensor detectors shows that the more accurate energy releases we measure, the lower rate of false alarm and higher detectivity we gain. Multi-sensor and adaptive alarm threshold (multi-criteria) become major development trend of fire detection <sup>[3][4]</sup>.

### 3. Application of thermodynamic model in smoke detection

Smoke is one of the major characters at incipient stage for most fires. Other energy releases, such as temperature change, light radiation etc., are too weak to be measured in the incipient stage. So the smoke amount can be regarded as the energy release  $\Delta E$ .

Suppose that the smoke amount is  $S$ , the test starts at the moment of  $T_0$  and ends at  $T_1$ , and the output analogue value of smoke detector is  $V(t)$ . We then have  $S = \int_{T_0}^{T_1} V(t) dt$ .

Optical smoke detectors with analogue value ranging from 0 to 255 were used in our test program. Statistical analysis was carried out on the basis of response curves against test fires of EN54-9 and some deceptive fire like sources. The result is given in table 1.

Table 1 Smoke amounts against test fires and non-fire sources

Fire source	Smoke amount□Digit*se cond□	Fire source	Smoke amount□Digit*sec ond□	Non-fire source	Smoke amount□Digit*se cond□
TF1	4095	TF4 (3)	2373	Steam	3910
TF2	37440	TF5	4992	Mosquito incense	3960
TF3	100880	TF6	0	Mosquito incense (ventilated)	2100
TF4 (1)	2688	TF7 (1)	18020		
TF4 (2)	2835	TF7 (2)	16492	Cigarette smoking	18170

From table 1, we know that the energy release  $\Delta E$  of non-fire sources except cigarette smoking is of the magnitude about  $10^3$ . And  $\Delta E$  for fire sources with the main product of smoke (TF2, TF3, TF7) are of the magnitude between  $10^4$  to  $10^5$ . However, for other sources, the smoke amount cannot be regarded as total energy  $\Delta E$  because, for example, the temperature change for fire sources of TF1, TF4, TF5 and TF6 is an important part of the energy release and can not be ignored. As a special case there is only temperature change but no smoke product in the experiment of TF6. Smoke detector cannot respond to TF6 no matter what fire detection algorithm is adopted. The reason is just that the energy release  $\Delta E$  cannot be predicted by smoke sensing. For the non-fire source of cigarette smoking, the energy release  $\Delta E$  reaches the magnitude that many fire sources reach as this experiment was carried out under a strict condition (smoking just in front of smoke detector). This implies that over smoking may lead to false alarm.

Fire alarm must be initiated in a real time. It is not permitted to obtain the total amount of smoke (total energy release) for making a fire alarm. Instead, the method of prediction of energy release is utilized in fire detection algorithms. Obviously, the amplitude and changing trend of smoke signal are the main factor of prediction. On the other hand, the longer the observation period lasts, the more accurate the prediction is. Therefore using adaptive alarm threshold and suitable observation period can effectively reduce the false alarm <sup>[2]</sup>.

A new algorithm of smoke detection based on the energy release prediction is shown in Fig. 3. The key point of the algorithm is that the detector makes the prediction of energy release i.e. smoke amount from time to time. The result of the prediction is  $\Delta\tilde{E}$ . For a given risk of alarm  $f_{risk}$ , the alarm threshold  $\Delta E_T$  can be obtained. With the equations of (4) to (6), the rate of false alarm, the detectivity and the rate of failure to alert can be calculated. Fire alarm decision can finally be made by the information of  $P_{fa}$ ,  $\Delta E_T$  and  $f_{risk}$ .

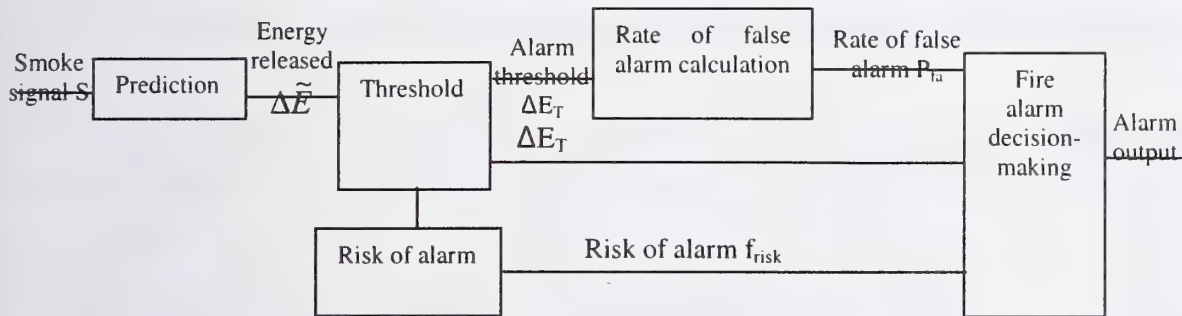


Fig. 3 Block diagram of the algorithm of energy release prediction for smoke detection

Energy release  $\Delta E$  is, in fact, the area covered by smoke curve. Future part of smoke curve can be predicted on the basis of present part of the curve. A simplest method is straight-line method with a little poor prediction accuracy. The risk of alarm  $f_{risk}$  can be set in accordance with the environmental conditions and protection requirements. A preset alarm threshold  $\Delta E_{T0}$  can be determined by experimental data and experiences. The alarm threshold is then  $\Delta E_T = \Delta E_{T0} * f_{risk}$ .

A BP neural network trained by the experimental data can be used to fit the probability function  $P(\Delta E, x)$ . The output of the neural network can directly be defined as  $P_{fa}$  and  $P_E$ .

For other detection algorithms of smoke detector,  $P_{fa}$  and  $P_E$  can also be deduced, provided that their equivalent alarm thresholds  $\Delta E_T$  can be obtained and the equivalent



neural network can then be trained. In this way many detection algorithms can be compared each other and examined objectively.

The algorithm related above is still under development. The non-smoke energy release cannot be acquired by smoke detector. Smoke detector is difficult to avoid false alarm by non-fire sources and failure to report the fires that are without smoke (such as TF6). Therefore, other type sensors (such as temperature sensor) must be combined in fire detector in order to reduce the rate of false alarm and the rate of failure to alert.

#### **4. Conclusions**

The application in smoke detector shows that the energy model is suitable for fire detection. The model provides theoretical relation of the rate of false alarm and the rate of failure to alert. Multi-sensor detection technique and multi-criteria data processing can estimate the energy releases more accurately. Reducing the rate of false alarm, in the view of sensor signal and signal processing, is possible by using this energy model and the algorithm of energy release prediction.

#### **References**

- [1] H. Luck and K.R. Hase, Signal Detection Aspects in Automatic Fire Detection, *Fire Safety Journal*, 6 (1983), pp.233-240.
- [2] Shu Wang and Zheng Dou, *Fire Detection and Fire Signal Processing*, Publishing House of Huazhong University of Science & Technology, 1998 (in Chinese).
- [3] Bukowski, R.W. and Reneke, P.A., New Approaches to the Interpretation of Signal from Fire Sensors, in *Proc. Of the 11th Int. Conf. on Fire Detection at the Duisburg University 1999 (AUBE'99)*, H. Luck ed., pp.11-21.
- [4] Gottuk, D.T., Peatross, M.J. etc., Advanced Fire Detection Using Multi-signature Alarm Algorithms, in *Proc. Of the 11th Int. Conf. on Fire Detection at the Duisburg University 1999 (AUBE'99)*, H. Luck ed., pp.237-246.

Hans-Christian Müller  
Duisburg Gerhard-Mercator-University  
Department of Communication Engineering  
Bismarckstrasse 81, 47048 Duisburg

## **A New Approach to Fire Detection Algorithms based on the Hidden Markov Model**

### **Abstract**

In this paper the theory and some experimental results of a new approach to fire detection algorithms are discussed. The algorithm is based on a signal classification principle, which is widely used in the field of speech recognition. The sensor signals are transformed into appropriate finite time series. The transformation is done in a preprocessing step that extract a suitable sequence from the signals to be classified. The time series are modeled by a Hidden Markov Model (HMM). The classification of a recognized sequence is the final step with respect to the decision making process.

### **1 Introduction**

Advances in semiconductor technology have influenced the development of fire detection algorithms to a high degree in recent years. The use of microprocessors in fire detection devices is nearly state-of-the-art. Improvement of detectivity has been achieved in modern fire detection systems independently of the design scheme with respect to central or distributed intelligence. Implementation of improved detection algorithms leads to reduced false alarm rates and good detection features in comparison with the classical threshold detector.

Modern fire detection algorithms are often based on a fuzzy logic or a neural network approach. They might include some sort of feature extraction methods applied to the sensor signals.

In the following we will introduce the concept of statistical models of sequential data with respect to the fire detection problem.

## 2 Hidden Markov Models

Let us consider an urn-and-ball system [1], [2]. We assume that there are  $N$  (large) glass urns in a room. Within each is a large quantity of colored balls. There are  $M$  distinct colors of the balls. The physical process to obtain observations is as follows. A genius is in the room, and, according to some random procedure, it chooses an initial urn. From this urn, a ball is chosen at random, and its color is recorded as the observation. The ball is then replaced in the urn from which it was selected. A new urn is then selected according to the random selection procedure associated with the current urn, and the ball selection process is repeated. The entire process generates a finite observation sequence of colors, which we would like to model as the observable output of an Hidden Markov Model (HMM).

Obviously, the simplest HMM that corresponds to the urn-and-ball process is one in which each state corresponds to a specific urn, and for which a (ball) color probability is defined for each state. The choice of urns is dictated by the state transition-matrix of the HMM.

Furthermore, it should be noted that the ball colors in each urn may be the same, and the distinction among various urns is in the way the collection of colored balls is composed. Therefore an isolated observation of a particular color ball does not immediately tell which urn it is drawn from.

### 2.1 Elements of an HMM

The above experiment consists of drawing balls from urns in some sequence. Only the sequence of balls is shown to us. An HMM for discrete symbol observation such as the urn-and-ball model is characterized by the following:

1.  $N$ , the number of states in the model. Although the states are hidden, for many practical applications there is often physical significance attached to the states of the model. Thus, in the urn-and-ball model, the states correspond to the urns. Generally, the states are interconnected in such a way that any state can be reached from any other state. However, other possible interconnections of states are often of interest. In the following individual states are labeled as  $\{1, 2, \dots, N\}$  and the state at time  $t$  is denoted as  $q_t$ .
2.  $M$ , the number of distinct observation symbols per state. The observation symbols correspond to the physical output of the system being modeled. For the urn-and-ball experiment the observation symbols are the colors of the balls selected from



the urns. We denote the individual symbols as  $V = \{v_1, v_2, \dots, v_M\}$ .

3.  $T$ , the length of an observation sequence.

4.  $O = (O_1 O_2 \dots O_T)$  the observation sequence, where  $O_t$  denotes the observation at time  $t$ .

5. The state transition probability distribution  $A = \{a_{ij}\}$  where

$$a_{ij} = P(q_{t+1} = j | q_t = i), \quad 1 \leq i, j \leq N$$

defines the probability of being in state  $j$  at time  $t + 1$  given that we were in state  $i$  at time  $t$ . For the special case where any state can be reached from any other state in a single step, we have  $a_{ij} > 0$  for all  $i, j$ . For other types of HMMs, we would have  $a_{ij} = 0$  for one or more  $(i, j)$  pairs.

6. The observation symbol probability distribution  $B = \{b_j(k)\}$ ,

$$b_j(k) = P(O_t = v_k | q_t = i), \quad 1 \leq k \leq M$$

defines the probability of observing the symbol  $O_t = v_k$  at time  $t$  given that we are in state  $j$ .

7. The initial state distribution  $\pi = \{\pi_i\}$ , in which

$$\pi_i = P(q_1 = i), \quad 1 \leq i \leq N$$

defines the probability of being in state  $i$  at the beginning of the experiment (i.e., at  $t = 1$ ).

It can be seen from the above that a complete specification of an HMM requires the specification of two model parameters,  $N$  and  $M$ , specification of observation symbols, and the specification of the three sets of probability measures  $A$ ,  $B$  and  $\pi$ . For convenience,  $\lambda = (A, B, \pi)$  will be used as a compact notation to denote an HMM.

Using the model, an observation sequence  $O = (O_1 O_2 \dots O_T)$  is generated as follows: We start our experiment at time  $t = 1$  by choosing one of the urns, according to the initial probability distribution  $\pi$ , then we choose a ball, the observation symbol from this urn. The state and the observation symbol at time  $t = 1$  are denoted as  $q_1$  and  $O_1$  respectively. After this we choose an urn (may be the same or a different from the urn at  $t = 1$ ) according to the transition probability distribution  $A$  and again select a ball (denoted as  $O_2$ ) from this urn depending on the observation symbol probability  $b_j(k)$  for that urn (state). The continuation of this procedure up to time  $t = T$  generates the observation sequence  $O = (O_1 O_2 \dots O_T)$ .

## 2.2 The Three Problems for HMMs

Most applications of HMMs are finally reduced to solving three main problems. These are:

- Problem 1: Given the observation sequence  $O = (O_1 O_2 \dots O_T)$  and a model  $\lambda = (A, B, \pi)$ , how do we efficiently compute  $P(O|\lambda)$ , the probability of the observation sequence, for a given model?
- Problem 2: Given the observation sequence  $O = (O_1 O_2 \dots O_T)$  and a model  $\lambda = (A, B, \pi)$ , how do we choose a corresponding state sequence  $Q = (q_1 q_2 \dots q_T)$  such that  $P(O, Q|\lambda)$ , the joint probability of the observation sequence and the state sequence is maximized?
- Problem 3: How do we adjust the HMM model parameter  $\lambda = (A, B, \pi)$  so that  $P(O|\lambda)$  or  $P(O, Q|\lambda)$  is maximized?

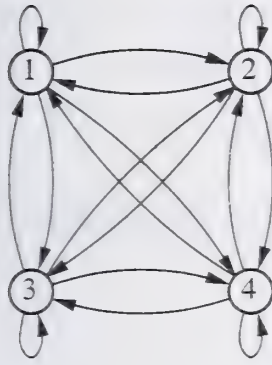
Problem 1 is the evaluation problem, namely, given a model and a observation sequence, how do we compute the probability that the observation was produced by the model? Problem 1 can be viewed as one of scoring how well a given model matches a given observation sequence. For example, if we consider the fire detection problem the solution of problem 1 allows to make an alarm decision.

Problem 2 is the one in which we attempt to uncover the hidden part of the model. Typical uses might be to learn about the structure of the model, to find the optimal state sequence for a given observation sequence.

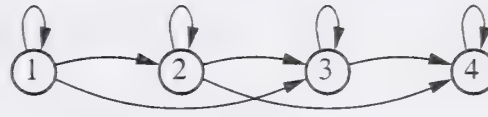
Problem 3 is the one in which we attempt to optimize the model parameters to best describe how a given observation sequence comes about. The observation sequences to adjust the model parameters are called training sequences because they are used to "train" the model. This problem is the crucial one for most applications of HMMs, because it allows us to create best models for real phenomena.

## 2.3 Types of the HMMs

One way to classify types of HMMs is by the structure of the transition matrix  $A$ . In the special case of ergodic or fully connected HMMs every state can be reached from every other state of the model in a single step.



(a)



(b)

**Figure 1:** Two types of HMMs

As shown in Figure 1(a), for an  $N = 4$  state model, we have

$$A = \begin{bmatrix} a_{11} & a_{12} & a_{13} & a_{14} \\ a_{21} & a_{22} & a_{23} & a_{24} \\ a_{31} & a_{32} & a_{33} & a_{34} \\ a_{41} & a_{42} & a_{43} & a_{44} \end{bmatrix} \quad \text{with } a_{ij} > 0 \text{ for all } 1 \leq i, j \leq 4$$

For some applications, particularly the one discussed here, other types of HMMs have been found to account for observed properties of the signal being modeled better than the standard ergodic model. One such model is shown in Figure 1(b). This model is called a left-right-model because the underlying state sequence associated with the model has the property that the system states proceed from left to right as time increases. Clearly, the left-right-type of HMM has the desirable property that it can model signals whose properties change in time in a successive manner (e.g., increasing sensor signal values obtained from a scattering light smoke sensor). The transition coefficients have the property

$$a_{ij} = 0, \quad j < i$$

Hence, no transitions are allowed to states whose indices are lower than that of the current one. Clearly, the initial state distribution  $\pi = \{\pi_i\}$  is given by

$$\pi_i = \begin{cases} 1, & i = 1 \\ 0, & i \neq 1 \end{cases}$$



because the state sequence must begin in state 1. Often, with left-right-models, additional constraints are placed on the transition coefficients. A constraint of the form

$$a_{ij} = 0, \quad j > i + \Delta i$$

is often used to make sure that large changes in state indices do not occur. In particular, for the example of Figure 1(b), the value of  $\Delta i$  is 2.

### 3 Realization

A discussion of the solution of the three problems of HMMs will exceed the scope of the paper. The solution of problem 3, the synthesis or training problem, is not necessarily part of a detection algorithm. The parameters of an HMM can be viewed as parameters of the detection algorithm which have to be adjusted by a preceding training procedure.

The solution of problem 1, the analysis problem, will be discussed later from the computational effort point of view which is of some interest as far as the practical realization is concerned.

#### 3.1 The parameters of the HMM

We are using a left-right-model with  $N = 10$  states. The number of distinct observation symbols per state is  $M = 15$ . Here, the observation symbols represent certain sensor signal values. The length of an observation sequence equals  $T = 12$ . We use a sampling rate of 0.2 Hz. Hence, the observation length corresponds to a duration of 1 minute.

The initial state distribution  $\pi = \{\pi_i\}$  is given according to the chosen left-right-model by a  $10 \times 1$  vector with only one nonzero component, i.e.  $\pi_1 = 1$ . The remaining parameter, the transition probability distribution, represented by a  $10 \times 10$  matrix, as well as the observation symbol probability distribution, represented by a  $10 \times 15$  matrix, are adjusted by a couple of training sequences, i.e., we used 30 training sequences taken from test fires of type TF1, TF3, TF4, TF5 and TF7.

#### 3.2 Solution of Problem 1

A straightforward way to determine  $P(O|\lambda)$  is by enumerating every possible state sequence of length  $T$ . There are  $N^T$  of such state sequences.

The probability of the observation sequence  $O = (O_1 O_2 \dots O_T)$  given the state sequence

$Q = (q_1 q_2 \dots q_T)$  and the model  $\lambda$  is

$$\begin{aligned} P(O|Q, \lambda) &= \prod_{t=1}^T P(O_t|q_t, \lambda) \\ &= b_{q_1}(O_1) \cdot b_{q_2}(O_2) \cdots b_{q_T}(O_T) \end{aligned}$$

The probability of such a state sequence  $Q$  can be written as

$$P(Q|\lambda) = \pi_{q_1} \cdot a_{q_1 q_2} \cdot a_{q_2 q_3} \cdots a_{q_{T-1} q_T}$$

The probability that the  $O$  and  $Q$  occur simultaneously, is the product of the above two terms

$$P(O, Q|\lambda) = P(O|Q, \lambda)P(Q|\lambda)$$

The probability of  $O$  given the model  $\lambda$  is obtained by summing this joint probability over all possible state sequences  $Q$ . Hence, we have

$$P(O|\lambda) = \sum_{\text{all } Q} P(O|Q, \lambda)P(Q|\lambda)$$

From the last equation we see that the summand involves  $2T - 1$  multiplications. Hence summation over all possible state sequences requires  $(2T - 1)N^T$  multiplications and  $N^T - 1$  additions. Even for small values,  $N = 10$  and  $T = 12$ , this means approximately  $2.3 \cdot 10^{13}$  multiplications. Clearly, a more efficient procedure is required to solve problem 1. Such a procedure exists and is called the forward procedure.

Consider the forward variable  $\alpha_t(i)$  defined as

$$\alpha_t(i) = P(O_1, O_2, \dots, O_t, q_t = i|\lambda)$$

i.e., the probability of the partial observation sequence,  $O_1, O_2, \dots, O_t$ , (until time  $t$ ) and the state  $i$  at time  $t$  given the model  $\lambda$ . We can solve for  $\alpha_t(i)$  inductively, as follows:

#### 1. Initialization

$$\alpha_1(i) = \pi_i b_i(O_1), \quad 1 \leq i \leq N$$

#### 2. Induction

$$\alpha_{t+1}(j) = \left[ \sum_{i=1}^N \alpha_t(i) a_{ij} \right] b_j(O_{t+1}) \quad 1 \leq t \leq T-1, 1 \leq j \leq N$$

#### 3. Termination

$$P(O|\lambda) = \sum_{i=1}^N \alpha_T(i)$$

Again, let us examine the number of multiplications involved with this procedure. The initialization step involves  $N$  multiplications. The induction step requires  $N$  multiplications plus one for the out of bracket  $b_j(O_{t+1})$  term. This has to be done for  $1 \leq j \leq N$  and for  $1 \leq t \leq T$ , which amounts to  $(N+1)N(T-1)$  multiplications in the induction step. The termination step requires no further multiplications. Hence the total number of multiplications is  $N + N(N+1)(T-1)$ . For  $N = 10$  and  $T = 12$  we need about 1200 computations for the forward procedure as compared to  $2.3 \cdot 10^{13}$  required by the direct computation of  $P(O|\lambda)$ .

### 3.3 The Algorithm

The algorithm we used works as follows: At each discrete time instant  $t$  (e.g., multiple integer of 5 seconds) an observation sequence  $O$  is taken from the sensor signal including the current signal value as well as the 11 preceding signal values. Then the a posteriori probability  $P(O|\lambda)$  is calculated according to the forward-procedure.

## 4 Experiments and Results

In this section we present some results taken from a computer simulation of the algorithm described above. The following plots show the output signal  $s(t)$  of a scattering light smoke sensor and the a posteriori probability  $P(O|\lambda)$  plotted as

$$P^*(O, \lambda) = \min(150, -\log[P(O|\lambda)])$$

The performance of the system in case of a testfire TF1 is in the following plot.

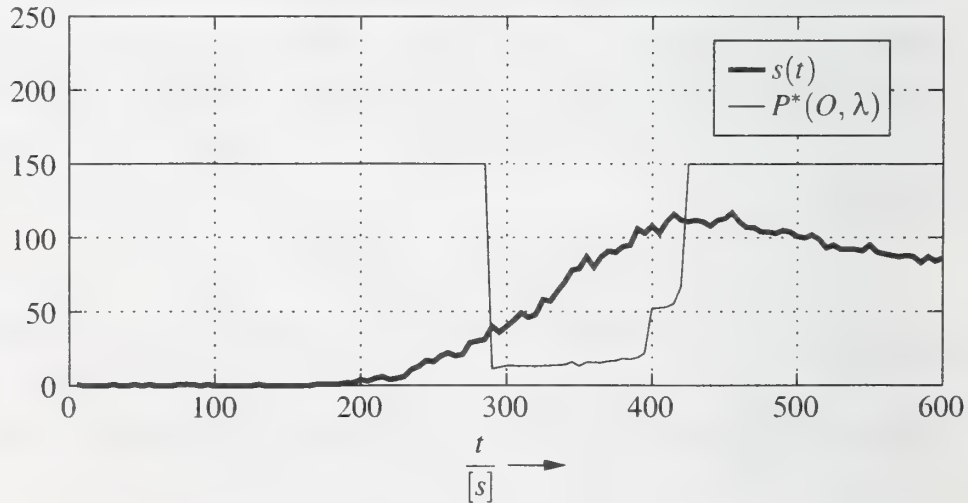
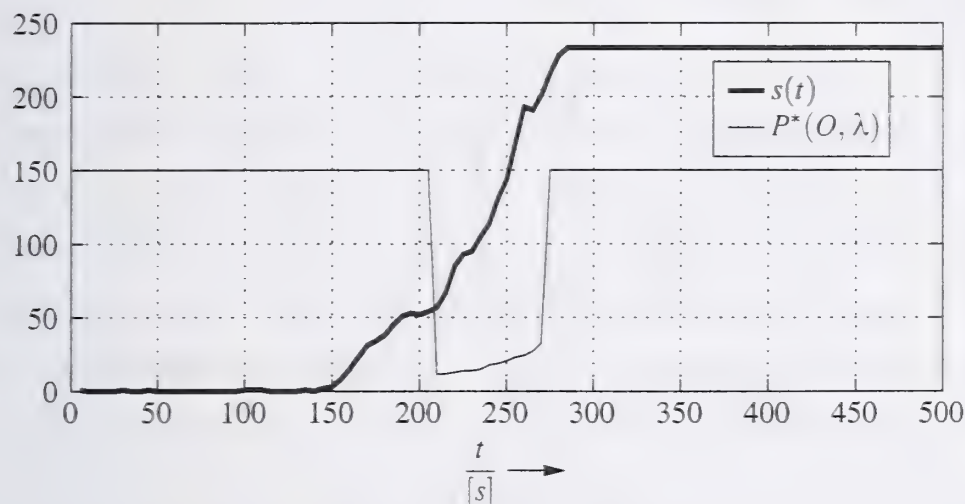


**Figure 2:** Sensor signal  $s(t)$  and the logarithm of the a posteriori probability  $P(O|\lambda)$  in case of testfire TF1



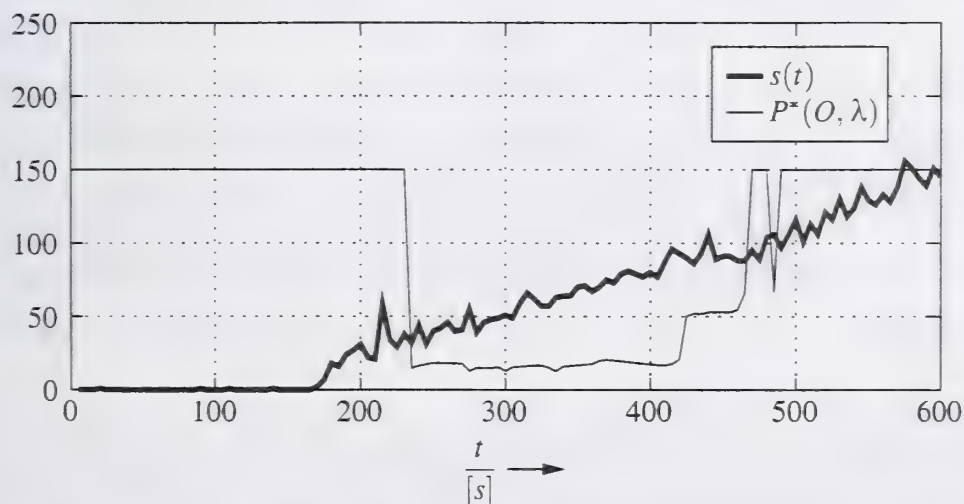
Obviously,  $P(O|\lambda)$  is maximum (or equivalent:  $P^*(O, \lambda)$  is minimum) about 100 seconds after the smoke sensor signal  $s(t)$  leaves the steady-state value.

Figure 3 shows the performance of the system in case of a smoldering fire, i.e. testfire TF2. Here, the maximum of  $P(O|\lambda)$  is reached 60 seconds after the smoke sensor signal  $s(t)$  leaves the steady-state value.



**Figure 3:** Sensor signal  $s(t)$  and the logarithm of the a posteriori probability  $P(O|\lambda)$  in case of testfire TF2

Figure 4 shows the performance of the system in case of a slowly developing fire, i.e. testfire TF7.



**Figure 4:** Sensor signal  $s(t)$  and the logarithm of the a posteriori probability  $P(O|\lambda)$  in case of testfire TF7

Again, the maximum of  $P(O|\lambda)$  is reached 60 seconds after the smoke sensor signal  $s(t)$  leaves the steady-state value.

Finally, in the last simulation presented here we used an artificial burst signal. Signals like this are most unlikely to occur in real fire situations, but may, for example, occur due to electromagnetic influences.

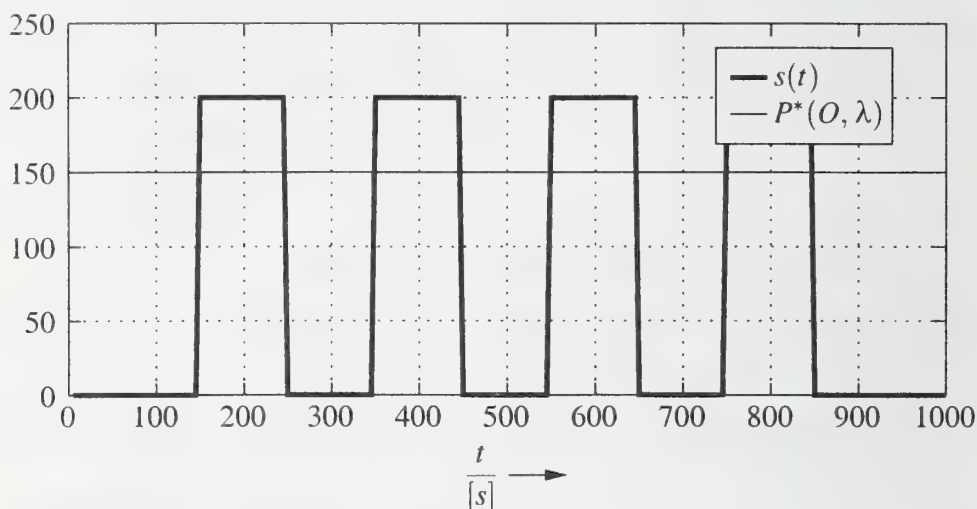


**Figure 5:** An artificial burst sensor signal  $s(t)$  and the logarithm of the a posteriori probability  $P(O|\lambda)$

Obviously, the maximum value of  $P(O|\lambda)$  (the minimum value of  $-\log(P(O|\lambda))$ ) is much smaller (greater) as compared to the last three examples. Note, a classical threshold detector will reach its alarm condition in case of the shown artificial burst signal.

## 5 Conclusion

In this paper we have derived a new approach for fire detection algorithms. The key element of our approach, which appears to be quite useful, is a Hidden-Markov-Model. To be more precise, we used a left-right-model. Simulation studies have been presented which show the ability to improve detection features in comparison with the classical threshold detector.

## References

- [1] Dugad, Rakesh and Desai, U. B.; *A tutorial on hidden markov models*; Indian Institute of Technology, Bombay Powai; 1996
- [2] Rabiner, Lawrence R; *Fundamentals of speech recognition*; Prentice Hall; 1993

Thomas Cleary and Kathy Notarianni

Building and Fire Research Laboratory, National Institute of Standards and Technology  
Gaithersburg, MD, 20899 U.S.A.

## **Distributed Sensor Fire Detection**

### **1. Introduction**

Most fire detection systems, even those with 100's of individual detectors reporting to a fire panel, are designed to alarm on a single detector, be it a single sensor or multi-sensor design. The stochastic nature of fire dictates that no single location for a detector is preferred. In current design, detectors are sited such that each detector "protects" a given fraction of the building space. While there may be some threshold alarm value adjustment if adjacent detectors start to sense fire conditions for particular designs, the concept of distributed sensor fire detection has been pursued no further. Distributed parameter systems, i.e., systems where the state vectors depend on spatial position, are frequently encountered in the field of process control and give rise to control theories dedicated to those systems. The fire detection problem is similar to control of distributed parameter systems in that both address a problem stated as: what are the number of measurements required and where are their locations to guarantee either early fire detection or stable control of the system? Also taking a cue from distributed parameter control where the distributed sensors need not be, and frequently are not, measuring the same state values (e.g., a mixture of temperature, concentration, pH, and pressure measurements, etc. for process control), different types of sensors distributed in space may afford an economical, optimized fire detection system. The concept put forth here is multi-sensor, multi-criteria detection with distributed sensing elements.

There are three conceivable reasons to integrate distributed sensing elements for fire detection. First, a sensor primarily used for another purpose may provide useful information related to early fire detection. An example might be a carbon dioxide sensor used for demand-controlled ventilation in a building, and located either in a return air duct common to several rooms, or in a single room. Second, cost may limit a particular sensor



to either a single location or a limited number of locations; other types of sensors would be needed to fill in the gap in space coverage. Third, a particular sensor may not be suitable for a particular location due to naturally-high ambient levels it would sense there (i.e., a CO sensor located next to a parking garage). This paper details a case study that utilized model simulations to assess the relative performance benefits of distributed sensing over single-station, single-sensor smoke detection and co-located multi-sensor detection.

## 2. Fire Model Runs

This study utilized 500 individual CFAST fire simulations performed by Notarianni [1]. CFAST is a multi-room zone fire model developed at NIST [2]. The space configuration considered was a seven room arrangement representing a single-floor apartment (Figure 1).

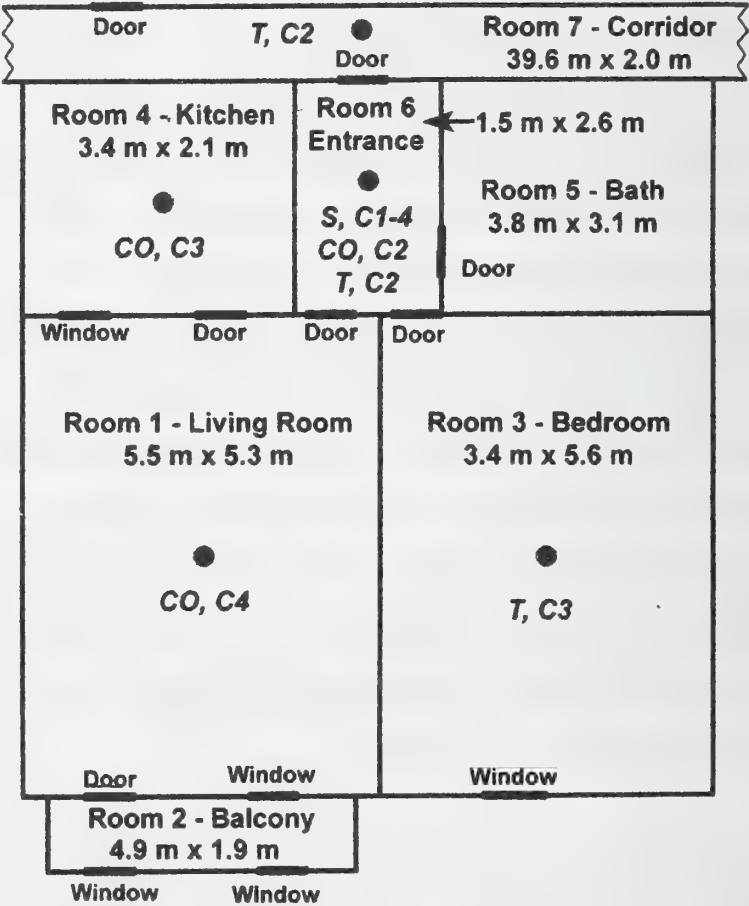


Figure 1. Schematic of apartment layout. The distribution of smoke (S), temperature (T), and carbon monoxide (CO) sensors are shown for the various cases (C#).

The 500 simulations encompassed a realistic distribution of potential fire scenarios. The set included a combination of scenarios that represent statistically, both the types of fires and the frequency at which they occur in a given occupancy type. Design fires were made up of fire events (heat release rate and location) and the characteristics of the material burning. Building geometry, properties of construction materials, and seasonal weather conditions, (outside ambient temperature) were used to fix initial and boundary conditions. Information about the uncertainty, variability, and correlational structure of the input parameters was used to define the fire scenarios. Fire growth rate inputs were one of the " $t^2$ " fires: slow, medium, or fast. A " $t^2$ " fire is a modeled fire where the heat release rate increases from zero as a function of time to the 2<sup>nd</sup> power. Standard pre-exponential values are defined as slow, medium, fast, etc. The fire location was moved to different rooms for different simulations. Model output included smoke concentration, CO concentration, and temperature in the upper layer as a function of time in each room. There are significant limitations in zone-model simulations with relation to detector response (instantaneous uniform mixing in the layers, no flow velocity information, etc.). Here it was assumed that the detector instantaneously sees the computed upper-layer value of smoke, CO, or temperature. Thus, the computed results were used as the sensor response for smoke, CO and temperature sensors. Given the model limitations and the assumption of instantaneous detector response, it was decided not to consider rate-of-rise of any of these computed values in the alarm rules. It is noted however that rate-of-change and other real sensor signal features contain a wealth of information that could be exploited in advanced pattern recognition algorithms developed for distributed sensor detection systems.

Figures 2-4 show the computed upper-layer values of smoke optical density, CO concentration and temperature as a function of time in each room for one simulated fire, a slow  $t^2$  fire located in the bedroom.

### **3. Detection Rules and Sensor Distributions**

Four sensor spatial configurations were examined along with 4 different rules governing the alarm state. Each sensor configuration and rule set constitutes a CASE for identification purposes. The sensor configurations are shown in Figure 1. Configuration 1 is the base case of a single smoke detector in the entrance (room 6) which represents the minimum

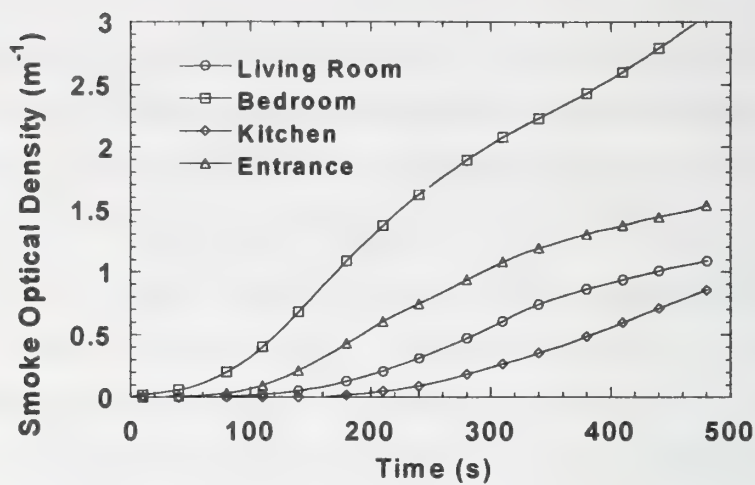


Figure 2. Smoke optical density for a slow  $t^2$  fire located in the bedroom.

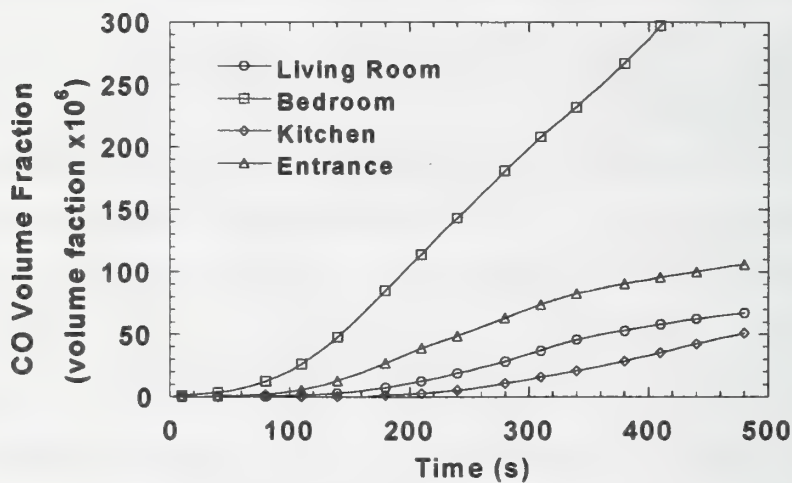


Figure 3. CO volume fraction for a slow  $t^2$  fire located in the bedroom.

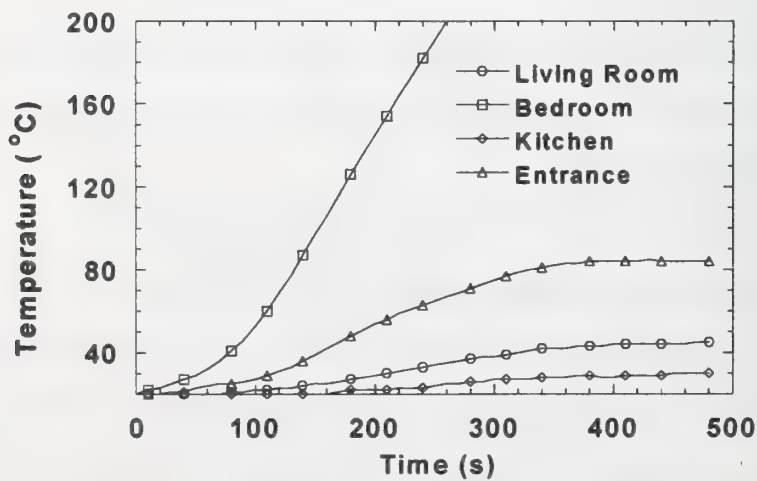


Figure 4. Upper-layer temperature for a slow  $t^2$  fire located in the bedroom.



code requirements for existing residential dwellings. Configuration 2 is a detector consisting of three sensors: smoke, CO, and temperature, co-located in the same space, the entrance (and presumably in the same detector housing). Configuration 3 is a smoke detector in the entrance, a heat detector in the bedroom, and a CO detector in the kitchen. A detector in the bedroom is a logical addition based on U.S. code requirements for new construction. The CO sensor in the kitchen is logical if gas appliances (water heater, dryer, etc.) are located there. Configuration 4 moves the heat sensor to the corridor, and moves the CO sensor to the living room.

The four rules consist of fixed thresholds or threshold adjustments based on other sensor signals. They are:

Rule 1 - If smoke optical density  $> 0.06 \text{ m}^{-1}$  ( 4 %/ft obscuration), then alarm is on

Rule 2 - If CO volume fraction  $> 1.0 \times 10^{-5}$  and smoke optical density  $> 0.015 \text{ m}^{-1}$  (1 %/ft obscuration), then alarm is on

Rule 3 - If  $\Delta T > 5 \text{ }^{\circ}\text{C}$  and smoke  $> 0.015 \text{ m}^{-1}$ , then alarm is on

Rule 4 - IF  $\Delta T > 15 \text{ }^{\circ}\text{C}$ , then alarm is on.

$\Delta T$  is the temperature difference between initial ambient room temperature and the upper-layer temperature. At each time step the rules were checked to see if an alarm condition was indicated. If so, the time to alarm was noted along with the rule that yielded the alarm.

The following Cases were examined:

CASE 1: Configuration 1 and Rule 1, (Base Case)

CASE 2: Configuration 2 and Rules 1-4

CASE 3: Configuration 3 and Rules 1-4

CASE 4: Configuration 4 and Rules 1-4.

#### 4. Results and Analysis

Figure 5 shows the alarm time versus simulation run for CASE 1. The mean alarm time was 88 s. It is more illustrative to compare other CASES to their improvement from the CASE 1. Figures 6-8 show the difference between the base case alarm time and the alarm time for CASES 2, 3, and 4 respectively. The mean alarm time for CASES 2, 3, and 4 were 50 s, 81 s, and 67 s respectively. The distributed sensor configuration with the temperature

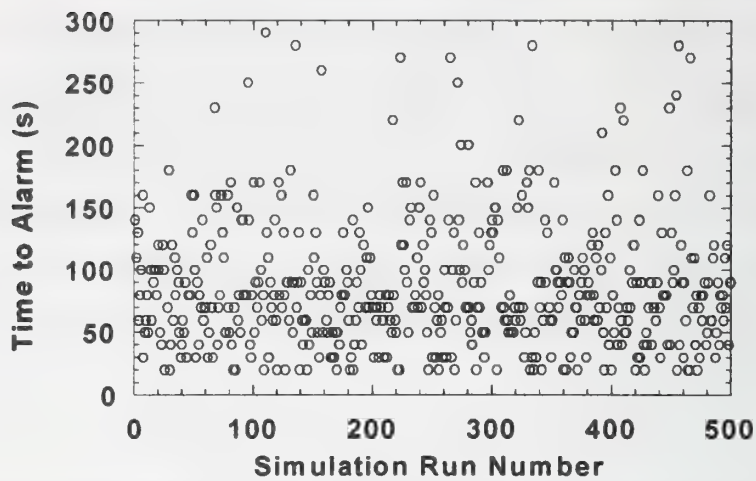


Figure 5. Time to alarm for CASE 1 (base case - a single smoke detector in the entrance).

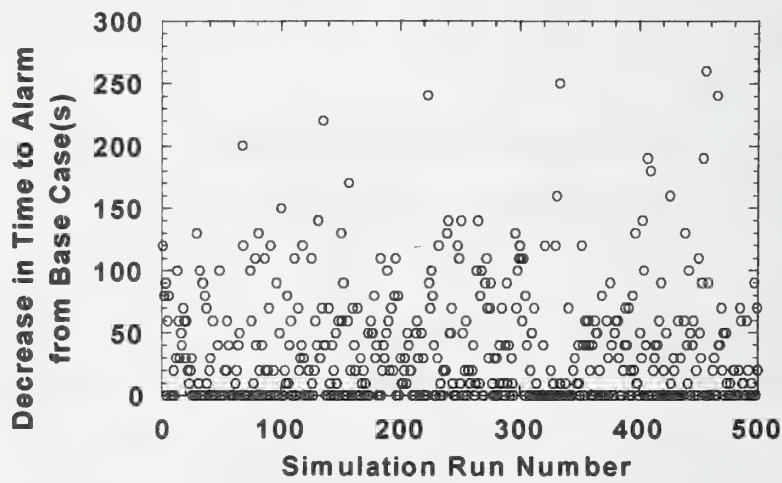


Figure 6. Decrease in time to alarm between CASE 2 (co-located smoke, CO, and temperature sensors in the entrance) and CASE 1 (base case).

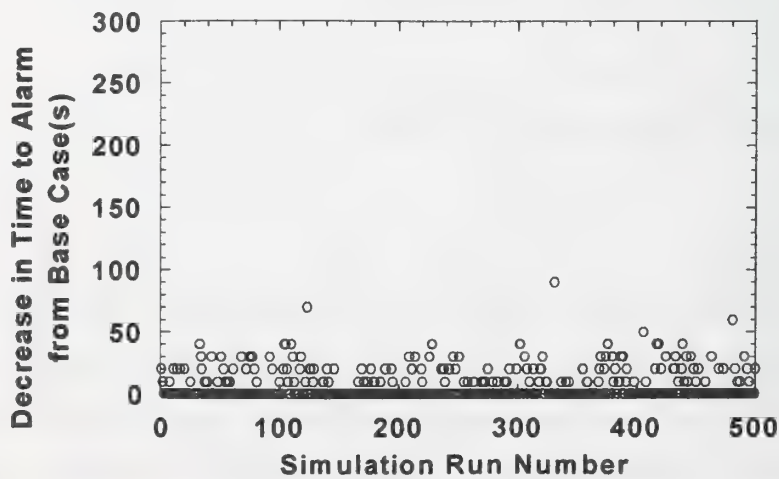


Figure 7. Decrease in time to alarm between CASE 3 (smoke, CO, and temperature sensors in entrance, kitchen, and bedroom respectively) and CASE 1 (base case).

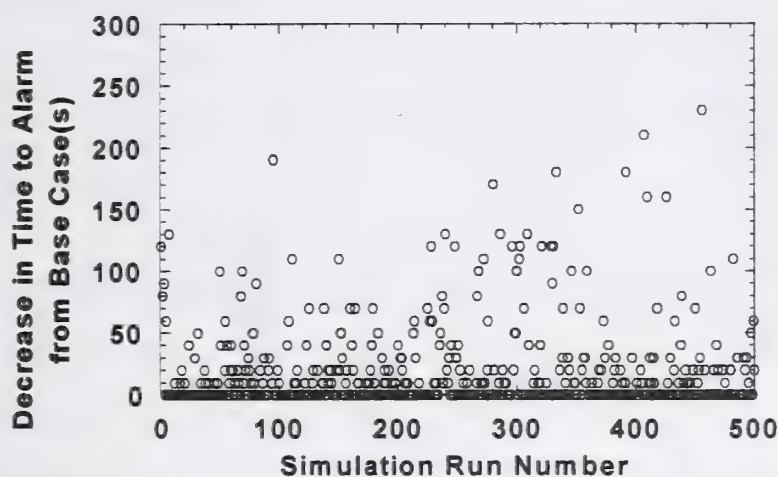


Figure 8. Decrease in time to alarm between CASE 4 (smoke, CO, and temperature sensors in the entrance, living room, and corridor respectively) and CASE 1 (base case).

sensor located in the bedroom, (CASE 3) performed only slightly better than the single smoke sensor CASE 1. The co-located sensor configuration, CASE 2, performed the best, on average, over all simulations.

Figures 9-11 show the decrease in alarm time from the base case (CASE 1) versus the rule that yielded the alarm in each simulation for CASES 2, 3 and 4 respectively. In Figure 9, notice that rule 2 (CO and smoke) was never first to yield an alarm in the co-located sensors configuration, and that significant reductions in alarm time were obtained with the temperature criterion (rule 4). Figures 10 and 11 show that rule 2 was first to yield an alarm a number of times in these distributed sensor configurations, though the decrease in time to alarm was less than 50 s for each time that rule was first.

The reason rule 2 was never the first to indicate alarm in Configuration 2, co-located sensors, is due to the selection of the CO and smoke yields used in the simulations. Smoke was always present in sufficient quantity to invoke rule 1 prior to CO volume fraction reaching the threshold in rule 2.

The preceding analysis considered only the reduction in alarm time for each fire scenario. A better metric would be to consider the life safety impact of the detection schemes. Here, a simple tenability criterion, a threshold upper-layer temperature in the room of (fire) origin, was used to compare the relative performance of the detection schemes. Two



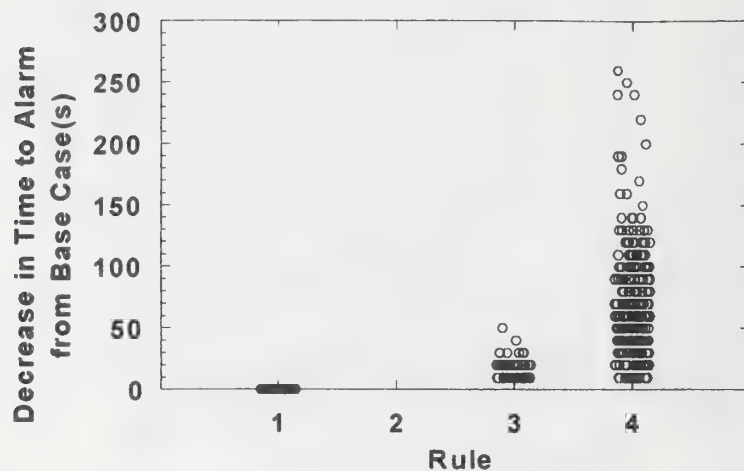


Figure 9. Decrease in base case time to alarm versus the rule indicated for CASE 2 - the co-located sensors in the entrance.

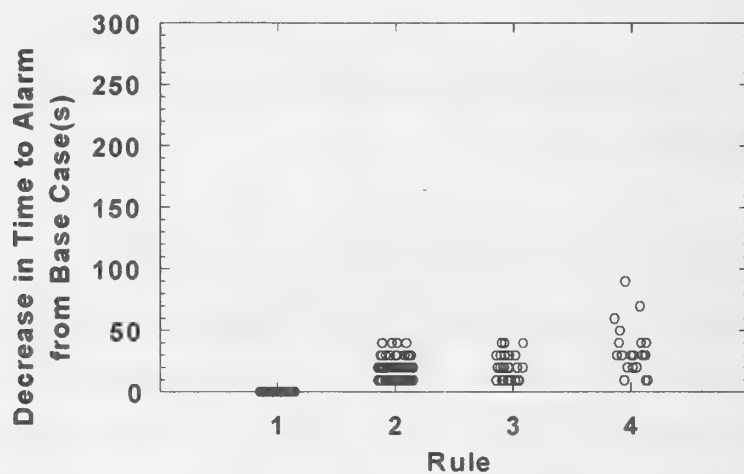


Figure 10. Decrease in base case time to alarm versus the rule indicated for CASE 3 - smoke, CO, and temperature sensors in the entrance, kitchen, and bedroom respectively.

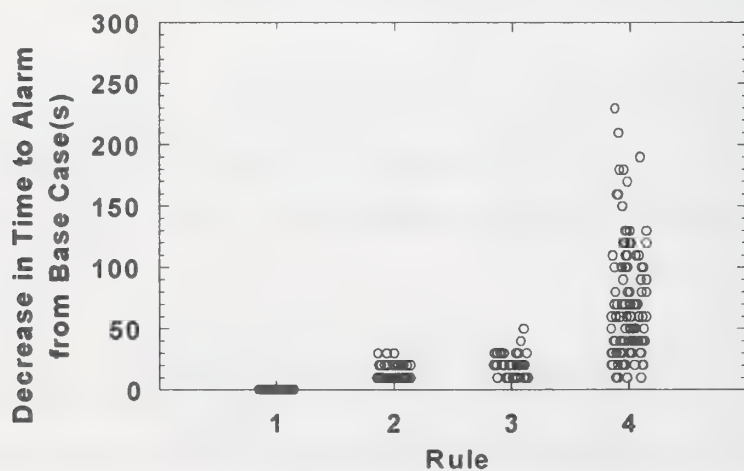


Figure 11. Decrease in base case time to alarm versus the rule indicated for CASE 4 - smoke, CO and temperature in the entrance, living room, and corridor respectively.

threshold upper-layer temperatures, 65 °C and 150 °C were specified as distinct limits indicating untenable conditions, with the lower value representing a more conservative criterion. A more complete hazard analysis would include multiple tenability criteria evaluated along egress paths.

Figures 12-15 show the difference between the time to reach the upper-layer threshold in the room of origin and the time to alarm for each simulation. A positive time difference represents the length of time after alarm but before a hazardous condition is reached in the room of origin, and conversely a negative time difference represents the length of time a hazardous condition exists in the room of origin before alarm. For both threshold temperatures all cases show positive and negative differences. The average difference over all simulation runs for each threshold and CASE is given in Table 1.

Threshold Temperature Criterion ( °C)	Average of T <sub>untenability</sub> - T <sub>alarm</sub> (s)			
	CASE 1	CASE 2	CASE 3	CASE 4
65	-2	35	5	19
150	61	98	67	81

Table 1. Average difference between time to reach threshold temperature in the room of origin and the time to alarm for all simulations.

For the 65 °C threshold, the base case average time difference was less than zero, meaning on average the room of origin reached hazardous conditions before alarm. For a 150 °C threshold, the base case average time difference increased to over a minute. For both threshold temperatures CASE 2, the co-located sensor configuration yielded the longest average time difference, 37 s longer on average than the base case. The next best was CASE 4, 20 s to 21 s longer on average than the base case. The distributed sensor configuration CASE 3 performed only slightly better than the base case. Maximizing the average time to escape hazardous conditions would be a goal of an optimized sensor configuration. Another constraint would be to reduce or eliminate negative time differences and increase small positive time differences between hazardous conditions and time to alarm (i.e., maximize the number of fire scenarios where an alarm allows for adequate escape from the hazard).

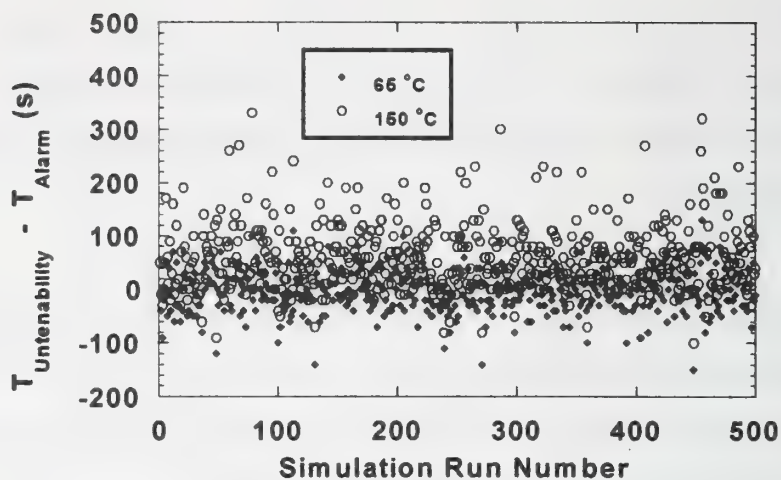


Figure 12. The difference between the time to untenable temperature in the room of origin and the time to alarm for CASE 1 (base case).

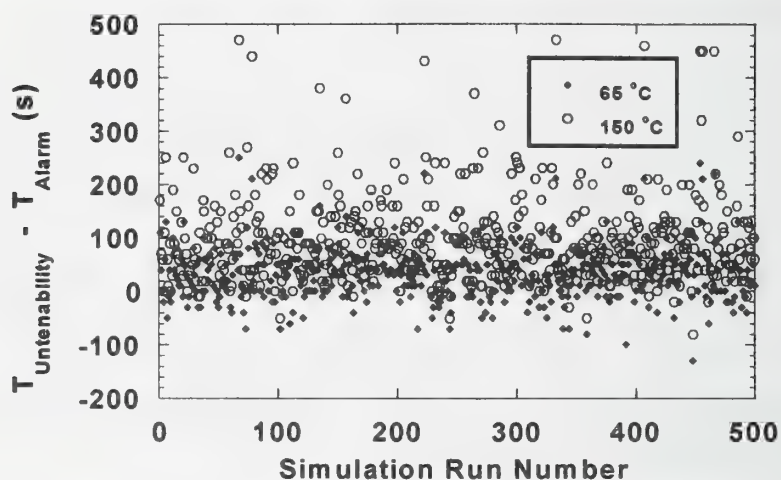


Figure 13. The difference between the time to untenable temperature in the room of origin and the time to alarm for CASE 2 (co-located sensors).

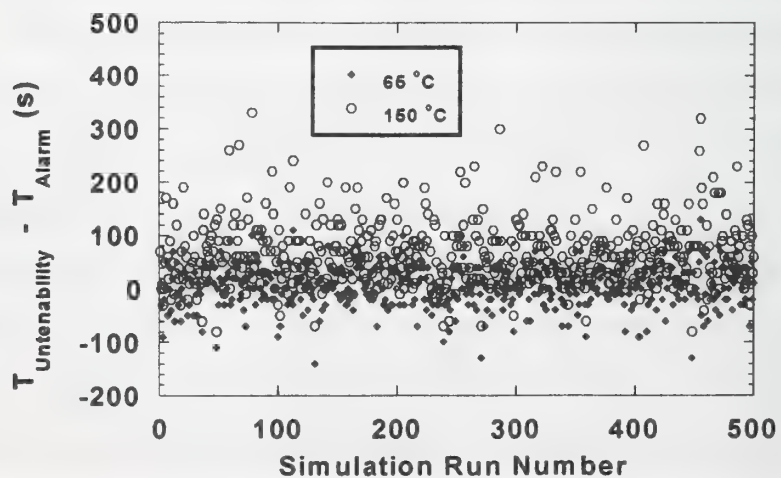


Figure 14. The difference between the time to untenable temperature in the room of origin and the time to alarm for CASE 3 (distributed sensors).



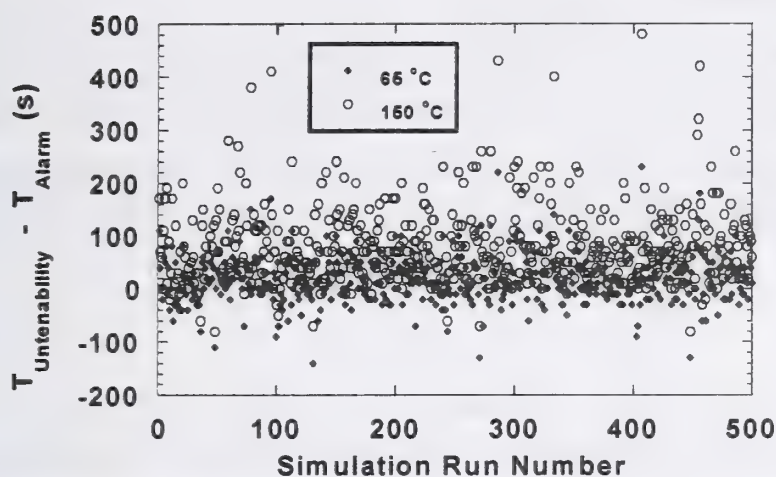


Figure 15. The difference between the time to untenable temperature in the room of origin and the time to alarm for CASE 4 (distributed sensors).

While the distributed sensor configurations did not perform as well as the co-located sensors configuration, the results were still encouraging. The rule base was not optimized for the distributed sensor configuration, nor were all three sensor/room combinations tried. Also, this set of simulations was skewed toward rapidly growing fires compared to fire sensitivity test fires developed for detectors (even a "slow"  $t^2$  fire reaches 29 kW in 100 s). Slower growing fires or smoldering fires would not have the rapid smoke and temperature rise associated with these simulated fires, and could produce higher CO yields. The fact that the apartment entrance was centrally located was particularly beneficial to the co-located sensor configuration.

## 5. Conclusions

From this modeling exercise and analysis, it is concluded the distributed sensing may improve time to alarm over single-station detectors, however, the location of sensors, their type, and the rules for processing multiple sensor signals need to be tailored for each specific application. More work is needed to develop simulation data that includes many more very slow growing fires with properties reflecting both smoldering and flaming conditions. Sensor environments obtained from simulations need to more closely follow actual temporal and spatial variations expected in real cases. With such data realistic sensor response models can be employed. Nuisance source simulation data is needed to assess the ability of sensor combinations and algorithms to reject nuisance alarms. HVAC flow needs to be included since it affects transport of combustion products. The most appropriate

models need to be selected and tested to assess their ability to produce "good" simulation data sets. If this research evolves to point where a rich set of statistically valid fire and non-fire simulations can be generated for given building configurations and occupancies, such data could be exploited by using it to develop and train distributed-sensor, pattern recognition algorithms for early fire detection.

## **6. References**

- [1] Notarianni, K. A., "The Role of Uncertainty in Improving Fire Protection Regulation," Ph.D. Thesis, Carnegie Mellon University, Pittsburgh, PA, May, 2000.
- [2] Jones, W. W., Forney, G.P., Peacock, R.D., and Reneke, P.A., "A Technical Reference for CFAST: An Engineering Tool for Estimating Fire and Smoke Transport," Tech. Note 1431, National Institute of Standards and Technology, Gaithersburg, MD, January, 2000.

Daniel T. Gottuk, Ph.D., P.E. and Lawrence A. McKenna, Jr.

Hughes Associates, Inc., Baltimore, Maryland USA

## **Spot And Aspirated Laser Smoke Detection In Telecommunications Facilities**

### **ABSTRACT**

Full-scale, in-situ comparison tests of spot and aspirated laser detection systems in an active telephone exchange were conducted to compare the response times of spot and aspirated smoke detection systems when exposed to a variety of smoke sources and ventilation conditions. The paper discusses the performance of multiple systems varying in detector type, detector spacing and detector locations (i.e., mounted on the ceiling versus on return air grills).

### **1.0 Introduction**

With the continuing advances in technology and the use of high value electrical equipment, the need for very early warning fire detection (VEWFD) has increased [1]. The increased use of VEWFD systems has resulted in more system options being available to the user. Currently, the two primary types of VEWFD systems are aspirated (air sampling) smoke detectors and laser-based spot-type smoke detectors. Also available are the standard photoelectric and ionization detectors set to very high sensitivities. Besides having several technologies to choose from, system designers must address the varying complexities of using these systems in diverse applications, such as semiconductor and telecommunication facilities, with little validation or test data.

Full-scale, in-situ comparison tests of spot and aspirated laser detection systems in an active telephone exchange were conducted to compare the response times of spot and aspirated laser smoke detection systems when exposed to a variety of smoke sources and ventilation conditions. The paper discusses the performance of multiple systems varying in detector type, detector spacing and detector locations (i.e., mounted on the



ceiling versus on return air grills). The work provides data intended to guide system designers in the selection and use of very early warning smoke detection systems.

## 2.0 Experiments

Reference 2 provides details of the experimental setup and procedure. The test space was one entire floor of a three-story building, 30.5 m (100 ft) wide, 54.9 m (180 ft) long ( $1672 \text{ m}^2$  ( $18,000 \text{ ft}^2$ )) 4.7 m (15.5 ft) high (Figure 1). The exchange was an active facility, which continued to operate throughout the course of the test program. The facility housed a DMS switching system, which covered approximately  $223 \text{ m}^2$  ( $2400 \text{ ft}^2$ ) of the south end of the building (designated the DMS equipment area), and a main frame and transmission equipment that covers approximately 30 percent of the remaining open floor space (designated the toll/frame area). Except for three small rooms on the periphery (total  $\sim 67.8 \text{ m}^2$  ( $730 \text{ ft}^2$ )) the test area was not subdivided, allowing free transport of gas/smoke throughout the entire space.

The test facility was maintained at normal conditions between  $22.2^\circ\text{C}$  and  $22.7^\circ\text{C}$  ( $72$  and  $73^\circ\text{F}$ ) and 45% relative humidity. Conditions in the test area were maintained via two independent ventilation systems: 1) a recirculation system with three pre-packaged fan/coil cooling units which served the DMS equipment area and 2) the general building HVAC which primarily served the larger toll/frame area. The layout of both systems is shown in Figure 2. The recirculation system serving the DMS equipment area consisted of three air conditioning units sharing a common discharge ductwork (AC1, AC-2, and AC-3 in Figure 2). This system provided the bulk of the airflow through the switch equipment. Compared to the toll/frame area, the airflow velocity in the DMS equipment area was high. Two ventilation conditions were investigated. The first condition consisted of all three recirculation units and the general HVAC unit operating (i.e., normal operation at  $12.2$  and  $5.9 \text{ m}^3/\text{s}$  ( $25844$  and  $12618 \text{ cfm}$ ), respectively). The second condition consisted of shutting down two of the three recirculation AC units in the DMS area yielding a supply flow rate of  $2.9 \text{ m}^3/\text{s}$  ( $6,224 \text{ cfm}$ ) from the remaining

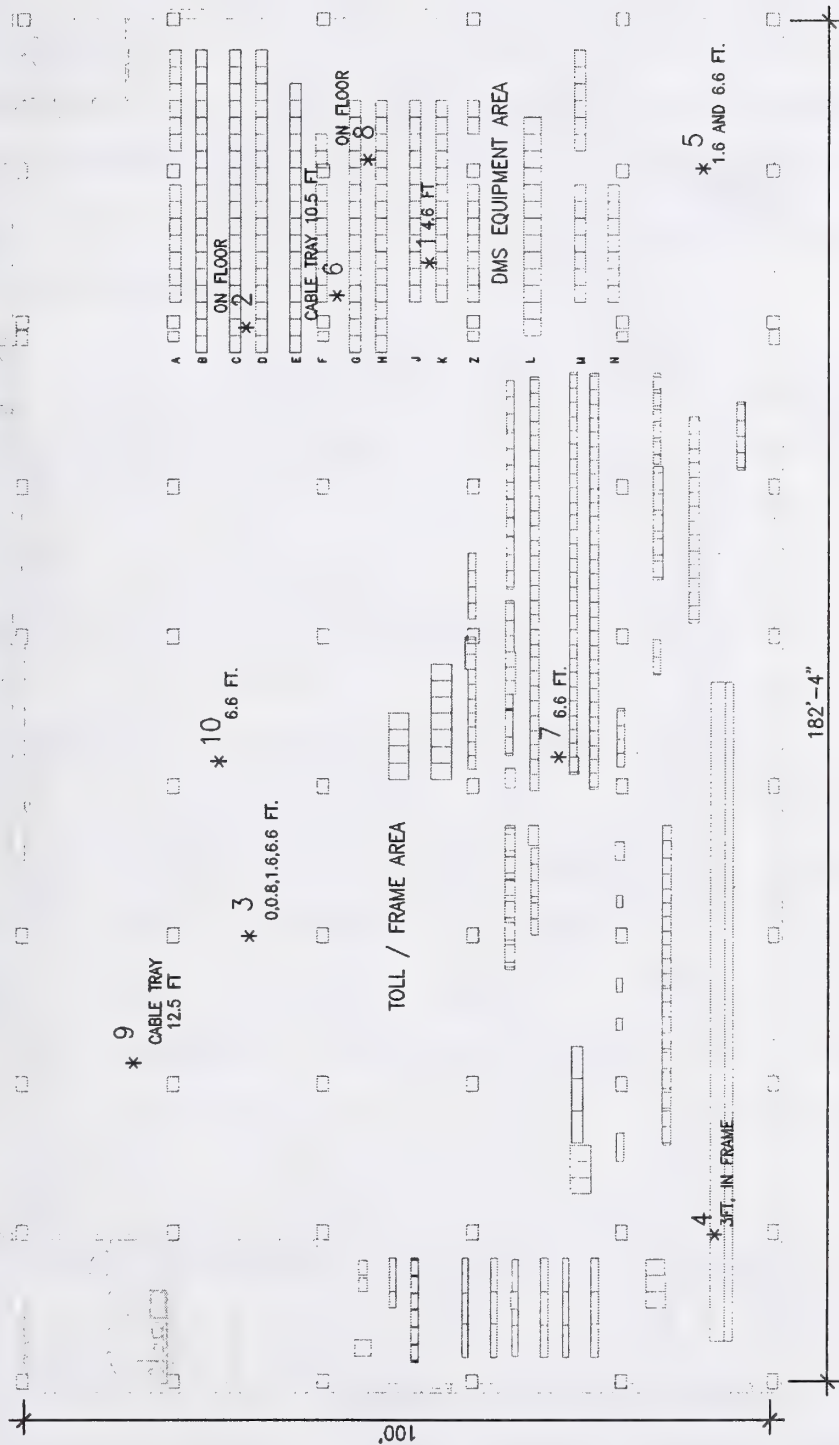


Figure 1 – Test Site with Smoke Source Locations and Equipment Layout

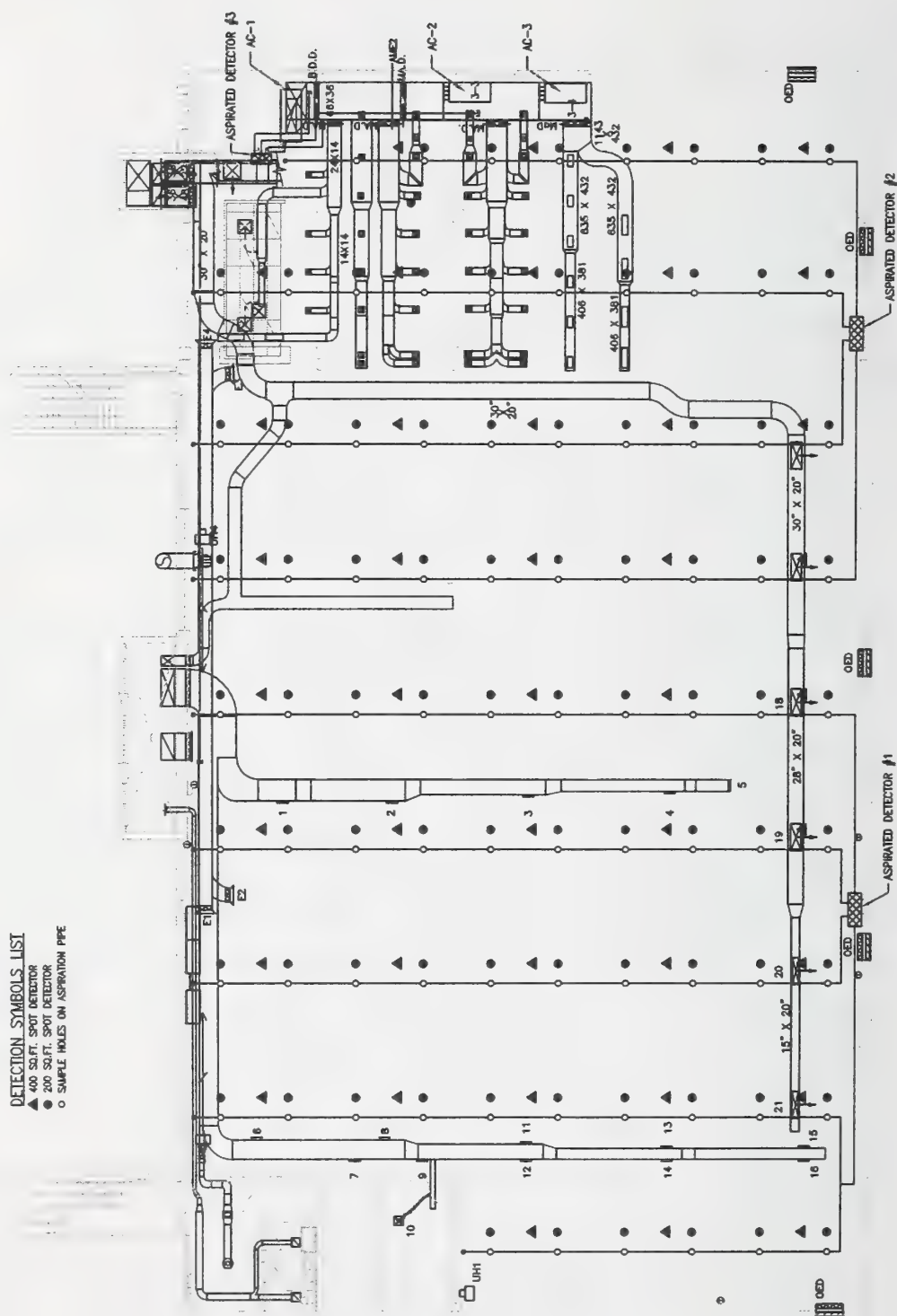


Figure 2 – Drawing of Device Locations and the Layout of the Ventilation Systems



AC unit (AC1) and the normal  $5.9 \text{ m}^3/\text{s}$  (12618 cfm) from the general HVAC supply. Two different types of commercially available laser based smoke detectors were evaluated in this test program: 1) spot type and 2) aspirated. Both types utilized the light scattering principal for smoke detection. The detector layouts were typical of that used in the telecommunication industry [3] and was driven by the  $6.1 \text{ m} \times 6.1 \text{ m}$  (20 ft x 20 ft) column spacing (bay) in the facility, which is typical of North American telecom buildings. Figure 2 shows the locations of the detection systems. All systems were designed and installed according to standard practices and commissioned by manufacturer authorized personnel.

The spot detection systems consisted of VIEW detectors (LPX-751) installed at ceiling level at both  $18.6 \text{ m}^2$  (200 sq ft) (hereinafter referred to as "200 SF") and  $37.2 \text{ m}^2$  (400 sq ft) (hereinafter referred to as "400 SF") spacing. Spot detectors were also mounted over the return grills of the ventilation systems (designated as Spot Returns). The 200 SF detectors covered regions  $3 \text{ m} \times 6 \text{ m}$  (10 ft by 20 ft). The 400 SF detectors covered areas that measured  $6 \times 6 \text{ m}$  (20 by 20 ft), corresponding to the coverage areas of the two closest 200 SF detectors. All of the detectors (including the aspiration system) were installed using four circuits and were monitored by two Notifier panels. The Notifier AFP-400 and AFP-300 control panels were programmed using the Veri•Fire 400™ Programming Utility, revision 3.51. VIEW detector sensitivity levels were fixed at the beginning of the test program to Pre-Alarm setting #4 (0.05 %/ft) and Alarm setting #3 (0.10 %/ft). The Cooperating Multi-Detector Sensing feature was enabled independently for the 200 SF and the 400 SF View systems using condition C, which involves two adjacent detectors. Alarm verification was not used.

The layout and installation of the air aspirated smoke detection systems were performed in conformance with current industry practice, as embodied in Reference 3. The aspirated systems consisted of three VESDA LaserPlus detectors installed to cover three regions of the test space: 1) the  $929 \text{ m}^2$  (10,000 ft<sup>2</sup>) of space at the north end of the space (toll/frame area); 2) the remaining  $743 \text{ m}^2$  (8,000 ft<sup>2</sup>) at the south end of the space (DMS equipment area); and 3) the return air inlets. The VESDA systems (1, 2 and 3) were numbered according to the designations described. The detector settings corresponded

to typical sensitivity levels used in telecommunication facilities: Alert was 0.0125 %/ft, Action was 0.022 %/ft, and Fire1 was 0.03 %/ft. No delay settings were used.

Five smoke sources were evaluated in this study, based on an understanding of past fire incidents in the targeted occupancies (telecommunications and data processing) as well as an understanding of the equipment and materials used in these occupancies that may become either the source of ignition energy, or first fuels for a fire [4-8]. The smoke sources consisted of the following:

1. Overheat of BSI 6266 wire samples,
2. Overheat of Bell Canada wire samples,
3. Mixture of potassium chlorate and lactose (BSI 6266 test [7]),
4. Internal printed wire board (PWB) failure [8], and
5. Conductive heating test of an EPDM insulated cable [8].

The smoke sources were evaluated at ten different locations throughout the test facility, as well as at various heights (e.g., floor level, 2 m (6.6 ft) and 3.8 m (12.5 ft) high). Figure 1 shows the smoke source locations. Some source locations were selected to specifically evaluate the effect of various ventilation conditions (e.g., high airflow in the DMS and relatively still air zones) and geometric considerations (e.g., obstructions due to duct work or cable trays). Three locations (7, 9 and 10) were randomly selected.

### **3.0 Results And Analysis**

In total, fifty-six (56) tests were conducted, encompassing variations in source type, source location, and ventilation conditions. Nineteen (19) BSI wire tests were conducted, ten (10) Bell wire tests, twenty (20) chlorate/lactose tests, five (5) PWB tests, and two (2) conductive heating tests. In thirteen of the tests, the smoke sources were either of such small size and duration or in a hard to detect location that no system reached a detection threshold. Of the remaining 43 tests in which at least one system reached a detection threshold, various analyses were conducted to compare the response performance of the different detection systems evaluated.

The analyses of response times was conducted based on two criteria. The first criterion is the time of first response. This time refers to the first time at which any detector within a system reaches any prealarm or alarm criteria. For the aspirated detectors, alarm condition "Alert" was always first even if "Fire1" was attained during the test. Spot detection systems sometimes transitioned directly from normal conditions to "Alarm" without signaling a "Prealarm" condition first. The time of first response criterion provides data from which one can assess the earliest possible notification provided by a detection system in response to a smoke source.

The second criterion used for evaluating system performance was the time to full alarm, either "Alarm" for the spot or "Fire1" for the aspirated systems. Depending on the end user and the particular facility application, an alarm condition may be the significant criteria for evaluating a detection system. As the results show, comparison of detection systems based on the two evaluation criteria can vary with respect to which system provides faster or more complete detection capabilities.

Results were evaluated for five different systems, defined as follows: (a) 200 SF Spot, (b) 400 SF Spot, (c) Spot Returns, (d) Aspirated Ceiling (1 and 2), and (e) Aspirated Returns (3). Using these five systems allowed results of key components of both the spot-type and the aspirated detection systems to be evaluated. Current practices would dictate that a ceiling mounted spot-type detection system (200 SF or 400 SF) would be the primary alternative to the AT&T specification of an aspirated system installed at the ceiling and at air return grills (i.e., full aspirated system 1, 2 and 3). The above system categories allow for such comparisons to be made while also evaluating other combinations, such as the benefits of including spot or aspirated detection at the air returns.

An example of results for selected system comparisons have been summarized below. Table 1 shows a summary of the comparisons between the 200 SF Spot system and the full Aspiration (1, 2, and 3) system based on time to first response and time to alarm results. The "Total Number of Tests" reported in the table represents the number of tests in which at least one of the systems being compared responded according to the



criterion being evaluated. As can be seen in Table 1, the 200 SF Spot system responded to more sources when evaluated according to either the time to first response or time to alarm criterion. The table also shows the number of tests in which each system responded faster than the other. The Aspirated (1, 2, and 3) system was first to respond in more tests (26 v. 17) than the 200 SF Spot system when compared according to the time to first response, but the 200 SF Spot system alarmed first in more tests (19 v. 13) when evaluated according to the time to alarm. For most system comparisons, excluding the cases in which one system did not respond, the difference in response times were generally within one to two minutes. Table 2 presents a similar summary of the comparisons between the 400 SF Spot system and the full Aspiration (1, 2, and 3)

**Table 1 – Comparison of First Response and Alarm Results for the 200 SF Spot and the Aspirated (Zones 1, 2, & 3) Detection Systems.**

FIRST RESPONSE	
Total Number of Tests Where System Achieved Either Pre-Alarm or Alarm	43
Number of times Aspirated system responded	34
Number of times 200 SF Spot system responded	40
Number of times Aspirated system responded first	26
Number of times 200 SF Spot system responded first	17
ALARM	
Total Number of Tests Where System Reached Alarm	32
Number of times Aspirated system alarmed	19
Number of times 200 SF Spot system alarmed	29
Number of times Aspirated system alarmed first	13
Number of times 200 SF Spot system alarmed first	19

**Table 2 – Comparison of First Response and Alarm Results for the 400 SF Spot and the Aspirated (Zones 1, 2, & 3) Detection Systems.**

FIRST RESPONSE	
Total Number of Tests Where System Achieved Either Pre-Alarm or Alarm	39
Number of times Aspirated system responded	34
Number of times 400 SF Spot system responded	31
Number of times Aspirated system responded first	28
Number of times 400 SF Spot system responded first	11
ALARM	
Total Number of Tests Where System Reached Alarm	24
Number of times Aspirated system alarmed	19
Number of times 400 SF Spot system alarmed	15
Number of times Aspirated system alarmed first	17
Number of times 400 SF Spot system alarmed first	7

system. Several observations regarding system response relative to smoke source type

and location can be made based on the test results. The aspirated detection systems (both ceiling and return detectors) were unable to detect most of the BSI wire tests. Considering all three aspirated detectors, only 6 of 19 BSI wire tests were detected. In comparison, the 200 SF Spot system responded in 13 tests and the 400 SF Spot system responded in 8 tests. All detection systems were unable to detect a majority of the Bell wire tests. Evaluating the detector responses when sorted per source location revealed that smoke from source Location 4 (the frame, which consists of horizontal racks of wire) was not detectable by either the spot or the aspirated return detectors. Except primarily for one PWB test, smoke from Location 9 was not detected by any of the systems. Location 9 was in the toll/Frame area on top of a cable tray and subject to high airflows.

Based on the criteria of time to full alarm, few alarm conditions were reached by any detection system for the Bell wire tests (4 of 10 tests). The Spot Return detectors reached alarm conditions in only 5 of all 53 tests reported. The Aspirated system (1, 2 and 3) and the 400 SF Spot system only reached alarm level in 3 of the 19 BSI wire tests. The 200 SF Spot system alarmed in 10 BSI wire tests.

A review of the response times showed that there is considerable variability in the alarm times from a given detection system due to changes in source type and location. Even for tests in which conditions were nominally the same, response times varied by up to a minute. For example, four lactose/chlorate tests were conducted in the same location with no changes in ventilation. The 200 SF Spot system and the ceiling and return aspirated systems had times to first response that varied by up to 48 to 72 seconds between tests. On a percentage basis with respect to the times to respond, these time differences represent roughly 30 to 70 percent variability. These differences may be partially attributable to the way in which the lactose/chlorate burned, but they also illustrate the variability that can be obtained due to subtle and imperceptible differences in events, such as ventilation conditions.

## 4.0 Conclusions

Based on the analyses of the detection system response times, the following conclusions were reached:

1. The 200 SF Spot detection system (ceiling mounted detectors) and the full Aspiration (1, 2 and 3) system (ceiling and return air grills) performed comparably. Each system demonstrated relative performance advantages depending on the criteria of performance. Considering the time to first response, the Aspiration system responded sooner in a majority of tests (26 v. 17); however, the 200 SF Spot system detected a greater number of sources (40 v. 34). Based on the time to alarm results, the 200 SF Spot system provided more responses (29 v. 19) than the aspiration system. The spot detection system also alarmed first in more tests (19 v. 13). Even though neither system was clearly superior in response time compared to the other, due to the high sensitivity of these systems, it is expected that they respond faster and to more incipient fires than conventional, standard sensitivity smoke detection systems.
2. The 400 SF Spot system provided a decreased level of performance (i.e., ability to detect the smoke sources and reach alarm points) compared to the 200 SF Spot system. Consequently, the performance of the 400 SF Spot system was also not as good as that of the full Aspirated (1, 2 and 3) system. However, the performance of the 400 SF Spot and the Ceiling Aspirated (1 and 2) systems were more comparable. Comparing the 400 SF Spot versus the full Aspiration (1, 2 and 3) system, the Aspirated system was able to respond (34 v. 31) and alarm (19 v. 15) to more fires than the 400 SF Spot system. Similarly, the full Aspirated system responded faster than the 400 SF Spot system when evaluated according to either the time to first response or time to alarm criterion (28 v. 11 and 17 v. 7, respectively).

The Ceiling Aspirated and the 400 SF Spot systems detected approximately the same number of sources when evaluated according to either the time to first response (31 v. 31) or time to alarm criterion (14 v. 15). The Ceiling Aspirated system typically responded and alarmed first (26 v. 11 and 13 v. 8, respectively),



typically ranging from 2 to 80 seconds faster than the 400 SF Spot system. The time difference was less than 60 seconds for the majority of the tests. Depending on the facility and the end-user requirements, these time differences may not be considered significant for the incipient-type sources evaluated.

3. There was no clear performance difference between the spot detectors and the aspirated detectors used at the return grills in these tests. The Aspirated Returns system and the Spot Return detectors provide approximately the same capability to respond and alarm to a fire (25 v. 29 and 10 v. 7, respectively). Depending on the criterion used for evaluation (time to first response or time to alarm), both systems were shown to respond faster than the other.
4. The inclusion of the spot detectors at the return air grills with the 200 SF Spot ceiling system provided little improvement in detection performance compared to the 200 SF Spot ceiling system used alone. Considering the time to first response, the Spot Returns detected fewer tests (25 v. 40 out of 43) and were slower to respond in most tests (4 v. 39) than the 200 SF Spot system. Based on the time to alarm results, the Spot Returns system also provided fewer alarms (7 v. 29 out of 31) and alarmed slower in most tests (2 v. 29) than the 200 SF Spot system. The biggest contribution provided by the Return detectors was the detection of 3 additional fires that were not detected by the 200 SF system.
5. The Aspirated 3 detector installed at the air handler return grills provided a small increase in detection capability for the full Aspirated system (1, 2 and 3) compared to the Ceiling Aspirated (1 and 2) system used alone. Considering the time to first response, the Aspirated Returns system detected fewer tests (25 v. 31 out of 34) and were slower to respond in most tests (7 v. 27) than the Ceiling Aspirated system. Based on the time to alarm results, the Aspirated system at the air returns also provided fewer alarms (10 v. 14 out of 19) and alarmed slower in the majority of tests (7 v. 12) than the Ceiling Aspirated system. All of the five tests, in which the ceiling system did not alarm and the return system did, were at a single source location close to the air returns.

6. The results reported in this test series, with respect to the value of return air intake detection, are counter to general practices and recommendations in the telecommunications industry [1,3]. HVAC practices in the telecommunications industry vary with different airflow patterns and volumetric flow rates depending on the heat loads imposed by the telecommunications equipment present in the room and the design concept used. The differences observed in this study may be attributed to the fact that the general practices were based on studies in which the HVAC systems consisted of a single return point and higher airflow rates.

## 5.0 References

- [1] "Fire Prevention in Telecommunications Facilities," in *Network Reliability: A Report to the Nation, Compendium of Technical Papers*, Federal Communications Commission Network Reliability Council, published by National Engineering Consortium, Inc., Chicago, IL, June 1993.
- [2] Gottuk, D.T. and McKenna, L.A., "Spot and Aspirated Laser Smoke Detection in Telecommunication Facilities," submitted to *Fire Technology*, 2000.
- [3] AT&T Fire Safety Practice 760-630-307, *Engineering, Design, and Installation of Air Sampling Smoke Detection (ASSD) Systems for Telecommunications Equipment and Data Processing Applications*, Issue 1, AT&T Corporation, Basking Ridge, New Jersey, September 1995.
- [4] *Hinsdale Central Office Fire Final Report*, Joint Report of the State Fire Marshal and Illinois Commerce Commission Staff, Springfield, IL, March 1989.
- [5] Taylor, Kenneth T., "Temporarily Disconnected," *Fire Journal*, Vol. 83, No. 3 (May/June, 1989).
- [6] McKenna, Lawrence A. Jr., "Reconstruction of the Power Plant Fire at the Pacific Bell Central Office at 420 South Grand Avenue, Los Angeles, CA, March 15, 1994," AT&T Environmental & Safety Engineering Center, Basking Ridge, NJ, November 1994.
- [7] British Standards Institute standard BS 6266, "Code of Practice for Fire Protection for Electronic Data Processing Installations," 1992.
- [8] McKenna, Jr., Lawrence A., Daniel T. Gottuk, and Phillip J. DiNenno, "Extinguishment tests of Continuously Energized Class C Fires," *Halon Options Technical Working Conference*, 12-14 May 1998.

## Strategies for the development of detection algorithms

### 1. Introduction

Multi-sensor/Multi-criteria based fire detectors require far more complicated detection algorithms as compared to simple threshold detectors, which are still used as single sensor based fire detectors. Cheap and powerful microprocessors are available to carry out this task. They may be implemented in each detector or alternatively as a central processing unit to carry out the fire or no-fire decision for all measured values being transmitted from various sensor-groups of a fire detection system.

A combination of smoke- and heat-sensors is at present frequently used in fire detection systems. The discussions not only on this congress show that a threefold sensor combination using smoke, heat and a gas sensors (for example *CO*) might be used in the foreseeable future.

The advantage of such a threefold combination is obvious for the simple reason that a more reliable alarm decision is possible if it is based on the observation of different physical phenomena associated with a genuine fire.

The combination of smoke- and heat-sensors is advantageous in case of open flame fires but the heat sensor does not help if the important class of smoldering fires is considered. A combination of smoke- and *CO*-sensor, however, would be beneficial in the latter case.

At present there are still some important restrictions to be taken into consideration for the design of new detection algorithms of higher complexity.

1. They possibly require much more computational power for each sensor combination. For hundreds of sensors per line this may quickly exceed the available computational power of a central processing unit since part of it is reserved for other administrative tasks (line protocols, handling of displays etc.).
2. Manufacturers of fire detection systems are for good reasons not too eager to replace their tried, tested and reliable central processing units by completely new devices with more powerful processors because a complete redesign is extremely expensive! For this reason the available processing power as well as the "Random Access Memory" (RAM) resources are usually rather limited.
3. The test authorities in Europe insist to understand at least the principle design rules of a detection algorithm. This is important as far as the selection of the detection method is concerned to avoid problems which may occur later in the certification process.

For these reasons it is recommendable to pursue a certain strategy and to keep in mind the given restrictions during the early design phase of a new detection algorithm.



# 2. Binary signal detection.

## 2.1 Principle solution of the detection problem.

Figure 1 shows a block diagram of a multi-sensor based detector and figure 2 illustrates the mode of operation of the decision-block from figure 1.  $H_0$  denotes the so called

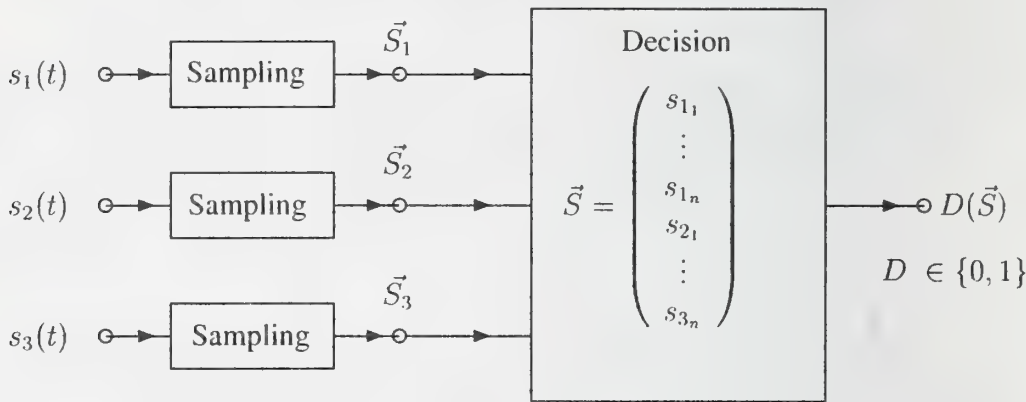


Figure 1: Block scheme of a multi-sensor based detector

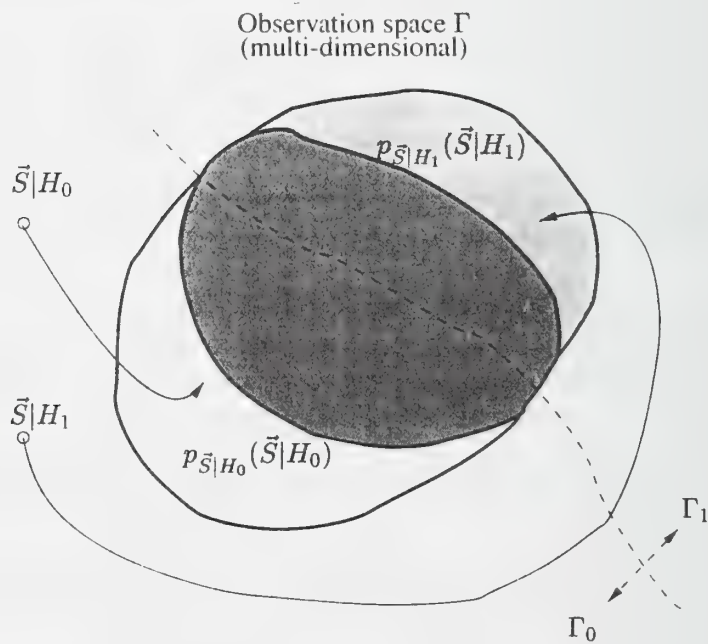


Figure 2: Observation space.

“zero-hypothesis”, i.e. the signals  $s_i(t)$  or signal vectors  $\vec{S}|H_0$  originate from no-fire situations. Correspondingly, hypothesis  $H_1$  denotes all signals  $s_i(t)$  or signal vectors  $\vec{S}|H_1$  originating from fire situations.

Each signal vector points to one specific location inside the multidimensional observation space, which is here schematically plotted as a two dimensional space.

In the aim to draw an unambiguous decision it is necessary to subdivide the observation space into two disjoint subspaces. This means:

if the signal vector points to the subspace  $\Gamma_1 \Rightarrow$  the decision is: alarm.

if the signal vector points to the subspace  $\Gamma_0 \Rightarrow$  the decision is: no-alarm.

Unfortunately, signal vectors  $\vec{S}|H_0$  and  $\vec{S}|H_1$  under either hypotheses may point to both subspaces  $\Gamma_0$  and  $\Gamma_1$ . Hence, we have not only two types of correct decisions but more-over two possible types of wrong decisions - a false alarm or a missed alarm.

*The most simple case:* threshold detector for one sensor. (Here the observation space is a one dimensional straight line.)

*Nearest more complicated case:* Two subsequently measured values from one sensor or one measured value from each of two sensors. (Here the observation space is a two dimensional plane.)

*and so forth:* one measured value from each of three sensors (with a three dimensional observation space.).

$n$  measured values from each of  $m$  sensors (requires a representation in a  $m \cdot n$  dimensional hyper-space).

The well known decision theory clearly states, how to divide the observation space into two disjoint subspaces taking into account certain optimization criteria. The "Bayes"-decision rule is as follows (see for example [1], [2]):

$$\Lambda(\vec{S}) = \frac{p_{\vec{S}|H_1}(\vec{S}|H_1)}{p_{\vec{S}|H_0}(\vec{S}|H_0)} \begin{matrix} H_1 \\ \geq \\ H_0 \end{matrix} \frac{q_0 \cdot K_\alpha}{q_1 \cdot K_\beta} = K \quad (1)$$

From the formula above follows that we need to know the conditional multivariate probability densities  $p_{\vec{S}|H_i}(\vec{S}|H_i) \quad \forall i \in \{0, 1\}$ . Unfortunately, these conditional probability densities are neither known nor determinable. Particularly, our knowledge concerning the signals of different sensors in no fire situations is very poor.

Intuitively, engineers would apply something similar to the above decision rule even if they have never heard of the "Bayes decision rule".

Consider for example a decision, which is based on one measured value from each of two sensors for smoke and  $CO$ -concentration. A reasonable subdivision of the total observation space could be chosen as shown in figure 3 where we have plotted a sequence of measured sample values  $s_1(t_i), s_2(t_i) \quad \forall i \in \{1, (1), n\}$  from a scattering light smoke sensor and a  $CO$ -measuring device which has been recorded during a TF2-smoldering-test-fire. Each pair of measured values is represented by one point in the  $s_1, s_2$ -plane.

Intuitively, an engineer would fix for example two threshold values  $sw_1, sw_2$  in such a way that all points in the plane which are above the thresholds indicate more likely a genuine fire than a no-fire situation and vice versa - according to the assumption of the engineer. This reasoning corresponds to the decision rule in eqn.(1) but there however, the conditional probability densities are assumed to be known and thus, the borderline between the subspaces would look quite different.

The "Bayes decision rule" moreover takes into account the probabilities of occurrence

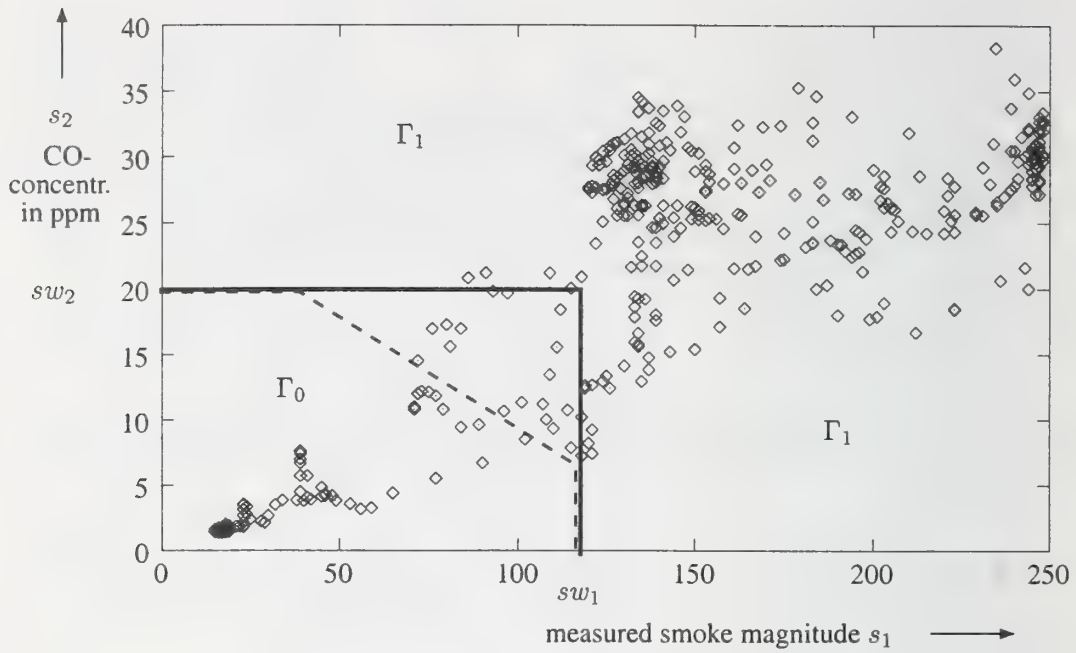


**Figure 3:** Intuitive selection of the subspaces  $\Gamma_0$  and  $\Gamma_1$ .

for fire- and no-fire situations ( $q_0$  and  $q_1$ ) and cost- or risk factors ( $K_\alpha$  and  $K_\beta$ ) assigned to correct or incorrect decisions.

Thus, the observation space is subdivided into two disjoint subspaces  $\Gamma_0$ ,  $\Gamma_1$  as indicated by the solid line in the plot of figure 3. The corresponding decision rule in mathematical terms is:

$$\text{if } ((s_1(t_i) > sw_1) \text{ or } (s_2(t_i) > sw_2)) \Rightarrow \text{alarm}, \quad (2)$$

which is a simple twofold threshold detector.

Slightly more complicated is a subdivision of the observation space as indicated by the dashed line in figure 3. This approach reflects the fact, that simultaneously existing smoke and  $CO$ -concentration indicates more likely a fire than solely the presence of smoke or  $CO$ -concentration. In this case it makes sense to trigger an alarm at lower magnitudes of both smoke and  $CO$ -concentration.

The corresponding decision rule in this case is as follows:

$$\text{if } ((s_1(t_i) > sw_1) \text{ or } (s_2(t_i) > sw_2) \text{ or } (s_1(t_i) + s_2(t_i) > sw_3)) \Rightarrow \text{alarm} \quad (3)$$

The joint evaluation of one sample from each of three sensors (like for example smoke, heat and  $CO$ -concentration) is more complicated because in this case it is necessary to fix a border-plane in the 3-dimensional space.

If we intend to include not only actual samples but also the last  $m$  sampled values of each of the  $n$  sensor signals then the confusing task is to find an adequate hyper-plane in an  $m \cdot n$  dimensional hyper-space. Thus, the task becomes more and more complicated with an increasing dimension of the observation vector and the question arises how to simplify the solution of the task.



## 2.2 Feature extraction methods

Feature extraction is a suitable method to simplify the decision problem considerably if we want to include the history of signals in our decision.

Feature extraction means to extract from each signal vector  $\vec{S}_j$ , consisting of  $n$  subsequently sampled values of the sensor signal, one (or a few) features  $m_{jk}$   $k \in \{1..l_j\}$  as shown schematically in figure 4.

Thus, we obtain a feature vector  $\vec{M}$  of dimension  $\sum_{j=1}^m \ell_j$ , which is considerably smaller than the dimension  $m \cdot n$  of the combined signal vectors. We can use the same decision method as previously described using the feature vector  $\vec{M}$ .

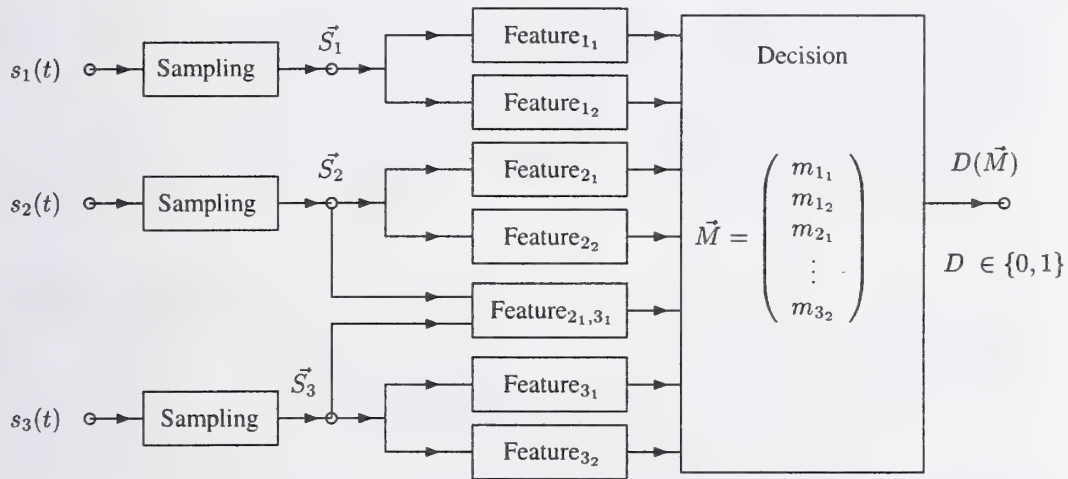


**Figure 4:** Schematic sketch of a detector with feature extraction.

Feature extraction is an important engineering task which requires to consider previously known individual characteristics of the sensors and their specific response in fire- and no-fire situations. Only a few examples are mentioned in the following:

- Determination of the average rate of rise.
- Suppression of the signal fluctuation which is considered to be irrelevant in no fire situations.
- Rate of rise limitation for sensor signals in those cases where step-like changes are unlikely to occur either physically or due to the features of the sensor (for example heat) but where step-like changes may occur due to data transmission errors or noise influence.
- Accumulation of signal amplitudes.
- Determination of significant spectral coefficients, if the signal fluctuation of sensors differs in fire- or no-fire situations.
- Joint evaluation of signal features from different sensors (correlation). e.t.c.

The few examples mentioned above show that feature extraction methods usually evaluate not only actual signal samples but include moreover the temporal development of signals. As an additional advantage we usually have a smaller variance of the features in comparison with the variance of the signals itself because features are calculated as some sort of average from several signal samples.

Feature extraction is applicable with more or less computational effort and storage-capacity efficient methods. One method to evaluate the temporal behaviour of signals is the so called “windowing”-method, i.e. feature extraction is based at each time instance with a new sample  $s_i(k)$  on the last  $n$ -samples (where  $k$  denotes a discrete time variable):

$$\vec{S}_i^T(k) = \{s_i(k), s_i(k-1), s_i(k-2), \dots, s_i(k-n+1)\}$$

If the next sample  $s_i(k+1)$  is drawn the eldest previously used sample  $s_i(k-n+1)$  is skipped and the new sample vector consists of the following components:

$$\vec{S}_i^T(k+1) = \{s_i(k+1), s_i(k), s_i(k-1), \dots, s_i(k-n+2)\}$$

Usually, we can find a recursive calculation from this vector for whatever feature to be calculated in the following form:

$$m_{ij}(\vec{S}_i^T(k+1)) = m_{ij}(\vec{S}_i^T(k)) + f[s_i(k+1), \overbrace{s_i(k), \dots, s_i(k-n+2)}^{\text{common components}}] - f[\underbrace{s_i(k), \dots, s_i(k-n+2)}_{\text{common components}}, s_i(k-n+1)] \quad (4)$$

Recursive calculations reduce the computational effort significantly but not the required storage capacity.

Since features are usually calculated as some sort of average on account of the random nature of the signals, the following alternative method is not only computationally efficient but saves moreover storage capacity.

$$m_{ij}(k) = a \cdot m_{ij}(k-1) + (1-a) \cdot f[s_i(k), s_i(k-1); \{s_j(k)\}] \text{ and } 0.9 < a < 1 \quad (5)$$

In this formula  $f(\cdot)$  denotes a so called “partial feature” which is calculated either from the actual sample  $s_i(k)$ , or from two subsequent samples of one sensor, or from one sample each of two sensors.

The updated feature  $m_{ij}(k)$  is calculated from its previous value  $m_{ij}(k-1)$  and the actually calculated partial feature  $f(\cdot)$ . This type of recursion is called “exponential windowing” and operates like a digital filter with  $RC$ -low-pass transfer-characteristic where the partial feature is the input signal and the output corresponds to the smoothed partial feature values. The denotation “exponential windowing” indicates, that the filter output corresponds to the sum of an exponentially weighted input sequence of the partial features with highest weight for the actual input and decreasing weights for previous partial features.

The constant  $a$  determines the 3dB-cut off frequency  $\omega_g$  of the low-pass characteristic or the “memory-depth” respectively.

$$\omega_g = -\frac{\ln(a)}{\Delta t} \quad \text{with } \Delta t, \text{ the sampling period.}$$

Apart from that, the use of integer or byte arithmetic saves storage capacity for random access variables as well as computation time because it is often possible to substitute multiplication- and division-operations by simple shift operations and integer or byte variables require less storage capacity by definition.

Although our electronic technology offers enormous processing power and giant storage capacity on one chip it seems to be important at present to regard the above mentioned aspects. The development of new control and indicating equipment with powerful central processors and large storage capacity requires time and enormous expenditures. But the use of tried and tested existing equipment with newly implemented detection algorithms sets hard limits with respect to storage capacity and computation time per detector.

A central processing unit in a fire detection system must carry out for example one decision/sec. based on feature extraction and preprocessing methods for hundredth of sensors or sensor combinations apart from various administrative tasks. For this reason only a few fractions of milliseconds remain as computation time for each sensor combination of a multi-sensor detector and the total amount of required RAM-storage capacity is proportional to the total number of detectors.

### 2.3 Automatic decision

The mode of operation of the decision-block in figure 1 or figure 4 we have already discussed in the previous section - i.e. the division of the observation- or feature-space into two disjoint subspaces. This task can be solved by two different approaches:

by a rule based decision                      or                      by a trained classifier.

For both of these methods there are various different realizations. Equations (2) and (3) represent without doubt simple rule based decisions. Clearly, the rule base becomes more complicated if more features are involved.

The advantage of a trained classifier is, that the designer does not need to think about various complicated rules for plenty of features because these rules are automatically determined during the training phase in a neural net for example. In other words the neural net automatically subdivides the multidimensional observation- or feature-space into the subspaces  $\Gamma_0$  and  $\Gamma_1$ .

Some proposals using neural nets as fire detectors are already to be found in the literature. For this reason it seems to be necessary to investigate the chances and shortcomings of this method - particularly, because there are software tools available which configure and train neural nets without any requirement for the user to understand much about the background.

## 3. Detectors with neural nets.

### 3.1 Realization of a neural net.

Each neuron has  $n + 1$  continuous valued inputs where  $n$  denotes either the total number of vector components of the input feature vector  $\vec{M}$  (or the signal vector  $\vec{S}$ ) which is applied to the input nodes or the number of neurons in the previous layer. Each neuron



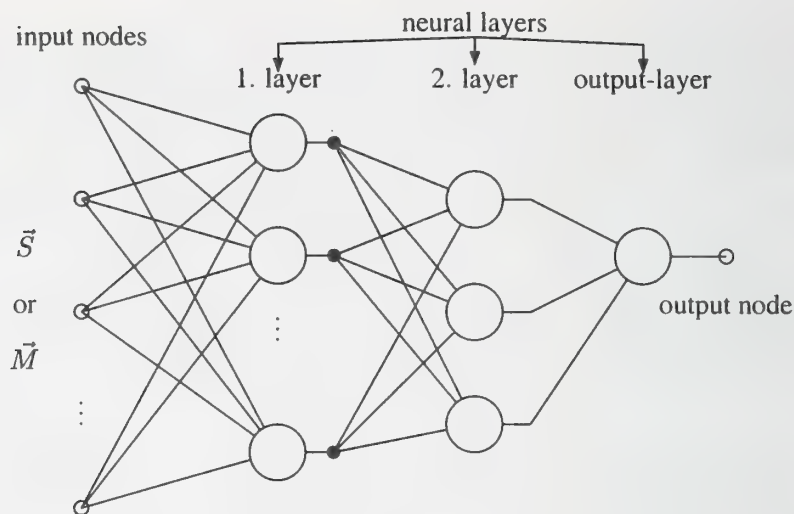


**Figure 5:** Sketch of a neural net.

computes a weighted sum of its input elements, subtracts a variable threshold and passes the result through a hard-limiting nonlinearity such that the output is between 0 and 1.

$$o_j(k) = \sigma \left( \sum_{i=0}^n w_{i,j} \cdot o_i(k-1) \right) \quad \text{with } o_0(k-1) = 1 \text{ and } o_i(0) = m_i \quad (6)$$

In the above formula  $k$  denotes the neural layer and the indices  $i, j$  the neurons in the  $k-1$ 'st and  $k$ 'th layer, respectively. The inputs of each neuron are weighted outputs (with weight  $w_{i,j}$ ) of the neurons of the previous layer (or the input node values). The nonlinearity  $\sigma(\dots)$  is of a "sigmoid type"; two representative examples of which are shown in figure 6.

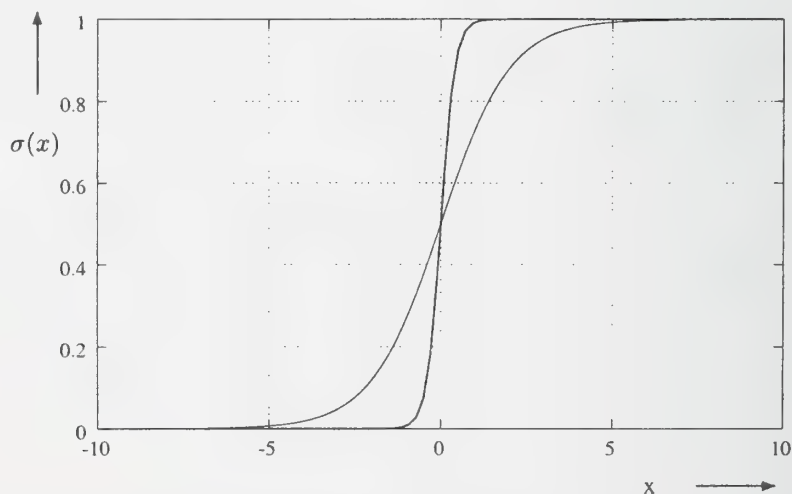


**Figure 6:** Hard-limiting nonlinearity of sigmoid type  $\sigma(x)$

A net as shown in figure 5 transforms the set of all input vectors to a set of output values in the range 0..1 with a more or less steep transition between 0 and 1. This corresponds nearly with the task to subdivide the observation space into two subspaces, i.e. to assign a value of 0  $\Rightarrow$  no-fire to all elements of a subset of the input vectors and a value of 1  $\Rightarrow$  alarm to the complementary subset of the input vectors.

If a binary decision (fire or no-fire) is required one neuron is sufficient in the output layer with its output values in the range 0..1. If we interpret the output values such, that for output values  $>0.5$  the probability for a fire is higher than for output values  $<0.5$ , we only need one additional threshold comparison to achieve an unambiguous decision.

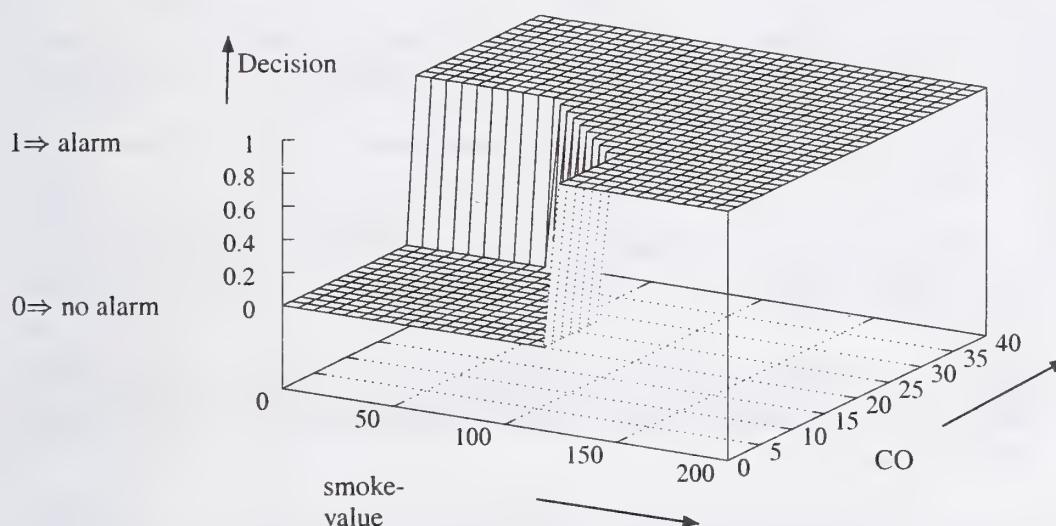


**Figure 7:** Decision function plotted above the observation space which corresponds to figure 3 or equation (3), respectively.

Thus, the output of a neural net defines an almost binary function above the observation space. For the simple example according to equation (3) and figure 3 the corresponding neural net output function is shown in figure 7. The precise modeling of this simple decision rule (equation (3)) requires 2 input nodes, 3 neurons in the first layer and 1 neuron in the second layer, which is the output layer in this case. Moreover, 9+4 weight factors are necessary which indicates the considerable effort. For this reason the rule-based solution is preferable in such simple cases.

### 3.2 Advantages and shortcomings of neural nets.

At first glance a neural net is attractive from the point of view that even in the case of observation- or feature-vectors of high dimension and perhaps confusing rules the neural net learns the underlying rules during a training phase. This requires to assign in advance the correct (or required) decision to any of the input vectors of the training set by a teacher.

All weights  $w_{i,j}$  are initialized by small random values. During the training phase the input vectors are randomly selected from the complete set and each corresponding output is calculated. From the difference between the calculated output and the required output all

weights in the net are updated (with the so called "error back-propagation algorithm" for example) such that **the mean square error** for all input vectors tends toward a minimum.

It has been shown that a trained neural net for certain assumptions classifies precisely according to the decision rule in equation (1) (see for example [3], p.14).

**The disadvantages are:**

1. the computational effort is enormous in comparison with other classifiers, not only during the training phase (which can be carried out off-line) but also during the classification phase,
2. the training procedure does not guarantee an optimal solution, i.e. the training phase must perhaps be repeated several times with different weight initializations,
3. only vague statements about the necessary number of neurons in different layers are possible,
4. the final classification performance depends very much on the correct selection of the observation vectors and even on the particular selection sequences during the training phase,
5. high partial errors may occur (while classifying single input vectors) although the mean square error indicates a good overall classification result. This might lead to false or missed alarms,
6. and last but not least - it is almost impossible to comprehend this classifying method in detail even if it works properly, because we do not know the classification rules after the training phase.

Some additional remarks concerning item 3 and the following:

**Item 3.:**

**3.1:  $n$ -neurons in the first layer and 1 neuron in the output layer  
(Two-Layer-Perceptron):**

Each neuron in the first layer subdivides the (2D)-observation space by a straight line, the (3D)-observation space by a plane and the ( $m$ D)-observation space by a hyper-plane, the inclination of which is determined by the corresponding weights  $w_{i,j}$ . With such a structure it is possible to separate open or simple enclosed regions in the observation space. The number of neurons in the first layer determine the details of the separated regions which are separated by polygons (see for example figure. 7 with 3 neurons in the first layer). The output neuron carries out some sort of logical OR operation which results in a final decision region that is the inclusion of all partial regions formed in the first layer.

This statement is true for sigmoid-nonlinearities with almost hard-limiting characteristic. For soft-limiting characteristics, the edges of the bounding polygons of the separated regions are smoothed.



### 3.2: Three neural layers with one neuron in the output layer (Three-Layer-Perceptron):

With a 3-layer structure it is possible to form arbitrary complex decision regions even with separated enclosed regions belonging to the same class.

Hence, more than 3 neuron layers are not necessary to solve an arbitrary complicated classification problem but it is not prohibited to use more than 3 layers.

#### Item 4.: The aggregate of observation vectors during the training phase.

One fundamental requirement to achieve a safe classification is, that the observation-vectors in the training set are representative for all possibly occurring fire situations and scattered over the whole observation-space during the learning phase, i.e. many **different** observation-vectors and their assigned class (fire or no-fire) must form the aggregate of the training set. Special attention must be paid to the subset of training vectors which cannot be assigned definitely to one or the other class or those vectors which point to approximately the same region in the observation space with contradictory meanings assigned by the teacher. The final classification of the trained network for contradictory training vectors is with higher probability in favour to those vectors, which appear more often in the training set with the same assigned meaning.

Contradictory training vectors can be avoided if the teacher observes the following rule in assigning the required class, which was already mentioned as part of the "Bayes"-decision rule in equation (1).

$$\text{Is } q_0 \cdot K_\alpha \begin{matrix} > \\ < \end{matrix} q_1 \cdot K_\beta ?$$

Here  $q_0$  denotes the probability of occurrence for such a vector during a no-fire situation and  $q_1 = 1 - q_0$  the probability of occurrence for a similar vector during a fire situation.  $K_\alpha$  and  $K_\beta$  are the corresponding cost-factors for wrong decisions; i.e.  $K_\alpha$  the cost-factor for a false alarm and  $K_\beta$  the cost-factor for a missed alarm.

The required class must be assigned to the hypothesis with the higher factor.

Moreover it is of importance to select the training-vectors at random and uniformly distributed from the complete training-vector aggregate.

#### Item 5.: Average classification-error and partial-errors.

The learning-progress during the training-phase is indicated by a decreasing mean square classification-error which is calculated according to the following sum:

$$\bar{F} = \frac{1}{N} \sum_{i=1}^N (o_{(i)} - t_{(i)})^2 \quad (7)$$

or, more simply, by a low-pass filtered sequence of the squared partial errors  $o_{(i)} - t_{(i)}$ . Here,  $N$  denotes the total number of training-vectors,  $o_{(i)}$  the classification value of the output neuron for the  $i$ -th training vector and  $t_{(i)}$  the corresponding correct or required output value assigned by the teacher.

$\bar{F} = 0$  can only be achieved after a sufficiently long training-phase if no conflicting vectors exist in the training-vector aggregate. Unfortunately, this does not hold for automatic

fire-detection problems otherwise false-alarms or missed alarms would not occur in practice. Consequently, the average classification error reduces during the training-phase and finally fluctuates around a minimum value  $>0$  and the learning phase is stopped if no more learning progress can be achieved.

Even if the average classification-error is sufficiently small, some partial errors may be high and thus lead to wrong classifications of the trained network in certain situations. Particularly, if the requirements mentioned in item 4 are neglected this may lead to missed alarms or unnecessary false alarms for 3-layer perceptrons with many neurons in the first and second layer.

For this reason a small mean square classification-error is not at all an adequate criterion. It is moreover urgently recommended to inspect closely all training-vectors with high partial-errors and their real classification after the training phase!

An adequate configuration of the neural net (number of layers and number of neurons per layer) may help to avoid such errors, though there is no other rule than: the least number of neurons and layers being sufficient and necessary to achieve a low mean square classification error.

Generally, neural nets are beyond doubt, powerful classifiers. Their use in automatic fire detection systems requires some caution, however, as shown by the remarks above - not to mention the problem of explaining with some plausibility their mode of operation to the authorities of a test institute for example.

#### **4. Test of new designed detection-algorithms.**

A performance test is an important part in the design process of a newly developed detection algorithm independent of the chosen type of detector. Personal computers in these days can be used as a powerful and rigorous test equipment. If the detection algorithm is software-implemented on the PC, it can be tested in time-lapse mode, using recorded data from fire-tests or, with artificially generated and randomly varied signal sequences for fire- and no-fire situations.

Though all manufacturers know the specific test procedures carried out by test institutes for certification, it is not recommendable to restrict the performance test to EN54-fires, for example, because in practice it is very unlikely that a fire develops according to EN54-conditions.

In our Institute, the sensor signals are recorded during the same test-fire from various sensor-heads, which are placed in different locations on the ceiling of the fire laboratory. Some of these locations are chosen arbitrarily unfavourable for detection purposes. Thus, the reproducibility conditions according to EN54 are usually not fulfilled for all sensor combinations but the recorded signals still represent fires to be detected.

Moreover, typical false alarm situations are either simulated or applied as recorded signals measured in more or less false alarm relevant environments.

We have already reported about a special test method which uses signal-models with stochastic variation of recorded signals (see for example: [4]). This method generates from a comparatively small set of recorded signals in fire- and no-fire situations arbitrarily many randomly varied test signals with similar characteristics (correlation features) than those of the recorded signals.

As a measure of quality, we compare the detection features of the newly designed algorithm either with a simple threshold detector or with the previously used detection algorithm of the manufacturer.

## Summary

After some introductory remarks concerning the chances and still existing restrictions in the development of improved multi-sensor-/multi-criteria detectors, the principle solution of a detection problem has been discussed.

The task becomes more and more complicated and confusing as more sensors and/or criteria are to be taken into consideration. It was shown that feature extraction simplifies the problem and the use of recursive methods reduces the necessary computational effort.

Special attention was paid to neural nets as classifiers with the principal advantage of learning even complicated rules automatically during a training phase with the aid of a teacher. But also the shortcomings and risks associated with neural nets as classifiers have been discussed.

The complexity of multi-sensor-/multi-criteria detectors requires careful performance tests. A few experimental tests with EN54-test fires are insufficient for a rigorous test in the opinion of the author.

Test methods using computer simulations with randomly varied test sequences for fire- and no-fire situations are proposed as an alternative.

## References

- [1] Bayes, Th.; *An Essay Towards Solving a Problem in the Doctrine of Chances*; Phil. Trans. 53, 370-418 (1764)<sup>1</sup>
- [2] van Trees, H.L.; *Detection, Estimation and Modulation Theory*; Part I; J. Wiley & Sons, New York 1968
- [3] Lippmann, R. P.; *An Introduction to Computing with Neural Nets*; IEEE ASSP Magazine, April 1987
- [4] Fischer, A., Müller, C.; *A simulation technique for the design of multi sensor based fire detection algorithms* ; Proceedings of the 10th International Conference on Automatic Fire Detection AUBE'95 in Duisburg, Germany; April 1995; ISBN 3-930911-46-9

---

<sup>1</sup>This 236 years old work of an english clergyman, who pondered about minimizing the gambling risk is until today the basis of decision theory!



Susan L. Rose-Pehrsson, Sean J. Hart, Thomas T. Street, Patricia A. Tatem,  
and Frederick W. Williams

Naval Research Laboratory, Chemistry Division, Washington DC

Mark H. Hammond

NOVA Research, Inc., Alexandria, Virginia

Daniel T. Gottuk, Mark T. Wright, Jennifer T. Wong

Hughes Associates, Inc., Baltimore, MD

### **Real-Time Probabilistic Neural Network Performance and Optimization for Fire Detection and Nuisance Alarm Rejection**

The U.S. Navy program, Damage Control-Automation for Reduced Manning is focused on enhancing automation of shipboard fire and damage control systems. A key element to this objective is the improvement of current fire detection systems. As in many applications, it is desirable to increase detection sensitivity, decrease the detection time and increase the reliability of the detection system through improved nuisance alarm immunity. The use of multi-criteria based detection technology offers the most promising means to achieve both improved sensitivity to real fires and reduced susceptibility to nuisance alarm sources. An early warning fire detection system is being developed by properly processing the output from sensors that measure different parameters of a developing fire or from analyzing multiple aspects of a given sensor output (e.g., rate of change as well as absolute value). The classification performance and speed of the probabilistic neural network deployed in real-time during recent field tests have been evaluated aboard the ex-USS SHADWELL, the Advanced Damage Control fire research platform of the Naval Research Laboratory.

The real-time performance is documented, and, as a result of optimization efforts, improvements in performance have been recognized. Early fire detection, while maintaining nuisance source immunity, has been demonstrated. A detailed examination of the PNN during fire testing has been undertaken. Using real data and simulated data, a variety of scenarios (taken from recent field experiences) have been used or recreated for the purpose of understanding potential failure modes of the PNN in this application.

## **1. Introduction**

The U.S. Navy program, Damage Control-Automation for Reduced Manning (DC-ARM) is focused on enhancing automation of shipboard fire and damage control systems. Improvement of current fire detection systems is a key element of the program. Increased detection sensitivity, decreased detection time and increased reliability of the detection system through improved nuisance alarm immunity are desired. The use of multi-criteria based detection technology [1] offers the most promising means to achieve both improved sensitivity to real fires and reduced susceptibility to nuisance alarm sources. A multi-year effort to develop an early warning fire detection system is currently underway. The system being developed uses the output from sensors that measure different parameters of a developing fire and a neural network for fire recognition. Two test series were conducted on the ex-USS SHADWELL [2] to evaluate and optimize candidate prototypes of the early warning fire detection system (EWFD). A third test series was used to validate the optimized system.

Improved fire recognition and low false alarm rates were observed using data from full-scale laboratory tests [3,4,5]. Several different sensor combinations were identified for use with a probabilistic neural network (PNN). Full-scale shipboard tests were conducted on the ex-USS SHADWELL to further develop detection algorithms and to expand the

fire/nuisance source database [6,7]. Using these two data sets, two candidate suites of sensors were identified for prototype development. Test Series 1 tested the real-time responses of the prototypes [8,9]. Two months later, under different environmental conditions, the optimized prototypes were tested with more fire and nuisance sources in Test Series 2 [10]. Test Series 1 and 2 were used to optimize the prototype, which was then evaluated in Test Series 3 [11,12].

Two data sets (laboratory and shipboard tests) served as the basis for a comprehensive PNN training data set used for the subsequent real-time applications. The classification of fire and nuisance events and the alarm speed were used to determine the performance of the multi-criteria fire detection system in the test series. The EWFD system with the PNN developed for real-time detection demonstrated improved classification performance as well as faster response times to fires compared to commercial smoke detectors. Some problems with the real-time implementation of the algorithm were identified and have been addressed. Using a variety of methods for speed and classification improvements, the PNN has been extensively tested and modified accordingly. As a result of these optimization efforts, significant improvements in performance have been recognized. The best classification performance observed for Test Series 1 and 2, while maintaining a fast detection speed, was observed with a sensor array consisting of ionization (ION), photoelectric (Photo), carbon monoxide (CO), and carbon dioxide (CO<sub>2</sub>) [11].

This paper describes the results of Test Series 3 for the ION, Photo, CO, and CO<sub>2</sub> sensors using magnitude and slope information, and background subtraction. A fire classification probability of 0.75 was used in Test Series 1 and 2 as the alarm threshold. The use of higher probability alarm thresholds has resulted in improved nuisance source rejection while still maintaining fast fire detection. The best probability cut off to maximize



detection and minimize false alarms was investigated. Finally, detailed examination of potential PNN failures during fire testing has been undertaken. Using real data and simulated data, several scenarios have been used or recreated for the purpose of understanding the potential failure modes of the PNN in this application.

## **2. Experimental**

The tests consisted of different fire scenarios and several different nuisance sources. In general, incipient size sources were used to challenge the detection limits of the commercial smoke detectors and to establish the minimum detection capability of new multi-criteria detection algorithms. The shipboard tests presented in this study were conducted on the second deck of the ex-USS SHADWELL in a space with a volume of approximately 144 m<sup>3</sup>. The sensors were mounted on the ceiling, 2.9 m above the deck. All of the sensors operated via gas diffusion to the unit. The fires were typically located about 4.3 m from the sensors and the nuisance sources were 1.5 m from the sensors. The heights of each source above the floor were selected to be representative of actual shipboard conditions.

All sensors were hard-wired to a National Instruments/LabVIEW data acquisition system that was used to acquire data and execute the PNN alarm algorithm in real time, save the data, and display the data. During tests, the data acquisition/processing system was synchronized in time with the commercial-off-the-shelf (COTS) Simplex smoke detection system currently installed on the ship. The shipboard system consisted of ionization detectors (Model 4098-9717) and photoelectric detectors (Model 4098-9714) monitored with a single alarm panel (Model 4020). The alarm sensitivity of these detectors was 4.2% obs/m for ionization and 8% obs/m for photoelectric. A more detailed explanation of the data acquisition system can be found in other reports [8,10,12].

The PNN analysis of sensor data included pre-processing, pattern calculation and scaling. The vector of input sensor responses, one number for each sensor in the array, comprises the set of data that is passed to the algorithm for pre-processing and PNN analysis during real-time deployment. All sensor measurements were background subtracted (i.e., values were evaluated as a change from an ambient baseline value). Data were collected every 2 seconds. The pattern magnitudes and slopes were computed and then autoscaled (mean zero and unit variance) using the means and standard deviations derived from the training set. The resulting scaled pattern was then submitted to the PNN algorithm for event classification (fire and nuisance) and determination of the probability of a fire event. The training set for the PNN consisted of 140 background subtracted response patterns generated in previous laboratory and shipboard tests. The training set data were compared at discrete times corresponding to the 1.63% obs/m alarm setting of a commercial photoelectric detector. This method of comparing signatures at particular alarm times provides a means of identifying parameters with respect to a practical benchmark. However, it also has the drawback of identifying signatures at a singular point in time, therefore, potentially missing key signature patterns.

Algorithm development and optimization was executed on a PC using routines written in MATLAB, version 5.2 (Mathworks, Inc., Natick, MA). Many of the routines were implemented using the PLS\_toolbox, version 2.0c (Eigenvector Technologies, Inc., Manson, WA). The classifier used in this study is a Probabilistic Neural Network (PNN) [13] that was developed at the Naval Research Laboratory for chemical sensor arrays [14]. Originally introduced to the neural network literature by Donald Specht in the 1980's, the PNN is a nonlinear, nonparametric classification algorithm that has been described as the neural network implementation of kernel discriminant analysis [15,16,17]. The PNN operates by defining a

probability density function (PDF) for each data class based on the training set data and the optimized kernel width parameter. The PDF defines the boundaries for each data class. For classifying new events, the PDF is used to estimate the probability that the new pattern belongs to each data class. The output probability can be used as a level of confidence in the classification decision, which can serve as a guide to reducing nuisance alarms. An improved PNN algorithm for chemical sensor array classification has also been developed at the NRL for use in real-time sensor systems [18].

### **3. Results and Discussion**

Test Series 3 was used to test a revised prototype that utilized four sensors: ION, Photo, CO, and CO<sub>2</sub> as described in Table 1. Thirty-nine tests were conducted that consisted of fire/nuisance sources used during previous tests as well as several new sources.

The detection rate of the PNN verses the false alarm rate is shown in Figure 1 for each probability cut off. If the probability of fire is required to reach 100%, then the false alarm rate is zero, but only 60% of the incipient fires generated in this test series are detected. As the probability cut off is reduced, the false alarm rate increases. At a probability cut off of 85%, 78% of the fires are detected and less than 20% of the nuisance sources are improperly classified. Both replicates of cutting steel with a torch were the only nuisance sources incorrectly classified. An alarm threshold of 85% provides a fire detection rate similar to both the COTS Photo and the combination of Photo and ION. When the COTS Photo and ION sensors are combined with an "OR" logic statement, the fire detection rate is better than either sensor used individually, however, the false alarm rate is also increased. The multi-criteria approach used here with the PNN classifier has a detection rate similar to the Photo+ION combination and a lower false alarm rate.



Table 1. Details of Prototype Fire Detectors.

No.	Component	Instrument Model No.	Manufacturer
1	Ionization smoke detector	1251 with base no. B501	System Sensor
2	Photoelectric smoke detector	2251 with base no. B501	System Sensor
3	Carbon monoxide (CO) 0-100 ppm	TB7F-1A	City Technology
6	Carbon dioxide (CO <sub>2</sub> ) 0-5000 ppm	2001V (EWFD1 and 2 only), 8002W Ventostat	Telaire/Engelhardt

The classification performance of the three EWFD prototypes is presented in Table 2. Each detector is presented as the number of tests correctly classified with respect to each of five categories; Overall, Total Fires, Flaming Fires, Smoldering Fires, and Nuisances. It should be noted that the overall and fire classifications are not 100 % for any detector because some of the fires were of such small size and duration (e.g., smoldering wire samples) that the detectors did not alarm. The EWFD system performed better than the COTS smoke detectors. The EWFD correctly classified more events than the COTS detectors in both flaming fires and nuisance source rejection. The EWFD performance to smoldering fires was not as good as the COTS Photo responses. The Photo+ION combination provides equivalent fire detection to the EWFD, but the nuisance alarm rate is poor. These results indicate that the PNN algorithm with the CO and CO<sub>2</sub> signatures provide improved detection performance than can be achieved by co-locating ionization and photoelectric smoke detectors. The EWFD system is faster than the COTS detectors for smoldering fires and is similar to the COTS ION for flaming fires.

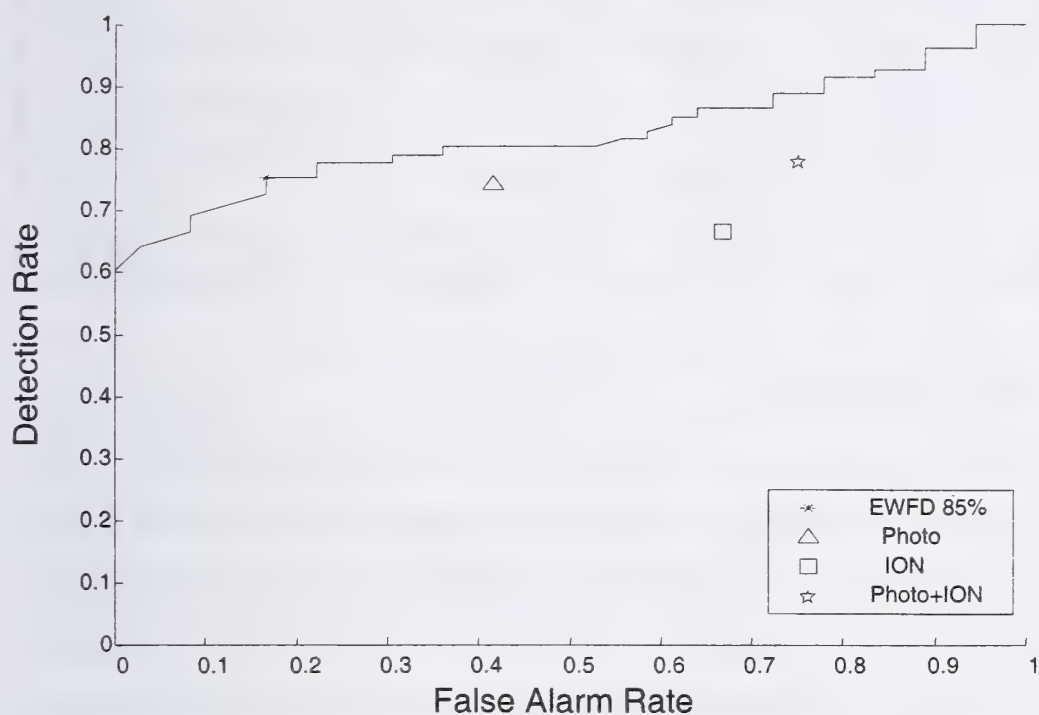


Figure 1. A Receiver Operator Curve (ROC Plot) showing the detection rate and false alarm rate for each PNN probability cut off. The 85% cut off level for the EWFD (\*) is compared to the detection rate and false alarm rate of the COTS Photo (•), COTS ION (□), and the combination Photo + ION (☆).

Table 2. Summary of Classification Performance of Test Series 3.

	Overall Total, % Correct (39)	Total Fires, % Correct (27)	Flaming Fires, % Correct (13)	Smolderin g Fires, % Correct (14)	Nuisance Sources, % Correct (12)
EWFD 1	79.5(31)	77.8(21)	100.0 (13)	57.1(8)	83.3(10)
EWFD 3	79.5 (31)	77.8 (21)	100.0 (13)	57.1 (8)	83.3 (10)
EWFD 5	76.9 (30)	74.1 (20)	100.0 (13)	50.0 (7)	83.3 (10)
COTS Ion	56.4 (22)	66.7 (18)	92.3 (12)	42.9 (6)	33.3 (4)
COTS Photo	69.2 (27)	74.1 (20)	84.6 (11)	64.3 (9)	58.3 (7)
Photo+ION	61.5(24)	77.8 (21)	92.3 (12)	64.3 (9)	25.0(3)

4. Failure Mode Simulations

A variety of simulations and tests were performed to evaluate several scenarios that could occur with a multi-sensor system and to elucidate PNN function, performance, and failure. Scenarios include increased noise on 1, 2, 3 channels while maintaining the integrity of the remaining channels, increasing the noise on all channels simultaneously, single sensor dropout (sensor value = 0), and single sensor erroneous values (values set to high or low values). The data used for testing were a heptane fire experiment performed in Test Series 1.

4.1 Noise simulations

The effect of noise added to the data was investigated by adding noise to each sensor alone, while maintaining the integrity of the others. The noise was added to the background data (data prior to ignition) in 13 steps from typical S/N levels to a S/N level of 3. The test simulates a false alarm when exposed to typical background air. Additionally, noise was added to two, three, and finally all sensor channels to probe the ability of the PNN to function under extremely adverse conditions. If the S/N is reduced to low levels, between approximately 3 and 5, then the PNN false alarms. When



the PNN predicts a fire at any point before the actual ignition time, this is considered to be a failure state, which cannot be tolerated.

To understand the effects of noise in the sensor arrays, the number of alarms before ignition as a function of S/N was investigated for noise added to 1, 2, 3, and finally all channels simultaneously. In general, the number of false alarms in background air increases as noise is added to more sensors simultaneously. The point immediately before the PNN fails is more important in terms of predicting and preventing future failures in the field. The pre-failure point is defined as the S/N level immediately before the PNN first fails. A summary of the pre-failure points is given in Table 3, in terms of the raw input data S/N. The pre-failure noise level is shown in bold. The S/N level for ION can drop to 4.8 if all the other sensors have typical noise levels. However, a S/N level below 5.8 will produce a false alarm if the S/N decreases on the CO<sub>2</sub> to 6.6. These pre-failure points may be used to estimate the raw data S/N levels that are tolerable in each sensor when one or more sensors may have excessive noise present.

#### **4.2 Extreme Sensor Failure**

Other sensor events that could occur in the field include sensor dropout (zero reading) and erroneous sensor values. There could be a case in the field where activities in the compartment cause temporary sensor responses of this kind, such as the use of hand radios for communication. Table 4 shows the results for each of these conditions on classification results. For sensor dropouts, the PNN will classify all but the most extreme cases. One or two sensors failing did not cause the EWFD system to fail. When sensor values are above the typical maximum values (constant high value), the PNN almost always produces an erroneous alarm condition. The erroneously high values used for each sensor were 120, 5.5, 50, and 2500 for Ion, Photo, CO, and CO<sub>2</sub>, respectively. When sensor values are below typical baseline values, the PNN results were variable. The below baseline values

used for each sensor were -60, -2.5, -30, and -1000 for ION, Photo, CO, and CO<sub>2</sub>, respectively. The PNN produced an alarm for half of the various situations tested. The response times under these conditions have not been investigated.

Table 3. Summary of PNN Pre-Failure Points Due to Added Noise.

Sensors	Ion S / N	Photo S / N	CO S / N	CO <sub>2</sub> S / N
<b>1 channel noise addition:</b>				
Ion	<b>4.8</b>	14.4	98.3	441.0
Photo	175.0	<b>4.2</b>	98.3	441.0
CO	175.0	14.4	<b>3.1</b>	441.0
CO <sub>2</sub>	175.0	14.4	98.3	<b>5.1</b>
<b>2 channel noise addition:</b>				
Ion and CO <sub>2</sub>	<b>5.8</b>	14.4	98.3	<b>6.6</b>
Ion and CO	<b>17.8</b>	14.4	<b>5.2</b>	441.0
Ion and Photo	<b>17.3</b>	<b>4.0</b>	98.3	441.0
Photo and CO	175.0	<b>6.0</b>	<b>7.4</b>	441.0
Photo and CO <sub>2</sub>	175.0	<b>4.3</b>	98.3	<b>68.8</b>
CO and CO <sub>2</sub>	175.0	14.4	<b>4.7</b>	<b>71.4</b>
<b>3 channel noise addition:</b>				
Ion, Photo, and CO	<b>47.5</b>	<b>5.4</b>	<b>5.7</b>	441.0
Ion, Photo, and CO <sub>2</sub>	<b>21.5</b>	<b>4.3</b>	98.3	<b>233.5</b>
Photo, CO, and CO <sub>2</sub>	175.0	<b>3.9</b>	<b>3.4</b>	<b>258.3</b>
Ion, CO, and CO <sub>2</sub>	<b>11.3</b>	14.4	<b>3.7</b>	<b>52.2</b>
<b>4 channel noise addition:</b>				
Ion, Photo, CO, CO <sub>2</sub>	<b>44.7</b>	<b>5.7</b>	<b>5.3</b>	<b>406.4</b>

Table 4. Summary of PNN alarm states for sensor dropout (zero-reading), sensor responses erroneously high and low.

<b>Sensor(s)</b>	<b>Dropout Missed Alarm</b>	<b>Sensor High False Alarm</b>	<b>Sensor Low Missed Alarm</b>
Ion	No	No	Yes
Photo	No	Yes	Yes
CO	No	Yes	No
CO <sub>2</sub>	No	Yes	No
Ion, Photo	No	Yes	Yes
Ion, CO	Yes	Yes	No
Ion, CO <sub>2</sub>	No	Yes	No
Photo, CO	No	Yes	Yes
Photo, CO <sub>2</sub>	No	Yes	Yes
CO, CO <sub>2</sub>	No	No	No
Ion, Photo, CO	No	Yes	Yes
Ion, Photo, CO <sub>2</sub>	Yes	Yes	Yes
Ion, CO, CO <sub>2</sub>	No	No	No
Photo, CO, CO <sub>2</sub>	Yes	Yes	Yes

## 5. Conclusions

The results of these studies have demonstrated the advantage of a PNN classifier with the multi-sensor, multi-criteria approach for fire detection. The current alarm algorithm resulted in better overall performance than the commercial smoke detectors by providing both improved nuisance source immunity with generally equivalent or faster response times.

Additional studies were performed that examined the effects of noise and erroneous sensor responses (sensor dropout, and high or low sensor values). The results of these experiments indicate that the PNN is robust to sensor noise and dropout. Unacceptable performance was not reached until the S/N level on a single sensor was reduced to 3-5. Noise introduced in multiple sensors produced mixed results with higher S/N levels producing poor PNN performance. The PNN classification results were not effected by single sensor dropout (flat-line zero). The remaining sensors and the PNN are capable of detecting the fires in the absence of one sensor. These effects are



entirely acceptable for a continuous early warning fire detection system until such time that the problem can be corrected.

## **6. Acknowledgements**

The Office of Naval Research under the U.S. Navy Damage Control-Automation supported this work for Reduced Manning Program, PE-603608N.

## **7. References**

1. Gottuk DT, Williams FW. Multi-Criteria Fire Detection: A Review of the State-of-the-Art. NRL Ltr Rpt Ser 6180/0472, September 10, 1998.
2. Carhart HW, Toomey TA, Williams FW. The ex-USS SHADWELL Full-Scale Fire Research and Test Ship. NRL Memorandum Report 6074, October 1987, Reissue, September 1992.
3. Gottuk DT, Hill SA, Schemel CF, Strehlen BD, Shaffer RE, Rose-Pehrsson SL, Tatem PA, Williams FW. Identification of Fire Signatures for Shipboard Multi-criteria Fire Detection Systems. NRL Memorandum Report, NRL/MR/6180-99-8386, June 18, 1999.
4. Shaffer RE, Rose-Pehrsson SL, Barry C, Gottuk DT, Williams FW. Development of an Early Warning Multi-Criteria Fire Detection System: Analysis of Transient Fire Signatures Using a Probabilistic Neural Network. NRL Memorandum Report, NRL/MR/6110-00-8429, February 16, 2000.
5. Rose-Pehrsson SL, Shaffer RE, Hart SJ, Williams FW, Gottuk DT, Hill SA, Strehlen BD. Multi-Criteria Fire Detection Systems using a Probabilistic Neural Network. Sensors and Actuators, B, 2000; 69(3): 325-335.
6. Wong JT, Gottuk DT, Shaffer RE, Rose-Pehrsson SL, Hart SJ, Tatem PA, Williams FW. Results of Multi-Criteria Fire Detection System Tests. NRL Memorandum Report, NRL/MR/6180-00-8452, May 22, 2000.
7. Rose-Pehrsson SL, Hart SJ, Shaffer RE, Wong JT, Gottuk JT, Tatem PA, Williams FW. Analysis of Multi-Criteria Fire Detection Systems Results for Test Series 1. NRL Memorandum Report, NRL/MR/6110-00-8484, September 18, 2000.

- 
8. Wright MT, Gottuk DT, Wong JT, Rose-Pehrsson SL, Hart SJ, Tatem PA, Williams FW. Prototype Early Warning Fire Detection System: Test Series 1 Results. NRL Memorandum Report, NRL/MR/6180-00-8486, September 18, 2000.
  9. Hart SJ, Hammond MH, Rose-Pehrsson SL, Shaffer RE, Wong JT, Gottuk DT, Wright MT, Street TT, Tatem PA, Williams FW. Real-Time Probabilistic Neural Network Performance and Optimization for Fire Detection and Nuisance Alarm Rejection: Test Series 1 Results. NRL Memorandum Report, NLR/MR/6110-00-8480, August 31, 2000.
  10. Wright MT, Gottuk, DT, Wong JT, Rose-Pehrsson SL, Hart SJ, Hammond MH, Tatem PA, Street TT, Williams FW. Prototype Early Warning Fire Detection System: Test Series 2 Results. NRL Memorandum Report, NRL/MR/6180-00-8506, October 23, 2000.
  11. Rose-Pehrsson SL, Hart SJ, Hammond MH, Wong JT, Gottuk DT, Wright MT, Street TT, Tatem PA, Williams FW. Real-Time Probabilistic Neural Network Performance and Optimization for Fire Detection and Nuisance Alarm Rejection: Test Series 2 Results. NRL Memorandum Report, NRL/MR/6110-00-8499, October 10, 2000.
  12. Wright MT, Gottuk DT, Wong JT, Pham H, Rose-Pehrsson SL, Hart SJ, Hammond MH, Tatem PA, Street TT, Williams FW. Prototype Early Warning Fire Detection System: Test Series 3 Results. NRL Memorandum Report, (In Preparation).
  13. Shaffer RE, Rose-Pehrsson SL, McGill RA. Probabilistic Neural Networks for Chemical Sensor Array Pattern Recognition: Comparison Studies, Improvements and Automated Outlier Rejection. NRL Formal Report 6110-98-9879, 1998.
  14. Shaffer RE, Rose-Pehrsson SL, McGill RA. A Comparison Study of Chemical Sensor Array Pattern Recognition Algorithms. *Anal Chim Acta* 1999; 384: 305-317.
  15. Specht DF. *Neural Networks* 1990; 3: 109-118.
  16. Masters T. *Practical Neural Network Recipes in C++*. Academic Press Inc, Boston, MA, 1993.
  17. Masters T. *Advanced Algorithms for Neural Networks*. John Wiley, New York, 1995.

---

18. Shaffer RE, Rose-Pehrsson SL. Improved Probabilistic Neural Network Algorithm for Chemical Sensor Array Pattern Recognition. *Anal Chem* 1999; 71(9): 4263-4271.



## **A New Type of Neural Fuzzy System and its Application in Automatic Fire Detection**

### **Abstract**

A new type of neural fuzzy system is proposed in this paper. With the advantages of network learning, this system solved the problem of defining training data set by human's experiential knowledge, which was impossible to be solved with conventional fuzzy principle. The construction and learning algorithm of this system, and extraction of inferential rules are discussed. Theoretical analysis and the application in automatic fire detection demonstrated that the new neural fuzzy system could be effectively used in the areas where inferential rules are changeable and difficult to be extracted.

### **1. Introduction**

Fuzzy system based on fuzzy logic simulates human's comprehensive inference and judgement and solve the problems of fuzzy information processing which is hard to be solved by normal methods. Fuzzy system has been widely used in industrial and domestic intelligent products. But the further development of fuzzy technique has been puzzled by the problem of extraction of inferential rules. The over changed and innumerable applications of inferential rules cannot be worked out through expert's experiences and knowledge based inductive and trial-and-error methods.

Artificial neural network which features nonlinear and large scale parallel processing, has recently made attractive progress. Simulating biological neural network makes its strong ability of adaptive learning, tolerance and robustness, and it is good in association, synthesis and dissemination. Combined with neural network, the fuzzy system can overcome the shortcomings of normal fuzzy system and improve the ability of learning and expression. The research work has made great progress since the middle of the 1980s and many combinations of fuzzy system with neural network have been introduced<sup>[1][2][3]</sup>. These combinations can be divided into two types.

One is the type of structure equivalence <sup>[3]</sup> where all the nodes and parameters have specified meanings corresponding to membership function and inference procedure of fuzzy system, and they can even transform each other. The structure equivalence system has therefore been widely used. The problem of this type of fuzzy system is that the number of inferential rules depends on the structure of network. It becomes unsuitable when the number of inferential rule is changeable.

Another form is the combination of network learning <sup>[2]</sup>, where all or part of the fuzzy system's fuzzification, linguistical rules, inference and defuzzification are realized with neural network. The physical meanings of neural network are not clear. Therefore the extraction of linguistical rules and the inference procedure are opaque and hard to understand. Particularly when linguistical rules and inference procedure are realized with neural network, and the inputs and outputs of the system are all fuzzy values, it is impossible to define the training data set by experiential knowledge. This has been the main problem hindering this type of fuzzy system from practical application.

A new combination system featuring network learning is proposed in this paper. The system, with the advantages of network learning system, solved the task of defining the training data set by human's experiential knowledge therefore could be used in those fuzzy systems where the number of inferential rules is of infinity. The extraction of inferential rules is also discussed in this paper.

## **2. The system's construction**

A typical fuzzy system mainly includes three parts: fuzzification, fuzzy logic inference and linguistical rules, and defuzzification. If linguistical rules are hard to extract or the number of the rules is large or even infinite, the system cannot be realized by normal fuzzy method. A multi-layer feed forward neural network can be used to store the linguistical rules and the inference of fuzzy logic. The network is a typical BP neural network with three layers (see figure 1), where the inputs and outputs are fuzzy values

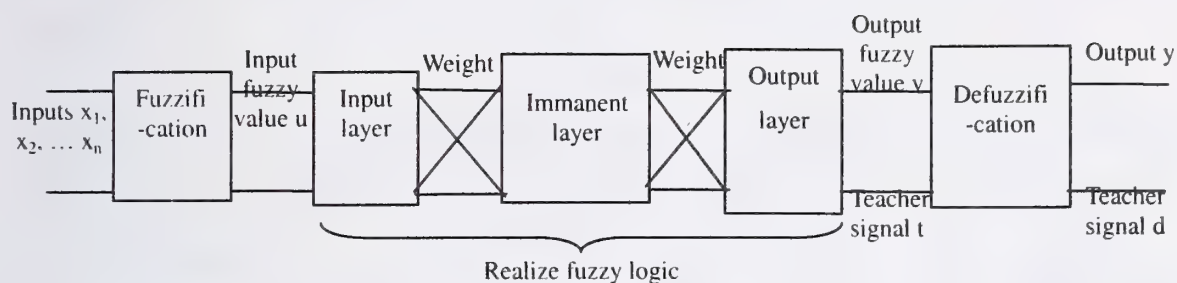


Fig. 1 A fuzzy system with inferential rules realized by a three-layer BP network

(respectively  $u$  and  $v$ ), the immanent layer of the network is used to realize the inference of fuzzy logic, and the weight between each layer are used to store the linguistical rules. The network has, in fact, the form of network learning<sup>[2]</sup>.

The kernel operation of realization of BP network is the procedure of learning. The output of the three-layer BP network is fuzzy value  $v$  rather than the final output  $y$  of the whole fuzzy system. So the teacher signal  $t$  is difficult to define. In general, experiential knowledge can be used to define the teacher signal  $d$  for final output  $y$ . It seems that deducing the teacher signal  $t$  from the teacher signal  $d$  would solve the problem. Unfortunately this cannot be realized. A typical procedure of defuzzification, for example the gravity center method is not a reversible procedure. The teacher signal  $d$  can be deduced from the teacher signal  $t$ , while the teacher signal  $t$  cannot be deduced from  $d$ . This is why the combination of network learning has difficulty in application.



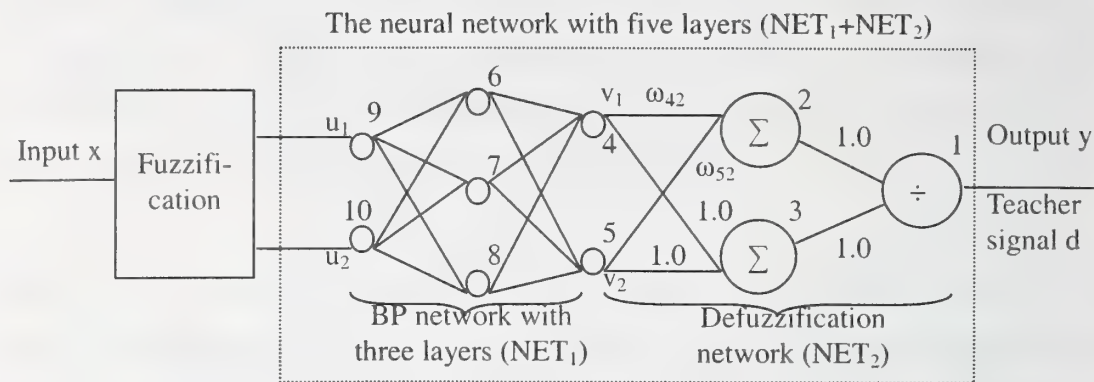


Fig. 2 A typical and simple neural fuzzy system

The system structure can be improved. According to the principle of structure equivalence, the part of defuzzification can be realized by a special neural network (see  $NET_2$  in Figure 2). And the network ( $NET_2$ ) can also be combined with a BP network of three layers ( $NET_1$ ) to form a larger neural network, which can be trained by the data set  $(u, d)$ . The fuzzy value  $u$  can be transformed from input values  $x_i$  through fuzzification. The fuzzification procedure can be done by directly training the BP network or by extracting the membership function through trial-and-error method. The whole system consists of two parts (see figure 2). One is the part of fuzzification. Another one is the five-layer neural network used to realize fuzzy logical rule inference and defuzzification. The system can be named as neural fuzzy system, and can also be regarded as a fuzzy neural network.

### 3. Algorithm of leaning

Suppose that the neural fuzzy system (see figure 2) has a single input  $x$  and a single output  $y$ . The fuzzy values  $u_1$  and  $u_2$  are the fuzzification results of input signal  $x$ . The system output  $y$  is the defuzzification result of fuzzy values  $v_1$  and  $v_2$  that are the result

of fuzzy logical inference. And the immanent layer of BP neural network has three neurons.

The fuzzification procedure has no relationship with the learning and application of the follow up network whatever fuzzification method is used.

For the algorithm, only the section from fuzzy values  $u_1$  and  $u_2$  to the system output  $y$  needs to be considered. Inside this section is the five layer neural network including three-layer BP network and two layers of structure equivalence network (see the dotted part of figure 2). For this combined neural network, the conventional error back-propagation algorithm should be effective. The problem is that the errors of neuron 4 and 5 are difficult to be estimated. With reference to the inferential procedure of BP algorithm, the learning algorithm of the five layers neural network can be inducted from the principle of maximum gradient reducing<sup>[3]</sup>.

Suppose the output of neuron  $i$  is  $O_i$  ( $i=1,2,...10$ ), the weighted sum of inputs is  $net_i$  ( $i=1,2,...10$ ), and  $w_{ij}$  is the connecting weight of neuron  $i$  and  $j$ , among which the value of  $w_{21}$ ,  $w_{31}$ ,  $w_{43}$ ,  $w_{53}$  is constantly 1.0. The neurons “ $\Sigma$ ” and “ $\div$ ” are different from the normal in that: the “ $\Sigma$ ” are add units, their outputs are the sum of all inputs, i.e. their excitation function is  $f(net)=net$ ; the “ $\div$ ” is a division unit with the output of quotient for two inputs. The mean-square error of the system is

$$E = \frac{1}{2} (d - o_1)^2, \quad (1)$$

where  $d$  – teacher signal.

Two weights  $w_{42}$  and  $w_{52}$  of the neural network need to be adjusted. And others are unchangeable:

$$O_1 = \frac{O_2}{O_3}, \quad O_2 = w_{42}O_4 + w_{52}O_5, \quad O_3 = O_4 + O_5. \quad (2)$$

$$\text{We have } \Delta w_{42} = -\eta \frac{\partial E}{\partial w_{42}} = \eta \cdot (d - O_1) \cdot \frac{O_4}{O_3}, \quad \Delta w_{52} = -\eta \frac{\partial E}{\partial w_{52}} = \eta \cdot (d - O_1) \cdot \frac{O_5}{O_3}. \quad (3)$$

$$\text{With generalized } \delta \text{ rule, a } \delta_k \text{ can be defined as } \delta_2 = (d - O_1) \cdot \frac{1}{O_3}. \quad (4)$$

In fact the above result can be worked out by using the procedure of generalized  $\delta$  rule.

That means  $\delta_2 = -\frac{\partial E}{\partial net_2}$ . Because neuron 2 is an add unit, the result of the procedure is

the same as formula 4. Although the weight of  $w_{43}$ ,  $w_{53}$  are fixed, the  $\delta$  of neuron 3 can still be calculated:

$$\delta_3 = -\frac{\partial E}{\partial net_3} = (d - O_1) \cdot \left( -\frac{O_2}{O_3^2} \right). \quad (5)$$

The  $\delta$  values of neuron 4 and 5 are:

$$\delta_4 = (w_{42}\delta_2 + \delta_3) \cdot f'_4(net_4), \quad \delta_5 = (w_{52}\delta_2 + \delta_3) \cdot f'_5(net_5). \quad (6)$$

If  $f(\cdot)$  is a sigmoid function, then

$$\delta_4 = O_4 \cdot (1 - O_4) \cdot (w_{42}\delta_2 + \delta_3), \quad \delta_5 = O_5 \cdot (1 - O_5) \cdot (w_{52}\delta_2 + \delta_3), \quad (7)$$

$$\text{and } \Delta w_{j4} = \eta \delta_4 O_j, \quad \Delta w_{j5} = \eta \delta_5 O_j \quad (j=6, 7, 8). \quad (8)$$

These are formal results because  $\delta_3$  has no actual significance, but the results are the same form as the ones of using the method of maximum gradient reducing, the derivation procedure of which is omitted in this paper. The purpose of using the similar deducing procedure as the general  $\delta$  rule uses is to make calculation and remembrance easy. The meaning of  $\delta_3$  is clearly different from other  $\delta$  values.

Since  $\delta_4$  and  $\delta_5$  have been obtained, the five layers neural network can now be trained directly by using the generalized  $\delta$  rule. And the conventional BP algorithm can be applied to learning procedure of the new network. The kernel procedure of learning algorithm based on the algorithm of maximum gradient reducing is still the back propagation of error. The algorithm has the same form as the BP algorithm has, except that the deducing method of  $\delta$  values of special neuron is different.

#### 4. Application in automatic fire detection

The neural fuzzy system was applied to signal processing of an optical smoke and heat combined detector. The block diagram of the experimental system is similar to figure 2. There is an operation of characteristic extraction before fuzzification. The system input signals are smoke and temperature. Two characteristics are extracted from each signal: signal amplitude and signal rising trend<sup>[4][5][8]</sup>. Let  $S$  and  $T$  be the signals of smoke and temperature,  $S_b$  and  $T_b$  be the base values of smoke and temperature. The characteristics of amplitude are  $S_\Delta = S - S_b$  for smoke and  $T_\Delta = T - T_b$  for temperature. The signal





phenomena caused by, for example, smoking, while the response time was shorter. The neural fuzzy system was of benefit to respond to incipient fire and to reduce the rate of false alarm effectively.

Table 2 Responses to fire, no fire and smoking situations

	TF1	TF2	TF3	TF4	TF5	TF6	TF7	No-fire	Cigarette smoke
Low threshold	260s	392s	397s	85s	93s	219s	107s	3 times of false alarm	False alarm
High threshold	308s	436s	624s	94s	120s	254s	175s	1 time of false alarm	No false alarm
Neural fuzzy system	252s	387s	365s	67s	79s	157s	99s	No false alarm	No false alarm

Note: The response time in this table is the time from the start point of test fire to the alarm point, in terms of second (s). “No-fire” is the data collected in a standard laboratory for about 24 hours, for reference only. “Low threshold” and “High threshold” are the data given by conventional detector working at high and low sensitivity respectively.

### 5. Conclusions

A new type of neural fuzzy system is constructed in this paper. Linguistical rules, fuzzy logic inference and defuzzification of the system are realized by using a neural network of five layers. And a learning algorithm similar to the BP algorithm is provided for training the network. The system not only has the advantages of network learning, but also overcomes the shortcomings that its training data model of inferential rules cannot be obtained by using experiences and knowledge. The new system has strong adaptability and can effectively solve the problem of extraction of inferential rules in many applications.

There was no effective method of fire signal characteristic extraction used for discrimination between fire and non-fire. So it has been difficult to find all inferential rules of automatic fire detection.

The new type of neural fuzzy system was applied to an experimental system of automatic fire detection. With this new neural fuzzy system, effective inferential rules can be obtained from a small amount of training data model. These rules, which are suitable for various types of fire and more effective than those obtained by conventional method, are implied into the weights of the neural network. Experimental result shows that the system can reduce false alarm effectively while does not fail to alert, and the alarm time becomes shorter. With this new system, the inferential rules can be automatically extracted for individual applications. The shortcoming that the inferential rules of existed fuzzy system are unchangeable can be overcome.

The system has stronger adaptive learning ability. In real field condition, the probability of real fire would be about zero during long time of observation. If the system reports an alarm during this period, it must be a false alarm and the data can be used as training data model for the system's learning. Then the system could obtain the inferential rules of reducing false alarm after learning. Theoretical analysis and experiments demonstrate that this new neural fuzzy system discussed in this paper can be effectively used in the applications where inferential rules are changeable and difficult to be extracted.

## References

- [1] Zhijian Zhou, Zongyuan Mao, Cross Study on Fuzzy Neural Network, Circuitry and System Journal, Vol. 3(3) 1998, pp.81-85 (in Chinese).
- [2] Liangjie Zhang, Yanda Li, New Development in Fuzzy Neural Network Technology, Vol. 24(1) 1995, Information and Control Journal, pp.39-45 (in Chinese).
- [3] Zhenyu Zhao, Yongmao Xu, The Basis and Application of Fuzzy Theory and Neural Network, Tsinghua University Publishing House, 1996 (in Chinese).
- [4] Shu Wang, Combined Exclusive Trend Algorithm of Fire Automatic Detection, Fire Safety Science, Vol. 5(1) 1996, pp.8-13 (in Chinese).
- [5] Shu Wang, A Trend Duration and Gradient Detector for Automatic Fire Detection, Fire Safety Journal, Vol. 27(3) 1996, pp.239-248.



- [6] Qing Zhang, Shu Wang, Zongkai Yang, Applications of Fuzzy Neural Network in Fire Detection, Circuitry and System Journal, Vol. 2(3) 1997, pp.51-55 (in Chinese).
- [7] Yoshiaki Okayama, A Primitive Study of a Fire Detection Method Controlled by Artificial Neural Net, Fire Safety Journal, Vol. 17 1991, pp.535-553.
- [8] Shu Wang and Zheng Dou, Exclusive Trend Detector with Variable Observation Windows for Signal Detection, Electronics Letters, Vol.33 No.17, August 1997, pp1433-1435.

Milan Dj. Blagojevich, Ph.D. Candidate, Dejan M. Petkovich, Ph.D., prof.,

Djordje Simich, Ph.D., prof.

Faculty of Occupational Safety, Department of Fire Protection, Nish, Yugoslavia

e-mail: milan@znrfak.znrfak.ni.ac.yu

### **A new algorithm for adaptive alarm threshold in fire detection system**

#### **ABSTRACT**

A basic approach in adaptive modeling of any data acquisition is based on the comparison of real time data with the data previously predicted from the adequate numerical model. In this paper we suggest the time sliding window principle, the length of which is variable in real time and depends on the calculated error. Due to equal time distance in data acquisition in fire detection systems, the number of acquired data and the length time sliding window are linearly interdependent. This approach demands that the borders of time sliding window vary in real time simultaneously with the window. This approach also leads to the best fit between real time and the predicted data when the difference between those two time series of data is used as a feedback.

Generally, the source of false alarms is the application of the fixed alarm threshold decision. This can be overcome using the method of the adaptive threshold. The decision method based on an adaptive threshold employs a threshold changing in time according to the values of the input data and a fixed threshold. The aim of this paper is to introduce the method for controlling fire detection systems in adaptive sense, based on the approximation of the signal with a suitable function.

#### **INTRODUCTION AND BACKGROUND**

The major characteristic of most known algorithms for treatment of alarm is based on a fixed value of alarm threshold. The decision that was made in such a way means that this decision is based on default (defined by the standard) value. However, selection of

adequate alarm threshold is not easy, because of the noise present during data acquisition, other disturbances or uncertainty. The selection of alarm threshold is subject to permanent compromise between the low rate of false alarming with small sensitivity to failure on the one hand, and the high rate of false alarming with high sensitivity on the other hand. This conventional logic practically leads to a discrete function which from the given set of data gives one predicted output value. The adaptive alarm threshold is based on the "history" of acquired data, usually known as time series. Unfortunately, when all of data are known, the fire is fully developed, and no prediction has any sense. The prediction of fire alarm has to be stated on the arbitrary set of previous, acquired data, the fewer of them the better. If we choose to view the set of data in the time window the length of which is constant, consequently we define time sliding window with constant length. Because of the nature of the process this window must have variable length.

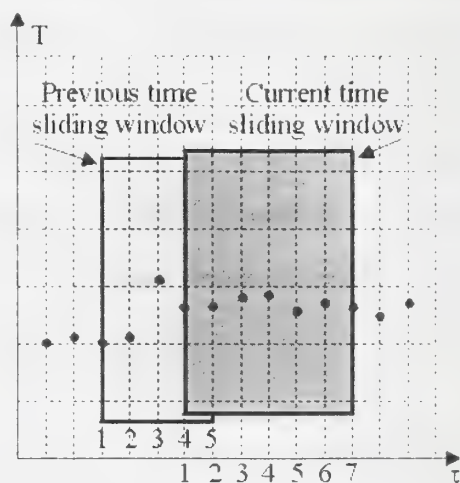


Fig. 1. Time sliding window

The length of time sliding window is variable in time and depends on the error, i.e. the difference between the predicted data and the data that are acquired at every time instant. Measuring of time in every sliding window begins from relative time zero. The method of variable length time sliding window includes feedback that corrects the errors in prediction and consequently enables:

1. System fault detection
2. Detection of an accident in the early stage
3. Adaptation of the alarm level
4. Prediction of a system behavior



## THE TIME VARIABLE SLIDING WINDOW ALGORITHM

In every time instant two values are significant: The first is the value of acquired data, and the second is the value of the velocity of change of data in time. In that case, the first is the temperature and the second is the gradient of temperature (rate of rise). Because of that, it is important to supervise both values, which means that the algorithm must have two major branches, in other words, there are two models. The first model includes approximation of the front edge of fire alarm signal when the adaptation of the alarm threshold is not necessary. The second model includes threshold adaptation based on the method we propose here. In both cases the false alarm can be detected.

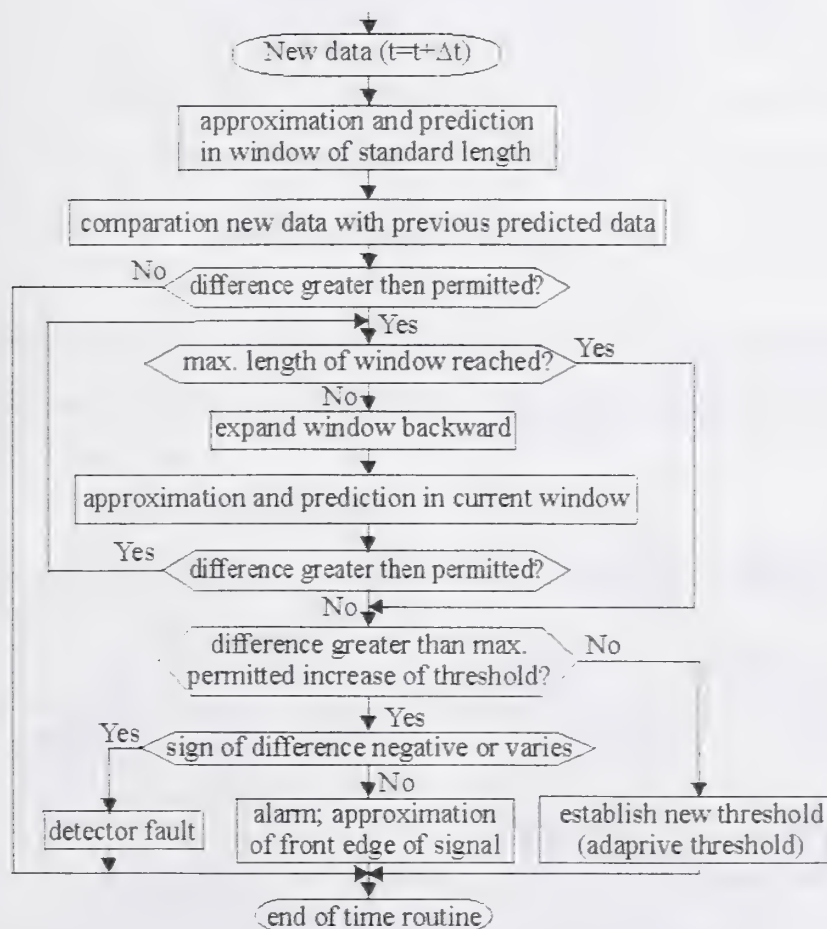


Fig 2. Time sliding window algorithm

The adaptation of the alarm threshold can be applied to the domain in which the two basic criteria are not reached: maximum permitted value of adaptation or critical rate of rise of the signal from the detector.

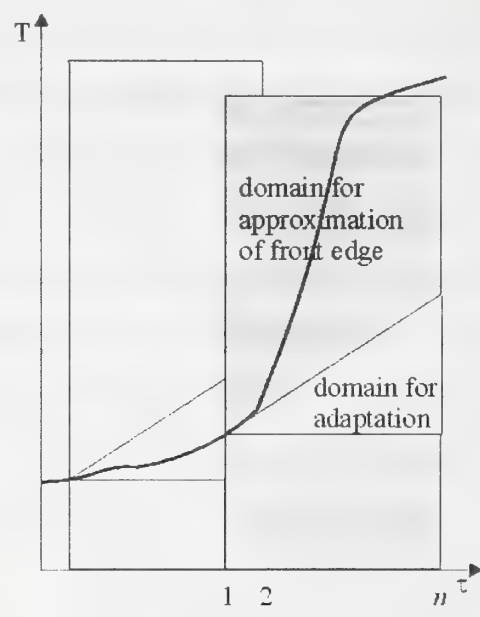


Fig. 3. Domains for approximation

The decision method based on an adaptive threshold employs a threshold changing in time according to the values of the input data and a fixed threshold (see Fig. 4.).

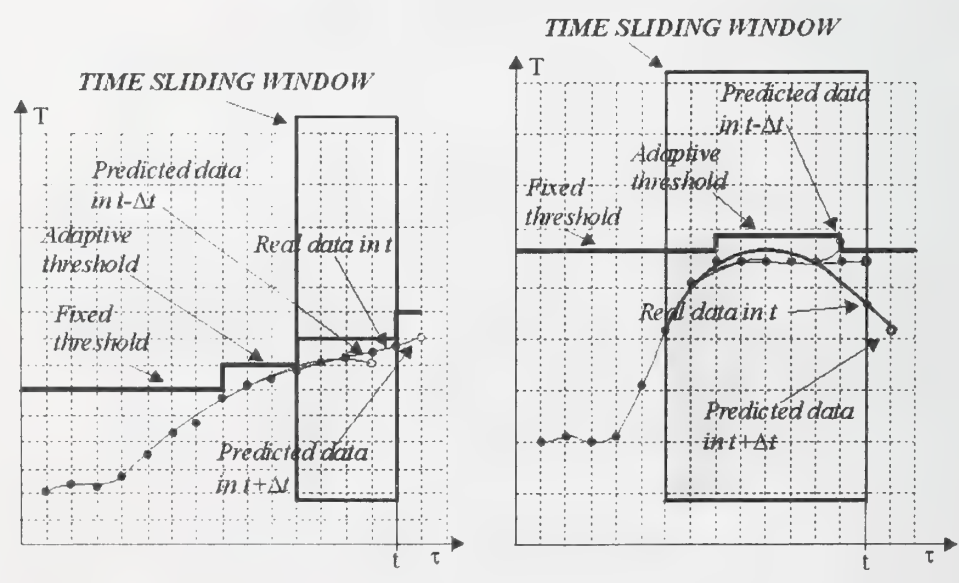


Fig. 4. Adaptive threshold in time sliding window

In fire detection systems where the collecting of data is stationary (polling in equal time distance), the simplest method, which is satisfactorily accurate, is the least squares method with the polynomial approximation of the detected signal. The various types of functions  $f(t)$  can be used to approximate the collected fire data. Functions that approximate the time dependent occurrence have  $m$  unknown parameters and can be constructed using the weighted residuals method, WRM. Some of the procedures are the least squares method, point matching method, etc. Also, spline polynomials are possible approximation for collected data and approximation of front edge of fire signal with conveniently chosen function.

The first step is to choose the order of polynomial,  $m$ , that is equal or less than the number of data in the current window, the time length of which is  $\tau = (m-1)\Delta t$ , and can be increased as window increase. Discrete time is  $K = m$  at the observed moment. From the numerical point of view, the length of the window is  $L \geq m$ . The left border of window can be calculated as  $P = K - L + 1$ .

The second step is to choose the appropriate method of fitting the curve (from a variety of WRM or spline) and determine  $m$  unknown parameters which, in turn, determine the function for approximation.

The third step is to calculate the value of the function in the next time step.

The fourth step is to estimate the difference between the real and predicted data followed by making a decision.

These steps will be repeated until the mathematical model that describes the real state of the system gives results is not satisfactory accurate. Finally, the only two states of the system are possible: accident or not accident.



## THE SMOOTHING SPLINE APPROXIMATION IN TIME SLIDING WINDOW

Spline functions are the category of very useful non analytic functions which consist of different polynomials on segments (and thereby segmental-analytic) linked in specific points which are called nodes. For prediction in time sliding window, in adaptable region, we have used a smooth cubic spline approximation of Schoenberg and Reinch with modification discussed in de Boor [4]. It is a natural cubic spline with knots at all the data abscissas, but it does not interpolate the data  $(x_i, f_i)$ . The smoothing spline is unique  $C^2$  function, which minimizes

$$\int_a^b S''(x)^2 dx \quad (1)$$

Minimization of (1) establishes a compromise between two conflicting goals:

1. to stay close to the given data, and
2. to obtain a smooth function.

These two conflicting goals may be expressed as

$$\sum_{i=1}^n \left| \frac{S(x_i) - f_i}{w_i} \right|^2 \leq \sigma \quad (2)$$

where  $w$  - weights,  $\sigma$  - smoothing parameter, and  $L$  - length of time sliding window (number of obtained data in window) in every time instant.

The parameter  $\sigma$  has to be chosen somehow and depends on the weights. In [4] proposes to choose  $\sigma$  somewhere within  $\sqrt{2L}$  of  $L$  in case  $\sqrt{2L}$  is a good estimate for the standard deviation of the data. That is,

$$L - \sqrt{2L} \leq \sigma \leq L + \sqrt{2L} \quad (3)$$

Simply,  $\sigma$  represent a knob which one may set or turn to achieve a satisfactory approximation to the data. More sophisticated choice for  $\sigma$  based on an estimate of the noise in the data obtained by a process called "cross validation".

In our approach, because of quasistationary nature of fire phenomena, we have defined weights of  $f_i$  in window uniformly from 0 to 1, where the data on the right border of the window has  $w=1$ . On the figure 5 the results of this approach on fictitious ("real" data) are shown.

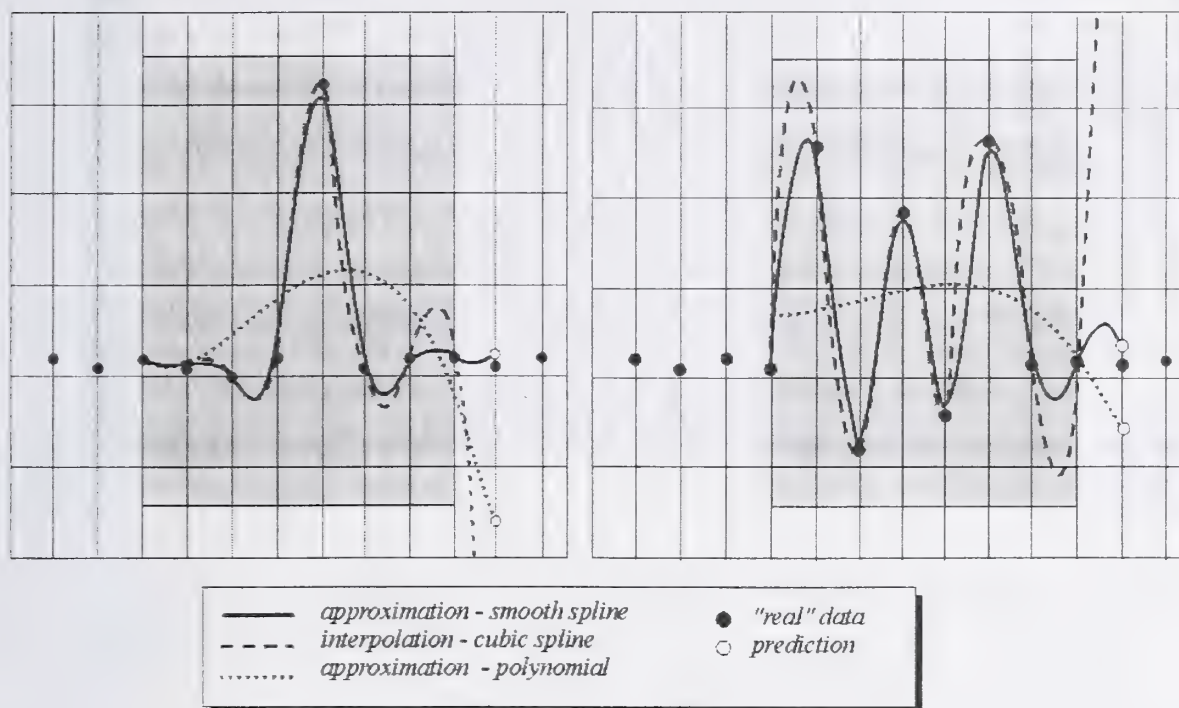


Fig. 5. Smooth spline approximation in time sliding window

The most advantage of spline polynomials usage is that this method of prediction is totally independent of time sliding window length. Application of functional analysis described in [6] shows that all comparisons in sense of vector calculus with various lengths of time sliding window, lead to almost identical values of parameters like relative difference, cosine etc.

Spline polynomials as possible approximation for collected data and approximation of front edge of signal with conveniently chosen function built in a simulation software. This software is being developed at the Faculty of Occupational Safety, Department of Fire Detection - Nish. The figure 6. shows a example of experimental data and related approximations in time sliding window.

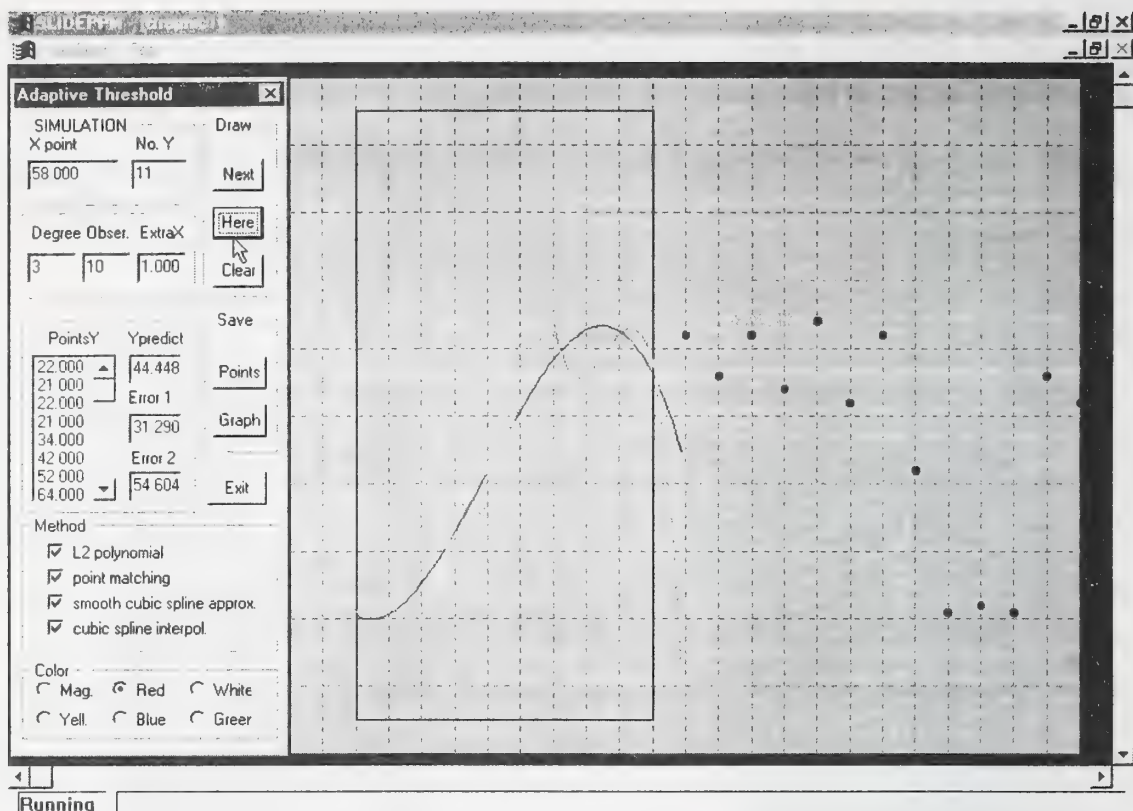


Fig. 6. User interface of simulation software

## CONCLUSIONS

The time sliding window method, which is applied for prediction of the development of fire, consists of two basic models. The first model uses a new function for approximation of front edge of fire signal, and the second, which uses smooth spline polynomials for adaptation of the alarm threshold. The method is built in software package for simulation and the first results are promising.

## REFERENCES

1. Blagojevich M., Petkovich D.: *Adaptive control and sliding window principle*, International Conference "System Identification and Control Problems - SICPRO 2000", Moscow, 2000.



2. Blagojevich M., Petkovich D.: *An approach to complex safety*, Problemi upravljenja bezopasnostju slozних sistem, Moscow, 1999.
3. Bukowski R., Reneke P.: *New approaches to the interpretation of signals from fire sensors*, Natl. Inst. Stand., MD USA, 1999.
4. de Boor C.: *A practical guide to splines*, Springer-Verlag New York, 1978., 235-243.
5. Forsythe, G.E.: *Generation and use of orthogonal polynomials for fitting data with a digital computer*, SIAM Journal on Applied Mathematics, 5, 74-78., 1957.
6. Peacock R., Reneke P., Davis W., Jones W.: *Quantifying fire model evaluating using functional analysis*, *Fire Safety Journal*, No. 33. 1999.
7. Reneke P., Peatross M., Jones W., Beyler C., Richards R.: *A comparison of CFAST predictions to USCG real-scale fire tests*, Natl. Inst. Stand., MD USA, 2000.
8. Shampine, L.F.: *Discrete least-squares polynomial fits*, *Communications of ACM*, 18, 179-180., 1975.
9. Blagojevich M., Petkovich D.: *New model for approximation of front edge of fire signal*, (will be published).

Pascal DUBOIS

CNPP, Saint Marcel, France

## **Electromagnetic compatibility and radio-linked systems**

### **Abstract**

In April 2000, the new European directive R-TTE (Radio and Telecommunications Terminal Equipment) came into effect. The manufacturers are now able to use this new directive to demonstrate by themselves, their product compliance with the relevant protection criteria.

We explain this new approach by analysing the requirements which are given in the relevant ETSI standards for the security systems, which used radio-frequency links. Then we'll make the comparison between the EMC requirements for a dedicated wired system, for a radio-frequency linked system and for a system using these two kinds of communication paths.

Finally, we'll compare the new R-TTE Directive EMC requirements with security and reliability requirements given in the standard draft for alarm system using radio-frequency links (PrEN 50 131-5-3 standard draft)

### **Introduction**

Since 1996, all the apparatus which have been placed on the European Community market, shall bear with the CE conformity marking. This marking presumed of the conformity of this device to the essential requirements of the relevant European directives. This CE marking allows, in a regulatory framework, the placing on the market, free movement and putting service in the European Community.

For electronic security systems, we can distinguish mainly, three European directives:

- The Electromagnetic Compatibility Directive (mainly: 89/336/EEC)
- The Low Voltage Directive (mainly 73/23/EEC)

- The Radio and Telecommunication Terminal Equipment Directive  
(1999/5/EEC)

## **1) Application field and essential requirements of these relevant directives**

### **1.1) The electromagnetic compatibility directive (89/336/EEC)**

**The electromagnetic compatibility Directive** applies to electrical and/or electronic apparatus, where apparatus means all electrical and electronic appliances together with equipment and installations containing electrical and/or electronic.

The **electromagnetic compatibility** means the ability of a device, unit or equipment or system to function satisfactorily in its electromagnetic environment without introducing intolerable electromagnetic disturbances to anything in that environment.

There are two essential requirements for this European directive:

- The disturbance, which is generating by the apparatus does not exceed a level allowing the radio and telecommunications equipments and other apparatus to operate as intended, and
- The apparatus has an adequate level of intrinsic immunity of electromagnetic disturbance to enable it to operate as intended

### **1.2) The low voltage directive (73/23/EEC)**

**The Low Voltage Directive** shall only apply if voltage between 50V and 1.000V for alternating current and/or between 75V and 1.500V for direct current is involved in the apparatus. This is the case for apparatus plugged on the main power network.

There are 11 essential requirements in this directive which can be resumed as follows:

- The manufacturers, or brand name , or trade mark should be clearly marked on the equipment or, if it is not possible, on it's packaging.



- The essential characteristics, the recognition and observance of which will ensure that electrical equipment will be used safely and in applications for which it was made, shall be marked on the equipment, or, if this is not possible, on an accompanying notice.
- The electrical equipment should be so designed and manufactured as to ensure that it can be safely and properly assembled and connected, and to ensure that protection against internal and external hazards are provided in such a way that persons and domestic animals are adequately protected against danger. These objectives should be met just as well, when the equipment is used in applications for which it was made, as in foreseeable conditions of overload.

### **1.3) The Radio and telecommunication terminal equipment directive(1999/5/EEC)**

This directive applies to apparatus which, in this background, has to be defined as followed:

**“apparatus”** means any equipment that is either radio equipment or telecommunication terminal equipment or both.

**“telecommunications terminal equipment”** means a product enabling communication or a relevant component thereof which is intended to be connected directly or indirectly by any means whatsoever to interfaces of public telecommunications networks (that is to say, telecommunications networks used wholly or partly for the provision of publicly available telecommunications services);

**“Radio equipment”** means a product, or relevant component thereof, capable of communication by means of the emission and/or reception of radio waves utilising the spectrum allocated to terrestrial/space radio-communication.

The essential requirements for all the equipments which are concerned by this directive are: - to meet the requirements of the electromagnetic compatibility directive

(89/336/EEC) and,

- to meet the low voltage directive (73/23/EEC), but with no low voltage limit applying.

In addition, there is another essential requirement which applies only to radio equipment, subscribing that radio equipment shall be so constructed that it effectively uses the spectrum allocated to terrestrial/space radio communication and orbital resources so as to avoid harmful interference.

## **2) The harmonized standards to meet these three European directives:**

The essential requirements to meet European directives are described in harmonized standards, which contain technical specifications and which are adopted by a recognised standards body under a mandate from the commission.

There are many harmonised standards for these European directives in the field of electronic security systems. If we consider the most complete case (in the sense of these three directives) for electronic security equipment, this latter may be made of :

- An enclosure,
- Alternative current inputs and/or outputs (generally: the main power input),
- Direct current inputs and/or outputs,
- A functional earth port,
- Signal and/or control inputs and/or outputs,
- Connections to telecommunications networks,
- Radio-frequency transmitting subsets, and
- Radio-frequency receiving subsets.

An illustration of this kind of equipment is given in illustration 1.

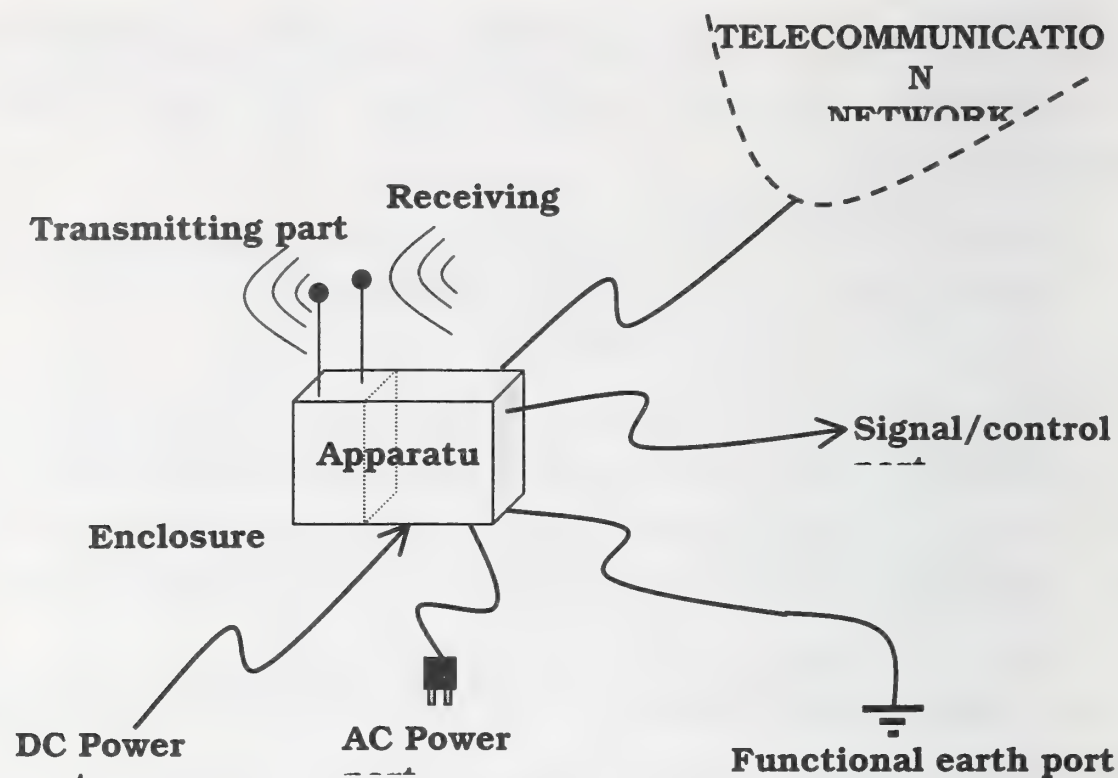


**Illustration n°1: most complete case of an electronic security equipment**

At the opposite, the most simple case for an electronic security equipment is an equipment without any external connection and powered with low voltage batteries (less than 75 V), for example: a domestic smoke detector (shown in illustration n°2).



**Illustration n°2: most simple case of an electronic security equipment**

At first, we can list the relevant standards which have to be applied to meet the three European directives for electronic security equipments:



**2.1) For the Low voltage directive:**

DIRECTIV E	KIND OF EQUIPMENT	SUBSE T	HARMONISED STANDARDS	Date of publication
LOW VOLTAGE DIRECTIV E (73/23/EE C)	Any radio equipment	ALL	EN 60 950 +Amendments A1, A2, A3 & A4	January 1993
	Any telecommunicatio n terminal equipment	ALL		
	Other equipments involving Voltage in the following ranges: between 50 and 1.000V for alternating current and/or between 75 and 1.500V for direct current	ALL		
	Any other equipment which is not part of those aforementioned	Low voltage directive does not apply		

**Table n°1: harmonised standards to meet the essential  
requirements of the low voltage directive in the case of an  
electronic security equipment**

**2.2) For the Electromagnetic compatibility directive:**

DIRECTIVE	KIND OF EQUIPMENT	SUBSET	HARMONISED STANDARDS	DATE OF PUBLICATION
<b>EMC DIRECTIVE (89/336/EEC) EMISSION ASPECTS</b>	Any radio equipment	ALL	no harmonised standard at this day	
	Any telecommunication terminal equipment	ALL	EN 50 081-1	1992
	Any other equipment	ALL	EN 50 081-1	1992

**Table n°2: harmonised standards to meet the essential requirements for the emission aspects of the electromagnetic compatibility directive in the case of an electronic security equipment**

DIRECTIVE	KIND OF EQUIPMENT	SUBSET	HARMONISED STANDARDS	DATE OF PUBLICATION
<b>EMC DIRECTIVE (89/336/EEC) IMMUNITY ASPECTS</b>	Any radio equipment	ALL	no harmonised standard at this day	
	Any telecommunication terminal equipment	ALL	EN 50 130-4	1995
	Any other equipment	ALL	EN 50 130-4	1995

**Table n°3: harmonised standards to meet the essential requirements for the immunity aspects of the electromagnetic compatibility directive in the case of an electronic security equipment**

### 2.3) The Radio and telecommunication terminal equipment directive

In the case of a radio equipment, the harmonised standards are not yet defined. But we already know that they will be defined in function of the transmitted power.

For the communication inside an alarm system, only short range devices are involved in the system and in this case we have good presumptions to say that the harmonised standards will be: - **ETS 300 220** series for the requirements related to the

spectrum utilisation

And - **ETS 300 683** standard for the EMC aspects for the short range devices operating on frequencies between 9 kHz and 25 GHz.

For the radio-telecommunication equipments (like GSM, DCS 1800, UMTS, TETRA, etc...) the standards are not yet harmonised in all over Europe, and in this case, national regulations may still be in force or, it may happen that there are restrictions on the use of the equipment in certain European countries.

For that reason, at this date, we can see different kinds of temporary CE marking as shown in illustration n°3.



**Illustration n°3: temporary CE marking in the case of a radio equipment**

These temporary CE marking may be split up into three parts:

- At first, the CE marking in itself ( **CE** ), as defined in the main European directive




- then: the number of the notified body (**N° XXXX**), which has intervened in the conformity evaluation according to European standards which are not yet harmonised

- and, at least: the warning sign (  ), which means that the frequency range which is used is not yet harmonised in Europe

In conclusion, for a radio device we have four different CE marking:

At this date, we have:

**CE** : in the case of frequency range which is used is already harmonised in Europe and standards which has been used to assess the conformity to the R-TTE directive are already harmonised


**CE ** : in the case of frequency range which is used is not yet harmonised in Europe and standards which has been used to assess the conformity to the R-TTE directive are already harmonised

**CE N° XXXX :**

in the case of frequency range which is used is already harmonised in Europe and standards which has been used to assess the conformity to the R-TTE directive are not yet harmonised

**CE N° XXXX **:

in the case of frequency range which is used is not yet harmonised in Europe and standards which has been used to assess the conformity to the R-TTE directive are not yet harmonised

When the relevant frequency ranges and standards to assess the conformity to the essential requirements of the R-TTE directive will be harmonised in Europe, it will only remain the simple  marking.

### **2.3.1) Requirements to meet the EMC directive and the EMC aspects of the R-TTE directive in a case of a short range device:**

In the field of electronic security systems, the short range devices are mainly the equipments which make up the radio-linked alarm systems such as: Radio-frequency linked intrusion and/or fire alarm systems, and the social alarm systems. There are two frequency bands which are allowed in Europe:

- 433,05 MHz - 434,79 MHz and
- 868 MHz – 870 MHz

These two frequency ranges are allocated for short range devices, which have an allowed maximum radiated power lying between 10 mW and 25 mW for the application of alarm systems.

For this kind of device, there are some restrictions for the use of the frequencies in certain European countries, that means that there is no harmonisation for the frequency bands. But, we know that the relevant standard which provides the requirements for a correct use of these frequency bands, is **ETS 300 220-1 [Radio Equipment and Systems (RES), Short range devices Technical characteristics and test method for radio equipment to be used in the 25 MHz to 1.000 MHz frequency range with power level ranging up to 500 mW; Part 1: Requirements related to spectrum utilisation]**. This latter mainly defines the maximum power level in function of the frequencies inside and outside the used frequency channel.

For the EMC requirements, the relevant European standard is **ETS 300 683 [Radio Equipment and Systems (RES) ElectroMagnetic**

**Compatibility (EMC) standard for Short Range Devices (SRD) operating on frequencies between 9 kHz and 25 GHz].**

This standard defines four kinds of EMC requirements:

- The Continuous phenomena applied to Receivers (CR)
- The Continuous phenomena applied to Transmitters (CT)
- The Transient phenomena applied to Receivers (TR)
- The Transient phenomena applied to Transmitters (TT)

It defines also 3 classes of equipment (1,2 & 3) in function of the impact on persons and/or goods in case the equipment does not operate above the specified minimum performance level under EMC stress. For the radio-frequency linked alarm systems, the corresponding class of equipment is the class 1 (Alarms application; Domestic security).

And at least, the standard defines 3 equipment types (I, II & III) in function of the technical nature of the primary function of the equipment, for the radio-frequency linked alarm system, the appropriate equipment type is I [transfer of messages (digital or analogue signals)].

The tests which are required to meet the ETS 300 683 for the radio linked alarm systems are described in the table n°4.

For the Radio-frequency electromagnetic field (80 MHz – 1.000 MHz), the standard specifies an exclusion band for the receiving equipments in which this test does not need to be performed. For the frequency bands which are allocated for the alarm systems, this exclusion band is defined as follows:

The lower frequency of the exclusion band is the lower frequency of the intended operating frequency band minus 5% of the operating frequency and the upper frequency of the exclusion band is the upper frequency of the intended operating band plus 5% of the operating frequency.



The other tests have to be performed with the same procedure as for the none radio equipments.

The performance criteria are defined in function of the kind of test (continuous or transient) and the class of equipment (for the alarm systems: class 1). For each test there are performance criteria during the test and after the test.

Phenomena	Application	Equipment test requirement		Reference document
		Fixed equipments	Remote control	
EMISSION REQUIREMENTS				
Emission measurements	Enclosure	Applicable to ancillary equipments	Applicable to ancillary equipments	EN 55 022
	DC power in/out	Applicable	Not applicable	EN 55 022 CISPR 16-1
	AC mains	Applicable	Not applicable	EN 55 022
IMMUNITY REQUIREMENTS				
RF electromagnetic field (80 MHz - 1.000 MHz)	Enclosure	Applicable	Applicable	EN 61000-4-3
Electrostatic discharge	Enclosure	Applicable	Applicable	EN 61000-4-2
Fast transients common mode	Signal and control ports, DC and AC power ports	Applicable	Not applicable	EN 61000-4-4
RF common mode (current clamp injection) 0,15 - 80 MHz	Signal and control ports, DC and AC power ports	Not applicable	Not applicable	EN 61000-4-6
Transients and surges	DC power input ports	Applicable	Not applicable	ISO 7637 Parts 1 & 2
Voltage dips and interruptions	AC mains power input ports	Applicable	Not applicable	EN 61000-4-11
Surges, common and differential mode	AC mains power input ports	Applicable	Not applicable	EN 61000-4-5

**Table n°4: EMC tests for short range devices according to ETS 300**

### **3) The European standard draft for radio linked alarm systems:**

For the radio-frequency linked alarm systems there are, on top of the essential requirements to meet the three relevant European directives and of the requirements related to spectrum utilisation, an European product standard draft in preparation at the CENELEC/TC79 level: **Pr EN 50 131-**

#### **5-3 (Alarm systems - Requirements for interconnections equipment using radio frequency techniques).**

This standard specifies reliability and security requirements for the radio frequency link in the field of alarm systems. It specifies four grades (1 to 4) based on different level of reliability and security, for which the higher level is obtained for the grade 4.

For the reliability aspects this draft proposes requirements about:

- the throughput rate, which requires that a minimum number of alarm messages that generate an alarm at the receiving equipment shall be 999 out of 1.000 for grades 1 & 2 and 9.999 out of 10.000 for grades 3 & 4.
- Immunity to unintentional message and component substitution
- Immunity to attenuation, in order to prevent any modification in the surround which may affect the RF link budget.
- Immunity to outband interferences
- Immunity to inband interferences (saturation)
- RF links monitoring

For the security aspects, there are mainly requirements about tampering:

- Immunity to intentional component substitution (for grades 3 & 4)
- Immunity to intentional message substitution (probability to discover an identification code in less than one hour (less



than 5% for grades 1 & 2, less than 0,5% for grade 3 and less than 0,05% for grade 4)

- Detection of interference (saturation of the receiver with an intentional signal at the same frequency as the operating frequency of the system)

Among all the requirements provided by the Pr EN 50 131-5-3, there are only two requirements which are comparable to those provided by the European directives.

There are about:

- o the RF electromagnetic field immunity test required by the

ETS 300 683 and,

- o the outband and the inband immunity test required by the Pr EN 50 131-5-3

If we compare these two tests, we can see that they are complementary. We have seen before that for the RF electromagnetic immunity test of the ETS 30 683, there are an exclusion band, inside which the test is not performed. In Pr EN 50 131-5-3, these tests have to be performed at the limit frequencies and/or inside this exclusion band in function of the grade as described in the table 5. The signal which is applied is different from the two standards, such as for the product standard (Pr En 50 131-5-3), the interference signal is very closed to the original one (at the difference of the frequency) and the performance criteria in the case of the product standard ask for 80% of good transmissions in the presence of the interference signal.

	$F_1$	$F_o$	$F_2$
<b>GRADE 1</b>	<b>3 V/m</b>	<b><math>L_o - 12</math> dB</b>	<b>3 V/m</b>
<b>GRADE 2</b>	<b>3 V/m</b>	<b><math>L_o - 12</math> dB</b>	<b>3 V/m</b>
<b>GRADE 3</b>	<b>10 V/m</b>	<b>10 V/m</b>	<b>10 V/m</b>
<b>GRADE 4</b>	<b>10 V/m</b>	<b>10 V/m</b>	<b>10 V/m</b>

**Table n°5: Outband & inband immunity test according to PrEN 50  
131-5-3**

In the table 5; -  $F_1$  means the lower frequency limit of the exclusion band

- $F_o$  means the operating frequency of the considered equipment
- $F_2$  means the higher frequency limit of the exclusion band
- $L_o$  means the level of the operating signal

These requirements show that higher is the grade, higher is the reliability level for the equipment which meets the PrEN 50 131-5-3 standard.

## **Conclusion**

So, we can conclude that there is a good complementarity between the essential requirements in the sense of CE marking and those from the product standard draft for the radio frequency links used in the wire free alarm systems.

Indeed the main aim of the essential requirements of the European directives is to assure that the equipment can be used safely and that this equipment would not cause any trouble to the other devices which are in its environment, whereas the aim of the CENELEC product standards is to

ensure that the devices have a good level of reliability, security and tamper resistance.



Karlheinz Schreyer

Siemens Gebäudesicherheit GmbH & Co. oHG, Munich, Germany

## **Radio Module Characteristics and Their Relevance to Fire Detection Systems**

### **1. Introduction**

Integrating wireless fire detectors into a fire detection system offers the user many advantages (see "Technical State of 868-870 MHz Radio Modules with SRD Band" in the same conference volume). Since this new technology must cover the same risks as conventional fire detection systems, the same requirements naturally apply to the quality of the radio link. With modern transmission processes and high-quality hardware, it has recently become possible to achieve the same quality as that of tried and trusted wired systems.

While the committed security expert is well able to discuss the advantages and disadvantages of any transmission process with the relevant supplier, the details which determine the hardware functionality of radio systems are almost certainly a mystery to him/her. This presentation attempts to shed some light on the most important technical terms and to explain their relevance to fire detection systems.

### **2. Propagation attenuation**

One of the first questions always asked is "What is the range of your radio link in the building?" In order to impress, various manufacturers therefore give the outdoor range. This value has very little meaning because there is no concrete reference basis. In a building, the waves are attenuated by more than a power of ten compared with unhindered propagation.

The attenuation of radio waves in a building depends entirely on the physical design properties and the distance between the transmitter and receiver. The manufacturer of a fire detection system cannot generally influence these matters and can only control the transmitted power and, above all, the sensitivity of the receiver. Instead of specifying distances, it would therefore be better to specify the attenuation budget, the attenuation reserve and the carrier frequency:

The attenuation budget is a measure of the range in the building.

2.1 Attenuation budget

The attenuation budget is the difference between the radiated transmitter power and the minimum received power required for good reception. The higher the value, the greater the range of the radio link, although it is important to remember that the attenuation in the masonry depends heavily on the frequency. A direct comparison can only be made between two values if the frequency is the same (see 2.3).

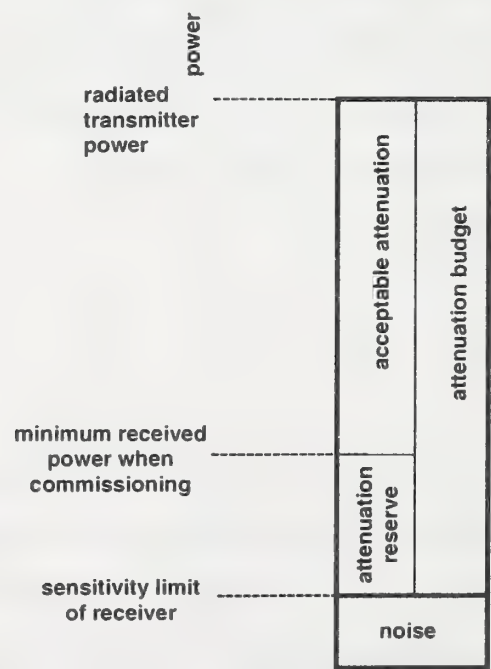


Figure 1 The attenuation budget

Some brochures highlight the transmitted power even though doubling it only means an increase of 3 dB in the attenuation budget while doubling the

20 dB more received sensitivity = 100 times greater transmitted

current drawn from the battery! Investing in receiver sensitivity makes greater sense (figure 1). For example, SIGMASPACE has an attenuation budget of approx. 115 dB.

## **2.2 Attenuation reserve**

For various reasons which could have a negative (or positive) effect on wave reflection, e.g. moving cupboards or plant pots, or even wet window panes, the propagation conditions in a building are constantly changing, so that a path which has a barely adequate power level should not be commissioned. A comparatively large attenuation reserve is essential in order to ensure a reliable link for a period of several years. In the case of SIGMASPACE, an attenuation reserve of more than 25 dB was chosen. This produces an

Effective attenuation = attenuation budget – attenuation

effective attenuation of approx. 90 dB.

## **2.3 Frequency-dependant attenuation**

If waves penetrate dense materials such as wood, concrete or masonry, then both electrical and magnetic field components interact with their atoms and molecules so that there is a linear increase in attenuation which is roughly in line with the increase in frequency.



Generally speaking, the higher the frequency, the smaller the aerials. Smaller ones draw less energy from the electromagnetic field than large ones.

Rule of thumb: If the frequency is doubled, it is at the expense of approx. 10 dB of the received signal in

### 3. Types of modulation

In addition to conventional amplitude (AM) and phase or frequency modulation (FM) (figure 2), a buzz word frequently used these days is “spread spectrum modulation”. It is explained in greater detail in section 6.



Amplitude modulation



Frequency modulation

Figure 2 Amplitude modulation und Frequency modulation

#### 3.1 AM and FM

For noise and distortion-free demodulation,

- the overall amplification in AM receivers must be precisely regulated to the demodulator operating point and
- the mixing frequency in FM receivers must be tuned precisely to the received signal.

Since interference and changes in the transmission path affect the received amplitude but not the frequency, FM is thought to be more robust.

FM less sensitive to interference

Note:

Narrow-band direct conversion receivers must also regulate their amplitude and can therefore respond to fluctuations in amplitude with distortion.

### **3.2 Spread spectrum modulation**

Within the comparatively narrow bandwidths in the ISM band at 433 MHz and in the SRD band at 870 MHz which have been approved for Europe, there is probably little sense in using this wide band transmission method for fire detection systems.

For further information regarding spread spectrum see section 6.

In Europe's narrow SRD band, spread spectrum modulation seems to make little sense for fire detection systems.

## **4. Transmitters**

In all likelihood, a "bad" transmitter", i.e. one which produces several spurious emissions will not have a negative impact on its own transmission path. It is more likely to interfere with other services or even other transmission paths for the same fire detection system, so that it results in inefficient utilisation of the frequency spectrum which, by its nature, is limited.

## **5. Receivers**

Receivers must filter out and amplify signals of the order of pW from the spectrum and in the process must not allow interference either from processes in neighbouring channels or electromagnetic influences. A truly enormous task. In order to tackle it, double detection receivers (heterodyne) are almost always used these days. Regenerative detectors are no longer in

general use and ultra wide band receivers which use correlators, have barely gone beyond the development stage.

## 5.1 Heterodyne with one or more intermediate frequencies

Figure 3 shows the major function blocks of a heterodyne receiver with an intermediate frequency (IF). In principle, the variants with two intermediate frequencies (double super) do not offer any advantage or disadvantage, they are simply design variants. They tend to provide better image frequency suppression and filtering.

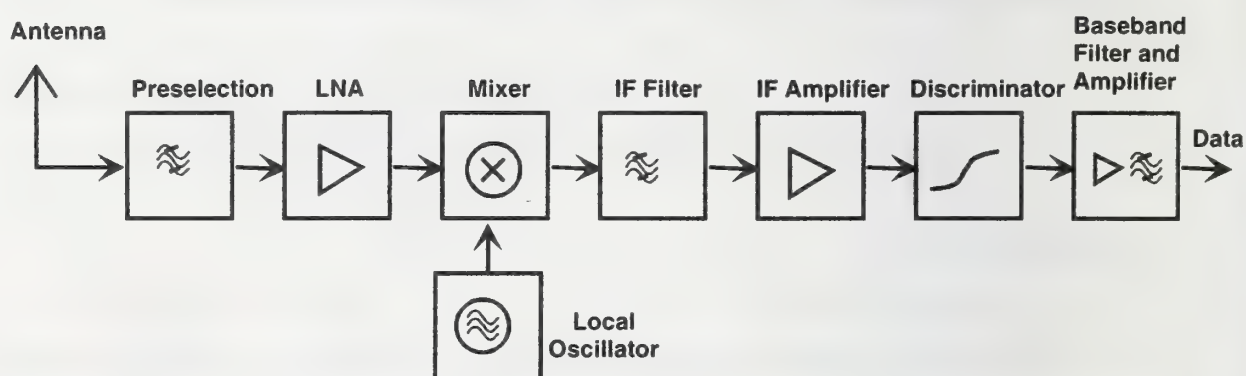


Figure 3 Circuit diagram of a heterodyne receiver

### 5.1.1 Preselection

In general, only high-quality radio modules have effective preselection which is fitted with effective components (e.g. surface wave resonators). While they attenuate the received signal by a few dB – which can be easily compensated by carrying out the next steps - they do improve:

- electromagnetic compatibility and therefore
- suppression of distant interference signals:

An oscillating antenna circuit consisting of inductances and capacitances is a rather poor compromise. Even with the antenna's selectivity, it only improves distance selection a little.



Effective preselection improves EMC and suppresses the image frequency.

### 5.1.2 Preamplifier and mixer

Preamplifiers are mainly used in places where very low signals need to be received. In doing so, they must not be overloaded with large signals missed by the preselection operation.

Along with the mixer and IF filter function blocks which follow it, the preamplifier determines the receiver dynamic range, i.e. the ability to register a small wanted signal in addition to a strong signal in one of the neighbouring channels (figure 4).

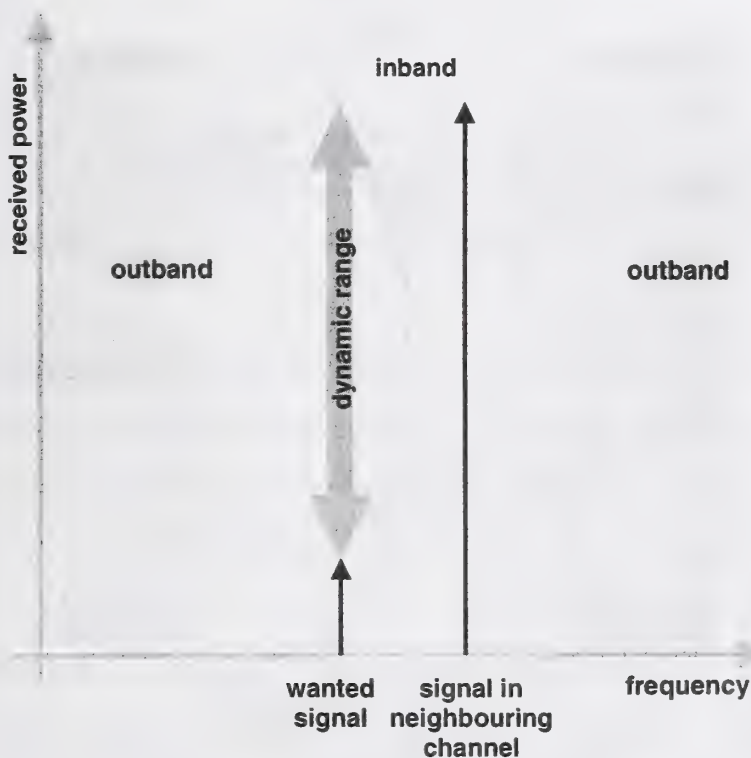


Figure 4 Dynamic range

In fire detection systems, the receiver dynamic range should be at least 60 dB.

Generally speaking, high-quality mixers and preamplifiers require comparatively high operating current. An acceptable level of energy consumption for the detector can only be guaranteed if the circuit concept is carefully chosen.

### 5.1.3 Local oscillator

The local oscillator must deliver a very clean signal, i.e. one which is free of spurious emissions or noise. For the mixer, every spurious emission, and even the oscillator signal noise, is seen as an additional mixer frequency, i.e. one with which it mixes unwanted signals from the spectrum into the IF (figure 5).

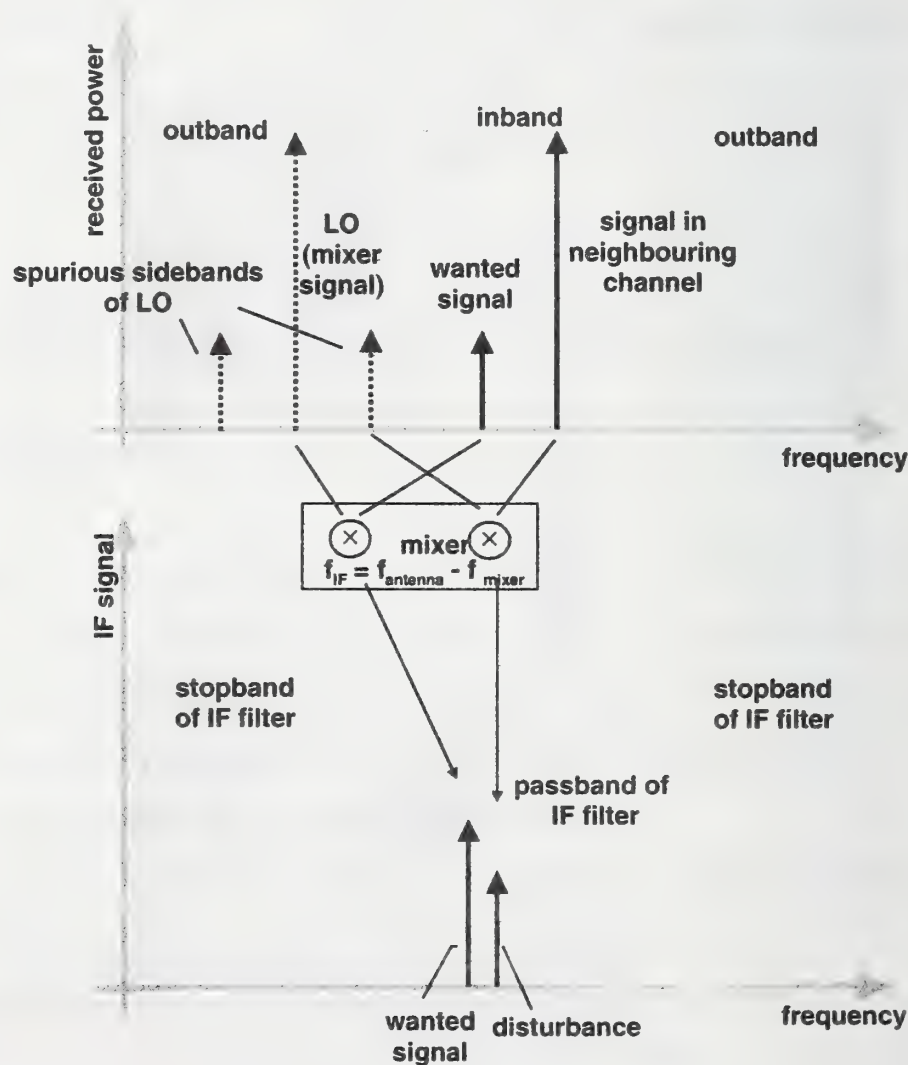


Figure 5 Unwanted mixed frequencies

Narrow-band receivers such as those required for the 25 kHz wide alarm channels in Europe's SRD band, demand very high quality in relation to the cleanness of the oscillator signal. This applies in particular to the immediate vicinity of the actual mixed frequency.

In high-quality receivers of approx. 900 MHz, the mixer frequency cannot be directly produced with the required precision in the local oscillator. A voltage controlled oscillator (VCO) supplies the output signal. It is linked to a lower oscillating quartz via a phase locked loop (PLL) (figure 6).

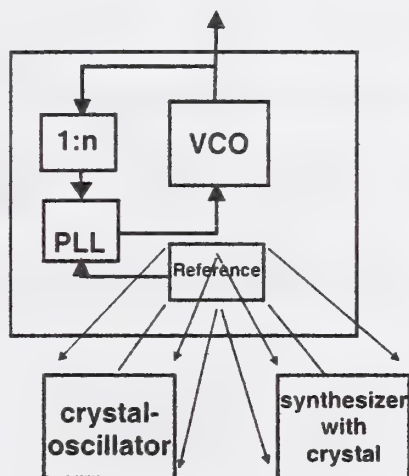


Figure 6 Basic structure of a local oscillator

Based on a single stable frequency, in transceivers, a synthesiser between the quartz oscillator and the PLL allows the creation of the transmission signal and the LO signal for the receiver mixer. For receivers which can operate in several channels, it supplies the variable reference frequency.

Unfortunately, synthesisers produce unavoidable spurious emissions. Precautions must therefore be taken to ensure that these do not couple to the mixer signal through the PLL. Otherwise other channels would mix and cause interference at the IF.

LO noise and spurious emissions should be suppressed 10 dB more than the required receiver dynamic range.



5.1.4 The discriminator

At this point, the only type of demodulator worth considering is the discriminator because amplitude modulation is not used in high-quality fire detection systems.

In principle, the discriminator is a frequency-dependent resistor. It converts the IF frequency variation into a variation in amplitude (figure 7).

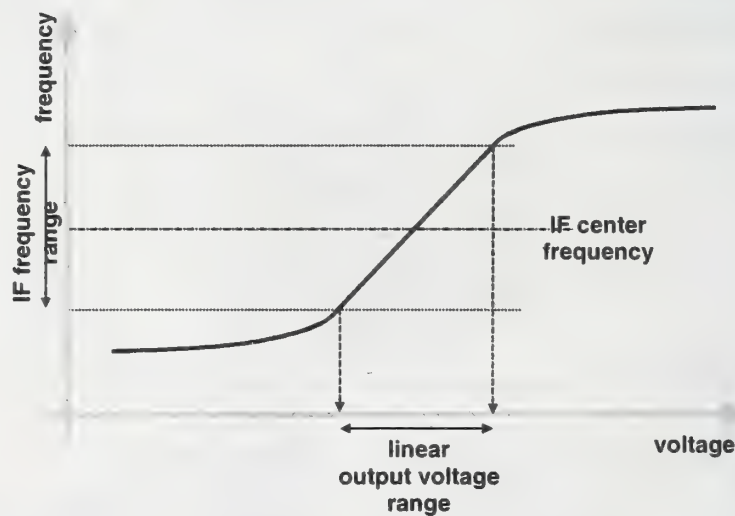


Figure 7 Discriminator curve

In order to achieve the greatest possible discriminator efficiency, the received signal must be mixed quite precisely at the middle of its linearity range. Broad-band receivers are somewhat less critical. Their quartz precision is generally sufficient to pinpoint the middle with sufficient accuracy. With narrow-band receivers, however, costly control mechanisms are required to tune the receiver to the transmitter.

Low priced broad-band solutions often also require frequency regulation because their reference oscillator is too imprecise. Simple versions of these regulation circuits are unable to transmit several “ones” or “zeros” in succession without becoming deregulated and verging on the limits of the discriminator’s linearity range. Direct current-free basic channel coding

(Manchester code, return to zero code) solves the problem, although it takes up double the bandwidth. Owing to the greater noise levels in broad-band receivers, they are somewhat less sensitive.

The maximum sensitivity and optimum utilisation of the spectrum can only be achieved with discriminators which can demodulate data which has a direct current

#### **5.1.5 Base-band filter and base-band amplifiers**

Owing to the current state of the art, base-band filters and amplifiers no longer have a negative effect on transmission quality, so there is no need for any further discussion.

### **5.2 Single chip double detection receivers**

In conventional double detection receivers, IF filtering cannot yet be integrated on silicon. At present, active filters can only be used up to approx. 100 kHz. Recently, therefore, two different receiver principles which can be satisfactorily integrated have appeared on the market, or will do so in the near future:

- Receiver with low IF
- Direct conversion

#### **5.2.1 Direct conversion**

In receivers with direct conversion (DC – not to be confused with the abbreviation for direct current!), the IF is at 0 Hz. With conventional discriminators, the resultant signal cannot be demodulated because both positive and negative frequency deflection of an FM signal is reproduced as a positive frequency in the “IF” (figure 8).

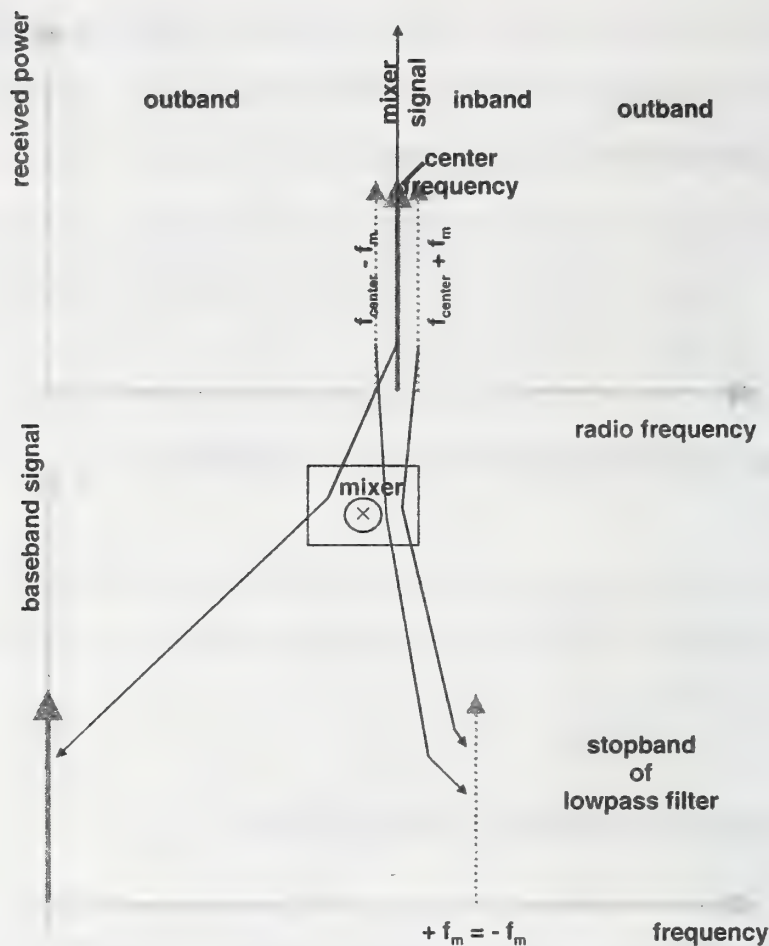


Figure 8 Mixing in direct conversion receivers

Figure 9 shows the amplitude-time curve of a 0/1 transition. The clearly recognisable irregularity originates from the phase change at the RF level.

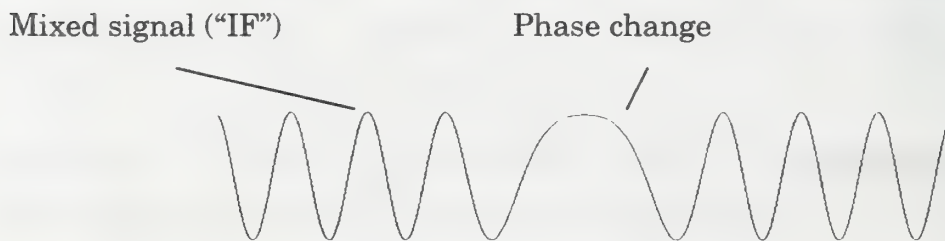


Figure 9 Amplitude-time diagram of a signal mixed at 0 Hz

However, demodulation is still possible because the phase between the mixer signal coming from the LO and the received signal changes when the received signal changes from  $f_m + \bullet f$  to  $f_m - \bullet f$ . DC receivers therefore have two mixers and two "IF filters" in the so-called I and Q branches. The I and



Q mixers are driven with a signal offset by 90 degrees (sine and cosine) in the process (figure 10).

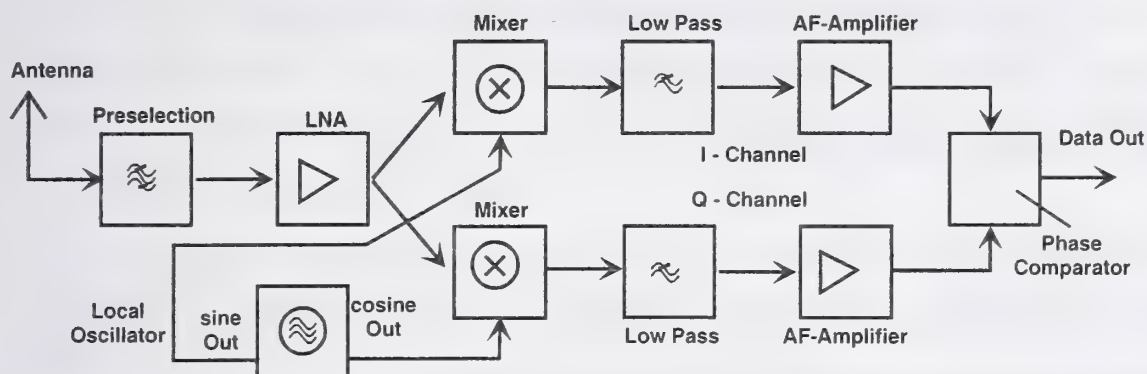


Figure 10 Circuit diagram of a direct conversion receiver

Figure 11 shows how the amplitude-time relationship changes between channels I and Q when the received signal switches from  $+\Delta f$  to  $-\Delta f$ . It is easy to see that this phase difference can be evaluated in principle.

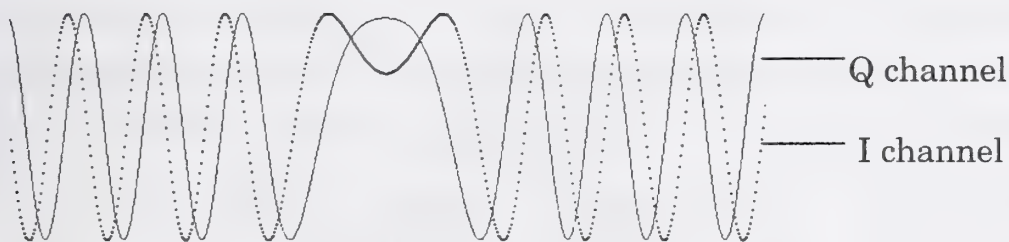


Figure 11 Amplitude-time diagram in the I and Q channel

DC receivers produce comparatively satisfactory results at low cost although they require a broader bandwidth for the same data rate. This results in somewhat lower sensitivity.

Fast-moving objects in the vicinity of the receiver could present a problem since mixing takes place in the receiver at precisely the received frequency. Needless to say, this mixing frequency cannot be completely attenuated and is radiated backwards, so to speak, through the aerial. If this signal meets a nearby object which is moving (ventilator) it is reflected. The resultant Doppler frequency (radar) superimposes itself on the receiving signal and causes interference.

DC receivers may react sensitively to moving objects in the

### 5.2.2 Receivers with low IF

In receivers with low IF, the received signal is mixed close to the base-band or even at half the RF bandwidth. In this range of just a few tens of kHz, good active filters can simply be realised on a chip.

With a very small intermediate frequency, the image frequencies come so close to the basic channel that they can no longer be suppressed with conventional filters. Figure 12 shows a suitable process which at first glance is similar to direct conversion. In one of the two channels, the AF phase is shifted by  $90^\circ$ . Both channels (I and Q) are then linked together in an addition stage. The base-band data become available following low pass filtering.

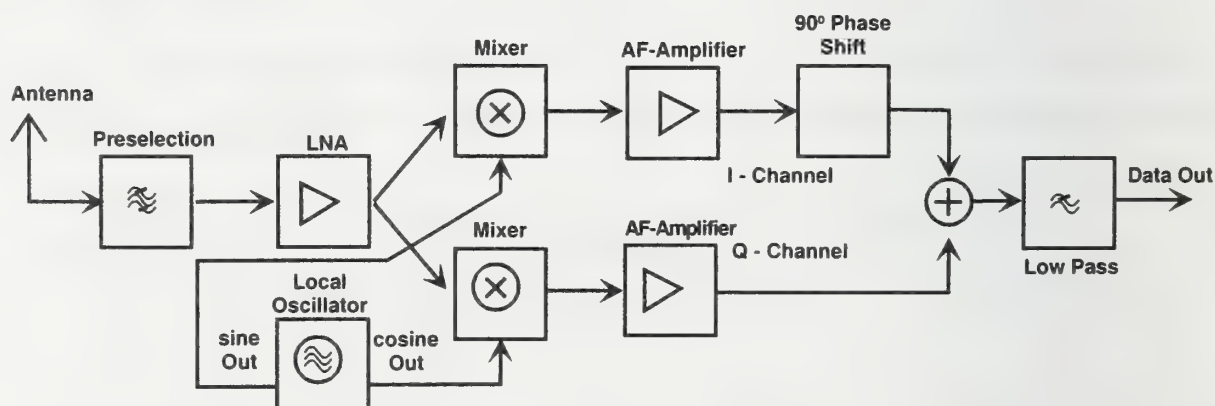


Figure 12 Circuit diagram of a receiver with low IF

Receivers with low IF make better use of the available spectrum than DC receivers.

## 6. Spread spectrum transmission

Originally spread spectrum transmission came from the military field. It was based on the idea of having the carrier frequency transmitted through a broad frequency range so quickly that it could no longer be detected by (conventional) enemy receivers.

If the carrier frequency does not change constantly but follows a specified digital algorithm, this is described as a “direct sequence spread spectrum” (DSSS).

When expanding the transmission band to a large spectral range, the level which can be measured by a non-synchronous receiver is reduced in proportion to the band spread (figure 13).

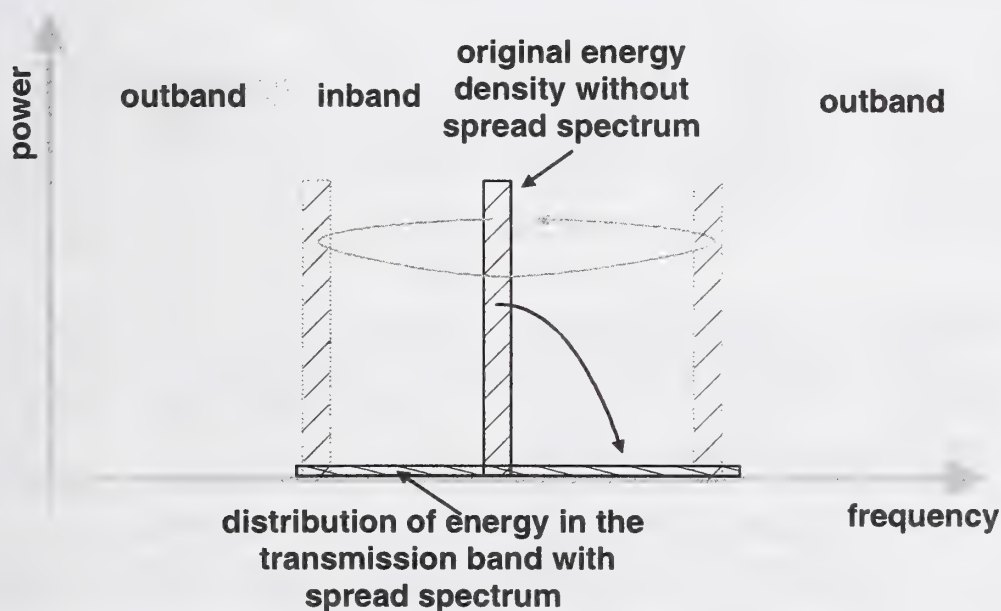


Figure 13 Energy distribution in the spread spectrum transmission channel

This factor is described as system gain  $G$

$$G = \frac{\text{Bandwidth RF}}{\text{Bandwidth baseband}} \quad [1]$$



It is the main parameter for spread spectrum transmission and characterises:

- the extent to which the average amplitude is reduced
- the extent to which transmission interferes with conventional receivers
- the extent to which a conventional transmission is mixed in with the spread spectrum transmission
- the extent to which spread spectrum transmissions interfere with one another
- the maximum dynamic range compared with other signals in the received band

Given the above conditions, 60 dB system gain would seem to be a reasonable minimum. At a data rate of 1 kBit/s this process would require a bandwidth of 1 GHz. At present, however, this is not realistic.

Another drawback of the system should also be mentioned. It is not easy to synchronise a receiver to a transmitter. Correlators which synchronise with a preamble are used for this.

The receiver ICs currently available still require too much energy to fit them in a fire detector. Apart from this, they only offer a comparatively modest system gain of approx. 30 dB.

<p><u>At present</u>, spread spectrum technology does not appear to be developed enough for use in fire detection</p>
---

### **Internet Technology: New Perspectives for Alarm Systems**

Internet technology is making rapid progress with a high pace of innovation and very short innovation cycles. Today, an 'internet year' is to be considered less than 90 days<sup>1</sup>. Prices of standard hardware and software components are dropping constantly and fast. This is the reason why it becomes more and more attractive to benefit from this technological progress and to make use of standard Internet technology for products and applications which had to rely on 'traditional' branch-specific technological solutions by now.

#### **1. Learning from other business segments**

A good example is the telecommunications industry. Communication systems based on traditional switching technology are now facing strong competition by new systems using new standardized protocols like Voice-over-IP (e.g., the ITU H.323 standard defines how to send voice packages via the Internet using the Internet Protocol (IP)) and Internet technology in general. The new systems reduce infrastructure costs by using the same technology for voice and data communication.

Furthermore they take advantage from Internet technology's steep innovation curve and resulting price/performance advantages. For example, Fast Ethernet boards declined in price by as much as 50 percent in the past year, while the price of legacy PBXs (private branch exchanges) declined by only 7 percent approximately (according to Cisco Systems Inc.; Internet Communications Software Group – Driving the Market for Converged Applications and Services (White Paper); July 2000).

As a consequence, established manufacturers of communication systems lost market share to new manufacturers coming from the IT business segment.

---

<sup>1</sup> In fact various numbers are mentioned with respect to how long an 'internet year' is. However, the innovation cycles are very short in any case.

## **2. What does this mean for building automation and alarm systems?**

The crude fact is: There is a challenge coming from IT business and if we do not face it, we will get in trouble. But let's look at it positively: It's not merely a challenge, it offers new chances. Internet technology opens new perspectives not only for building automation (HVAC) systems but for alarm systems with higher demand on reliability as well.

There are mainly two aspects of using Internet technology for alarm systems: Internet technology for system communication and Internet technology for providing new services.

## **3. Internet technology for system communication**

First, the technology can be used for internal communication between system components. This will become attractive for two reasons. On the one hand, the cost of Internet technology hardware components will drop dramatically because of mass scale production, e.g., a processor chip with an Internet Protocol stack on board will probably cost less than five dollars in the near future. On the other hand, standard software implementations of all the relevant protocols are available on the market and, furthermore, numerous software packages are offered, based on the Internet Protocol suite and implementing interesting services of all kinds, e.g. encryption, authentication etc. There is no need to make this software, one can buy it off-the-shelf instead, saving lots of development effort.

In order to understand the situation properly it will help to have a look at the OSI 7-layer communication model (see Table 1).

If two devices want to communicate with each other a common protocol is needed in order to make sure that they understand each other, i.e. 'they have to speak the same language'. The messages to be exchanged have usually application specific content and the protocol to be used is a protocol belonging to the application layer of the layered OSI communication model. In order to transport the message from one device to the other, services provided by lower level protocols are used.



	Layer	Function of the layer
<b>7</b>	Application Layer	User level applications (e.g. WWW (HTTP), FileTransfer (FTP))
<b>6</b>	Presentation Layer	Adaptation of formats (empty for Internet technology)
<b>5</b>	Session Layer	Synchronization, administration (almost empty for Internet technology)
<b>4</b>	Transport Layer	Peer-to-peer communication (e.g. TCP (Transport Control Protocol), UDP (Universal Datagram Protocol))
<b>3</b>	Network Layer	Routing and switching (e.g. IP (Internet Protocol))
<b>2</b>	Data Link Layer	Access method to the physical media (e.g. Ethernet, Token Ring)
<b>1</b>	Physical Layer	Physical media and transport of bits (e.g. Coax, Twisted Pair)

Table 1: OSI 7-layer communication model

What does it mean if we say we want to use Internet technology for system communication? First of all, it means that the Internet Protocol (IP, Layer 3) and probably TCP or UDP (Layer 4) shall be used. This decision allows us to use a lot of software components based on TCP/IP or UDP/IP available off-the-shelf on the market, as it was already described above.

### 3.1 TCP/IP is not enough

However, this decision alone does not guarantee that two devices understand each other. Therefore, a common protocol on the application layer is needed. There are many possibilities to choose from. As there is the general tendency away from proprietary protocols to open standardized protocols (for obvious reasons), BACnet is one of the candidates for the common language among the devices. A little bit deviating from the OSI model, BACnet defines its own network layer protocol and uses UDP/IP as one of its possible data link layers.

When a common application layer protocol has been found, the other open question is what to use below IP as data link and physical layer. In order to profit as much as

possible from widespread technology, Ethernet is the best choice. Ethernet is an established, worldwide standard supported by IEEE and ISO. It has been broadly used in office environments and is penetrating the industrial environment as well. The high number of users ensures the downward price of its components. The long-term exposure to Ethernet technology has produced an expansive knowledge base and unparalleled resources. However, for industrial usage Ethernet has some drawbacks which are seriously stressed by its critics. But these drawbacks can be avoided or overcome today.

### **3.2 Ethernet and real-time behavior**

Ethernet as used in an office environment uses a media access method known as CSMA/CD (carrier sense multiple access with collision detection) that cannot guarantee a deterministic behavior of the network. This can be overcome by using an appropriate network topology with so-called Switched Ethernet technology. The switches make sure that every device connected to the network can operate full-duplex with a guaranteed bandwidth. Thus, the network supports real-time communication with guaranteed response times. In addition, there are several options how to assign priority levels to messages. The fact, that it is possible to build networks with guaranteed response times based on Ethernet technology has been proved many times in industrial automation applications today. One should keep in mind that the requirements with regard to real-time behavior are usually much higher in industrial automation than in alarm systems. Furthermore, it is for sure that the real-time behavior of the Internet (including Ethernet technology) will be further improved because there is high demand for transporting real-time video information via the Internet.

The bandwidth of standard Ethernet is 10 Mbit/s which is quite high compared with other bus systems used for alarm systems today. If that should not be enough, Fast Ethernet is available today with a bandwidth of 100 Mbit/s and Gigabit Ethernet (1 Gigabit/s) is emerging. The IEEE standardization group has even started work to define 10 Gigabit/s Ethernet.

### **3.3 Ethernet and reliability**

Reliability is not only an issue for alarm systems but for industrial automation as well. It is not acceptable that single faults may cause a complete stand-still of a production line easily resulting in million dollar losses. For that reason the issue of making an Ethernet-based control network reliable has also been solved already in industrial automation. There are several solutions for making an industrial Ethernet redundant and fault-tolerant, some of them can even cope with double faults in the system.

More and more often customers ask whether it is possible that existing company-owned TCP/IP network infra-structure can be used for the alarm system as well, in order to save efforts for installation of a separate network. The answer is: yes and no.

As mentioned before, a standard office LAN (local area network) based on Ethernet is not suited for time-critical applications. The network topology would have to be adjusted. For several reasons, it may be the better solution to install a separate security network for safety-critical and time-critical applications which may be connected to the office network via a TCP/IP-Gateway (the terms router or bridge may also be used, although all of them have different functions). The big advantage of using Internet technology for both the security network and the office network is that information which is not time-critical can easily travel across the border between the sub-networks. From a PC in the office network it is then possible to get always up-to-date information about the status of the alarm system. In automation technology this concept is known as the sensor-to-boardroom integration. All plant devices act as servers providing information to anyone anywhere.

### **3.4 Ethernet and robustness**

Some critics of Ethernet for industrial use argue that the connectors (in an office environment cheap RJ45 connectors are used) are not suited for an industrial environment. But this problem has been solved already, too. Several alternative Ethernet connectors are available for rugged environments.



### **3.5 Internet technology has an influence on the system architecture**

As prices drop, the level on which Internet technology can be used profitably drops. While Ethernet and IP communication is used on the management system level (management layer) already today, it starts to be profitable on the control panel level (control layer) now. Even some IP-based sensors are available today, but currently this is not yet profitable for low-cost sensors. However, we see no reason why Internet technology should not move down to the sensor level (device layer) in some years time.

Using Internet technology will of course also have an impact on the overall system architecture of an alarm system. Today a simple alarm system installation usually consists of a control panel with hundreds or even thousands of sensors connected to it. If you think of a multi-functional alarm system for fire detection, intrusion detection, and maybe access control, it is necessary to install lots of cables in the building for the different sensors to be connected with the control panel(s). From our point of view an architecture for a new system that makes use of Internet technology would be a more decentralized architecture with the sensors connected to smaller system units spread over the building and connected via Internet technology. This could probably help to reduce installation and maintenance costs of the system.

The progress in wireless technology may be another influence on future system architecture. Again, using Internet technology has the advantage that e.g. Wireless LAN technology or next generation mobile communication technology, like UMTS (Universal Mobile Telecommunication System), can easily be integrated into the future alarm system architecture because it is for sure that these new technologies will support the transport of IP packages and Internet technology in general.

### **4. Internet technology for providing new services**

Besides system communication, the other important aspect of Internet technology is the provision of opportunities to add value for the customer by offering really new services. In the following, we can just try to give a few examples.

#### **4.1 Remote control and remote service via web technology**

First of all, web technology (using the standardized application layer protocol HTTP (HyperText Transfer Protocol)) allows to access the alarm system anytime from anywhere. Of course, access shall be restricted to authorized personnel. No problem, just take an authentication software package, perhaps some encryption package or whatever you need off the Internet technology shelf. In the alarm system an embedded web server is needed. Again, hard- and software are available on the market in various sizes at various prices. On the client side the big advantage is that every device supporting standard web browser technology can be used for access, whether a PC, a PDA (Personal Digital Assistant), a wireless 'web pad' or – soon – a UMTS mobile phone.

Remote Access by web technology enables you to offer remote control and remote services to your customers, perhaps the service being your USP (unique selling point) giving you an advantage over your competitor. For your service organization remote access offers a huge cost reduction potential. Of course, remote service can also be implemented without web technology. But with web technology you can buy most of the components needed on the market and there is no need to implement and maintain a proprietary solution.

By using Internet technology it is also quite easy to integrate audio- and video-information into an alarm system. There are standards, e.g. the H.323 standard we already mentioned before, which define how to transmit multimedia information over IP-based networks. Not to forget the messaging services which come for free with Internet technology, like Electronic Mail. Alarm or system fault messages can be forwarded by E-Mail, Fax or SMS (Short Message Service for sending and receiving short text messages with a mobile phone). All this offers many opportunities how to offer added value to the customers.

#### **4.2 Software download and application service providing**

Another simple application layer protocol is FTP, the File Transfer Protocol. Based on this protocol, it will easily be possible to download software or data from remote into the system in order to update the system software. If the alarm system is connected with

the Internet (whether the public Internet or a VPN (Virtual Private Network) of the system vendor or any service provider) it becomes possible to offer services to the customer which do not have to be installed on the alarm system. Instead, they are located on a so-called application server owned by the alarm system vendor or a service provider. Such ASPs (application server providers) are just emerging rapidly in the office world. An ASP offers software which can be used via the Internet, but does not have to be installed on the customers computer. The customer can choose to pay a monthly flat-rate for the license to use the software or to pay per use. For an alarm system the customer may want to run a diagnostic program from time to time providing some information about the status of the sensors and detectors. Because he runs the program only if needed, he may prefer to run it from the application server and to pay for it by use. An alarm system installer may prefer not to install a planning and provisioning tool on his own computer but to use the tool from the application server, where he always gets the most recent version supporting all new system features. For the system vendor or service provider it is much more convenient to update the version of the application program on his own application server than to update hundreds of application programs which are installed on the systems of the customers.

#### **4.3 New possibilities for improved risk calculation and priority analysis**

Due to the closer integration of the alarm system's control network with the office network and the transparency between those networks it will be much easier than before to combine information related to the alarm system with information available from the customer's office network. In case of fire alarm, for example, information about the material stored in a warehouse could be taken into account, in order to perform a more detailed risk calculation and priority analysis. This information could help in the decision whether a building has to be evacuated immediately, or in the decision about the best strategy for fire fighting.

Of course, it would be great if the fire fighters could get more detailed information about the situation on-site, before they arrive there. Our vision is, that the fire fighters have access to detailed information from the alarm system via a mobile Internet terminal in their trucks (e.g. using mobile Internet access via UMTS). They can get every



information they need to fight the fire effectively, whether there are specific risks, how to get most quickly to the center of the fire etc. Even transmission of live video images from the site is possible. This vision is not far away.

## **5. Summary**

We have to be aware that if the alarm system manufacturers will not take the opportunities offered by Internet technology for offering new services to the customers, some vendors of IT technology will start to offer more and more safety and security related services. There is a clear trend from delivering only technology to delivering applications and services.

The customers, of course, like systems which are based on open standards and standardized interfaces because this helps to protect the customers' investments, to manage complexity and to reduce risks of change. The use of standard hardware and software components and the new system architecture of multifunctional integrated alarm systems supported by Internet technology will significantly reduce installation and maintenance costs of the systems.

The experiences made with using Internet technology in industrial automation have produced reliable, robust solutions with real-time behavior which are equally suited for use in alarm system applications.

Internet technology opens new perspectives for alarm system manufacturers.

## **Technical State of 868-870 MHz Radio Modules in the SRD Band**

### **1 Introduction**

Wireless detection systems are becoming more and more the norm in modern building technologies. Their competitive advantages are their cost-efficiency and flexibility with which the system parameters can be set and the detector zones be configured. Due to the fact that they have to compete with wired (conventional) systems they need the same standard of safety and reliability. This and other economical aspects are challenging the development of today's wireless detection systems.

### **2 Attenuation of RF-transmission calculation**

The attenuation factors inside a building are an important factor for safe planning and running of the system because radio transmission is limited in range. Mistakes which are made in early project stages lead, without fail, to much customer dissatisfaction.

The attenuation is a measure of how much the radio wave is weakened . It is needed to determine the placement and number of the wireless cell components in advance to guarantee a safe radio transmission. Beside this it is very important for the sales to make an accurate offer.

Which factors have to be taken into account for safe planning?

#### **2.1 Theoretical**

##### **Field attenuation**

The spreading of electromagnetic at frequencies above 30 MHz is like light beams. If a light beam hits an object's surface, it is illuminated with the strength  $E$ . With increasing (doubling) of the distance the light beam has to lighten a

surface which is four times as big as the original surface. Therefore the illuminate strength decreases proportional to the surface increase i.e. to a quarter of the original strength  $E$ .

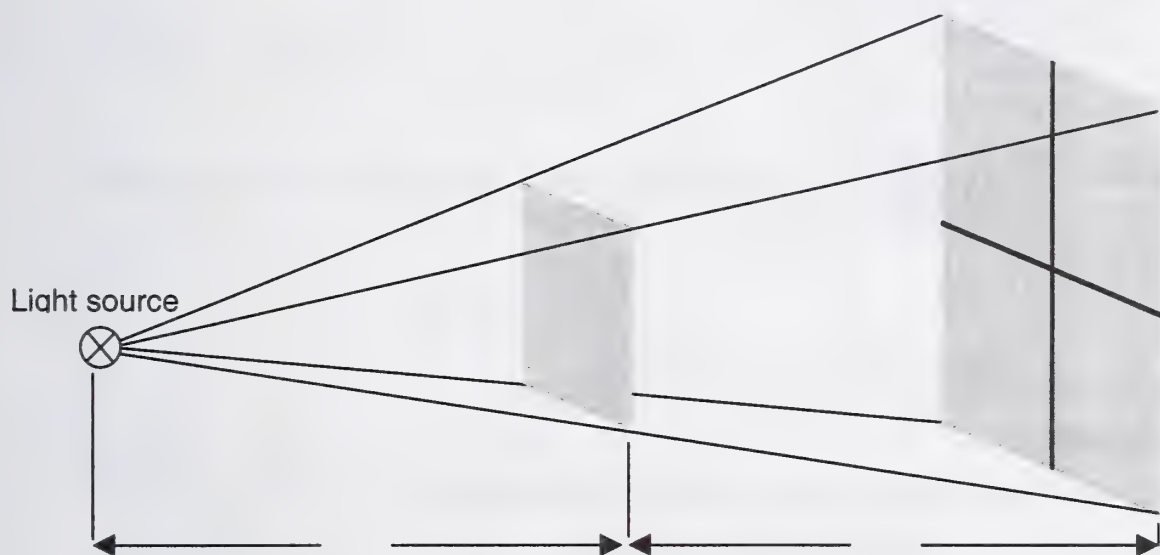


**Figure 2.1:** Relation light strength to distance

The behaviour of radio waves is quite similar.

One of a radio signals features which differs from sun light is its coherence (coherent = waves of one wavelength in phase). Sunlight (incoherent) runs without coupling in all directions form it's source.



## SUNLIGHT

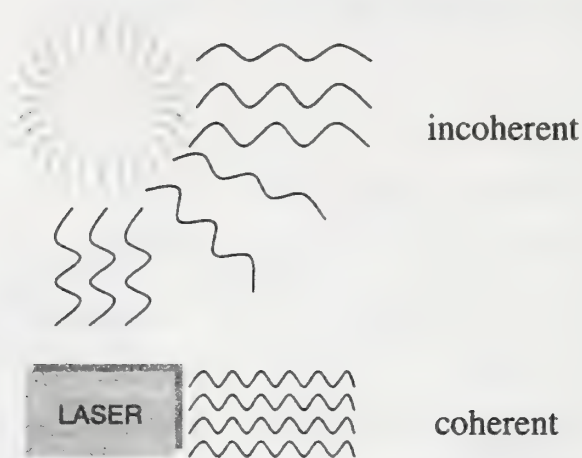
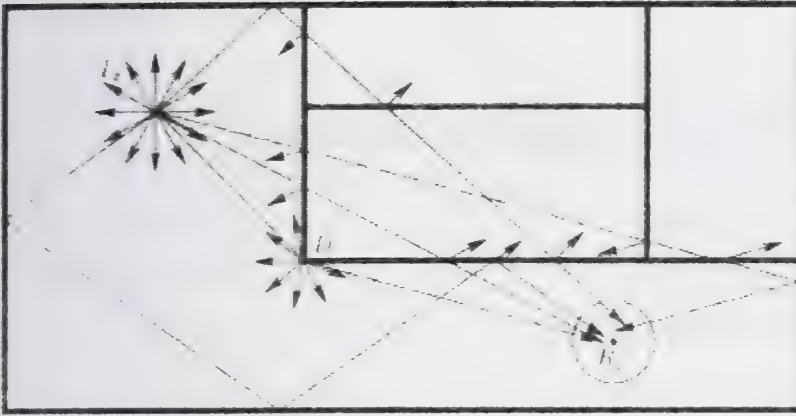


**Figure 2.2:** Coherent and incoherent light.

### Reflection

When like in the algebra, several vectors meet together one point the resulting vector is the sum of all. Depending on the vector orientation vectors are added or subtracted (sun light beams always amplify each other, e.g. switching on of two lamps). In the worst case the vectors subtract from each other and the resulting vector is zero (which is called fading).

In this case no signal can be received on the radio wave.



The sending of radio waves is always spherical around the sender (Tx).  
 At every spherical obstacle we get again spherical reflections (D).  
 Therefore the amount of radiowaves which hit the receiver (Rx) have a variety of strength and orientation.  
 The resulting signal is the sum of them.

### Superimposition of radio waves at 870 MHz

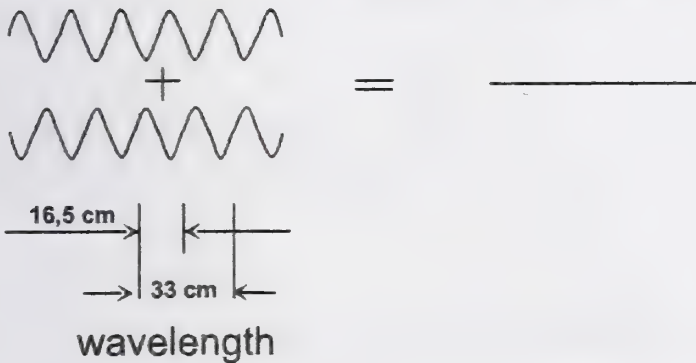


**Figure 2.3:** Wave reflection inside buildings

It's hard to give a prediction inside buildings with its large amount of vector reflections.

There are further ways to calculate the range using computers. These models take account of other influences which have an impact on the transmission of radio waves. Some computer programs use a combination of the beam analysis method and the reflection method.

Putting empirical collected data in a data sheet together we get:

Relation of field strength and distance

- **Outdoors:**
  - Field strength  $\propto 1/r^2$
  - Double distance: Reduction of  $\propto 6\text{dB}$
- **Indoors:**
  - Field strength  $\propto 1/r^5$
  - Double distance: Reduction of  $\propto 16\text{dB}$

Attenuation = f (distance) *Indoor examples*

Distance (m)	40	30	25	20	15	10	5
Attenuation (dB)	90	83	79	74	67	57	40

Figure 2.4: Relation of field strength and distance

By the rule of thumb we can calculate that in an outdoor environment with every doubling of the distance between transmitter and receiver we get an attenuation increase of 6 dB. In an indoor environment it is 16 dB.

Obstacles

When radio beams hit an obstacle which prevent the direct way to the receiver two things can happen. Depending on the thickness and material the beam gets either reflected or gets through the material or both.

Unfortunately the relative permittivity is in most cases unknown. Therefore the best way to insert the right values is to take empirically developed attenuation figures.

SIEMENS empirically developed attenuation values for building materials can be found in the next table:



# Relation of attenuation and material

<ul style="list-style-type: none"> <li>Room separator</li> </ul>	<ul style="list-style-type: none"> <li>very low</li> </ul>	<ul style="list-style-type: none"> <li>&lt; 1 dB</li> </ul>
<ul style="list-style-type: none"> <li>Brick, concrete dry</li> </ul>	<ul style="list-style-type: none"> <li>low</li> </ul>	<ul style="list-style-type: none"> <li>⌘ 6 dB</li> </ul>
<ul style="list-style-type: none"> <li>Sandstone</li> </ul>	<ul style="list-style-type: none"> <li>moderate</li> </ul>	<ul style="list-style-type: none"> <li>⌘ 10dB</li> </ul>
<ul style="list-style-type: none"> <li>Wood wall</li> </ul>	<ul style="list-style-type: none"> <li>moderate</li> </ul>	<ul style="list-style-type: none"> <li>⌘ 10dB</li> </ul>
<ul style="list-style-type: none"> <li>Brick wet</li> </ul>	<ul style="list-style-type: none"> <li>moderate</li> </ul>	<ul style="list-style-type: none"> <li>⌘ 10dB</li> </ul>
<ul style="list-style-type: none"> <li>Plaster plates coated</li> </ul>	<ul style="list-style-type: none"> <li>moderate / high</li> </ul>	<ul style="list-style-type: none"> <li>⌘ 15dB</li> </ul>
<ul style="list-style-type: none"> <li>Reinforced concrete</li> </ul>	<ul style="list-style-type: none"> <li>high</li> </ul>	<ul style="list-style-type: none"> <li>⌘ 30dB</li> </ul>
<ul style="list-style-type: none"> <li>Heavy wet brick wall</li> </ul>	<ul style="list-style-type: none"> <li>very high</li> </ul>	<ul style="list-style-type: none"> <li>&gt; 40dB</li> </ul>

Figure 2.5: Relation of attenuation and materials

S

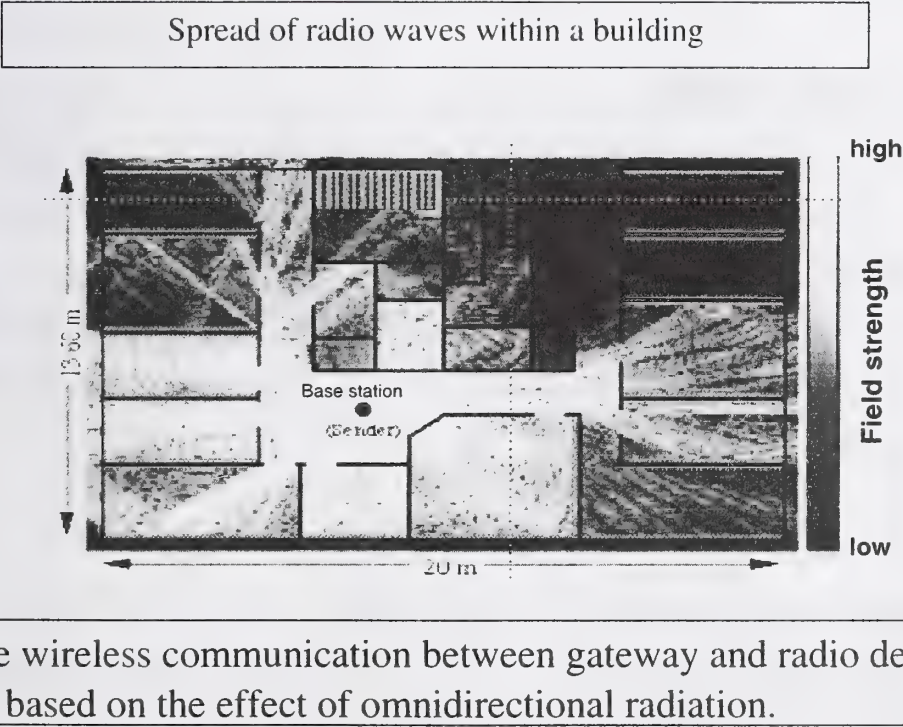


Figure 2.6: Spread of radio waves within a building

## **2.2 Practical**

As we can see in the above picture the direct way has mostly the highest field strength. In areas where reflection of the radio wave is needed the resulting field strength is different in every room depending on addition and subtraction of the field strength vectors.

### **Combination method by using the computer**

A common way to do the calculation is by using a computer.

The method which is used is called combination method, because it combines the beam analysis method and the reflection method. Both methods have advantages and disadvantages, the combination of both delivers an acceptable result.

Unfortunately the calculation with a computer is currently very time intensive and only possible with high performing computers. The procedure allows the definition of the obstacle material through which the beam has to go through. All insertions of information into the computer need much time.

### **Attenuation addition method**

A way to calculate the attenuation inside of buildings quite simply is the addition of empirical developed single attenuation factors (just distances and obstacles and neglecting the reflection).

This is quite an easy method for every layman to calculate the maximum distance between transmitter and receiver where just a few environment factors have to be taken into account.

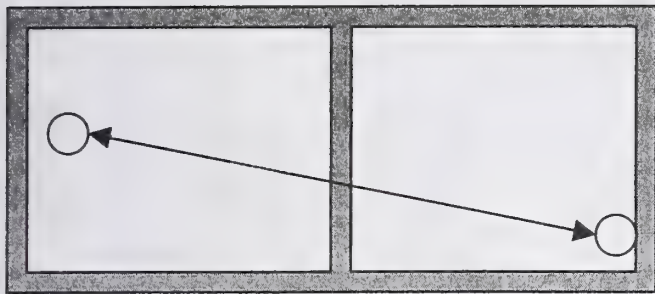
#### **Principle:**

The difficulties for the proper methodology are the right definition of the material which the radio wave has to go through when the direct way is disturbed, and the calculation of the distance between transmitter and receiver or the reflection path between both.

As seen in the previous chapter table 2.4 and 2.5 give the empirical developed overview.

Finally all numbers are added up to the total amount of attenuation.

Example:



Distance:        20m                    74 dB

Obstacle:       concrete dry        6 dB

Amount:                                80 dB

The disadvantage of this method is that the reflections are not included but it gives a suitable start for making a sales offer and doing the project.

In cases of uncertainty a measurement of the range of a radio cell is imperative.

This has also to be done at new installations to guarantee customer satisfaction.

### 3 Handling of radio frequency fading

As described in the previous chapters the reason for fading is that the resulting vector is zero therefore no signal can be received.

When watching the radio reception over a whole day we find strong deviations because of changing reflection circumstances inside the rooms.



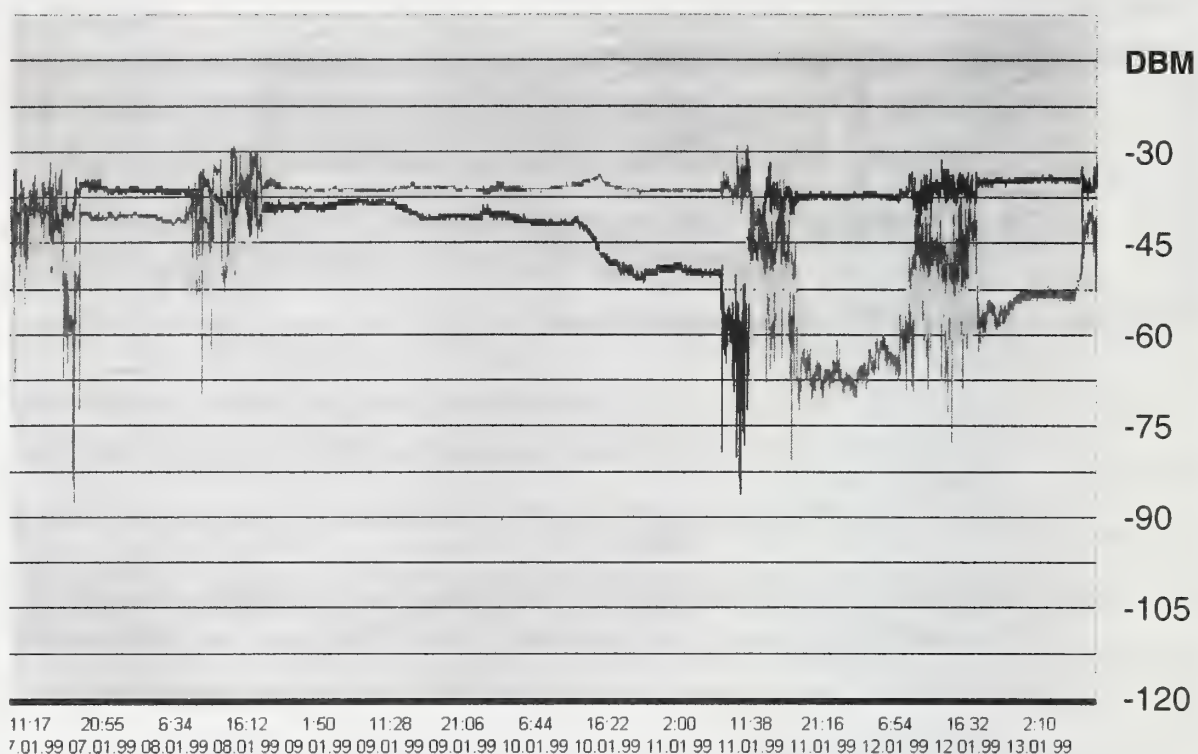


**Figure 3.1:** Transmission quality of a radio cell watched over a whole week. The reasons for the differences in reception quality are the movements inside the building and therefore changes of the reflections. ( tests with just a single hand covering of the radio module show a disturbance of the signal).

How can a radio system avoid this variation in reception?

### 3.1 Aerial diversity

One solution to avoid this is to equip the radio module with two aerial which are orthogonally oriented to each other. Due to the different vector orientation the module can take the antenna which has the best reception of the signal.

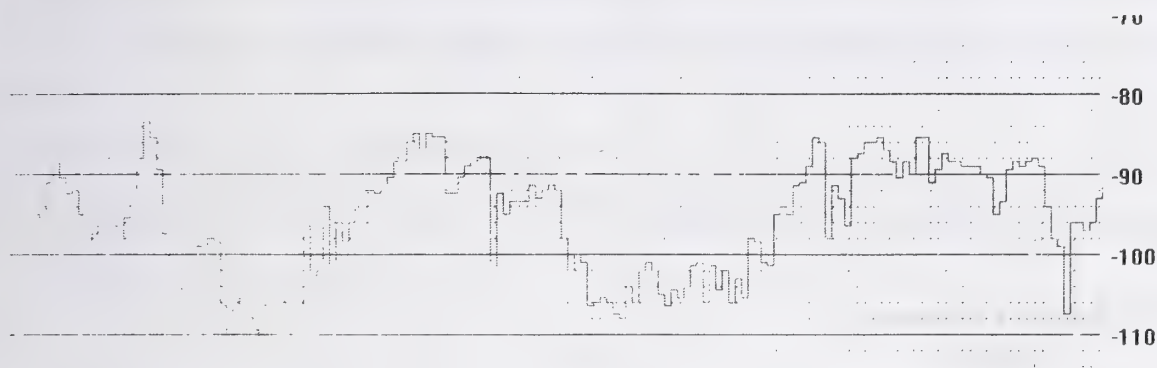


**Figure 3.2:** Transmission difference with two antennas

(e.g. We can see similarities in our daily life, with our ferrite-rod aerial radio. To get the best reception we rotate the ferrite-rod (orientation) until the radio receives best.)

### 3.2 Channel switching

S

## Alternate frequency channels

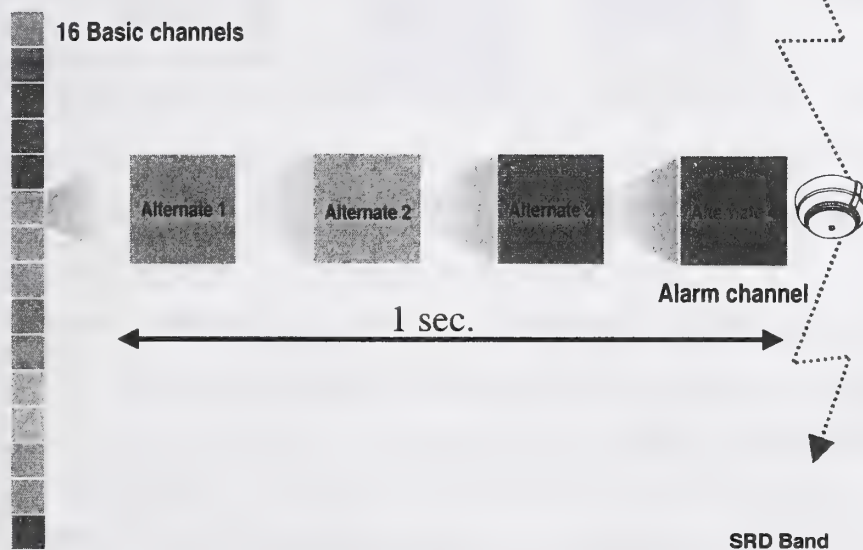


**Figure 3.3:** Channel switching changing the wave length through changing the frequency.

Another way to avoid short-term reception loss is to change the frequency. This has an impact on the wavelength and the sum of vectors between transmitter and receiver.

\*This can be achieved with SIGMASPACE/ TeleRex in a maximum of four times at fixed preprogrammed channels.

**3.3 Bypass of information**

**SIEMENS**

**Telegram bypass for radio disturbances**

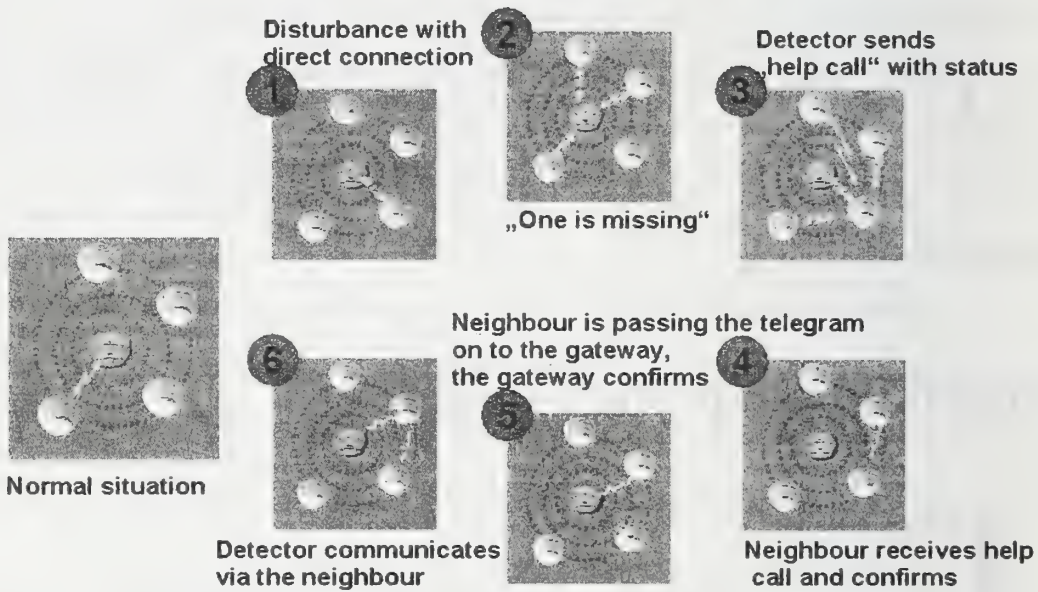


**Figure 3.4:** Bypass of information

In cases where the transmission from transmitter to receiver is disturbed a technique is to bypass the message via a neighbour radio module and use this as a repeater. The above picture explains how this can work.

\*With all these procedures installed in our wireless system SIGMASPACE/TeleRex we have achieved a very high transmission quality. Beside that, disturbances are detected within 100 seconds!



#### **4 Conclusion**

Many challenges are testing the progress of modern wireless systems in the building technology infrastructure. Only when the technique dominates totally can it replace wired systems in the future.

This presentation has shown how at SIEMENS these challenges are accepted. We are looking to a sound future of wireless building technology systems.

## **APPENDIX**

### **Application SIGMASPACE/TeleRex**

All building danger alarms as defined under DIN VDE 0833 and a range of additional technical information can be displayed and processed with one system, the SIEMENS SIGMASYS/AlgoRex danger alarm system.

To enhance the flexibility and suitability characteristics of SIGMASYS/AlgoRex, SIEMENS developed SIGMASPACE/TeleRex, a wireless detector system which is integrated into SIGMASYS/AlgoRex. The products allow SIGMASYS/AlgoRex to protect each individual customer's building and keeps pace with the customer's changing environment and requirements.

SIGMASYS hazard detection equipment is able now to keep pace with every customer requirement through the simplest and quickest of system extensions with SIGMASPACE/TeleRex detectors.

The advantages of SIEMENS' wireless system in a nutshell:

- installation neatness – through wireless connection
- flexibility– through use of the most modern radio technology
- functional security- through two patented disturbance handling procedures
- detection reliability – through SIEMENS' 1<sup>st</sup> class detector experience
- profitability– through simple installation and long battery life
- automation – through automatic radio system configuration

As an example how a typical configuration of SIGAMSYS/AlgoRex with SIGMASPACE/TeleRex can look, see below picture.

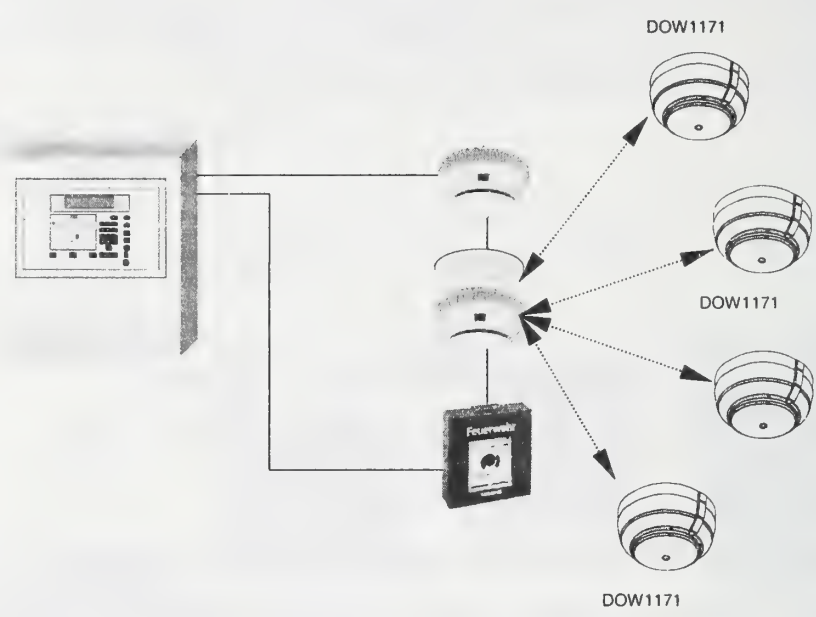


**Figure 5.1:** Typical configuration SIGAMSYS/AlgoRex with SIGMASPACE/TeleRex

As can be seen in figure 5.1. the SIGMASY/AlgoRex control unit is wired connected to the detector and the call point. In the middle we see the SIGMASPACE/TeleRex, which is the interface between wired and wireless technology.. The gateway is the master of every radio cell. SIGMASPACE/TeleRex uses wired and wireless technology it is called a hybrid system.

**Features**

Only approved (VdS EN 54-7) hybrid system in the SRD band with text alarm location message.

- Transmission power: 5mW
- Frequency: 870MHz
- Attenuation budget: 115dB
- Wireless distance: approx. 40m in buildings

Oliver Linden, Hans Hölemann

University of Wuppertal - FB 14 - Section: Fire and Explosion Protection

Gauss Str. 20, 42097 Wuppertal, Germany

### **Testing Methods for Gas Sensor Based Fire Detectors**

*VdS Testing Methods - Advantages and Disadvantages -  
Suggestions for Improvement*

#### **Abstract**

*Within the past years fire detection technology has developed at a high speed of innovation. Computerization and the use of sophisticated fire detection algorithms gained more and more importance at taking advantage of the wide range of opportunities multisensor detectors show. Despite this development testing methods still remain to be the same. European testing standards and testing equipment that have been created for fire detectors decades ago are undergoing adoption to state of the art of fire detection technology step by step. Against this background the new VdS testing methods for gas sensor based fire detectors have been created basing on the European standard EN 54.*

#### **1 Introduction**

Nowadays, fire detection technology is characterized by an increasing use of multisensor-detectors. In particular optical smoke sensors, ionization chambers and heat sensors are combined. By the continuous development of gas sensors, which are based on different physical and chemical principles, there is - in the meantime - the possibility to further improve multisensor-detectors by the additional use of gaseous fire criteria. Using suitable detection algorithms gas sensors can contribute to reduce the rate of deceptive alarms.



Furthermore, gas sensors seem to be suitable for the use in some special applications, in which conventional fire detectors are - due to the predominant environmental factors - not to be used or in which they cannot react sufficiently fast.

Gas sensor based fire detectors as well as conventional smoke- and heat detectors have to be subjected to a testing procedure in accordance with EN 54 to receive VdS approval. In this context, the University of Wuppertal, section fire and explosion protection, supports VdS Schadenverhütung at the development of a new testing procedure in design, realization, and testing out.

This paper gives an outline of VdS testing methods [1] for gas sensor based fire detectors. The advantages and disadvantages of the testing procedure will be illustrated and possible future solutions will be derived.

## **2 VdS Testing Methods for Gas Sensor Based Fire Detectors**

In co-operation with industry and the University of Wuppertal and supported by the Institute of Applied Physics in Giessen, VdS Schadenverhütung has developed test guidelines for the testing of gas sensor based fire detectors.

As presented below the VdS-test procedure can be broken down into various modules:

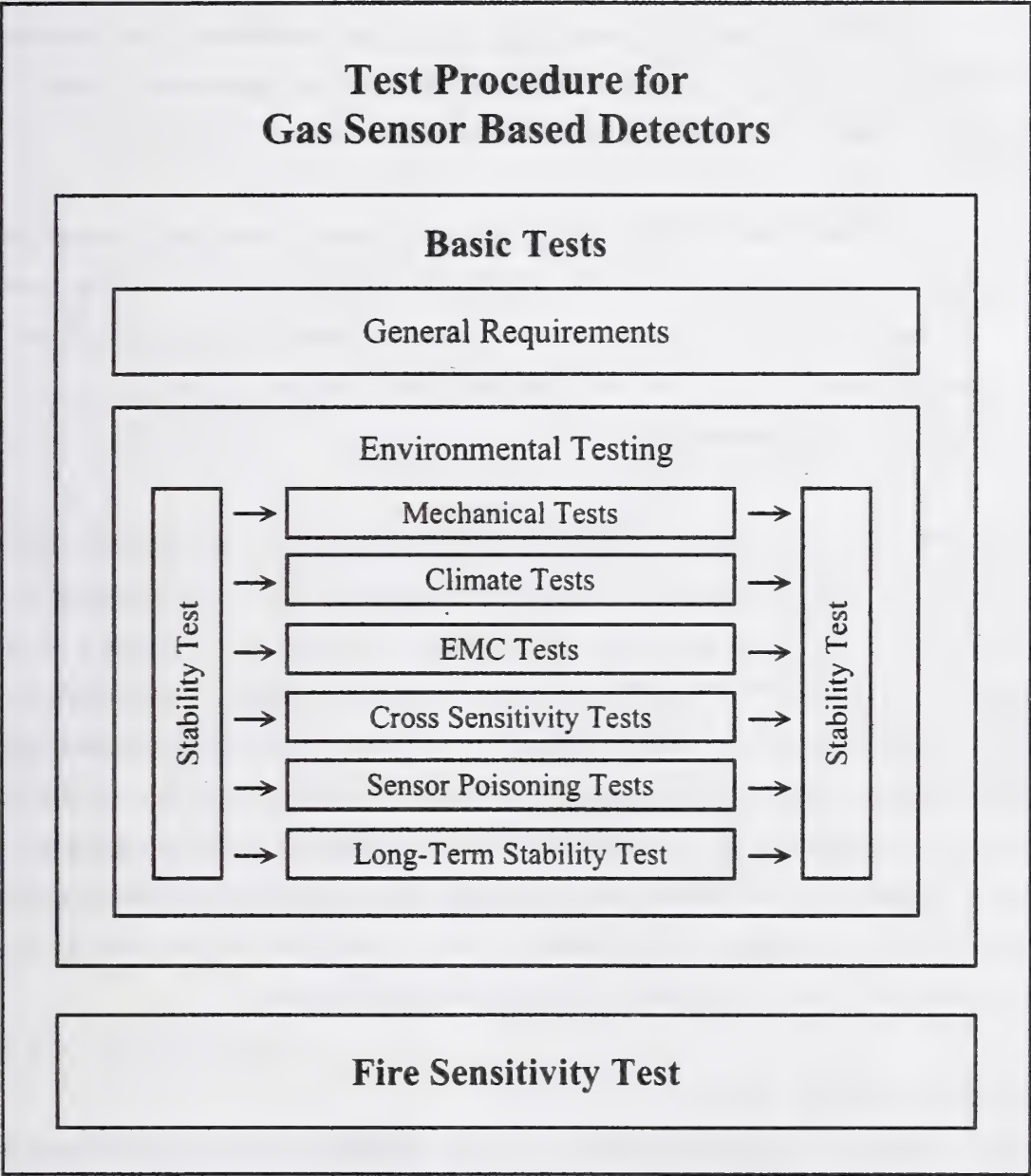


Figure 1: VdS test procedure for gas sensor based fire detectors

## 2.1 Environmental Testing

The requirements of the test methods, which is to assure the efficiency and the reliability of the individual components of fire detection systems, are described in the DIN EN 54 series of standards [3]. This series of standards also includes the functional testing of fire detectors with gas sensors (gas sensor based fire detectors). Section 1.3 of DIN EN 54, Part 1 stipulates:

*“The fire detection system must not only work satisfactorily under the conditions of the fire event but also under environmental conditions which will normally occur in practice. The stipulated tests have the purpose to provide evidence for the performance of the system and its components under such conditions.”*

The definition of this objective allows us to conclude that it is not necessarily sufficient to test fire detectors based on a new technology using a selection of existing tests in accordance with EN 54. Rather, it may be considered as an appeal to find out whether - and if so, which - additional tests may be necessary for the application of new technologies in fire detection in order to make sure that a detector will operate satisfactorily “also under environmental conditions, which will normally occur in practice”. Against this background, new tests have been included in the test schedule for gas sensor based fire detectors and these have been chosen with respect to the well-known problems of *sensor poisoning* and *cross-sensitivities* found in many gas sensors.

### Cross Sensitivity Tests

The occasionally insufficient selectivity of gas sensors includes the risk that gas sensor based fire detectors might be put in the alarm status by a large number of non-fire specific parameters [2]. For this reason, two deceptive alarm tests have so far been defined, where the detector must not emit an alarm signal. For the time being, the following parameters apply to the existing tests:



Deceptive parameter	Concentration	Test period
Ethanol (similar to [4])	500 ppm	1 h
Ammonia (similar to [5])	50 ppm	1 h

### Sensor Poisoning Tests

In order to largely exclude "poisoning phenomena" of gas sensors in practical use, additional tests are carried out to determine the effect of sensor poisons. It should thus be determined, whether certain substances will irreversibly damage the sensors or negatively impact on the function of the test specimen or even prevent the detector's use altogether. For the time being, two potential sensor poisons have been chosen:

Sensor poisons	Concentration	Test period
Ozone	500 ppb	1 h
Hexamethyldisiloxane (HMDS) (similar to [4])	10 ppm	1 h

In future it will probably be necessary to subject gas sensor based fire detectors to further tests for deceptive alarms and poisoning - depending on the sensors' principle. The ozone test concentration determined so far corresponds approximately to the maximum value which can be measured in the ambient air in summer. There are considerations to increase the requirements for this test.

## 2.2 Stability Test

According to the VdS testing methods and similar to the smoke (heat) channel for testing smoke (heat) detectors, a gas mixing apparatus is used for testing the signal reproducibility. This way of performing the stability test is - nowadays - the only one and logical means to establish defined testing methods for gas sensor based fire detectors within a short period of time.

Wolfgang Krüll

Gerhard-Mercator Universität Duisburg, Germany,

Department of Communication Engineering

## **A modular data acquisition system for the measurement of fire characteristics**

### **1. Introduction**

This article describes the development of a computer-aided data acquisition system as a component of an installation in a fire detection laboratory. With this laboratory standardized test fires (EN54) are possible as well as fundamental experiments. Besides the required measuring techniques (measurement of smoke density according to the ionization current principle and the extinction principle, temperature and weight loss) the system offers the possibility of implementing new measuring instruments and sensors relatively simply due to its modular structure. Thus this system can accommodate new measuring instruments of interest in the future. The motivation for developing this new data acquisition system was to submit a proposal for a standardized data acquisition in other laboratories which can accommodate various existing and possible new standards. The goal was to launch a flexible hardware and a user friendly expandable software. Thus the source code of the program has to be understandable not only for experts such as e.g. C++ programs. On the other hand we wanted to replace the existing system with a much more comfortable system.

### **2. The fire lab**

The existing fire lab consists of the main fire room with a base of 10.5 m \* 9.0 m and two observation rooms, situated over the other. The ceiling in the main fire room is vertically adjustable (2.87 m ... 6.57 m). Therefore, the fire lab provides the opportunity to perform standardized test fires as well as basic experiments with different room heights and volumes. The technical equipment is placed in the upper observation room as well as on top of the adjustable ceiling. The top of the ceiling can be walked on if the ceiling is in the maintenance position. Non-inflammable plates (0.6 m \* 0.6 m) on the under-

side of the ceiling can be removed. This enables easy equipment assembly.

Requirements for the data acquisition system to be developed:

1. Computer-based data acquisition system

The data acquisition hardware should be placed on top of the vertically adjustable ceiling. That has the advantage that new devices can be installed easily and quickly. Further computing facilities should be placed in the observation room.

2. The existing devices should be connected directly and trouble-free. Figure 1 shows the structure of the data acquisition system to be realized.

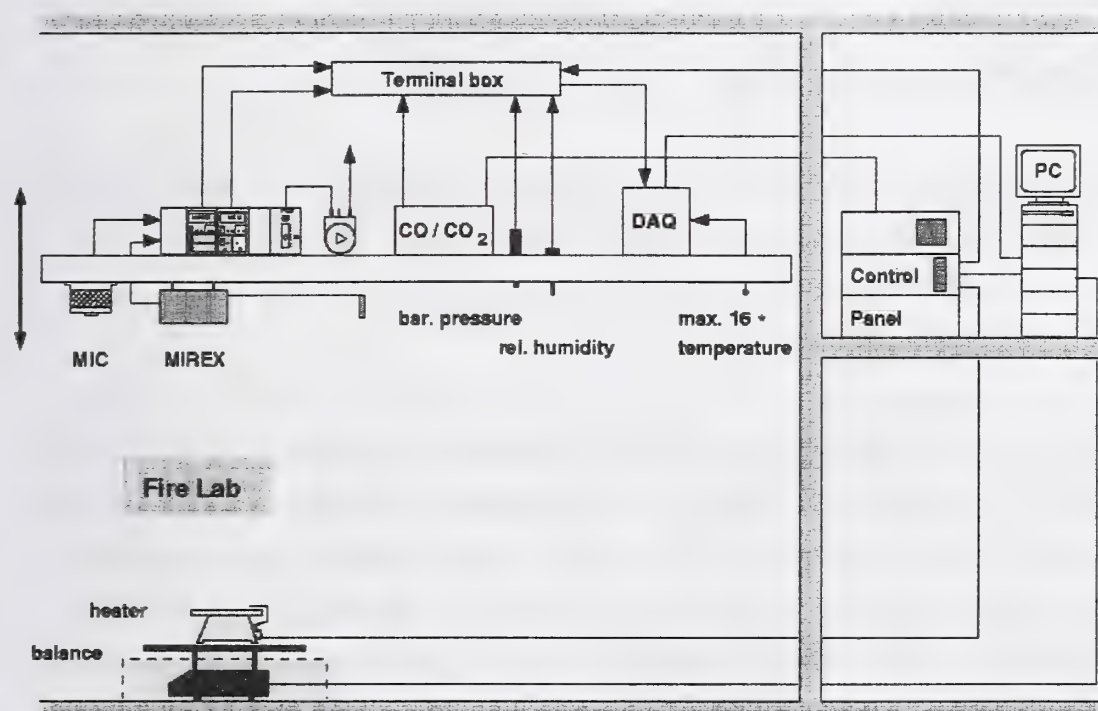


Figure 1: Structure of the data acquisition system to be realized

- Basic measuring equipment meeting the requirements of the European standard EN 54:  
Measuring ionization chamber (MIC), smoke density measuring instrument according to the extinction principle (MIREX), temperature sensor (Pt100), balance, controller for the heater and measurement of the heater temperature
- Further devices for basic experiments:  
The reduction of false alarms is only possible if (as much as possible) information about normal surrounding conditions of fire detectors is known (e.g. relative air



humidity, barometric pressure, temperature distribution under the ceiling). The inclusion of gas detection within multi-sensor detectors requires a new reference measuring technique. Therefore measurement of the CO and CO<sub>2</sub>-concentration is recommended. Appropriate measuring instruments are installed.

3. The hardware should be produced and tested by a well-known manufacturer. A trouble-free installation and a world-wide support had to be guaranteed.
4. The software to be developed should be written in a programming language which is adapted to the chosen hardware. The software should have the ability to monitor the measured data online.

### **3. Modular hardware design**

The implemented system consists of the following components:

- Data Acquisition System (hardware and software)
- Computing Facilities
- Measuring Devices
- Control Panel

To develop a high quality data acquisition system for measurement and control it is important to understand the function of all components. In this field signal conditioning is especially important because existing sensors provide multiple electrical signals in various forms. The data acquisition system has to be adapted to measure all these different signals. The type and number of sensors (thermocouple, RTD, voltage or current output of a device) define the components of the system. Interesting is for example the number of channels (single-ended or differential), the resolution of the analog signals and the sample rate.

The chosen modular SCXI-system is produced by National Instruments Corporation. The data acquisition system consists of a module housing (SCXI-2000), a data acquisition card (SCXI-1200) with 24 additional digital inputs and outputs for the adaptive control of devices (e.g. controlling the air conditioning system) during a test fire, a 16-channel-multiplexer (SCXI-1122) for temperature sensors (Pt 100) with a terminal box and a 32-channel-multiplexer (SCXI-1100) for voltage channels with a 32-channel-

terminal-box (BNC-2095) with BNC-connectors (for various measuring instruments). Figure 2 shows the structure.

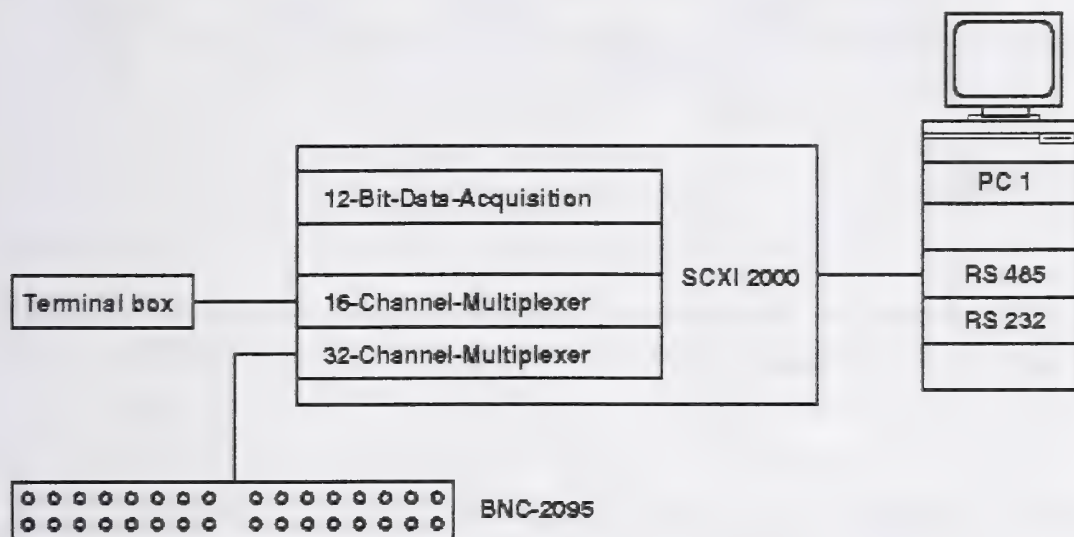


Figure 2: Structure of the chosen data acquisition system

The realized system concerns a modular structured system which is expandable at any time and is connected to the central computer via RS-485 serial communication. The advantages of data transmission via RS-485 over the conventional RS-232 are:

- longer distance (max. 1200 m)
- faster data transmission (max. 1 Mbps), data throughput will usually be limited by serial communication rates
- lower error probability during data transmission (by symmetric signals)

The appointed computer is a standard-PC (Pentium 3 / 500 Mhz) with 256 MB RAM and an additional RS-485 serial interface, the operating system is Windows-NT. The presented flexible data acquisition system is an integral component of a computer network (see figure 3). The archived data can be accessed by all installed computers.

The control panel in the observation room contains the display unit for CO and CO<sub>2</sub>, the components for controlling the heater, a module with the power switch, fuses and switches to drive the connected measuring instruments with the option to install further devices in the housing. It is connected to the central computer via a RS-232 serial communication.

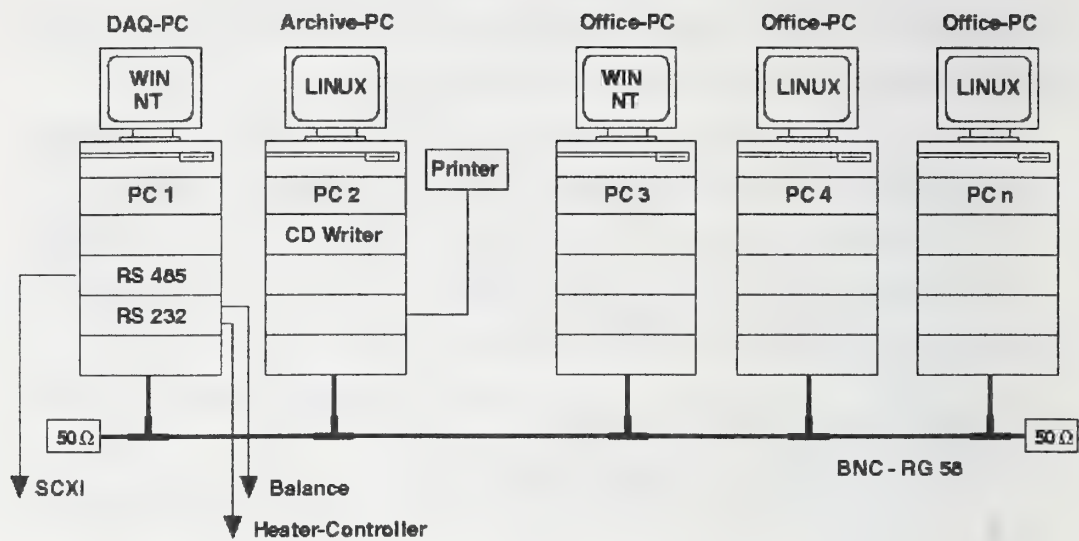


Figure 3: Structure of the computer network

#### 4. Data acquisition software

The software integrates the sensors, signal conditioning, and data acquisition hardware into a complete and functional system. The developed software enables controlling of test fires with the ability to monitor measured data online. Filesaving and documentation are possible as well as the following representation and analysis of the measured values. The software is designed with the graphic programming language „LabView" and afterwards compiled into a not editable, only executable program by the „Application builder". This executable application runs at compiled execution speeds and does not require a separate run-time system. A non-changeable user friendly software is provided to the user, so that the source code is protected against undesignedly modifications. Modifications can be made only by an authorized person.

##### 4.1 Review of use of the graphic programming language „LabView"

The graphic programming language „LabView" was developed by „National Instruments Corporation" for controlling data acquisition hardware and has broad in the application field of automation and instrumentation. The use of „LabView" as



programming language offers the advantage that a clear, easily understandable surface is provided, which can be served without detailed knowledge.

The programs are titled „Virtual Instruments (VI)“ and consist of two parts:

- the front panel user interface with indicators and operative functions for the interactive control of the software system
- the diagram with the wiring of the applied functions

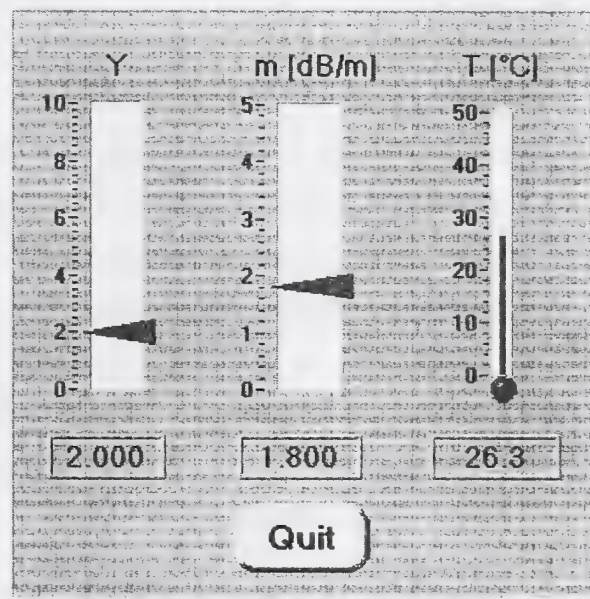
Graphic programming with „LabView“ is accomplished in two steps: VIs are built instead of written programs:

- component placement (indicators and controls) in the front panel window:  
Objects are chosen from the „Controls palette“, e.g. numeric displays, meters, thermometers, charts, and graphs. Parallel to the component placement in the panel window corresponding symbols are generated in the diagram. When the VI is complete the front panel is used to control the system while the VI is running. Figure 4 and 5 show an example.

- component placement and wiring of the components in the diagram window:

Component placement and wiring is similar to constructing a graphical block diagram. Objects are chosen from the „Functions palette“ e.g. arithmetic or logic functions and file I/O operations. These interconnections are used to transport data from one component to the next as well as controlling the program sequence at the

same time. A component does not start processing until valid data are available at all inputs. This type of programming is called dataflow programming because the interfaces transmit data as well as controlling the program sequence.



Picture 4: Panel with three indicators.  
Checking start conditions

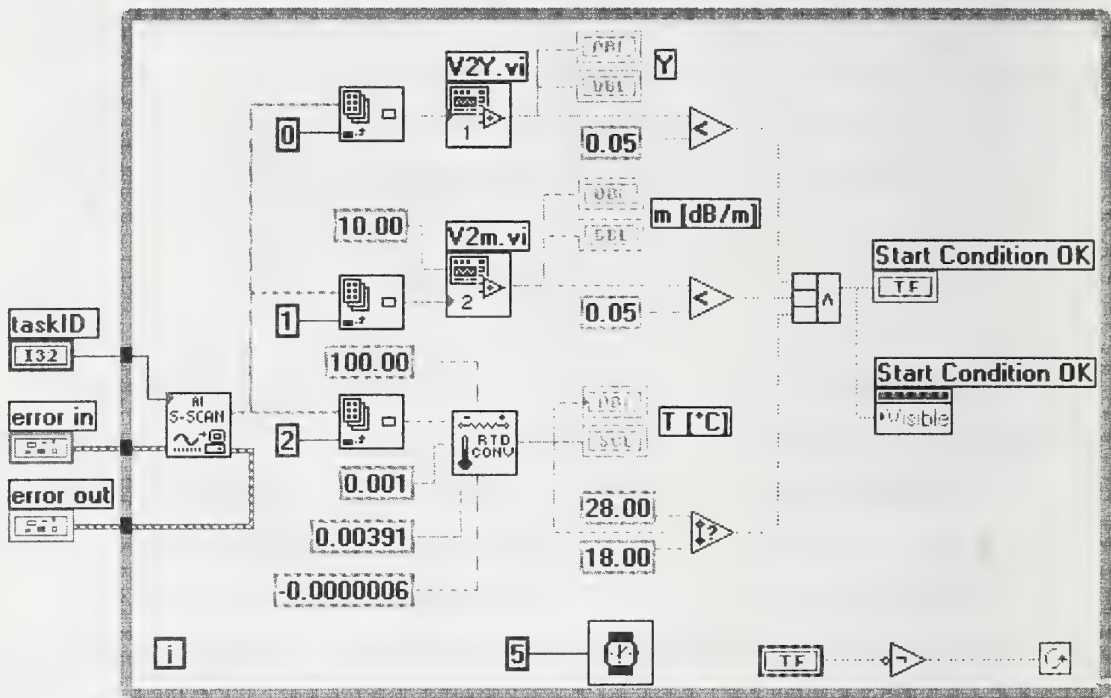


Figure 5: Diagram for the front panel shown in figure 4

A running VI is controlled by the flow of data between blocks, and not by the linear architecture of sequential lines of a text. Any VI can run independent or as part of another VI. It is possible to create diagrams that have simultaneous operations. „LabView“ has the ability to create VIs in a modular design. Created VIs can have their own icons, so that a hierarchy of VIs and SubVIs can be designed.

An example for a diagram with custom made SubVIs (with the icons „V2m.vi“ and „V2Y.vi“) and „LabView“-functions is shown in figures 5, 6 and 7. The diagram shown in figure 5 belongs to the front panel shown in figure 4.

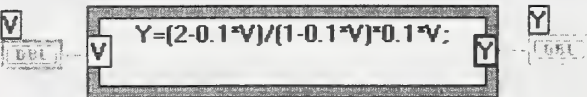


Figure 6: „SubVI“ converting MIC-voltage to „Y“

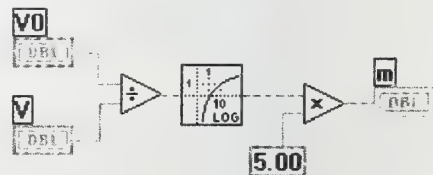


Figure 7: „SubVI“ converting MIREX-voltage to m [dB/m]

Smoke density measured with the „Measuring Ionization Chamber (MIC)“:

$$Y = \frac{(2-X)}{(1-X)} \cdot X \quad [1]$$

$$X = \frac{U}{10V}$$

$X$ : relative chamber current change

$Y$ : smoke density

$U$ : measured  $X$ -value

Smoke density measured with the „Extinction measuring equipment (MIREX)“:

$$m[dB/m] = \left(\frac{10}{d}\right) \cdot \log\left(\frac{1}{T}\right) \quad [2]$$

$$T = \frac{U}{U_0}$$

$m$ : extinction module

$d$ : active light path in smoke

$T$ : transmission

$U$ : received light intensity with smoke

$U_0$ : received light intensity with smoke

It is possible to modify, interchange, and combine created VIs with other VIs to meet application needs. Only the programmer can use these two levels. Operators may only use the front panels. Thus operators cannot modify programs.

## 4.2 Review of the developed data acquisition program

Beginning with the selection of the test fire to be recorded, the installation and selection of sensors, the representation of the measured values up to archiving and editing all functions are controlled by the system. The program is arranged in such a way that operating errors are largely excluded. Before a measurement can be started, the operator has to load a „profile“ (see figure 8) to provide the program with all necessary information:

- selection of the test fire to be recorded
- additional information:
  - operator, name of the project, additional remarks, etc.
  - sampling rate
  - data path
  - channel configuration:
    - status (inactive, to be measured, to be measured and displayed)
    - label (name of the sensor)
    - data range (minimum and maximum voltage level) of the sensor



After provide the program with these parameters it is possible to start the measurement. Measurement includes the following functions:

- checking start conditions according to EN 54 (see figure 4)
- offset adjustment of the input amplifiers
- data acquisition, scaling and online monitoring of selected measured signals (see figure 9)
- controlled fixing of the „end of test“ condition  $t_e$  and check of the reproduction requirements according to EN 54 part 9 as well as EN 54 part 7
- hand controlled setting of the „end of test“  $t_e$  is possible
- filesaving

Following the measurement and filesaving it is possible to load and print prepared data (see figure 10) . Recorded data consist of two parts:

- the header with detailed information of the measurement
- measured values as a table

Its advantage is the representation of the measured values with a „LabView“ program as well as with a conventional spread sheet program (e.g. EXCEL).

## **5. Conclusion**

The application of the chosen hardware, the programming language „LabView“ and the developed data acquisition software offers a high-performance data acquisition system, which is readily expandable. A further advantage of „LabView“ as programming language is the compatibility with the installed hardware which both come from the same supplier. „LabView“ was designed by „National Instruments Corporation“ to control data acquisition hardware. It is applied in various industry branches very successfully. World-wide support is guaranteed.

In „LabView“ the interaction between a user and the application proceeds in panels. The topics of these panels are specified by the respective application. Panels can generate other, overlapping panels. But only one panel is active at a time. The source code of a

„LabView“-program is not a linear program in a top-down design. Thus it is not sequentially readable as with other text-based program codes (e.g. C++). The program consists of numerous partly serial sequences, loops or other child panels (SubVIs). „LabView“ is a multitasking system. Thus it is possible to create diagrams that have simultaneous operations with the result that large and complex programs require a high degree of discipline from the developer during programming.

Even though the designed data acquisition program is very large, it is possible to expand or modify the program to adapt it to different standards which create additional requirements. The source code of the introduced software is understandable. Created VIs can be combined with other VIs to meet new application needs.

The modular structure of the introduced hardware and the developed software offer the possibility of also adapting this system for use in other laboratories as well as for special requests.

- [1] Delta Electronics : Instruction Manual for Smoke Measuring Equipment,  
MIC Type EC-912
- [2] Delta Electronics : Instruction Manual for Smoke Measuring Equipment,  
MIREX Type EC-910







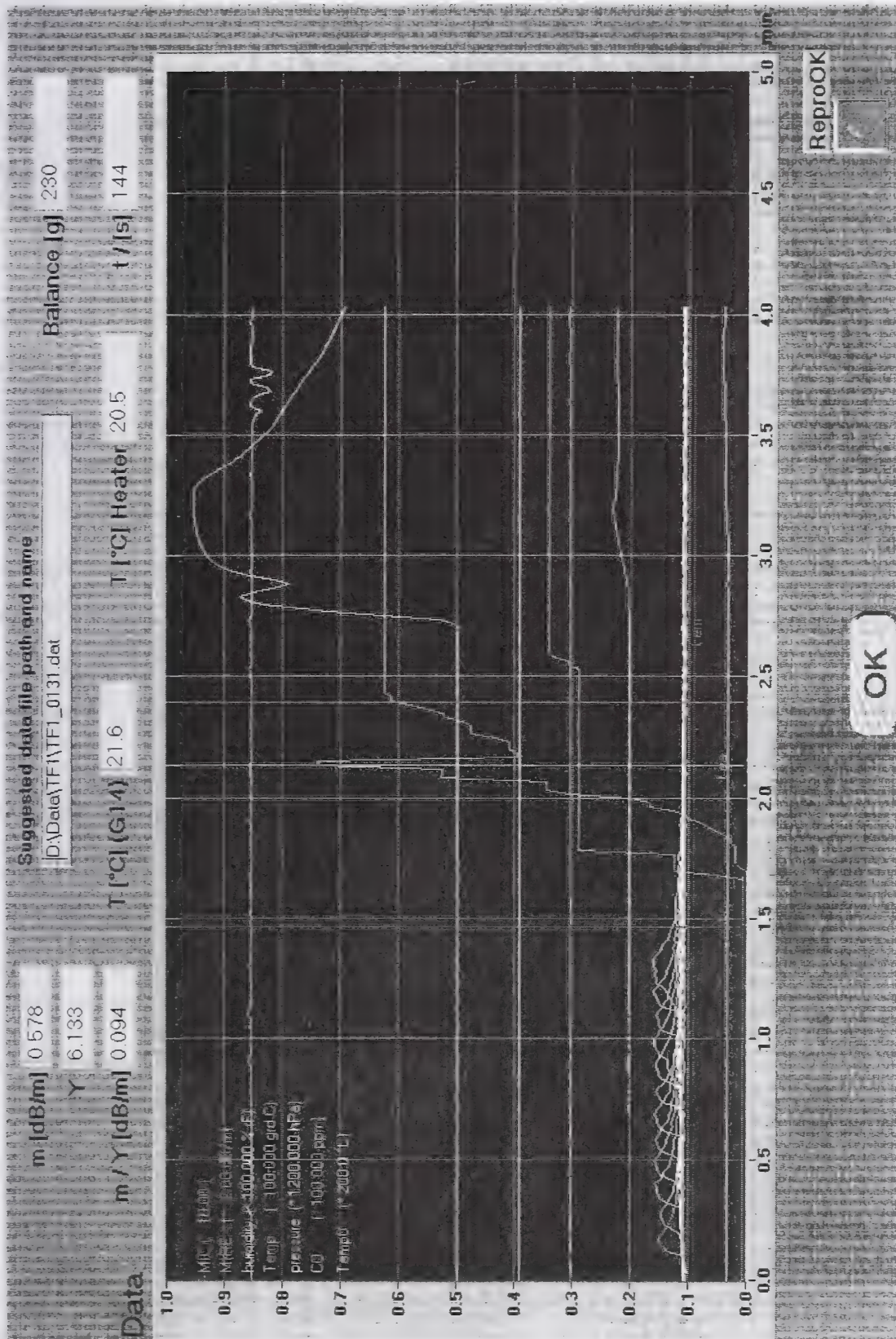


Figure 9: Representation of measured values during a fire test





J. R. Qualey III, L. Desmarais, J. Pratt

Simplex Time Recorder Co., 100 Simplex Drive, Westminster, MA 01441

## **Response-Time Comparisons of Ionization and Photoelectric/Heat Detectors**

### **1. Introduction**

Despite the recent introduction of new technologies, the vast majority of smoke detectors sold and in service today are based on either the photoelectric or the ionization principle. In the twenty-five years since smoke detectors began to attain widespread acceptance as essential life/safety fire protection devices [1], it has become generally accepted that "ionization smoke detection is more responsive to invisible particles (smaller than 1 micron in size) produced by most flaming fires" [2]. It is also generally accepted that photoelectric detection is "more responsive to visible particles (larger than 1 micron in size) produced by most smoldering fires", "somewhat less responsive to smaller particles typical of most flaming fires", and "less responsive to black smoke than lighter colored smoke" [2]. However, the relative merits of the two detector types continue to be a subject of discussion [3].

We recently reported the results of fire tests comparing the response time performance of three models of ionization smoke detector (from three different manufacturers) to a photoelectric smoke detector model [4]. As an extension of that work, we conducted an additional series of fire tests comparing the performance of two ionization detector models used in the earlier study to the performance of a single model of photoelectric/heat detector. The photoelectric/heat detector combines a thermistor-based heat detector with a photoelectric smoke detector which is otherwise identical to the model used in the earlier study. These series of fire tests are the latest in an ongoing investigation which Simplex is conducting to help develop



objective criteria for which smoke detector technologies are most appropriate for different applications.

Consistent with the results of the earlier investigation comparing ionization smoke detectors to photoelectric detectors, the results reported here show that in UL 268 Smoldering Smoke tests, photoelectric detection occurred many minutes earlier than ionization detection. The results also show that in UL 268 Flammable Liquid Fire tests and TF-5 type liquid heptane fire tests, photoelectric and ionization detection occurred at about the same time. The three heat detector modes evaluated (15 °F/min ROR, 20 °F/min ROR, and 135 °F fixed temperature) generally did not exceed their alarm thresholds in either the TF-5 type fire tests or the UL 268 Smoldering Smoke and Flammable Liquid Fire tests. However, the maximum rate-of-rise measured for the heat detectors in the TF-5 type tests suggest that the heat detection component would be useful for fires with a heat release rate (HRR) somewhat larger than that generated in the test.

## **2. Test Procedures**

Two commercially-available ion smoke detectors were compared to a commercially-available photoelectric/heat detector which incorporates a thermistor-based heat detector. For each test, the basis of comparison was the response-time-difference between the ion detector under test and an adjacent photoelectric/heat detector. The comparisons were conducted using standardized test fires in Simplex's UL 268 Fire Test Room.

For each test series, six samples of the ion detector under test were surface mounted on the fire room ceiling. Four of the ion detectors were arranged in a 15-foot square array and two were placed in the right and left positions of the ceiling "Test Panel" specified by UL 268 [5] (ceiling positions Ion 5 and Ion 6 in Fig. 1). A photoelectric/heat detector was placed adjacent (approximately 6-in. separation) to each of the ion detectors in the square

array. A fifth photoelectric/heat detector was mounted midway between the Ion 5 and Ion 6 ceiling positions. For each test, the distances from the detector locations to the test fire are given in the results table for that test (Tables 1 - 8). For all tests, each photoelectric, and ion detector was placed so that its "least favorable position for smoke entry" was oriented towards the test fire location.

Three different fire types were used to evaluate each ion detector model. The first test-type was the UL 268 "Smoldering Smoke Test" found in section 40 of UL 268. This test used 10 sticks of ponderosa pine (3" x 1" x  $\frac{3}{4}$ ") on a laboratory hotplate to produce a slow, smoldering fire. The second test-type was the UL 268 "Flammable Liquid Fire - Test C" found in section 39.4 of UL 268. This test used 38 milliliters of a mixture of 65% heptane and 35% toluene by volume to produce a hot, flaming fire. Both of these UL 268 fire tests were performed according to the test method outlined in UL 268, 4<sup>th</sup> Ed. paragraph 39.6. As specified in UL 268, photo beam and measuring ionization chamber (MIC) data were collected during all tests and analyzed to ensure that the buildup rate and the light-transmission vs. MIC curves conformed to the requirements of UL 268.

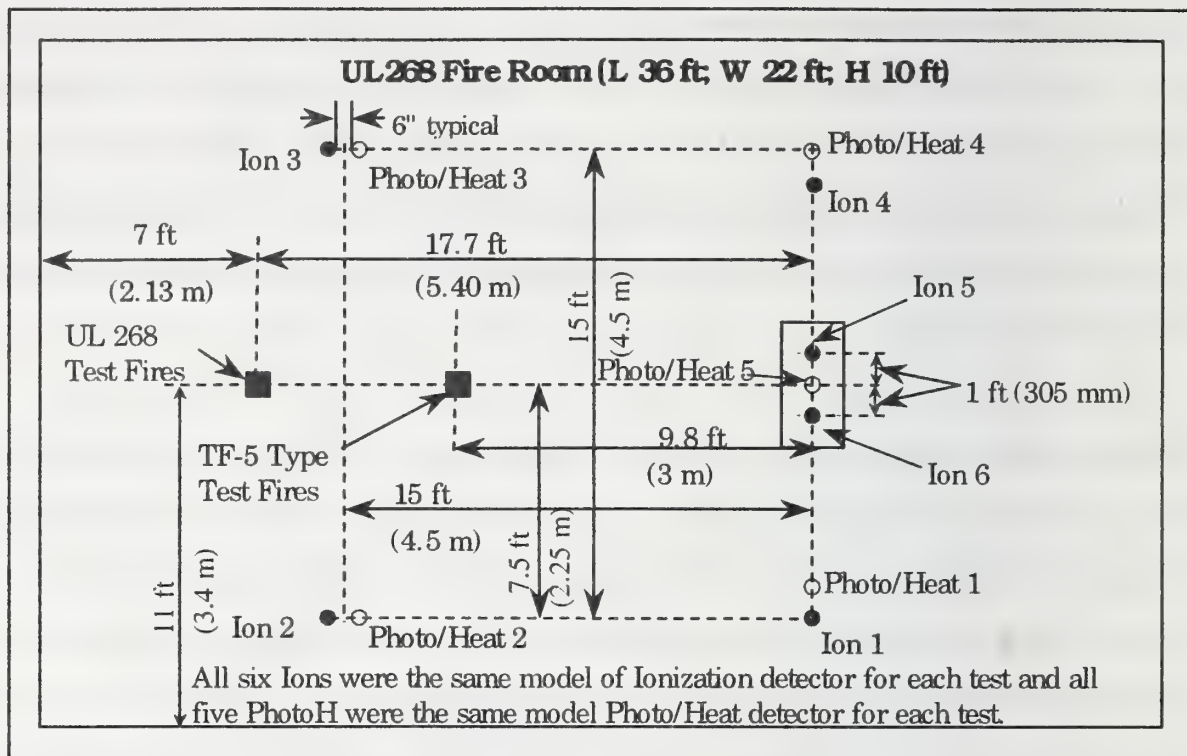


**Figure 1. Detector Positions for Fire Tests**

The third test type was similar to the “TF-5 - Liquid (Heptane) Fire” described in Appendix K of pr EN 54-7 (Draft A3). The ceiling of the UL 268 fire room is 1 meter less than that specified by prEN 54-7 so the amount of the heptane (97%)/toluene (3%) mixture was reduced to 463 ml to prevent heat and fire damage to our test facility. The fuel was burned in a round receptacle 33 cm in diameter and 7.5 cm deep to attain the required smoke density build-up rate. The test fire location was selected so that ceiling positions Ion 5, Ion 6, and Photo 5 were contained in the prEN-54-specified volume.

The fire room was instrumented with an NIR obscuration meter and MIC which met the prEN 54-7 criteria. Optical density (m-value in dB/m) and MIC data (y-value) were collected and analyzed for each test to determine if the “m against y” and “m against time” tolerance limits of prEN 54-7 were met. The TF-5 type fires typically came close to or met the tolerance limits as shown in Fig. 2.



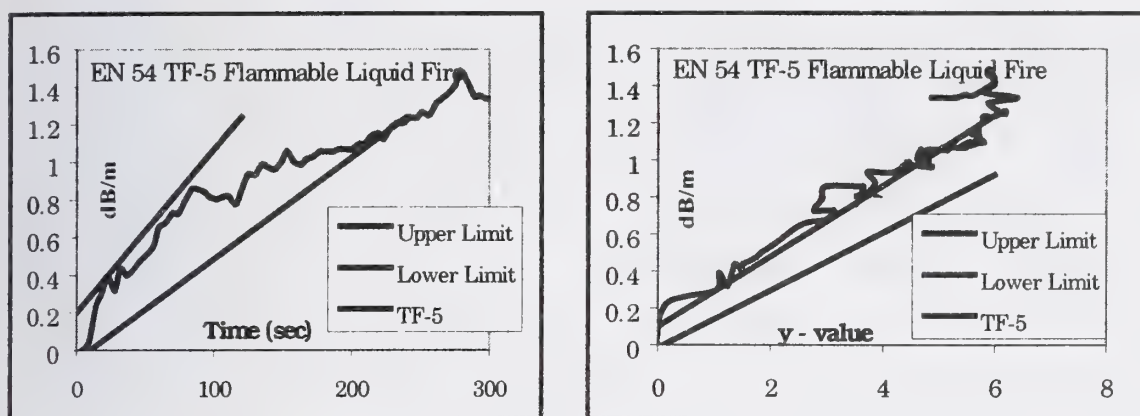


**Figure 2.** pr4EN 54-7 Fire TF-5 Tolerance Limits

### 3. Description of Devices Tested

Two ion sensor models from different manufacturers were tested. Ion detector Type A is currently sold by Simplex for use in Simplex fire alarm systems. Ion detector Type B was previously sold by Simplex for use in Simplex fire alarm systems. Each type of ion detector consists of a detector/base combination which sends a digital representation of smoke density to a Simplex control panel. The alarm activation time of each ion detector was evaluated at 0.5 %/ft (the most sensitive of its four standard settings) and at its default installation sensitivity of 1.3 %/ft. All six detectors of each ion type were selected at random from stock. Each ion detector was used as calibrated by its manufacturer.

The five photoelectric/heat detectors used were standard Simplex UL-listed units taken at random from stock. This detector type consists of a sensor/base combination which sends digital representations of smoke density and temperature to a Simplex control panel. The alarm activation time of the photoelectric component was evaluated at 0.5 %/ft (the most sensitive of its eight standard settings) and its default installation sensitivity of 2.5 %/ft. Each of the five photoelectric/heat detectors was calibrated in a Simplex UL 268 Sensitivity Test Box using Simplex's standard manufacturing calibration procedure.

The thermistor-based heat sensor element of the photoelectric/heat detector is a fixed temperature/rate-of-rise type whose sensitivity can be selected at the control panel. In the present investigation, the alarm activation time of the heat detector component was evaluated using two rate-of-rise (ROR) sensitivities (15 °F/min and 20 °F/min) and one fixed-temperature (FT) sensitivity (135 °F). In addition, maximum ROR data for each heat detector component was collected for each TF-5 type test

#### **4. Data Collection**

In each test, a digital representation of each ion and photoelectric/heat detector's output voltage was transmitted to a PC-based data acquisition system. Ion, photoelectric, and heat detector response times were calculated by post-processing the data. The algorithms used, together with a 4 second polling interval and alarm thresholds based on the device calibration, simulated the performance of the Simplex Model 4010 fire panel operating with no pre-alarm and no alarm verification delay. A chief advantage of using this method for obtaining detector response times was that it enabled the determination of detector response times at multiple sensitivities during a single test fire, thus decreasing the total number of test fires. For each combination of ion detector type and test fire type, four trials were conducted.

The ion and photoelectric detectors were compared at two combinations of sensitivity levels. The comparison at the same sensitivity of 0.5 %/ft was selected because these are the most sensitive standard Simplex sensitivities of these two detector types. The comparison of the ion detector at 1.3 %/ft to the photoelectric detector at 2.5 %/ft was selected because these are the default sensitivities of these two detector types and therefore represent a typical Simplex installation.

## 5. Fire Test Results

The results for the comparison of ion detector Type A and the photoelectric/heat detector are summarized in Tables 1 - 4. Unless otherwise noted, each alarm time entry is the average of 4 trials. The detector positions are indicated in parentheses beneath the distance from the fire. Note that, for each test type, only one average photoelectric alarm time is listed for ceiling positions 5 and 6. This is because the ion detectors at ceiling positions 5 and 6 were compared to a single photoelectric detector midway between them at ceiling position 5. For the smoldering smoke tests, the individual Type A ion and photoelectric detector response times measured for the four trials generally varied over a range of a few hundred seconds at each ceiling position. For the UL 268 Flammable Liquid Fire and the TF-5 type tests, the range of variation was on the order of ten seconds. Each table includes the difference between the average response times of the ion and photoelectric detectors for each ceiling position.

The average response-times recorded for the Type A ion detector at 1.3 %/ft and the photoelectric/heat detector at 2.5 %/ft are listed in Table 1 for the UL 268 Smoldering Smoke and Flammable Liquid Fire tests. Note that not all ion detectors alarmed in each smoldering smoke test. For each ion detector position, the number of tests for which no alarm (N/A) was observed is indicated in parentheses beneath the average response time value. Table 2 lists the average response-times of the ion and the photoelectric detectors in the UL tests when both were set to a sensitivity of 0.5 %/ft.



UL 268 Tests		Distance from Test Fire					
Ionization Type A: 1.3		(Ceiling Position #)					
%/ft		8.0 ft		17.7 ft		19.2 ft	
Test	Devi	(2)	(3)	(5)	(6)	(1)	(4)
UL 268 Smold.	Ion A	3459	3317	3843	3614	3864	3591
Smoke	(N/A)			(3)		(2)	
Averages of 4 Trials	Photo	2421	2253	2916		2726	2823
Diff. of Avg. Time (Ion - Photo)		1038	1064	927	698	1138	768
UL 268 Flamm.	Ion A	31	36	61	56	65	65
Liquid	Photo	26	29	55		57	57
Diff. of Avg. Time (Ion - Photo)		5	7	6	1	8	8

**Table 1.** Ion Detector A, UL 268 Tests: Default Sensitivity Alarm Times  
(in sec.)

The data for the smoldering smoke tests show that typically the photoelectric detectors set to 2.5 %/ft responded 12 - 18 minutes earlier than the Type A ion detectors set to 1.3 %/ft. Table 2 shows that when both were evaluated at 0.5%/ft, the photoelectric detectors typically responded 25 - 30 minutes faster than the Type A ion detectors. As Tables 1 and 2 show, in the UL 268 Flammable Liquid Fire tests, there was no significant difference in response time between the photoelectric and Type A ion detectors whether compared at their default sensitivities (2.5 %/ft and 1.3 %/ft) or the same, higher sensitivity (0.5 %/ft).

<b>UL 268 Tests</b>		<b>Distance from Test Fire</b>					
<b>Ionization Type A: 0.5 %/ft</b>		<b>(Ceiling Position #)</b>					
<b>Photoelectric: 0.5 %/ft</b>		<b>8.0 ft</b>		<b>17.7 ft</b>		<b>19.2 ft</b>	
<b>Test</b>	<b>Devi</b>	<b>(2)</b>	<b>(3)</b>	<b>(5)</b>	<b>(6)</b>	<b>(1)</b>	<b>(4)</b>
<b>UL 268 Smold. Smoke</b>	Ion A	3318	3236	3691	3471	3677	3474
	Photo	1556	1577	2008		1854	2002
Diff. of Avg. Time (Ion - Photo)		1762	1659	1683	1463	1823	1472
<b>UL 268 Flamm. Liquid</b>	Ion A	29	31	60	56	65	63
	Photo	18	20	45		53	52
Diff. of Avg. Time (Ion - Photo)		11	11	15	11	12	11

**Table 2.** Ion Detector A, UL 268 Tests: 0.5 %/ft Sensitivity Alarm Times  
(in sec.)

<b>TF-5 Type Tests</b>		<b>Distance from Test Fire</b>					
<b>Ionization Type A: 1.3 %/ft</b>		<b>(Ceiling Position #)</b>					
<b>Photoelectric: 2.5</b>		<b>9.1 ft</b>		<b>9.8 ft</b>		<b>12.3 ft</b>	
<b>Test</b>	<b>Devi</b>	<b>(2)</b>	<b>(3)</b>	<b>(5)</b>	<b>(6)*</b>	<b>(1)</b>	<b>(4)</b>
<b>Modified TF-5 Fire</b>	Ion A	19	20	26	22	38	32
	Photo	55	58	69		76	67
Averages of 4 Trials							
Diff. of Avg. Time (Ion - Photo)		-36	-38	-43	-47	-38	-35
<b>Max ROR result</b> (°F/min. Avg. of 4	ROR	14	7	14		12	10
<b>Max. Temperature</b> (°F. Avg. of 4 trials)	FT	115	89	114		101	99

**Table 3.** Ion Detector A, TF-5 Type Tests: Default Sensitivity Alarm  
Times (in sec.)

Maximum ROR and Fixed Temperature Values

Table 4 lists the average response times in the TF-5 type tests of the Type A ion detectors evaluated at 1.3 %/ft and the photoelectric detectors evaluated at 2.5 %/ft. Table 4 lists the average response times in the TF-5 type tests of the ion and the photoelectric detectors when both were set to a sensitivity of 0.5 %/ft. In the TF-5 type tests, Type A ion detectors evaluated at 1.3 %/ft

responded in 19 to 38 seconds; about 40 seconds faster than the photoelectric detectors set at 2.5 %/ft. When the sensitivity levels were set to 0.5 %/ft for both types, there was no significant difference in TF-5 test response time between the photoelectric and Type A ion detectors. It is interesting to note that in both the UL 268 Flammable Liquid Fire tests and the TF-5 type tests, there were no significant differences in the Type A ion detector alarm times whether set at 0.5% or 1.3 %/ft.

TF-5 Type Tests		Distance from Test Fire					
Ionization Type A: 0.5 %/ft		(Ceiling Position #)					
Photoelectric: 0.5		9.1 ft		9.8 ft		12.3 ft	
Test	Devi	(2)	(3)	(5)	(6)*	(1)	(4)
Modified TF-5 Fire	Ion A	16	19	24	22	35	30
Averages of 4 Trials	Photo	15	17	19		23	23
Diff. of Avg. Time (Ion - Photo)		1	2	5	3	12	7

**Table 4.** Ion Detector A, TF-5 Type Tests: 0.5 %/ft Sensitivity Alarm Times (in sec.)

The results for the comparison of ion detector Type B and the photoelectric/heat detector are summarized in Tables 5 - 8. Each alarm time entry is the average of 4 trials. For the four smoldering smoke tests, the response times measured for the individual Type B ion and photoelectric detectors generally varied over a range of a few hundred seconds at each ceiling position. For the UL 268 Flammable Liquid Fire and the TF-5 type tests, the range of variation was on the order of ten seconds.

The average response-times recorded in the UL 268 Smoldering Smoke and Flammable Liquid Fire tests for the Type B ion detector at 1.3 %/ft and the photoelectric/heat detector at 2.5 %/ft are listed in Table 5. Table 6 lists the average response times of the ion and the photoelectric detectors in the UL tests when both were set to a sensitivity of 0.5 %/ft. The data for the



smoldering smoke tests show that the photoelectric detectors set to 2.5 %/ft responded 8 - 14 minutes earlier than the Type B ion detectors set to 1.3 %/ft. When both were evaluated at 0.5%/ft, the photoelectric detectors typically responded 17 - 25 minutes faster than the Type B ion detectors. In the UL 268 Flammable Liquid Fire tests, there was no significant difference in response time between the photoelectric and Type B ion detectors whether compared at their default sensitivities (2.5 %/ft and 1.3 %/ft) or the same, higher sensitivity (0.5 %/ft).

UL 268 Tests		Distance from Test Fire					
Ionization Type B: 1.3 %/ft		(Ceiling Position #)					
		8.0 ft		17.7 ft		19.2 ft	
Test	Devi	(2)	(3)	(5)	(6)	(1)	(4)
UL 268 Smold. Smoke	Ion B	3350	3368	3470	3518	3602	3553
	Photo	2566	2534	3008		2871	2970
Diff. of Avg. Time (Ion - Photo)		784	834	462	510	731	583
UL 268 Flamm. Liquid	Ion B	25	22	50	50	56	55
	Photo	29	32	56		58	58
Diff. of Avg. Time (Ion - Photo)		-4	-10	-6	-6	-2	-3

**Table 5.** Ion Detector B, UL 268 Tests: Default Sensitivity Alarm Times (in sec.)

Table 7 lists the average response times in the TF-5 type tests of the Type B ion detectors evaluated at 1.3 %/ft and the photoelectric detectors evaluated at 2.5 %/ft. Table 8 lists the average response-times of the ionization and the photoelectric detectors in the UL tests when both were set to a sensitivity of 0.5 %/ft. The Type B ion detectors evaluated at 1.3 %/ft responded in 19 to 27 seconds in these tests; about 45 seconds faster than the photoelectric detectors set at 2.5 %/ft. When the sensitivity levels were evaluated at 0.5 %/ft for both types, there was no significant response-time-difference between the photoelectric and Type A ion detectors. For both the

UL Flammable Liquid Fire tests and the TF-5 type tests, there were no significant differences in the Type B ion detector alarm times whether set at 0.5% or 1.3 %/ft .

UL 268 Tests		Distance from Test Fire					
Ionization Type B: 0.5 %/ft		(Ceiling Position #)					
Photoelectric: 0.5		8.0 ft		17.7 ft		19.2 ft	
Test	Devi	(2)	(3)	(5)	(6)	(1)	(4)
UL 268 Smold. Smoke	Ion B	3159	3211	3340	3343	3450	3395
	Photo	1676	1697	2331		1929	2198
Diff. of Avg. Time (Ion - Photo)		1483	1514	1009	1012	1521	1197
UL 268 Flamm. Liquid	Ion B	21	21	49	48	55	54
	Photo	19	18	49		55	49
Diff. of Avg. Time (Ion - Photo)		2	3	0	-1	0	5

**Table 6.** Ion Detector B, UL 268 Tests: 0.5 %/ft Sensitivity Alarm Times (in sec.)

The heat detector fixed temperature and ROR functions generally did not exhibit a significant response in the UL 268 Smoldering Smoke and UL 268 Flammable Liquid fire tests. In the TF-5 type fire tests, the fixed temperature and ROR functions did not generally exceed their alarm thresholds, but, these quantities reached significant levels which are tabulated in Tables 3 and 7 for the Type A ion tests and Type B ion tests, respectively.

TF-5 Type Tests		Distance from Test Fire					
Ionization Type B: 1.3 %/ft		(Ceiling Position #)					
Photoelectric: 2.5		9.1 ft		9.8 ft		12.3 ft	
Test	Devi	(2)	(3)	(5)	(6)	(1)	(4)
Modified TF-5 Fire	Ion B	19	21	20	20	27	26
Averages of 4 Trials	Photo	67	58	72		71	65
Diff. of Avg. Time (Ion - Photo)		-48	-37	-52	-52	-44	-39
Max ROR result (°F/min. Avg. of 4	ROR	9	7	13		13	10
Max. Temperature (°F. Avg. of 4 trials)	FT	100	93	115		106	104

**Table 7.** Ion Detector B, TF-5 Type Tests: Default Sensitivity Alarm Times  
(in sec.);

Maximum ROR and Fixed Temperature Values

TF-5 Type Tests		Distance from Test Fire					
Ionization Type B: 0.5 %/ft		(Ceiling Position #)					
Photoelectric: 0.5		9.1 ft		9.8 ft		12.3 ft	
Test	Devi	(2)	(3)	(5)	(6)*	(1)	(4)
Modified TF-5 Fire	Ion B	16	17	18	17	23	23
Averages of 4 Trials	Photo	16	18	16		25	23
Diff. of Avg. Time (Ion - Photo)		0	-1	2	1	-2	0

**Table 8.** Ion Detector B, TF-5 Type Tests: 0.5 %/ft Sensitivity Alarm Times  
(in sec.)

## 6. Discussion: Photoelectric/Heat vs. Ion Response

A series of UL 268 Smoldering Smoke (gray smoke), UL 268 Flammable Liquid Fire (black smoke), and TF-5 type Liquid (Heptane) Fire (black smoke) tests were conducted to compare the performance of two models of commercially available ion detectors (designated Type A and Type B) to the performance of a commercially available photoelectric/heat detector. The



basis of comparison was the length of time required for each detector to exceed its alarm threshold.

In the smoldering smoke tests, at both combinations of sensitivity tested, both models of ion detector took considerably longer to respond than the photoelectric component of the photoelectric/heat detectors. This result strongly supports the generally accepted view [2] that photoelectric detector technology possesses an advantage over ion detector technology with regards to smoldering smoke response.

In the UL 268 Flammable Liquid Fire tests, the performance of the photoelectric component of the photoelectric/heat detector was fully equivalent to that of both ion detector models at both combinations of sensitivity. The detectors of all three types typically alarmed in about a minute or less.

In the TF-5 type tests, the ion detectors (both types) responded about 40 - 45 seconds earlier than the photoelectric detectors when both technologies were evaluated at their default sensitivities (2.5 %/ft for the photoelectric and 1.3 %/ft for the ions). In Figure 3, the 8-bit digital representation of smoke density is plotted versus time for an ion detector and an adjacent photoelectric detector for typical UL 268 Flammable Liquid Fire and TF-5 type tests. The 0.5 and 1.3 %/ft alarm thresholds of the ionization detectors are indicated by dashed lines. Solid lines indicate the 0.5 and 2.5 %/ft photoelectric alarm thresholds of the photoelectric/heat detectors. In the UL 268 Flammable Liquid Fire tests, ion and photoelectric technologies responded approximately at the same time. In the TF-5 type fires, the photoelectric detectors generally responded more slowly than they did in the UL 268 Flammable Liquid Fire tests. The ion detectors took about the same length of time in both types of fire. The slower performance of the photoelectric detectors in the UL 268 Flammable Liquid Fire tests is

possibly due to the fuel mixtures used. In the TF-5 fire, the heptane fuel (smoke yield .037 g/g) contains only 3% toluene (smoke yield .178 g/g) [6]. It seems likely, therefore, that the 65% heptane/35% toluene fuel mixture used in the UL 268 Flammable Liquid Fire test will produce a greater proportion of visible smoke than the TF-5 fire. Since ion detectors have a greater sensitivity to the invisible particles produced by a hot flaming fire, the conditions of the TF-5 type fire would therefore be more favorable for ion detectors than the UL 268 Flammable Liquid Fire test.

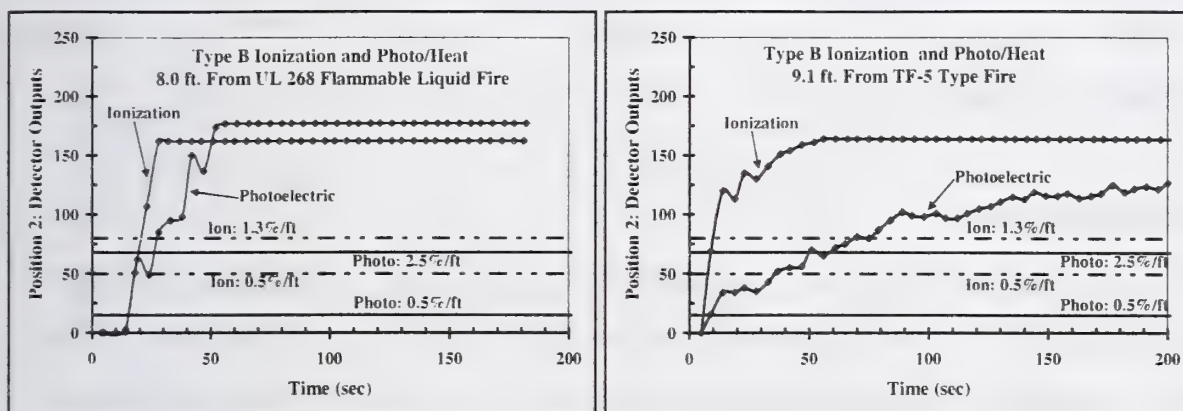


**Figure 3.** Detector Outputs for TF-5 and UL 268 Flammable Liquid Fire Tests

With the 4 second sample time used, the two technologies yield equivalent response times of about 20 seconds at the higher sensitivity of 0.5 %/ft. At the lower default sensitivities (1.3 %/ft for the ion, 2.5 %/ft for the photo), the faster response of the ion detector to the TF-5 fire products becomes more obvious. This interesting result illustrates the importance of fully specifying the experimental conditions when performing technology comparisons.

The three heat detector modes evaluated (15 °F/min ROR, 20°F/min ROR, and 135 °F fixed temperature) generally did not exceed their alarm thresholds in the fire tests performed. Furthermore, the response of the fixed temperature and ROR functions, though negligible in the UL 268 Smoldering Smoke and Flammable Liquid Fire tests, was significant in the

TF-5 type tests. For example, the ROR heat detection function came relatively close to alarming at the 15 °F/min setting in the TF-5 fire tests. Two factors probably contribute most to this performance differential. First, in the TF-5 type tests, all detectors were closer to the fire than in the two UL 268 tests. Second, the heat release rate (HRR) of the TF-5 type test was much greater than for either UL 268 test. Using the heat release rate (HRR) calculation described in the SFPE Handbook [7], the HRR of the TF-5 type fire was estimated to be 123 kW and the HRR of the UL 268 Flammable Liquid Fire test was estimated to be 12.7 kW. The HRR of the UL 268 smoldering fire was estimated to be about 1.5 kW, based on the hotplate characteristics.

## **7. Conclusions**

In this investigation, the response of the photoelectric smoke detection technology to smoldering smoke was much faster than the response of the ion technology. The photoelectric response to the black smoke produced by the UL 268 Flammable Liquid Fire was generally as fast as (or faster than) the ion response. In the TF-5 type fire tests, the photoelectric response lagged the ion response by only about 45 seconds when both were evaluated at their default sensitivities (1.3 %/ft for ion, 2.5 %/ft for photoelectric). However, the photoelectric response to the TF-5 type fire was typically as fast as the ion response when both were evaluated at the same sensitivity (0.5 %/ft). Furthermore, the TF-5 type fire test results also indicate that, even in the absence of visible smoke, the photoelectric/heat detector would be effective for the detection of fires with a heat release rate or duration slightly greater than that of the TF-5 type test fire used. Therefore, these results strongly support the conclusion that photoelectric and photoelectric/heat technologies possess a clear overall performance advantage over ion technology if the most likely sources of fire danger are smoldering fires (as some believe [3]) or flaming hydrocarbons.



## References

- [1] Bukowski, R.W. and Mulholland, G.W.; Smoke Detector Design and Smoke Properties; NBS Technical Note 973 U.S. Department of Commerce, National Bureau of Standards, Nov. 1978.
- [2] Section A-1-4, Appendix A Explanatory Material; NFPA 72 National Fire Alarm Code 1996; p. 196.
- [3] Fleming, J; Photoelectric vs. Ionization Detectors - A Review of the Literature; Proceedings Fire Suppression and Detection Research Application Symposium, February 25-27, 1998, Natl. Fire Protection Association, Quincy, MA, 1998, pp. 18-59
- [4] Qualey, J, Desmarais, L, and Pratt, J.; Fire Test Comparisons of Ion and Photoelectric Smoke Detector Response Times; Fire Suppression and Detection Research Application Symposium, Orlando, FL, February 7 - 9, 2001.
- [5] UL268: Standard for Smoke Detectors for Fire Protective Signaling Systems; 4th Ed., 12/30/96, (Rev. 1/4/99), Underwriters Laboratories, Inc., Northbrook, IL, 1999
- [6] Babrauskas, V.; Burning Rates, Section 3, Chapter 1, SFPE Handbook of Fire Protection Engineering, Second Edition, 1995, pp. 3-1 to 3-15.
- [7] Tewarson, A.; Generation of Heat and Chemical Compounds in Fires, Section 3, Chapter 4, SFPE Handbook of Fire Protection Engineering, Second Edition, 1995, pp. 3-53 to 3-124.

J N Smithies

FRS, Building Research Establishment Ltd., Garston, Watford, U.K.

M J Spearpoint

Department of Civil Engineering, University of Canterbury, Christchurch,  
New Zealand.

### **The Performance of Mains-Powered Residential Smoke Alarms with a Backup Energy Source**

#### **Abstract**

Mains-powered residential smoke alarms are considered more reliable than equivalent battery-powered devices since it is not necessary to have an annual battery replacement and there less chance that the home occupier will remove the battery for some reason. However, the reliability of residential smoke detection systems comprising of mains-powered devices can be further improved by the use of a backup energy source. This allows a smoke alarm to continue operating if the mains supply becomes unavailable.

This paper examines the long-term performance of a range of energy sources that are used as backup for mains-powered smoke alarms. The paper reports on the results from a research programme that has be running for over four years in which energy sources have been tested in both standby and alarm modes.

## **1 Introduction**

### **1.1 Background**

The benefit of using smoke alarms is recognised in the 1992 revisions to the UK's Approved Document B of the Building Regulations [1] which recommends that all newly constructed dwellings should have a linked mains-powered domestic smoke alarm on each floor. As noted in BS 5839 Part 6 [2], the reliability of systems comprising of mains-powered smoke alarms can be improved by the use of a backup energy source. This allows a smoke alarm to continue operating when the mains supply is unavailable.

The majority of homes in the UK now have at least one domestic smoke alarm installed [3, 4]. These devices are only of benefit to the occupants in a fire when they are operating correctly. A US study of domestic smoke alarms [5] found that around one fifth were not operational, mainly because of non-functioning power sources. Nearly all of these non-operating devices had missing, flat or disconnected batteries. The use of smoke alarms powered by the mains electricity supply eliminates the problems of battery removal and flat batteries.

In the UK, the mains AC electricity supply can be considered a reliable source. However, there are cases where the supply may become accidentally or deliberately disconnected. The frequency and duration of any disconnections will depend on several factors such as the location of the property and the type of tenant. The use of a backup energy source would allow a smoke alarm to continue operating until the mains supply is re-established. A backup power supply will also maintain the operation of a smoke alarm should the mains power be lost during a fire (early on, before the alarm is heard) or as a result of the fire being due to an electrical fault that interrupts the supply.

Should a mains-powered smoke alarm with a backup energy source become disconnected from the AC power it will continue to function using the backup energy source. The capacity of the energy source determines how long the smoke alarm can operate and raise an alarm in case of fire. If the backup supply voltage drops below a



particular threshold, an audible warning is given. If the voltage continues to drop, it will reach a certain point where the sounder will no longer be able to function but the low power warning will continue to operate. A further drop in the voltage will result in failure of the low power warning. The particular voltage levels at which these events occur vary between devices but typical values are 7.5 V for the low power warning to commence, 4.5 V for the sounder to fail and 3.5 V for the low power warning to fail.

A range of mains-powered smoke alarms is available in which various types of backup energy source are used. Each type of backup source has particular advantages and disadvantages. Backup supplies can be considered to consist of two broad categories; primary and rechargeable as described below. This paper considers the different types available and compares their performance. It is not the intention, nor is it possible, to declare that any one type of backup source is 'better' than any other as the selection of backup energy sources depends on many factors:

1. Cost - the type of backup source has an influence on the initial purchase cost of the smoke alarm and also subsequent maintenance where the backup supply may need servicing or replacing,
2. Shelf life - the life of the source while not in use and any storage requirements,
3. Operating power capacity - the available power when no mains power is being supplied,
4. Alarm power capacity - the available capacity during an alarm,
5. Recharge time - the length of time for the backup supply to recharge after full or partial usage where appropriate,
6. Safety - any risks to the user or maintenance personnel during normal operation or if the backup energy source is misused,
7. Environmental considerations - the cost and requirements for the eventual disposal of the smoke alarm that includes its accompanying backup power source.

## **1.2 Primary cells**

Cells with irreversible reactions are commonly known as primary cells and are available in a number of forms: zinc carbon, zinc chloride, alkaline manganese and lithium. The

standard 9V PP3 primary cells, in particular zinc carbon and alkaline have been used in smoke alarms for many years and have been shown to operate effectively, powering smoke alarms for extended lengths of time. However the user can remove primary cells and although several manufacturers have designed their mains-powered smoke alarms to limit removal of this form of backup energy source, it is not possible to eliminate such abuse.

Zinc carbon cells (or 'Leclanché' cells) were the first primary batteries made available for household use. The zinc chloride battery is a development of the zinc carbon battery and it is used where the higher energy of alkaline is not required. Currently alkaline manganese is the most commonly used primary cell and although it is suited to high current drain applications, the very low self-discharge current also allows for low drain uses such as smoke alarms. Lithium cells are available in a range of chemistries that are suited to different current drain applications. The cells have a very long shelf life due to extremely low self-discharge rates. Standard size PP3 lithium manganese dioxide batteries are available which can be fitted to smoke alarms that accept primary cells. It is reported that these cells should be able to power a smoke alarm for between five [6] and ten years [7].

### **1.3 Rechargeable cells**

There are several types of rechargeable technology available as a backup power sources for smoke alarms; Nickel cadmium (NiCd), super-capacitor and rechargeable lithium.

NiCd batteries are used extensively in a range of applications such as rechargeable power tools and portable electronic equipment. The type of NiCd cell used in many smoke alarms cannot be removed by the user although PP3 size NiCd cells are available that could be used as a rechargeable substitute for primary cells. The recharge time of NiCd cells is relatively long compared with other technologies and they can exhibit a 'memory effect' where continual partial discharging and recharging can reduce their capacity. Cadmium is a 'heavy' metal and should not be allowed to contaminate the environment and the disposal of devices containing NiCd batteries may require special procedures particularly where large numbers are involved.

The super-capacitor (or memory capacitor) technology was introduced into the smoke alarm market in around 1991. The performance of the super-capacitor may be influenced by temperature although in normal domestic environments this should not be a problem. Compared with other rechargeable technologies the recharge time of the super-capacitor is relatively quick however their power capacity is less. The cells are environmentally friendly, as they do not contain any toxic material.

Rechargeable lithium cells are the latest technology to be used as a backup power source and they reportedly do not exhibit the memory effect. They also do not contain heavy metals, however, lithium should not be put in a persons mouth or swallowed. Lithium is potentially explosive which can cause particular problems for recycling and in landfill sites.

#### **1.4 Testing arrangements**

This study was carried out in collaboration with the Building Research Housing Group (BRHG), a group of local authorities and housing associations with interests in public housing needs. The BRHG members supplied a representative selection of mains-powered domestic smoke alarms to FRS for the study. These devices were tested both when connected to the mains AC supply and in standby mode with the backup supply voltage measured either daily or weekly depending on the type of source and the testing procedures. In addition, some stand-alone smoke alarms (i.e. devices that use primary cells as their only source of power) were also tested as part of the study.

## **2 Backup supply performance**

### **2.1 Primary cells**

*Figure 1* shows typical voltage discharge profiles for three types of primary cell installed in mains-powered smoke alarms operating in standby mode. After about 8 months the device containing zinc chloride cell began to give the low power warning. However, the battery continued to supply a sufficiently high enough voltage to power the device for at least another 1000 days while continuing to give a low power warning.



The early battery warning and the extent of the standby capacity of the zinc chloride cell were somewhat unexpected. It appears that this particular device had its low power warning threshold set too high.

Three test modes are shown for the alkaline cells; (1) optical sensor smoke alarm without weekly test, (2) ionisation sensor with a sounder tested for five seconds once per week, (3) stand-alone dual optical/ionisation sensor smoke alarm without weekly test. The smoke alarm containing the optical sensor gave a low power warning after 855 days however the other two devices have yet to reach their low power warning thresholds.

The results for the lithium primary cell exhibits an almost flat profile with no appreciable reduction in the voltage demonstrating that it can continue to fully power a smoke alarm for at least four years.

## **2.2 Rechargeable NiCd**

*Figure 2* shows the performance of a NiCd backup energy source in an ionisation smoke alarm over a series of discharge cycles. The first discharge cycle gave a standby time of around 75 days. After the third discharge the cell shows a degraded performance with the low power warning given at an earlier time than previously.

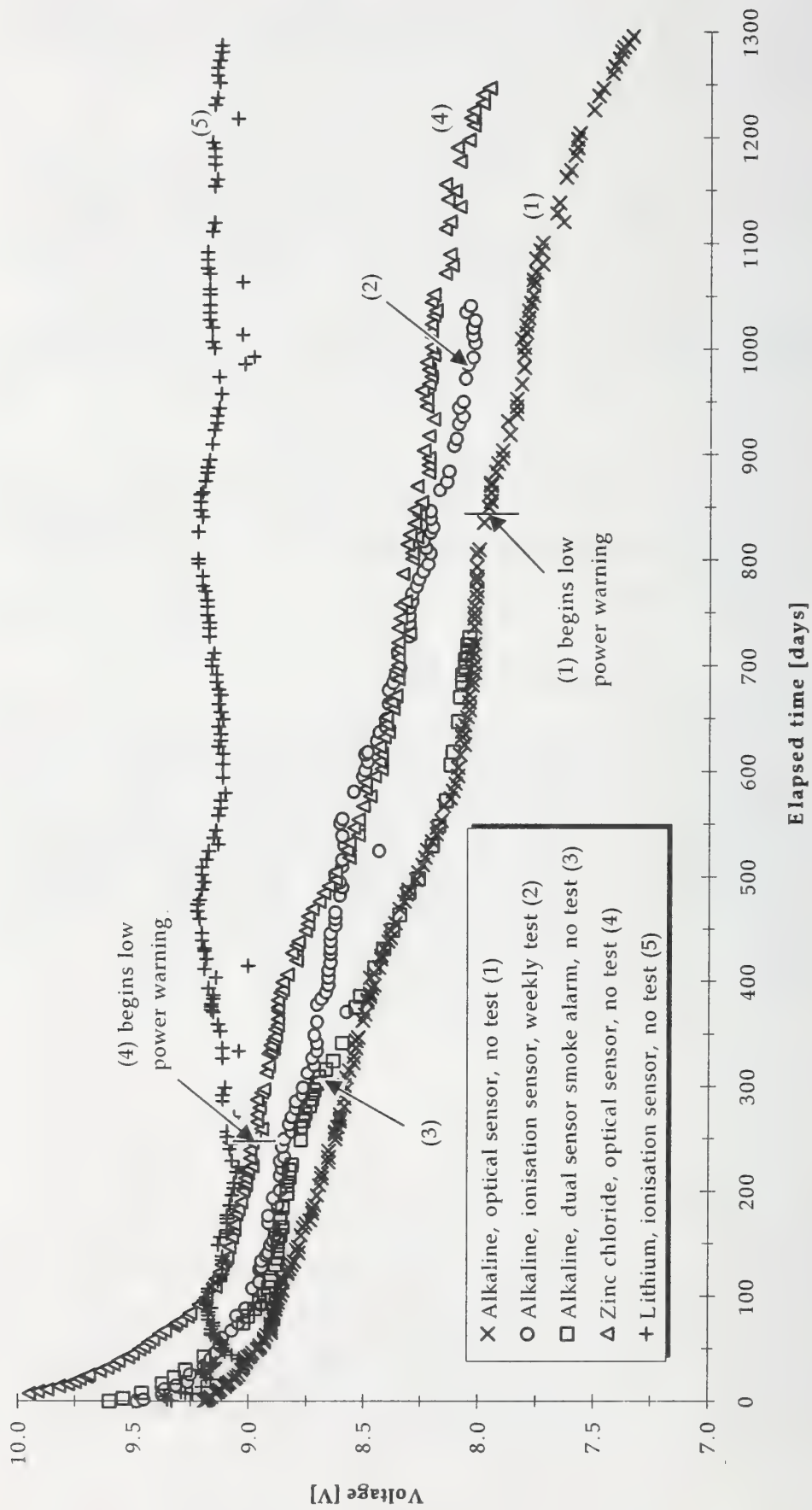


Figure 1. Primary cell voltage discharge curves.

By the eighth discharge cycle the voltage soon falls to a level at which the low power warning is given however this period extends further than the earlier discharge cycles. Similar behaviour was recorded in several smoke alarms having a NiCd backup supply.

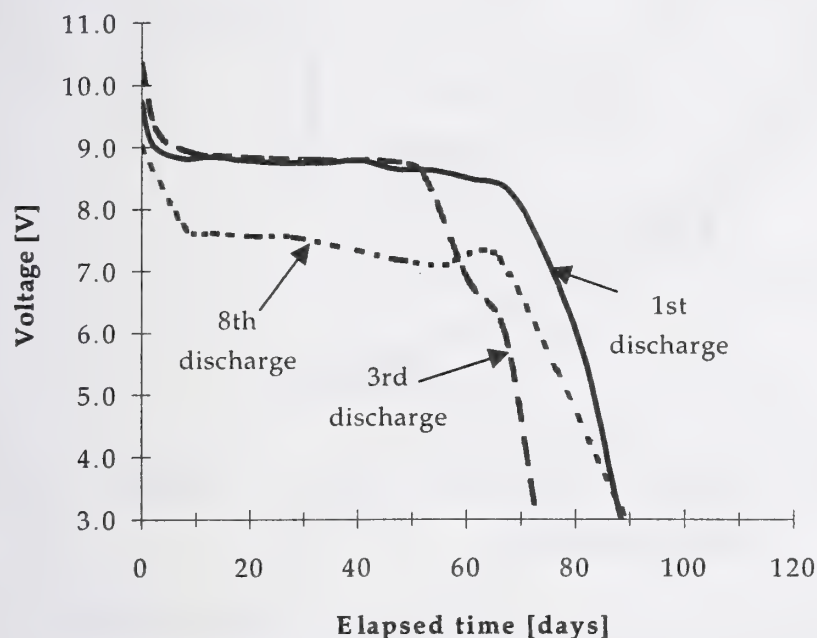


Figure 2. Voltage discharge curves for a NiCd backup source.

From these results it is clear that the NiCd cells will exhibit a memory effect. The repeated discharging and recharging the cells leads to a reduced capacity. However these tests present a demanding requirement on the performance of the cells that may not be encountered in the field. Where smoke alarms using a NiCd backup source were continuously connected to the mains supply it was found that the capacity of the cell was not affected.

### 2.3 Super-capacitors

Figure 3 shows the voltage discharge curves for optical sensor and ionisation sensor smoke alarms with super-capacitor backup energy source. Both devices show similar profiles and on average give eight days backup until the low power warning is given.



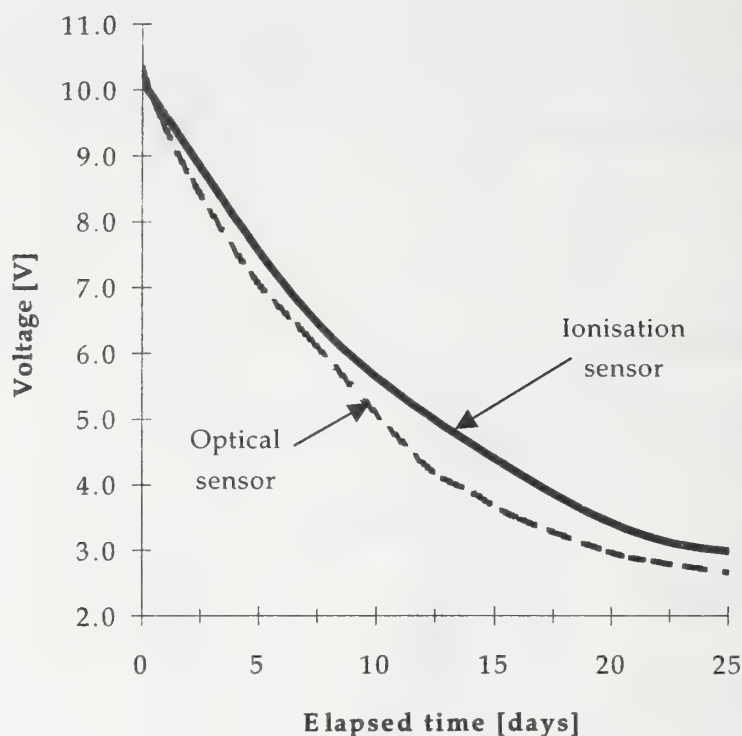


Figure 3. Voltage discharge curves for super-capacitor backup sources.

During the testing it was noted that several devices containing super-capacitors did not fully charge during installation and one device failed during the test procedures. These faults were identified with early models and the manufacturer has since resolved these problems. The majority of the smoke alarms using the super-capacitor backup supply (including devices that were subjected to repeated discharge cycles) functioned well and users in the field report acceptable performance from their installations.

#### 2.4 Rechargeable lithium

The performance of the rechargeable lithium cell is shown in *Figure 4*. The first discharge of the cell gave approximately 265 days of backup capacity. However by the sixth discharge cycle the capacity had fallen to only 6 days. It is clear from these tests that the capacity of the rechargeable lithium cell deteriorates significantly when it is repeatedly discharged and recharged. As with the NiCd cells, these tests present a demanding requirement on the performance of the cell.

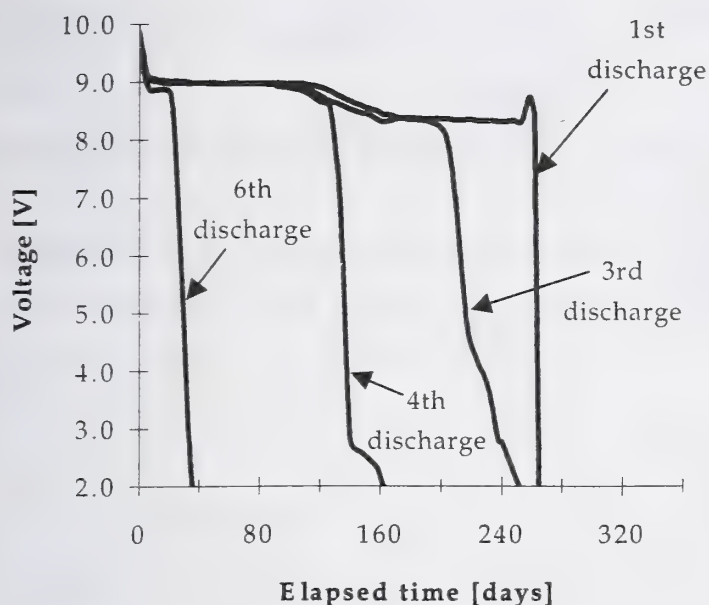


Figure 4. Voltage discharge curves for a rechargeable lithium backup source.

## 2.5 Summary of results

The results of the standby mode tests are summarised in Table 1. What is somewhat surprising is the length of time that primary cells are able to supply a smoke alarm in standby mode. These extended periods of operation have meant that complete discharge times of the sources cannot be reported here. The times quoted for the NiCd and rechargeable lithium cells are typical values since their performance was found to vary with each discharge cycle.

## 3 Conclusions

Primary cell batteries provide an effective backup supply to mains-powered smoke alarms. The standby capacity of a cell has the potential to extend for several years depending on the particular technology. The use of primary cells may not eliminate the problem of battery removal and they may need to be replaced if they become sufficiently discharged.

Backup power source	Specifications	Time to low power warning [days]	Time to sounder power failure [days]	Time between low power warning and sounder failure [days]
Zinc chloride cell	Optical sensor, no weekly test	245	> 1250	> 1005
	Optical sensor, no weekly test	855	> 1295	> 440
Alkaline primary cell	Ionisation sensor, 5 second weekly sounder test	> 1040	-	-
	Optical/ionisation sensor, no weekly test	> 725	-	-
Lithium primary cell	Ionisation sensor, no weekly test	> 985	-	-
Nickel cadmium <sup>(1)</sup>	Optical sensor, no weekly test	148	160	12
	Ionisation sensor, 5 second weekly sounder test	68	78	10
Super-capacitor	Optical sensor, no weekly test	7 ½	12	4 ½
	Ionisation sensor, no weekly test	8 ½	16	7 ½
Rechargeable lithium <sup>(2)</sup>	Ionisation sensor, no weekly test	253	265	12

- No data available

(1) Typical values before memory effect

(2) Initial value before degradation

*Table 1. Summary of backup power source standby mode performance.*

The potential memory effect and the disposal difficulties of NiCd cells place some limitations for their use as backup power sources for smoke alarms. They are more suitable in applications where disconnections from the AC supply are expected to be infrequent. The super-capacitor backup power source is suited to situations where expected periods of disconnection from the mains supply will be relatively short. They can be repeatedly discharged and recharged without any memory effect. Rechargeable lithium cells have a standby capacity somewhere between a typical NiCd cell and an alkaline cell. Although they reportedly do not suffer from the memory effect, the results presented in this paper show that their performance does degrade with repeated



discharge cycles. Compared to the primary cells, all of the rechargeable backup sources have a much shorter time between the onset of the low power warning and the voltage falling below the sounder operation threshold.

New backup power source technologies are being developed and current technologies are being advanced. Some of these developments may find their way into future designs of smoke alarms with potential improvements in their backup energy source performance.

#### **4 Acknowledgements**

The authors would like to thank those members of the BRHG and those smoke alarm manufacturers who supplied test devices and supporting information as part of this project. The authors would also like to thank Roger Harrison for his continued assistance in monitoring the smoke alarms.

#### **References**

1. Department of the Environment and The Welsh Office. The Building Regulations, Approved Document B, 1992 edition. HMSO, 1991.
2. Fire detection and alarm systems for buildings, Part 6: Code of practice for the design and installation of fire detection and alarm systems in dwellings. BS 5839: Part 6: 1995. British Standards Institution.
3. Marriott M D. Reliability and effectiveness of domestic smoke alarms. Fire Engineers Journal, June 1995.
4. Arvidsson T & Gale M. Homing in on smoke alarms. Fire Engineers Journal, November 2000, pp.53-55.
5. Ahrens M. Batteries not included. NFPA Journal, May/June 1998 pp.98-106.
6. Walsh J. Mains powered smoke alarms. Fire Surveyor, February 1990, pp.9-12.
7. Wolf A. The 10-year battery. NFPA Journal, January/February 1999, pp.49-52.

Thomas Cleary, Michelle Donnelly, and William Grosshandler

Building and Fire Research Laboratory, National Institute of Standards and Technology  
Gaithersburg, MD, 20899 U.S.A.

### **The Fire Emulator/Detector Evaluator: Design, Operation, and Performance**

#### **1. Introduction**

Grosshandler introduced the concept of a "universal fire emulator/detector evaluator" (FE/DE) at *AUBE '95*, and development of such an apparatus began at NIST soon thereafter [1]. The FE/DE has proven to be a very flexible design. The main function of the device is to reproduce the environment (temperature, air velocity, aerosol and gas species concentrations) a detector would be exposed to during fire and non-fire events. It has been used primarily for fire detection, but may prove useful in testing other types of sensors such as those used for indoor air quality assessment, building HVAC control, or hazardous gas monitoring. The FE/DE is a single-pass "wind tunnel" that allows for the control of the flow velocity, air temperature, gas species, and aerosol concentrations at a test section wherein detectors and sensors are exposed to these environmental conditions.

While others have developed tunnels to test specific aspects of fire detector performance, the FE/DE is the only apparatus designed to reproduce all relevant conditions needed to assess the performance of spot-type particulate, thermal and gas sensor detectors or combination detectors. It has been used in a study of the smoke entry lag of commercial analog-output photoelectric and ionization detectors, where a two-parameter model was developed that allows for the prediction of the analog detector response given smoke concentration and velocity at the detector opening as a function of time [2]. It was used to emulate the smoke temperature and flow velocity conditions developed in a modeled detector sensitivity room fire test [3]. Experimental results of analog-output detector response to test smoke from a propene soot generator, oil aerosol from a smoke detector testing device, and aerosolized Arizona test dust were presented at *AUBE '99* [4]. Recent work at NIST that utilized the FE/DE is described in several

papers presented at this conference: *AUBE '01* (see other papers in this proceedings). Below is a description of the FE/DE hardware, performance range, and selected experimental results.

## 2. Experimental Apparatus

A schematic of the FE/DE is shown in Figure 1. Room air is drawn into the opening, and exhausted to a hood at the end of the duct. The air velocity at the test section is controlled over a range of flows between 0.02 m/s to over 2 m/s by means of the computer-controlled axial blower. Air is first propelled through the annular finned heating elements, then travels along the duct to the test section. The flow is conditioned before it reaches the test section by passing through a 10 cm long aluminum honeycomb with 5 mm rectangular openings. The goal is to provide a nominally flat flow profile indicative of what would be experienced by a detector in a ceiling jet flow. The flow is monitored at the test section by a thermo-anemometer capable of recording flows as low as 0.05 m/s with a stated uncertainty of 4 % of the reading. For lower velocities, or non-isothermal flows, other means must be employed such as pitot probes, hot-wire anemometry, or laser doppler velocimetry. Figure 2 shows the mean centerline axial velocity as a function of distance from the top of the duct for a range of fan speeds. The flow profile is nearly top-hat, and at each stationary position the velocity fluctuates indicating turbulent flow. The horizontal bars indicate a two standard deviation range in the mean velocity measured by the thermo-anemometer. Transition from laminar to turbulent flow is expected at velocities above 0.08 m/s based on the duct Reynolds number. Heat is added to the flow by a series of 9 annular finned heating elements. Each element is rated at 5 kW for a total maximum heat input of 45 kW. Power to the heating elements is controlled by a feedback controller that receives set-point values from a computer file and compares them to the air temperature exiting the heaters. (An air temperature difference between the heater exit and test section location is due to heat losses to the duct section between those two points. Therefore, it is not practical to use the test section temperature for feedback control.) A rate of temperature rise in air flow of 0.5 °C/s is achievable at the test section, up to maximum of about 80 °C. Air temperatures and duct wall temperatures are recorded at the test section with type-K thermocouples. Figure 3 shows the air temperature response to a programmed sequence



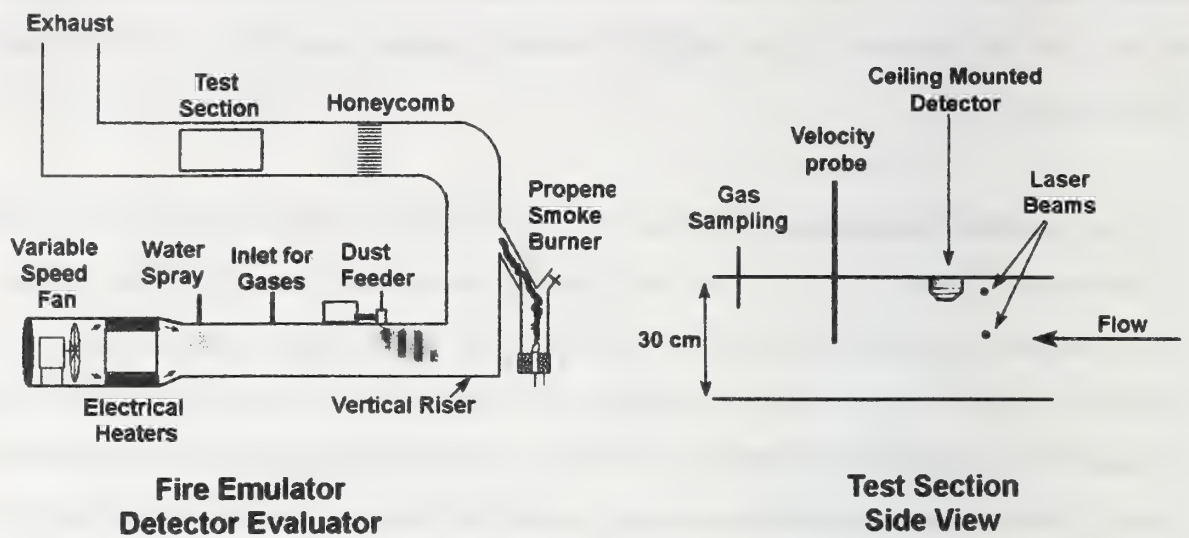


Figure 1. Schematic of the fire emulator/detector evaluator.

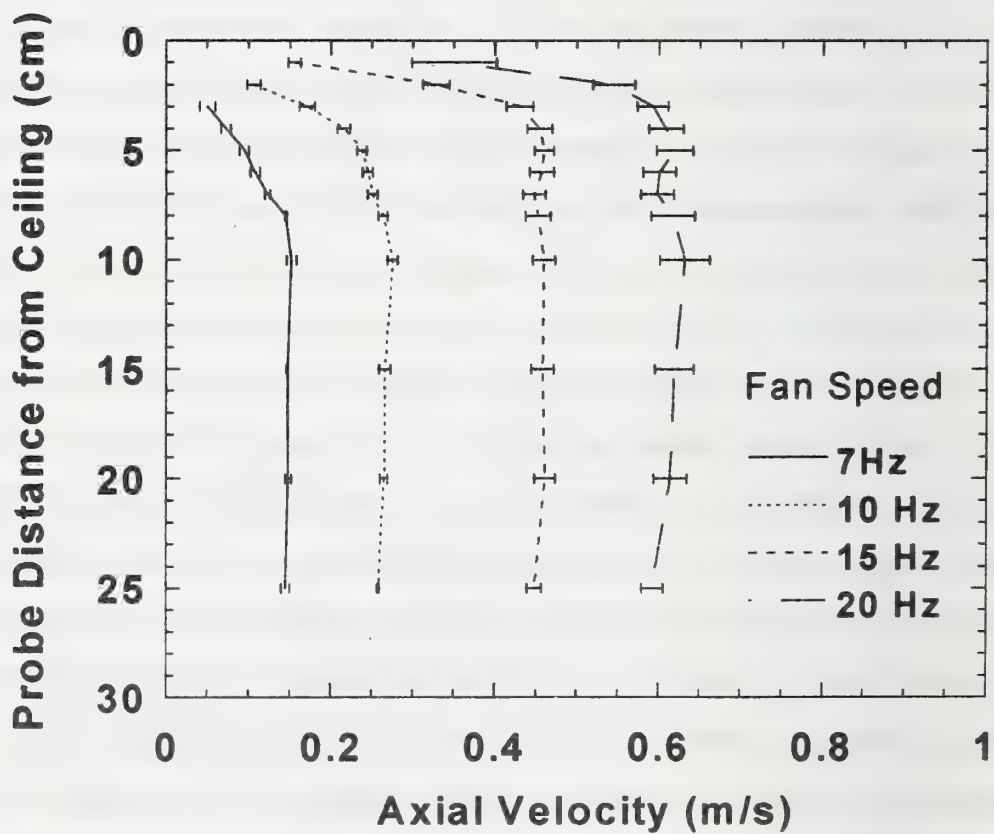


Figure 2. Axial velocity at the duct centerline as a function of distance from the ceiling.

of temperature set point values sent to the heater controller, and fan speed settings. This sequence was designed to reproduce velocity and air temperature rise at a detector location predicted from a modeled test fire (the particular example is for location 11 described in reference [5] found in these proceedings). The graph shows the air temperature for four repeated runs, along with the heater set point values. Figure 4 shows the flow velocity at the duct center at the test section for these repeated runs along with the fan speed settings.

CO, CO<sub>2</sub>, or other gas blends may be metered into the flow via electronic mass flow controllers. Superheated water may be sprayed into the flow after the heater section to fix humidity between ambient room and saturation conditions depending on the spray flow. Water, CO, CO<sub>2</sub>, and hydrocarbon gas concentrations at the test section are monitored by non-dispersive infrared (NDIR) analyzers. The ability to control gas concentrations independently benefits both fire and nuisance alarm scenario emulation. For example, both CO and CO<sub>2</sub> may be normally present in ever-changing concentrations in a building due to the external environmental sources such as attached parking garages, or internal sources such as the diurnal CO<sub>2</sub> variation due to occupancy and ventilation levels.

Various types of smokes and non-combustion aerosols may be introduced into the flow, including flaming soot, smolder smokes, dust, nebulized liquid mists, and cooking aerosols. Laser light transmission measurements across the duct at the test section are used to calculate the light extinction coefficient or optical density of the aerosol. Extinction coefficient or optical density is the typical "concentration" measurement of smoke or other non-fire aerosol. A HeNe laser at 632.8 nm wavelength is the light source, and a stabilizer utilizing a liquid crystal polarizer maintains a nearly constant laser intensity. The beam is split and introduced at two heights: the center of the duct, and 5 cm below the ceiling. Each light beam is reflected off two mirrors inside the duct and directed at a photodetector placed on the opposite side of where the beam enters the duct. The total light transmission path length inside the duct is 1.5 m. The photodetector output voltage is linear with respect to the transmitted light intensity. The standard relative uncertainty due to random fluctuations in the output is 0.06 % of the

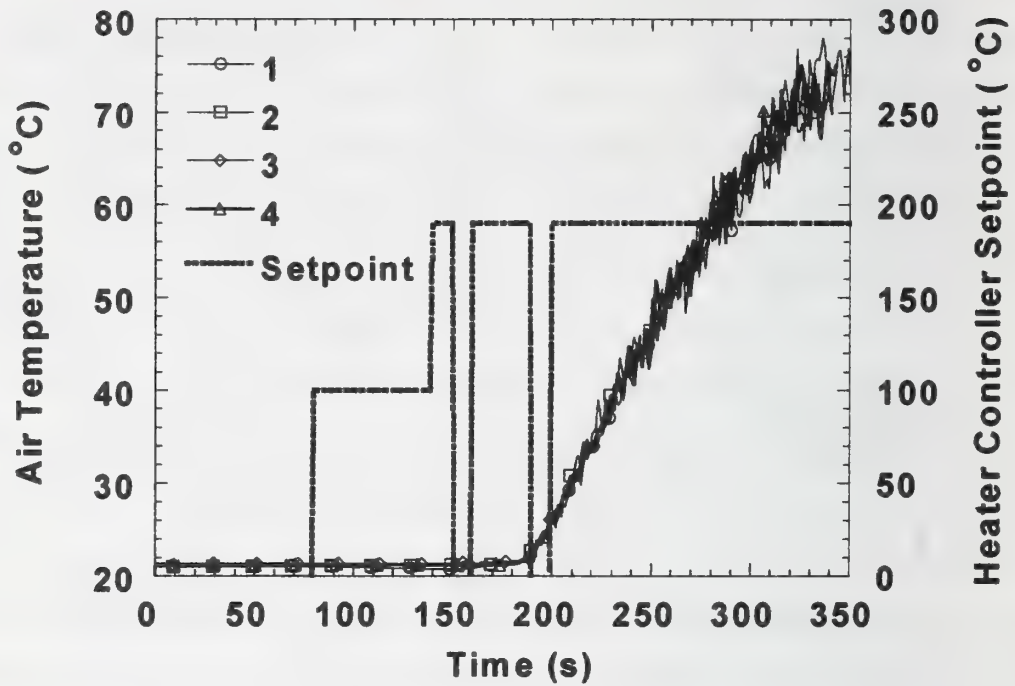


Figure 3. Temperature at a detector location for repeated emulations of a modeled fire.

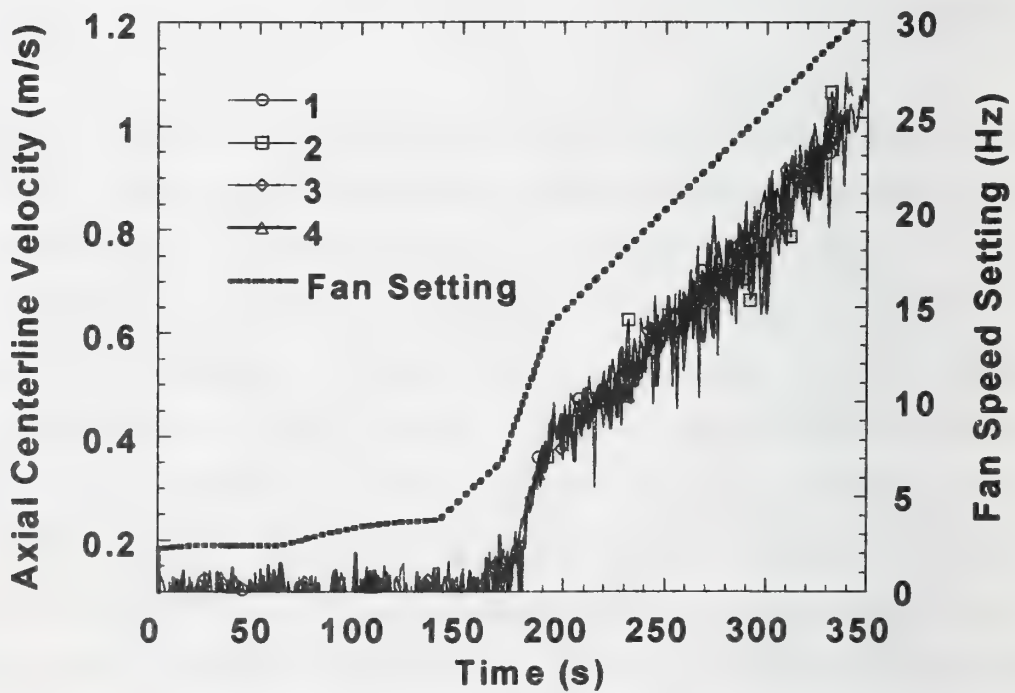


Figure 4. Velocity at a detector location for repeated emulations of a modeled fire.



measured light transmittance (light intensity divided by smoke-free initial light intensity). The extinction coefficient is computed by dividing the natural logarithm of the transmittance by the path length through the smoke and multiplying by (-1). A measuring ionization chamber (MIC) can be located in the test section to provide a reference chamber current measurement more appropriate for ionization detectors than light extinction.

### **3. Smoke Aerosols**

The flaming and smoldering smokes produced cover a wide range of physical properties and concentrations. The propene smoke generator provides black soot typical of flaming hydrocarbon or plastics fire smoke. The generator is directly attached to the FE/DE duct at the vertical riser section. The concentration of smoke in the flow is varied by changing the fuel flow of the burner, and opening or closing dampers allowing more or less flow from the burner to enter the duct. Examples of emulated flaming fire conditions are given in references [5,6] in these proceedings. Propene smoke generated in the FE/DE was collected for the light scattering study in reference [7]. A steady concentration of smoke was provided at the test section (fan speed set at 7 Hz), then collected for light scattering experiments. Figure 5 shows the light transmittance of the upper laser beam traversing the test section and the MIC current output. Here, data gathering began after steady conditions were achieved, as indicated by the transmittance and MIC output. The smoke collection time for the smoke used in the light scattering experiment was from 30 s to 390 s.

Pyrolyzing wood smoke was generated by heating 8 beech wood blocks, 3.5 cm x 2.0 cm x 1.0 cm on an electric hotplate placed inside the duct at the bottom of the vertical riser (Figure 6). This scenario is similar to the fire sensitivity test fire 2 in EN 54 part 9 [8]. The hotplate was operated at full power for this test (750 kW), and the fan speed was set to 7 Hz. For this test the hotplate was turned on at 30 s and turned off at 1300 s. Smoke generated from the heated wood blocks was also collected and studied in the light scattering and size distribution experiments described in [7]. Figure 7 shows the light transmittance of the upper laser beam traversing the test section and the MIC current output for this scenario. The MIC output started to drop at approximately 550 s while the

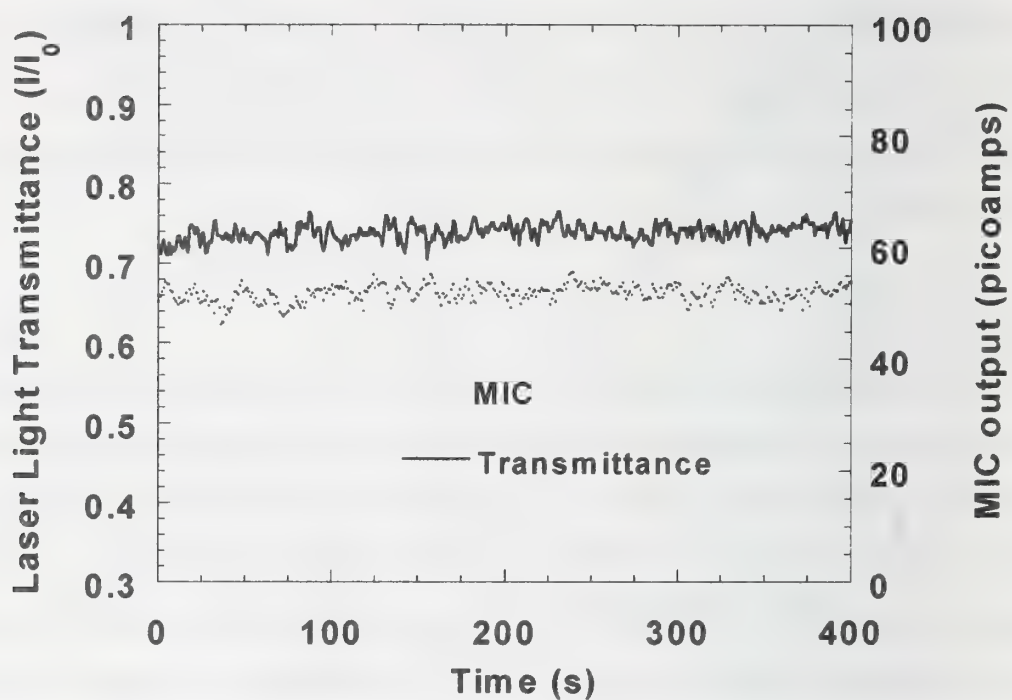


Figure 5. Transmittance and MIC output for steady propene smoke concentration.

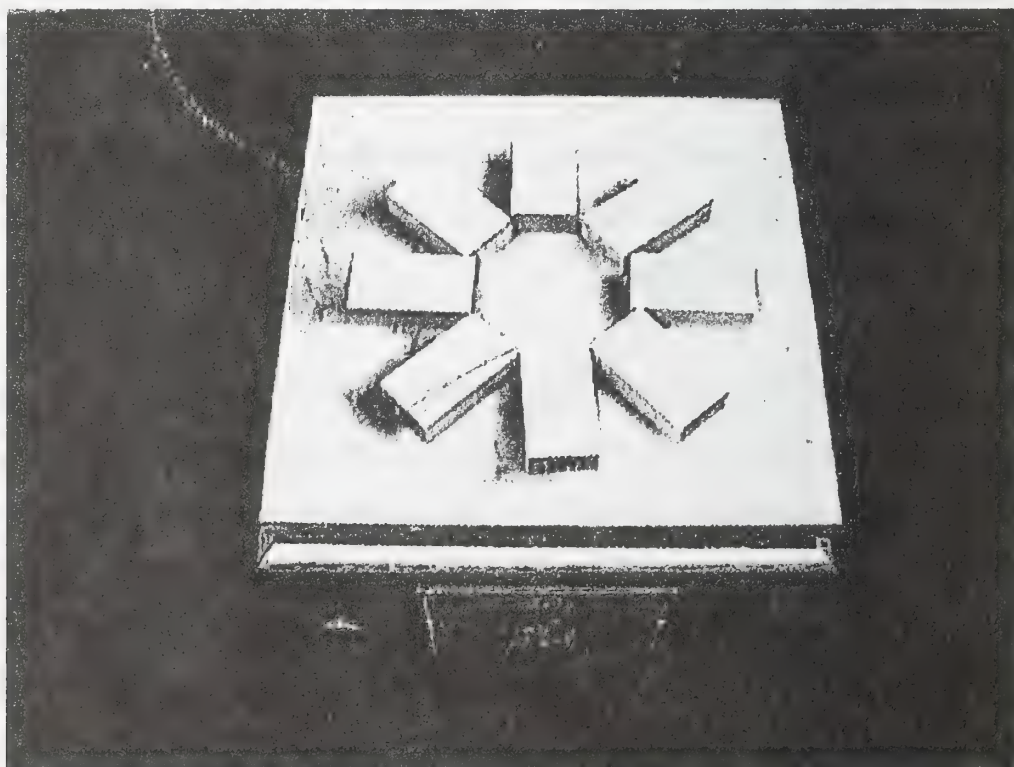


Figure 6. Electric hotplate with arranged wood blocks prior to testing.

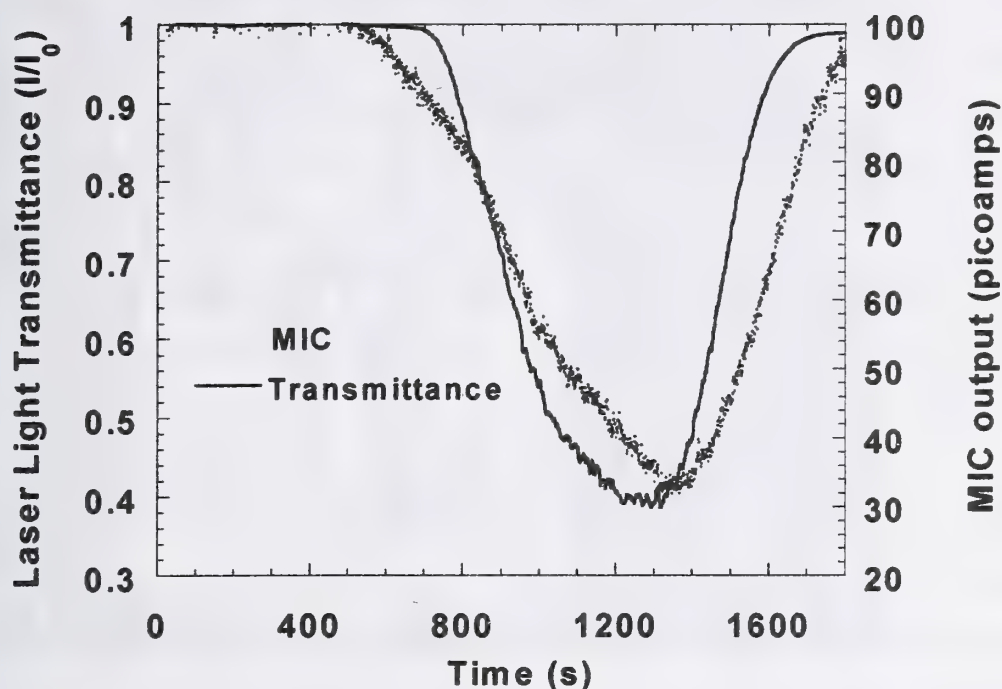


Figure 7. Transmittance and MIC output for pyrolyzing wood blocks source.

transmittance began to drop around 700 s, and both were continuously changing throughout the test. Smoke for the light scattering and size distribution measurements was collected over a time period from 800 s to 1160 s. Over this collection period, the transmittance dropped from 0.9 to 0.4.

Smoldering cotton smoke is generated by a staged-wick-ignition device (Figure 8) that ignites wicks by applying power to electrical heating wires in a prescribed computer-controlled sequence to affect a specific rate of smoke build-up at the test section. Eight groups of up to four individual wicks can be ignited in sequence to provide the controlled rate-of-rise in smoke concentration at the test section. The cotton smolder source is similar to the cotton smolder test fire 3 in EN 54 part 9 [8]. Smoke generated from the smoldering wicks was also collected and studied in the light scattering and size distribution experiments described in [7]. Successive application of power to each of the eight sets of four wick igniters was performed at 12 s intervals to achieve the smoke buildup; data collection began 30 s prior to the start of the ignition sequence. Figure 9



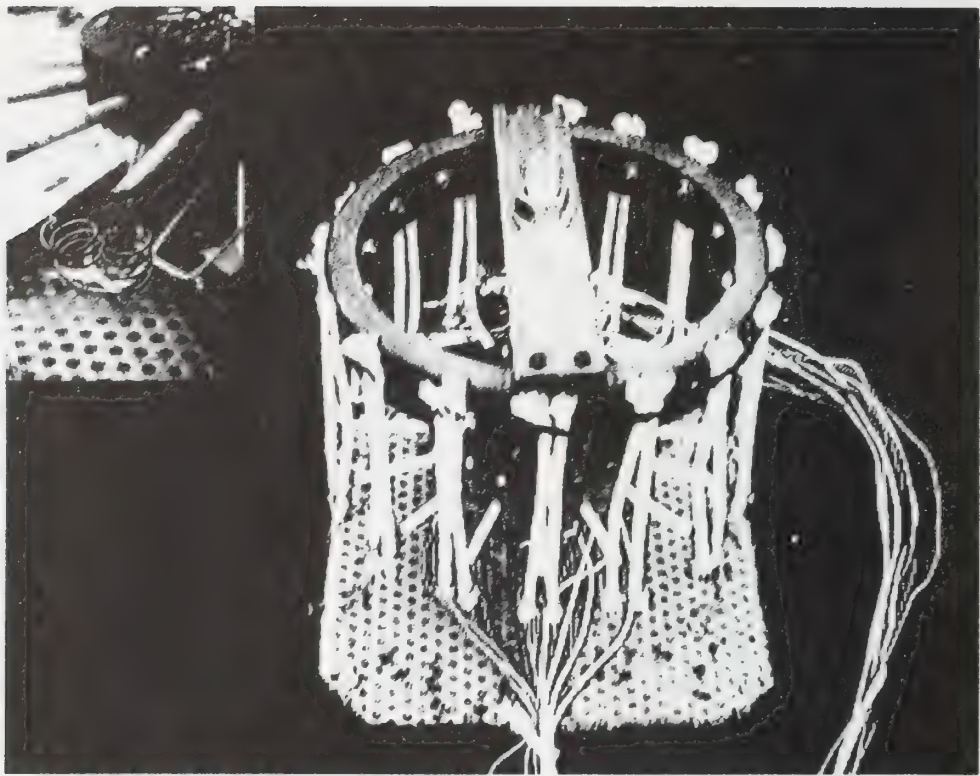


Figure 8. Staged-wick ignition device with close-up of an igniter.

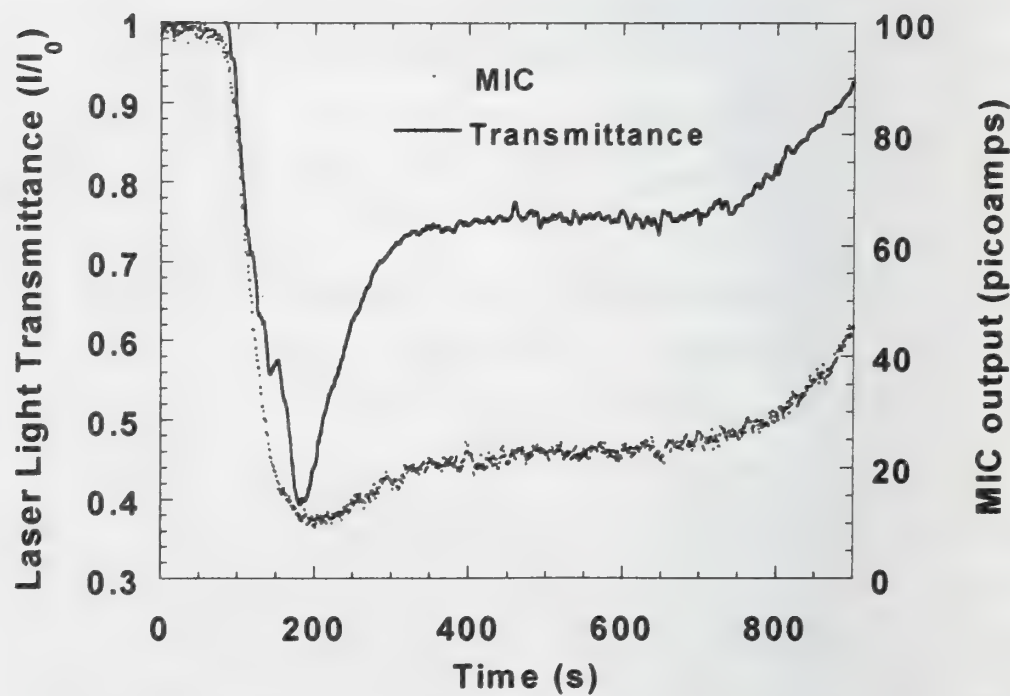


Figure 9. Transmittance and MIC output for cotton smolder smoke.

shows the shows the light transmittance of the upper laser beam traversing the test section and the MIC current output for this scenario. The transmittance and MIC current initially drop at the same rate. It then appears that the MIC output loses sensitivity at a light transmittance below 0.6. At about 190 s, the transmittance reached its lowest value. All 32 wicks have ignited and each are approaching the steady burning rate period. Between 350 s to 750 s the wicks burn at a steady rate as evidenced by the transmittance and MIC output values. After 750 s the first set of four wicks start to burn out, followed by successive groups of four later. Smoke for the light scattering and size distribution measurements in [7] were collected over a time period from 360 s to 720 s.

An illustration of the relative difference in the properties of these test smokes as related to the response of light scattering and ionization detectors is shown in Figure 10 where the ratio of the normalized MIC output ( $(I_0-I)/I_0$  where  $I_0$  is the initial chamber current and  $I$  is the present value of the chamber current) to extinction coefficient over the collection times for each of the smokes is plotted. The ratio is steady for cotton smolder

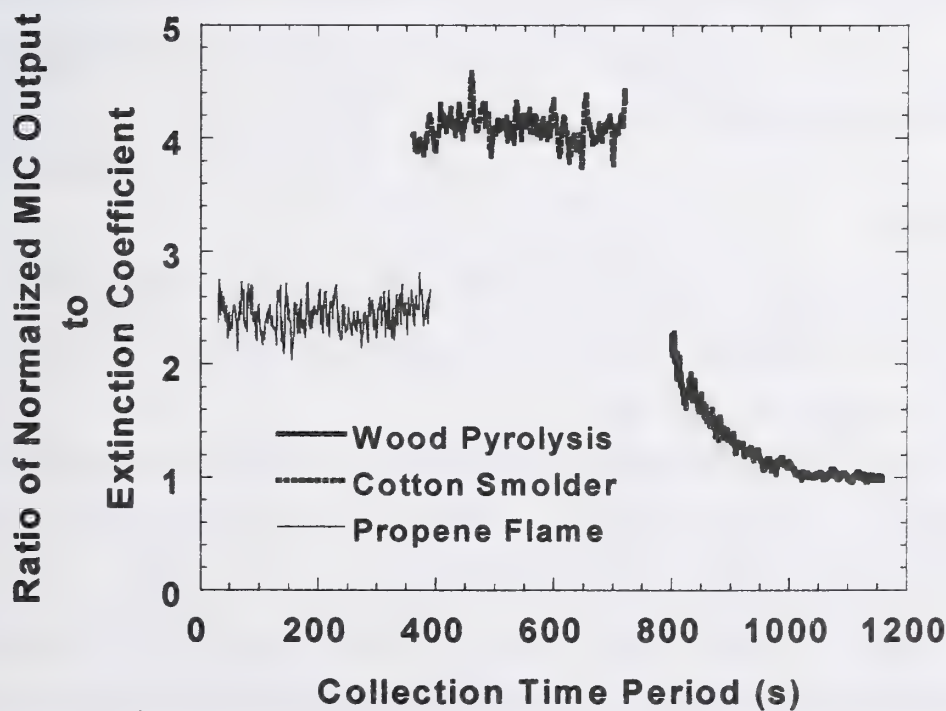


Figure 10. Ratio of normalized MIC output to extinction coefficient for FFE/DE test smokes collected for light scattering and size distribution measurements.

and propene smoke with means of 4.2 and 2.5 respectively, following a collection time period when the extinction coefficient was a constant value of  $0.2 \text{ m}^{-1}$  in both cases. The ratio computed for the wood smoke varied from about 2 to 1 over the collection time period. The ratio for wood smoke during the brief collection time when the extinction coefficient was  $0.2 \text{ m}^{-1}$  was 1.3. Comparing the two non-flaming smokes, the ratio is 3.2 times higher for the cotton smoke at that fixed extinction coefficient. This implies that at a fixed concentration, an ionization sensor will be more sensitive to cotton smoke compared to the wood smoke. The size distribution measurements in reference [7] offer an explanation for this effect based on the observation that the cotton smoke size distribution is shifted to smaller particle size compared to wood smoke. More work is planned to characterize other fire smokes and nuisance aerosols produced in the FE/DE

#### 4. Conclusions

The FE/DE is capable of emulating a wide range of fire and non-fire environments to which a spot-type detector could be exposed. Air flows, temperatures, smoke and combustion gas concentrations from growing fires can be emulated accurately in the FE/DE up to levels where detectors should alarm. The flaming and non-flaming fire smokes generated cover a range of concentrations and physical properties that impact smoke detector response.

#### 5. References

- [1] Grosshandler, W.L., "Toward the Development of a Universal Fire Emulator/Detector Evaluator," *Fire Safety Journal* 29, 113-128, (1997).; also in AUBE '95 Proceedings, pp. 368-380.
- [2] Cleary, T., Chernovsky, A., Grosshandler, W., and Anderson, M., "Particulate Entry Lag in Spot-Type Smoke Detectors," Sixth International Symposium on Fire Safety Science, University of Poitiers, France, July, 1999.
- [3] Cleary, T., Anderson, M., Averill, J., and Grosshandler, W., "Evaluating Multi-sensor Fire Detectors in the Fire Emulator/Detector Evaluator," Proceedings of the 8th Inter. Conf. on Fire Science and Eng., Interflam '99, Edinburg, Scotland, June 1999.



- [4] Cleary, T., Grosshandler, W., and Chernovsky, A., "Smoke Detector Response to Nuisance Aerosols," Proceeding of the 11th International Conference on Automatic Fire Detection "AUBE '99", March 16-18, 1999, Gerhard Mercator University, Duisburg, Germany, Luck, H., Ed., pp 32-41, 1999.
- [5] Cleary, T., Donnelly, M., Mulholland, G., and Farouk, B., "Fire Detector Performance Predictions in a Simulated Multi-room Configuration," Proceeding of the 12th International Conference on Automatic Fire Detection "AUBE '01", March 26-28, 2001, National Institute of Standards and Technology, Gaithersburg, MD, USA, Grosshandler, W., Ed., 2001.
- [6] Cleary, T., and Donnelly, M., "Aircraft Cargo Compartment Fire and Nuisance Source Tests in the FE/DE," Proceeding of the 12th International Conference on Automatic Fire Detection "AUBE '01", March 26-28, 2001, National Institute of Standards and Technology, Gaithersburg, MD, USA, Grosshandler, W., Ed., 2001.
- [7] Weinert, D., Cleary, T., and Mulholland, G., "Size Distribution and Light Scattering Properties of Test Smokes," Proceeding of the 12th International Conference on Automatic Fire Detection "AUBE '01", March 26-28, 2001, National Institute of Standards and Technology, Gaithersburg, MD, USA, Grosshandler, W., Ed., 2001.
- [8] EN 54: Components of Automatic Fire Detection Systems, European Committee for Standardization, Parts 1-9, 1988

## **Fire Protection Systems for Traffic Tunnels Under Test**

### **1. Introduction**

Underground transport facilities are sensitive links in the economic chain that carry thousands of people and tons of goods every day and they are growing in importance. Therefore a breakdown in operations can have catastrophic consequences. That is why safety precautions are vitally important and the work involved is commensurate with the high potential risk. By far the greatest risk is a fire out of control. There is great danger to life from toxic combustion gases, exceedingly high temperatures, total loss of visibility, limited means of escape and the panic reactions of drivers and passengers. The emergency services are usually hindered by vehicles and by the smoke and gas generated by the fire which at the same time causes serious damage to the infrastructure of the transport facility.

The dramatic events in the Mont Blanc and Tauern tunnels triggered a wide public debate on the safety of road and rail tunnels leading to demands for comprehensive safety precautions to safeguard the survival of travellers, to keep damage to the facility to a minimum and to maintain its availability.

Structural and organizational measures such as refuges, escape tunnels, effective smoke-venting and rescue concepts are an important first step. Equally important for the prevention of a catastrophe are

- fire detection which is fast, reliable and indicates the precise fire location without being influenced by high-speed air currents

- automatic activation of traffic control systems, the alerting of the emergency services, a fire spread assessment at the scene of the accident, the activation of ventilation systems etc.
- the activation of extinguishing systems to keep the fire in check until the fire department arrives at the scene of the accident.

As with all high-risk installations, those underground call for systems offering the highest reliability. Furthermore, early and certain detection and immunity to false alarms is of the greatest importance. What previously was a very basic form of fire detection for tunnels has, in recent years, developed into a special discipline which has had a powerful influence on the entire security concept for underground transport facilities.

## **2. Aim and purpose**

Concepts for electronic security systems have existed for years and have been consistently upgraded. However, the question is, how the effectiveness, the reliability and immunity to interference of the systems proposed can be practically tested using the previously made physical calculations. Similarly, the test environment, i.e. the location or the premises as well as the technical installations play a decisive role in such tests. The following description deals with these tests with emphasis on fire detection and extinguishing.

## **3. Test Infrastructure**

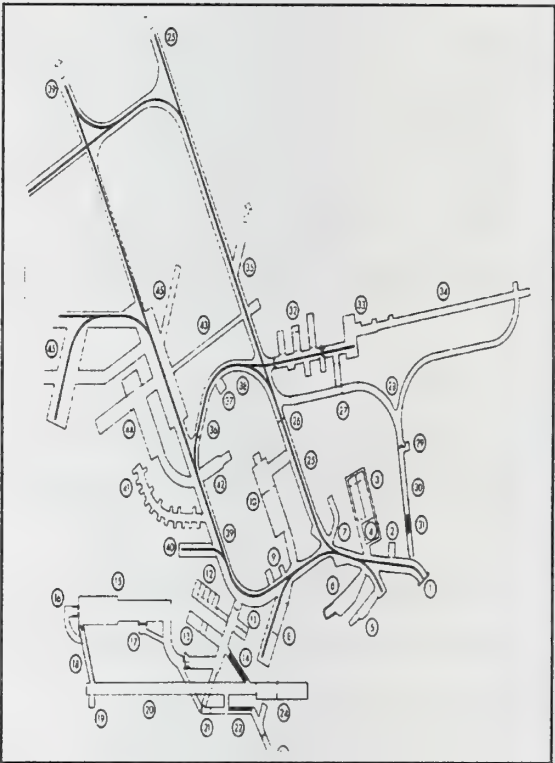
The Hagerbach tunnels near Sargans in Switzerland offer almost ideal conditions for the tests. Hagerbach comprises approx. 4500 m of underground



tunnels of various lengths equipped in different ways. It is mainly used for research into new methods of tunnel construction as well as demonstrations (see “The Siemens Magazine – New World No. 3“, August 1999).



Entrance to the Hagerbach (Switzerland)  
test tunnel



The plan of the test tunnels.  
The tunnel  
complex consists of approx.  
4500 m tunnel sections of  
varying lengths and equipped  
in different ways

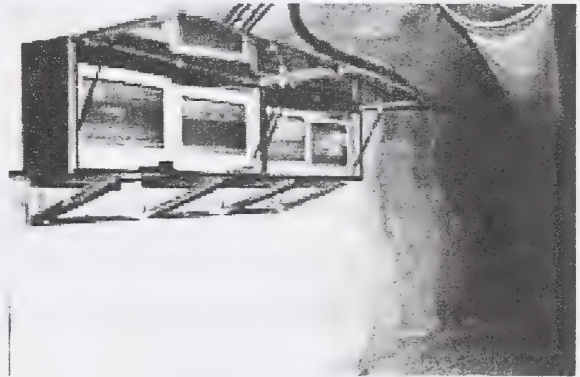
The extract air tunnels with wind speeds of up to 5 m/s, are particularly good for genuine fire and extinguishing tests. For this purpose the floor of the used air tunnel was concreted and fitted with a sump to collect the waste water resulting from extinguishing tests. Various temperature sensors, which can be located wherever required, measure convection and radi-

ant heat. The air speed is also measured. The early warning flame detectors signal the first open fire in a series of tests. The entire test area for fire and extinguishing tests is monitored by video cameras. The control centre was set up some distance away and monitors the test equipment and measuring devices and records all test, measuring and graphics data.

In addition to pool fires for the simulation of rail and road vehicle accidents, a specially-designed dummy vehicle is used to re-create various fire sequences as well as the assessment of the effect of extinguishing in different extinguishing configurations.



Test set-up in tunnel with dummy vehicle.



The control center with its monitors.

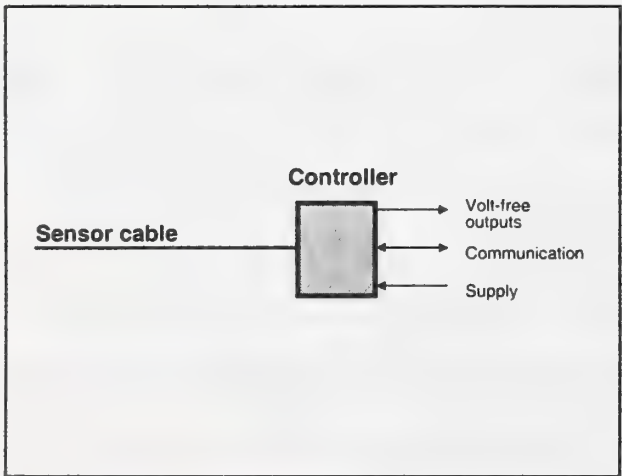
As the test tunnel with a height of 3m and a width of 3m is smaller than a standard tunnel, the measurements were scaled down to provide a mathematically correct basis for proper tests. Thus the procedure could be used for the application of test results for tunnels with different dimensions, lane directions and ventilation conditions. The “Scaling Up / Down” calculation is part of the VdS test for the FibroLaser II calculation program (see also section 4.2).

## 4. Testing systems

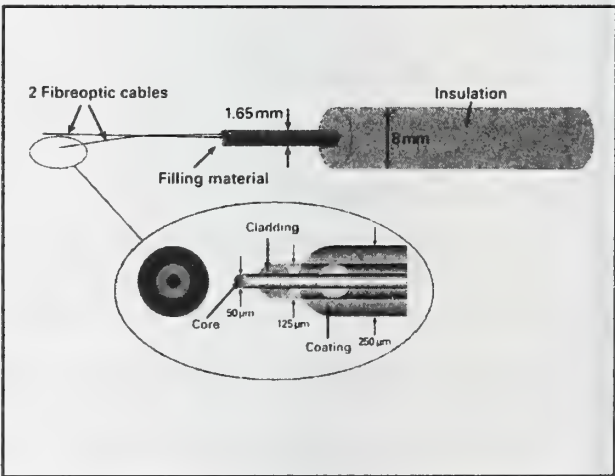
### 4.1 Fire detection with FibroLaser II

The FibroLaser II fire detection system is used for fire detection in tunnels. The system is an intelligent heat detector connected to a fire detection control unit and as required can provide detailed alarm information for further processing. FibroLaser II has a simple system architecture:

- Fibreoptic sensor cable up to 4 kilometers long
- Controller with laser light generation and software-supported evaluation
  - Volt-free outputs for alarm and fault messages
  - Communication interface for the setting of the optimized operating parameters for the tunnel concerned during commissioning and for a link to the control and visualization units with no retro-active effect
  - Power supply 24V DC or 220V AC (100W)



System architecture FibroLaser II  
sensor cable



Design of FibroLaser II



The sensor cable consists of a steel capillary tube with an outer diameter of 1.65 mm. The capillary tube contains 2 separate quartz fibers each with an outer diameter of 0,25 mm. The remaining space in the capillary tube is filled with an anhydrous, heat-conductive material.

The steel capillary tube is encased in a plastic coating with a diameter of up to 8 mm. This plastic coating makes handling easier during installation and provides mechanical stability as well as sensitivity to strictly radiated heat.

The FibroLaser II fire detection system is VdS listed. FM and UL listings are pending.

The FibroLaser II sensor cable was installed at different locations along the roof and walls of the tunnel in the test set-up in order to be able to record all reactions to convection and radiant heat. In addition, by placing the sensor cable of FibroLaser II in cable raceways in the vicinity of the tunnel test section, it is possible to determine heat detection capability in bunches of cables, cable ducts etc.

#### 4.2 Calculation program for FibroLaser II

The planning of tunnel fire detection systems is very demanding as wind speeds have to be taken into account in addition to traffic conditions and geometric dimensions.

A calculation program (patent applied for) has been developed to check the effectiveness of the fire detection system as planned and works out the response time of the FibroLaser II on the basis of the tunnel dimensions, the fire load and wind speeds etc. Known or assumed parameters are entered in the input template of the calculation program. The result is presented in table form or as graphics.

The series of fire tests in the Hagerbach tunnels has provided valuable basic data which, supplemented with results from fire tests in real tunnels has yielded the basis for the mathematical model of the calculation program.

The calculation program is VdS listed. As already mentioned, this review includes the "Scaling Up / Down" process.

#### 4.3 Fire detection with video

Fire detection with video or so-called "cold fire detection" is frequently mentioned in publications at the moment. However, so far no video system has been produced for application in tunnels which can independently guarantee reliable and false alarm free fire detection and which has international approval. Nevertheless, video technology is making great strides.

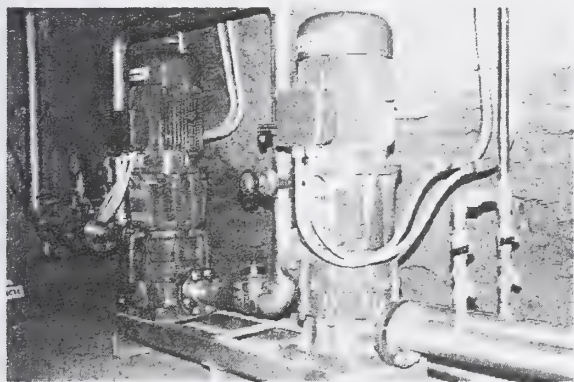
For this reason provision has been made in the Hagerbach installation to enable new developments in video technology to be tested.

#### 4.4 Extinguishing

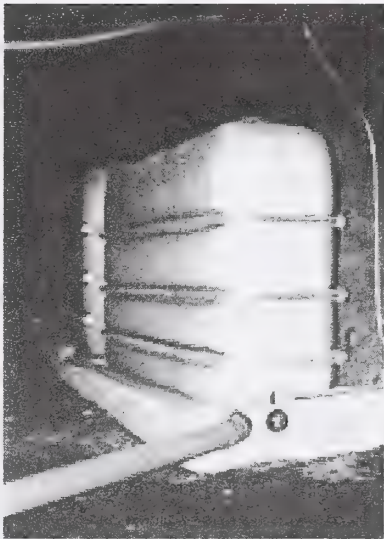
Extinguishing systems for tunnels are specially designed water spray systems with nozzles modified to the type of tunnel in order to guarantee the best extinguishing effect. The extinguishing system is automatically actuated at the fire location by the FibroLaser II system. This means that extinguishing is only triggered at the fire location and that no other vehicles in the tunnel are involved. This procedure also allows us to keep extinguishing water supplies and the amount of waste water to a minimum.

Extinguishing systems in tunnels must be able to withstand the special ambient conditions such as below-zero temperatures or corrosive exhaust gases. Furthermore, the extinguishing system must be able to bring the fire under control in spite of powerful air currents.

Water pipes for servo-mechanical nozzles are mounted along the roof and walls of the tunnel section of the test installation. This simplifies the evaluation of the various extinguishing configurations. The pressurized water is supplied via an arrangement of pumps which enables not only the water pressure to be varied, but also different rates of flow. It is also possible to introduce additives into the extinguishing water. The waste water from the extinguishing system is collected in sumps and correctly disposed of. Gas detectors monitor the water collecting points for impermissible gas concentration



The extinguishing water pump station



Tanks for the disposal of waste water

VdS approval of the extinguishing system described is pending.



#### 4.5 Systems engineering

In the field of systems engineering emphasis is on practical tests for operating sequences.

System specialists work out the interfaces, interactions, data communication and control system technology in accordance with customers' specifications.

### **5. First findings from the test series**

The series of tests at the Hagerbach test tunnels have the following objectives:

- Validation of the calculation program for the optimum application of FibroLaser II
- Examination of the "Scaling Up / Down" method, which enables configuration of the detection system irrespective of the size of the tunnel
- Optimization of tunnel extinguishing in the form of a water spray deluge system with minimum water consumption

When validating the calculation program, (PC software) particular attention is paid to examining the following thermodynamic phenomena:

- Combustion behavior according to the type of combustible and the fire surface

- The influence of the wind on the rate of combustion and on the mixing of combustion gases
- The radiated power of the fire on the FibroLaser sensor cable
- The convection heat exchange with the FibroLaser sensor cable

Previous tests have shown that the tunnel wind, especially that from the emergency ventilation, which in the event of a fire is switched on to disperse the smoke, has a decisive influence on the course of the fire and detection. Furthermore, it has been proved that the linear detection of the radiated heat of a fire is the only relevant alarm criterion at higher wind speeds. As the radiated heat is not influenced by the tunnel wind, the fire location can also be precisely determined.

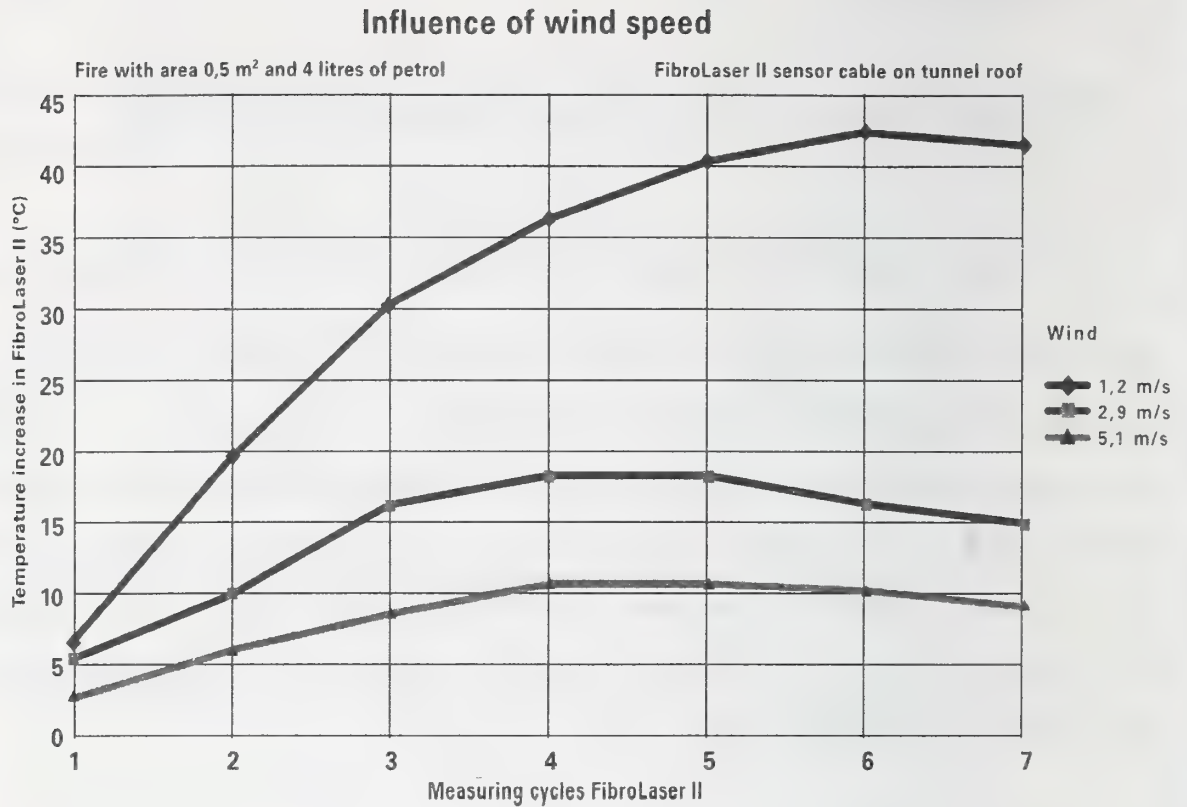


Diagram of fire test results

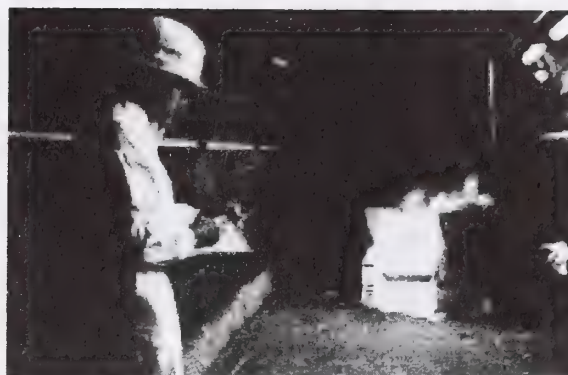
The diagram above shows the results of fire tests in the Hagerbach test tunnels with a petrol fire (4 liters) covering 0,5m<sup>2</sup> and various wind speeds. This size of fire is equivalent to that involving one car.

The diagram clearly shows the influence of wind on detection and the combustion time. In this particular case only the field of radiation is detected. The combustion gas temperatures beneath the roof of the tunnel lie below the measured values in the FibroLaser sensor cable.





Fire test with dummy vehicle  
without tunnel wind at fire source



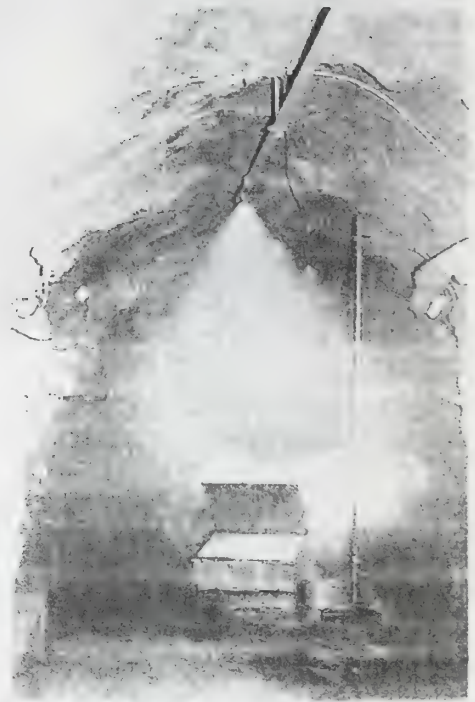
Fire test with dummy vehicle and a  
tunnel wind of  $\sim 5\text{m/s}$  at fire source

An important aspect for the interpretation of the Hagerbach tests is the "Scaling Up / Down" procedure. Tests in small or large tunnels must be comparable and it must be possible for the calculation program to process them irrespective of tunnel geometry. Experience shows that empirical values are the decisive parameters for the conversion of the specific radiation volume and the specific calorific output of a fire.

Tunnel fire extinguishing is based on an optimized water spray deluge system with a nozzle concept that achieves its protection aim with minimum water consumption. Fire tests with a dummy vehicle and realistic combustibles (plastics, petrol, rubber etc.) show that the protection aim must be to bring the fire under control in the vehicle where it originated and to prevent fire spreading to the surrounding area. It has proved to be essential to extend the coverage area of flooding to zones of approx. 30m, whereby basically the extinguishing system in the zones adjacent to the zone in which extinguishing has been actuated should also be actuated. With FibroLaser II it is possible to locate the fire to within about 3-4m and to register the spread of hot gases.



Extinguishing test with fire in the dummy vehicle and a tunnel wind of ~ 3 m/s at fire source



Extinguishing test with fire in the dummy vehicle and a tunnel wind of ~ 5m/s at fire source

## 6. International activities in tunnel protection

Following the tragic accidents in spring 1999, groups of experts were formed in a number of countries to check existing tunnels and to work out plans for the realization of comprehensive concepts for tunnel safety. It is hoped that some of these projects will be financially supported by national authorities. The scope of these concepts stretches from structural measures such as escape tunnels, the design of ventilation systems, electronic security systems and extinguishing systems, to training centres for the emergency services.

Within the framework of such schemes Siemens Building Technologies Ltd., Cerberus Division can make a solid contribution towards the protection of tunnels.

The author of this paper, Rudolf Maegerle, is Head of Application Support at Siemens Building Technologies Ltd., Cerberus Division and is also responsible for the development and application of new products.



## **Concepts for the test of volumetric fire detectors**

### **Abstract**

This paper covers the question, if it is possible to apply to volumetric fire detectors a testing concept, which was introduced in intrusion detector testing. The concept follows a so-called 'solid-state' approach, leading to the stimulation of detectors by means of electronically controllable signals in such a way that the detector cannot distinguish between an artificial stimulation and a situation with a real fire. The application of this technique for the test of video fire detectors and other fire detectors, possibly coming up in the future is discussed.

### **1 Introduction**

Since many years for traditional types of fire detectors test procedures and suitable test apparatus exist, which are specified in national and international standards. These standards rely on evaluating the detectors performance in a) a set of basic tests, which determine the response threshold of detectors before and after environmental tests and b) check the detector in a set of full scale tests [1]. The corresponding test equipment and fire test rooms are available in all major test laboratories.

In a project sponsored by the European Commission, for the basic test of intrusion detectors, testing concepts were worked out and prototypes were set-up, which aim at an apparatus for the determination of the response threshold of such detectors. Although intrusion detectors are designed for the detection of the motion of a human within the detection range, the stimulation of such detectors within the test is carried out without any motion inside the test chamber [2].

The apparatus is designed to be the counterpart of the smoke and heat tunnel, which enables to determine the response threshold for smoke and heat detectors.

One key feature of this equipment is the fact that all physical stimulation signals can be controlled by electronic signals. Thus in a certain range any arbitrary stimulation of the detector is produced. So a stimulation following very closely to a normal motion of humans can be realised.

After the introduction of such a 'solid state' testing concept for intrusion detector tests, the question came up to what extent such a method could be applied to the test of fire detectors. In detail: Is it possible (and reasonable) to consider a test equipment, which determines the relative or absolute response threshold of a smoke detector e.g. without producing any smoke or flames. An investigation into these questions led to some first answers and the following considerations.

## **2 The stimulation concept**

In a full scale test fire detectors have to prove their ability to respond to a set of artificial fires in a more or less well defined environment. To some degree such tests do not rely on the special operating principle of detectors, so a kind of black-box testing is given.

The concept of 'solid state' detector stimulation can be considered as a white-box testing method. Such test methods must perfectly match the required detector type and its design parameters. Different detector types need to be stimulated by different test set-ups. The test apparatus therefore might require a sophisticated construction. Also some essential design details of detectors have to be known in order to select the proper stimulation method and to efficiently carry out such tests. But a clear benefit of such tests is that the detector stimulation is to a very high extent easily adaptable to different test scenarios and superior repeatability is given. Electronic control of the detector stimulation provides also a means of down-scaling the tests with respect to detection range and test chamber dimensions. So the test equipment might be reduced in size to a minimum.

### **3      Applicability to point-type detectors**

This paper essentially covers test methods on volumetric detectors. For point-type detectors test methods are in use for many years, so significant improvements cannot be expected. For newer detector types such as gas detectors the situation is a bit different, improvements of test methods are under discussion.

An important example of such improvements in the test methods for point-type detectors is a test facility, developed at NIST, called in short FE/DE [3]. The apparatus is essentially based on the smoke & heat tunnel and is able to stimulate fire detectors in a very flexible and controlled way. Also the evaluation of gas detectors and multi-sensor detectors is implemented. The stimulation of fire detectors with this system covers the detector response in fire alarm and in some false-alarm situations.

Another reason for the restriction of the following considerations only on volumetric detectors is given by practical limitations for the stimulation of point-type detectors. If an optical point smoke detector for instance is considered, the detector principle requires that inside of the detector housing and inside its measurement chamber the stimulation has to be produced. This chamber is of course always optically shielded very well against environmental light so that an optical stimulation from the outside cannot work.

One might take into consideration that a scattering effect might be realised by inserting a fibre, which carries an optical receiver and transmitter, producing a defined radiation intensity as a function of the received radiation level whilst keeping the signal form. Today's technology allows for such intelligent fibres, but without precise information of the design of the tiny measurement chamber, without a suitable opening and without micro manipulation techniques such a stimulation cannot repeatably be produced.

On the other hand it has to be expected that advances in sensor and processor technology and improvements in signal processing will in the future lead to new cost-effective products with volumetric operating principles.



Volumetric principles open up the possibility of including much more information about the spread of a fire than point type detectors due to the additional spatial information. Also the location estimation of a fire can be enhanced using a volumetric detection.

#### **4 Some testing aspects concerning early volumetric detectors - flame detectors**

For flame detectors a standardised test method is in use since many years. The concept of 'solid state' stimulation could be realised using an appropriate IR /UV source and a modulator for producing the flickering effect of flames. Various options exist for the light modulator. A solid-state solution would implement a micro-mirror spatial light modulator, which offers full digital control, wide spectral response from IR to UV and cut-off frequencies up to 500 Hz [4].

But the limited advantages of easier control, more flexibility of the detectors stimulation and the expected costs do not predict lots of success for such a concept over the existing test method. For other volumetric detectors a possible introduction of an alternative testing concept is much more promising.

#### **5 Volumetric ultrasonic fire detector and a corresponding test concept**

By Appleby and Ellwood [5] in 1995 a number of volumetric fire detection techniques were described. One very interesting technique makes use of the Doppler effect of ultrasonic waves produced by the convection of hot air above a fire. Although such ultrasonic fire detectors don't play any role in fire detection up to now, the potential advantages of the described testing concepts are highlighted very well.

The Doppler signal of such a detector is dependent on the type of the heat source, so a stimulation of an ultrasonic fire detector has to produce a signal form very close to that gained in a real open fire. For an ultrasonic detector the concept of 'solid state' stimulation signals can be applied without problems. Scaling down the scenario with a scale down factor of 5 to 10 leads a compact test chamber.

The stimulation can be produced by means of an IQ modulator, an ultrasonic transducer and a suitable microphone, which have to be located in front of the detector.

If appropriate generation of the I- and Q-signals is provided, the ultrasonic transducer is able to generate any arbitrary low-frequency Doppler signal in the specified frequency range. Typical ultrasonic frequency bands for long range operation and low-cost cover the range of about 25 kHz to 40 kHz Doppler. As the ultrasonic Doppler signals exhibit dominant spectral components of about 40 Hz, it is sufficient to produce Doppler signals with a cut-off frequency of less than 300 Hz. Main cost driving components for such a test apparatus will be the microphone, alignment components for the detector and a test enclosure covered with absorbers.

## **6 Testing of state-of-the-art video fire detectors**

The application areas for video fire detection systems are developing fast. Detecting smoke plumes in forests, fire in aircraft hangars have been the first applications. Video surveillance in manufacturing plants and tunnels are additional areas [6], [7]. Video fire detection systems usually consist of a video control unit to which a number of video cameras are connected and which perform the detection algorithms. Such a system structure opens up the possibility of repeatable test procedures, which follow the same principles as for video motion detection systems [8]. The signals of a predefined set of digital video sequences are fed into the control unit instead of the video camera outputs. By this means perfectly repeatable stimulation signals are fed into the system. Such sets include fire and non-fire situations.

Also the determination of response threshold values can be carried out. Different methods for its determination might be applied. One example of such a method makes use of the response time of the video detection system to a typical fire test scenario as the key parameter for the response threshold determination. A more sophisticated, but also more time consuming onset would use a set of test fire videos produced with different amounts of burning material.

The response threshold can then be defined by that test fire video sequence with the minimum of burning material leading to a detector response.

## **7 Self contained video fire detectors**

Self contained video fire detectors, which integrate the video signal processing components in the detector housing are no product for the mass market of the year 2001. But in the far future the situation might change. Self contained video motion detectors are already on the way. They can make use of CMOS image sensors offering superior performance in several aspects on CCD chips, e.g. in terms of power consumption of less than 35 mW. For the moment the higher price level is the one exception of the long list of benefits. But it is expected that the price level will follow the same development as for CCD chips. It can also be expected that fire detection algorithm might then be offered as an add-on to such components or perhaps as their main function.

In such a situation the presently used techniques for video fire detector tests will not always work because CMOS image sensor and signal processing circuitry will due to cost reasons be implemented on the same chip. So in general an access to internal input signals to the signal processing components is not given. Advanced locally adaptive CMOS image sensor designs already combine local pixel signal processing features, where the local image processing circuits are located inside the pixel cells.

So for such detectors an external stimulation has to be provided using a real or an artificial image. It is proposed to provide such an image by a screen placed in front of the video detector. Onto such a screen video sequences should be played back using a suitable display. The response threshold determination method then need no changes compared to normal video detectors. Because of the usual small focal length of the cameras the screen might be placed quite close to the detector without the risk of a blurred image, so scale-down factors of 10 to 20 might be applied given a rather small size of the corresponding test chamber.



## **8 Microwave detector testing**

Let us assume that also microwave fire detectors find their way in applications with the need for hot spot detection. How could a testing concept look like for such detectors? A more repeatable stimulation than by means of a real fire with enough embers might be carried out using a hot plate of defined temperature placed in front of the detector at a fixed distance and orientation. The problem is to find a material with high emissivity and easy, electrically controllable temperature.

These problems can be overcome in stimulating the detector by means of a microwave signal generator and an antenna at the location of the hot plate. Such tests could be carried out in a small chamber, equipped with microwave absorbing material or in a fire test room. The main requirement is, that few details on the evaluated microwave band have to be known in order to select the proper antenna and signal generator settings.

## **9 Conclusion**

For point smoke detectors a solid-state test concept seems to be far from applicable. For volumetric fire detectors the situation is different. For IR and UV flame detectors the application is possible, but leads to no significant improvements. For future fire detectors, such as self contained video fire detectors and microwave detectors the 'solid state' approach is quite promising.

## **References**

- [1] EN54 Components of automatic fire detection systems, European Committee for Standardisation, Parts 1-9, 1988
- [2] Willms, I., Berentsen, M., Rexfort, C. Solid state simulation of movements for the test of volumetric intrusion detectors, International Carnahan Conference on Security Technology, Madrid, 1999
- [3] Cleary, Th., Grosshandler, W., Chernovski, A. Smoke detection to nuisance aerosols, AUBE '99, Duisburg 1999

- [4] Dürr, P., Gehner, A., Dauderstädt, U. Micromirror spatial light modulators, International Conference on Micro Optical Mechanical Systems, Mainz, 1999
- [5] Ellwood, S.H., Appleby, D. Volumetric fire detection using imaging of fire products and transport phenomena, AUBE'95, Duisburg, 1995
- [6] Lloyd, D. Video Smoke Detection, Fire Safety Engineering 2000, 7
- [7] Löpfe, M. Status of video and smoke detection. EUSAS Workshop on Fire Protection in Tunnels, Männedorf, 2001
- [8] Pritchard, D.A., Virgil, J.T. On the development of a digital video motion detection test set, IEEE International Carnahan Conference on Security Technology, Madrid, 1999

Thomas Cleary and Takashi Ono\*

Building and Fire Research Laboratory, National Institute of Standards and Technology  
Gaithersburg, MD, 20899 U.S.A.

\*Department of Electrical Engineering, College of Science and Technology  
Nihon University, Tokyo Japan

## **Enhanced Residential Fire Detection by Combining Smoke and CO Sensors**

### **1. Introduction**

The advantages of multi-sensor detection in general, and gas sensing in particular, suggest that a combined carbon monoxide-smoke fire detector could benefit the consumer by providing better fire detection through discrimination of some common nuisance sources, while warning of hazardous CO concentration in the living space. Heskestad and Newman [1] reported that the cross-correlation of CO concentration and measuring ionization chamber (MIC) measurements taken during room fire experiments was capable of detecting fires similar to EN 54 test fires with high sensitivity. Gottuk *et al.* [2] performed a number of fire and nuisance source room experiments, and showed that by combining CO and ionization signals, many nuisance sources were discriminated, while most fire source were detected. Ishii *et al.* [3] developed a detection algorithm using CO concentration, smoke concentration, and temperature measures in an artificial neural network. Here, three fire sources and four nuisance sources were emulated in the fire emulator/detector evaluator (FE/DE). Analog output photoelectric and ionization detector signals, along with an electrochemical CO cell's signal were gathered during the tests from sensors located in the FE/DE test section. The sensor signals from these tests were used to test a multi-parameter, rule-based fuzzy logic detection algorithm.

### **2. Fuzzy Logic Detection Algorithm**

Residential smoke detectors are typically ionization type or photoelectric type. There are dual sensor designs that contain both ionization and photoelectric sensors in the same housing, however, they function separately. The benefit of monitoring both photoelectric and ionization sensor outputs lies in their differing relative response to both fire smokes



and nuisance aerosols. In combination with a CO measurement, potentially better fire detection and nuisance source discrimination is possible compared to a CO and ionization detector combination. Here, photoelectric, ionization and CO sensor signals were combined in a rule-based, fuzzy logic algorithm designed to discriminate between the emulated fire and nuisance source test results. The signal feature considered was the instantaneous value of the measured output. Hence, this algorithm is considered a static classification algorithm.

An overview of the fuzzy logic methodology and computations are described below. A more detailed treatment for the application of this methodology related to fire detection is given by Mueller [4]. Here, photoelectric, ionization, and CO signals were the input variables, and assigned to classes low, medium and high depending on their values. The state of alarm (fire) was the output variable, and assigned to class true or false. A rule base consisting of 27 rules of the form below was specified.

***IF Photoelectric = (low, medium, or high) and Ionization = (low, medium, or high) and CO = (low, medium, or high) THEN fire = (TRUE or FALSE).***

Each variable has a degree of membership in each class ranging from 0 to 1, given by defined membership functions. The membership functions for the variables photoelectric, ionization, and CO are shown in Figures 1-3. The final shape was obtained by an iterative process of testing the algorithm against the FE/DE test signals then adjusting membership functions. A commercial analog output photoelectric, ionization, and heat combination detector was used to obtain the photoelectric, and ionization sensor signals. The photoelectric and ionization sensor signals represent integer values from 0-255 spanning the sensor range; the membership function spans a portion of this range, where a zero-offset has been subtracted from the values. Figures 4-6 show the response of these sensors to steady concentrations of flaming soot, dust, and nebulized oil aerosol [5]. A linear fit through the data for each sensor is given along with the correlation coefficient. Error bars represent  $\pm 1$  standard deviation about the mean for each data point (an indication of aerosol source stability). The CO sensor signal was obtained from the voltage drop across a resistor attached to the terminals of an electrochemical CO cell. The voltage drop may be converted to CO volume fraction by multiplying it by 0.13 (volume fraction/volt).

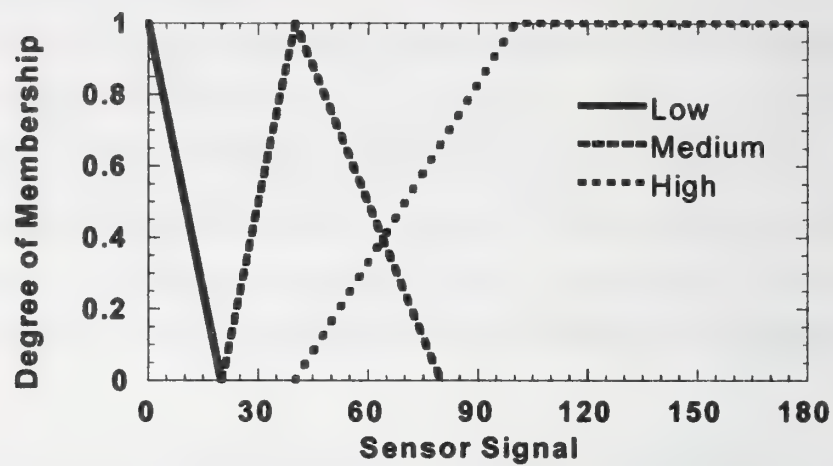


Figure 1. Membership functions for photoelectric sensor output.

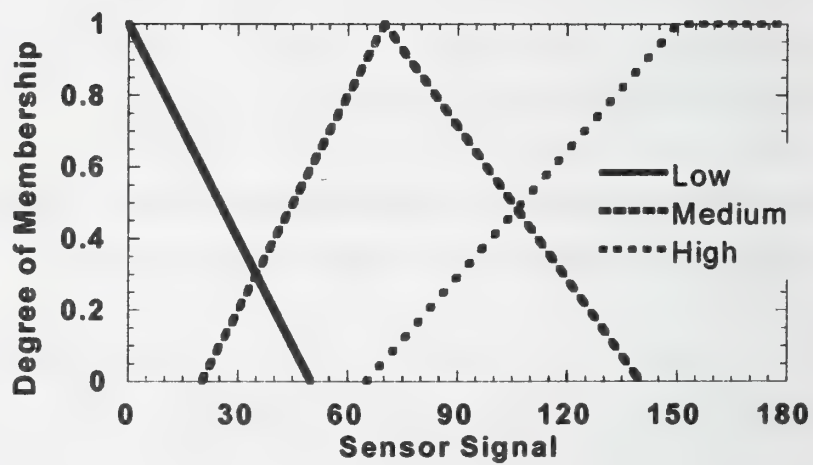


Figure 2. Membership functions for ionization sensor output.

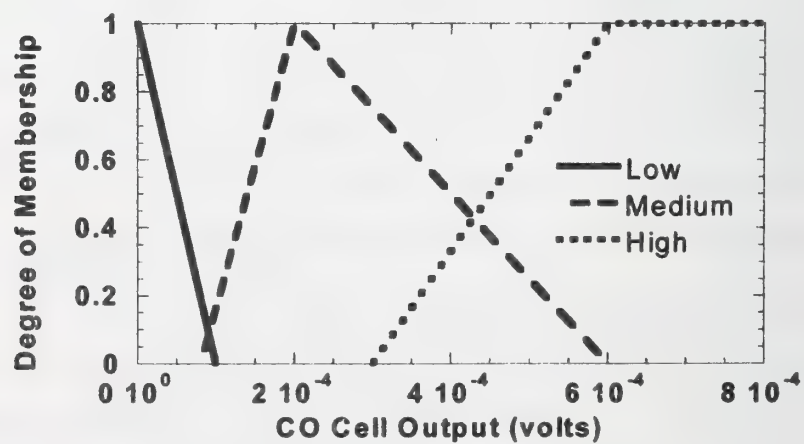


Figure 3. Membership functions for CO cell output.

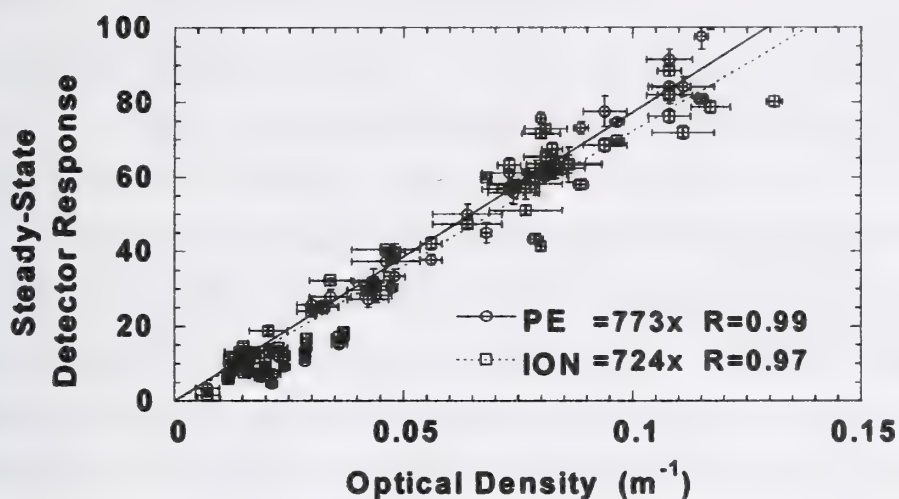


Figure 4. Photoelectric and ionization detector response to propene smoke.

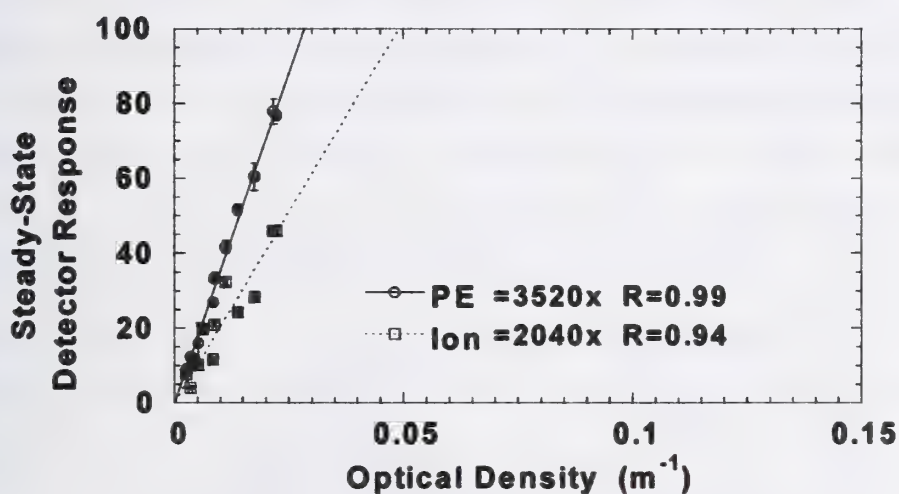


Figure 5. Photoelectric and ionization detector response to nebulized oil.

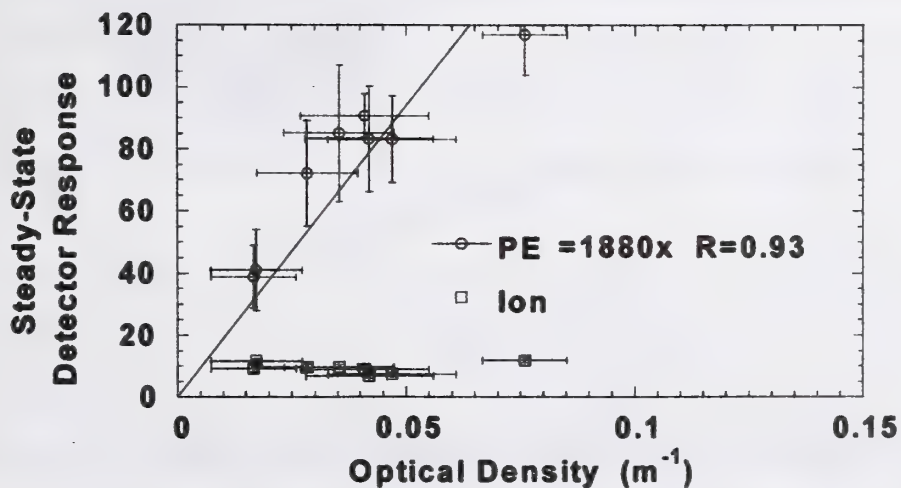


Figure 6. Photoelectric and ionization detector response to Arizona test dust.



The degree of membership in each class for the input variables is used to evaluate the output variable's degree of membership. A weighted average of this set is used to determine if an alarm is reached by comparing it to a threshold value.

By computing the results over the entire range of photoelectric, ionization and CO sensor outputs, a surface plot reflecting the boundary between no alarm, and alarm conditions was constructed. In Figure 7, all space on and above the surface reflects computed alarm conditions, while the space below reflects the computed no alarm conditions. At an ionization signal of about 70 and higher and a photoelectric signal of 80 and higher, no CO concentration was required for alarm. At lower ionization and photoelectric signal values, CO cell voltage must be above zero to indicate alarm. No alarm was indicated when ionization signal fell below 34. No single sensor value was sufficient to cause alarm by itself over the range considered.

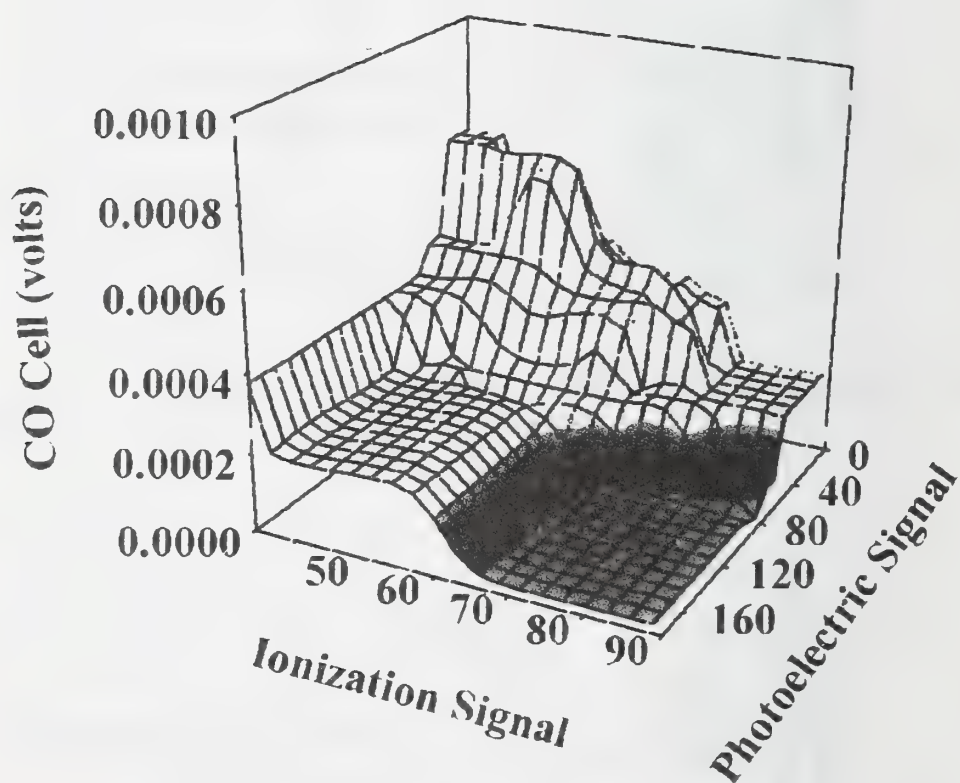


Figure 7. Boundary surface between alarm and no-alarm conditions.

### 3. Fire and Nuisance Source Signals and Algorithm Output

Three fire smokes (flaming fire, smoldering cotton, and pyrolyzing wood blocks) and 4 nuisance sources (Arizona test dust, toasting bread, heated cooking oil, and cigarette smoke) were produced in the FE/DE, and sensor data for the analog output detector and CO electrochemical cell were gathered (see other papers by Cleary *et al.* in this proceedings for details on the FE/DE). Residential photoelectric and ionization detectors were placed on the ceiling of the FE/DE test section just down stream from the analog output detector and CO cell. Alarm times for these detectors were recorded during the tests. Each source is described below, along with the photoelectric, ionization, and CO sensor outputs and the alarm algorithm computations over the length of the test.

The flaming fire source was produced by heating the air, ramping the fan speed, and increasing soot from the propene smoke generator to emulate conditions from a burgeoning pool fire. Figure 8 shows the photoelectric, ionization, and CO sensor signals along with residential detector alarm points and the computed fuzzy alarm algorithm. The photoelectric, ionization, and CO signals all begin to rise at about 280 s. The residential ionization detector alarms first, followed by the algorithm computation (indicated by the transition from an arbitrarily low computed value to a high value), then the residential photoelectric detector.

Cotton smolder smoke was generated by igniting 10 cotton wicks inside the FE/DE at the bottom of the vertical riser with the fan speed set at 5 Hz (corresponding to a mean flow velocity of 0.05 m/s). Figure 9 shows the sensor signals and alarm algorithm computation. The photoelectric signal climbs more steeply than the ionization signal and peaks at a higher value. For this source, the algorithm computation alarms first, followed by the residential photoelectric detector, then the residential ionization detector less than 10 s later.

Smoldering wood smoke was generated by heating 8 blocks of wood on an electric hotplate placed in the FE/DE at the bottom of the vertical riser (this source was a scaled down version of EN 54 test fire 2) with a fan speed of 7 Hz. Figure 10 show the sensor signals and alarm algorithm computation. While all signals begin to rise between 600 s to 700 s, the photoelectric signal rises much more steeply and reaches its maximum value. The

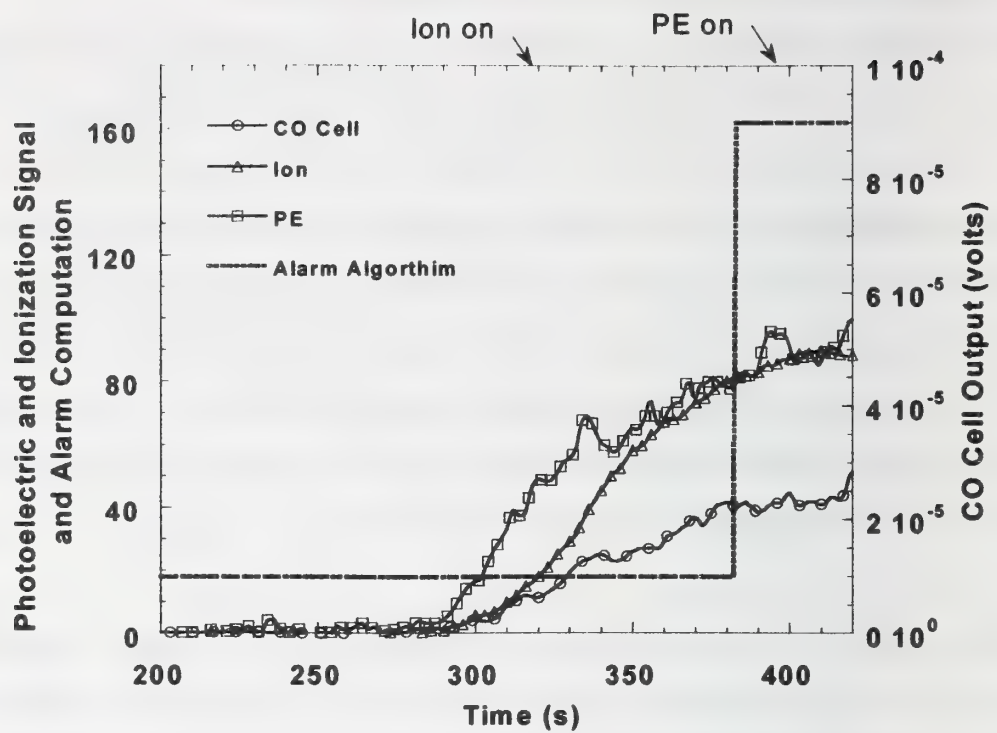


Figure 8. Sensor signals and algorithm computation for flaming fire scenario.

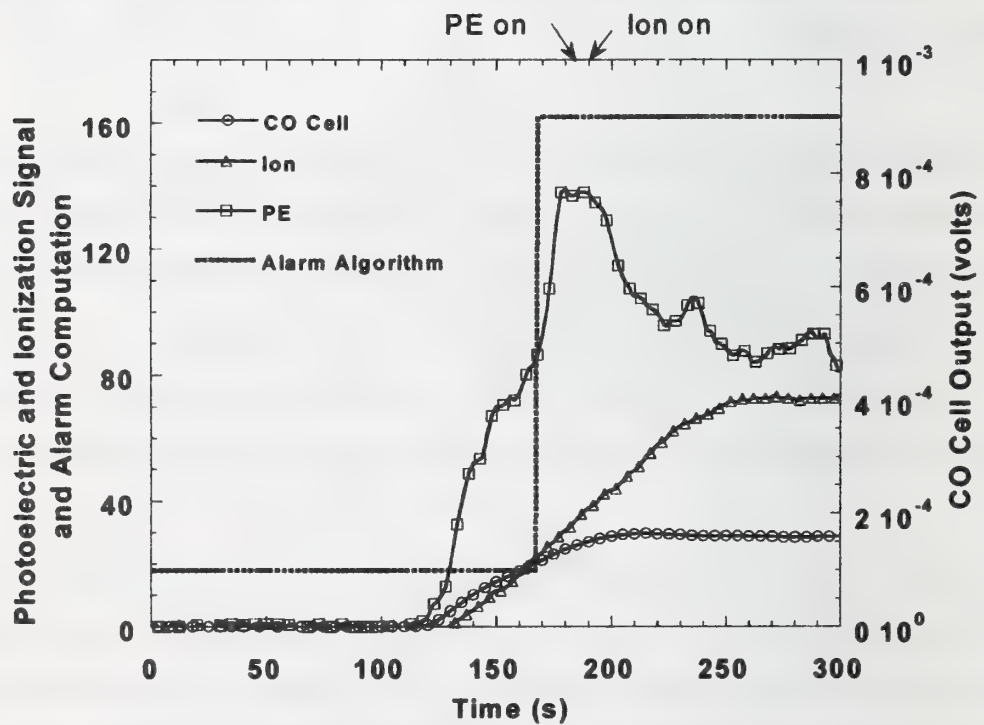


Figure 9. Sensor signals and algorithm computation for smoldering cotton source.



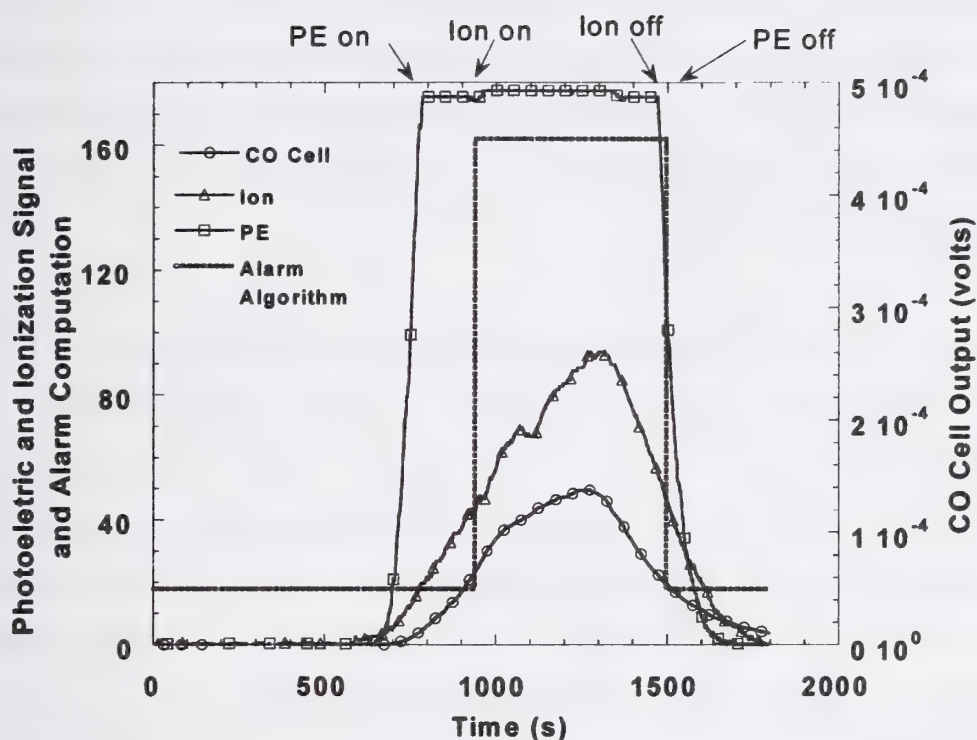


Figure 10. Sensor signals and algorithm computation for pyrolyzing wood source.

residential photoelectric detector was the first to alarm, followed about 200 s later by the residential ionization detector and the algorithm computation.

The dust exposure was produced by introducing Arizona test dust into the FE/DE duct by a powder-delivery feeder at a constant rate, with a fan speed setting of 10 Hz. Figure 11 shows the sensor signals and the alarm computation. The photoelectric and ionization signal began to rise at 80 s with the photoelectric signal reaching its maximum value less than 10 s later. The ionization signal reached a much lower steady maximum 30 s to 40 s after beginning to rise. No appreciable rise in CO cell voltage was observed. The residential photoelectric detector was the only one to alarm. The algorithm computation stayed low throughout the test.

Cigarette smoke was produced by igniting a single unfiltered cigarette that had its unlit end attached to an air ejector (designed for this test to provide a continuous draw on the cigarette ) placed at the bottom of the vertical riser. Smoke emitted directly from the burning coal, and drawn through the cigarette by the air ejector was blown to the test

section by a duct flow from a fan speed setting of 5 Hz. Figure 12 shows the sensor signals and alarm computation. Smoke from the cigarette reached the test section and the sensors began to rise at about 70 s. Although all signals rise, the alarm computation stayed low and neither residential detector alarmed. (In one repeated test, the residential photoelectric detector did alarm at 500 s)

Cooking oil placed in a glass dish and heated on an electric hotplate (which was placed at the bottom of the vertical riser) produced a nuisance cooking aerosol. For this test condition the fan speed was set to 5 Hz. Figure 13 shows the sensor signals and alarm computation for this test. The ionization signal was the first to rise, starting at about 400 s. The photoelectric signal began to rise at 700 s and reached its maximum before 1000 s. At about 1000 s, the CO cell voltage began to rise, signifying that the cooking oil was beginning to pyrolyze. The residential photoelectric detector alarmed at 920 s, while the residential ionization detector alarmed at 1360 s, and the algorithm computation alarmed at 1435 s. Given the CO production and heavy smoke later in the test, this "nuisance" cooking source, in reality, transitioned to a hazardous condition that a detector should sense and alarm.

Smoke from toasting bread was produced by placing two slices of white bread into a two-slice toaster placed at the bottom of the vertical riser and setting the fan speed at 5 Hz. This toaster was modified by wiring the pop-up mechanism down so that as long as electrical power was applied, the bread continued to toast. Figure 14 shows the sensor signals and alarm computation for this test. The ionization signal was the first to rise, starting at about 60 s, followed by the photoelectric signal around 160 s, and the CO cell voltage at 220 s. The residential ionization detector was the first to alarm at 131 s followed by the algorithm computation and residential photoelectric detector at 235 s and 238 s respectively. Before 200 s there was no appreciable visible smoke emitted from the toaster, but soon thereafter, heavy smoke was produced followed by significant increase in CO production between 300 s and 400 s. Similar to the cooking oil test above, the power was left on long enough such that this nuisance source transitioned to a hazardous condition that should be detected.

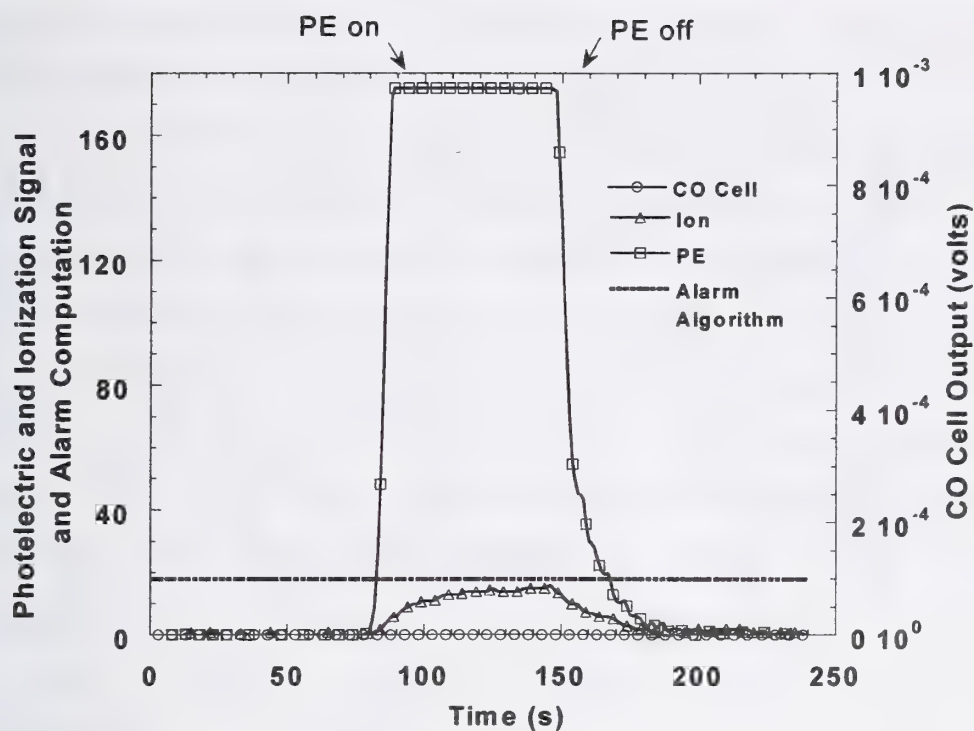


Figure 11. Sensor signals and algorithm computation for dust exposure.

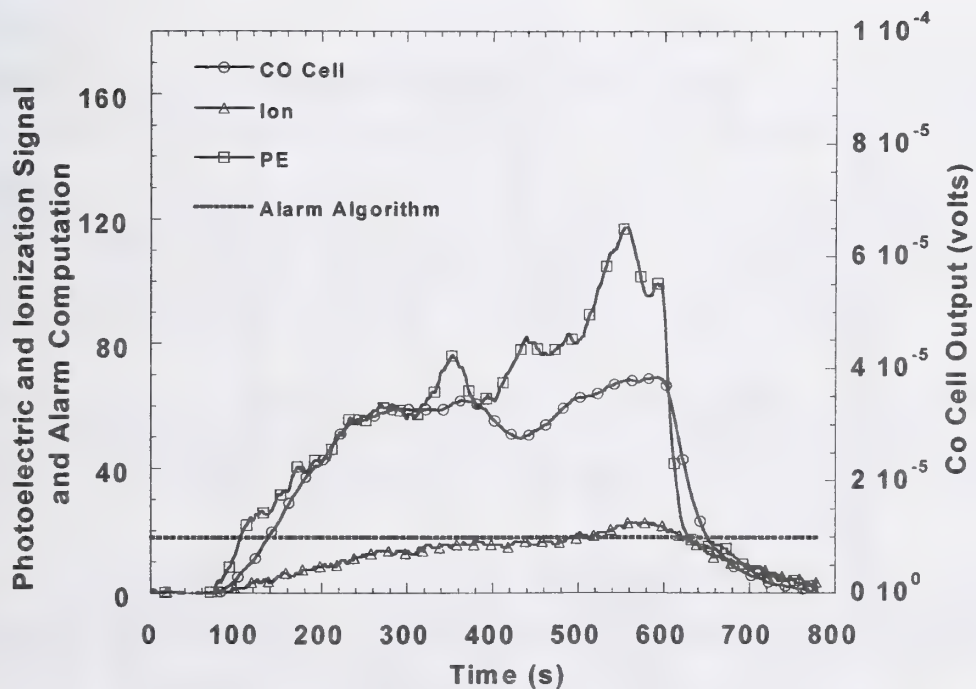


Figure 12. Sensor signals and algorithm computation for cigarette smoke exposure.



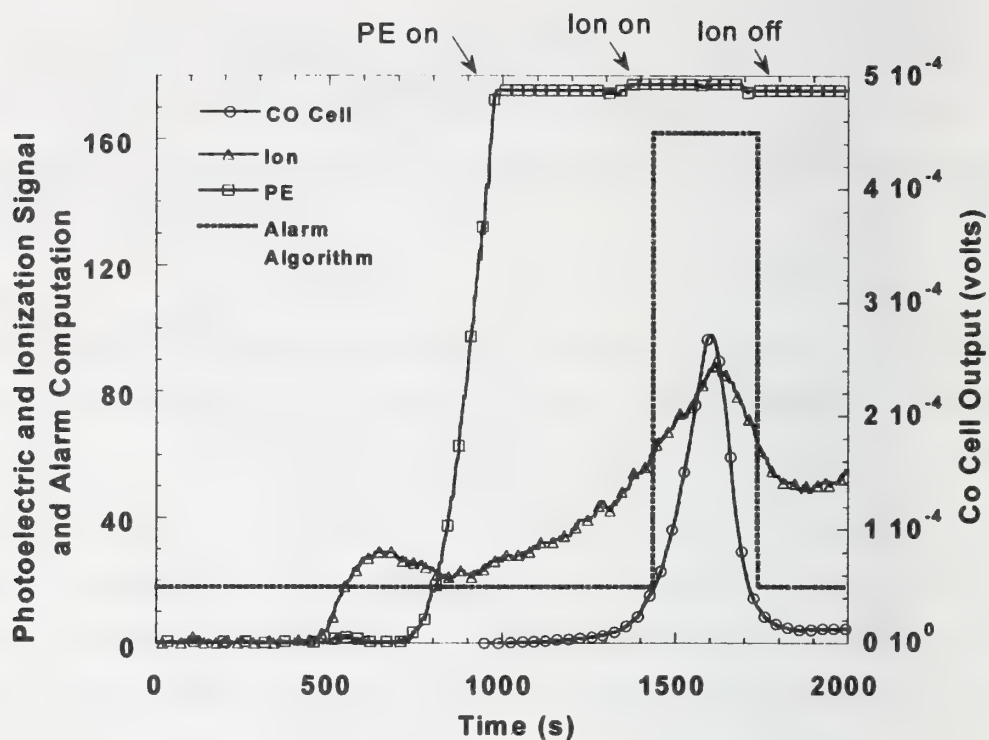


Figure 13. Sensor signals and algorithm computation for heated cooking oil source.

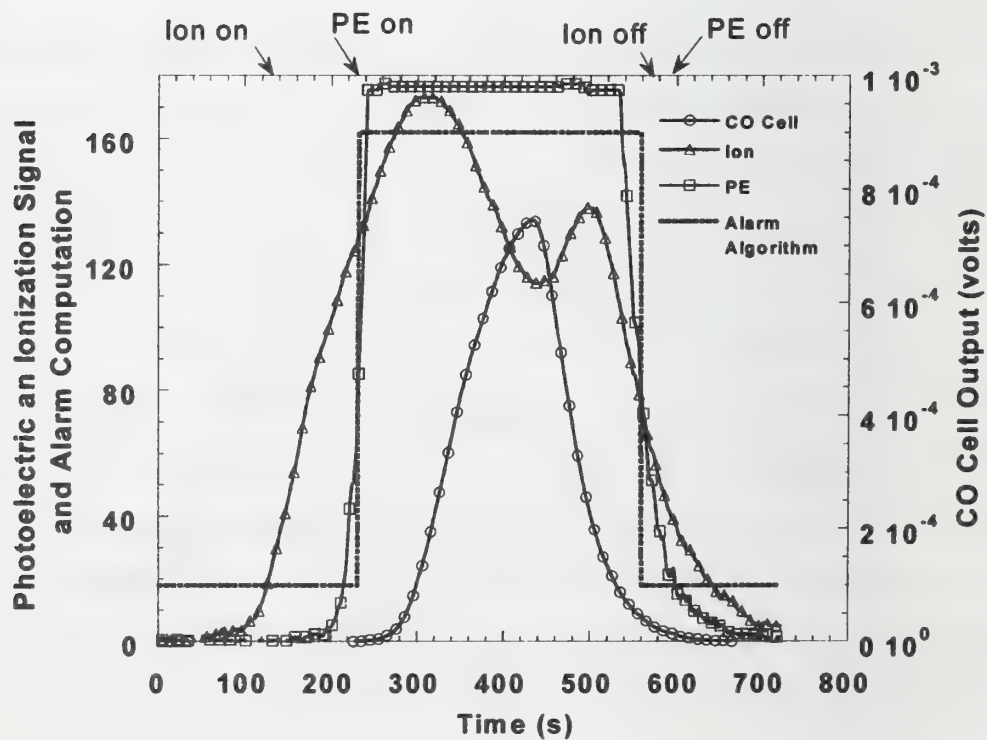


Figure 14. Sensor signals and algorithm computation for toasting bread source.

#### **4. Conclusions**

By combining photoelectric, ionization, and CO cell sensor signals in a rule-based, fuzzy logic alarm algorithm, a robust, multi-sensor detection scheme suitable for residential applications was achieved. The alarm algorithm was able to identify emulated fire conditions earlier than both residential detectors for the smoldering cotton source, earlier than the residential photoelectric detector for the flaming fire source, and approximately the same time as the residential ionization detector for the pyrolyzing wood source. The alarm algorithm did not indicate alarm during dust or cigarette smoke exposure, and did indicate alarm during the transition to hazardous conditions for the pyrolyzing cooking oil and burning toast sources. The fact that the algorithm employed signals from existing sensor technologies already in use in homes today suggests that this approach is viable in the near future.

#### **5. Acknowledgements**

The authors would like to thank Edwards Systems Technology for the use of their detection equipment. Part of this work was funded by a contract from the U.S. Dept. of Housing and Urban Development as part of their Healthy Homes Initiative project.

#### **6. References**

- [1] Heskestad, G., and Newman, J. S., "Fire Detection Using Cross-Correlations of Sensor Signals," *Fire Safety Journal*, Vol. 18, No. 4, 355-374, 1992.
- [2] Gottuk, D.T., Peatross, M.J., Roby, R.J., and Beyler, C.L., "Advanced Fire Detection Using Multi-signature Alarm Algorithms," *International Conference on Automatic Fire Detection "AUBE '99"*, 11th, March 16-18, 1999, Gerhard Mercator University, Duisburg, Germany, Luck, H., Editor, pp. 237-246, 1999.
- [3] Ishii, H., Ono, T., Yamauchi, Y., and Ohtani, S., "Fire Detection System by Multi-Layered Neural Network with Delay Circuit," *4<sup>th</sup> International Symposium, Intl. Assoc. for Fire Safety Science*, Boston, MA, Kashiwagi, T., Editor, pp. 761-772, 1994.
- [4] Mueller, H., "Rule Based Detection Algorithms," *Proceedings of VdS Conf. on Gas Sensors for Fire Detection*, November 15-16, Cologne, Germany, 2000.
- [5] Cleary, T., Grosshandler, W., and Chernovsky, A., "Smoke Detector Response to Nuisance Aerosols," *Proceeding of the 11th International Conference on Automatic Fire Detection "AUBE '99"*, March 16-18, 1999, Gerhard Mercator University, Duisburg, Germany, Luck, H., Ed., pp 32-41, 1999.

## **A Diode Laser Multigas Analyzer for Advanced Detection of Fires**

### **1. Introduction**

An ideal instrument for early fire detection would combine high sensitivity, rapid response, automatic self-testing and a low false alarm rate while generating information specific to the location and nature of the fire. Current fire detection strategies in large buildings call for many point sensors such as standard smoke detectors. In these systems, the false alarm rate becomes unacceptably high because the overall rate is the sum of the false alarm rate from each sensor. Even if sensors are inexpensive, routine maintenance and testing can be very costly when hundreds of detectors are in use. Some new systems use multiple point air sampling and a centralized, highly sensitive smoke detector; this approach reduces false alarm rates but is expensive to install, particularly in existing structures.

Near-infrared diode lasers allow detection of trace gases by optical absorption spectroscopy. It is possible to provide rapid, part per million (or better!) quantitation of combustion products including CO, HCN, HCl, CO<sub>2</sub>, CH<sub>4</sub>, acetylene, HF, and perhaps formaldehyde. Detection of incipient fires is possible. The approach being studied shows high selectivity for each gas detected; the concentration of each species is measured separately. False alarm rates can be reduced dramatically because a positive indication of a fire requires observing higher than normal concentrations of more than one target gas.

The type of diode lasers useful for fire sensing was originally developed for long haul fiber optic communications. These miniature devices are rugged, reliable, operate at low power, and require absolutely no maintenance. Near-infrared diode lasers are compatible with conventional, inexpensive fiber optics. Thus, we envision a fire sensing system in which the light from several lasers housed in a central location is distributed via a fiber optic system to hundreds of remote measurement locations. Feasibility calculations imply that light from one laser can be distributed among 800 such measurement points.



Most implementations of our diode-laser-based fire sensing technique will rely on simultaneous quantitation of three or four key gases selected from carbon dioxide, carbon monoxide, hydrogen cyanide, hydrogen chloride, and acetylene. Carbon dioxide is included because it provides a known non-zero background level that can be used as a continuous check of instrument operation. This solves one of the problems found with instruments designed to report rare events: how to provide frequent verification of proper operation? Carbon dioxide levels will fluctuate, but it is unreasonable to expect the concentration to drop significantly below 350 ppm. Such a loss of signal would be indicative of system error. Carbon monoxide and hydrogen cyanide are particularly important because these gases are implicated in most smoke inhalation deaths.[1-4] Hydrogen chloride is a key signature compound produced during pyrolysis and combustion of PVC-containing plastics.[5] Acetylene is a soot precursor. In addition, detection of HCN, HCl, and HCCH is useful for fire sensing because all of these compounds have extremely low background levels in nearly all environments. Finally, measuring CO and CO<sub>2</sub> levels may also prove useful for indoor air quality monitoring and can be incorporated into energy conservation schemes for building-wide HVAC systems.

Initial experiments demonstrated that modulation frequency multiplexing is the optimum method for simultaneous (or near simultaneous) detection of multiple gases. In this approach, one laser is used for each gas detected. The output from each laser is combined into a single optical fiber. It is possible, however, to distinguish the signals due to each laser—hence the concentration of each gas—by modulating each laser at a slightly different frequency. Selective demodulation of the photodetector output allows discrimination among the absorbance signals. This approach is similar to radio where a tuner picks out one station among a myriad of broadcast signals.

Our current research is building on these results by constructing and testing a prototype system for simultaneous detection of CO, CO<sub>2</sub>, and HCN. It should be possible to build rugged, reliable, multigas sensors for the detection of incipient fires. Output from each laser can be distributed to hundreds of measurement locations using a fiber optic distribution network.

## 2. Gas Detection Using Near-Infrared Diode Lasers

For diode-laser-based fire detection, the sensitivity toward each compound is determined, in large part, by the smallest optical absorbance that can be measured. Absorbance,  $\alpha$ , is a dimensionless quantity defined by Beer's Law,

$$\frac{I}{I_0} = e^{-\alpha} \text{ where } \alpha = \sigma N \ell, \quad (1)$$

where  $I$  is the laser intensity reaching the detector,  $I_0$  is the laser intensity in the absence of absorption,  $\sigma$  is the absorption cross section,  $N$  is the number density of the absorbing species, and  $\ell$  is the absorption path length. Since absorption cross sections and optical path lengths are known, measurement of absorbance allows determination of concentration.

Conventional spectrometers such as FTIR instruments or diode array devices can measure absorbances down to  $\alpha \sim 10^{-3}$ , whereas using diode lasers we and other groups[6-19] have demonstrated minimum detectable absorbances as small as  $10^{-7}$ . For the deployment scheme planned for fire detection, where the laser output is distributed among many measurement points, the *theoretical* lower bound is defined by laser/detector shot noise and equals a minimum detectable absorbance better than  $10^{-6}$  (1 Hz bandwidth). We estimate that each of the optical measurement locations in our fire detection scheme will achieve minimum detectable absorbances of  $10^{-5}$ .

The detection method we employ with diode lasers is a high frequency version of what is described in the literature by the terms "wavelength modulation spectroscopy," "derivative spectroscopy," or "harmonic detection." [6-14] The absorbance measurement is shifted to high frequency to avoid laser excess ( $1/f$ ) noise. A small sinusoidal modulation is superimposed on the diode laser injection current. This current modulation produces a modulation of the laser wavelength, since the laser wavelength is tuned by changing the current. As the laser beam passes through the sample gas, absorption converts the wavelength modulation into amplitude modulation. The AM components of the laser intensity induce synchronous modulation of the photodiode current at the modulation frequency,  $f$ , and higher harmonics,  $nf$ . Phase-sensitive electronics isolate and quantify (demodulate) the photocurrent component at a selected harmonic. The demodulated signal

lineshape looks like the  $n^{\text{th}}$  derivative with respect to wavelength of the direct transmission spectrum. Absolute absorbances are obtained by dividing the demodulated AC signal by the detector DC output; high sensitivity absorbance measurements are possible using a single optical beam.

Another important advantage of wavelength modulation spectroscopy is that the technique responds only to the type of narrow, isolated absorbance features characteristic of gas phase compounds. Attenuation of the laser beam by particulates, or losses due to scattering do not generate false positive signals. Since the actual absorbance is proportional to the ratio of the AC to DC components of the detector output, measurements can tolerate a ten- to hundred-fold loss in overall light intensity (the DC signal), yet provide accurate gas concentrations. If the DC level falls below some predetermined minimum, then the instrument will report an error.

### **3. Characteristics of Near-Infrared Diode Lasers**

Diode lasers are ideally suited to spectroscopic detection of gases because the lasers are wavelength tunable and are highly monochromatic. Coarse tuning can be accomplished by varying the laser temperature using an inexpensive thermoelectric cooler, which can be an integral part of the laser packaging. High resolution wavelength tuning is obtained by varying the laser injection current. AC modulation of the laser current is a simple method to implement wavelength modulation.

Gases important for fire detection can be detected using InGaAsP lasers which were originally developed for long haul, fiber optic communications. These lasers can be fabricated at any wavelength between 1.2 and 2.0  $\mu\text{m}$ , and each device has a tuning range of about  $\pm 2$  nm. This relatively limited tuning range requires a separate laser for each gas detected in most cases.

InGaAsP lasers operate at room temperature and are compatible with standard silica fiber optics and with high efficiency InGaAs photodiode detectors that also operate at room temperature. The lasers are hermetically sealed in miniature (approx.  $1'' \times \frac{1}{2}'' \times \frac{1}{2}''$ ) DIP



or butterfly IC packages and consume less than 100 mW of electrical power while producing from 2 to 5 mW of near-infrared light.

Spectral purity of the laser output is important for gas detection applications. The simplest style of diode laser often emits several nearby wavelengths simultaneously and is not suitable for the proposed application. In the case of InGaAsP diode lasers, single mode (single frequency) operation can be obtained with distributed feedback or "DFB" lasers that include a grating etched along the gain region. The laser output has a wavelength spread of only  $0.003\text{ cm}^{-1}$  compared with gas absorption linewidths of  $0.1\text{ cm}^{-1}$ ; in contrast, laboratory spectrometers such as FTIR devices typically show resolution of  $1\text{ cm}^{-1}$ , or worse. Extremely narrow laser linewidths allow selective probing of a single absorption line, even in the presence of many other gases. This point is crucial to the success of the proposed fire detection technique: wavelength selectivity increases the sensitivity for detecting each target compound while also minimizing the risk of false alarms.

#### 4. Feasibility Demonstration

Figure 1 is a schematic diagram of the apparatus first used to test modulation frequency multiplexing for simultaneous detection of multiple gases. The feasibility study focuses on simultaneous measurement of CO and CO<sub>2</sub> with a separate laser used for each gas. The CO laser is modulated at 50 kHz while the CO<sub>2</sub> laser is modulated at 40 kHz. Output from the lasers is injected into a single

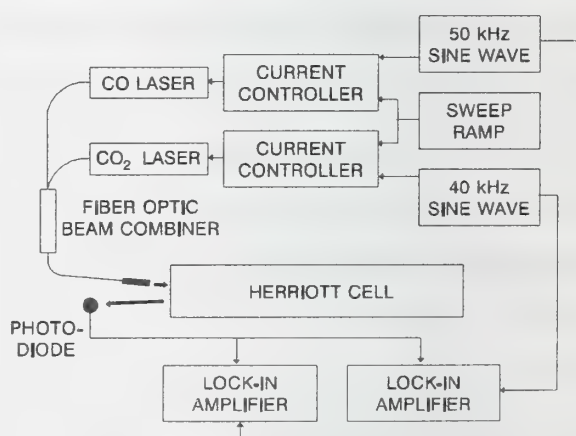


**Figure 1** - Schematic diagram of apparatus used to test modulation frequency multiplexing for the simultaneous detection of two gases.

mode fiber using a  $2 \times 1$  fiber optic beam combiner. The resulting light exits the fiber, is collimated by a graded index (GRIN) lens and directed into the Herriott [20] cell containing 50 torr each of CO and CO<sub>2</sub>. After traversing 26 passes within the cell (13.9 m), the beam exits and is focused onto an InGaAs photodiode. Output from the photodiode is applied to

a pair of lock-in amplifiers set to operate at  $2f$ ; one is referenced to the 50 kHz modulation source, the other to the 40 kHz source.

Wavelength modulation spectra are acquired by sweeping both laser current supplies and digitizing the output from the two lock-in amplifiers. The DC currents from each supply are adjusted such that the peak due to CO appears at the left hand side of each scan with the CO laser while the CO<sub>2</sub> peak appears at the right hand side of each scan with the CO<sub>2</sub> laser. This approach—scanning full wavelength spectra and offsetting the positions of the two peaks—is useful for determining signal-to-noise ratios and for examining potential cross-talk between the two absorbance measurements.

Measurements show that the limiting noise source is not due to the multiplexing scheme but to unwanted optical interference fringes which change slightly in magnitude during the time required to collect all pertinent data. Specifically, Fig. 2 compares CO spectra taken when only the CO laser was on (lower trace) and when both lasers were on (upper trace). The WMS signal corresponds to a peak absorbance of 2.7% (measured in a separate experiment). We define the noise as the standard deviation of the right hand baseline region. Spectra in Fig. 2 imply that the minimum detectable absorbance changes from  $1.2 \times 10^{-5}$  when only the

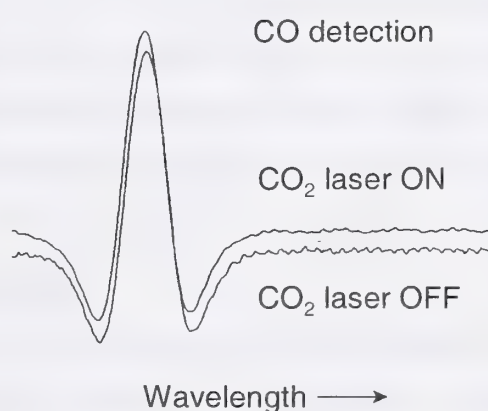


**Figure 2** - Modulation frequency multiplexing detection of carbon monoxide in a 50:50 mixture of CO and CO<sub>2</sub>.

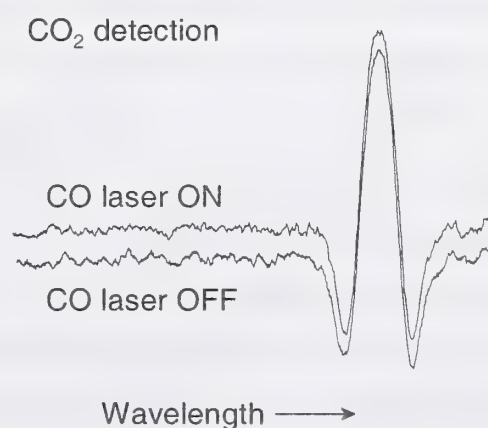


**Figure 3** - Modulation frequency multiplexing detection of a carbon dioxide in a 50:50 mixture of CO and CO<sub>2</sub>.

CO laser is used to  $1.8 \times 10^{-5}$  when both lasers are on. For these data, measurements are extrapolated from the 20 Hz bandwidth used to a 1 Hz detection bandwidth. In contrast, the data in Fig. 3, which shows CO<sub>2</sub> spectra, indicate the minimum detectable absorbance actually improves from  $1.6 \times 10^{-5}$  to  $0.8 \times 10^{-5}$  when the CO laser is activated.

Examination of the baseline regions in both sets of spectra, Figs. 2 and 3, shows that regular interference fringes dominate random noise. This feature is seen most clearly in the lower trace of Fig. 2. The presence of etalons is consistent with Southwest Sciences' prior experience with nearly all diode laser applications and explains why we target a minimum detectable absorbance of  $1 \times 10^{-5}$  (1 Hz) for field applications even though theoretical noise limits are  $\sim 1 \times 10^{-8}$  for typical laser powers and detector characteristics. More importantly, these feasibility results imply that there is probably no performance penalty associated with frequency modulation multiplexing. Additional shot noise associated with having more than one laser impinging on the detector is exceeded by the etalons.

As the last test of frequency modulation multiplexing, Fig. 4 verifies no measurable cross-talk between the two demodulations. The CO and CO<sub>2</sub> spectra were acquired simultaneously using the apparatus depicted in Fig. 2. There is no excess noise or residual signal due to the CO peak in the CO<sub>2</sub> trace and *vice versa*.

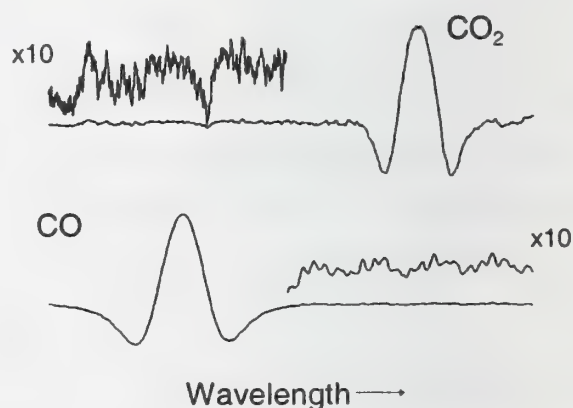


**Figure 4** - CO and CO<sub>2</sub> spectra acquired using modulation frequency multiplexing.

The spectra acquired to demonstrate modulation frequency multiplexing (*e.g.*, Figs. 2-4) were not been scaled to the DC laser power,  $I_0$  in Eq. (1). But, long term operation of commercial instruments would require dividing the WMS signal by the laser power in order to get the correct absorbance. Measurement of  $I_0$  is straightforward when only one laser is impinging on the detector; we just measure the total photocurrent passing through the photodiode. For applications of



modulation frequency multiplexing, we anticipate using an indirect measurement of laser power: modulation of the laser current introduces amplitude modulation as well as wavelength modulation, and the magnitude of the amplitude modulation signal is an easily calibrated measure of the laser power.

## **5. Construction and testing of a commercial prototype**

The next step in demonstrating the effectiveness of the diode-laser-based technology for early detection of fires is construction of a stand-alone prototype system for field testing. That work, now in progress, includes simultaneous detection of carbon monoxide, carbon dioxide, and hydrogen cyanide. Target detection limits for the three gases are 30 ppm for CO and CO<sub>2</sub>, and 1 ppm for HCN. Key aspects of the prototype system include:

- Modularity. Each laser system operates independently while reporting gas concentrations and operating to a central computer using standard serial communications protocols.
- Digital signal processing (DSP) technology. A stand-alone, DSP single board computer controls each laser system and provides numerical demodulation of the detector signals as well as data reduction of the resulting wavelength modulation spectra. The DSP hardware including four analog-to-digital converters (200 kHz, 16 bits), four digital-to-analog converters (also 200 kHz and 16 bits), and two RS-232 serial ports provides a compact, low cost control and signal processing platform.
- Line locking. Stable, long-term performance of each laser system is guaranteed, in part, by using small optical cells filled with the target gases to provide a wavelength standard for active wavelength control of each laser.
- 1f power measurements. Accurate measurement of wavelength modulation spectra requires separate measurement of the 2f signal and "DC" power components of each laser's contribution to the overall photodiode output. The present approach uses the amplitude modulation that occurs synchronously with the laser's wavelength modulation to provide a frequency-dependent signature for measuring separately each laser's power reaching the photodiode.

Each DSP system is programmed to act as a digital lock-in amplifier. The laser modulation waveform is a modified square wave (the upper trace in Fig. 5). In theory, the  $2f$  signal is  $(a + b) - (c + d)$  where the time periods  $a$ ,  $b$ ,  $c$ , and  $d$  are noted in Fig. 5. In practice, this simple computation requires no

electronic phase delays between the modulation waveform and the photodetector output. A more useful approach, and the one used in the

prototype instrument, requires digitizing the detector output at twice the frequency used for the modulation waveform—indicated by the vertical digital lines—and obtaining the vector dot products of the digitized signal with a pseudo-sine vector and with a pseudo-cosine vector. The  $2f$  signal is the sum of the two dot products weighted by a demodulation phase. This calculation is repeated at each wavelength step in order to generate a complete  $2f$  spectrum.

This demodulation approach is applied to both the signals from the reference cell and from a multipass cell similar to the Herriott cell used in the feasibility study. The signal from the reference cell is used for line-locking; a small offset is applied to the laser current control in order to keep the peak of the reference spectrum at the center of each scan. Figures 6 and 7 show the CO reference cell (line-locking) signal and the sample cell signal for 1000

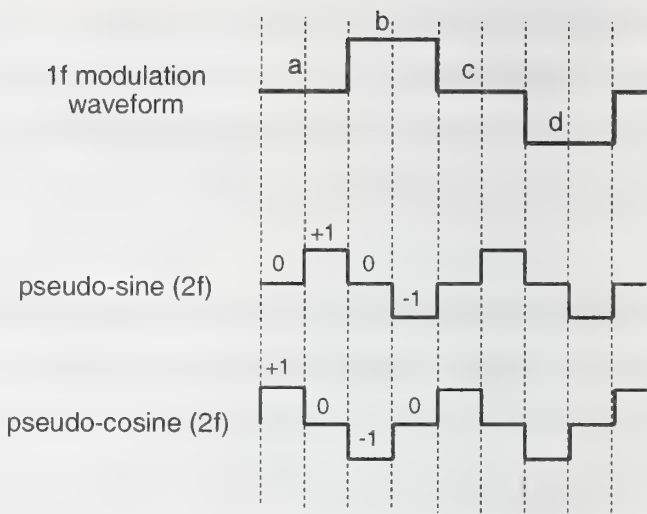


**Figure 5** - Modified square wave modulation waveform (top) and the “in phase” (center) and “out of phase” (bottom) demodulation waveforms used for generating an all-digital wavelength modulation spectrum.

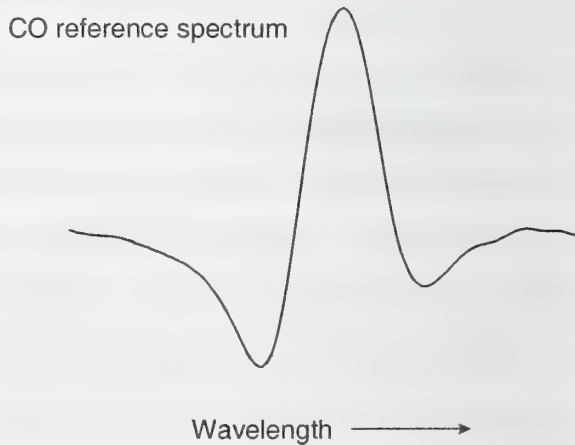


**Figure 6** - CO reference cell  $2f$  spectrum used for line-locking.

ppm CO, respectively. The spectrum in Fig. 7 shows the effects of unwanted optical interference fringes (etalons) which distort the line shape as well as introduce some high frequency noise. These etalons reflect mechanical problems in the alignment of the fiber optic collimating lens used to direct the combined laser beams into the sample cell. We anticipate that a modified lens mount should improve alignment stability and reduce the size of the etalons.

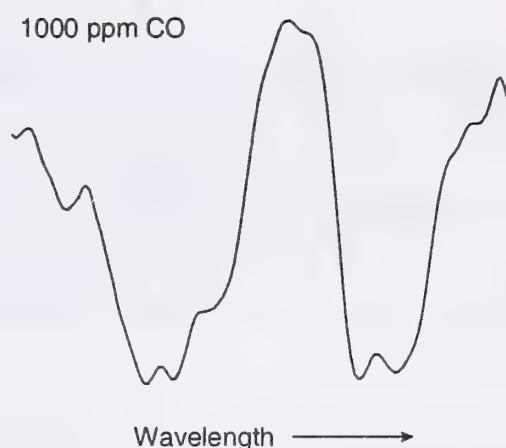


**Figure 7** -  $2f$  spectrum of 1000 ppm CO.

Gas concentration measurements are obtained from spectra such as Fig. 7 by representing each raw  $2f$  spectrum as the sum of the “true”  $2f$  profile, a DC offset, a baseline slope, and a baseline curvature term. This separation is shown pictorially in Fig. 8. The numerical decomposition can be performed quickly using a fast multilinear regression cast as a simple matrix equation:

$$raw = A \cdot x, \quad (2)$$

where  $A$  is the “library” matrix with columns comprising a representative  $2f$  spectrum, the DC baseline offset, the baseline slope, and the baseline curvature, respectively. Vector  $x$  contains the coefficients identifying the amounts of the four terms that make up a given raw spectrum. Solution of the matrix equation (2) is straightforward,

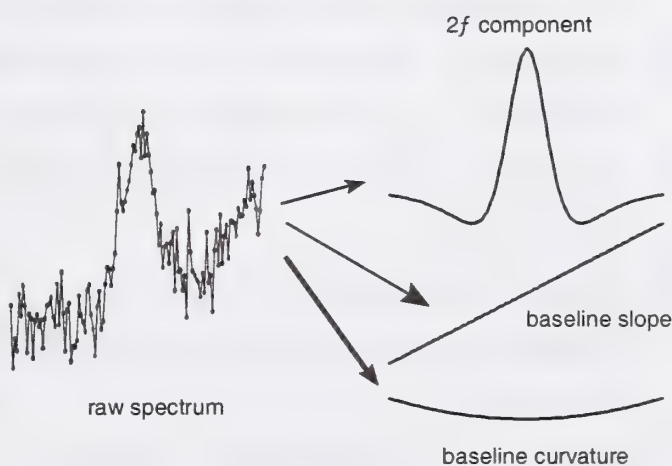


**Figure 8** - Decomposition of raw  $2f$  spectrum into the target  $2f$  component plus a baseline slopes and curvature terms. The baseline offset term is not shown.



$$x = \left( \mathbf{A}^T \mathbf{A} \right)^{-1} \mathbf{A}^T \cdot \text{raw} , \quad (3)$$

and the matrix  $(\mathbf{A}^T \mathbf{A})^{-1} \mathbf{A}^T$  can be calculated beforehand. In practice, only the first element of vector  $x$  is important – the magnitude of the  $2f$  component within the raw spectrum – which is simply the dot product of the first row of  $(\mathbf{A}^T \mathbf{A})^{-1} \mathbf{A}^T$  and the vector *raw*. The first row of  $(\mathbf{A}^T \mathbf{A})^{-1} \mathbf{A}^T$  is stored on disk within the host computer and is downloaded to the DSP board soon after the RS-232 link is established.

Long term detection limits are presently an order of magnitude worse than the target levels due to problems in maintaining optical alignment in the sample Herriott cell. We are now redesigning one of the key optical mounts with the expectation of significant improvement in pointing stability and, concurrently, gas detection sensitivities.

## 6. Acknowledgment

This work supported by NIST under Phase 1 and 2 SBIR contract 50-DKNB-7-90149.

## 7. References

- [1] Levin, B. C. and Gann, R. G., in *Fires and Polymers*, ACS Symposium Series 425, Nelson, G. L., Ed., (American Chemical Society, Washington, 1990), p 2.
- [2] Tsuchiya, Y., Proc. First International Symposium on Fire Safety Science, Grant, C. E. and Pagni, P. J., Eds., (Hemisphere, 1986), p. 349.
- [3] Lundgren, B., and Stridh, G. in *Fires and Polymers*, ACS Symposium Series 425, Nelson, G. L., Ed., (American Chemical Society, Washington, 1990), p 35.
- [4] Pitts, W. M., Twenty-Fourth Symposium (International) on Combustion, (Pittsburgh, 1992), p. 1737.
- [5] Hartzell, G. E., Grand, A. F., and Switzer, W. G., in *Fires and Polymers*, ACS Symposium Series 425, Nelson, G. L., Ed., (American Chemical Society, Washington, 1990), p 13.
- [6] Silver, J. A., Appl. Opt. 1992; 31: 707-717.
- [7] Bomse, D. S., Stanton, A. C., and Silver, J. A., Appl. Opt. 1992; 31:718.
- [8] Silver, J. A., and Stanton, A. C., Appl. Opt. 1988; 27: 4438.
- [9] Silver, J. A., Bomse, D. S., and Stanton, A. C., Appl. Opt. 1991; 30: 1505.

- [10] Bomse, D. S., Appl. Opt. 1991; 30: 2922.
- [11] Silver, J. A., and Hovde, D. C., "Near-Infrared Diode Laser Airborne Hygrometer," Rev. Sci. Instrum. 1994; 65: 1691.
- [12] Stanton, A. C., and Silver, J. A., Appl. Opt. 1988; 24: 5009.
- [13] Stanton, A. C., and Hovde, D. C., Laser Focus World 1992; 28: 117.
- [14] Silver, J. A., and Stanton, A. C., Appl. Opt. 1988; 27: 1914; U. S. Patent No. 4,934,816.
- [15] Cooper, D. E., and Carlisle, C. B., Opt. Lett. 1988; 13: 719.
- [16] Reid, J., Shewchun, J., Garside, B. K., and Ballik, E. A., Appl. Opt. 1978; 17: 300.
- [17] Reid, J., Garside, B. K., Shewchun, J., El-Sherbiny, M., and Ballik, E. A., Appl. Opt. 1978; 17: 1806.
- [18] Reid, J., El-Sherbiny, M., Garside, B. K., and Ballik, E. A., Appl. Opt. 1980; 19: 3349.
- [19] Cassidy, D. T., Appl. Opt. 1988; 27: 610.
- [20] Herriott, D., Kogelnick, R. H., and Kompfner, R., Appl. Opt. 1964; 3: 523.

## **Requirements to Gas Sensors in Fire Alarms for Residential Use**

### **1. Introduction**

There are fire alarms for two basically different areas of application: The fire alarms for professional application and the fire alarms for residential use. The fire alarms for the professional application are usually operated by a central unit, which analyses and passes the alarms on. Fire alarms for residential use however are single devices for the application in households, which are operated without central unit. Alerting is effected by integrated acoustic and/or optical components.

Fire alarms, which are offered for the two areas of application specified above, differ strongly in their technical level of development. Within the professional area, the frequency of false alarms could be clearly reduced by the introduction of multiple sensor alarm units e.g. the combination of light scattering and thermal sensors. The use of gas sensors as an additional component in multiple sensor alarm units has been discussed very intensively for several years. This invention will further reduce the rate of false alarms. For this there are very promising beginnings, which are already transferred partly into products which are ready for the market.

In contrast to this the technical development of fire alarms for residential use is far back. The majority of the world-wide used alarm units are of the ionization type, a smaller proportion are light scattering smoke detectors. The multiple sensor technology is not represented in fire alarms for residential use so far.

There is a strong motivation for reducing the frequency of false alarms and thus for using multiple sensor alarm units for residential use. It is well-known that unfounded alarming can reduce the acceptance for fire alarms and so the owner often deactivates the alarm unit. To that extent there are serious reasons to increase the reliability of fire



alarms for residential use by the application of the multiple sensor technology in particular also by using gas sensors.

This article considers the requirements for gas sensors, which arise from their use in private homes.

## **2. Environmental conditions**

When talking about environmental conditions temperature and humidity have to be mentioned first. In private homes 0°C to +50°C as well as 10% to 90% RH seem to be sufficient. However if garages are added for example, these values have to be extended at least to -25°C to +70°C, which is also typical for industrial applications, as well as 10% to 95% RH.

Besides environmental conditions in operation, also terms of transport are to be considered. The gas sensor may not be destroyed or damaged during the transport, e.g. from the manufacturer to the dealer or from the dealer to the user's home. Extreme conditions may occur: The alarm unit can be situated in a car for several days. During a day in stout sun 100°C can be achieved or -40°C in cold winter nights. These conditions have to be taken into account, when defining packaging of the detector.

Since a fire alarm unit is a safety-relevant device, it has to get over all these scenarios without damage or it has to announce its malfunction. The status signal of malfunction however is only the second best solution.

## **3. Sensitivity, Selectivity, disturbance variables, deceptive alarms**

For a gas sensor for this application it is important that it is sensitive to one or more combustion gases. At the same time however it has to be insensitive on possible disturbance variables. The gases CO, CO<sub>2</sub>, NO/NO<sub>2</sub> and H<sub>2</sub> seem to be suitable for fire recognition. The following table 1 shows some concentrations of combustion gases which were determined within fire tests according to EN54.

For the application in dwellings the test fires TF1 to TF4 are relevant primarily. A pure plastic fire (TF4) is rather improbable. Textiles (TF3) and wood (TF1/2) will always be involved. As a result it can be counted on a significant high CO-concentration in fire situation. CO<sub>2</sub> and NO/NO<sub>2</sub> occur in higher concentration at open liquid fires than at cellulose fires.

	CO [4]	CO [3]	CO [5]	CO <sub>2</sub> [5]	CO <sub>2</sub> [3]	NO <sub>2</sub> [3]
TF1	230		90	1800		
TF2	50	80	100	880	350	0,15
TF3	300	100	90	1560	600	0,03
TF4	15	19			1500	0,75
TF5	15	27			2100	0,9
TF6	5	25			2000	1,7

Table 1: Measured values of gas concentrations for different fires in ppm [1]

Concerning the measured combustion gases, electrochemical cells, semiconductor gas sensors, NDIR/DIR sensors, optodes and pellistors are suitable for fire detection. Semiconductor gas sensors however have problems with reproducible measuring of small concentrations of CO, as they occur at TF4, TF5 and TF6. Due to their poor sensitivity pellistors are only suitable for certain fire scenarios with high CO production (cellulose fires).

NDIR/DIR sensors provide the best selectivity due to the physical measurement principle of infrared absorption. Optodes and electrochemical cells also provide a very good selectivity on combustion gases. For electrochemical CO cells in particular the highest cross-sensitivities are observed on NO/NO<sub>2</sub> and H<sub>2</sub>. These however are also combustion gases and thus they are no real disturbance variables.

Semiconductor gas sensors and pellistors show a very large sensitivity to all inflammable gases and vapours. This can lead to substantial disturbance variables by

solvents, lacquer vapour, alcohol vapour, cleaning agents and so on and thus cause false alarms.

At present piezo-electric gas sensors (quartz micro balance) are not suitable for fire detection due to their sensitivity and spectrum of the measurable substances.

Capacitive and resistive gas sensors only got importance in measuring humidity. So far suitable gas sensitive coatings for fire detection are missing, for both types (piezo-electric gas sensors and capacitive /resistive gas sensors).

When using CO concentration as an indication for a fire situation, all other sources of CO potentially cause false alarms. The CO levels, which have to be detected for fire alarm, are in many cases significantly lower than the Threshold Limit Value (TLV) (table 1). Figure 1 shows the CO signal when ten persons smoking in a room of 197 m<sup>3</sup>. The CO level is about the same as it can be expected at open liquid fires (TF5/6). Only the combination with an optical smoke detector avoids a false alarm. Other possible sources for CO are e.g. exhaust gases of vehicles and feature fireplaces.



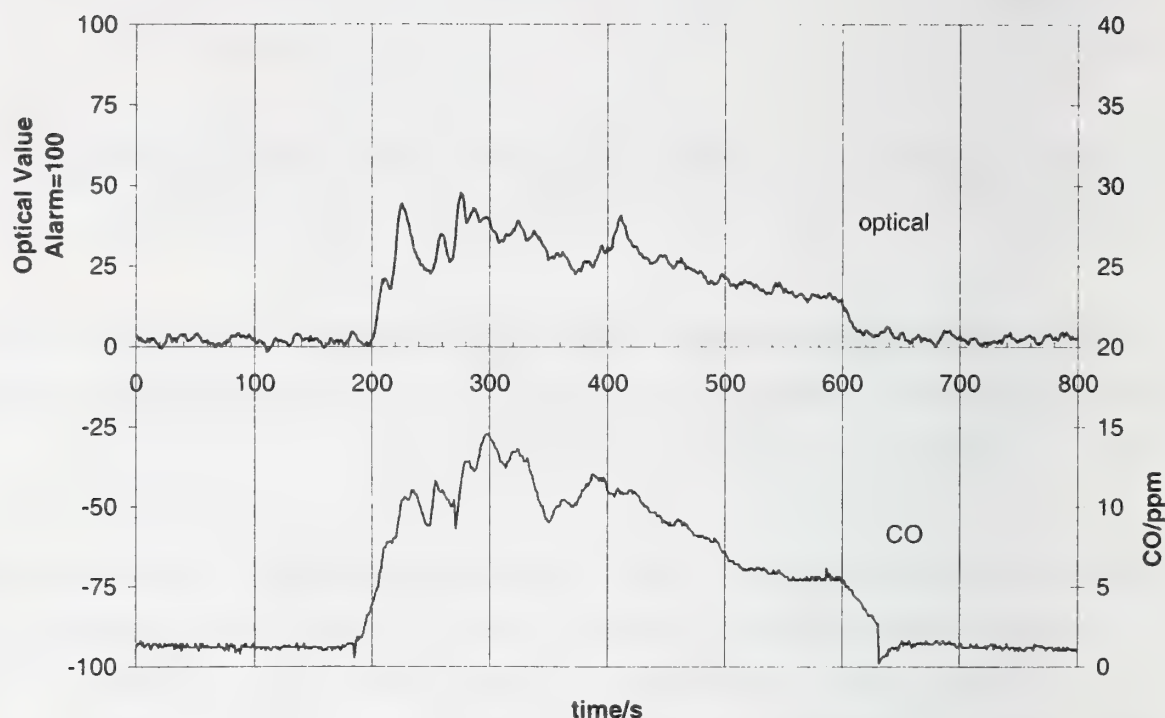


Figure 1: Optical and CO signal when ten persons smoking in a room of 197 m<sup>3</sup>.

On the other hand the CO-Signal prevents false alarms from dust, steam, fog and other optical disturbance variables. So an additional gas sensor and in particular a CO sensor considerably improves false alarm behaviour of an optical smoke detector. But a CO sensor on its own would be a poor fire detector.

#### 4. Power consumption

A further important point is the power consumption of the gas sensor in operation. Since fire alarms for residential use are battery powered usually, a very small power consumption is admissible regarding an acceptable lifetime of the battery.

For this reason all gas sensors, which are operated at high temperatures (semiconductor gas sensors, pellistors) and therefore use an integrated heating have to be regard critically. Meanwhile there exist some approaches to reduce power consumption by micromechanical structure and pulsed operation to make battery operation possible [8].

Particularly electrochemical cells and optodes with a power consumption of some  $\mu\text{W}$  are best suited for battery-operated devices.

## **5. Operational reliability, Maintenance**

Since in the private area no regular maintenance schedule can be supposed, the lifetime of the sensor must be at least as long as the battery life. This also implicates that fire alarms for residential use are not periodically checked in a way that the sensor is actually exposed to test gas. Here the operability of the alarm unit has to be guaranteed with other measures. This can e.g. be ensured by a self test feature of the gas sensor.

Thus there are two types of self test e.g. for electrochemical cells: Measurement of cell impedance represents a very good indication for the operability of the sensor. In gas measuring equipment for industrial application this is usually regarded sufficient. More sophisticated cells provide the capability to produce hydrogen by electrolysis. This hydrogen causes a real gas signal in the cell. Thus it is guaranteed that the cell actually reacts to gas. This self test can be executed regularly and automatically (e.g. once a day). However it is not suitable for calibrating the cell.

Effects of poisoning by substances from the environment (e.g. silicone) are well-known for semiconductor gas sensors and pellistors. These may cause insensitivity of the sensor. The only chance, to recognise such a poisoning is to test the sensor with real gas. However such a test does not seem to be practicable for fire alarms in private homes.

## **6. Conclusion**

From technical view only an optical smoke detector in combination with an electrochemical cell, with a NDIR/DIR-sensor or with optodes seem to be suited for fire detectors for residential use. The advantage of the NDIR/DIR sensors concerning their high selectivity must be paid by an accordingly high expenditure for the structure, which will not be interspersable however for fire alarms in private homes. Electrochemical cells are high sophisticated and reliable. Optodes on the other hand offer the advantage that several gases (e.g. three) can be measured with one component, which is also clearly smaller than usual electrochemical cells.

## 7. References

- [1] Oppelt, Ulrich: Auswerteverfahren für die Multisensorik für eine sicherere Meldungsentscheidung bei Brandereignissen, AUBE 1999
- [2] Hippauf, Barbara: Interner Untersuchungsbericht Institut für Meß- und Automatisierungstechnik, Universität der Bundeswehr, Neubiberg, 5/95
- [3] Linden, O.: Messungen im VdS Brandraum. BUGH Wuppertal, 10/98
- [4] Fischerauer G., Mauder A., Müller R.: Acoustic Wave Devices (SAW and BAW) in Sensors Vol. 8, Wiley-VCH 1995.
- [5] Grosshandler, William L.: A Review of Measurements and Candidate Signatures for Early Fire Detection  
NISTIR 5555 Building and Fire Research Laboratory, 1995
- [6] Hensel, A.: Further development of optode membranes for the selective detection of combustion gases. VdS-Conference: Gas Sensors for Fire Detection, Cologne 2000.
- [7] Pichlmaier J.: Kalibrierung von Gassenoren in befeuchteter Atmosphäre und Modellierung des Feuchteinflusses auf kapazitive SO<sub>2</sub>-Sensoren, VDI-Verlag, Düsseldorf 1994.
- [8] Katsuyuki Tanaka, Shin-ichi Matsumoto, Munehiro Ito, Kazuo Onaga: Development of Semiconductor CO Sensor for Battery Operation, 8<sup>th</sup> International Fair and Congress for Sensors, Transducers & Systems, Nürnberg 1997



Sensor Type	Gases	Sensitivity range	Temperature range	Selectivity	Power consumption	Life cycle	Currently used in security systems
Electrochemical Cell	CO, NO <sub>x</sub> , NH <sub>3</sub> , Cl <sub>2</sub> , H <sub>2</sub> S, SO <sub>2</sub> , HCl, ..	0-300 ppm, 0-200 ppm	"-20 to +50°C"	+	< 10 $\mu$ W	1-7a	<input checked="" type="checkbox"/>
Semiconductor Gas Sensor, Metal Oxide	CO, NO <sub>x</sub> , Cl, NH <sub>3</sub> , H <sub>2</sub> S, ..	0-100 ppm, 0-1000 ppm	"-20 to 80°C"	--	35 mW to 10 W	1-5a	Residential use only
Capacitive and resistive Sensors (Polymer layer)	H <sub>2</sub> O, SO <sub>2</sub> [7]	10 to 95% RH, 10-500 ppm SO <sub>2</sub>	u.d.	-	100 $\mu$ W to 100 mW	u.d.	Humidity
NDIR, DIR	CO <sub>2</sub> , CO, NH <sub>3</sub> , N <sub>2</sub> O,	1,7 ppm, <1 ppm	"-20 to 80°C"	++	100 $\mu$ W to 100 mW	5-10a	<input checked="" type="checkbox"/>
Optodes [6]	NH <sub>3</sub> , NO, (CO <sub>2</sub> , H <sub>2</sub> O)	< 1 ppm	u.d.	+	< 10 $\mu$ W	u.d.	
piezo-electric gas sensors (SAW, BAW) [4]	organic substances	0-10 %	u.d.	-	10 to 1000 mW	u.d.	
Thermokathalytic Sensors (Pellistor)	CO, combustible gases	0-2000 ppm Iso-butane, 0-5% CO	"-20 to 80°C"	--	~500 mW	1-5a	<input checked="" type="checkbox"/>

Table 2: Survey Gas Sensors (u.d.: under development)

Jeffrey S. Goldmeer

Southwest Sciences, Inc., Santa Fe, NM, USA

## **A Rugged LED-Based Sensor for Fire Detection**

### **1. Introduction**

An ideal instrument for early detection of aircraft cargo compartment fires would combine high sensitivity, rapid response time, automatic self-testing, and would have a zero false alarm rate. In addition, such systems could provide continuous data to the pilots, giving them the ability to monitor the growth and possible extinction of a fire after activation of the on board suppression system. Current aircraft cargo compartment fire detection systems, which are primarily smoke detectors, do not meet this ideal. These detectors have false alarm rates, defined as the percentage of alarms with no verified smoke in the cargo compartment, as high as 99%, resulting in over 150 unscheduled landings in the last four years [1]. Current gas detection systems also fall short of the ideal; tests of commercially available CO detectors showed various failures that included false alarms at low CO levels, and worse, no alarms at dangerous CO levels [2].

Southwest Sciences is developing a novel optical absorption spectroscopy technique for fire detection. Key gases produced by incipient fires are detected by optical absorbance measurements using inexpensive, rugged mid-infrared Light Emitting Diodes (LEDs). Fully engineered sensors will achieve rapid response with low false alarm rates, will be small, lightweight, fully automatic, self-checking, and use little power. The reduction in false alarms is accomplished by measuring the concentrations of multiple gases in order to detect incipient combustion. This multi-parameter detection approach has been examined by NIST [3].

Target gases for the Southwest Sciences' instrument include carbon monoxide (CO), carbon dioxide (CO<sub>2</sub>), hydrogen cyanide (HCN) and acetylene (C<sub>2</sub>H<sub>2</sub>). Carbon dioxide is an important gas to monitor because its non-zero ambient concentration allows the detection system to automatically confirm correct performance. In addition, in flaming

combustion carbon dioxide concentrations are well in excess of ambient levels (350 ppm) and can reach concentrations in excess of 1500 ppm [4]. In contrast smoldering fires tend to produce large amounts of carbon monoxide [5, 6]. Monitoring both CO and CO<sub>2</sub> reduces false alarm rates because the ratio of these gases due to combustion is known [7] and should be significantly different from the ratio due to emissions from biological cargo. Acetylene has a zero ambient concentration and plays a critical role in the development of soot [8, 9]. Hydrogen cyanide, which also has a zero ambient concentration, is produced during the thermal degradation of nitrile containing plastics and foams [10, 11, 12]. Thus, the presence of either hydrogen cyanide or acetylene could indicate the occurrence of a fire.

This paper reports on absorbance measurements of CO and CO<sub>2</sub> using this innovative technique and examines the feasibility of detecting hydrogen cyanide and acetylene.

## 2. Experimental Hardware

### 2.1 Mid-IR LEDs & Detectors

A benchtop LED-based absorption spectroscopy gas detection system (*Patent Pending*) was built with off-the-shelf components. Compact mid-infrared LEDs that operate at a center wavelength of 4.6  $\mu\text{m}$  were used as the light sources for this sensor (Fig. 1). They are inexpensive, rugged, and compact (~ 5 mm dia.). The LEDs have a spectral bandwidth of 0.85  $\mu\text{m}$  (FWHM) and an output power of 11  $\mu\text{W}$ . Each LED package includes a 1 cm diameter parabolic reflector used to direct the output. Because the emission bandwidth is much greater

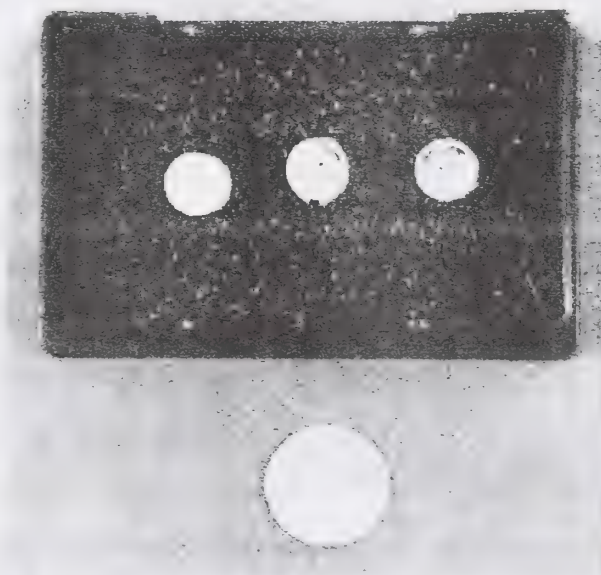


Figure 1 - Mid-IR LEDs



than the target absorption bands ( $\sim 0.2 - 0.3$  microns), bandpass filters were used to achieve selective detection of the target species. Three such filters were used in the tests reported in this paper:  $3.91 - 4.09 \mu\text{m}$  (reference),  $4.16 - 4.45 \mu\text{m}$  ( $\text{CO}_2$ ), and  $4.53 - 4.77 \mu\text{m}$  ( $\text{CO}$ ).

Mid-infrared LED output was measured with an infrared detector. Initially a thermoelectrically cooled mercury cadmium telluride (HgCdTe) infrared detector, which is well suited for continuous monitoring applications, was used. After a failure with this detector, a liquid nitrogen cooled indium antimonide detector was used. Both detectors have good spectral response to  $5\mu\text{m}$  and a  $1.0 \text{ mm}^2$  active area.

## 2.2 Prototype Detection System

A schematic diagram of the gas detection system (*Patent Pending*) is shown in Fig. 2. This system uses two LEDs that are each pulsed at 10kHz with a 50% duty cycle. Light from the LEDs is bandpass filtered and combined using a cadmium telluride (CdTe) flat, and then focused onto the detector using two plano-convex, calcium fluoride

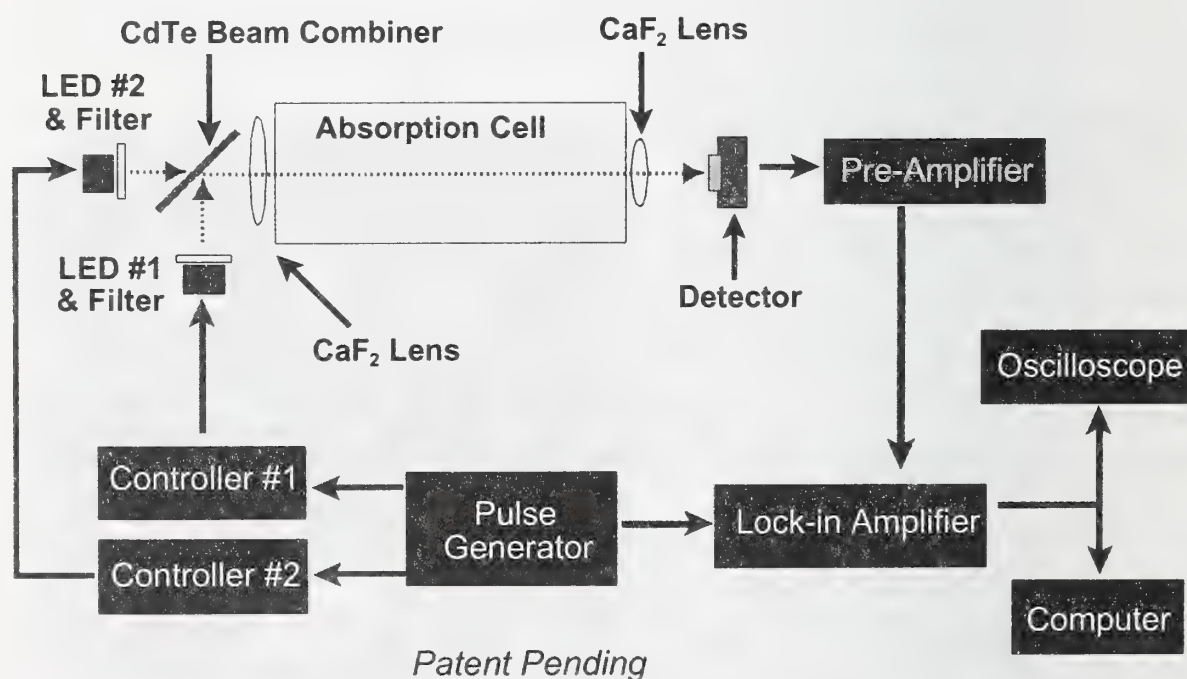


Figure 2 – Schematic of the prototype detection system

lenses. The light passes through an absorption cell that has a path length of 35.5 cm before reaching the detector. The pre-amplified signal from the detector is sent to a lock-in amplifier that provides phase-sensitive detection at the LED modulation frequency. The output from the lock-in can be viewed directly, or captured using an analog-to-digital data acquisition board in a personal computer.

### 3. Spectroscopic properties

Spectroscopic detection of CO and CO<sub>2</sub> is possible using commercially available LEDs having a 4.6  $\mu\text{m}$  center wavelength. The  $\nu_3$  band of CO<sub>2</sub>, centered around 4.27  $\mu\text{m}$ , and the CO fundamental vibrational band, centered at 4.67  $\mu\text{m}$ , are both strong absorption features, and are sufficiently well separated to allow selective detection of the two gases using bandpass filters in combination with the LEDs, Fig. 3.

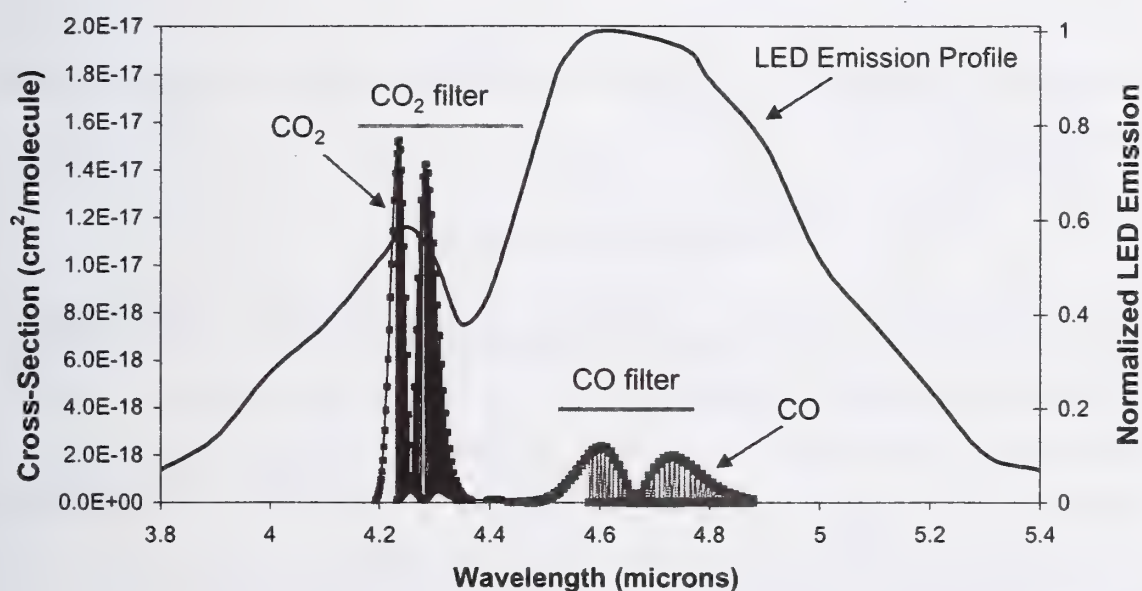


Figure 3 - LED emission profile, CO and CO<sub>2</sub> filter bandwidths, and absorption bands of CO and CO<sub>2</sub>.

This technique utilizes a broad emission (from the LEDs), covering a large portion of an absorption band, instead of a single line feature that would be used for a high-resolution tuned diode-laser. Effective cross-sections can be calculated by integrating molecular

line strength data (from the HITRAN database [13]) across a bandpass filter transmission window:

$$\sigma_{\text{EFF}} = \sum S(T) / \Delta\nu_{\text{FILTER}} \quad (1)$$

Although individual molecular line strengths,  $S(T)$ , are functions of temperature, the resulting effective cross-section ( $\sigma_{\text{EFF}}$ ) is invariant to temperature over the expected range (300-1000K). The effective cross-section is related to an effective absorbance ( $\alpha_{\text{EFF}}$ ) through the Beer-Lambert Law:

$$\alpha_{\text{EFF}} = \sigma_{\text{EFF}} N L \quad (2)$$

in which ( $L$ ) is defined as the optical path length, and ( $N$ ) is the number density of the absorbing gas. Measured cross-section and absorption values are compared against experimentally derived data in the next section.

#### 4. Experimental Results

Two techniques were used to measure the concentrations of CO and CO<sub>2</sub>: direct absorption measurements using a single LED and differential absorption measurements using two LEDs.

##### 4.1 Direct Absorption Measurements

In these experiments, measurements were performed using a single LED modulated at 10 kHz, and with a lock-in amplifier set to a one second time constant. For carbon dioxide, data was obtained with the test cell evacuated (0 ppm CO<sub>2</sub>) to provide a baseline ( $I_0$ ), and then filled with air (~ 350 ppm CO<sub>2</sub> at 600 Torr). (The ambient pressure at Southwest Sciences, located in Santa Fe at 7000 feet above sea level, is 600 Torr.) The experimentally determined absorbance (0.17) was within 10% of the effective absorbance (0.16) computed using Eq. (1) and (2). The experimental absorption cross-section was  $7.1 \times 10^{-19} \text{ cm}^2/\text{molecule}$  in comparison to the computed effective cross-section of  $6.4 \times 10^{-19} \text{ cm}^2/\text{molecule}$ .

For carbon monoxide, measurements were made with the cell filled with 100% nitrogen (0 ppm CO) to provide a baseline ( $I_0$ ). Calibration data were obtained with varying concentrations of CO that ranged from 20 to 10,000 ppm. All measurements were made



at 296 K and at 600 Torr. Figure 4 shows the measured absorbance data plotted against CO concentration. A linear best fit of these data is then used to compute an experimental cross-section ( $7.4 \times 10^{-20} \text{ cm}^2/\text{molecule}$ ), which is within 1.3% of the numerically predicted cross-section ( $7.5 \times 10^{-20} \text{ cm}^2/\text{molecule}$ ). The excellent agreement between the experimental and theoretical values validates the numerically computed effective cross-section and absorbance. Figure 4 also shows the FAA's CO minimum performance standard,  $200 \pm 50 \text{ ppm}$  [1,14,15].

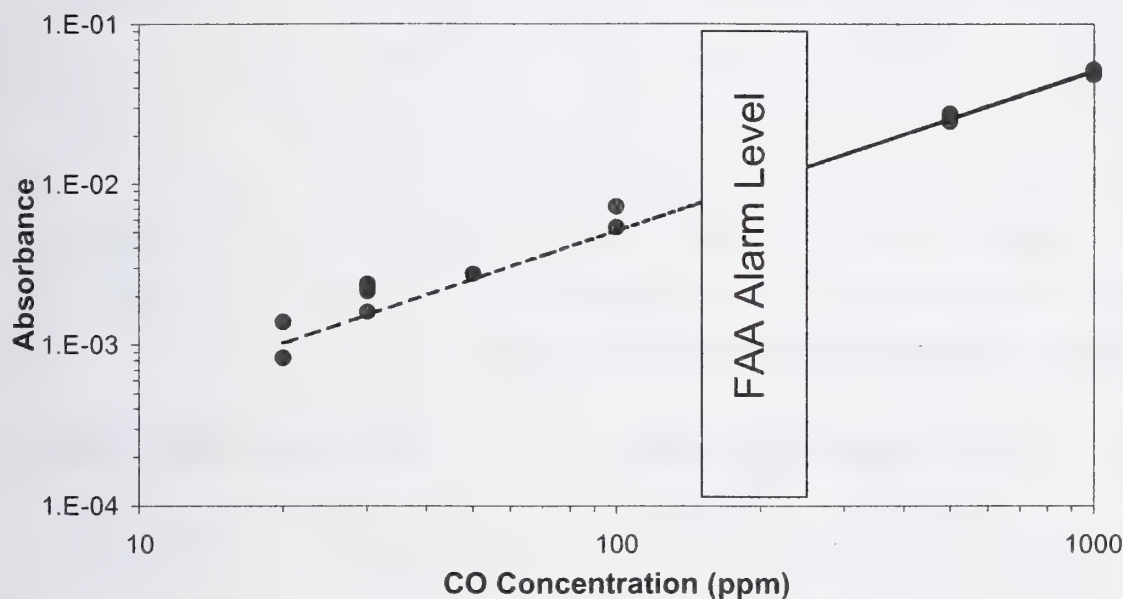


Figure 4 - Direct absorption measurements and the FAA's CO minimum performance standard for CO [1,14,15]

#### 4.2 Differential Absorption Measurements

One approach to reducing the fire detector false alarm rates is to increase the detector sensitivity, making it possible to differentiate between ambient levels and fire generated concentrations of the key gases. Standard absorption spectroscopy techniques, such as direct absorption, measure small changes on a large baseline signal making detection of trace levels more difficult. Our approach uses a novel (*Patent Pending*) modulation method that improves detection sensitivity and helps to distinguish among the target gases and to reject signals due to background gases such as water vapor. This is to be accomplished by measuring small changes on a zero baseline. Specifically, the goal of

this technique is to discern small concentration changes, potentially as small as the limit set by the intrinsic detector noise.

This technique uses two LEDs (as shown in Fig. 2) pulsed 180 degrees out of phase, and uses the difference between the two LED intensities at the detector to measure absorbance by a gas. The LED emissions are filtered to provide a reference signal and an absorption signal. Initially, the LED input currents are adjusted such that the detection signal level ( $I_0$ ) is the same for each LED/filter combination with no absorbing gas present in the cell, as shown in Fig. 5. When the lock-in amplifier processes these signals, the resulting output is zero because the signals cancel each other out. When there is an absorbing gas, such as CO or CO<sub>2</sub> present in the cell, the sample beam intensity decreases while the reference intensity is unchanged and the lock-in amplifier displays a non-zero output. The technique is effective because it allows measurements of small absorbances against zero baseline and minimizes the dynamic range requirements of the lock-in amplifier.

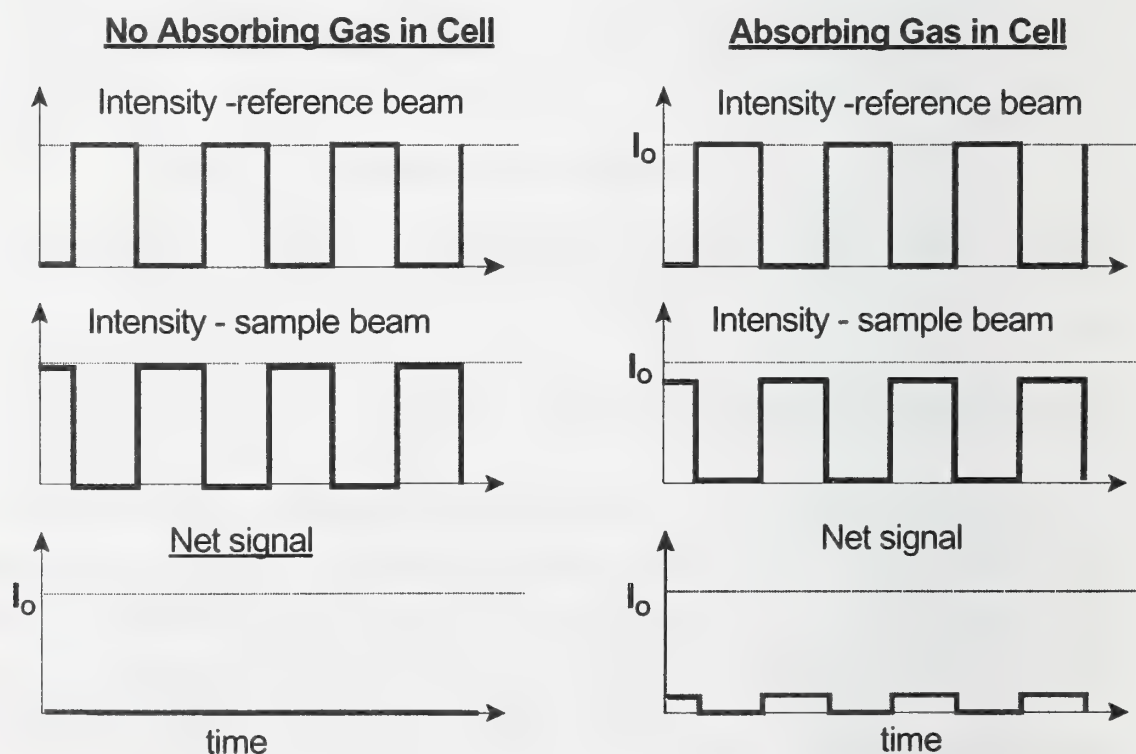


Figure 5 - Differential absorption measurement technique

Calibration measurements were made with concentrations of CO that ranged from 10 to 10,000 ppm. The differential technique was able to measure a CO concentration of 10 ppm, which is lower than the direct absorption measurements. Thus, the differential absorption technique has a higher sensitivity than the direct absorption technique! All measurements were made at 296K and at 600 Torr. Figure 6 shows the measured change in intensity plotted against CO concentration and the FAA's CO minimum performance standard,  $200 \pm 50$  ppm [1,14,15]. The detection limit for the differential absorption technique is below the FAA's CO alarm level [14,15] and below the 8 hour weighted average exposure (40 ppm) established by National Institute for Occupational Safety and Health [16].

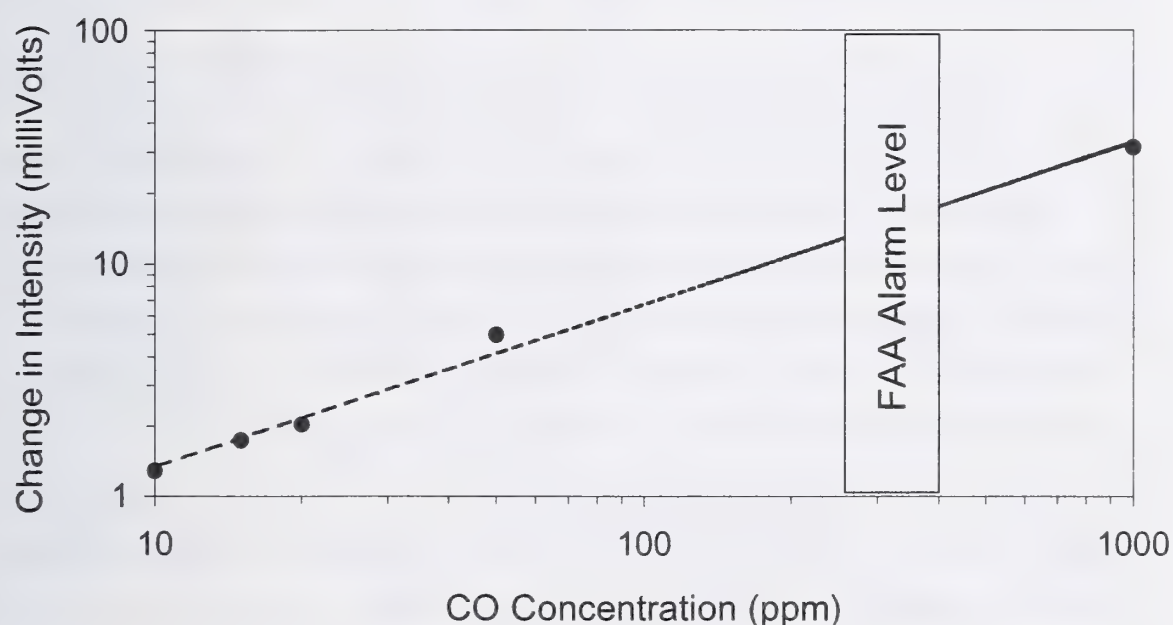


Figure 6 - Differential absorption measurements and the FAA's minimum performance standard for CO [1,14,15]

#### 4.3 Cross Talk

Successful implementation of Southwest Sciences' fire detection method requires sensitive and *selective* detection of the target gases. Selectivity refers to measurement of one gas in the presence of the others. Our results show trivially small cross talk between CO and CO<sub>2</sub>. Filling the sample cell with 0.8 atm of CO<sub>2</sub> shows a false



positive response equivalent to 50 ppm CO; that means selectivity for CO in the presence of CO<sub>2</sub> is 16,000:1. We expect no detectable false positive CO signals for all realistic CO<sub>2</sub> concentrations. In the other direction, filling the cell with 10,000 ppm CO gives a false CO<sub>2</sub> signal of 77 ppm. This corresponds to a selectivity of 130:1. The small false positive CO<sub>2</sub> signals are unimportant relative to the large CO<sub>2</sub> background: 430 ppm of CO – a substantial CO concentration that will certainly exceed alarm threshold – would introduce a false CO<sub>2</sub> signal equal to only 1% of the 350 ppm CO<sub>2</sub> background.

## 5. Spectroscopic Modeling

### 5.1 Feasibility of measuring HCN and C<sub>2</sub>H<sub>2</sub>

These gases have absorbance bands in the mid-IR that can be reached with commercially available LEDs and filters. There is strong overlap between HCN and C<sub>2</sub>H<sub>2</sub> absorbances, which may prevent this technique from selectively measuring these gases. However, even if these gases cannot be detected separately, monitoring for HCN and C<sub>2</sub>H<sub>2</sub> is useful because trace amounts of either gas, which have a zero ambient concentration, would clearly indicate the presence of combustion. Using the validated numerical simulation, the effective cross-sections for both gases are nearly identical to each other ( $6.1 \times 10^{-20}$  cm<sup>2</sup>/molecule and  $8.1 \times 10^{-20}$  cm<sup>2</sup>/molecule for C<sub>2</sub>H<sub>2</sub> and HCN, respectively) and to CO ( $7.3 \times 10^{-20}$  cm<sup>2</sup>/molecule). This translates into a minimum detectable concentration of similar to that of CO – 10 ppm.

### 5.2 Interference by Water Vapor

Cross-section calculations, Eq. (1), also allow us to predict potential interference by background gases. Water vapor, because it is ubiquitous in air and has numerous infrared absorption bands is the most important background gas. Spectroscopic modeling computations show that there is no significant interference by water vapor for detection of carbon monoxide, carbon dioxide, hydrogen cyanide, or acetylene. These computations use the spectral line parameters in the HITRAN database [13], which are

known to be accurate for these low molecular weight gases (including water vapor) at temperatures near ambient. Under worst case conditions – 100% humidity at 310 K which might occur in an open cargo bay on the ground during the summer at a coastal location – the optical absorbance due to water vapor contributes a false positive signal of 15 ppm CO. This concentration is below the OSHA maximum workday exposure [16] and is well below FAA CO minimum performance levels ( $200 \pm 50$  ppm) [14,15]; moisture levels during flight will be at least a factor of three lower.

## 6. Conclusions

A new, innovative technique (*Patent Pending*) has been utilized for measuring trace gas concentration. The mid-IR LEDs used in this system are ideally suited for continuous monitoring in situations that require a small, low-cost alternative to conventional systems, such as in aircraft cargo compartments. Using multiple LEDs, the system has the ability to separately measure the instantaneous concentration of multiple gases, greatly reducing the likelihood of false alarms, and increasing the likelihood for detecting incipient fires. In addition, continuous monitoring of carbon dioxide, which has a non-zero ambient concentration, can be used for real-time testing of instrument performance.

This instrument could be used for early fire detection in aircraft cargo compartments and other inaccessible locations within an airframe. This type of instrument could be integrated into a sophisticated aircraft control system, such as the *Aircraft Command in Emergency Situations* system prototyped by Boeing [17]. The commercial applications of the proposed instrument extend to fire safety in any location requiring fast and accurate detection of a fire, including, but not limited to: storage warehouses, industrial settings, large office buildings, shopping malls, etc. This technology could also be applied to spacecraft fire safety, providing fire detection for long-duration manned space missions. Additionally, the same technology used for fire detection can be used for air quality monitoring, for a wide range of gases in almost any setting.

## 7. Acknowledgements

Dr. Goldmeier would like to acknowledge financial support provided by the NASA Glenn Research Center's Small Business Innovation Research (SBIR) Program (NAS3-00058), as well as technical assistance from Drs. David Bomse, Daniel Oh, Jeffrey Pilgrim, Joel Silver, and Alan Stanton at Southwest Sciences.

## 8. References

1. Blake, D. Aircraft cargo Compartment Smoke Detector Alarm Incidents on U.S. Registered Aircraft, 1974-1999. DOT/FAA/AR-TN00/29, 2000.
2. Hedrick, R. L., and Billick, Irwin. Chamber tests of Residential CO Alarms. Gas Research Institute 1997.
3. Grosshandler, W. A Review of Measurements and Candidate Signatures for Early Fire Detection. NISTIR 5555, January 1995.
4. Milke J., and McAvoy T. Analysis of Fire and Non-fire Signatures for Discriminating Fire Detection, Fire Safety Science - Proceedings. Fifth International Symposium 1997; 819-828.
5. Pfister, G., Fire Safety Journal, 1983; 6: 165-174.
6. Jackson. M. and Robins, I. Gas Sensing for Fire Detection: Measurements of CO, CO<sub>2</sub>, H<sub>2</sub>, O<sub>2</sub>, and Smoke Density in European Standard Fire Tests. Fire Safety Journal 1994; 22: 181-205.
7. Milke, J. Using Multiple Sensors for Discriminating Fire Detection. Proceedings - Fire Suppression and Detection Research Applications 1999; 150-164.
8. Glassman, I. Soot Formation in Combustion Processes. Proceeding of the Combustion Institute 1988; 22: 295-310.
9. Kennedy, I.M. Models of Soot Formation and Oxidation. Progress in Combustion Science 1997; 23: 95-132.
10. Levin, B., and Gann, R. Fires and Polymers, ACS Symposium Series 425, American Chemical Society 1990.
11. Lundgren, B., and Stridh, G. Fire and Polymers, ACS Symposium Series 425, American Chemical Society 1990.



12. Hathaway, G., et al. Proctoer and Hughes' Chemical Hazards of the Workplace, Van Nostrand Reinhold, NY, 3<sup>rd</sup> ed. 1991.
13. L. S. Rothman, et al. *Journal of Quant. Spectrosc. Radiat. Transfer*, 1992: 48.
14. Cargo Compartment Fire Detection Instruments. Federal Aviation Administration TSO C1c, 1987.
15. Cargo Compartment Fire Detection Instruments. Society of Automotive Engineers, Inc., (SAE) Aerospace Standard (AS) Document No. AS 8036, 1985.
16. Recommendations for Occupational Safety and Health. Department of Health and Human Services (NIOSH) Publication No. 92-100, 1992.
17. Reynolds, T.L. Improvements in Aircraft passenger Safety: High Costs, Diminishing Returns. Interior Safety of Passenger Transport Seminar, Institution of Mechanical Engineers, London, England, November 1992.

## **Measuring results of a combined optical, thermal and CO detector in real sites and classifying the signals**

### **1 Introduction**

One of the major problems of fire detectors is the number of deceptive alarms. Though the detectors themselves are not unreliable, they are sensitive to other aerosols and their large number in the field can lead to a significant amount of false actions of the fire brigades. It is fact, that deceptive signals, mainly caused by aerosols or dust, without any danger of fire, happen much more often than real fire situations. Various statistics prove, that fire brigade actions preponderate for other reasons than fire. The number of deceptive alarms depends on the application and the installation site, but there is also a human factor in not properly recognizing critical installation areas. The aim is, to find solutions for a better enhance disturbance behavior of today's detectors. For special applications like fire detection in airplanes or in coil processing plants, there are already sophisticated special solutions. But these solutions cannot be transferred easily to general purpose applications.

The range of applications for fire detectors can be broadened by using additional information from the signals provided by the fire accident. This additional information can be obtained from time analysis of the smoke density signal, from information on the installation site or from additional signals of other sensors. This paper reports on measurements with a new fire detector that comprises a light scattering detector, a temperature sensor and a CO-gas sensor.

**2 Influence of variations of light scattering on the signals from a light scattering detector**

Figure 1 shows the electrical signal of a light scattering detector over a time course of 9 hours in a normal environment without any signal processing or filtering.

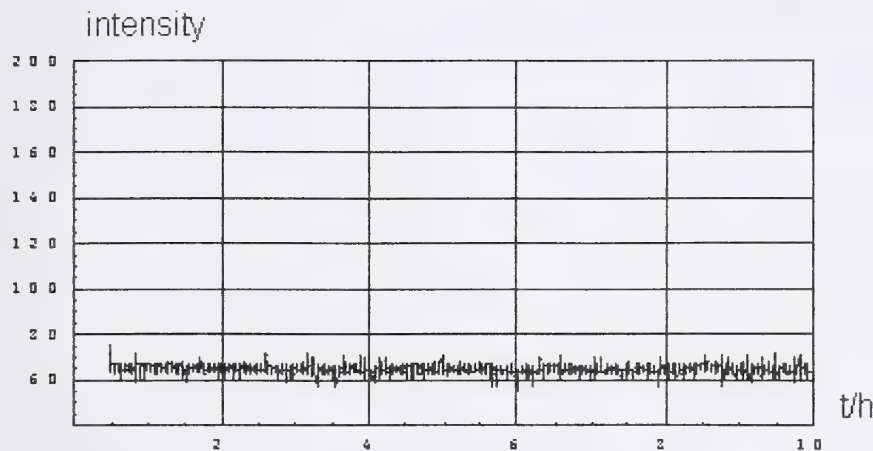


Fig. 1: Light scattering signal in normal environment

An analysis of the signal with a  $\chi^2$ -test shows, that a Gaussian distribution can be assumed for this sample. With an typical signal to noise ratio  $S/N=20$  and sample rate of one second the threshold will be exceeded once in  $2 \times 10^{316}$  years. This dramatically changes with signals sampled from a susceptible environment. Fig. 2 shows for the signal taken in a smokers room as an example.

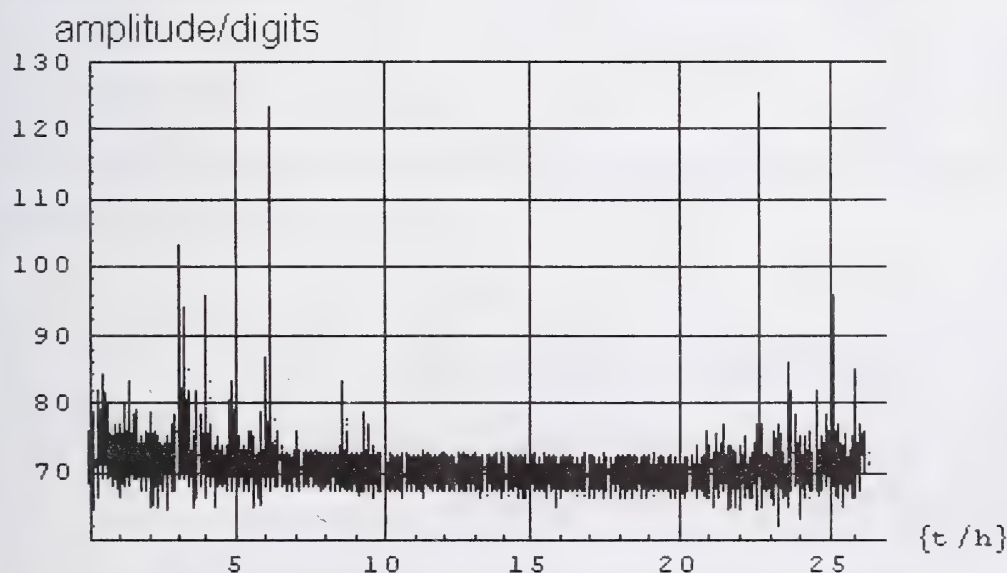




Fig. 2: Raw signal from a smokers room

Distinct signals peaks are recognizable in the distribution density diagram. The values around zero have been suppressed, to highlight the distribution of the disturbance signal.

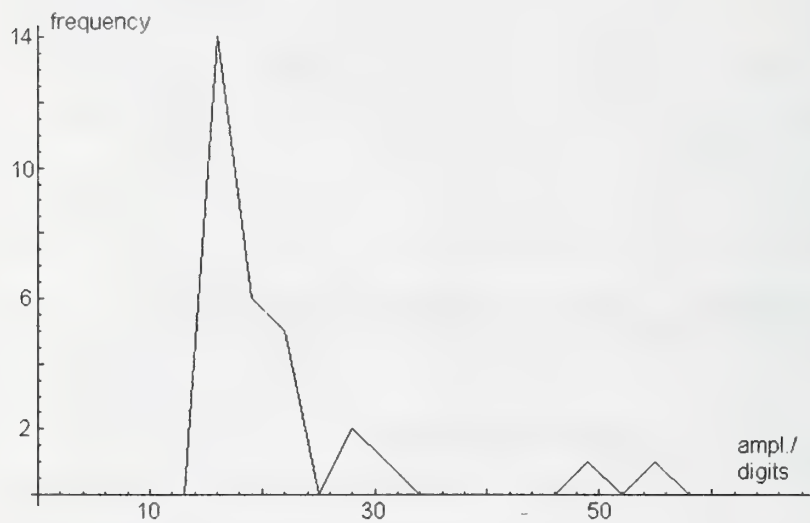


Fig. 3: Distribution density from signals of a smokers room

To estimate the probability of a deception alarm, the distribution density was approximated with a logarithmic normal distribution density function.

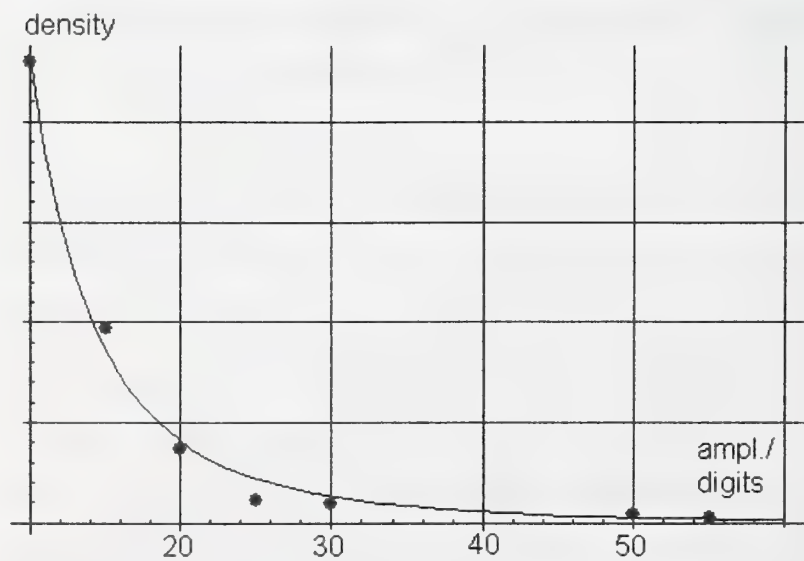


Fig. 4: Approximation of the measured distribution density with a logarithmic normal distribution density function

With this model one can estimate for a given alarm threshold, when a false alarm will occur.

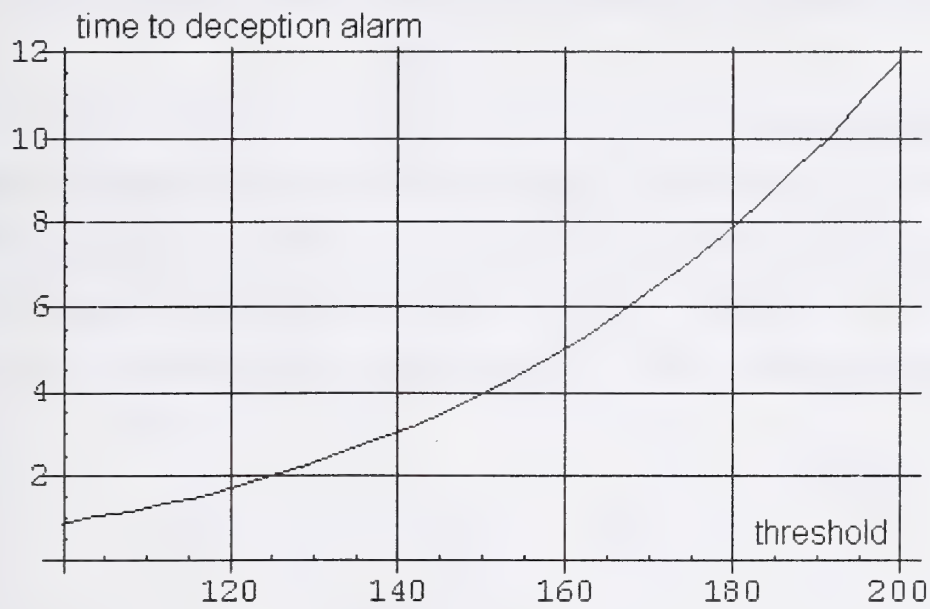


Fig. 5: Schematic rate of deception alarms depending of the alarm threshold

It can be seen, that the deception alarm rate decreases more than proportional. Doubling the threshold lowers the false alarm rate by a factor of 10. This consideration was done with raw signals, still without any aspects of signal analysis, and shows, what improvement can be expected using additional information to raise the threshold for the optical alarm signal. So the use of more than a single sensor is an attractive possibility for obtaining additional information. To get an impression about the usability of combined sensors in fire detection, a new detector comprising a light scattering chamber, a temperature sensor and a CO gas sensor was investigated with test fires of EN54 and some additional defined fires and artificial produced disturbances.

The CO sensor was an electrochemical cell. The properties of electrochemical cells have been significantly improved over the last few years. The life time of today's cells is specified with more than 5 years and the costs lie in a range now, making their use in fire detectors attractive. The selectivity is sufficient and the power consumption is low in contrast to

metal oxid sensors, which need power to heat them. To analyze the new fire detector further, it has been analyzed under different environmental conditions for a longer time beside the pure fire tests.

### 3 Fire tests

The new detector was tested in a fire room with standard test fires. Table 1 shows the CO sensor values at the end of the fires defined by EN54. In case of a fire situation a significant concentration of CO is expected, at smoldering fires (TF 3) it is particularly high (Fig 6).

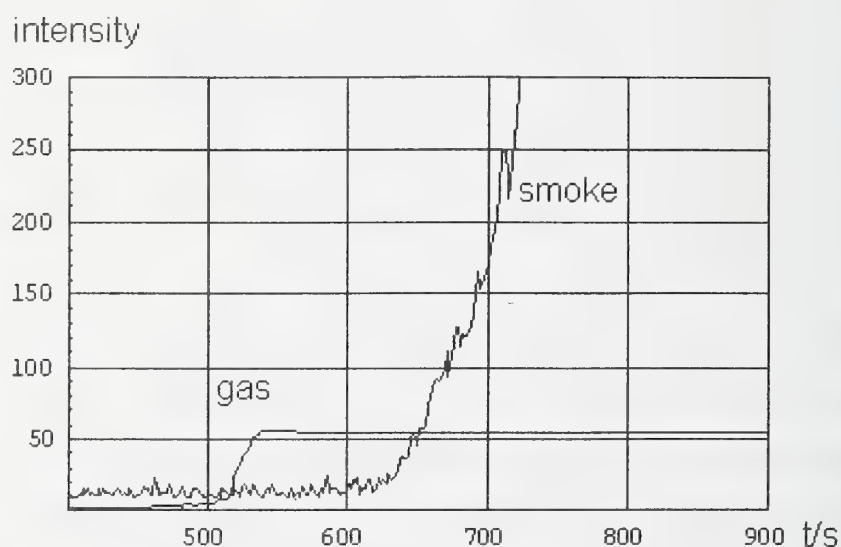


Fig. 6: CO and smoke signal of smoldering cotton fire (EN54)

One has to be aware that CO can also be measured at other occasions than a fire, e.g. in environments with cars with operating engine.



Test fire according EN54	CO-concentration at the end of fire in ppm
TF1 open wood fire	20 ... 35
TF2 smoldering wood fire	10 ... 47
TF3 glowing smoldering cotton fire	130
TF4 flaming plastics (polyurethane)	25
TF5 flaming liquid, n-heptan	14 ... 33
TF6 Aethanol	1,5 ... 10
TF7 Decalin	16 ... 27
cable fire	3 ... 6
paper bin fire	35

Table 1: CO-concentration at standard fires

Installations at real sites should reveal, therefore, which signals are to be expected, and whether the combination of the values of the scattering, temperature and CO concentration signals can give information about the origin of the sensor output.

#### 4 Measuring arrangement

To analyze different applications for the new fire detector, it was exposed to various influences. In some situations the optical detector may react insensible, while the other sensors will be very reactive and vice versa. The list below shows some critical factors, to which a fire detector has to adapt in normal environments.

- cigarette smoke
- draught in entrance areas
- heater fans in industrial halls
- high humidity, dew
- fog
- all kind of dust (color, particle size)

- various climates and temperature cycling (operating  $< 0^{\circ}\text{C}$ )
- fibers
- insects
- damp, smear films, solvents
- gasoline gases
- emanation in plastic manufacturing
- direct sunlight

For the selection of test sites as much different surroundings as possible were chosen. The results presented here include a smokers room, a welder room, a hall with open sides to the free air, a repair garage for cars and a normal industrial environment. Fig 7 shows the data acquisition system. The fire detectors were installed together with a customary fire panel. They sent all the actual sensor values on demand. The data were collected about every 5 minutes, depending from the number of detectors in the loop, and are temporarily stored in the fire panel. In case of an alarm or a pre alarm (75% threshold) the measurement ensemble was immediately transmitted, in order not to loose the values of the alarm situation. Furthermore the values of this special detector

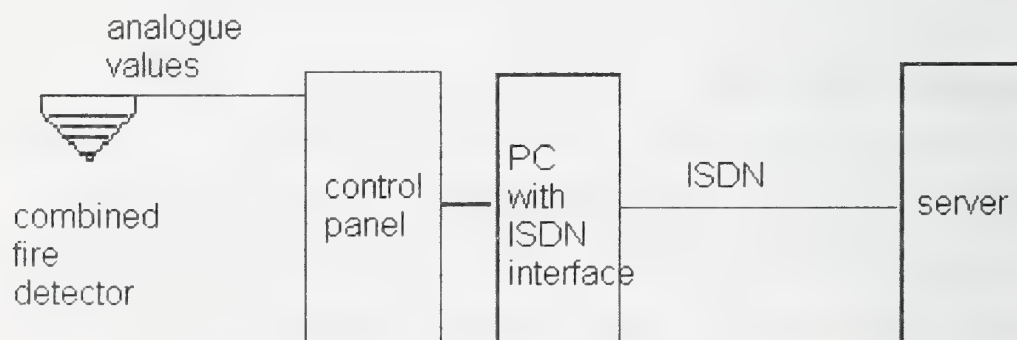


Fig. 7: recording of measuring values

in the loop were sampled with a higher sampling rate. Every hour, the stored values were transmitted to a personal computer, where the data were packed and saved in a sequential file on a mass storage. Once a day, these data were transmitted via an ISDN data link to a server at the development

location for further data analysis. For a detailed evaluation some data collection was also done in real time.

**5 measuring values**

The following figures show typical curves from the critical application areas with disturbance signals. A closer view at the data of the welding cabin shows, that the optical and CO signals are mainly short peaks. This could not only be seen in amplitude analysis but also in a time analysis. Specific experiments in the fire room show, that the emission of CO is less with electric welding than with autogenous welding.

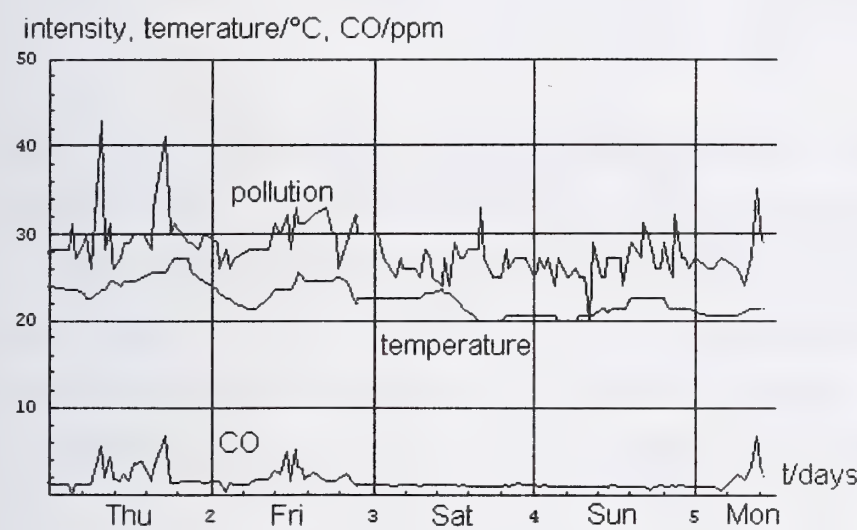


**Fig 8: Measurement curve in a smokers room for 4 days**



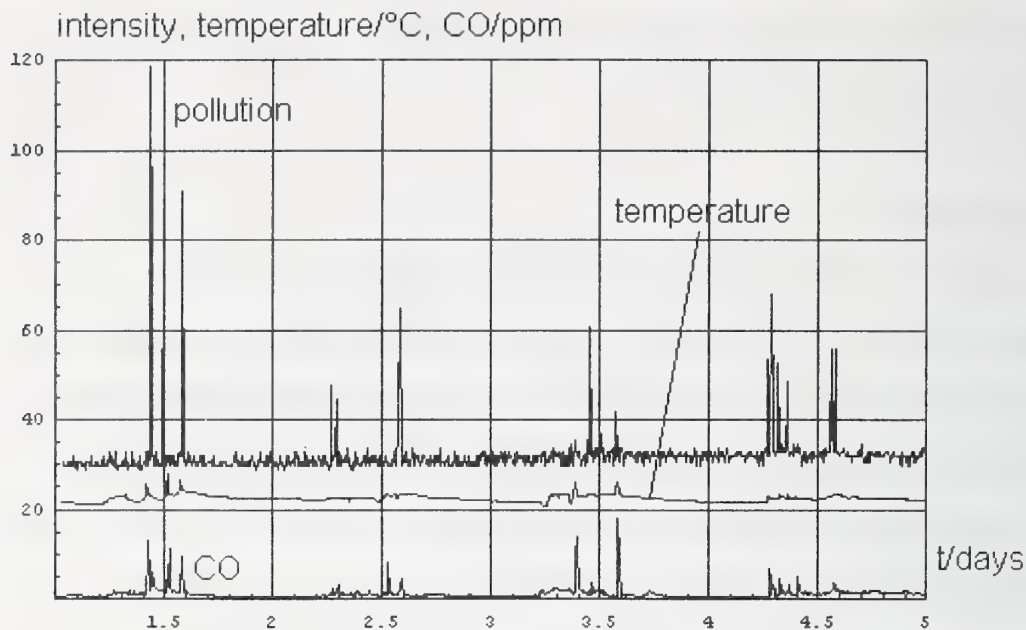


Fig. 9: measurements in a welding cabin

Contrary to welding, the cars driving in and out of a repair garage gave a significant CO signal. The values are higher than the values at the majority of the test fires. It is interesting, that the light scattering signal does not show significant amplitude values.

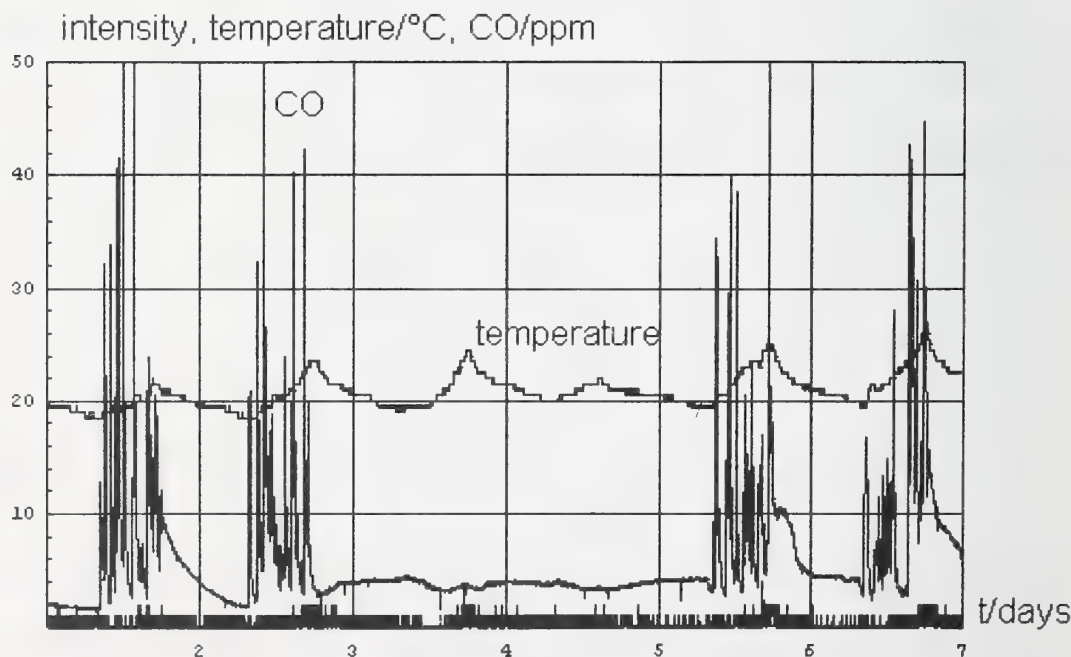
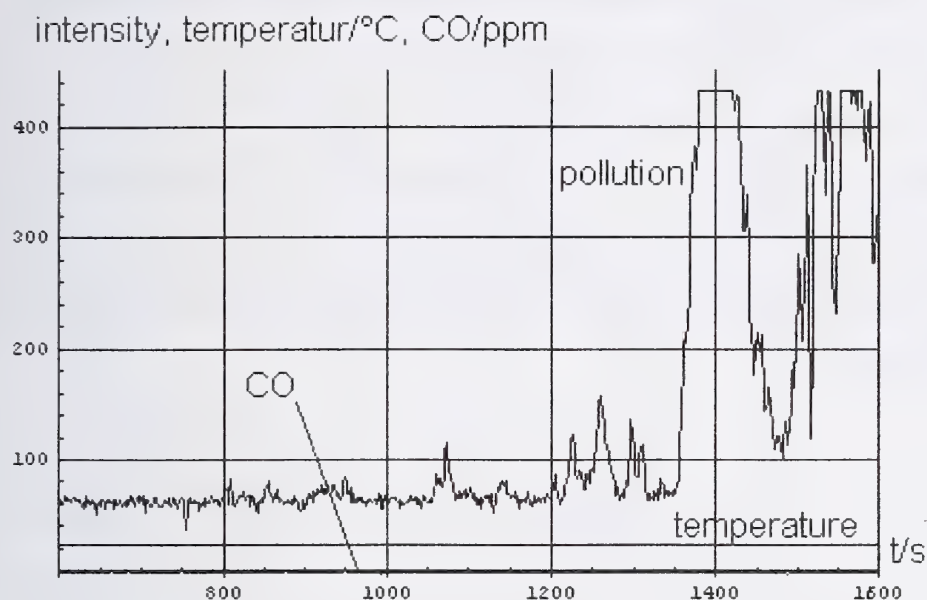


Fig. 10: signal curve in a garage

All shown disturbance values were especially chosen, because aerosol as well as CO occurs simultaneously even though in different amplitudes. However many disturbance effect only the optical part of the fire detector. For this belongs beside the general creeping dust accumulation, making the detector more unstable, all kind of dust and foggy substances corrupt the



optical signals. An extreme example is an experiment with disco fog (Fig. 11). Similar to dust, there is no CO signal as well as there is no increase in temperature.

Fig. 11: experimental measuring with disco fog

## 6. Classification of the signals

The single signals of the detector have been divided into rough classes. The classes were named as “nothing”, “some”, “more”, “much”, “very much”.

“Nothing” means, there is no signal which can be assigned to the event, “some” means a signal in accordance to the event, but it is too small to make a decision on this signal without a priori knowledge. “More” means a value near but not reaching the alarm threshold. “Much” stands for alarm and “very much” is a value far beyond the alarm. The presence of disturbance signals increase the risk of false alarms dependent on the probability of

their occurrence. In table 2 it is seen, that at all test fires except the alcohol fire CO is generated in a measurable amount. Therefore it seems, that CO could be used for the validating a fire situation, but contrary it cannot be concluded that it is possible the CO signal alone for suppressing disturbance signals. With disturbance signals like cigarette smoke and welding CO concentrations are measured similar to some test fires. The combination of the light scattering signal and the CO signal is also not clear enough to make a distinction between fire and deception. The temperature and the optical signal cannot distinguish clearly between smoldering fires and disturbance signals caused by dust and aerosols. It is the nature of the deception signals caused by combustion processes have a similar behavior as caused by injuring fires.



event	scatter signal	temperature	CO signal	remarks
TF1	some	more	more	
TF2	very much	nothing	much	
TF3	very much	nothing	very much	
TF4	much	some	more	
TF5	much	more	more	
TF6	nothing	very much	nothing	
TF7	very much	some	more	
dico fog	very much	nothing	nothing	
cigarette	some	nothing	more	CO conc. similar to TF1
welding autogenous	some	nothing/some	more	CO conc. to TF1
welding electro	much	nothing	some	
car garage	nothing	nothing	very much	high CO- values
diesel aggregate	some	nothing	very much	

Table 2: classifying of signals

Fig. 12 shows the recording of value triples. The large points show the values of the test fires, the smaller points represent the values of disturbance signals. In this three dimensional graph the disturbance signals could be separated from the fire signals, there is no overlap. Disturbance signals with a high amplitude in only one category could be suppressed with clever positioning a threshold area. The obtainable gain can be estimated from fig. 5 and is expected to be in one order of magnitude.

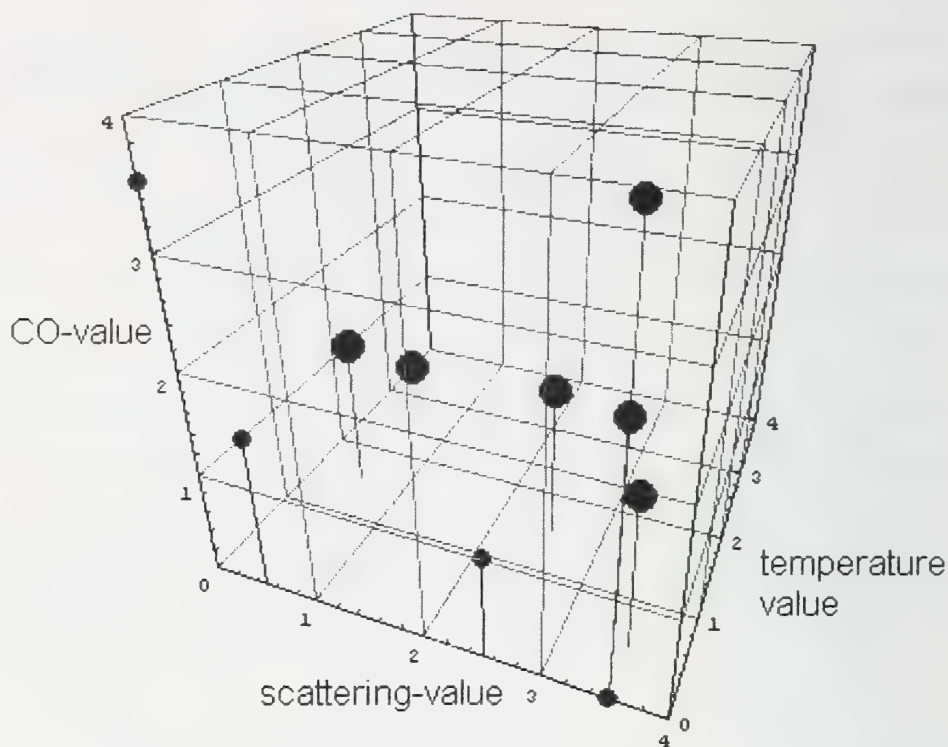


Fig. 12: Classifying of disturbance and fire signals (small points: disturbance signal, large points: signal from fire)

## 7 Conclusion

Measurement triple of new fire detector combining optical, temperature and CO sensors were be presented. Using all three signals in environments with disturbance signals caused by dust and aerosols a significant improvement of disturbance rejection can be expected. Deception signals caused by combustion processes resemble real fires with a high grade. Improved rejection of deception signals could be reached by selecting a threshold area between the different triple values of fire and non fire signals. Not mentioned in this report was the potential to validate signals by a time domain analysis. With the a priori knowledge about the application field, the detector combining optical, temperature and CO sensors promised a significant improvement in reliability in many disturbance areas.

## **Measurements for fire detection by mean of gas sensors in an insulation material factory**

### **Abstract**

The characteristics of fire detection systems is improved by a proper application of gas sensors. Particularly in surroundings, where dust or smoke produced by industrial processes cause false alarms in conventional smoke detectors, gas sensors show advantages.

Analysis of the background level in comparison to the firesignals is necessary in many fields of application. As an example tests carried out in a plant producing pulp-based insulation material are described. As a result statements on the suitability of gas sensors for fire detection are made. Investigations on long term stability started.

### **1 Einleitung**

Gassensoren haben sich bereits in vielen verschiedenen Anwendungsgebieten etabliert, so z.B. in der Klimatechnik, zur Messung explosionsfähiger Atmosphären oder zur schnellen Gasdetektion. In der Brandmeldetechnik konnte sich diese Technologie bisher nicht durchsetzen, obwohl es bereits 1983 Ansätze für den Einsatz von Halbleitergassensoren in der Brandmeldetechnik gab [1]. Dies liegt zum einen am relativ hohen Preis der Sensorelemente und zum anderen an der geringen Langzeitstabilität, dem problematischen Ansprechverhalten sowie dem hohen Stromverbrauch der meisten Sensoren.

Durch die konsequente Weiterentwicklung der Sensortechnik in den letzten Jahren ist es jedoch möglich geworden, preiswerte und zuverlässige Gassensoren mit immer geringerem Energieverbrauch in großen Stückzahlen anzubieten. Hieraus eröffnet sich



die Möglichkeit, freigesetzte Gase zur Detektion von Bränden zu nutzen. Versuche im Brandraum des VdS Schadenverhütung, Köln haben gezeigt, daß Gassensoren als Detektorelemente bei sich langsam entwickelnden Schwel- und Glimmbränden wesentlich schneller und signifikanter ansprechen, als herkömmliche Brandmelder auf Basis einer Detektion von Flammen, Rauch oder Wärme [2]. Die Freisetzung von Gasen bei verschiedenartigen Bränden, wie z.B. Zigarettenglimmbrand und offenen Benzinbrand, ist ebenso unterschiedlich wie charakteristisch. Durch die simultane Erfassung und Auswertung verschiedener Brandgase kann eine Täuschung der Brandmelder durch brandähnliche Vorgänge, wie z.B. Schweißen oder Rauchen, verhindert werden. Erfolgreich eingesetzt werden solche mit  $H_2$ -,  $CO$ - und  $NO_x$ -sensitiven Sensoren bestückten Melder bereits in Bekohlungsanlagen von Braunkohlenkraftwerken.

Der Einsatz von Gassensoren in der Brandmeldetechnik bringt jedoch auch Probleme mit sich. Die Langzeitstabilität vieler Sensoren ist noch relativ unbekannt. Der Einfluß von aggressiven Dämpfen und abgelagerten Stäuben auf den Sensoren ist ebenfalls wenig untersucht. Für eine sichere Branddetektion ist weiterhin der Abstand zwischen den betriebsbedingten Hintergrundsignalen und den vom Brand verursachten Signalpegeln entscheidend. Untersuchungen zu diesem „Hintergrundrauschen“ von Gassensoren in den verschiedensten möglichen Einsatzgebieten sind bisher nicht bekannt. Diese Probleme sollen im Rahmen des Forschungsprojektes „Untersuchungen über den Einsatz von Gassensoren in der Brandmeldetechnik“ an der Bergischen Universität – GH Wuppertal bearbeitet werden [3].

## **2 Ziele des Projekts**

Um die Vor- und Nachteile der verschiedenen Sensorprinzipien herauszufinden, wird durch Langzeitversuche mit Gassensoren und herkömmlichen Detektoren das „Hintergrundrauschen“ in verschiedenen potentiellen Anwendungsbereichen erfaßt. Hierbei sollen zum einen die Signale von brandgasspezifischen Sensoren ( $CO$ ,  $CO_2$ ,  $H_2$ ,  $NO_x$ ,  $CH_4$ ) in der Umgebungsluft erfaßt werden. Zum anderen werden Stör- und Täuschungsgrößen, sowie Sensorgifte in den Umgebungen ermittelt, der

Wartungsaufwand untersucht und das Verhalten der Sensoren bei unterschiedlichen klimatischen Bedingungen (Temperatur und Luftfeuchtigkeit) beurteilt. Stör- und Täuschungsgrößen können beispielsweise auch Abgase von Kraftfahrzeugen oder Gabelstaplern sein.

Gleichzeitig zu den Messungen des „Hintergrundrauschens“ wird eine Literaturrecherche zu den Hintergrundkonzentrationen in der allgemeinen Umgebungsluft sowie in verschiedenen Anwendungsbereichen durchgeführt. Hierbei werden vor allem Messungen des Landesumweltamtes und des berufsgenossenschaftlichen Instituts für Arbeitsschutz (BIA) zu Hilfe genommen.

Da an den Meßstandorten neben dem Hintergrundrauschen im allgem. keine Brände aufgezeichnet werden können, werden mit der Meßapparatur typische Brände sowie genormte Testfeuer in Brandräumen aufgezeichnet und mit dem „Hintergrundrauschen“ an den Meßstandorten verglichen.

Um die bei der Interpretation der Meßergebnisse vermuteten Querempfindlichkeiten und Täuschungsgrößen näher zu untersuchen, werden die Sensoren in einer Prüfkammer gezielt mit Täuschungssubstanzen beaufschlagt. Dabei handelt es sich um Substanzen, die zum Teil schon bekannt sind, zum Teil aber auch aus den Langzeitversuchen heraus vermutet werden.

### 3 Aufbau der Meßapparatur

Für die Durchführung dieser Langzeitversuche werden die verschiedenen Sensorprinzipien in unterschiedlichen baulichen Ausführungen eingesetzt. Im einzelnen kommen folgende Sensoren zum Einsatz:

Sensor	Zielgas	Querempfindlichkeiten	Meßbereich	Hersteller Besonderheiten
Halbleitersensor mit Zinndioxidsubstrat (1. SnO <sub>2</sub> )	NO <sub>x</sub> ; O <sub>3</sub>	Alkohole; HC	ppm	Herst: UST [4] Interdigitalstrukturen der Substratkontakte
Halbleitersensor mit Zinndioxidsubstrat (2. SnO <sub>2</sub> )	HC NO <sub>2</sub>	NH <sub>3</sub>	ppb – ppm	Herst: UST [4]

Halbleitersensor mit Galiumoxidsubstrat ( $\text{Ga}_2\text{O}_3$ )	$\text{H}_2$	$\text{CH}_4$ ; Lösungsmittel	ppm	Herst: SIEMENS [5] Hochtemperatursensor für Überwachung von Gasturbinen
elektrochemische Zelle (EC-CO)	CO	Ethanol; $\text{H}_2$	0-500 ppm	Herst: Sensoric [6]
elektrochemische Zelle (EC-NO)	NO	keine Angabe	0-100 ppm	Herst: Sensoric [6]
elektrochemische Zelle (EC-NH <sub>3</sub> )	NH <sub>3</sub>	keine Angabe	0-100 ppm	Herst: Sensoric [6]
Infrarot-Meßzelle mit Referenzdetektor (IR-CO <sub>2</sub> )	CO <sub>2</sub>		0-5000 ppm	Herst: Sensor Devices [7]; Verwendung zur MAK-Überwachung
Infrarot-Meßzelle mit Referenzdetektor (IR-HC)	HC		0-4 %	Herst: Sensor Devices [7]; Verwendung zur UEG-Überwachung

Zusätzlich wird auf jedem Sensorarray ein Rauchmelder nach dem Streulichtprinzip mit separatem Ausgang der Meßgrößen genutzt. Weiterhin gemessen werden Temperatur und relative Luftfeuchte.

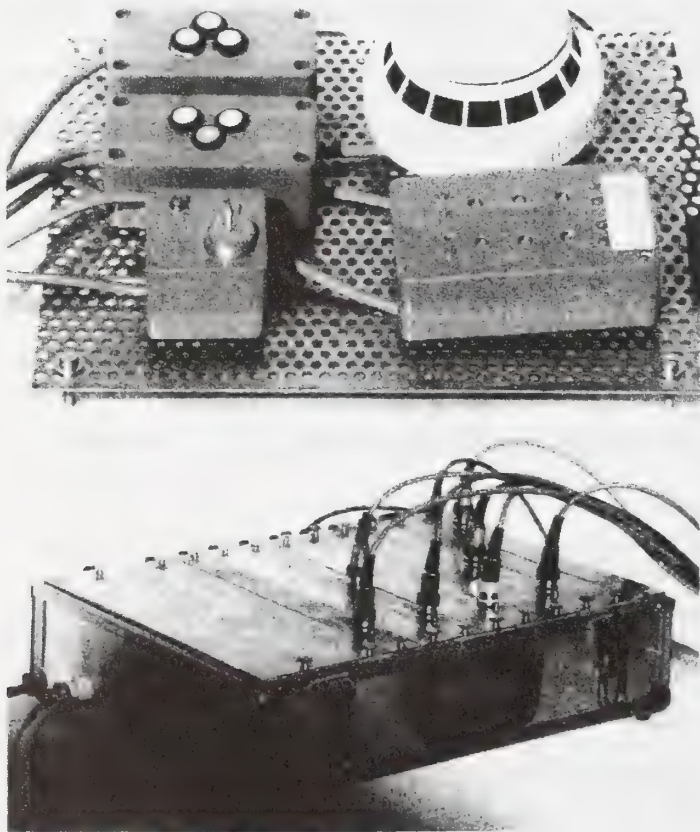


Abb. 1 – Sensorarray und Meßkoffer

Alle Sensoren sind in einem Sensorarray gemäß Abb. 1 zusammengefaßt. Die einzelnen Sensoren des Arrays werden an einen Meßkoffer angeschlossen, der bis zu 2,5m abgesetzt vom Sensorarray angeordnet werden kann und die komplette Sensorelektronik enthält. Die Meßapparatur wird über einen Lowcost Industriebus (M-Bus) an einen Personalcomputer angeschlossen. Der M-Bus ist eine protokollunabhängige Zweidraht-Schnittstelle mit integrierter Fernspeisung für den Anschluß mehrerer mikroprozessor-basierter Endgeräte.



## **4 Anwendungsbereiche**

Die Umgebungen, die mit dem Meßsystem untersucht werden, umfassen sowohl allgemeine Anwendungsbereiche wie Büros, Tagungsräume und Heimbereiche als auch spezielle Anwendungsbereiche. In den allgemeinen Anwendungsbereichen wird besonderes Augenmerk auf Raucher- und Nichtraucherbereiche und die Einflüsse von Kopierern, Drucker und Reinigungsmitteln gerichtet. Als spezielle Anwendungsbereiche werden Bereiche der Lagerwirtschaft, öffentliche Gebäude mit hohen Menschenansammlungen und industrielle Fertigungseinrichtungen mit rauen Umgebungsbedingungen mit überdurchschnittlicher Staub- und Aerosolbelastung untersucht. Es handelt sich hierbei um Bereiche, in denen herkömmliche Brandmelder große Probleme bereiten.

Zur Zeit sind bzw. waren Meßapparaturen in einem Motorenprüfstand, in Büro-, Labor- und Heimbereichen, in der Automobilindustrie (Härteanlagen, Erodieranlagen, Emulsionsaufbereitung, Garagen), über verschiedenartigen Schweißarbeitsplätzen und in einem Dämmstoffwerk installiert. In dem folgenden Abschnitt werden exemplarisch die Ergebnisse der Messungen in einem Dämmstoffwerk vorgestellt.

## **5 Untersuchungen in einem Dämmstoffwerk**

### **5.1 Dämmstoffe**

Die Dämmplatten bestehen aus Altpapierflocken, die mit Jutefasern verstärkt werden. Zudem werden diverse Zusatzstoffe in geringen Mengen beigegeben: Ligninsulfonat wird als Bindemittel eingesetzt, Tallharz und Aluminiumsulfat wirken wasserabweisend, ein Borsäure/Boraxpuffer dient einerseits als Brand- und Glimminhibitoren, andererseits auch als Pilzschutzmittel (Fungizid).

#### Herstellung:

Altpapier wird zerkleinert und im Wirbelstrom mit Borax und Borsäure vermischt. Die Jutesäcke werden zu Fasern zerrissen, danach werden Aluminiumsulfat, Tallharz und Ligninsulfat beigegeben. Die Komponenten werden vermischt und in einer

Verfahrensstraße zu Platten gepreßt, mit heißem Wasserdampf getrocknet und formatiert.

Beim Zerkleinern des Altpapiers und beim Zerkleinern der Dämmstoffplatten sowie im gesamten Verfahrensablauf entsteht viel Staub. Im Laufe einer Woche bildet sich schnell eine Staubschicht von 3 bis 5cm. Vor allem auf den Stahlträgern lagert sich der fertigungstechnisch bedingte Staub ab. Am Wochenende kommt es zeitweise durch Vogelflug zu Staubaufwirbelungen, durch die ein Fehlalarm der Ionisationsmelder verursacht wird. Die Nutzung von Gassensoren als zusätzliches Branderkennungskriterium erscheint daher als sinnvoll.

Die Anlagen starten bei normaler Produktionslage gegen 8.00 Uhr morgens. Zur Mittagszeit werden die Anlagen vorübergehend heruntergefahren und laufen nach Beendigung der Mittagspause bis ca. 18.00 Uhr.

## **5.2 Branderkennung**

Die Branderkennung erfolgt zur Zeit über Ionisationsrauchmelder, die an eine Brandmeldeanlage angeschlossen sind. Ein eventueller Alarm läuft tagsüber (während der Betriebszeiten) bei dem Pförtner und nachts direkt bei der Feuerwehr auf.

## **5.3 Meßorte und Installation**

Im Dämmstoffwerk wurden zwei Meßapparaturen installiert. Ein Sensorarray wurde über einer Mühle zum Recycling von Altpapier aufgehängt. Die Papiermühle stellt den kritischsten Ort in diesem Dämmstoffwerk dar. Bei diesem Verfahrensschritt kommt es zum größten Staubanfall innerhalb des Produktionsprozesses verbunden mit starken Vibrationen. Das zweite Meßsystem wurde in dem sog. Technikum aufgebaut, wodurch Vergleiche zwischen den Hintergrundsignalen zweier ähnlicher Anlagen und den Meßwerten von Testbränden gezogen werden können. Das Technikum stellt die Versuchsabteilung dar, in der die gesamte Produktionsanlage verkleinert noch einmal aufgebaut ist (Abb. 2), um Untersuchungen zur Verbesserung der Dämmstoffe und der Produktionsprozesse durchführen zu können. Dort werden insbesondere auch

verschiedene Stoffe zum Brand- und Glimmschutz getestet, wozu Brände in den Dämmstoffen ausgelöst werden.

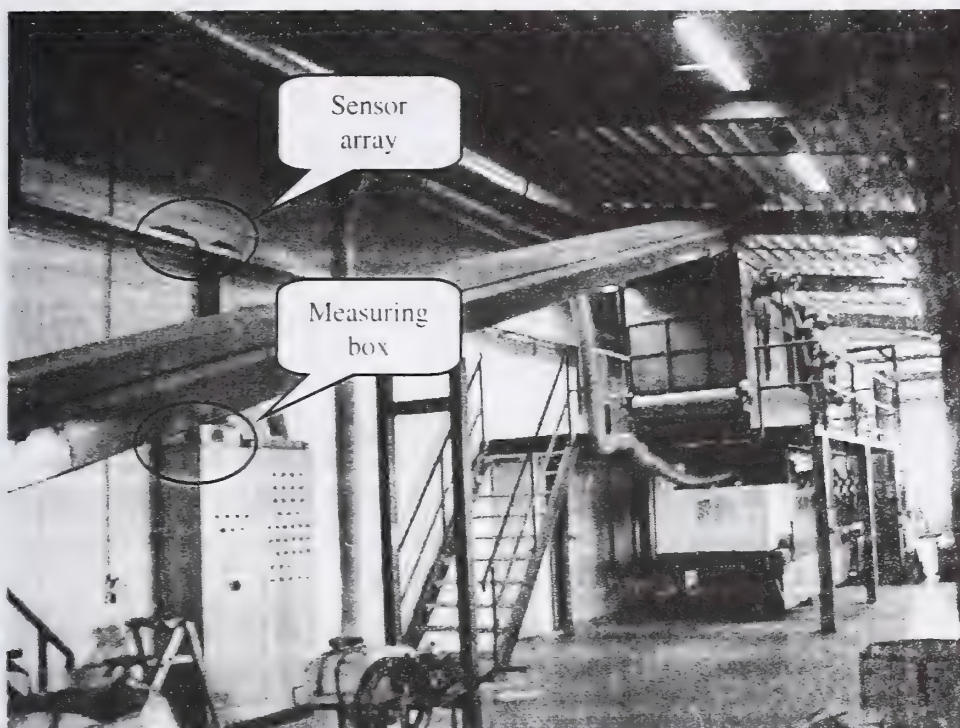


Abb. 2 – Meßapparatur im Technikum

## 5.4 Meßergebnisse

Die Abbildungen 3 und 4 zeigen einen typischen Wochenverlauf ausgewählter Sensorsignale im Technikum mit einem Testbrand am Montag um 13.00 Uhr. Hieraus werden die Signalabstände sowie die Klassifikation der Sensoren abgeleitet. Auf der linken Ordinate ist jeweils das Sensorsignal über der Zeit aufgetragen. Die rechte Ordinate gibt die äquivalenten Konzentrationen für die ermittelten Sensorsignale bezogen auf das Zielgas des jeweiligen Sensors an, denen der Signalpegel bei Beaufschlagung mit dem reinen Gas entsprechen würde.

Das oberste Diagramm von Abb. 3 zeigt den Wochenverlauf des  $\text{Ga}_2\text{O}_3$ -Sensors. Da Wasserstoff ein typisches Brandprodukt ist, sollte dies auch im Projektverlauf näher untersucht werden. Es ist jedoch in diesem Anwendungsfall ein unerwarteter Absinken des Leitwertes zu beobachten, das sich nur geringfügig von den Hintergrundsignalen unterscheidet. Es kann davon ausgegangen werden, daß wahrscheinlich  $\text{NO}_x$  detektiert



wurde. Der ansonsten relativ starke Hintergrundpegel ist durch das Cracken von organ. Hilfsstoffen (Lösungsmitteln) an der heißen Sensoroberfläche zu erklären.

Der erste  $\text{SnO}_2$ -Sensor besitzt eine hohe Sensitivität für das reduzierende Gas  $\text{NO}_x$ , was sich in der kurzzeitigen Leitwertabnahme zeigt. Der auf das Brandereignis folgende starke Leitwertanstieg ist auf das Freiwerden von Kohlenwasserstoffen durch den Glimmbrand zurückzuführen. Kohlenwasserstoffe sind typische Brandprodukte bei

Schwelbränden und eignen sich deshalb sehr gut zur Detektion in rauher Atmosphäre.

Ammoniak bzw. Amine sind ebenfalls Gase, die durch ihr oxidierendes Verhalten auf der Sensoroberfläche sehr gut zur Detektion von Bränden genutzt werden können. Einen entsprechenden zur Ammoniakdetektion optimierten Sensor stellt der zweite  $\text{SnO}_2$ -Sensor dar. Auch hier hebt sich das Signal des Brandes deutlich vom Hintergrundsignal ab. Die zyklischen Schwankungen der Signale der Halbleitersensoren sind auf Änderungen der absoluten Luftfeuchte zurückzuführen. Diese Beeinflussung wurde bereits mehrfach nachgewiesen. Die Temperaturschwankungen können als Ursache ausgeschaltet werden, da die Sensoren temperaturgeregelt sind.

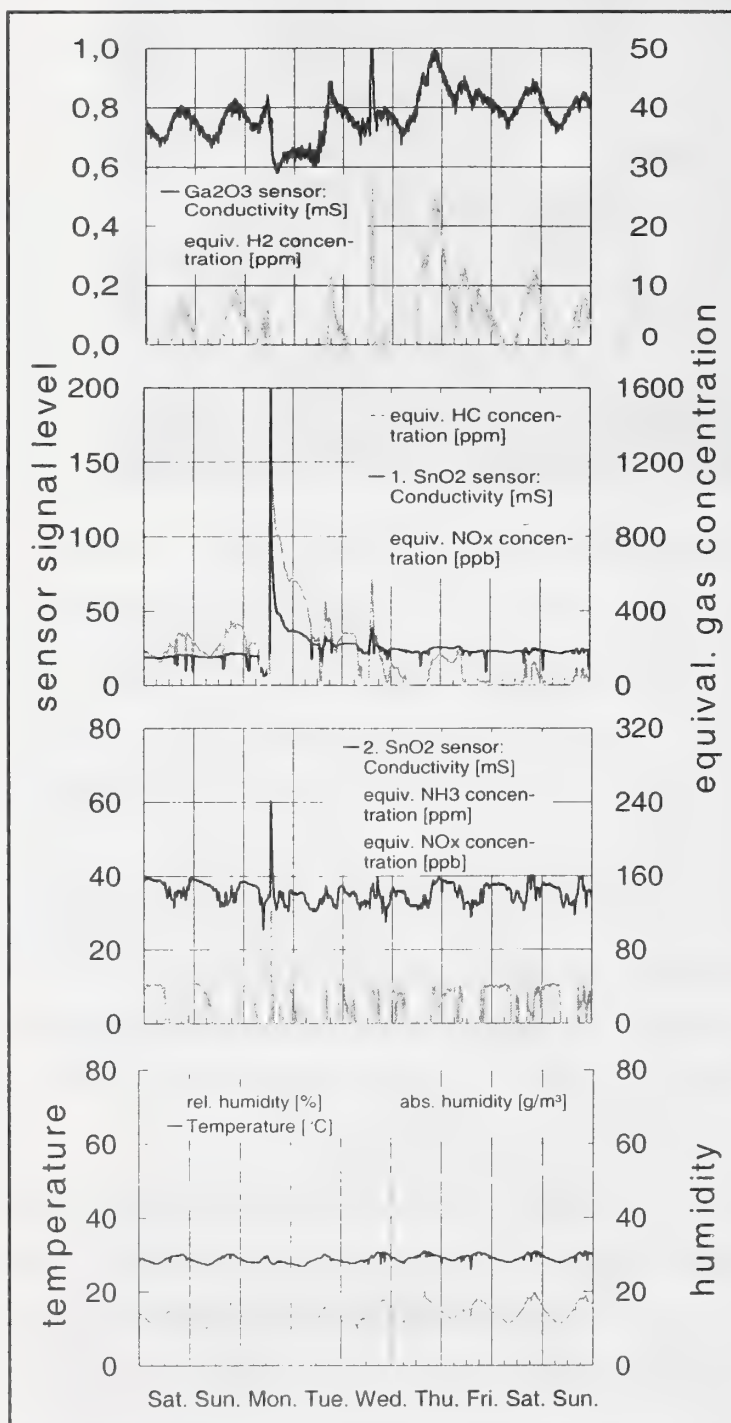


Abb 3 – Signalverlauf der Halbleitersensoren

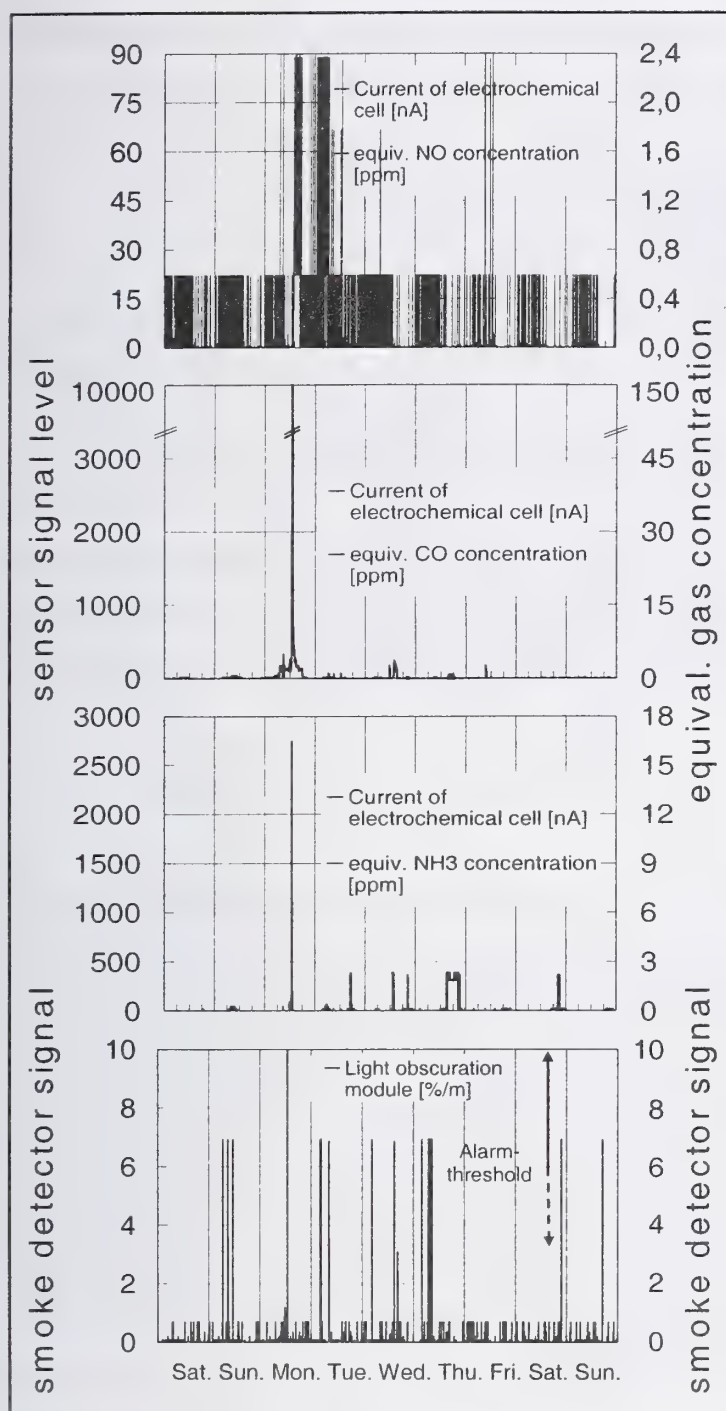


Abb 4 – Signalverlauf der elektrochemischen Zellen und des Rauchmelders

In Abbildung 4 sind die Signale der elektrochemischen Sensoren als zweite Gruppe der Gassensoren dargestellt. Als erstes Diagramm ist der Signalverlauf einer NO-empfindlichen Zelle dargestellt. Zwischen dem Brandereignis und den sonstigen Hintergrundsignalen ist ein sehr hoher Abstand zu sehen. Das langsame Abklingen des Brandsignals läßt vermuten, daß nach dem Brand nicht alle Schwelrückstände beseitigt wurden, so daß es in der Folgezeit zu weiteren Ausgasungen kam.

Die elektrochemischen Sensoren für CO und NH<sub>3</sub> besitzen die größten Signalabstände bei diesem Testfeuer.

Um die gewonnenen Daten mit dem Verhalten der bisher üblichen Brandmeldetechnik vergleichen zu können, wurden die Meßwerte des OT-Melders ebenfalls aufgezeichnet. Der

Temperaturverlauf ist im untersten Diagramm von Abbildung 3 dargestellt und zeigt während des Brandes keinen signifikanten Anstieg. Die Rauchdichte dieses Melders ist dem untersten Diagramm von Abbildung 4 zu entnehmen. Darin ist der übliche Alarmbereich dieser Melder eingetragen. Die Alarmschwellen liegen herstellerabhängig

zwischen 3 bis 6 %/m. Deutlich zu erkennen ist eine Alarmauslösung während des Brandereignisses. In der dargestellten Woche hätte dieser Melder jedoch zusätzlich 14 weitere Alarme ausgelöst. Zu diesem Zeitpunkt war dieser Melder 3<sup>1</sup>/<sub>2</sub> Monate installiert.

Die Signale der Infrarotmeßzellen sollen hier nicht weiter dargestellt werden, da sie keinerlei charakteristisches Verhalten auf das Brandereignis zeigten. Dies liegt beim CO<sub>2</sub>-Sensor an den stark schwankenden Signalpegeln während des Betriebes. Die CO<sub>2</sub>-Konzentration ist abhängig von Lüftung und der Anzahl der Personen, die sich im Raum aufhalten. Der HC-Sensor besitzt eine zu geringe Auflösung, um Konzentrationen der einzelnen Kohlenwasserstoffe im ppm-Bereich nachweisen zu können. Andere Ereignisse, wie Freisetzung von Lösungsmitteln, treten viel stärker in Erscheinung als das Brandereignis.

## 6 Ergebnisdiskussion

Die bisher vorgestellten Ergebnisse zeigen die zeitlichen Verläufe der Sensorsignale. Um eine endgültige Aussage über die Eignung der verschiedenen Sensoren treffen zu können, müssen die Signalabstände der einzelnen Sensortypen sowie deren sensorische und technischen Eigenschaften näher betrachtet werden. Eine grafische Übersicht der Brandsignalpegel der einzelnen Sensortypen im Vergleich zum maximalen Hintergrundsignal (Basis = 1) ist Abbildung 5 zu entnehmen, wobei sich deutlich die prinzipielle Eignung beider Sensorprinzipien zeigt.

Bei Halbleitersensoren ist vor allem der erste Typ zu bevorzugen. Er zeigt einen sehr starken Leitwertanstieg auf Schwelbrände. Auch sein Ansprechverhalten auf NO läßt eine Vermutung nahelegen, daß mit ihm auch offene Flammenbrände detektiert werden können. Sein vom Hersteller spezifiziertes Verhalten auf Ozon läßt jedoch auch Probleme an warmen Sommertagen erwarten, so daß Systeme mit nur einem Halbleitersensor schwierig beherrschbar sein werden. Das Verhalten der unterschiedlichsten Halbleitersensoren wird im weiteren Verlauf des oben genannten



Projektes noch näher untersucht, wenn eine größere Anzahl verschiedener Sensoren den genormten und neu konzipierten Testfeuern ausgesetzt werden.

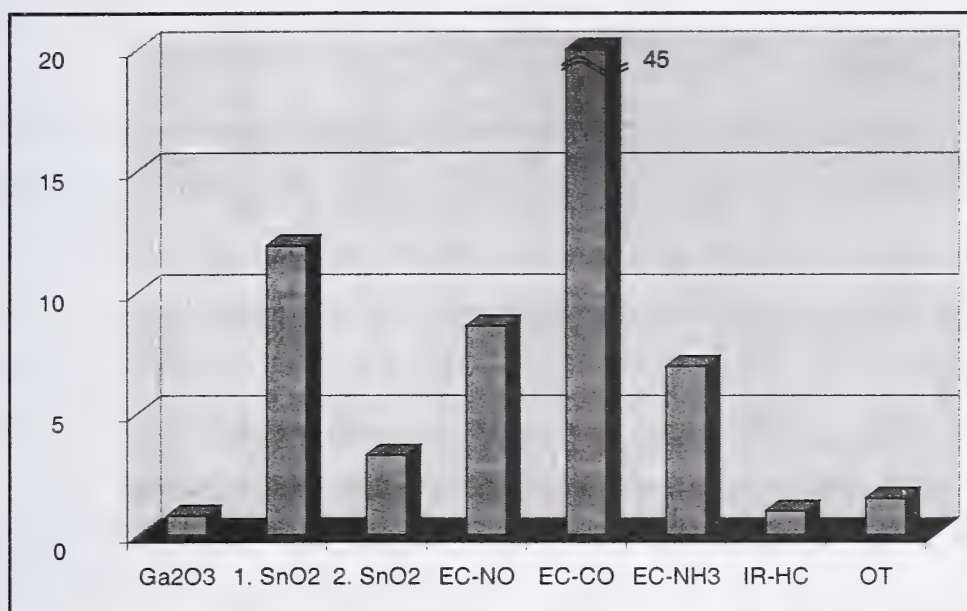


Abb. 5 – Brandsignal bezogen auf den maximalen Hintergrundpegel

Bei den elektrochemischen Zellen erweist sich eine CO-empfindliche EC-Zelle als am besten geeignet. Diese Aussage sollte jedoch nicht verallgemeinert werden, da CO ein Gas ist, das regulär bei vielen Produktionsprozessen frei wird. So zeigte sich bei einer Versuchsanordnung, die in einer Härtereie installiert war, daß ein Hintergrundpegel von knapp unterhalb des MAK-Wertes permanent vorherrscht. Beim automatischen Beschicken der Öfen kann dieser Wert kurzzeitig überschritten werden, was dem Alarmpegel des hier durchgeführten Versuchsbrandes entspricht. Desweiteren sind EC-Sensoren für dauerhaften Einsatz in Atmosphäre, die mit dem Zielgas belastet ist, eher ungeeignet. Dort wird die prinzipbedingt begrenzte Lebensdauer solcher Zellen erheblich verkürzt.

Die klimatischen Einflüsse spielen im hier beschriebenen Anwendungsfall nur eine untergeordnete Rolle, da die Luftfeuchte nur geringe Änderungen aufweist und mit einem Mittelwert von ca. 50% rel. Feuchte bzw. 15g/m<sup>3</sup> abs. Feuchte konstante Betriebsbedingungen für die Sensoren darstellt. Auch die Temperatur sollte keinen Einfluß auf das Arbeitsverhalten der Sensoren besitzen. Der Betrieb in einer geschlossenen Werkhalle läßt selbst im Winter keine für elektrochemische Sensoren kritischen Temperaturen von unter -10°C erwarten.

Auch im Sommer besitzt die Temperatur nur untergeordnete Bedeutung. Bei Temperaturen von bis zu 45°C muß dies nur bei der Wahl der Installationsorte entsprechender Brandmeldetechnik Beachtung finden, da Wärmepolster eine frühe Detektion verhindern.

Der eingesetzte optische Rauchmelder bestätigt die Erfahrungen des Betreibers mit der konventionellen Brandmeldetechnik. Fehlalarme durch Staubaufwirbelungen sind keine Seltenheit und Schwelbrände wurden bisher nur unzureichend detektiert bzw. erst nach Übergang zu einem offenen Brand erkannt.

## **7 Fazit**

Als Ergebnis der Versuchsreihe wird eine Ergänzung der bestehenden Brandmeldeanlage durch gassensorische Branddetektoren als sinnvoll erachtet.

Eine Kombination von konventionellen Rauchmeldern mit Gassensoren eliminiert deren Staubempfindlichkeit. Hierbei bieten sich insbesondere elektrochemische Sensoren für CO und NH<sub>3</sub> an. Für diesen Sensortyp spricht weiterhin die geringe Stromaufnahme, was eine Integration in bestehende Brandmeldesysteme vereinfacht. Nachteile dieser Kombination sind der relativ hohe Preis der Sensoren sowie die sehr begrenzte Lebens- bzw. Einsatzdauer. Weiterhin wird das Detektionsverhalten gegenüber Schwelbränden im Vergleich zu einem reinen Rauchmelder nicht beschleunigt.

Eine weitere Möglichkeit besteht im Einsatz sog. Schwelbrandmelder auf Basis mehrerer Halbleitergassensoren. Deren Sensorelemente sind relativ kostengünstig und besitzen eine hohe Lebensdauer. Nachteilig wirkt sich der hohe Energieverbrauch sowie die komplexe Auswertung der Sensorsignale aus.

Zur Zeit wird ein erster kommerziell erhältlicher Schwelbrandmelder mit Halbleitergassensoren [8] im Bereich der Papiermühle getestet und seine Signale im Meßsystem aufgezeichnet.

## Literaturnachweis

- [1] Pfister, G.: Detection of smoke gases by solid state sensors – A focus on research activities; Fire Safety Journal; 6 (1983); Seite 165 – 174
- [2] Linden, O.; Hölemann, H.; Research on the Suitability of Gas Sensors for fire Detections; EUSAS-Workshop No. 10, The Detection of Combustible Gases in Connection with Fire Detection; Rauischolzhausen; 1998
- [3] Kubon, Ch.; Hölemann, H.; Linden, O.; Research on the suitability of gas sensor based fire detectors for various applications; VdS-Fachtagung, Gassensorik in der Brandmeldetechnik; Köln; 2000
- [4] N.N.: Gassensoren GGS, Produktinformation und Applikationshinweise; UST Umweltsensortechnik GmbH, Geschwenda; 1998
- [5] Fleischer, M.; Seth, M.; Kohl K. D.; Meixner H.; A study of surface modification at semiconducting  $\text{Ga}_2\text{O}_3$  thin film sensors for enhancement of sensitivity and selectivity; Sensors and Actuators B – chemical; 35-36 (1996); Seite 290 ... 296
- [6] N.N.: Technical Data CO 3E 300, NO 3E 300, NH3 3E 200; SENSORIC Gesellschaft für angewandte Elektrochemie mbH; Bonn; 1998
- [7] N.N.: Datasheet – IR-Gassensor GS30; for  $\text{CO}_2$  and HC; Sensor Devices GmbH, Dortmund; <http://www.home.t-online.de/home/sensor-devices>; 1998
- [8] Petig, H.; Kelleter, J.; Schmitt, D.; Gas Sensor Fire Detector Prove Effective in Coaling Plants; Global Risk Report; Allianz Versicherungs AG; 4 (1999); Seite 19 ... 22



M. Harms, J. Goschnick

Institute for Instrumental Analysis, Karlsruhe Research Center GmbH,  
Hermann-von-Helmholtz-Platz 1, 76344 Eggenstein-Leopoldshafen,  
Germany, Phone +49-7247-822580, Fax +49-7247-824606,  
Email: michael.harms@ifia.fzk.de

R. C. Young

National Aeronautics and Space Administration, Kennedy Space Center,  
Florida 32899, USA

## **Early Detection and Distinction of Fire Gases with a Gas Sensor Microarray**

### **1. Introduction**

The necessity of gas-analytical instruments for fire detection has been discussed in the past and is widely accepted at present. Conventional fire detectors usually work on a poor information basis, incapable of identifying the nature of the fire. Therefore, false alarms are often set off as gas concentrations, smoke densities or a high air temperature are mal-interpreted. This leads to the fact that many people do not consider fire alarm systems as reliable. Moreover, false alarms cause high costs due to the security measures triggered. For these reasons much faster and more reliable detectors are needed that are based on an additional discrimination power able to distinguish between the different occasions of gas release, but on the other hand incur no more costs than a conventional instrument.

The measurement of the electrical conductivity of semi-conducting metal oxides represents one way of realizing cheap and sensitive detection of gaseous components. Provided an array of metal oxide gas sensors is used, a high discrimination power in gas analysis can be realized. Using this principle, a novel type of gas sensor microarray based on the segmentation of a monolithic metal oxide layer by a set of parallel electrodes, has been devel-

oped at the FORSCHUNGSZENTRUM KARLSRUHE, that allows a sensitive detection and discrimination of gases at a very low cost.

## **2. Detection Principle**

The principle of conductivity measurement at n-semi-conducting metal oxide fields for detection of gaseous atmospheric components has been well-known for about 40 years [1]. If a metal oxide surface is held at a temperature of some hundred degrees Celsius, adsorption and catalytic reactions of nearly all types of gases take place at the surface (see Fig. 1). The release of electrons by catalytic reactions (e.g. the oxidation of adsorbed hydrocarbons) or immobilization of conduction band electrons by adsorptive species, cause a gas specific change of the electrical conductivity of the metal oxide surface if the ambient gas composition is changed. If oxidizable gases such as methane are adsorbed on the surface, catalytic oxidation takes place, with electrons released to the conductivity band. As a result of adsorption and dissociation of gaseous oxygen molecules, negative oxygen ions are consumed during oxidation. Therefore, their level is kept low in the presence of air containing hydrocarbons or other oxidizable gases. However, if the latter disappear from the ambient atmosphere of the metal oxide surface, the level of adsorbed oxygen ions rises to saturation, causing the conductivity to drop accordingly. By different mechanisms, not only oxidizable gases can be detected, but reducible ones as well – such as  $\text{NO}_2$  and  $\text{O}_2$  - or less active gases - as  $\text{CO}_2$  [2]. Nearly all gases are detectable except for rare gases and other extremely passive gases, such as nitrogen.

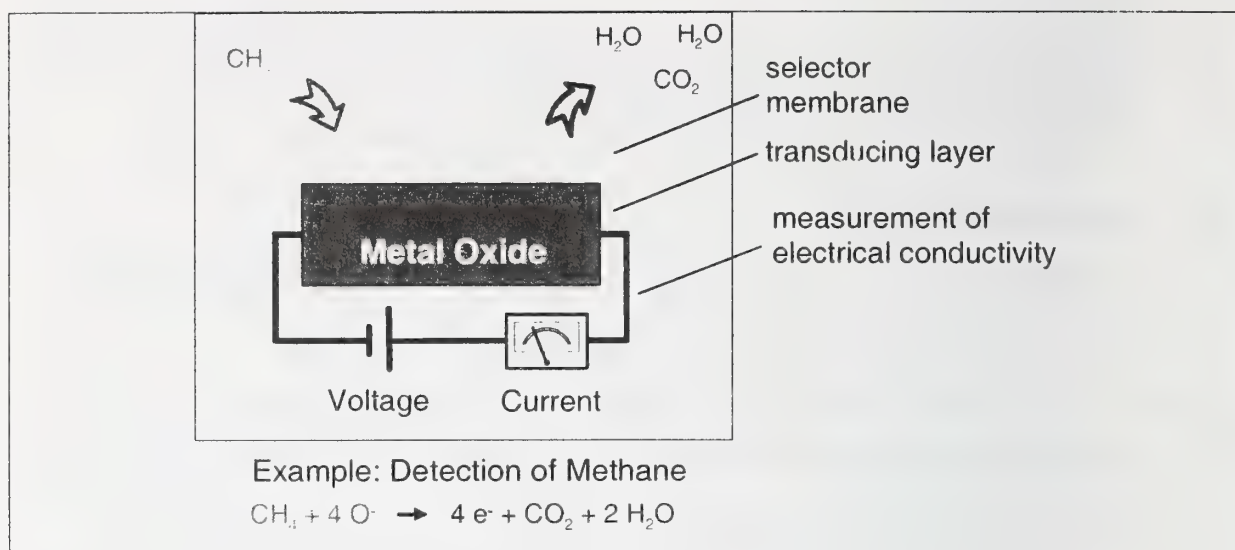


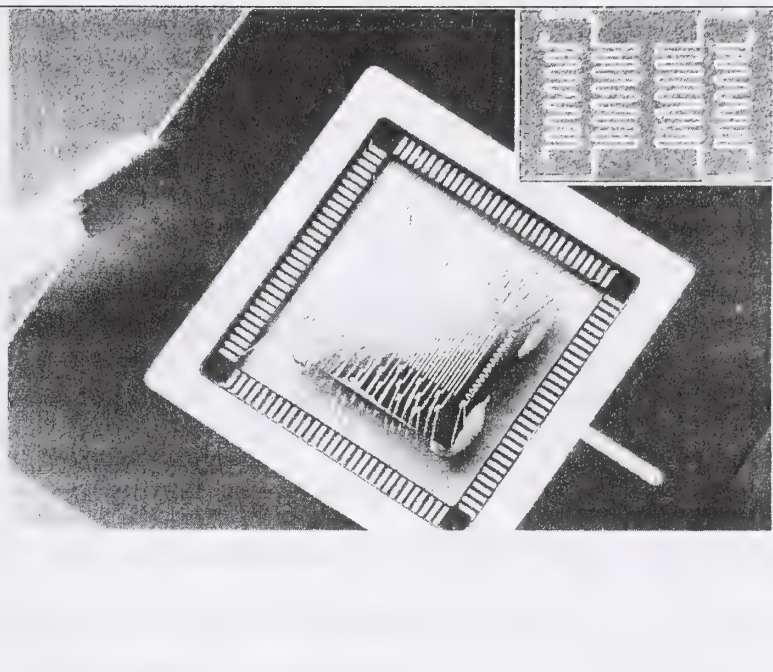
**Fig. 1:** Gas detection principle of metal oxide conductivity sensors. The detection of methane is shown as an example.

### 3. Gas Sensor Microarray

The great diversity of detectable gases can turn out to be a disadvantage for a single sensor if high selectivity for a particular atmospheric component is required. A sensor system with the ability to differentiate between gases can be set up if a multitude of different sensors is combined. Provided the sensitivity spectrum of each sensor, the so-called selectivity, is different from the other sensors of the array, exposures of the array to gases or gas ensembles result in a conductivity pattern, characteristic of the type and quantity of the gases contained in the gas mixture. The technological novelty of the microarray invented at the FORSCHUNGSZENTRUM KARLSRUHE, however, is the arrangement and differentiation between the gas sensors. Contrary to conventional macroarrays and other gas sensor microsystems, a single monolithic metal oxide film alone forms the basis of the whole array. This film is separated into 38 sensor segments by parallel electrode strips to measure the electrical conductivity of the individual segments [3]. The necessary operation temperature (usually between 200°C and 400°C) is provided by four meandering heating elements, placed at the reverse side of the chip (see Fig. 2). The heating power is controlled by two platinum thermoresistors, placed on the upper side of the chip. The whole array is coated with a permeable  $\text{SiO}_2$  layer of variable thickness across the 38 sensor segments.



**Fig. 2:** Gas sensor microarray mounted in its housing. The front side consists of the metal oxide detector field, separated into 38 sensor elements by 39 electrode strips. The reverse side carries four separate heating elements (on the upper right side).



#### 4. Gradient Technique

The gradient technique serves to differentiate gas detection selectivity via the 38 individual sensor segments. The thickness of the ultra-thin gas-permeable  $\text{SiO}_2$  membrane layer deposited on top of the metal oxide film varies across the array (s. Fig. 3). Additionally, a controlled temperature gradient, e.g. of 50 K, is maintained across the array. Depending on the nature of the gases, due to diffusion through the membrane and the warmth caused by gas reactions at the metal oxide interface, gas detection selectivity is gradually modified from sensor segment to sensor segment. Therefore, the exposure to single gases or gas ensembles (like odors) cause characteristic conductivity patterns at this gradient microarray. The dependence of the conductivity pattern on the type and quantity of ambient gases allows gas discrimination and quantification.

Hence, this gradient microarray can be applied to realize an electronic nose system at a low cost: the Karlsruhe Micro Nose (KAMINA). Micro-fabrication is uncomplicated and thus inexpensive, especially thanks to the simple but high level integration of the sensor elements into the gradient

array structure. Further functional advantages are reliability, stability and sensitivity of the gas-analytical performance.

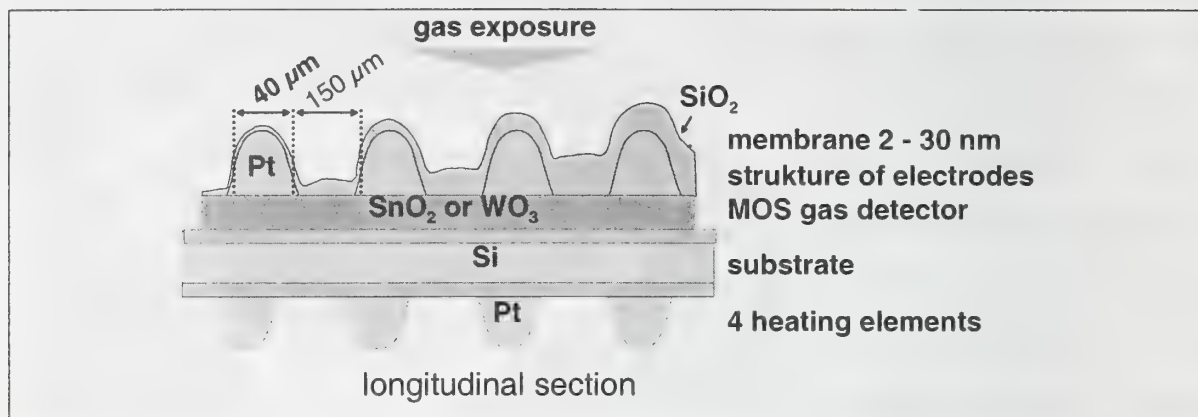


**Fig. 3:** Longitudinal section of the microarray. A  $\text{SiO}_2$ -membrane of a few nanometer. Thickness covers the metal oxide layer including the electrode structure. The thickness of the membrane varies across the sensor array in order to differentiate between the selectivity of the individual sensor segments.

## 5. Experimental

In the first stage of the fire detection study, two different kinds of microarrays were tested using defined concentrations of fire relevant gases. Representing typical components of fire gases, benzene, formaldehyde, tetrafluoromethane, hydrogen cyanide, and carbon monoxide were chosen as test gases. Two types of microarray chips were used in order to determine the most appropriate one for this kind of application: one was coated with tin dioxide doped by 1 % platinum (SP chip) and the other with tungsten trioxide (WO chip). Furthermore, the best operation temperature for the microarray was determined. In this stage, gas concentrations in the range of 1 – 100 ppm were used. The concentrations were set by a computer-controlled mixing system, producing defined pulses of test gases alternating with clean air at a r. h. of 60 %. The signal response to the test exposures was used to determine the analytical performance of the microarray chips including sensitivity, detection limits, and response times. The gas concentrations were

checked by applying conventional analytical methods (e.g. PID, FTIR). The experiments were repeated four weeks later using the selected chip with its optimal operation temperature in order to determine long time stability. Gas concentrations in the range of 0.5 – 250 ppm were then used. Additionally, the gas discrimination power was tested using the standard pattern recognition algorithms Principal Component Analysis (PCA) and Linear Discrimination Analysis (LDA). Signal reproducibility was examined in an experiment exposing the microarray to five gas pulses of 10 ppm. Furthermore, the influence of changing humidity on the microarray was tested.

The studies were completed by practical tests using the KAMINA. Several materials were burnt in a furnace and the gases formed were examined. In addition to response behavior, possibilities were investigated of distinguishing between different burning materials. In another experiment, the ability was tested to differentiate between solvents and the gases of overheated wire insulation. Furthermore, the system was trained to distinguish between fire gases and diesel engine exhaust.

## **6. Results and Discussion**

### **6.1 Microarray test with defined single gas exposures**

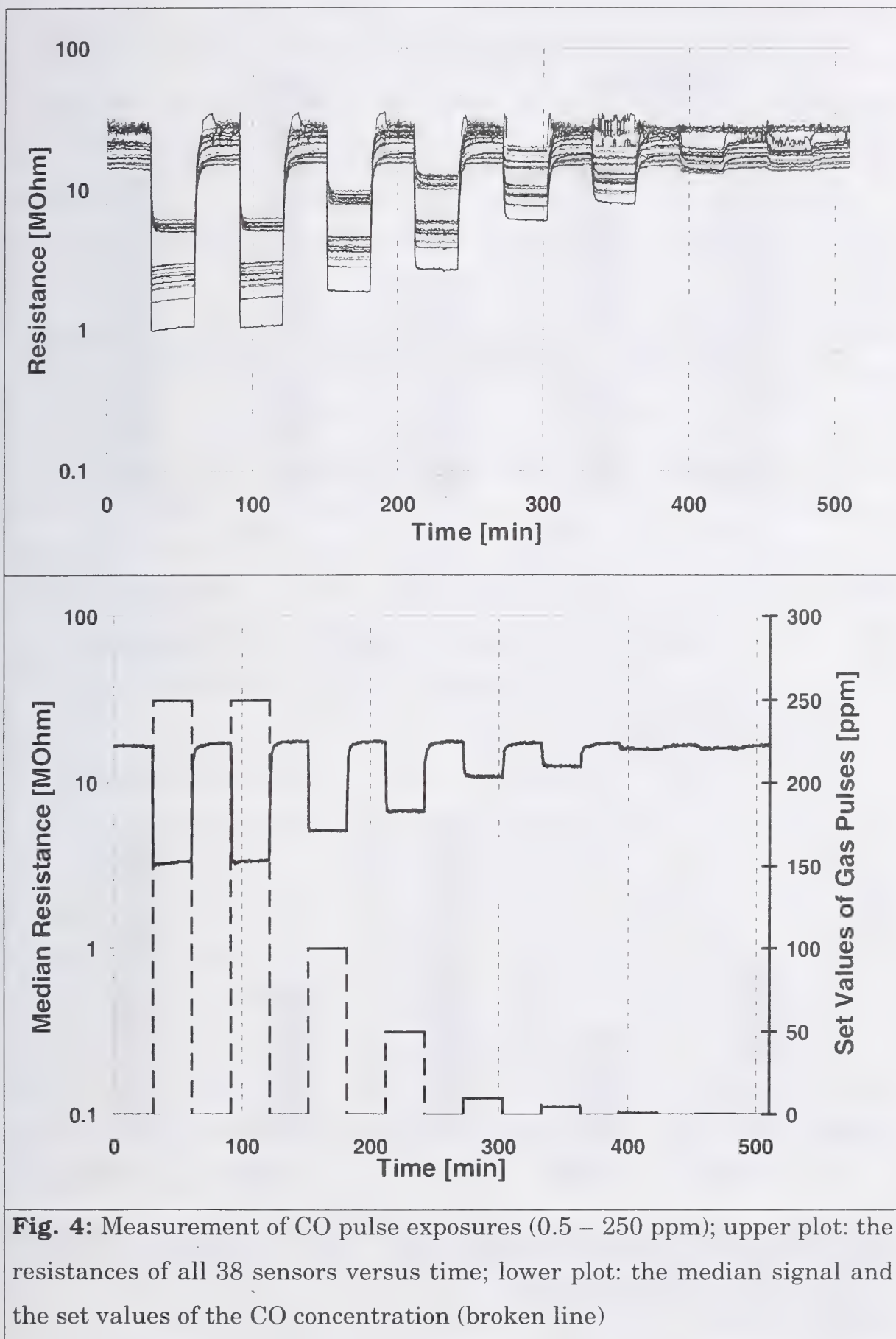
Measurements of the microarray's response to single model gas exposures showed that the SP chip was the most appropriate microarray for fire gas analysis. The optimal temperature span for chip operation turned out to be 200 – 250 °C. The following results have been achieved using SP chips.

Fig. 4 shows the resistances of all 38 elements versus the elapsed time or the median in a typical pulse exposure experiment. In this example, the gas sensor microarray was tested with pulse exposures of CO concentrations in the range of 0.5 to 250 ppm. During the time in between the testing gas pulses, the microarray was exposed to clean humid air of 60 % r. h., with the sensor response immediately following the rising CO concentration. The  $t_{90}$  response times were usually below 1 min. Using the KAMINA, response



times of a few seconds are possible. As contrary to conventional laboratory electronics, the KAMINA has an output rate of 1 signal per second. A sensor signal for 0.5 ppm CO was produced.

The signal  $S$  is defined as the relative conductivity change with respect to the reference gas (clean humid air)  $S = [R_o / R] - 1$  with  $R_o$  = reference resistance. Fig. 5 shows the median signal of all sensor elements. It can clearly be seen that the median signals of all gases (formaldehyde, benzene, tetrafluoro methane, hydrogen cyanide, carbon monoxide) are above the significance level, which is defined as triple noise level. Moreover, the comparison of the signal from the first test to that of a repeated test (one months later) only shows a slight decrease of the sensor response. This means sensor stability is reasonably good. Moreover, separate long term investigations with alcohol exposures have shown that this kind of sensitivity loss only occurs during the first 100 days after fabrication, while later sensitivity nearly remains constant (it was tested up to 400 days).



**Fig. 4:** Measurement of CO pulse exposures (0.5 – 250 ppm); upper plot: the resistances of all 38 sensors versus time; lower plot: the median signal and the set values of the CO concentration (broken line)

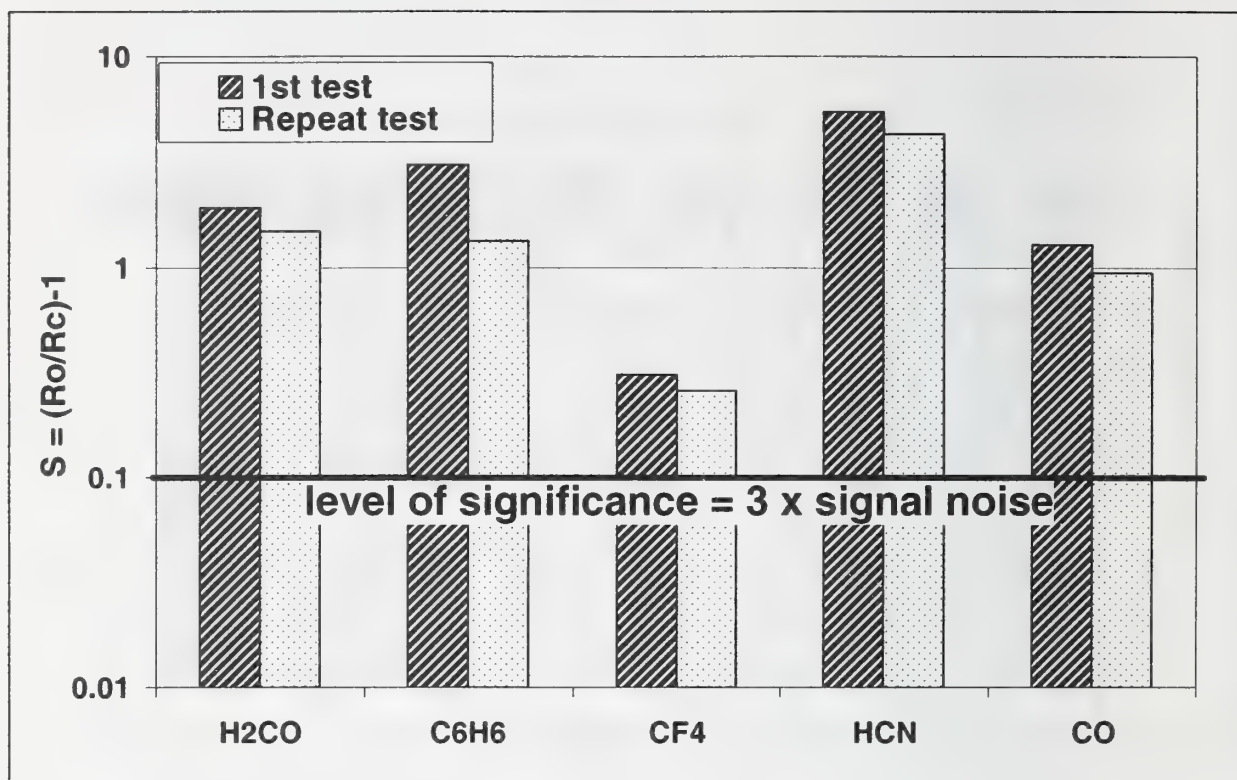


**Fig. 5:** Median signal of the SP chip ( $T = 200 - 250\text{ }^{\circ}\text{C}$ , gas concentration 10 ppm); comparison of the 1<sup>st</sup> to a repeated test after 1 month

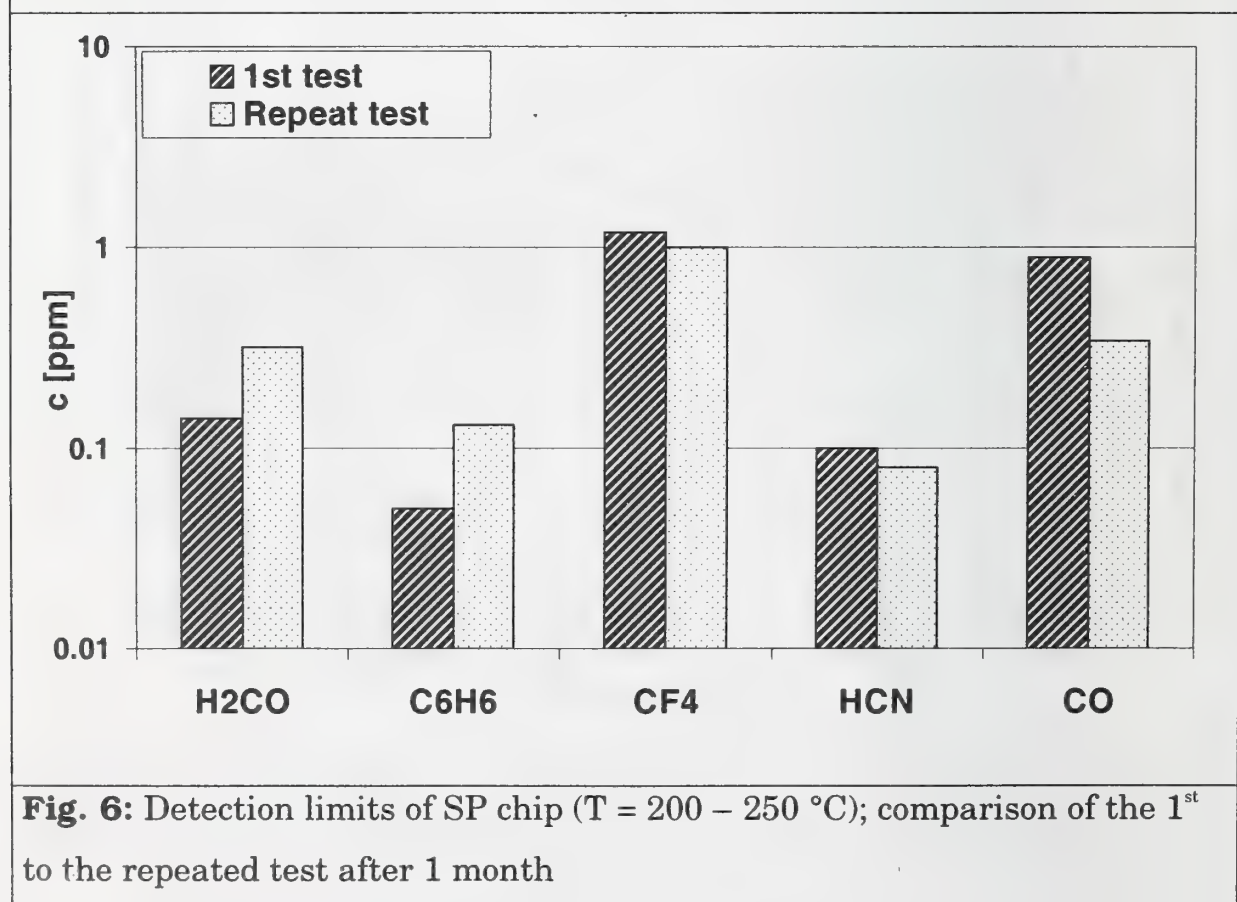


**Fig. 6:** Detection limits of SP chip ( $T = 200 - 250\text{ }^{\circ}\text{C}$ ); comparison of the 1<sup>st</sup> to the repeated test after 1 month



Furthermore, reproducibility was examined measuring sequences of five 10 ppm pulses for every gas. The mean deviation of the sensor signal was 3.6 %, at a maximum of 6 %. No cross sensitivity to humidity could be detected in the range of 40 –90 % r. h. Only a statistical scatter of the median signal with a standard deviation of 8 % was measured in the examined humidity range.

Fig. 6 shows the detection limits of the test gases. The detection limit of  $\text{CF}_4$  was 1 ppm as  $\text{CF}_4$  is less active and only the adsorption of the molecule established a change of the metal oxide conductivity. All other detection limits were far below 1 ppm. Especially hydrogen cyanide could be detected very easily. Repeated tests showed that the detection limits mostly remained constant: the detection limits of benzene and formaldehyde were a little higher than before, whereas the detection limits of  $\text{CF}_4$ , HCN, and CO were even slightly lower. These results again stand for good long time stability.

## 6.2 Distinction between different burning materials

The most important feature of an intelligent electronic nose system, as the gradient microarray, is the ability to distinguish between various kinds of gases. Therefore any difference in the composition of the gas ensemble released by different kinds of burning materials should cause the signal pattern of the microarray to respond in a characteristic way according to the burning material. Even the heat-up phase before burning should give rise to a characteristic signal pattern according to the specificity of the gas. However, the spreading of the fire changes the composition and the temperature of the burning materials which in return results in a continuous variation of the fire gases. Nevertheless, the signal inventory of the microarray obtained from real fire gases was examined in terms of its significance of discrimination of burning materials.

The signal patterns of the microarray consisting of resistances normalized “to the signal median” were examined by an LDA model. In Fig. 7 the resulting LDA diagram clearly depicts separate fields of clean air, fire gases

from wool and PVC. Fire gases from wood, PE, PS and PU form a further field, which is separate from the other ones. Thus, first of all the occurrence of fire gases can be clearly distinguished from clean air and it does seem possible to make predictions about the types of burning materials with the help of the microarray. The spread of the signals within their cluster is due to the pattern variation in the course of a burning process. In all fire experiments the microarray responded to the gases within a few seconds only.

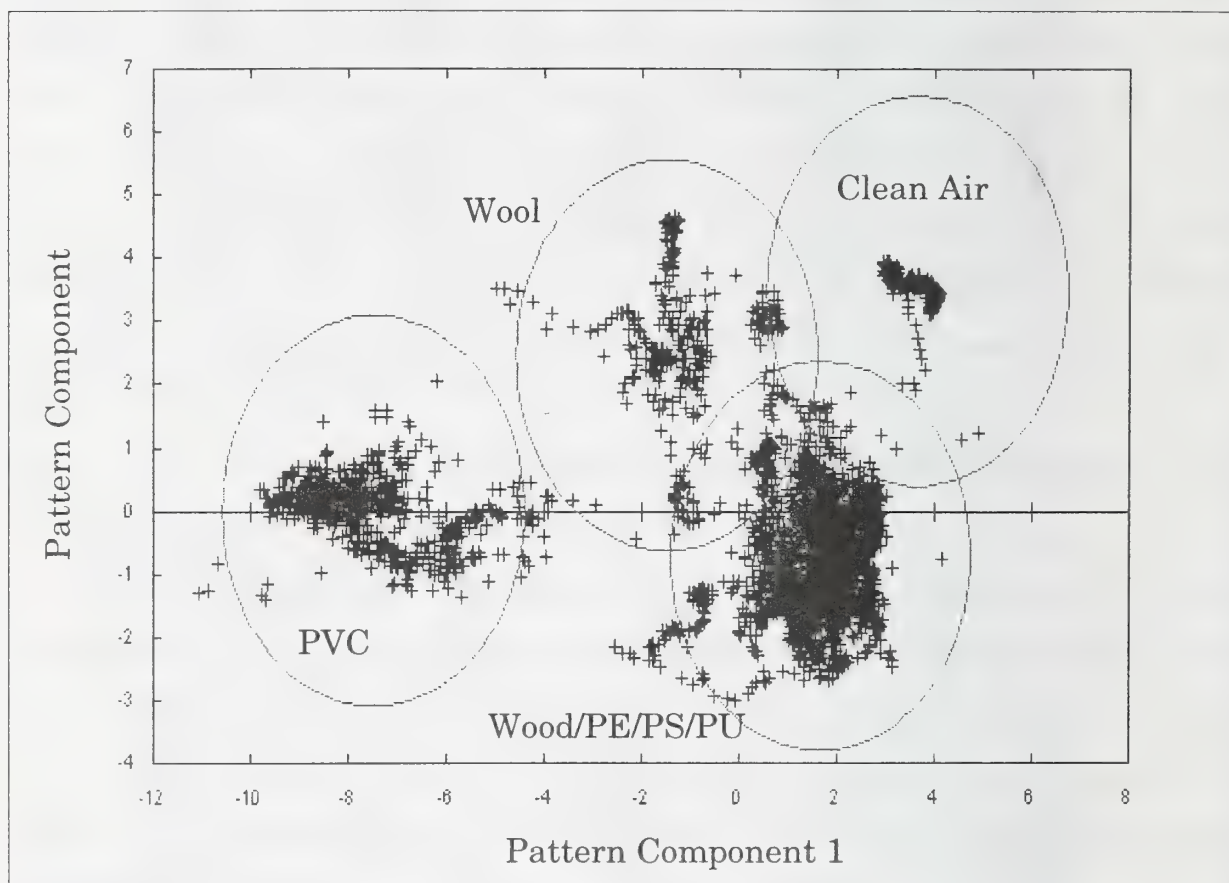


**Fig. 7:** LDA of the signal inventory obtained while the microarray was exposed to real fire gas. The resistances were normalized to the median signal. Discrimination between fire gases of different burning materials and clean air is attain to high extent (PE: polyethylene, PS: polystyrene, PU: polyurethane, PVC: polyvinyl chloride). A gradient microarray with 38 sensor segments based on Pt-doped  $\text{SnO}_2$  was used for the measurement. The surface temperature of the array chip was hold at 250 – 300 °C. The area limits describe a confidence range of 95 %.

### **6.3 Distinction between solvents and overheated wire insulation**

An important feature of a fire detector is its selectivity in terms of recognition of fire events, thus preventing false alarms caused by other sources that emit solvent vapors, such as cleaning processes. Fig. 8 shows the result of a test carried out with different kinds of overheated wire insulation as they could occur in pre-fire situations and a selection of solvents. The microarray very quickly responded to every single sample. By using the signal pattern evaluation technique of an LDA, not only differentiating between the classes fire gases and solvents but also distinguishing between individual solvents and insulation materials became possible. Hence, a reliable detection of overheated wire insulation is feasible. However, more data has to be collected from pre-fire situations and situations in which there is no danger of fire, but similar gas components are in the air. Although the gradient microarray hardware already provides a sufficient gas discrimination power, a broad data base is necessary to design appropriate recognition of signal patterns, ensuring a reliable detection of pre-fire situations.



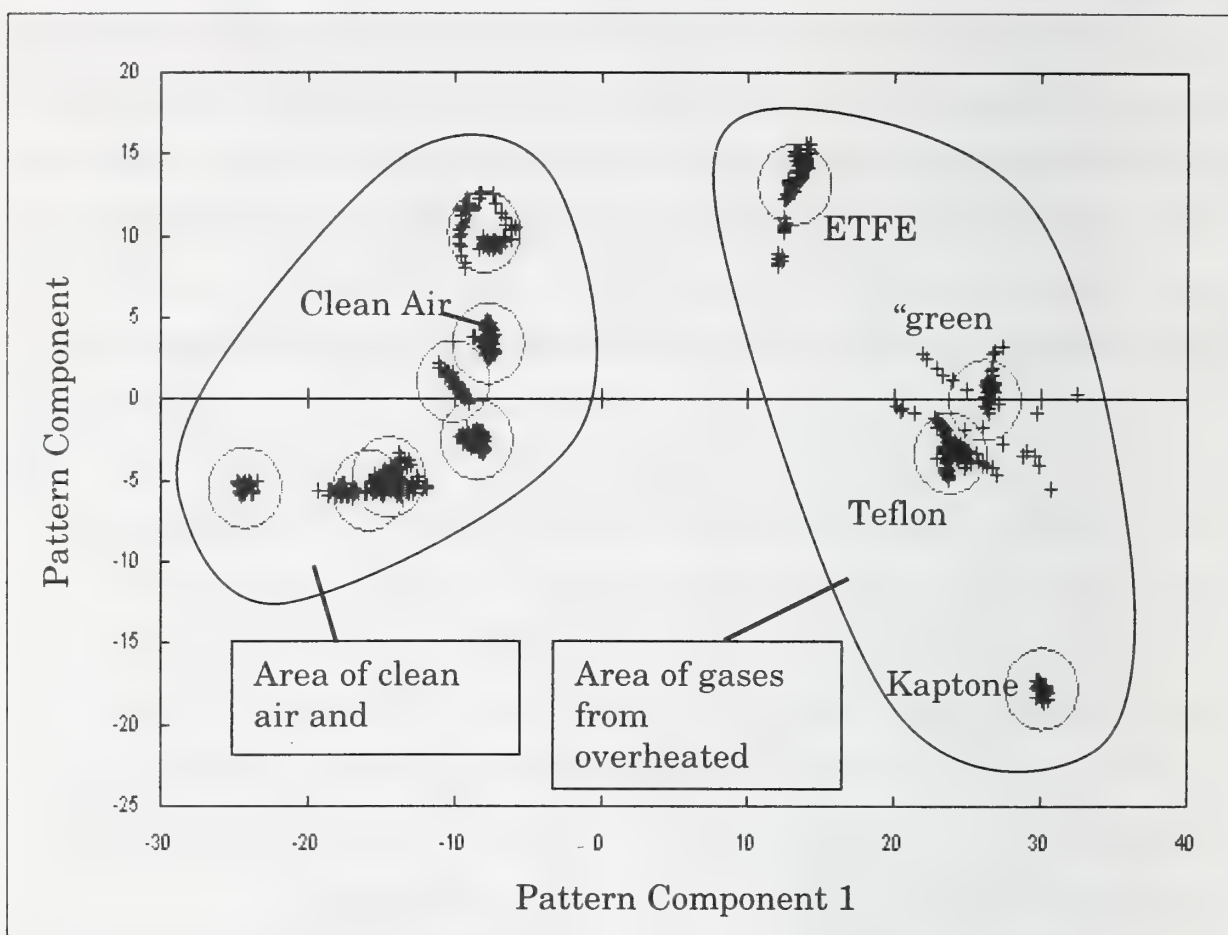


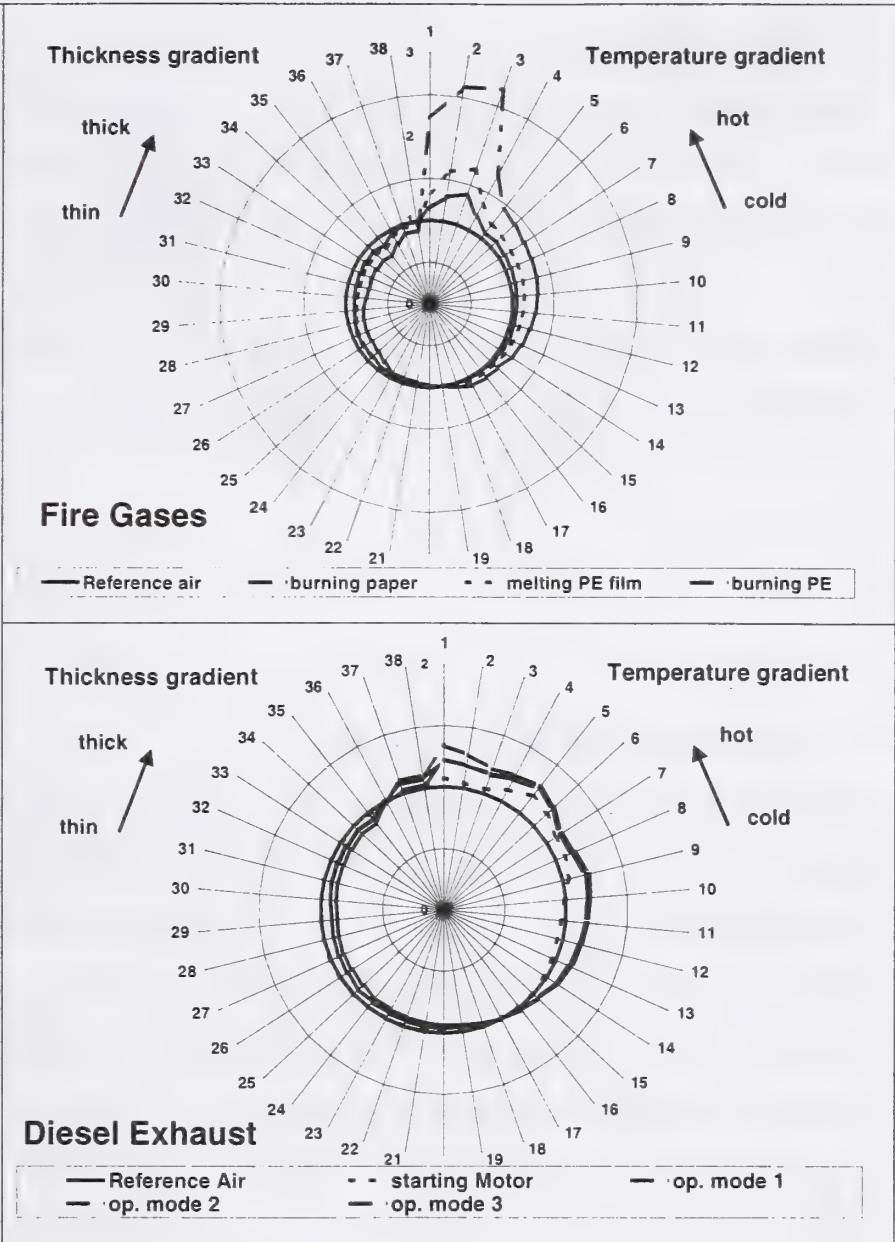
**Fig. 8:** Distinction between clean air, solvents and overheated wire insulation in an LDA diagram; solvents (isopropanole, ethanole, xylene, toluene, acetone, WD40) are clearly depicted separately from pre-fire gases of hot wires mantled with kaptone, fluorine-containing and unknown materials. A gradient microarray based on Pt-doped  $\text{SnO}_2$  was used for measurement. Its temperature was kept at 250 - 300 °C. The area limits describe a confidence range of 95 %.

#### 6.4 Distinction between fire gases and diesel exhaust

A deficiency of conventional fire detectors is false alarm set off by particle contaminated exhaust gases of engines, e.g. diesel engines. This problem was dealt with in another test. The following signal patterns (s. Fig. 9) were produced during measurements of the exhaust of a diesel engine and of gases from paper and polyethylene fire.

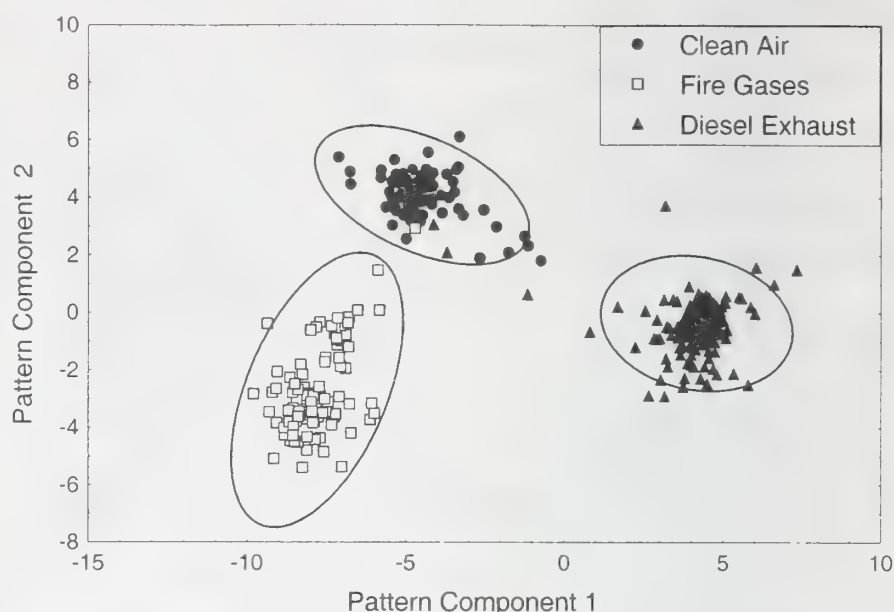
**Fig. 9:** Radar plots of fire gases and diesel exhaust signal patterns, normalized by the median signal.

The lower plot shows the signal patterns resulting from measurements of different operation modes of the diesel engine.



From these simple radar plots the difference between the patterns can be told. Accordingly, a corresponding LDA (s. Fig. 10). shows clear separate fields representing clean air and the two gas ensembles caused by burning materials and the output of a diesel engine.

**Fig. 10:** Result of LDA to distinguish between fire gases and diesel exhaust based on the data of fig. 9.



## 7. Summary and Conclusions

Typical fire gases were sensitively detected in laboratory tests on defined conditions with a gas sensor microarray equipped with 38 sensor segments based on platinum-doped tin dioxide. The determined detection limits were 1 ppm for CF<sub>4</sub> and far below 1 ppm for CO, hydrogen cyanide, benzene and formaldehyde. All these model gases could be clearly distinguished according to their signal patterns. Furthermore, the microarray showed very short response times within the range of a few seconds only. In several practical tests with fire gases or precursor gases of fires, the gas discrimination power of the microarray was tested, namely its signal pattern results caused by the gradient differentiation of the array's sensor segments were checked. Possible interfering gases for the detection of pre-fire and fire gases, such as solvents or diesel exhaust, could reliably be distinguished from other true fire gases. Furthermore gas discrimination of the gradient microarray has proved to be successful for discrimination between different burning materials. Hence, the gas sensor microarray with its unique sensor element gradient differentiation offers a promising basis for development of a gas analytical fire detector.



## 8. References

- [1] Göpel, W. and Schierbaum, K.-D., Chemical and Biochemical Sensors. in: Göpel, W., Jones, T. A., Kleitz, M., Lundström, J. and Seiyama, T., Sensors, Vol. 2, VCH, Weinheim, New York, 1991
- [2] Madou, M. J. and Morrison, S. R., Chemical sensing with solid state devices. Academic Press, Inc. (London) Ltd., 1989
- [3] Althainz, P., Goschnick, J., Ehrmann, S. and Ache, H. J., Multisensor microsystem for contaminants in air. Sensors and Actuators B 1996; 33: 72-76

Martin Berentsen, Thomas Kaiser  
Fachbereich 9, Fachgebiet Nachrichtentechnik  
Gerhard-Mercator-Universität, Germany  
Bismarckstrasse 81, 47048 Duisburg  
e-mail: berentsen@sent5.uni-duisburg.de, th.kaiser@uni-duisburg.de

## **FIRE LOCATION ESTIMATION USING TEMPERATURE SENSOR ARRAYS**

### **1. ABSTRACT**

This paper reconsiders how to estimate the location of a fire in a closed room with an array of temperature sensors. The very important question is: "Where is a fire located?". The answer is of interest for research on fire detection and for a deeper understanding of the case of fire for prevention and extinguishing. The answer to this question can be given with two small arrays of temperature sensors. Here, "small" means in the same dimensions like a standard fire detector. The data signal processing for the fire location estimation can be done by a digital signal processor (DSP). It seems to be possible to give a rough fire location estimation with such an array in the same time which is required by a standard fire detector to give a fire alarm.

### **2. INTRODUCTION**

One of the main concerns in fire research is to detect a fire in a short time with a low false alarm rate. It is also of interest *where* a fire is located. For example two scenarios will be given. First an automatic fire extinguishing in a sensible area like a ware house or a computer room. The damage in such an area can be minimized with knowledge of the fire location and a more exact automatic extinguishing can be done. Hence, the cost can be reduced. The second scenario is a fire extinguishing by a fireman in a smoky room. Knowledge of the fire location before entering the room minimizes the extinguishing time. It can also minimize the danger for his life while entering a room with such deadly smoke.

Now we take a look at a fire in an early stage. The hot gases are rising up from the fire place near the floor to the ceiling shown in figure 1 a). Under the ceiling they propagate in a circular shapes as shown in figure 1 b).

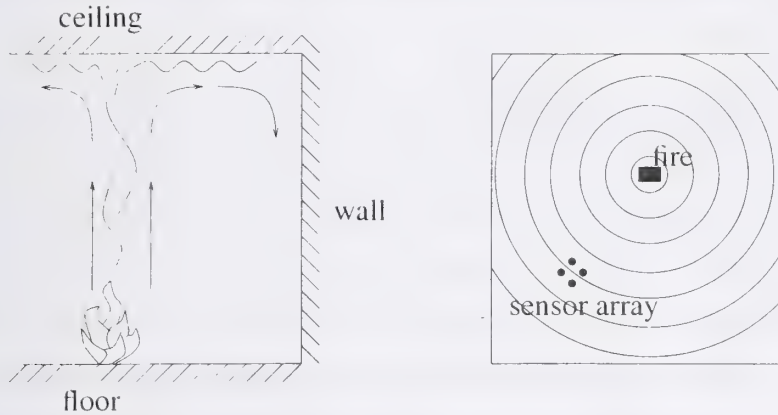


Figure 1: a) fire in a closed room (sideview) b) circular wave shapes (topview)

Due to more or less strong turbulences and interferences caused by the rooms walls the shapes will not be perfectly circular. If we take now an average in time we expect an almost circular shape. This observation is fundamental for the following idea. However, these circular behavior seems to be time limited. When a fire grows up, the hot gases become more turbulent, and the propagation becomes more and more non-circular shapes.

Here, our basic approach. For the following considerations some boundary conditions must be fulfilled:

- The ceiling should be flat with a low heat conductivity.
- The flow current velocity  $\vec{v}$  of the hot gases should be nearly constant under the ceiling in the early state of fire.
- The fire is near the floor level
- The walls are of the same temperature.
- The fire is not located directly at a wall.
- Other air currents, e.g. caused by a heating system, should be neglected.



These assumptions are needed to validate the waveform as of almost circular shape. With these assumption the hot gases grow up vertically from the fire and reach the ceiling with the shortest distance. From this point the circular shapes starts under a nearly flat ceiling. In this case the estimation can be reduced from a three dimensional problem into a two dimensional problem.

In the following always an array of four sensors is used. The sensors are arranged in a quadratic way and located at the points  $(x_n, y_n)$ ,  $n = 1(1)4$  with a distance  $d = 5\text{cm}$ . The active part of the sensor (diameter  $0.13\text{mm}$ ) is mounted  $8\text{mm}$  under the ceiling. These parameters differs from earlier publications on this topic [3], [4], [7]. Modern ceramical NTC resistors are used in a temperature range from  $0^\circ\text{C}$  up to more then  $150^\circ\text{C}$ . Thus, a high dynamic of these sensors is required. The used sensors have a low response time around  $0.11\text{s}$  in air [8]. Also a low tolerance is required, which is guaranteed here by careful selection.

### 3. THEORETICAL FUNDAMENTALS

The propagation of the hot gases under the ceiling can be seen as a temperature wavefront  $T(x, y, t)$  with  $(x_0, y_0)$  as the location of the fire. With a flat ceiling a radius  $r$  can be defined as

$$r = (x - x_0)^2 + (y - y_0)^2.$$

Since the wavefront  $T(x, y, t)$  is assumed to be of a circular shape it is only a function of the radius and time. Hence, we use the notation  $T(r, t)$  instead of  $T(x, y, t)$  in the following. For a sensor on a fixed point  $(x_n, y_n)$  the temperature function  $T(t)|_{r_n}$  is only a function of time. Sampling is required for the data processing. The frequencies in the case of fire are limited up to  $\approx 10\text{Hz}$  [2], so that we assumed to use a sample frequency of  $f_A = 20\text{Hz}$ . So the temperature samples from  $b$  sensors at the location  $(x_n, y_n)$  can be seen as

$$T_n(k) = S_n(k) + N_n(k), \quad n = 1(1)b$$

where  $S_n(k)$  is interpreted as a deterministic signal caused by the fire and  $N_n(k)$  as noise caused by the unavoidable turbulences. If the range  $r$  is large between the fire place projection under the ceiling  $(x_0, y_0)$  and the location of the sensor array  $(x_n, y_n)$ , the temperature wave under the ceiling can be seen as a quasi planar wavefront from the perspective of the array with the dimensions  $d \times d$  and  $d \ll r$ .

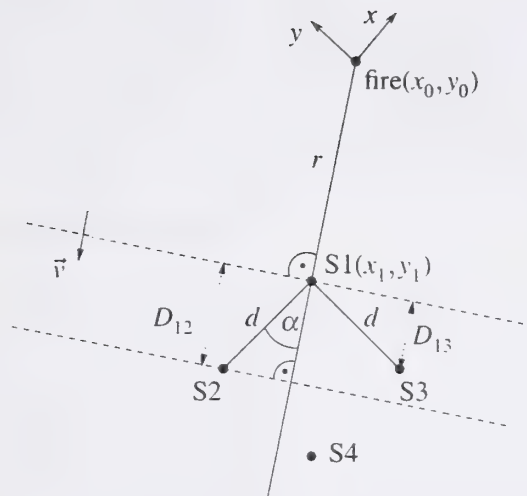


Figure 2: geometrical arrangement of the sensor array

In figure 2 the sensor array with sensors  $S_n, n = 1(1)4$  is shown in the distance  $r$  from the fire place projection under the ceiling. The wavefront is shown as quasi planar with the velocity  $\vec{v}$ .

Figure 2 also shows, that with knowledge of the geometric order of the sensors in the array and the assumption of a quasi planar wavefront with the velocity  $\vec{v}$  first reaches the sensor S1, then S3, then S2 and last S4. With this model a time delay can be defined between S1 and S2 as  $D_{12}$  and also  $D_{13}$  as delay between S1 and S3.

With knowledge of this coherence and our signal model the problem of estimation the direction can be reduced using the geometry of the sensor array to a time delay estimation problem

$$T_1(k) = S(k) + N_1(k)$$

$$T_n(k) = \alpha_n S(k - k_{1n}) + N_n(k), \quad n \neq 1$$

with the delays  $k_{1n}$ . The deterministic signal  $S(k) = S_1(k)$  as a part of  $T_1(k)$  is interpreted as a time delayed signal  $S(k - k_{1n})$  also in  $T_n(k), n \neq 1$ .

We have investigated several signal processing algorithms known on time delay estimation, e.g. the PATH-algorithm, the SCC-algorithm, the SCOT-algorithm, the WIENER PROCESSOR, the ROTH PROCESSOR, the ML-algorithm and the Adaptive Time Delay Estimation method. For details see [9]. In the following only the SCC-algorithm (Simple

Cross Correlation) is explained to understand the principles of time delay estimation. The cross correlation between the first and the  $n$  sensor output is

$$R_{1n}(\kappa) = E\{T_1(k)T_n(k + \kappa)\}, \quad n = 2(1)4.$$

By the assumption of uncorrelated noise  $N_n(k)$  in the signal model, it can be written as

$$R_{1n}(\kappa) = E\{S(k)S(k - k_{1n} + \kappa)\}, \quad n = 2(1)4.$$

The maximum of  $R_{1n}(\kappa)$  occurs for  $\kappa = k_{1n}$ , since the argument takes for arbitrary  $s(k)$  a positive value. For estimation of  $k_{1n}$  now only the cross correlation has to be estimated and its maximum has to be found. Normally the estimation  $\hat{R}_{1n}(\kappa, k)$  is given by averaging the temperature sample vectors from  $T_1(k)$  and  $T_n(k)$ .

$$\hat{R}_{1n}(\kappa, k) = \frac{1}{L} \sum_{l=m}^{L+m-a} T_1(l)T_n(l + \kappa), \quad n = 2(1)4, \quad k = \frac{m}{M},$$

$$m = 0(M)K - L, \quad \kappa = -\kappa_{max}(1)\kappa_{max}.$$

In the following the hat indicates an estimation. The in-stationarity of the signals is taken into account by the time dependence  $k = \frac{m}{M}$  of  $\hat{R}_{1n}(\kappa, k)$ . The measured signals are composed to non overlapping blocks with the length  $L$ . The estimation is only calculated each  $M$ th time.  $\kappa_{max}$  should be not too large to minimize required calculation power.

After knowing the estimated time delays, we just need the relations between these delays and the parameters  $r$ ,  $\alpha$  and  $\vec{v}$ . We have assumed that the fire is far away from the array, so that  $r \gg d$  and we can see them as quasi planar wavefronts. So the velocity vector can be seen as

$$|\vec{v}| \frac{k_{12}}{f_a} = d \cos \alpha$$

$$|\vec{v}| \frac{k_{13}}{f_a} = d \sin \alpha.$$

So the parameters  $\alpha$  and  $\vec{v}$  can be written as

$$\alpha = \arctan\left(\frac{k_{13}}{k_{12}}\right)$$

$$|\vec{v}| = f_a \frac{d \cos \alpha}{k_{12}}.$$

Actually the fourth sensor  $S_4$  is unused, so it can be used to estimate another pair of delay times. These delay times can be also used to calculate an estimated angle and velocity



to verify and also to improve the first calculation. For the location estimation a second estimated angle information is required. In our case we place another angle estimation unit in the same observation room. With these two estimated angles  $\alpha_1$  and  $\alpha_2$  a location of the fire can be calculated.

#### 4. FIRE EXPERIMENTS

All fire experiments were carried out in the fire detection laboratory of the GERHARD-MERCATOR-University Duisburg. The fire room of the laboratory has a ground size of  $10.5\text{m} \times 9\text{m}$  and the variable ceiling (it can be varied from 2.87m up to 6.57m) was fixed at 3.40m. Some first experiments [3],[4] with spirit fire were carried out to test out the generic work of the location estimation algorithm. After an optimizing process for some boundary conditions on the algorithm parameters seven kinds of test fire were done. The test fires are listed in table 1 by name, number and burning material.

TF1	Open wood fire (beechwood)
TF2	Smoldering (pyrolysis) wood fire (beechwood)
TF3	Glowing smoldering fire (cotton)
TF4	Flaming plastic fire (polyurethane)
TF5	Flaming liquid fire (n-Heptane)
TF6	flaming liquid fire (metylated spirit)
TF7	Flaming liquid fire (dekalene)

Table 1: Test fires by name and material

To verify the different algorithms with test fires a fixed angle between the sensor arrays and the fire location was used. For the fire experiments two sensor arrays are mounted under the ceiling. The physical parameters are  $\alpha_1 = 45^\circ$ ,  $\alpha_2 = 45^\circ$ ,  $r_1 = 3\text{m}$  and  $r_2 = 3\text{m}$ , the fire was always located at  $(x_0, y_0) = (0, 0)$ .

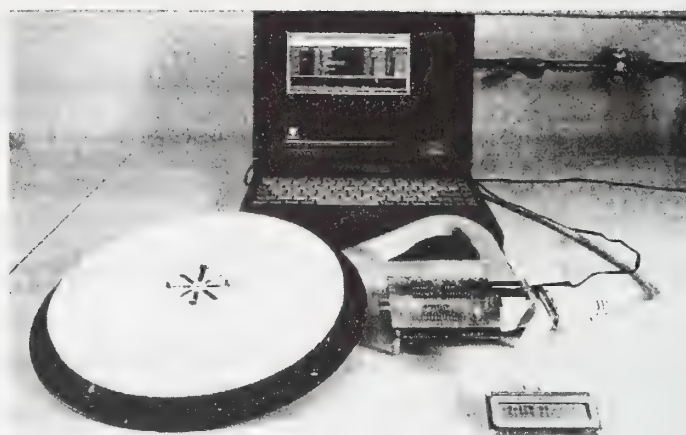


Figure 3: Sensor array, signal processor and PC

The measurement system, shown in figure 3, uses a disc with a diameter of 23cm. In its center the temperature array containing four sensors is placed. The figure also shows the used Digital Signal Processor (DSP) board, liquid crystal display and data acquisition computer. For a detector solution with DSP we minimized the required calculation power and used memory. The sample rate was shifted down to  $f_A = 20$  Hz. The observation window length  $L$  was minimized to 40 samples. All shown angle estimations are calculated with the *SCC*-algorithm. The reason for this selection was the first portation of this algorithm into a DSP for an automatic angle estimator. In [9] is shown that the error between the *SCC*-algorithm and other, more calculation intensive algorithms is small enough for a first solution.

To verify the results from the DSP solution an additional computer-based simulation with the algorithm under test has been done. The estimation algorithms has been tested with all of the listed kinds of test fires. But exemplified by three of these fires should be shown that the estimation works. Only the first 80 seconds of a test fire are shown in the following figures, because the goal of the estimation was to give a first fire location estimation at the time of fire alarm. For example the detection time for a TF6 and an European standard temperature detectors of class A1 is around 60 seconds. The detector must give an alarm after the room temperature increases by 29° Celsius. The alarm here is given by a temperature of 50° Celsius depending on a room temperature of 21° Celsius before the fire starts.

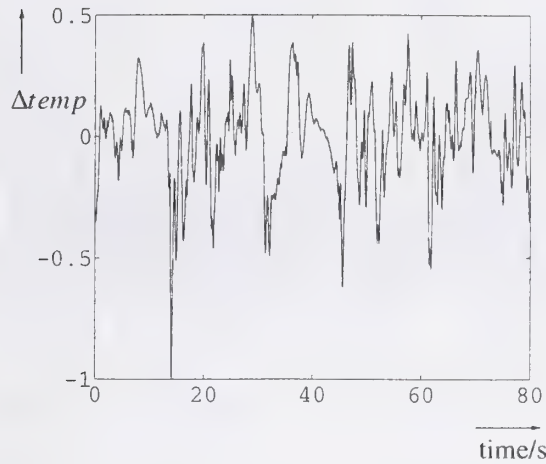


Figure 4: TF2 temperature data

Figure 4 shows the temperature curve from a sensor which is typical for smoldering fire type TF2. This signal and the following signals shown in figure 6 and figure 8 showed no temperature dc offset, so they can be interpreted as shown after a high pass filtering. These signals includes the lightning of the fire in their first ten seconds.

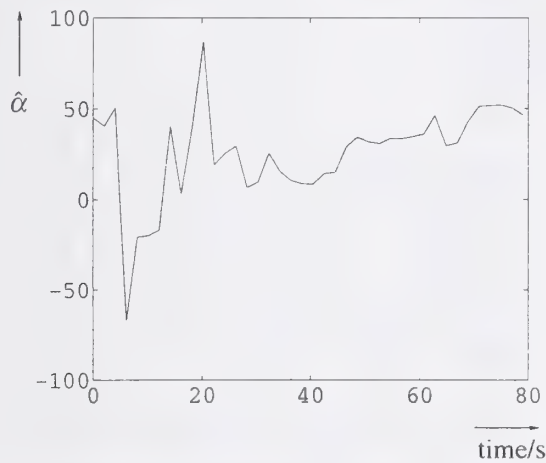


Figure 5: Estimated angle  $\hat{\alpha}$  for a TF2

The figures 5, 7 and 9, shows the estimated angle value  $\hat{\alpha}$  for the first 80 seconds of a fire. There is an angle  $\hat{\alpha}$  value for every two seconds depending on a 40 sample correlation window length  $L$  and a  $f_A = 20$  Hz sample rate. The estimated angle  $\hat{\alpha}$ , shown in figure 5 varies  $\Delta\alpha = -12 \dots +8$  degrees around true real value after 60 seconds.

Figure 6 shows the temperature curve from a sensor which is typically for a flaming fire



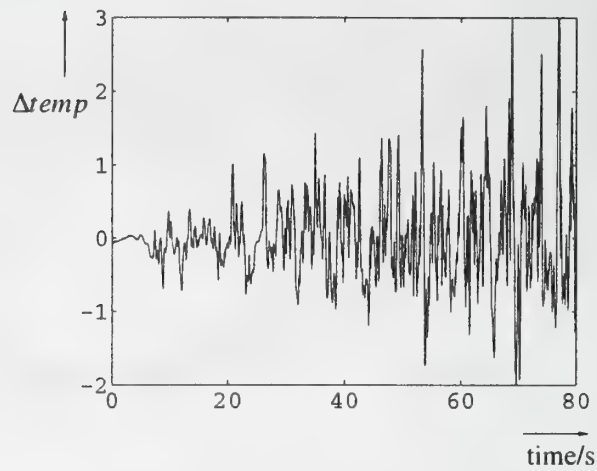


Figure 6: TF4 temperature data

type TF4. The typical increasing temperature values over the time indicate that the time is limited for estimating the fire place. This is caused by increasing the turbulences of the hot gases under the ceiling from the increasing fire.

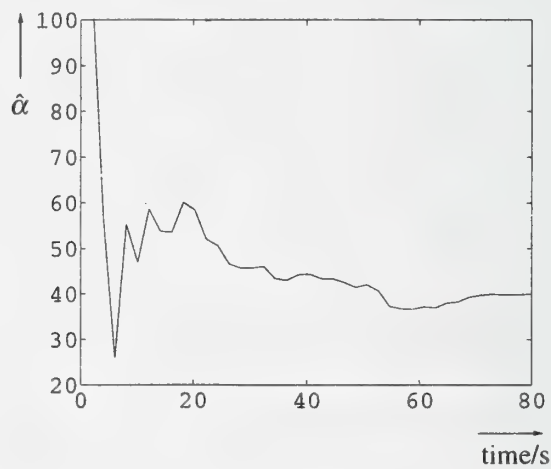


Figure 7: Estimated angle  $\hat{\alpha}$  for a TF4

The estimated angle  $\hat{\alpha}$ , shown in figure 7 varies  $\Delta\alpha = -10 \dots +3$  degrees around the real value after 40 seconds.

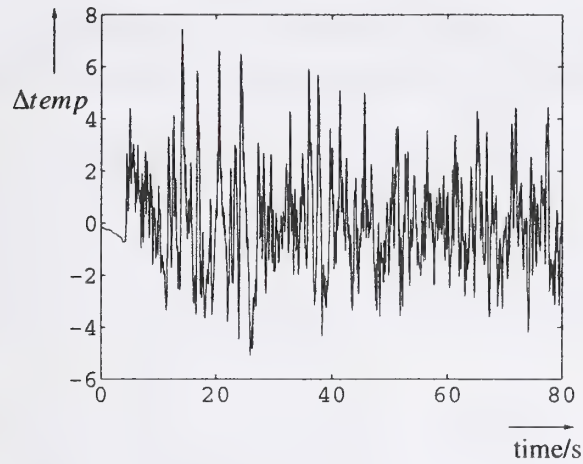


Figure 8: TF6 temperature data

Figure 8 shows the temperature curve from a sensor which is typically for a flaming liquid fire type TF6.

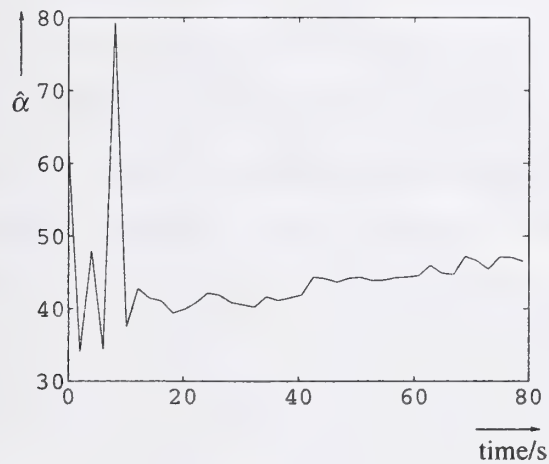


Figure 9: Estimated angle  $\hat{\alpha}$  for a TF6

The estimated angle  $\hat{\alpha}$ , shown in figure 9 varies  $\Delta\alpha = -8... + 4$  degrees around the real value after 20 seconds and  $\Delta\alpha = -5... + 3$  degrees after 40 seconds.

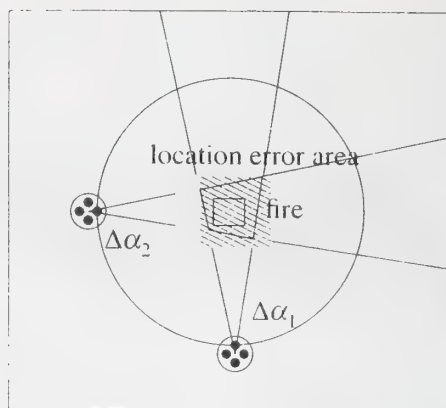


Figure 10: The location estimated error area

Figure 10 shows the error area of the location estimation in the fire laboratory under our test conditions. For example the TF6 is a flaming liquid fire in a quadratic basin with  $43.5\text{cm} \times 43.5\text{cm}$  and the error area from the estimation is in the same dimensions.

## 5. CONCLUSION

A method to locate a fire using two temperature arrays was proposed. A first DSP solution was shown and its results were verified by fire experiments. It was shown that it is possible to give a first fire location estimation in the same time as needed for detecting the fire with a class A1 detector. Unknown is the time for an useful location estimation of smoldering fires of type TF2 and TF3. For the future it is planned to port some other promising time delay estimation algorithms to the DSP solution for a higher accuracy. It is also planned to test some other sensor types e.g. pyroelectric sensors for their useful work in such a detector type.

## References

- [1] G. C. Carter, "Coherence and Time delay Estimation", Proceedings of the IEEE, vol 75, no.2, pp.236-255, February 1987
- [2] G.Cox. R. Chitty, "Some Stochastic Properties of fire Plumes", Fire and Materials, vol. 6, no. 3+4, 1982



- [3] L. Eikermann, "Ortsbestimmung von Bränden unter der Verwendung eines Temperatursensorfeldes", Studienarbeit, Gerhard-Mercator-Universität Duisburg, 1997
- [4] L. Eikermann, "Weitere Untersuchungen zur Ortsbestimmung von Bränden", Diplomarbeit, Gerhard-Mercator-Universität Duisburg, 1997
- [5] D. Wang, "Untersuchungen möglicher Fehlerquellen bei der Ortsbestimmung von Bränden", Studienarbeit, Gerhard-Mercator-Universität GH Duisburg, 1997
- [6] H.Luck: "Theoretische Grundlagen der Nachrichtentechnik 3,4", Vorlesung an der Gerhard-Mercator-Universität Duisburg.
- [7] T. Kaiser, "Ortsbestimmung von Bränden mit Temperatursensorgruppen", AUBE99 proceedings, pp.52-66, 1999
- [8] A. Telljohann "Vorarbeiten zum Aufbau eines Prototypen zur Ortsbestimmung von Bränden", Studienarbeit, Gerhard-Mercator-Universität Duisburg, 1999
- [9] R. Sprenger "Ein erster Ansatz zur signalprozessorbasierten Brandortbestimmung", Diplomarbeit, Gerhard-Mercator-Universität Duisburg, 1999
- [10] T. Kaiser "Fire Detection with Temperature Sensor arrays", IEEE Carnahan Conference proceedings, 2000

N. Miyamoto, T. Someya, and T. Omori

Energy & Environmental Technology Laboratory, Tokyo Gas Co., Ltd., Minato-ku,  
Tokyo, Japan

## **FIELD MODELING OF AN INITIAL STAGE OF FIRE IN A COMPARTMENT**

### **-Comparison with a Fire Experiment Measured in an Enclosure**

#### **1. Introduction**

Wider installation of the fire detector is effective in preventing disastrous fire. Given a broad variety of fire, effects of the fire and situation of a fire-containing room on fire detection should be well understood, thereby making more effective implementation of fire detectors possible.

The present study focuses on an early stage fire, during which an initiated fire in the compartment develops to trigger a fire detector installed, to elucidate fire phenomena and predict accurately heat transfer and diffusion of combustion-generated intermittent chemical species. To this end, simulation of compartment fire is performed using the field model approach. Existing work of field model fire simulation has largely simplified complex fire phenomena involving turbulent buoyant flow, unsteadiness, chemical reaction of combustion, thermal radiation between the high temperature flame and solid walls, among others.

It has been recognized, however, that in the initial stage of fire, combustion, fluid flow, unsteady heat conduction of building walls, radiative heat transfer from the fire source to the combustion gas as well as walls, and convective heat transfer all play major roles. Hence, putting early stage-fire simulation into practice need to integrate these important factors without oversimplification and by balancing with constraints from computational resources and allowable time frames.

2. Brief Description of Fire Experiment

According to the European standard of fire alarm test method [1], response time of the ceiling-mounted fire sensor provided is measured when a prescribed amount of combustible is ignited in an enclosure for fire experiment (Fig. 1). Six different types of fuel, designated TF1 for wood through TF6 for ethanol, are prepared to represent fire ranging from flaming fire to smoldering. Here, experimental data for TF6 collected in a thermal detection test [2] are employed for validation of numerical simulation results.

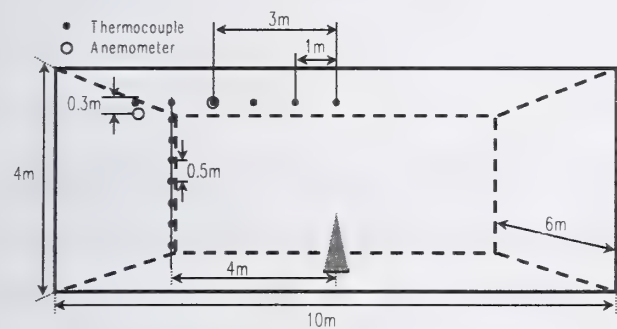


Fig. 1 Schematic diagram of Test Fire Cell

Table 2 Experiment condition

Comartment size	10 mü ~6 mü ~4 m(H)
Fuel	Ethanol 2500cc
Pan size	0.435 mü ~0.435 mü
Heat release rate	100 kW
Thermocouple placement (K type)	
Ceiling temperature (horizontal array)	5cm under ceiling 1m horizontal intervals from fire
Vertical temperature (vertical array)	4m away horizontally from fire 0.5m vertical intervals from ceiling
Anemometer placement (Ultrasonic anemometer)	
Velocity nearby ceiling	5cm under ceiling 3m away horizontally from fire
Velocity nearby wall	30cm under ceiling 5cm from wall

Table 1 Properties of walls, ceiling and floor

Surface	Material	Thermal conductivity	Thickness	Density
		W /mK	m	kg/m³
Walls	Concrete(Light)	0.523	0.1	1,350
Ceiling	Flexible board	0.616	0.1	723
Floor	Concrete	1.63	0.1	2,250

For representative flame combustion, 2500 cc of TF6 ethanol fuel fills a square pan having side length of 43.5 cm placed on a scale that is centrally located on the floor. The thermal properties of the wall material used in the test compartment are summarized in Table 1. When the fuel is spark ignited, ethanol temperature rises by receiving heat from the flame by convection and radiation as well as conduction through the pan walls. After the liquid temperature reaches the boiling temperature of ethanol (351.7 K), all the heat input is consumed by evaporation and both the temperature and the evaporation rate stay constant thereafter. The measured combustion rate using the scale is converted to the heat generation rate and is presented in Fig. 2.



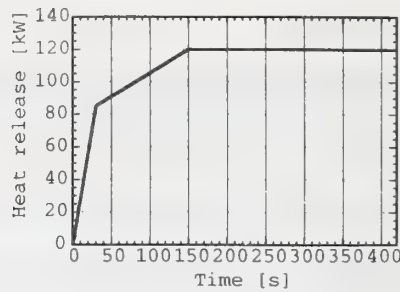


Fig. 2 Heat release rate history

### 3. Numerical Simulation

#### 3-1. Combustion model

The heat generation rate increases with time in the initial stage of fire studied here and, therefore, its effects should be properly accounted for when one wishes to gain accurate prediction of temperature rise inside the room. To this end, the eddy break up model of Magnussen for combustion [3] is employed. The computations are made under the condition that vaporized ethanol with minimum heat generation of 26.8 MJ/kg, latent heat of evaporation of 0.85 MJ/kg, and specific heat of liquid of 2.42 kJ/kg·K, flows uniformly from the fuel pan into the room. The incoming velocity is set equal to the experimental data.

#### 3-2. Radiative Heat Transfer

Ethanol undergoing liquid surface combustion generates glowing flame with a measured absorption coefficient of approximately 0.4 to 0.5  $\text{m}^{-1}$  [4]. The present investigation adapts 0.5  $\text{m}^{-1}$  for the absorption coefficient that is specified in a rectangular parallelepiped region above the fuel pan.

At 7 minutes after ignition, the concentration of carbon dioxide ( $\text{CO}_2$ ) below the ceiling is measured to be about 1.1 % in standard wet gas condition, while that of water vapor ( $\text{H}_2\text{O}$ ) is 1.6 %. Using the measured gas temperature of 90 °C and by assuming 2.7 m as the thickness of gas layer, the mean light path is estimated to be 2.8 m. The absorption coefficient calculated from the emissivity of gas using the Hottel chart is 0.08  $\text{m}^{-1}$ .

As to the absorption coefficient underneath the ceiling, two values –  $0.1 \text{ m}^{-1}$  (Case 1) accounting for a small amount of soot, and  $0.2 \text{ m}^{-1}$  (Case 2) – are specified to assess effects of soot radiation.

### 3-3. Incoming Turbulent Energy of the Fuel

Application of the standard  $k$ - $\epsilon$  model to an intensely buoyant thermal plume flow that may arise in fire situations has been found to give overprediction in the axial temperature of plume. This has been attributed to the suppressed momentum and heat diffusion near the fire source [5]. Yoshie et al. [6] obtained closer agreement with the experimental correlation of Yokoi [7] when larger incoming kinetic energy of turbulence  $k$  was specified at the height seven times the radius of the fire source, which leads to enhanced diffusion. Effects of this practice are examined in the present study by varying the incoming value of  $k$  for the following three cases: 0.0001 (Case 3, baseline case), 0.02 (Case 4), and  $0.05 \text{ m}^2/\text{s}^2$  (Case 5).

Table 3 simulation cases

Case	K_pr.	k_inlet
1	0.1	0.0001
2	0.2	.
3	0.1	0.02
4	.	0.05

### 3-4. Numerical Method

Simulations are conducted using the CFD package CFX 4.2 [8] with the standard  $k$ - $\epsilon$  model of turbulence and under the weakly compressible assumption. Radiative heat transfer is analyzed using CalcRad [9]. Convective heat transfer to the wall is calculated by the generalized logarithmic law-based wall function. The convection terms are discretized using the hybrid finite-difference method and the pressure-velocity correction follows the SIMPLEC algorithm. The time step  $\Delta t$  is gradually increased as explained in Table 4. The initial increment  $\Delta t$  is set small so that relatively fast changes in the room temperature distribution may be sufficiently resolved. Due to the geometrical symmetry having the seat of fire centrally located in the room, the computation is carried out for a quarter domain only. The incoming flow boundary condition is set at the fuel pan and the drain is treated as a pressure boundary. The

simulation model is depicted in Fig. 3. The mesh systems displayed in Fig. 4 have

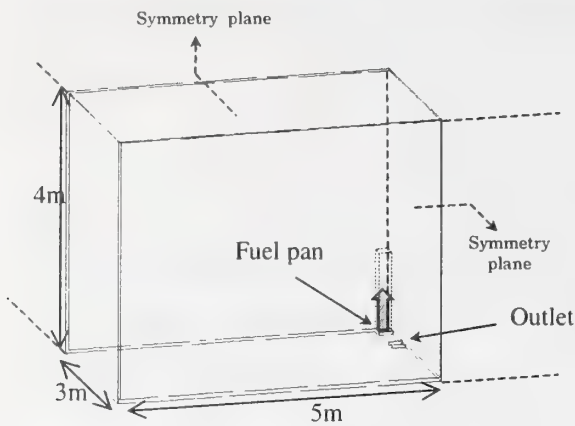
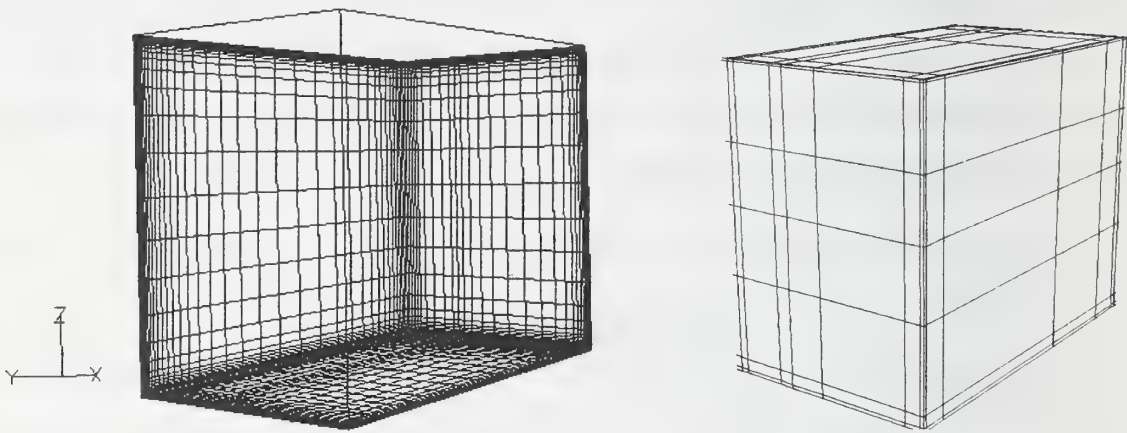


Fig. 3 Simulation model

Table 4 Simulation condition

Time [s]	0	1	3	10	20	40	420
$\Delta t$ [s]	0.1	0.2	0.5	1.0	2.0	5.0	
Heat Transfer to Walls	Wall Function(Log law)						
Absorption coefficient [ $m^{-1}$ ]	Flame		0.5				
	Gas layer		0.1				



36,176 grid points consisting of 38 (x)  $\times$  28 (y)  $\times$  34 (z) divisions for the CFD mesh and 38  $\times$  28  $\times$  34 nodes for radiation calculations. The first CFD grid near the ceiling is located 0.5 cm below the wall. All the computations are run using a SGI Origin 2000 with a single CPU, which consumes about 25 hours per case.

4. Results and Discussion

4-1. Comparison of the Simulated Cases

Figure 5 shows the time history of combustion gas temperature at the point 5 cm underneath the ceiling and 4 m horizontally separated from the fire source. It is seen that the result of Case 1 almost overpredicts the experimental data. On the other hand, in Case 2 for which the absorption coefficient is 0.2 m<sup>-1</sup>, the computed temperatures



increasingly underestimate the measured values with time, indicating the excessively large absorption coefficient. The predicted result of Case 3 with the larger turbulence energy is overall in good agreement with the experiment, except for the temperature overshoot up to 10 °C during  $t = 100$  and 300 seconds. Further increasing turbulence energy (Case 4) leads to much higher temperature with degraded convergence properties stemming from somewhat unstable computation. Based on these observations, the computational results of Case 3 that achieve the best agreement with the measured data are considered for further discussion.

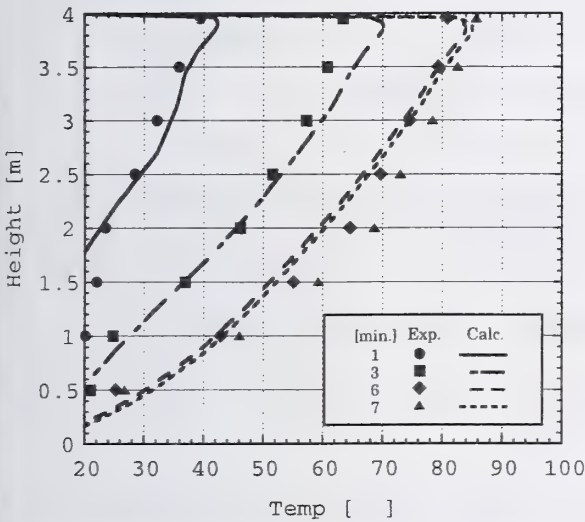


Fig. 6 Transition of vertical temperature distribution (4m from fire)

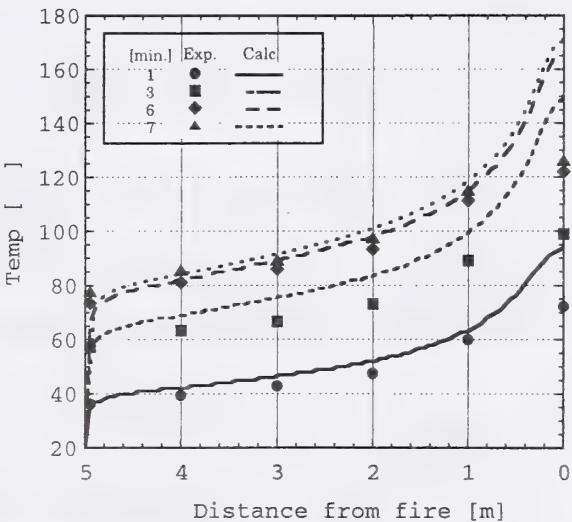


Fig. 7 Transition of horizontal temperature distribution near ceiling

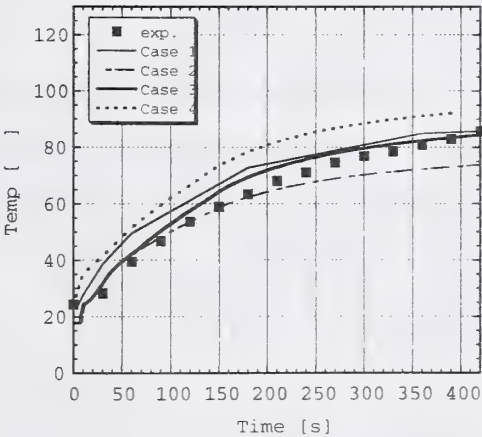


Fig. 5 Comparison of Simulation cases (ceiling, 4m from fire)

#### 4-2. Variation of Vertical Distribution of Air Temperature with Time

The vertical temperature distributions of air at 1, 3, 6, and 7 minutes after ignition at the horizontal location 4 m away from the fire source are represented in Fig. 6. The numerical predictions are seen to be globally in good agreement, although the temperature below the ceiling at 3 minutes is overestimated by roughly 7 °C and the mid-height temperature undershoots by almost 8 °C at 7 minutes.

#### 4-3. Time Variation of the Near-Ceiling Temperature Distribution of Combustion Gas

In Fig. 7, the horizontal gas temperature distribution at the monitoring point 5 cm below the ceiling from the fire source toward the wall is shown. Except for the computed higher temperature seen right above the fire, the numerical prediction agrees well with the measured results beyond the location 1 m away from the fire.

The European Standard EN54 [1] imposes that the fire detector be positioned on the ceiling and 3 m horizontally away from the location of test fire. The computed temperature will trigger properly a detector with a given temperature sensitivity.

#### 4-4. Flow Velocity

Table 5 provides the measured and computed velocities at 7 minutes after ignition at the location below the ceiling and 3 m separated horizontally from the fire source, and the near wall (distance 5 cm apart) location 30 cm away from the ceiling. The simulation is seen to slightly attain the higher flow speed in both positions. However, in the actual experimental situations in which there are instrumentation and other protrusions on the ceiling area, the flow speed may have been reduced compared to the unobstructed ceiling condition and, in turn, the two sets of data should come closer to be in good agreement.

4-5. Time Elapse to Fire Detector Activation Temperature

The fire detector is designed to activate when the combustion gas temperature at its mounted location reaches 65 °C. Figure 8 depicts the time elapsed from ignition for triggering the alarm. Note the enlarged scale of temperature centered on 65 °C. The activation time in the experiment is roughly 170 seconds, while in the simulation it is about 40 seconds shorter to have 130 seconds. The difference may stem from the manner the combustion rate is approximated: in the simulation it varies linearly with time, as shown in Fig. 2. More realistic fuel consumption pattern should be utilized for achieving better agreement.

Table 5 Velocity comparison at time=390 s

Location	Exp.	Calc.
Ceiling	0.59	0.61
Wall	0.28	0.37

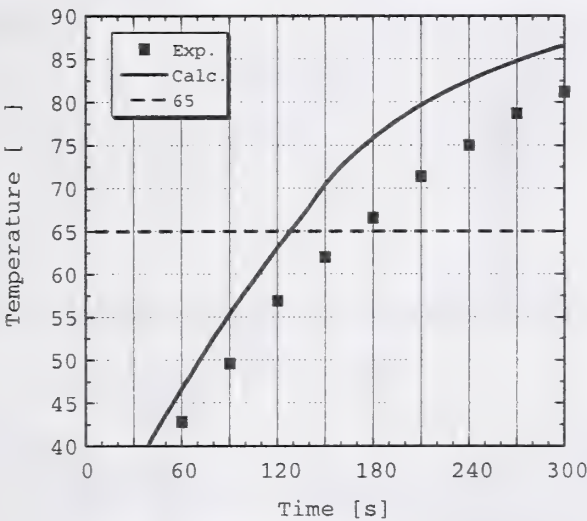


Fig. 8 Comparison of alarm time



4-6. Variation of Indoor Air Temperature

Changes in the air temperature in the symmetry plane (corresponding to the central vertical plane of the room) together with a plane 5 cm below the ceiling are displayed in Fig. 9. The temperature range exceeding 100 °C is colored in red. After the thermal plume rising from the fire source impinges on the ceiling, it spreads over the ceiling wall in a concentric fashion. Upon hitting the vertical walls, the flow turns downward until it loses momentum and reverses its direction upward due to the buoyancy force. The nearer the ceiling jet is from the fire source, the larger the momentum contained therein. This manifests into the descending combustion gas that penetrates farther down near the fire source (toward the right of the figure). This demonstrates the course of developing thermal stratification properly captured in the present simulation results.

5. Conclusion

The early stage-fire experimental situation using ethanol fuel (TF6) that conforms to the

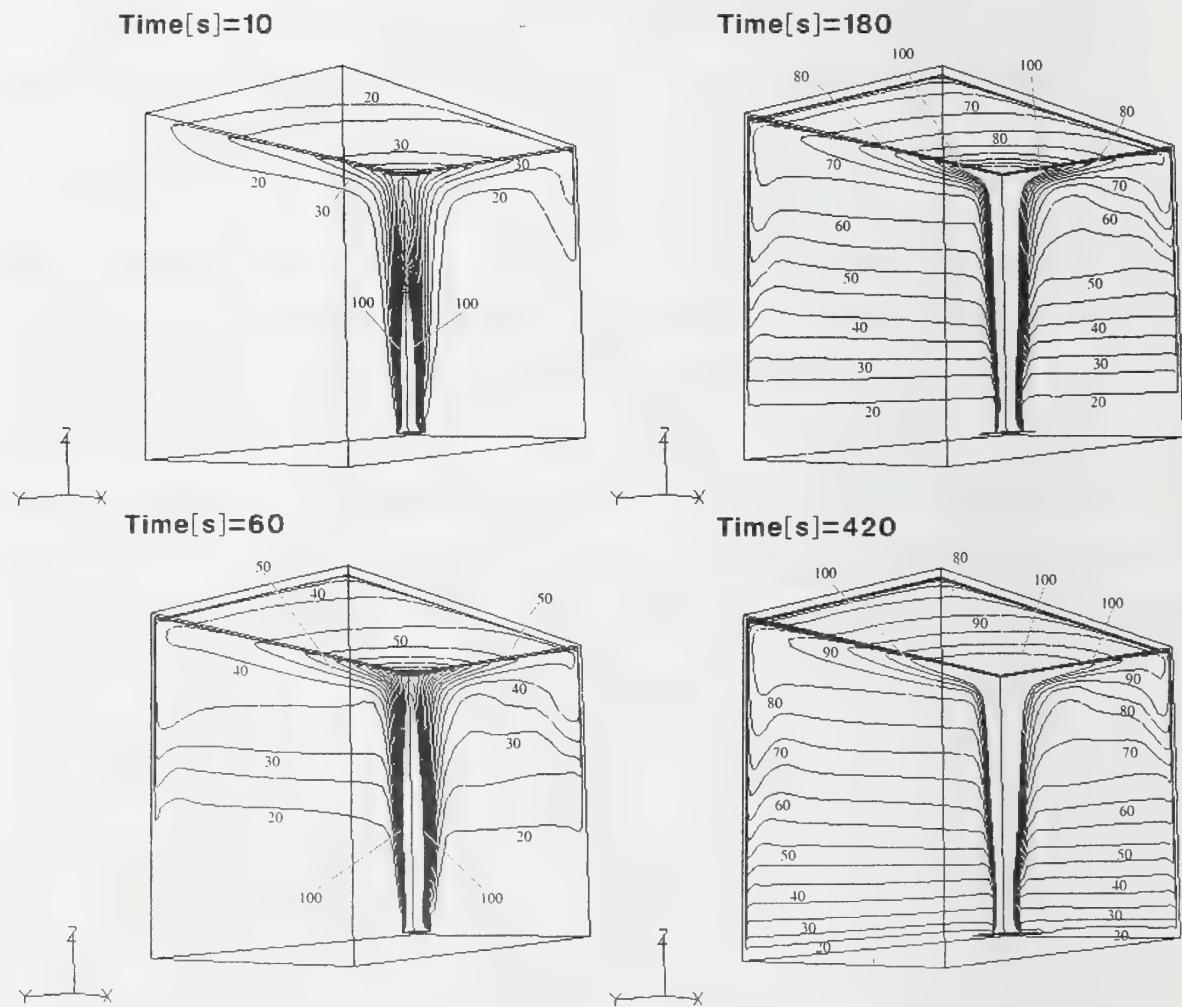


Fig. 9 Transient temperature distributions

EN 54 semi-enclosure is simulated numerically by way of the field model approach. The following conclusion is drawn from the results obtained:

1. In the stagnation region where impingement of the thermal plume on the ceiling takes place, the predicted temperatures are significantly higher compared with the measurement data. However, excellent agreement is achieved in the ceiling jet region that is located about 1 m away from the stagnation point.
2. For the numerical simulation of the TF6 fire experiment, the absorptivity of combustion gas layer for thermal radiation is roughly  $0.1 \text{ m}^{-1}$  that is given by the Hottel chart.
3. With the eddy break up model used for modeling combustion, higher turbulence energy should be assigned as the boundary condition for the incoming fuel. For TF6, good agreement with the experimental result in the ceiling jet region is found by setting  $k = 0.02 \text{ m}^2/\text{s}^2$ .
4. The present numerical simulation captures successfully a series of phenomena characteristic of the early-stage compartment fire: When the ascending thermal plume from the fire source impinges on the ceiling, it transforms to the ceiling jet that spreads concentrically. The ceiling jet, after it shortly heads downward upon hitting the vertical walls and then loses momentum, rises due to the buoyancy effects. These lead to the well-developed thermal stratification as time elapses.

## References

- [1] British Standard Institution, Components of automatic fire detection systems: Part 9. methods of test of sensitivity to fire. EN 54 1984.
- [2] Doi, M., Manmoto, A. and Yamauchi, Y. Prediction of response time of the thermal sensor using the RTI-C model. Proc. Fire Society of Japan 1999; 50-53 (in Japanese).
- [3] Magnussen, B. F. and Hjertager, B. H. On mathematical modeling of turbulent combustion with special emphasis on soot formation and combustion, 16<sup>th</sup> Symp. (Int.) on Combust. 1976; 719-729.
- [4] Tanaka, T. Introduction to Building Fire Safety Engineering 1993; 138-141 (in Japanese).

- [5] Nam, S. and Bill, R. G. Jr. Numerical simulation of thermal plumes. *Fire Safety Journal* 1993; 21: 231-256.
- [6] Yoshie, R. CFD Analysis of Fire Plumes (2nd Report). *Proc. Arch. Inst. Japan* 1998; 147-148 (in Japanese).
- [7] Yokoi, S. Study on the prevention of fire-spread caused by hot upward current. *Report of the Building Research Institute* 1960; No. 34.
- [8] CFX Release 4.2 User Guide. 1994; AEA Hyprotech K.K.
- [9] Omori, T., Yamaguchi, S. and Taniguchi, H. Accurate Monte Carlo simulation of radiative heat transfer with unstructured grid systems. *11<sup>th</sup> Int. Symp. on Transport Phenomena* 1998; 567-573.



Thomas Cleary, Michelle Donnelly, George Mulholland, and Bakhtier Farouk\*

Building and Fire Research Laboratory, Natl Inst of Stds and Tech Gaithersburg, MD  
20899, USA

\*Mechanical Engineering and Mechanics Department, Drexel University  
Philadelphia, PA 19104, USA

## **Fire Detector Performance Predictions in a Simulated Multi-room Configuration**

### **1. Introduction**

Modeling fire detector performance requires detailed information on the environment surrounding the detector, the species transport (heat, particulate smoke, and gases) from the surrounding to the sensing surface or volume, and the sensor response. The details of the environment surrounding a detector can be gathered from full-scale fire experiments, however, that approach affords very little flexibility. One may be able to find information gathered from standard fire sensitivity tests or other single-room fire tests, but not for complex configurations. In a performance-based approach, an ideal situation is one where modeling replaces full-scale experiments wherever possible. Luck and Sievert [1] refer to the environment surrounding the detector as the "outer world", where all aspects important for fire detection must be modeled including both fire and non-fire conditions. Once the detector environment is known, the species transport to a detector's sensing surface or volume and its response can be modeled if sufficient detailed information on a particular detector exists. An alternative approach is to perform detector exposure experiments in the fire emulator/detector evaluator to ascertain sensor responses for modeled, realistic fire scenarios.

### **2. Modeling Detector Fire Environments**

Modeling of detector environments has evolved from the ceiling jet correlations applied to (thermal) detector activation, zone modeling, to more detailed computational fluid dynamics models. Davis [2] has developed a zone fire model "Jet" which has a ceiling jet correlation embedded in the computational algorithm to facilitate better temperature, smoke and species concentrations, and flow conditions at detector locations. The model

formulation has been used in a sensor driven fire model that utilizes thermal and/or smoke sensor outputs to predict fire conditions [3]. Andersson and Holmstedt [4] performed a computational fluid dynamics (CFD) study to predict temperature and smoke light extinction at a detector location in a simulated EN 54 part 9 fire sensitivity test. Davis *et al.* [5] used CFD computations to study complex ceiling geometry effects on detector activation. Cleary *et al.* [6] used the Fire Dynamics Simulator, (FDS; a computational fluid dynamics fire model based on large eddy simulation technique, developed by NIST [7]) to predict the smoke, thermal and flow environment at a detector located in a simulated EN 54 part 9 test room subjected to test fire 4.

Here, the fire model FDS was used to predict the fire environment at multiple detector locations in a three room suite. Specifically, FDS was used to compute velocity, temperature, smoke and CO gas concentrations at detector locations in each room of a simulated fire located in one of the three rooms. A diagram of the room layout, fire and detector locations is shown in Figure 1. Room 1 is the fire room, where the fire source is located at the floor in the center of the room. The ceiling height is 2.90 m and the door openings are 0.91 m wide by 2.44 m high. Supply and return HVAC vents (0.3m wide by 0.9 m high) are located in the walls at a height 0.3 m from the ceiling, and have fixed flows between 0.04 m<sup>3</sup>/s and 0.2 m<sup>3</sup>/s. The return in room 2 acts as an open vent. The ambient temperature was 20 °C and the surfaces were adiabatic (i.e., no heat loss to wall or ceiling). The computational grid spacing was  $x = 150$ ,  $y = 75$ , and  $z = 27$ , for a total of 303,750 cells and a physical grid spacing of 17.2 cm, 20.8 cm, and 10.7 cm for  $x$ ,  $y$ , and  $z$  directions respectively.

The simulated fire consisted of a flaming fire that starts out with a heat release rate similar to the EN54 TF4 flaming polyurethane foam mat fire. It transitions to a "medium  $t^2$  fire" after the mat fire reaches its peak output at 200 s (Figure 2). The radiative fraction was set at 0.35 with a heat of combustion fixed at 16 kJ/kg. The smoke and CO yields of 0.03 g smoke/g burned and 0.01g CO/g burned are in the range of what would be expected from a flaming plastics fire. The detector locations represent two separate detector spacings of 9.1 m (30 ft.) for locations 1, 3, 8, and 9, and 6.4 m (21 ft.) for locations 1, 2, 4, 5, 6, 7, 10, 11, and 12. The environment was simulated for 500 s with

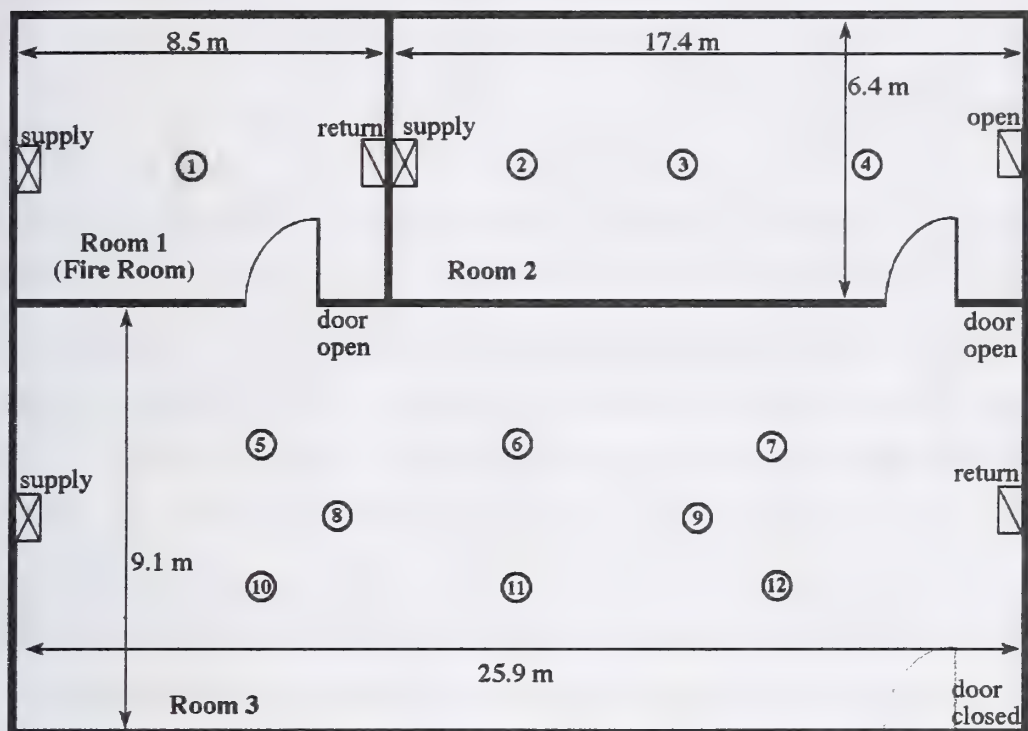


Figure 1. Three room suite layout; circled numbers are detector locations.

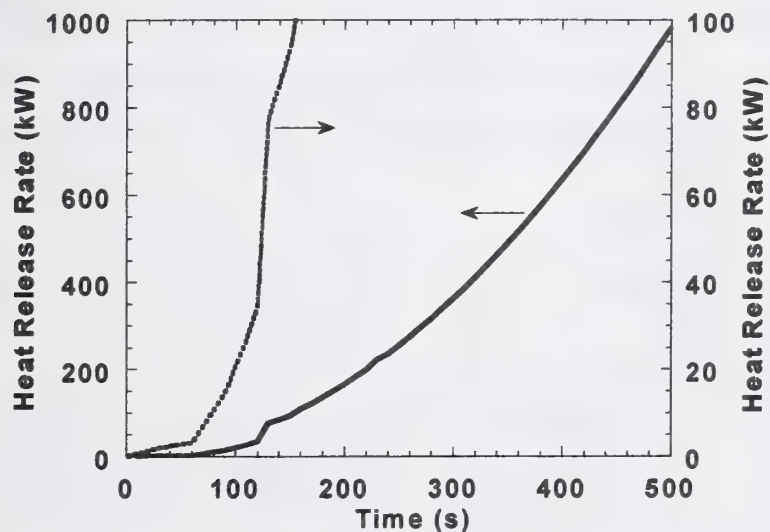


Figure 2. Heat release rate curve used in FDS computation.

the temperature, smoke and CO concentrations, and the x and y flow velocity vectors recorded at each detector location (i.e., the computational grid at the ceiling which encompasses a typical detector's vertical position). The x and y velocity vectors were used to compute the scalar horizontal flow speed as a function of time at each detector



location. The smoke concentration was converted into an extinction coefficient by multiplying the smoke concentration in grams per m<sup>3</sup> by a specific extinction coefficient for soot of 8.7 m<sup>2</sup>/g [8].

Figures 3 and 4 show the temperature, flow speed, CO volume fraction, and smoke extinction coefficient computed at detector location 1 (L1) in the fire room. In Figure 3, the temperature rise curve has the same shape as the heat release rate curve. The plume centerline temperature at the ceiling was computed from Heskestad's strong plume correlation at ambient background temperature of 20 °C [9];  $\Delta T = 25 Q_c^{2/3} z^{-5/3}$ , where  $\Delta T$  is the excess temperature (°C),  $Q_c$  is the convective heat release rate, and  $z$  is the height of ceiling from the fuel source. The fact that the correlation predicts higher ceiling temperatures early may be due to the coarse grid size used in the FDS calculation and the fact that the plume correlation was developed from steady-state fires. The under-prediction later in the computation is due to the fact that the correlation is valid for unconfined plumes, and the effects of entrainment of hot layer gases is not accounted for. The horizontal flow speed is somewhat vague since the plume velocity is turning

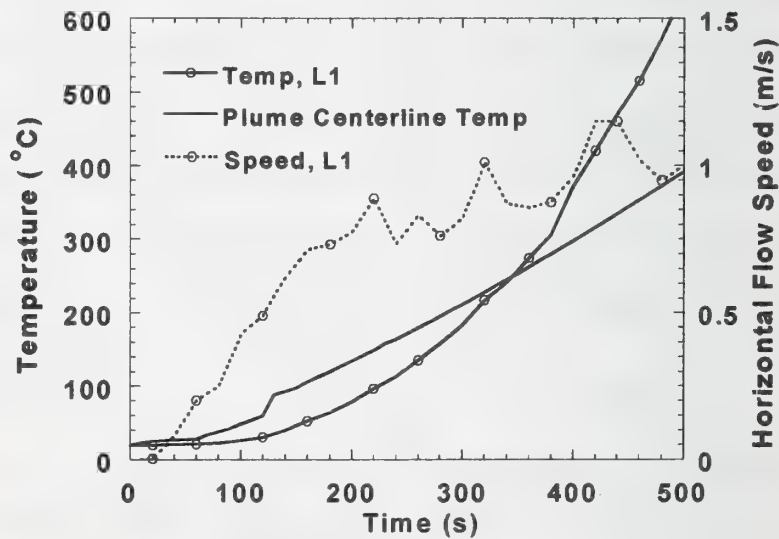


Figure 3. Temperature and flow speed at detector location 1 in the fire room.

from mostly vertical to horizontal directly above the plume. In Figure 4, the CO volume fraction gradually rises (noticeably starting at 60 s) to a peak volume fraction greater than  $500 \times 10^{-6}$  at the end of the simulation time. The extinction coefficient started

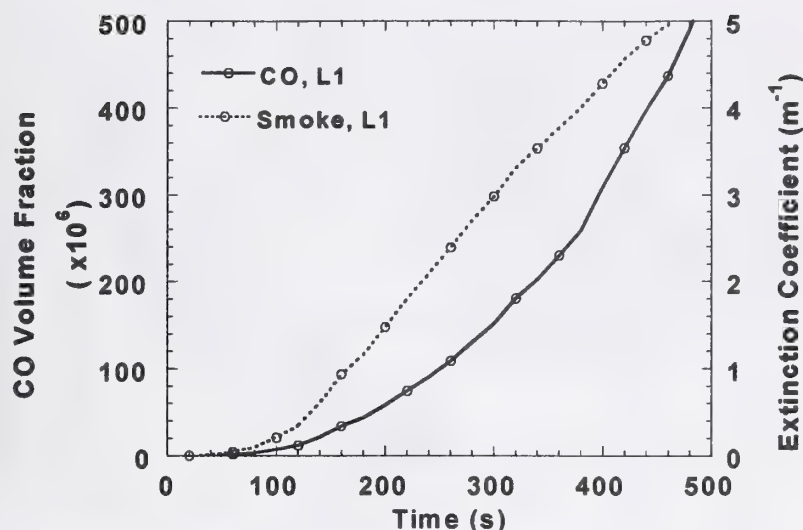


Figure 4. CO volume fraction and smoke extinction coefficient at detector location 1.

to rise at 60 s and continued to rise above  $5 \text{ m}^{-1}$  by the end of the simulation. For comparison, an extinction coefficient of  $0.13 \text{ m}^{-1}$  is equivalent to a smoke obscuration of 4 % per 0.3 m (1 ft).

Figures 5 and 6 show the temperature, flow speed, CO volume fraction and extinction coefficient values computed at detector locations 5, 8, and 10. These locations were grouped together due to their proximity to one another and to the door opening from

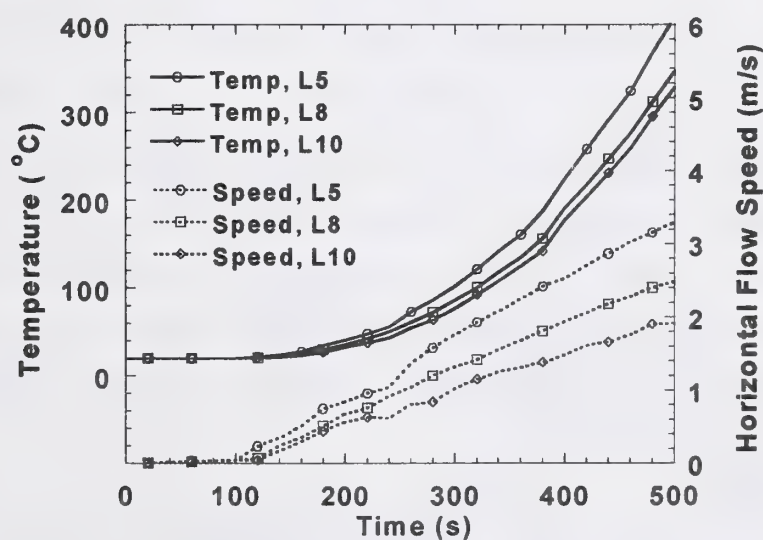


Figure 5. Temperature and flow speed at detector locations 5, 8, and 10 in room 3.

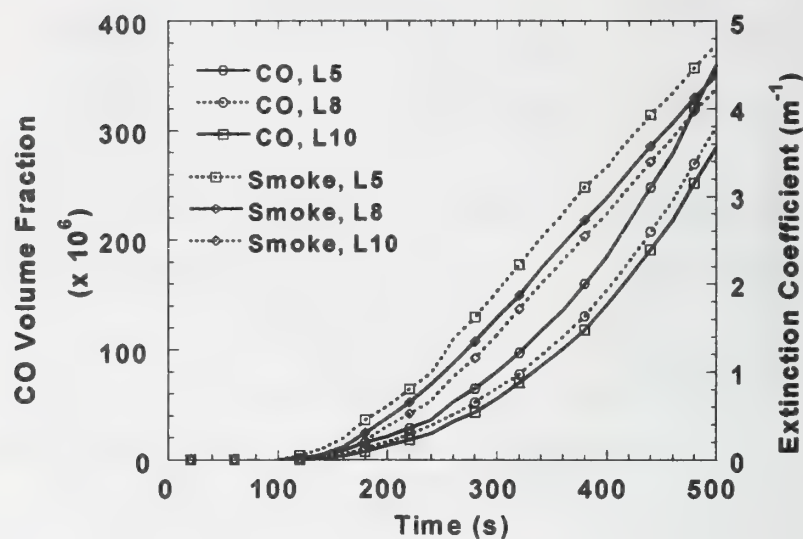


Figure 6. CO volume fraction and smoke extinction coefficient at locations 5, 8, and 10.

room 1. In Figure 5, note that the flow speeds reach levels of over 0.8 m/s before temperatures rise by 25 °C, and peak between 1.9 m/s, 2.5 m/s, and 3.3 m/s for locations 5, 8, and 10 respectively. These flow speeds are created from the jet issuing from the doorway. In Figure 6, the CO volume fraction curves look similar to the CO volume fraction in room 1 except that the initial rise started at 120 s and the peak volume fractions were lower than at location 1. Smoke extinction followed a similar path compared to location 1, however, initial rise was delayed by 40 s to 80 s.

Figures 7 and 8 show the computed values at detector locations 6, 7, 9, 11, and 12. Again, these were grouped due to their proximity. As expected, all computed values begin to rise later than at locations closer to the fire. Except for location 11 after 300 s, the temperatures, flow speeds, CO volume fraction and extinction values are quite similar, however, shifted in time by 20 s to 60 s. The flow speed at location 11 continued to rise after 300 s, achieving a speed of 1.5 m/s at the end of the simulation, which suggests it was seeing the effects of the doorway jet more directly than the locations 6, 7, 9, and 12.

Figures 9 and 10 show the computed values at detector locations 2, 3, and 4, all located in room 2, and the furthest from the fire source. All computed values began to rise



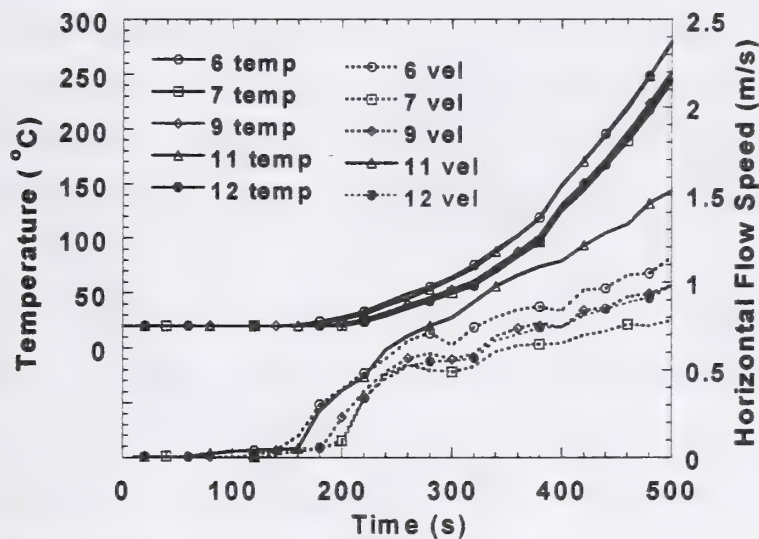


Figure 7. Temperature and flow speed at locations 6, 7, 9, 11, and 12 in room 3.

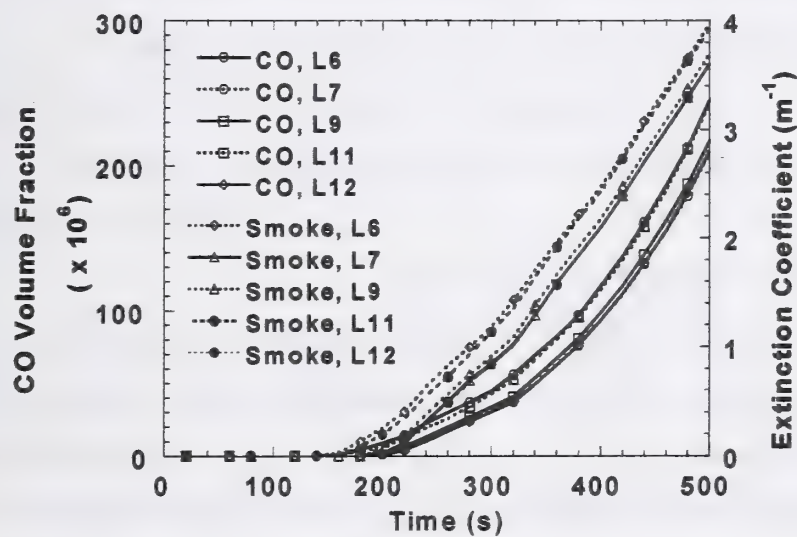


Figure 8. CO volume fraction and extinction coefficient at locations 6, 7, 9, 11, and 12.

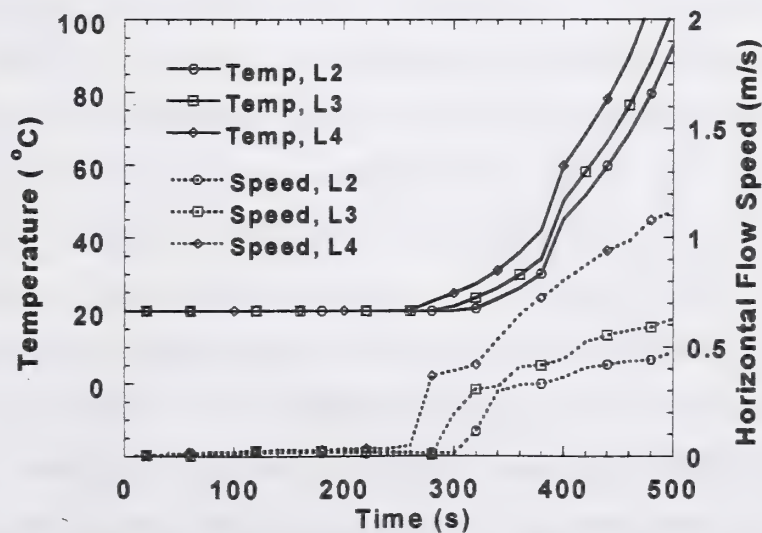


Figure 9. Temperature and flow speed at locations 2, 3, and 4 in room 2.

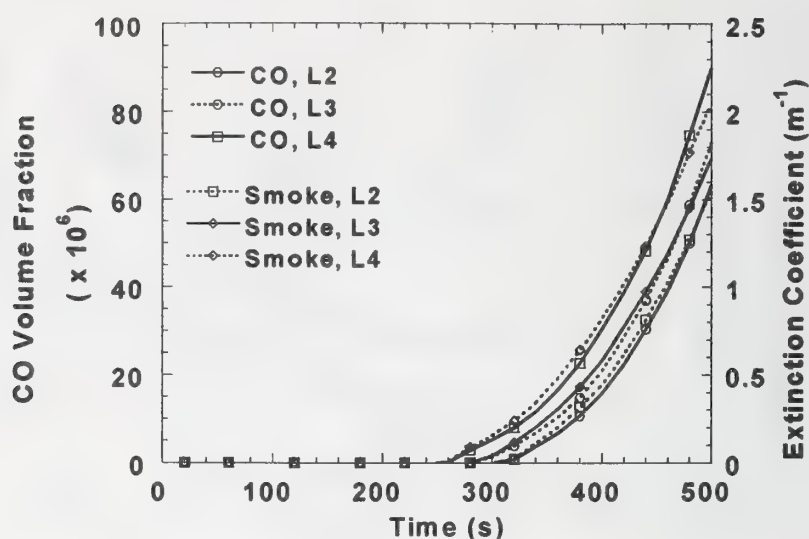


Figure 10. CO volume fraction and extinction coefficient at locations 2, 3, and 4.

260 s and 320 s. The maximum speed at location 4 was nearly twice as large as the maximum at location 3, owing again to its relative position to the doorway opening and the jet issuing from room 3.

### 3. Fire Emulator/Detector Evaluator Tests

The fire emulator/detector evaluator (FE/DE) was used to reproduce the computed flow speed, temperature rise, CO and smoke concentrations at select detector locations. The FE/DE is a single-pass wind tunnel where room air is drawn into the opening, and exhausted to a hood at the end of the duct. It was designed specifically to reproduce the environment surrounding a detector during fire or nuisance events [10,11]. In the FE/DE, air velocity at the test section can be controlled over a range of flows between 0.02 m/s to over 2 m/s by means of a computer-controlled axial blower. The flow is conditioned before it reaches the test section by passing it through a 10 cm long aluminum honeycomb with 5 mm rectangular openings. The goal was to provide a nominally flat flow profile indicative of what would be expected by a detector in a ceiling jet flow. The flow was monitored at the test section by a bi-directional probe located at the duct centerline. For fixed fan speeds, the flow profile is nearly top-hat with a velocity that fluctuates indicating turbulent flow. Thermal energy is added to the flow by forcing it through a series of 9 annular finned heating elements. Each element is rated at 5 kW for a total maximum heat input of 45 kW. Power to the heating elements is controlled by a feedback controller that receives set-point values automatically from a

computer file and compares them to the air temperature exiting the heaters. An air temperature difference between the heater exit and test section locations is due to heat losses to the duct section between those two points. A rate of rise in air temperature of 0.5 °C/s is achievable at the test section, up to maximum temperature of about 80 °C. Air temperature at the test section was recorded with type-K thermocouples.

CO, CO<sub>2</sub>, or other gas blends may be metered into the flow via electronic mass flow controllers. CO, CO<sub>2</sub>, H<sub>2</sub>O, and hydrocarbon gas concentrations are monitored by non-dispersive infrared analyzers. The standard uncertainty in the CO volume fraction measurement is stated as  $2.5 \times 10^{-6}$ . The ability to control gas concentrations independently benefits both fire and nuisance alarm scenario emulation. For example, both CO and CO<sub>2</sub> may be normally present in ever-changing concentrations in a building due to the external environmental sources such as attached parking garages, or internal sources such as the diurnal CO<sub>2</sub> variation due to occupancy and ventilation levels. The FE/DE can be programmed to reproduce such conditions as part of an evaluation of a fire detector that includes gas detection.

Various smoke and non-combustion aerosols may be introduced into the flow. Here, a propene smoke generator, which provides black soot typical of flaming hydrocarbon or plastics fire smoke, was used. The concentration of smoke in the flow is varied by changing the fuel flow of the burner and opening or closing dampers allowing more or less flow from the burner to enter the duct. Laser light transmission measurements across the duct at the test section were used to calculate the extinction coefficient of the propene soot. A He-Ne laser at 632.8 nm wavelength is the light source, and a stabilizer utilizing a liquid crystal polarizer maintains a nearly constant laser intensity. The beam is split and introduced at two heights: the center of the duct, and 5 cm below the ceiling (here, the extinction measurement from the beam 5 cm below the ceiling was used). Each light beam is reflected off two mirrors inside the duct and directed at a photodetectors placed on the opposite side of where the beam enters the duct. The total path length inside the duct is 1.5 m. The photodetector output voltage is linear with respect to the transmitted light intensity. The standard relative uncertainty due to random fluctuations in output is 0.06% of the measured light transmittance.



A multi-sensor, analog output fire detector was used to record continuous photoelectric and thermal sensor signals during the emulated conditions. These outputs are actually 8 bit numbers from an analog to digital converter. Here, offsets were subtracted so the outputs are zero to start. A CO sensor removed from a residential CO detector was placed in the FE/DE test section during the tests and the voltage drop that developed across a resistor placed between the two sensor electrodes was recorded.

The simulated detector environments that were emulated in the FE/DE and reported here are detector location 2 in room 2, and detector location 11 in room 3. The computed values at these locations represent the range of flow speeds and temperature rise achievable in the FE/DE. The length of simulation time emulated depends on the flow and temperature rise; the complete 500 s simulation at location 2 was emulated, while only the first 330 s of the simulation at location 11 was emulated. Figure 11 shows the duct velocity and fan settings for two repeats of a test that was designed to emulate conditions developed at location 2. The fan setting was controlled such that the duct velocity matched the simulated flow speed as indicated. Figure 12 shows the duct velocity and fan setting for a test designed to emulate conditions developed at location 11. Again, good agreement between the simulated flow speed and the duct velocity was achieved.

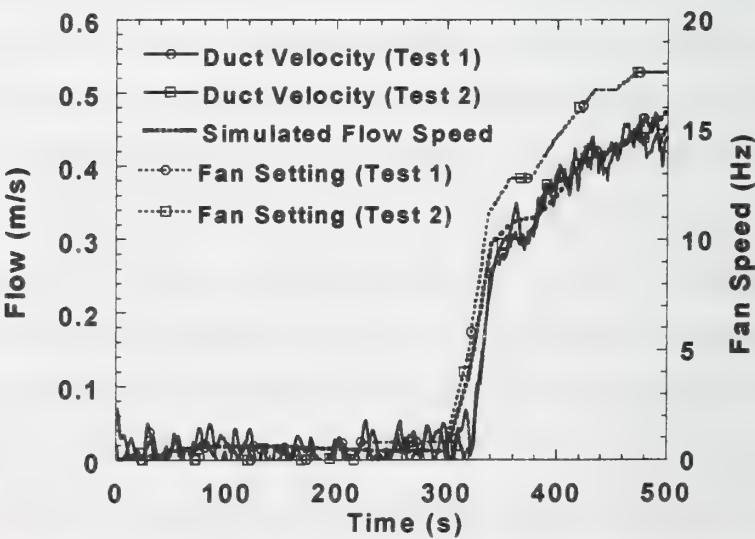


Figure 11. Duct velocity and fan setting for emulated conditions at location 2.

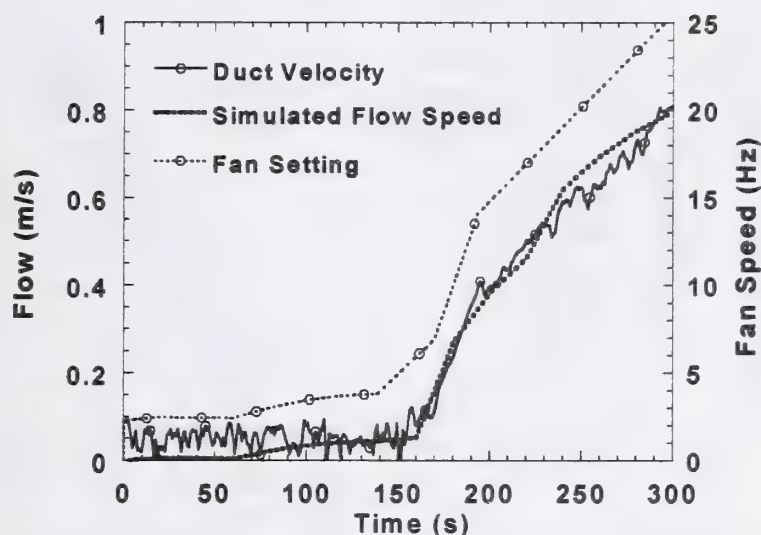


Figure 12. Duct velocity and fan setting for emulated conditions at location 11.

Figure 13 shows the duct air temperature at the test section and the thermal sensor output for repeated tests of the location 2 emulation. The computed temperature and the emulated temperature compare favorably until about 450 s when the emulated temperature starts to deviate from the computed temperature which continued to climb. The thermal sensor lagged the thermocouple temperature due to its response characteristics. Figure 14 shows the duct air temperature and thermal sensor output for the location 11 emulation. Good agreement between the computed temperature and the emulated temperature was maintained until about 330 s when the simulated temperature rose above the operational range of 80 °C of the FE/DE. Note that the lag between the

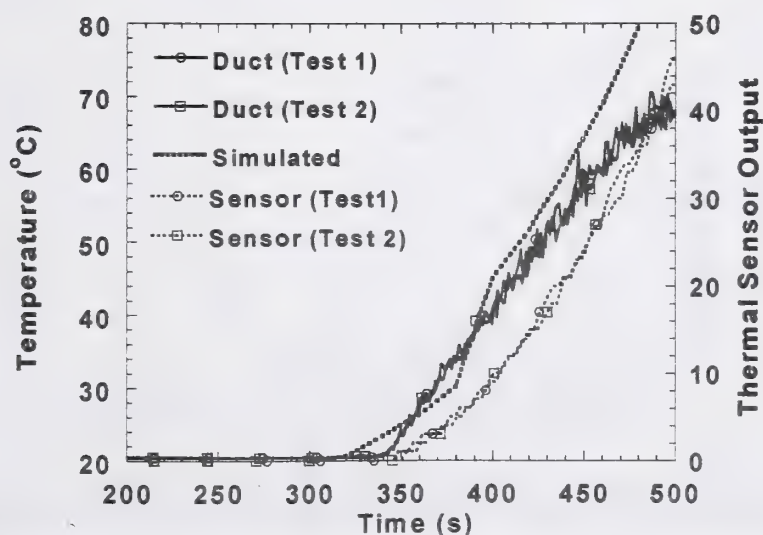


Figure 13. Duct temperature and thermal sensor output for conditions at location 2.

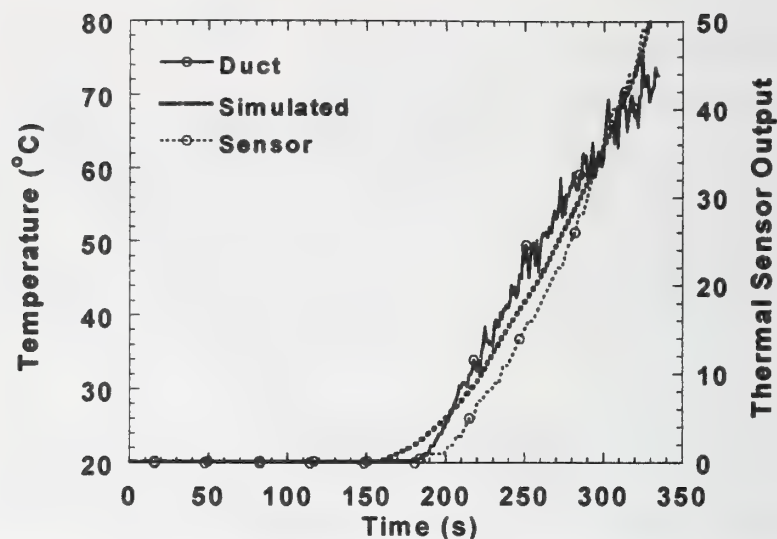


Figure 14. Duct temperature and thermal sensor output for conditions at location 11.

thermal sensor and the thermocouple is less pronounced. This is most-likely due to enhanced convective heat transfer to the thermal sensor in this emulation due to the higher duct flow velocities.

Figures 15 and 16 show the duct CO volume fraction for location 2 and location 11 emulations respectively. The agreement between the duct CO volume fraction and the computed value is not very good. This is due in part to the fact that the lower limit of the selected mass flow controller used to introduce the CO gas into the duct was too high

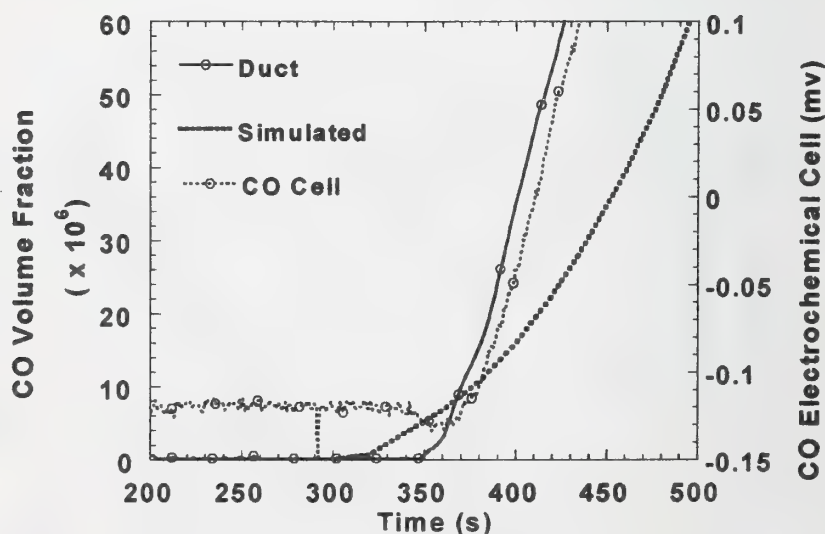


Figure 15. Duct CO volume fraction and CO cell volts for emulated conditions at location 2.



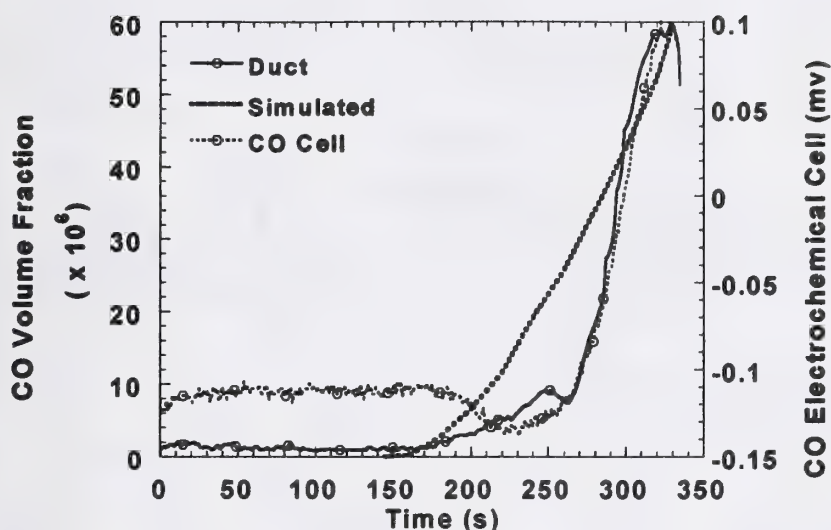


Figure 16. Duct CO volume fraction and CO cell volts for emulated conditions at location 11.

to produce smooth continuous flows of CO needed to achieve the target concentrations. For comparison, the electrochemical cell output is shown, and it compares favorably with the duct CO concentration, with only a short lag time between the curves.

Figures 17 and 18 show the duct extinction coefficient and the computed extinction coefficient for emulation tests of location 2 and 11 respectively. The smoke produced by the propene burner is sufficient to emulate the computed extinction coefficients at

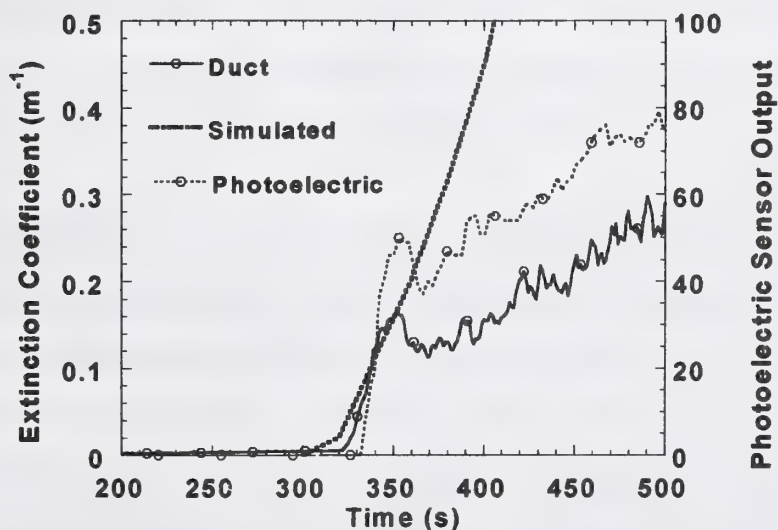


Figure 17. Duct smoke extinction and photoelectric sensor output for emulated conditions at location 2.

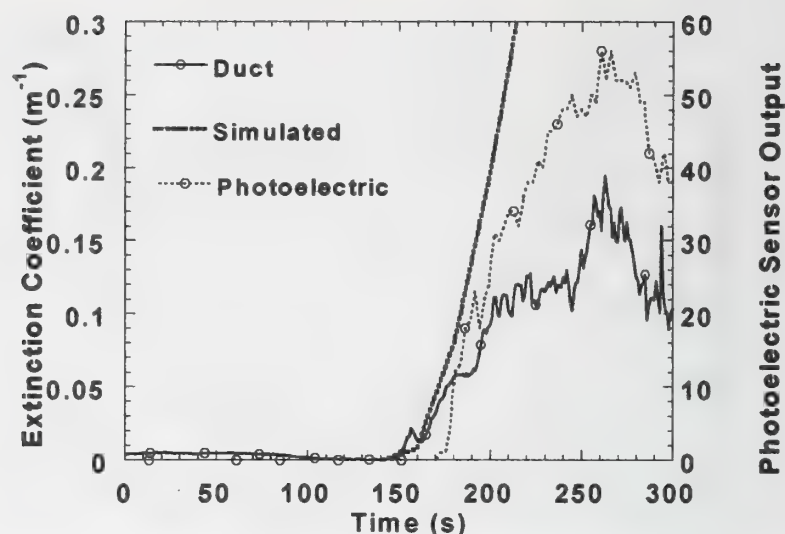


Figure 18. Duct smoke extinction and photoelectric sensor output for emulated conditions at location 11.

each location up to about  $0.15\ m^{-1}$ . Owing to the ever increasing flow velocity, the smoke production cannot keep up with the simulated smoke build-up. However, a high smoke concentration that produces a large extinction coefficient is not necessarily relevant to detector performance. The photoelectric sensor output tracked the duct extinction coefficient in each emulation. Here, the duct flows are sufficiently high to reduce the smoke entry lag to negligible times.

The particular simulated fire scenario chosen pushed the operation of the FE/DE to its limits. Refinement of the FE/DE for these emulated conditions is required to overcome the temperature, smoke production, and CO flow limitations.

#### 4. Conclusions

From this work, it is concluded that multi-room fire simulation with the FDS software can yield environmental conditions a detector or sensor may experience during an actual fire. The FDS code computes the smoke, heat, and gaseous species transport needed to predict detector performance. The specific fire scenario simulated here was chosen to produce rapidly changing smoke and gas concentrations, heat, and flow velocities at detector locations. Such a fire test would be quite expensive to perform a single time since the fire room approaches flashover conditions during the computational time. Once a detector environment is specified, the FE/DE can reproduce the important

variables of the environment in a repeatable fashion, and actual detectors or sensors can be exposed to the defined environment for performance evaluation.

## 5. References

- [1] Luck, H., and Sievert, U., "Does an Overall Modelling Make any Sense in Automatic Fire Detection?", Proceeding of the 11th International Conference on Automatic Fire Detection "AUBE '99", March 16-18, 1999, Gerhard Mercator University, Duisburg, Germany, Luck, H., Ed., pp 1-9, 1999.
- [2] Davis, W., "The Zone Fire Model Jet: A Model for the Prediction of Detector Activation and Gas Temperatures in the Presence of a Smoke Layer", NISTIR 6324, National Institute of Standards and Technology, Gaithersburg, MD, May, 1999.
- [3] Davis, W., and Forney, G., "A Sensor-Driven Fire Model, Version 1.1", NISTIR in preparation, National Institute of Standards and Technology, Gaithersburg, MD, January, 2001.
- [4] Andersson, p., and Holmstedt, G., "CFD-Modelling Applied to Fire Detection - Validation Studies and Influence of Background Heating," Proceeding of the 10th International Conference on Automatic Fire Detection "AUBE '95, April 4-6, 1995, Gerhard Mercator University, Duisburg, Germany, Luck, H., Ed., pp 429-438, 1995.
- [5] Davis, W., Forney, G., and Bukowski, R., "Developing Detector Siting Rules from Computational Experiments in Spaces with Complex Geometries," Fire Safety Journal, Vol. 29, pp 129-139, 1997.
- [6] Cleary, T., Anderson, M., Averill, J., and Grosshandler, W., "Evaluating Multi-sensor Fire Detectors in the Fire Emulator/Detector Evaluator," Proceedings of the 8th Inter. Conf. on Fire Science and Eng., Interflam '99, Edinburg, Scotland, June 1999.
- [7] McGrattan, K., Baum, H., Rehm, R., Hamins, A., and Forney, G., "Fire Dynamics Simulator - Technical Reference Manual," NISTIR 6467, National Institute of Standards and Technology, Gaithersburg, Maryland, January, 2000.
- [8] Mulholland, G., and Croarkin, C., "Specific Extinction Coefficient of Flame Generated Smoke," Fire and Materials, Vol. 24, pp 227-230, 2000.
- [9] Heskestad, G., "Engineering Relations for Fire Plumes," Fire Safety Journal, Vol. 7, pp. 25-32, 1984.
- [10] Cleary, T., Grosshandler, W., and Chernovsky, A., "Smoke Detector Response to Nuisance Aerosols," Proceeding of the 11th International Conference on Automatic Fire Detection "AUBE '99", March 16-18, 1999, Gerhard Mercator University, Duisburg, Germany, Luck, H., Ed., pp 32-41, 1999.
- [11] Cleary, T., "Performance Characterization of Multi-sensor, Multi-criteria Fire Detectors in the Fire Emulator/Detector Evaluator: Particulate, Thermal, and Gas Sensing Combinations," Proceedings of VdS Conf. on Gas Sensors for Fire Detection, November 15-16, Cologne, Germany, 2000.



## Fire Sensor Modelling and Simulation

### 1. Introduction

In automatic fire detection it is desirable to know exactly how fire sensors incl. their housing work.

A fire sensor in its housing is the *link* between *physical quantities* in the sensor housing environment and the usually *electrical signals* generated by the sensor. The *physical quantities* (fig. 1) in the room to be watched are converted into *elec-*

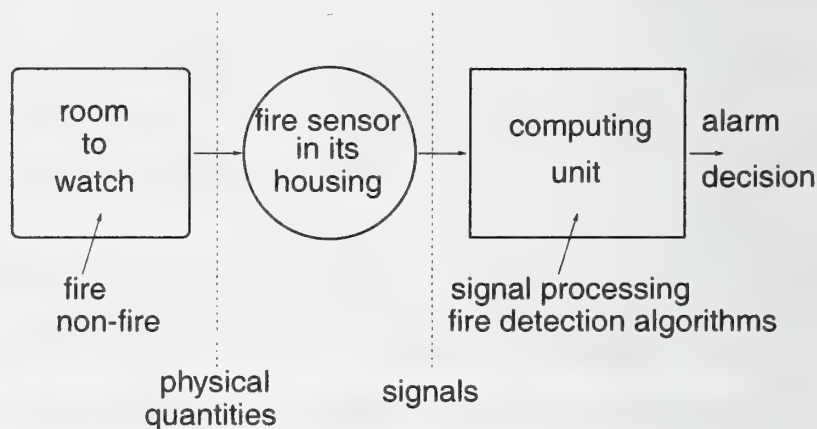


Figure 1: Automatic Fire Detection

*trical signals* by the *sensor element* itself. The physical quantities must penetrate through the housing, which surrounds the sensor element in order to protect it against touch, damage, dirt, etc. and, in case of optical sensors, against disturbing external light.

The actual measurement of the physical quantities as well as the process of enter-

ing the housing *have some influence on the measuring result*. Exact knowledge how these mechanisms work is required in order to correctly describe fire sensors and interpret their signals in a correct way.

The *computing unit* (fig. 1) represents the "intelligence" of a fire detection system. It processes the sensor signals, it combines those of a group of sensors if necessary, watches for sudden changes or crossed thresholds etc. in order to form an *alarm decision*.

The sensor in its housing together with the computing unit represent the *fire detector*.

When it becomes possible to model and simulate the *fire sensor in its housing* then *complete fire detectors* can be simulated in computer program on the base of physical quantities which have been measured and recorded during test fires. This is even possible for a new fire detector while it is under development if the basic model is correct.

## 2. The sensor element

The sensor element is the device that actually measures physical quantities and converts them into an electrical signal.

### 2.1. Ionisation chamber type smoke sensor

The ionisation chamber can be described according to HOSEMANN [12]

$$y = \frac{1}{\eta} \int_{d=0}^{\infty} d dN^{(H)}(d) \quad (1)$$

$y$  = smoke density

$\eta$  = chamber constant [12]

$d$  = particle diameter

$$N^{(H)}(d) = \text{particle size distribution}$$

Though there are more accurate theories available HOSEMANN's formula [12] is used for simplicity. The chamber current  $i_k$ , which depends on the smoke density  $y$  according to

$$y = \frac{i_0}{i_k} - \frac{i_k}{i_0} \quad (2)$$

$i_0 = \text{chamber current without smoke}$

is also somewhat influenced by the velocity of the air through the chamber. This effect is not contained in HOSEMANN's formula. It can be described:

$$i_k(v) = i_k(v=0)f_v\left(\frac{v}{v_{Er}}\right) \quad (3)$$

$$f_v(x) = \begin{cases} 1 - \frac{1}{2}x & x < 1 \\ \frac{1}{2x} & x \geq 1 \end{cases} \quad (4)$$

$v_{Er} = \text{constant}$

## 2.2. Optical smoke sensors

Optical smoke sensors i.e. the scattered light sensor and the light extinction sensor, can be described using the MIE theory [16, 13]

$$I = I_0 \int_{d=0}^{\infty} \frac{V_{St} \lambda^2}{8\pi^2 r^2} (i_1\left(\frac{\pi d}{\lambda}, \underline{m}, \Theta\right) + i_2\left(\frac{\pi d}{\lambda}, \underline{m}, \Theta\right)) dN^{(H)}(d) \quad (5)$$

$$\sigma_{ext} = \int_{d=0}^{\infty} C_{ext}(d) dN^{(H)}(d) \quad (6)$$

$I$  = intensity of scattered light

$I_0$  = intensity of incoming light

$d$  = particle diameter

$V_{St}$  = scattering volume

$\lambda$  = wavelength of incoming light

$\pi$  = 3.1415926...

$r$  = distance between observer and scattering volume

$i_{1,2}$  = MIE scattering functions [13]



- $\underline{m}$  = complex refractive index  
 $\Theta$  = scattering angle  
 $\sigma_{ext}$  = extinction coefficient  
 $C_{ext}$  = extinction cross section [13]  
 $N^{(H)}(d)$  = particle size distribution

## 2.3. Elektrostatic sensor

Electrostatic sensor can be described according to [9]

$$i = K \int_{d=0}^{\infty} P_D\left(\frac{d}{2}\right) q_T\left(\frac{d}{2}\right) dN^{(H)}(d) \quad (7)$$

$$P_D(a) = \min \left\{ \frac{b(a)Uh}{vd_C^2}; 1 \right\} \quad (8)$$

$i$  = sensor current

$K$  = sensor constant

$a$  = particle radius

$d$  = particle diameter

$q_T(a)$  = electrical charge on a particle

$N^{(H)}(d)$  = particle size distribution

$b(a)$  = electrical mobility of a particle

$U$  = voltage of sensor

$v$  = velocity of air through the sensor

$h, d_C$  = geometrical sizes

## 2.4. Semiconductor gas sensors

Semiconductor gas sensors usually present an electrical output quantity according to:

$$g = c_1 K_1 + c_2 K_2 + \dots + c_n K_n + c_T (T - T_0) \quad (9)$$

- $g$  = sensor output signal
- $c_i$  = sensitivity constants
- $K_i$  = volume concentration of gases
- $T$  = temperature
- $T_0$  = reference temperature, usually room temperature

### 3. Particle filtering

The sensor housing can be interpreted as particle filter. It is a particle-size distinctive filter according to the five principles described by OGAWA [20, 21]:

- Inertia Deposition: decreases number of large particles
- Interception: decreases number of large particles
- Diffusion: decreases number of small particles
- Electrostatic attraction: decreases number of small particles
- Gravity settling: decreases number of large particles

Particle deposition also occurs in the inside of the sensor housing. Altogether, these effects result in a kind of particle size bandpass so that the particle size distribution in the inside of the housing differs from the particle size distribution outside:

$$N_i^{(H)}(d) = N^{(H)}(d)f_{BP}(d) \quad (10)$$

$d$  = particle diameter

$N_i^{(H)}(d)$  = particle size distribution, inside

$N^{(H)}(d)$  = particle size distribution, outside

$f_{BP}(d)$  = bandpass function

Another way to achieve this is the following: In an abstract point of view, if the particle size distribution can be described by a set of parameters  $p_1, \dots, p_n$  the

particle bandpass transforms these parameters into another set  $p_{1i}, \dots, p_{mi}$ . For example, we can assume a logarithmic normal distribution with the parameters  $n_0$  (volumetric number concentration),  $\mu$  (geometric mean particle diameter), and  $\sigma$  (geometric standard deviation) which turn into  $n_{0i}$ ,  $\mu_i$ , and  $\sigma_i$ , respectively.

## 4. Entry lag

Entry lag was first described by HESKESTAD [11] and has been extended by CLEARY e.a. [5]. It is modelled as an air velocity dependent system with the impulse response

$$h(t) = A\varepsilon(t - t_0)ce^{-c(t-t_0)} \quad (11)$$

$$c = k_c v^{d_c} \quad (12)$$

$$t_0 = k_t v^{d_t} \quad (13)$$

$A$  = constant, area under the function

$$\varepsilon(t) = \begin{cases} 1, & t \geq 0 \\ 0, & t < 0 \end{cases}$$

$e$  = Euler number

$k_c, d_c, k_t, d_t$  = parameters

$v$  = velocity of air through the sensor housing

## 5. Combining things into a general model

For a complete spot-type fire sensor the following general model based on the model proposed by FISSAN and HELSPER [8] is proposed:

The model (fig. 2) consists of the four parts A, B, C, D while B is distributed into the two parts B1 and B2. The vektor  $\vec{x}$ , representing the model input, is a combination of all physical quantities important for fire detection. Fig. 3 shows an example.



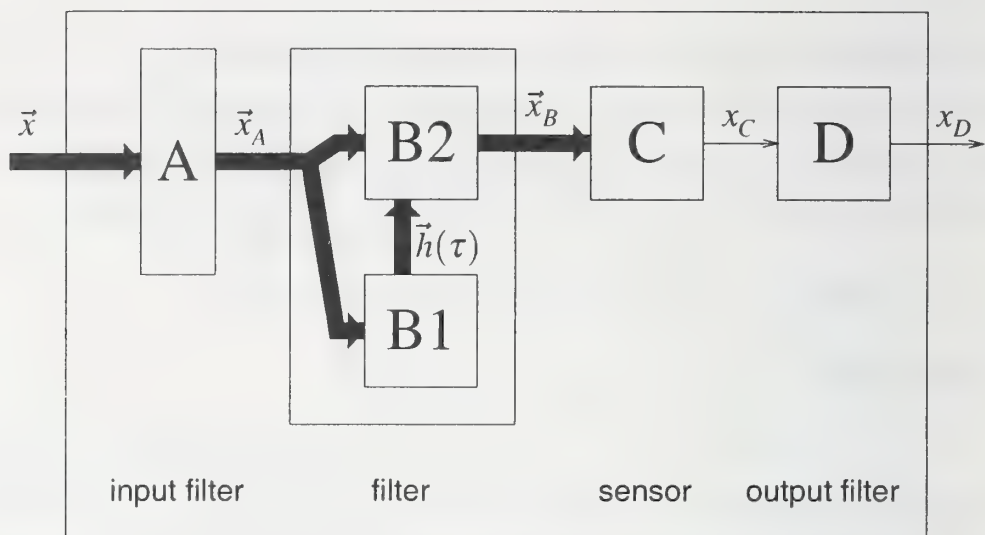


Figure 2: fire sensor in its housing

$i$	$x_i$	comment
1	$n_0$	volumetric particle number concentration
2	$\mu$	geometric mean particle diameter
3	$\sigma$	geometric standard deviation
4	$\underline{m}$	complex refractive index
5	$v$	velocity of air
6	$T$	temperature

Figure 3: Example of physical quantities in vector  $\vec{x}$

Part A is a memoryless system. Its output vector  $\vec{x}_A$  is a vectorial function of  $\vec{x}$  i.e. each component of the output vector may depend on each component of the input vector. The idea is that part A represents the particle filter.

Part B is a system with memory modelling the entry lag. It is based on the theory of linear and time-invariant systems though the system is not necessarily linear or time-invariant. First, part B1 constructs a function  $h_i(\tau)$  for each component of the input vector. Then, this function is used as an impulse response in part B2. So the output vector  $\vec{x}_B$  consists of components which are the results of the convolution of the respective component of  $\vec{x}_A$  with the associated impulse response. Note that the impulse response may be time dependent because it is formed by part B1

which gets time dependent input signals.

Part C describes the sensor element itself. This means that it combines the components of its input vector  $\vec{x}_B$  into a single-component output signal  $x_c$  according to the physical laws describing the sensor (MIE theory, HOSEMAN theory etc).

Part D is an output filter representing for example sensor signal amplifier characteristics (lowpass, limiter). It is optional.

## 6. Simulation results

Simulation results presented reflect the state of the study from July 2000 and are preliminary. The study is continued. Simulations are based on particle measurements by TAMM, MIRME, e.a. [23, 17] which result in a particle size distribution in the form of  $N^{(H)}(d, t)$  during the test fires. All tests have been made in the fire detection laboratory at the Gerhard-Mercator-Universität Duisburg. Also, the air velocity has been recorded.

In the following figures 4 to 6, the measured output signals of industry-standard fire sensors are compared to the simulated signals according to the model proposed above. As an example, test fire TF1 according to EN54/9 [7] is shown. The results for other fires are similar.

## 7. Conclusion

A new, complete, and highly modular model for fire sensors including the housing has been introduced. The model is based on the work from HESKESTAD, FISSAN and HELSPER, CLEARY a.o. and has been designed to be suitable for computer simulation. Simulation results have been presented and compared to signals measured with industry-standard fire detectors.

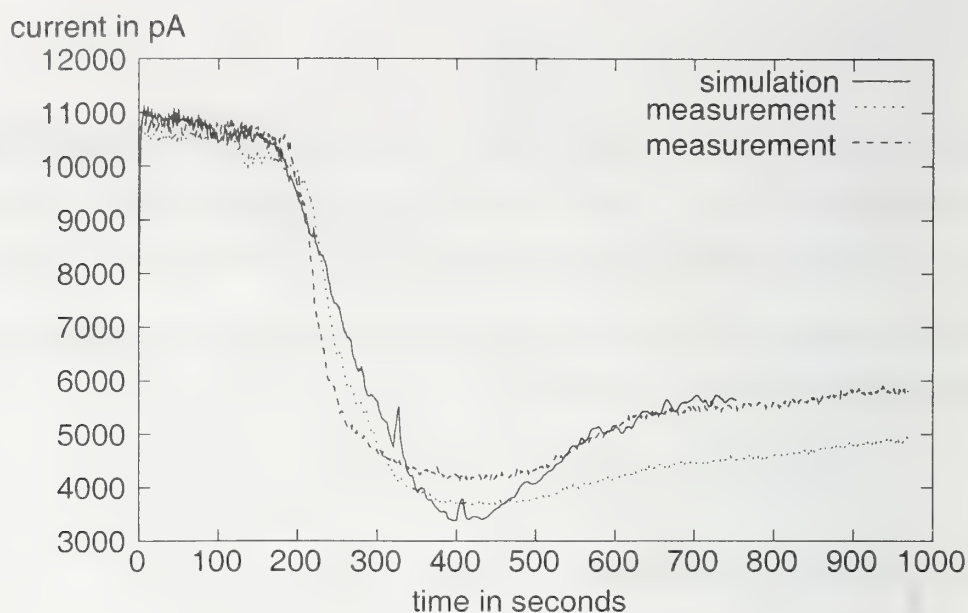


Figure 4: ionisation chamber response during TF1

## References

- [1] N.G. BERNIGAU, H. LUCK: *The Principle of the Ionization Chamber in Aerosol Measurement Techniques – A Review*. Journal of Aerosol Science Vol 17 No 3, 1986, pp. 511-515
- [2] J. BJÖRKMAN, D. BAROUDI, M. KOKKALA, R. LATVA, M. TUOMISSAARI: *Determination of Characteristic Parameters of Point-type Smoke Detectors*. in: H. LUCK (HERAUSGEBER): Tagungsband der 11. Internationalen Konferenz über automatische Brandentdeckung AUBE'99, Duisburg, März 1999, Agst Verlag Moers 1999, S. 22-31
- [3] C.F. Bohren, D.R. Huffman: *Light Scattering and Absorption by Small Particles*. Wiley, New York 1983
- [4] TH. CLEARY, W. GROSSHANDLER, A. CHERNOVSKI: *Smoke Detector Response to Nuisance Aerosols*. In: H. LUCK (HERAUSGEBER): Tagungsband der 11. Internationalen Konferenz über automatische Brandentdeckung AUBE'99, Duisburg, März 1999, Agst Verlag Moers 1999, S. 32-41



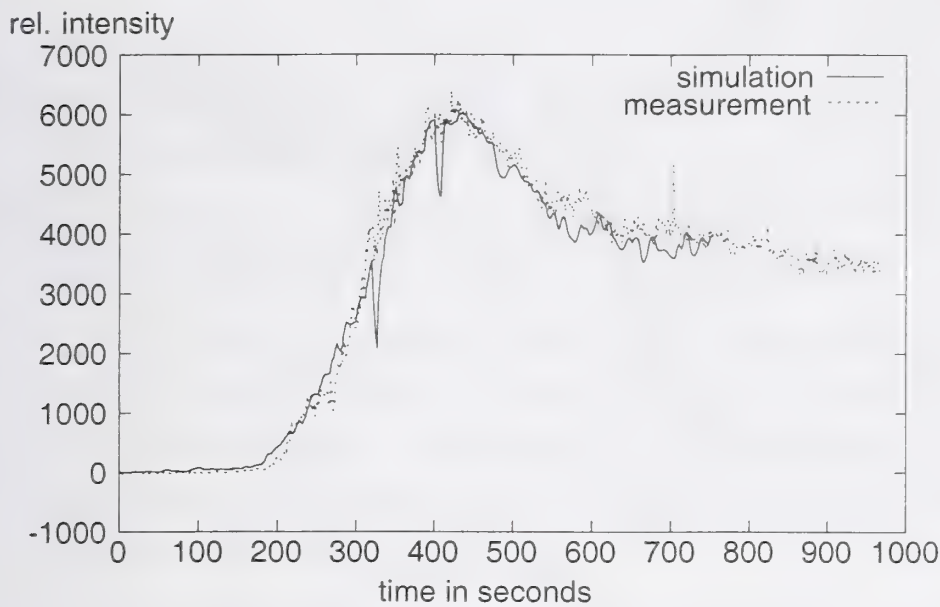


Figure 5: scattered light sensor response during TF1

- [5] TH. CLEARY, A. CHERNOVSKI, W. GROSSHANDLER, M. ANDERSON: *Particulate Entry Lag in Spot-type Smoke Detectors*. In: Proceedings of the Sixth International Symposium on Fire Safety Science, Poitiers, 1999
- [6] I. COLBECK, B. ATKINSON, Y. JOHAR: *The Morphology and Optical Properties of Soot produced by different fuels*. Journal of Aerosol Science Vol 28 No 5 July 1997, pp. 715-723
- [7] CEN EUROPÄISCHES KOMMITTEE FÜR NORMUNG: *EN 54 Teil 9, Bestandteile automatischer Brandmeldeanlagen, Erprobungstest*. 1984
- [8] H. FISSAN, C. HELSPER: *Zur Reaktion von Rauchdetektoren auf Brandkenngrößen*. In: H. LUCK (HERAUSGEBER): Tagungsbericht des 8. internationalen Vortragsseminars über Probleme der automatischen Brandentdeckung AUBE'82, Duisburg, Oktober 1982, S. 20-37
- [9] F. GOCKEL: *Messung der elektrischen Ladung bei Testbränden*. In: H. LUCK (HERAUSGEBER): Tagungsband der 11. Internationalen Konferenz über automatische Brandentdeckung AUBE'99, Duisburg, März 1999, Agst Verlag Moers 1999, S. 160-169

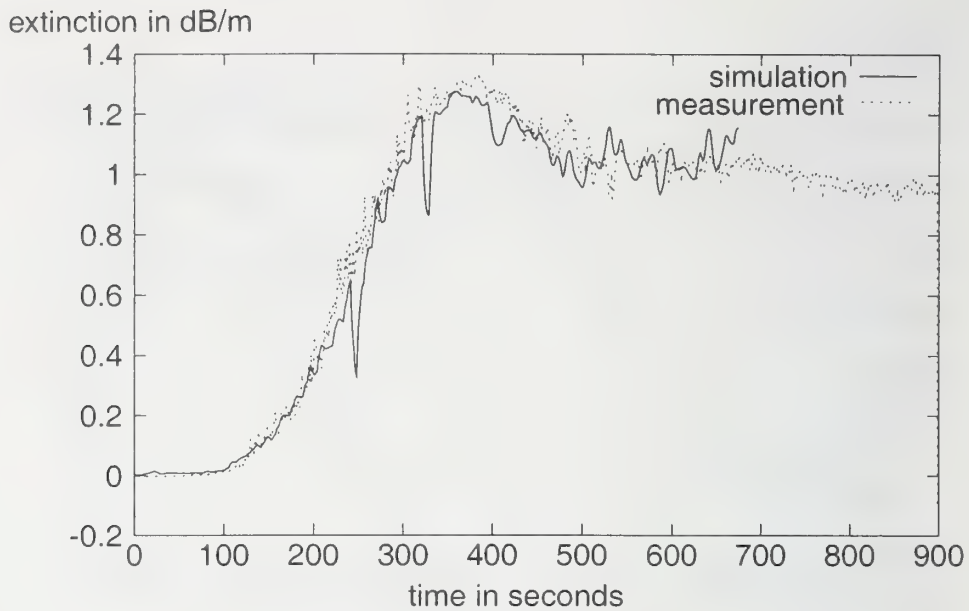


Figure 6: light extinction sensor response during TF1

- [10] C. HELSPER, H. FISSAN, J. MUGGLI, A. SCHEIDWEILER: *Verification of Ionization Chamber Theory*, Fire Technology 19, 1, 1983, pp. 14-21
- [11] G. HESKESTAD: *Generalized Characterization of Smoke Entry and Response for Products-of-Combustion Detectors*. In: V. ASCHOFF, H. LUCK (HERAUSGEBER): Tagungsbericht zum 7. internationalen Vortragsseminar über Probleme der automatischen Brandentdeckung AUBE'75, Aachen, 1975, S. 267-310
- [12] J.P. HOSEMANN, H. GILSON: *Meßkammer nach dem Kleinionenanlagerungsprinzip zum quantitativen Nachweis von Aerosolpartikeln*. Forschungsberichte des Landes Nordrhein-Westfalen Nr. 2336, Westdeutscher Verlag Opladen, 1973
- [13] M. KERKER: *The Scattering of Light*. Academic Press, New York 1969
- [14] C.D. LITTON: *A Mathematical Model for Ionization Type Smoke Detectors and the Reduced Source Approximation*. Fire Technology 13, 4, 1977, pp. 266-281
- [15] G. MEYER: *Ein mathematisches Modell für Ionisationsrauchmelder*. In: H. LUCK (HERAUSGEBER): Tagungsbericht des 8. Internationalen

Vortragsseminars über Probleme der automatischen Brandentdeckung  
AUBE'82, Duisburg, Oktober 1982, S. 38-62

- [16] G. MIE: *Beiträge zur Optik trüber Medien, speziell kolloidaler Metallösungen*. Annalen der Physik, Band 25, Folge 4, Nr. 3, 1908, S. 377-445
- [17] A. MIRME, E. TAMM, U. SIEVERT: *Performance of an Optical and an Ionisation Smoke Detector Compared to a Wide Range Aerosol Spectrometer*. In: H. LUCK (HERAUSGEBER): Tagungsband der 11. Internationalen Konferenz über automatische Brandentdeckung AUBE'99, Duisburg, März 1999, Agst Verlag Moers 1999, S. 380-391
- [18] G.W. MULHOLLAND: *Smoke Production and Properties*. in: PH.J. DINENNO (EDITOR): The SFPE Handbook of Fire Protection Engineering, National Fire Protection Association, Quincy 1995, pp. 2/217-227
- [19] J.S. NEWMAN: *Prediction of Fire Detector Response*. Fire Safety Journal 12, 1987, pp. 205-211
- [20] A. OGAWA: *Separation of Particles From Air and Gases*. Vol. 1, CRC Press, Boca Raton, Florida 1984
- [21] A. OGAWA: *Separation of Particles From Air and Gases*. Vol. 2, CRC Press, Boca Raton, Florida 1984
- [22] F.N. SIMON, G.D. RORK: *Ionization Type Smoke Detectors*. Rev. Scient. Instrum. 48, 2, 1976
- [23] E. TAMM, A. MIRME, U. SIEVERT, D. FRANKEN: *Aerosol Particle Concentration and Size Distribution Measurements of Test-Fires as Background for Fire Detector Modelling*. In: H. LUCK (HERAUSGEBER): Tagungsband der 11. Internationalen Konferenz über automatische Brandentdeckung AUBE'99, Duisburg, März 1999, Agst Verlag Moers 1999, S. 150-159



B. Farouk, G. W. Mulholland\*, and K. B. McGrattan\*

Department of Mechanical Engineering and Mechanics, Drexel University  
Philadelphia, PA

\*Building and Fire Research Laboratory, National Institute of Standards and  
Technology, Gaithersburg, MD

### **Simulation of Smoke Transport and Coagulation for a Standard Test Fire**

#### **Abstract**

Large eddy simulations of a standard test fire (EN 54-9, TF4) were carried out. The development of the large-scale air movements and temperature fields generated by the enclosure fires are calculated. In addition, the smoke transport and time evolution of the size distribution of smoke aerosol due to coagulation are also predicted. The mass and number densities of smoke particles are computed at a detector location, as specified in the standard test fire procedure. Recent measurements of the number and mass densities of smoke using electrical aerosol spectrometry compared favorably with the model predictions.

#### **Introduction**

Smoke detector response is sensitive to both the concentration of smoke ingested and the size distribution of the aerosol in a fire scenario. The local smoke characteristics actually sensed by the detector must be related to the physical and geometrical properties of the fire and the enclosure, so that the response of a smoke detector can be understood.

Generally the ionization detectors are found to be more sensitive to the *number density* of the smoke. As a class, smoke detectors using the ionization principle provide somewhat faster response to high energy (open flaming) fires, since these fires produce larger numbers of the smaller smoke particles. On the other hand, photoelectric smoke

detectors respond to the volume (*mass*) *density* of the smoke particles rather than the number density.

Prediction of smoke transport and coagulation has been attempted in the past [1, 2] where the evolution of size distribution of smoke aerosol under the influence of coagulation as well as the large scale fluid motion and temperature fields were studied. Specifically, Lagrangian particles or 'thermal elements' were used to model the burning of fuel in the fire plume. Each thermal element (blob) represents a given mass of smoke (containing many smoke particles), which is proportional to the instantaneous heat release rate. The transport of the thermal elements is also used to model smoke movement (without smoke coagulation) in a Lagrangian sense. The evolution of the size distribution in space was calculated deterministically from the solution to the Smoluchowski equation.

A promising methodology for the prediction of large-scale gas movement, temperature field and smoke movement in fire plumes and enclosure fires has been recently introduced [3]. The model and computational methodology have reproduced mean temperature and buoyant velocity correlations for large fire plumes [4]. In this paper, we present numerical results for the velocity and temperature fields induced by a standard test fire (EN 54 part 9) [5] by applying the above model, which incorporates large eddy simulation techniques. The simulations reported here are for the test fire TF4 (open plastic fire) [5]. The smoke particles are again represented by a large number of the thermal elements - continuously introduced at the burning surface, while the fuel is being consumed. Based on prescribed rates of smoke yield ( $Y$  kg/kg of fuel consumed), the smoke transport within the enclosure is reported. While the ionization detectors are found to be more sensitive to the local number density of the smoke, the photoelectric detectors are more sensitive to the mass density. Hence it is necessary to determine both the mass and the number densities of the aerosol reaching a detector. A smoke coagulation sub-model based on the Smoluchowski equation [6] is incorporated to track the mean number density of smoke particles in each blob with time. The mean size of the smoke particles in each thermal element increases with time due to coagulation. The smoke mass and number-densities at a specified detector location are computed directly

from the number of thermal elements and the corresponding number densities of smoke particles in each thermal element (blob), present at the detector location. The time evolution of the mass and number densities of smoke at the detector location are compared with the recent measurements reported by Mirme et al. [7]. The model predictions for smoke coagulation compare favorably with the reported measurements.

### **Problem description**

The test fire TF4 in EN 54-9 [4] is an open plastic fire, which is allowed to burn freely with no restriction of air supply in an enclosure. The overall enclosure dimensions and the detector location are specified in the test procedure. For the present simulations, a 9.5 m x 6.3 m x 4.0 m enclosure was considered (see Figure 1 below). A small vent is considered at a bottom corner of the enclosure to allow for constant pressure condition during the combustion process. The fire source is located at the center of the enclosure (0.5 m x 0.5 m) on a 0.25 m high pedestal. The walls, floor and ceiling are considered to be thermally insulated. The rate of heat release  $\dot{q}(t)$  for the TF4 fire is estimated from the measurements reported by Ahonen and Sysio [8].

### **Model description**

A fire plume is a three-dimensional transient buoyant flow that can be modeled by the motion of a thermally expandable ideal gas [8]. The Navier-Stokes equations are solved for such a fluid driven by a prescribed heat source. Following Rehm and Baum [9] the pressure is decomposed into three components, a background (average) pressure, a hydrostatic contribution, and a perturbation to the hydrostatic pressure. High-frequency acoustic oscillations are eliminated while large temperature and density variations typically found in fires are retained. The resulting equations are thus referred to as weakly compressible and are valid for low Mach number flows. Constant pressure specific heat of the gas is considered in the formulation. An elliptic partial differential equation for pressure perturbation is formulated by taking the divergence of the momentum equation. Further details of the mathematical formulation can be obtained in [3].



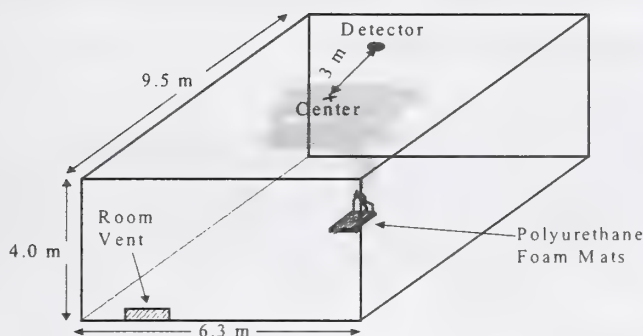


Figure 1. Schematic of the test fire laboratory

### Large eddy simulation technique

The present application of the large eddy simulation (LES) techniques to fire is aimed at extracting greater temporal and spatial fidelity from simulations of fire performed on the more finely meshed grids allowed by modern fast computers. The small-scale eddy motion is modeled via a sub-grid description. One such representation is the Smagorinsky model. There have been numerous refinements of the original Smagorinsky model but it is difficult to assess the improvements offered by the newer schemes. In this study, we have used the Smagorinsky model, which produces satisfactory results for most large-scale applications where boundary layers are not important [3].

### Combustion model

A sub-grid thermal element model (TEM) is formulated to represent the fire. A large number of Lagrangian elements (blobs) are introduced into the plume, releasing heat as they are convected by the thermally induced motion [3]. The overall heat release rate  $\dot{q}(t)$  from the fire is discretized as thermal elements that represent pyrolyzed fuel. At a specified surface, such as the fuel bed, thermal elements are ejected at a rate of  $\dot{n}''$  blobs per unit time per unit area. The heat release rate of a single thermal element 'j' is given by

$$\dot{q}_{p,j} = \frac{\dot{q}''(t_0)}{\dot{n}''} \frac{1}{t_b} \quad (1)$$

where  $\dot{q}''(t_0)$  is the instantaneous heat release rate per unit area of the fuel bed and  $t_b$  is the burnout time ( $t - t_0 < t_b$ ) of the thermal element and  $t_0$  is the time the element is

ejected from the burning surface. The burnout time is obtained from the plume correlations of Baum and McCaffrey [4].

#### Smoke transport model

A specified percentage of the fuel consumed (smoke yield,  $Y$  kg/kg of fuel) is assumed to be converted to smoke particulate. The smoke transport is simulated by tracking the motion of the thermal elements. The smoke mass in any thermal element (blob) introduced at time  $t_0$  is given by

$$m_s = \frac{\dot{q}''(t_0) Y}{\Delta H_c \dot{n}''} \quad (2)$$

where  $\dot{q}''(t_0)$  is the instantaneous heat release rate,  $Y$  is the smoke yield and  $\Delta H_c$  is the heat of combustion of the fuel. Again,  $\dot{n}''$  is the number of thermal elements injected per unit time per unit area of the burning surface. In the present model, the total smoke mass in each blob remains constant as it is convected by the buoyant plume. At any instant, the smoke mass density at the detector location can be determined if the total number of smoke blobs in the detector volume is known. The smoke mass density is the summation of smoke masses of the individual thermal elements in a grid cell of volume  $\delta x \delta y \delta z$ .

$$C_m(t) = \frac{\sum m_{s,j}}{\delta x \delta y \delta z} \quad (3)$$

#### Smoke coagulation model

The most important physical mechanism acting to change the smoke aerosol sized distribution once it leaves the flame zone of a fire is coagulation. The particles present at high concentration levels collide as a result of Brownian motion and stick together. The time evolution of coagulating particles for a uniform system is described by the Smoluchowski equation

$$\frac{\partial n(v,t)}{\partial t} = \int \Gamma(v-v', v') n(v-v', t) n(v', t) dv' - 2n(v, t) \int \Gamma(v, v') n(v', t) dv' \quad (4)$$

where  $n(v, t) dv$  is the number concentration in the particle volume size range  $v$  to  $v + dv$  and  $\Gamma(v, v')$  is the coagulation frequency. In this analysis, we assume that  $\Gamma(v, v')$  is a constant. The total number concentration,  $N(t)$  and the volume concentration  $V(t)$  are obtained as the first two moments of the size distribution. Integrating equation (3) with respect to volume leads to the following differential equation:

$$\frac{dN}{dt} = -\Gamma N^2 \quad (5)$$

Smaller particles collide and stick decreasing the number concentration, but the volume concentration is unchanged. For the present calculations, the time evolution of the number density of smoke particles  $n_s(t)$  in a given thermal element is modeled as [5]

$$n_s(t) = \frac{n_s^0}{(1 + \Gamma N^0 t)} \quad (6)$$

where  $n_s^0$  is initial number of smoke particles in a thermal element at the time of its injection,  $\Gamma$  is the coagulation frequency and  $N^0$  is the initial number concentration of smoke particles (number of particles/volume) in the flame zone. For the present calculations, the value of  $G$  ( $G = \Gamma N^0$ ) is estimated from measurements reported in literature. The initial number of smoke particles  $n_s^0$  in a thermal element (injected at time  $t_0$ ) is calculated from

$$n_s^0 = \frac{\dot{q}(t_0) Y}{\Delta H_c \dot{m} \left( \frac{1}{6} \pi D_p^3 \rho_s \right)} \quad (7)$$

where  $D_p$  is the initial smoke particle diameter and  $\rho_s$  is the soot density. The smoke number density is the summation of smoke masses of the individual thermal elements in a grid cell of volume  $\delta x \delta y \delta z$ :

$$C_N(t) = \frac{\sum n_{s,j}}{\delta x \delta y \delta z} \quad (8)$$

where  $n_{s,j}$  is defined in equation (12) above for the  $j$ -th particle.

## Results and discussion

We present the results for a hypothetical fire with a 'fixed heat release rate' first. The computational domain is a parallelepiped region with a rectangular base (9.5 m x 6.3 m) and a height of 4.0 m. The origin of the Cartesian coordinate system is at the right bottom corner. A uniform mesh (64 x 32 x 32) was used for the simulations. This gives a cell size with dimensions 0.15 m x 0.20 m x 0.12 m. All simulations were carried out for a period of 300 s. For all calculations presented, only 65% of the energy from combustion is considered to be the convective heat release. The rest of the energy, converted to radiation, did not play any role in the simulations as none of the surfaces



were specified in the model as thermally active. The heat of combustion of the fuel ( $\Delta H_c$ ) was taken as 20,000 kJ/kg. A smoke yield value of  $Y = 0.05$  kg/kg of fuel consumed) was used for the present simulations. Figure 2 shows the time-dependent convective heat release rate for the simulation with 'a fixed heat release rate'.

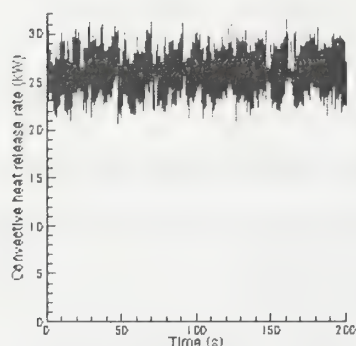


Figure 2. Convective heat release rate for the 'fixed heat release rate' case.

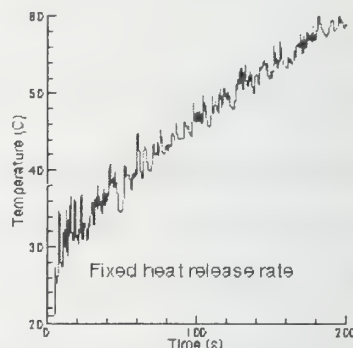


Figure 3. Predicted temperature profile at the detector location

According to EN54 – 9 specifications, the detectors and measuring instruments are to be located along a 3 m radius from the center of the fire source. A detector location was chosen near the ceiling ( $z = 3.9$  m) at  $x = 2.25$  m,  $y = 3.15$  m (see Figure 1). For the present mesh, one computational cell was found to be large enough to represent a detector. The temperature rise at the detector location is shown in Figure 3 as a function of time. The temperature at the detector location continues to increase as the heat release rate is held fixed in the simulations. A large number of thermal elements were introduced into the flow field to properly characterize the smoke transport and coagulation. Five thermal elements were introduced per each cell covering the burning area per time step ( $\Delta T = 0.05$  s). All thermal elements introduced were tracked for the entire period of the calculations (200 s) unless they leave the enclosure by the small vent (see Figure 1).

The predicted smoke number density variation (averaging time = 3 s) at the detector location for the 'fixed heat release rate' case is shown in Figure 5. Coagulation effects

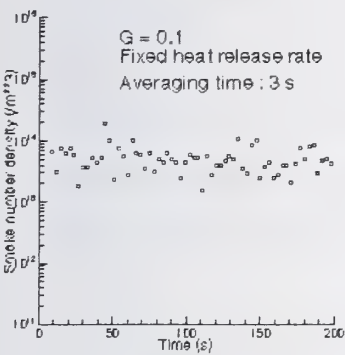


Figure 5. Predicted smoke number density  $C_m(t)$  at the detector location for the 'fixed heat release rate' case

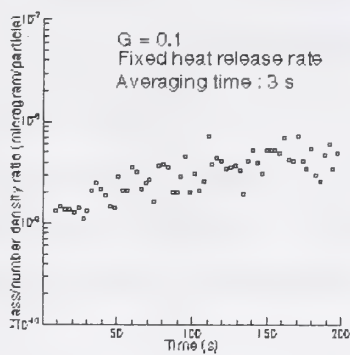


Figure 6. Ratio of smoke mass/number densities  $C_m(t)/C_N(t)$  at the detector location for the 'fixed heat release' case

were considered by setting  $G = 0.1 \text{ s}$ . The time-averaged evolution of the ratio of the smoke mass/number densities at the detector location is shown in Figure 6. The ratio increases initially as the buoyant plume reaching the detector develops. The effect of aging on the smoke particles is evident after about 150 s when the ratio of mass/number densities starts decreasing.

The simulations of the test fire (TF4) are presented next. The EN54 –9 specifications suggest a fuel source of soft polyurethane foam mats (0.5 m x 0.5 m). The heat release rate for the fuel source is obtained from the measurements of Ahonen and Sysio [7]. The heat of combustion of the fuel ( $\Delta H_c$ ) was taken as 20,000 kJ/kg and the smoke yield value was  $Y = 0.05 \text{ kg/kg}$ . Figure 7 shows the time-dependent convective heat release rate for the simulations of test fire TF4.

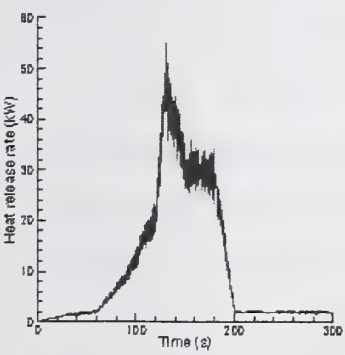


Figure 7. Convective heat release rate for the TF4 fire

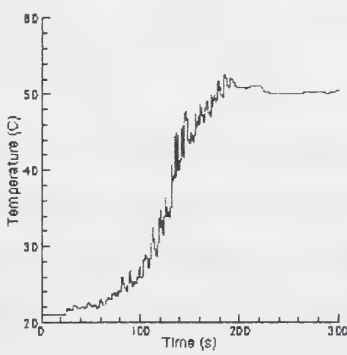


Figure 8. Predicted temperature profile at the detector location for the TF4 fire

The TF4 fire simulations were carried out for a period of 300 s. The large eddy simulations capture the evolution of the characteristic structure of the fire-plume and the associated buoyant flow field. The temperature rise at the detector location is shown in Figure 8 as a function of time. The temperature (non-averaged) at the detector location remains unchanged for the first 20 s, then increases rapidly. After the fuel source is fully consumed, the temperature is found to decrease gradually.

The predicted time variation of the smoke mass density (averaging time: 3 s) at the detector location is shown in Figure 9 for the TF4 fire. The smoke mass density increases continuously for the about 120 s (see Figure 7 for the corresponding rise in heat release rate) then levels off as the strength of the fire decreases. The recirculating flow generated in the test section maintains the level of smoke mass density at the detector location. When the calculations are carried out with no coagulation model ( $G = 0$  s), the predicted evolution of smoke-mass and number densities are similar and the ratio of mass/number densities at the detector location is invariant.

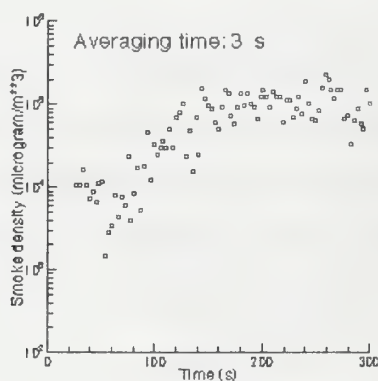


Figure 9. Time-averaged (3 s intervals) prediction of the smoke density  $C_m(t)$  at the detector location for the TF4 fire

Recent measurements of the TF4 fire smoke characteristics are reported in Mirme et al. [7]. An electrical aerosol spectrometer (EAS) was used to measure the smoke aerosol characteristics including number and mass densities. The EAS is able to measure the extremely fast changing aerosol in a broad particle size range. The measured time variation of the smoke number density (top curve) and the smoke mass density (bottom curve) are shown in Figure 10.



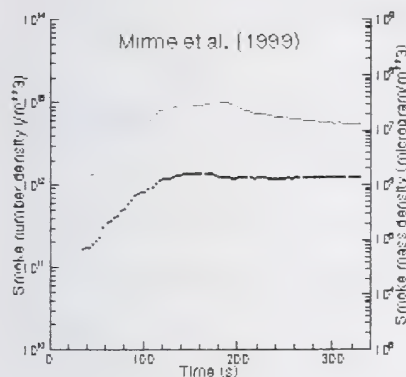


Figure 10. Measured time variation of the fire sensor readings for the plastic fire (TF4), Mirme et al.

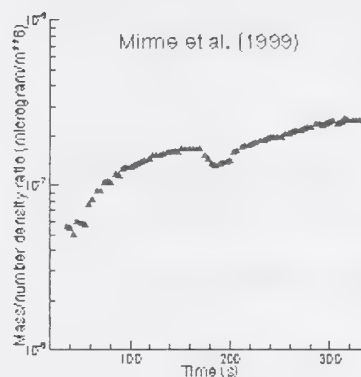


Figure 11. Measured time variation of the ratio  $C_m(t)/C_N(t)$  for the plastic fire (TF4), Mirme et al.

The ratio of the measured smoke/mass number densities is shown in Figure 11. Both the mass and number densities detected tend to increase as the fire grows with the growth rate of mass density higher than the growth rate of the number density.. While the growth rate of the mass density levels off, the number density keeps decreasing as the aerosol ages.

The model predictions for smoke coagulation for the TF4 fire (for different values of the coagulation frequency,  $G$  s are now presented and qualitative comparisons with the measurements (shown in Figures 10 and 11) are made. Figure 12 below shows the predicted time-averaged (averaging time: 3 s) smoke number density for the TF4 fire at the detector location with  $G = 0.1$  s. As the fire gains strength, the number density predicted increases, then starts decreasing as the coagulation effects become apparent. The trend observed in the measurements (Figure 10) is similar to that shown in the predictions in Figure 12. However, differences exist quantitatively between the measurements and the predictions. While the peak value of the measured smoke number density is about  $10^{13}$  /m<sup>3</sup>, the predicted peak value of the smoke number density is about  $10^{14}$  /m<sup>3</sup>. Also the coagulation rate predicted with  $G = 0.1$  s appears to be somewhat faster than the rate observed in the measurements (Figure 10, top curve).

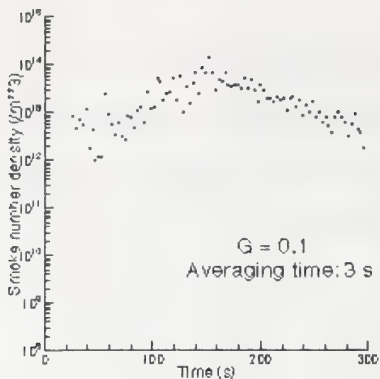


Figure 12. Time-averaged (3 s intervals) predictions of the smoke number density  $C_N(t)$  at the detector location ( $G = 0.1 \text{ s}^{-1}$ ) for the TF4 fire

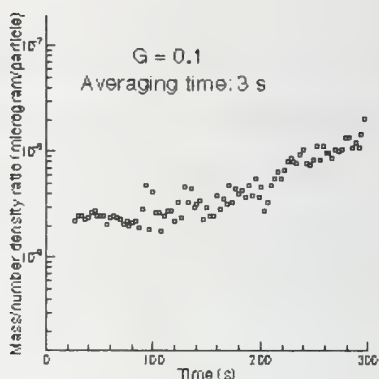


Figure 13. Time-averaged (3 s intervals) prediction of the ratio  $C_m(t) / C_N(t)$  at the detector location for the TF4 fire

The predicted evolution of the ratio of mass/density number densities is shown in Figure 13 with  $G = 0.1 \text{ s}^{-1}$ . The measured ratio (as shown in Figure 11) increases as the fire develops which signifies onset of coagulation effects. In the predictions, the  $C_m(t) / C_N(t)$  ratio remains somewhat invariant for the first 100 s and then starts increasing. This is consistent with the number density variation shown in Figure 11. Predictions were also obtained with a slower coagulation frequency,  $G = 0.01 \text{ s}^{-1}$ . The predicted time variation of the ratio  $C_m(t) / C_N(t)$  is shown in Figure 14. As expected the ratio

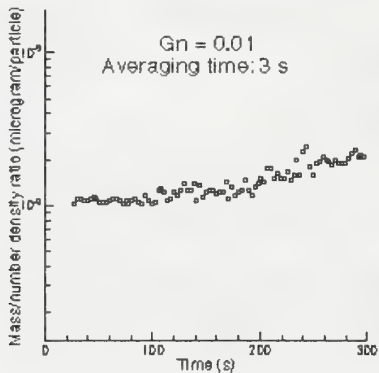


Figure 14. Time-averaged (3 s intervals) prediction of the ratio  $C_m(t) / C_N(t)$  at the detector location ( $G = \Gamma N^0 = 0.01$ )

shows a much gradual rise with time now, indicating that the model simulates the prescribed physics realistically. Better qualitative and quantitative agreement with the

measurements can be obtained by systematically varying the adjustable parameters in the model, namely, the coagulation frequency,  $G$  and the smoke yield  $Y$ .

## Conclusions

Numerical simulations of smoke transport and smoke coagulation in the fire TF4 (EN54 part 9) were conducted. The simulations were based on the heat release rate as prescribed in the test fire. The present results provide interesting insights to the smoke movements as seen by a detector placed near the ceiling of an enclosure.

## Acknowledgements

One of the authors (BF) gratefully acknowledges support from the Building and Fire Research Laboratory at NIST, Gaithersburg, MD where he served as a Guest Researcher during the academic year 1999-00

## References

- [1] Baum, HR, Rehm RG and Mulholland GW, 'Computations of Fire Induced Flow and Smoke Coagulation' 19<sup>th</sup> Symposium (International) on Combustion, The Combustion Institute, 1982, p. 921-931
- [2] Baum HR, Rehm RG and Mulholland GW, 'Prediction of Heat and Smoke Movement in Enclosure Fires', Fire Safety Journal, 1983, 6, p. 193-201
- [3] McGrattan KB., Baum HR. and Rehm RG., 'Large Eddy Simulation of Smoke Movement', Fire Safety Journal, 1998, 30(2), p. 161-178
- [4] Baum HR., and McCaffrey BJ., 'Fire Induced Flow Field – Theory and Experiment' Fire Safety Science – Proceedings of the Second International Symposium, 1989, p. 129-148
- [5] Jackson MA, and Robins I, 'Gas Sensing for Fire Detection: Measurements of CO, CO<sub>2</sub>, H<sub>2</sub>, O<sub>2</sub>, and Smoke Density in European Standard Fire Tests', 1994, Fire Safety Journal, 22, p. 181-205
- [6] Mulholland GW, 'Smoke Production and Properties', NFPA Fire Protection Handbook, Sec. 2, Ch. 15, 1993
- [7] Mirme A., Tamm, E. and Siever, U, 'Performance of an Optical and an Ionization Smoke Detector Compared to a Wide Range Aerosol Spectrometer', Internationale Konferenz über Automatische Brandentdeckung, AUBE 1999, Proceedings, p. 380-391
- [8] Ahonen, AI, and Sysio PA, 'A Run-in Test Series of a Smoke Test Room – Tests according to the proposal prEN 54-9', Research Report 139, Technical Research Center of Finland, 1983
- [9] Rehm RG. and Baum HR., 'The Equations of Motion of Thermally Driven Buoyant Flows', Journal of Research, National Bureau of Standards, 1978, 83(3), p. 297-308



## **A Sensor-Driven Fire Model**

### **1. Introduction**

Modern building fire sensors are capable of supplying substantially more information to the fire service than just the simple detection of a possible fire. Nelson, in 1984, recognized the importance of tying all the building sensors to a smart fire panel [1]. In this paper, a sensor-driven fire model is described that is designed to achieve a smart fire panel configuration such as envisioned by Nelson. A sensor-driven fire model makes use of signals from a variety of detectors such as smoke, heat, gas, etc. to detect, verify and predict the evolution of a fire in a building. In order to accomplish this task, the fire model must be able to discriminate between fire and non-fire conditions, must be able to recognize detector failure for both fire and non-fire scenarios, and must be able to determine the size, location, and potential hazards associated with a growing fire.

The fire model must be flexible by having the capability to handle fire scenarios in rooms where there may be anywhere from a suite of detectors to no detectors. In the latter case, detectors in adjacent rooms would provide the necessary sensor input to the model. For the suite of detectors, the model must be able to take advantage of the increased amount of information in order to provide earlier and more reliable detection. The model must also be able to accommodate detector failures due to a growing fire and still continue to provide estimations of fire growth and location. Finally, the model must be able to handle a large number of rooms and must complete its calculation cycle in a time interval that is shorter than real time.

## 2. Sensor-Driven Fire Model

Version 1.1 of the sensor-driven fire model, SDFM, is designed to predict the heat release rate (HRR) of a fire based on signals from either smoke or heat detectors positioned below the ceiling that sample the ceiling jet produced by the fire. The estimated HRR is then used by a variant of the zone model CFAST to predict layer temperature and heights in the fire room and in the adjacent rooms in the building. Based on the predicted layer temperature and height, room conditions such as limited visibility and flashover potential can be deduced. In non-fire situations, the SDFM is designed to look for sensor failure, to discriminate between nuisance signals and fire induced signals, and to monitor the condition of detectors that degrade over time.

The model will spend virtually all its time monitoring the building detectors in the no fire mode. In this mode, the signal received from each detector will be compared with the historic detector record to identify any deviation from normal operation. Detector failure modes will be checked and sensor signals that fall into these modes will result in a trouble (sensor failure) signal being sent to the appropriate monitoring location. Version 1.1 of the sensor-driven fire model has only a simple checking algorithm available that detects sensor failure based on either no signal or a saturated signal from the detector.

When the model receives a detector signal that indicates a HRR increasing with time and has reached a target threshold, the model will try to verify that it is a true fire by assessing the signals received by other available detectors in the area. Such detectors might include CO or CO<sub>2</sub> detectors as well as heat or smoke detectors. If other detectors do not support the fire signal, a trouble signal will be issued and the program will revert to its normal detector polling. If no other detectors are available in the room or if other sensors also support the presence of a fire, a fire alarm will be issued.

The target threshold for the model to start checking for a fire is based on two alternative methods of defining a fire signal. The first method used by the model is to

compare the sensor signal with a user prescribed signal. This signal would be one that has been developed by observing the response of the detector to small test fires. The second method would be based on looking at the time history of the detector signal once an estimated HRR based on the detector signal has been reached. If the detector signal indicates a time growing hazard that has reached a particular HRR, a fire alarm will be issued. This second method may allow for earlier detection of fires as well as fewer false alarms since it depends on a time history as well as a signal magnitude.

The determination of a HRR from a detector signal requires knowledge about the characteristics of the detector and its position with respect to the fire. Detector characteristics include the calibration curve for the analog/digital signal generated by the detector as a function of temperature or smoke/gas concentration and the delay time introduced by thermal lag or flow conditions into the sensing element. Once the detector characteristics have been defined, the HRR may be estimated using modeling correlations coupled with a zone fire model. In the following discussion, it will be assumed that only one detector is present in each room. The detector will be located close to the ceiling where it can be considered in the ceiling jet. Presently, version 1.1 of SDFM contains algorithms to estimate HRR from either the excess temperature or the smoke concentration in the ceiling jet [2 3 4].

### **3. Estimating the extent of fire hazards**

Once a HRR has been obtained for one or more of the identified fire sources, this information will be passed to a version of CFAST in order to calculate layer height, temperatures and smoke concentrations in each room of the structure. From this information, hazards such as limited sight, high temperatures, toxic gases and potential for flashover may be identified on a room by room basis for the current fire conditions.

The layer temperatures and smoke concentrations calculated using CFAST are also used to estimate fire spread from the room of origin to adjacent rooms. The signals



from sensors in these adjacent rooms are compared with calculated signals based on the estimated layer temperature and smoke concentration predicted by CFAST. If the ceiling jet temperature as estimated from sensor signals is 30% higher than the upper layer temperature predicted by CFAST, it is assumed that a fire has broken out in the adjacent room. If the predicted upper layer temperature exceeds the flashover temperature, 500 °C, it is assumed that a fire has started in that room. In addition, with a known HRR history, projections can be made using CFAST to estimate fire growth and spread. The present version of SDFM does not have this capability.

#### 4. Model Verification

Since the SDFM is designed to operate in a space with a large number of rooms, verification of the algorithms becomes a major problem. One method of verification will be to use the results of multiple room fire experiments and to test the predictions of the SDFM against these experiments. The number of these fire experiments is quite limited, so an additional method of verification is being used. The Virtual Cybernetic Building Testbed at NIST is a computer platform where the building ventilation, heating and cooling, and sensor activities in a multiple room building can be simulated.

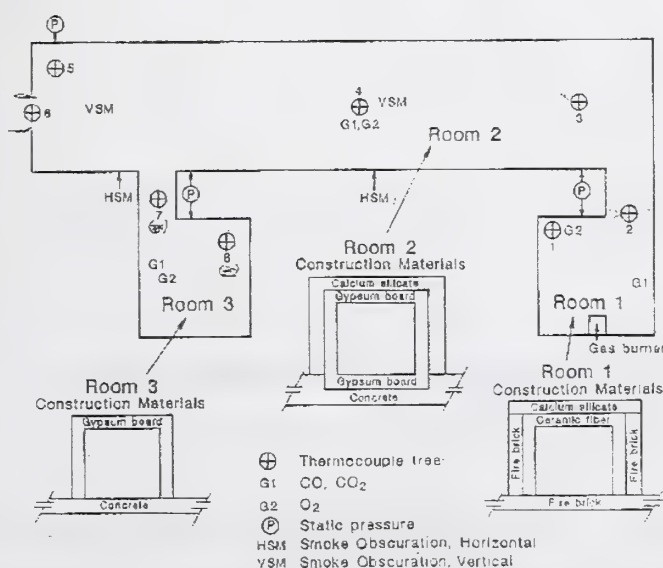


Figure 1 Three-room test plan view.

The present structure modeled in the test-bed contains three rooms and will soon be increased to nine rooms. Using CFAST [5] or FDS [6], a fire scenario can be generated for the testbed room geometries and the resulting sensor signals used as the model input for the SDFM. In this way, the SDFM can be tested using a virtual fire source and receive signals which are representative of what may happen in an actual fire scenario in the virtual building.

Two fire experiments were selected to provide initial verification of the SDFM. The first is a three room, single level experiment where the fire source was a methane burner [7]. The second experiment is a seven room, two story full scale fire test (Sharon 2) where the major fuel source was wood pallets and flashover was achieved in the burn room [8]. Thermocouple data was available for both experiments and

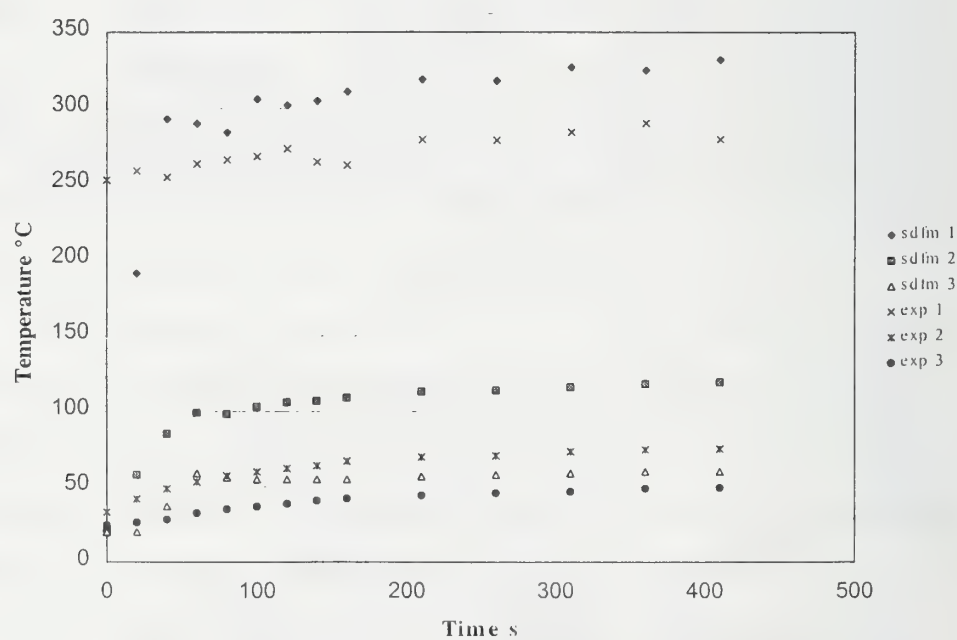


Figure 2 Calculated (sdfm) vs measured (exp) upper layer temperature for each room – 1, 2, 3.

single thermocouples near the ceiling were used for the SDFM inputs to mimic the response of ceiling mounted heat detectors

A plan view of the Three-room test is shown in figure 1. The test was modeled as a three-room structure with two short corridors connecting the rooms being modeled as doors. While multiple thermocouple trees and sensors were available in each room, only one thermocouple per room was used to provide a sparse data set for comparison with room conditions. A sparse data set does not provide sufficient information to locate the fire and therefore provides a test of the default positioning algorithm used in the SDFM. The experiment consisted of a methane burner operating at 2.8 kW for the first 330 s of the test. The 2.8 kW fire was increased to 103 kW at 340 s into the test. The SDFM detected a fire in the burn room at 350 s into the test. The initial fire of 2.8 kW was below the threshold setting for fire detection in the SDFM.

Figure 2 provides a comparison of the predicted upper layer temperatures of the

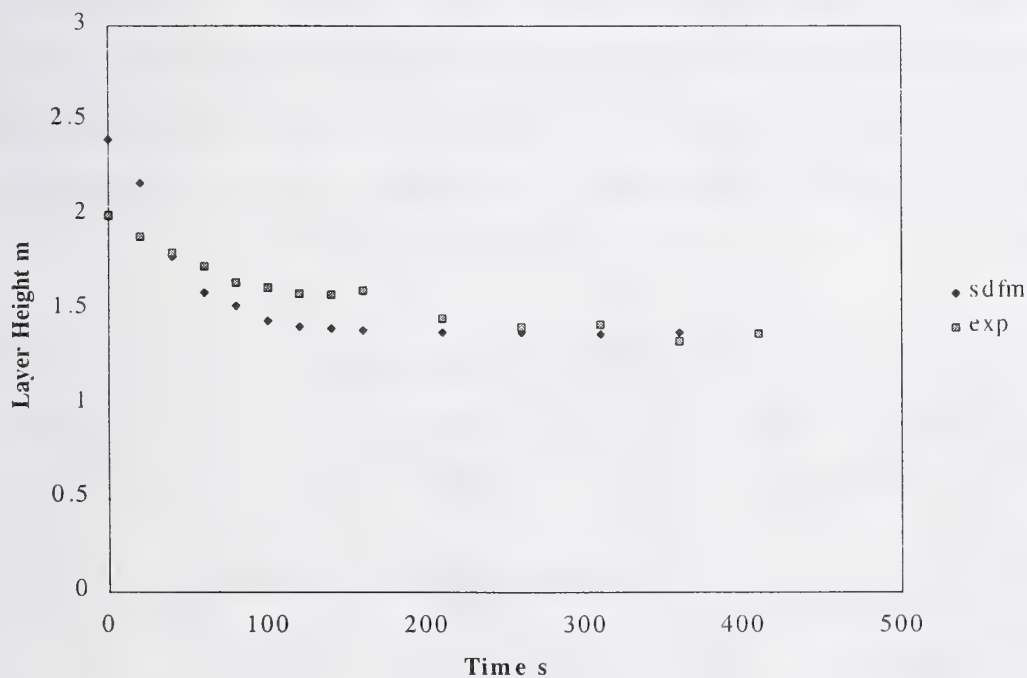


Figure 3 Upper layer height comparison for room 2

SDFM with the calculated upper layer temperatures of the experiment. The plots start from time 0 that is the time that the SDFM detected a fire (350 s into the experiment). The SDFM predictions are higher than the calculated upper layer temperatures of the



experiment for the second room but are in good agreement for rooms one and three. The average 95 % confidence interval for this data based on five identical experiments is  $\pm 18\text{ }^{\circ}\text{C}$ ,  $\pm 6^{\circ}\text{C}$ , and  $\pm 4\text{ }^{\circ}\text{C}$  for rooms 1, 2, and 3 respectively. The layer height comparisons for room 2 are given in figure 3. The experimentally measured layer heights are based on observations of the height of the smoke layer in the experiment and are not inferred from temperature measurements. Agreement between the observed layer heights and calculated layer heights are quite good. The average 95% confidence interval for this measurement is  $\pm 0.2\text{ m}$ .

The SDFM is designed to provide information concerning the fire threat that fire fighters might encounter in a building. The fire threats presently in the model include: a smoke layer less than 2 m above the floor (limited visibility), a smoke layer above a temperature of  $50\text{ }^{\circ}\text{C}$  and layer height below 1.5 m (toxic gas/thermal hazard), and a smoke layer at a temperature higher than  $500\text{ }^{\circ}\text{C}$  (flashover). For the three-room experiment, the upper layer temperature did not reach flashover and no flashover warnings were issued. A comparison of the SDFM predictions with the experimental measurements is given in the table below. The SDFM was run with a reporting interval of 20 s.

Room	1 EX	1 SD	2 EX	2 SD	3 EX	3 SD
Visibility Limited	na	20 s	20 s	40 s	na	60 s
Toxic Gas - Thermal Hazard; Layer	na	100s	190 s	100 s	na	nr
Toxic Gas - Thermal Hazard; Temperature	0 s	20 s	50 s	100 s	460 s	80 s

**Table 1** Comparison of time of occurrence for three hazard predictions. The symbol “na” stands for not available and “nr” is not reached. 1 EX is the first room experimental results while 1 SD is the first room model prediction.

Experimental layer heights were given for only room 2 in the experiment. Hence, the toxic gas/thermal hazard warning has been separated into two parts, one the smoke layer temperature in excess of  $50\text{ }^{\circ}\text{C}$  and the other for a layer height less than 1.5 m.

In room 1, the SDFM provided a toxic gas/thermal hazard warning as quickly as it could (based on temperature) and is in good agreement with the experimental measurement.

In room 2, the limited visibility warning was in good agreement with the experimental measurements. The toxic gas/thermal hazard warning was issued roughly 90 s ahead of the criteria being met experimentally. This difference is due to the experimental layer height staying just above the 1.5 m layer height criterion while the calculation predicted a layer height that is just below the 1.5 m criterion (see figure 3).

In room 3, the layer temperature in the experiment remains just below the 50 °C criterion while the calculated value is just above the 50 °C criterion (see figure 2) for an extended time period. The small differences in the experimental and calculated temperatures account for the large difference in the time to issue the warning. Based on the results for rooms 2 and 3, the warning levels used to issue hazard warnings should be set at a lower value than the hazard level so that small differences in the calculations will not delay potential hazard warnings.

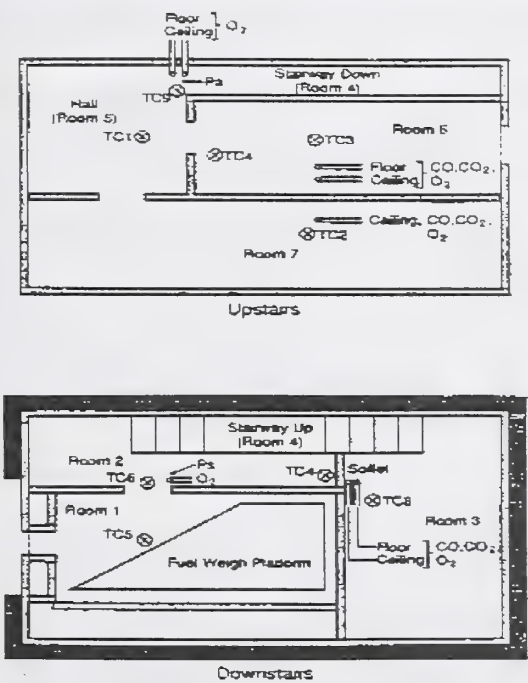
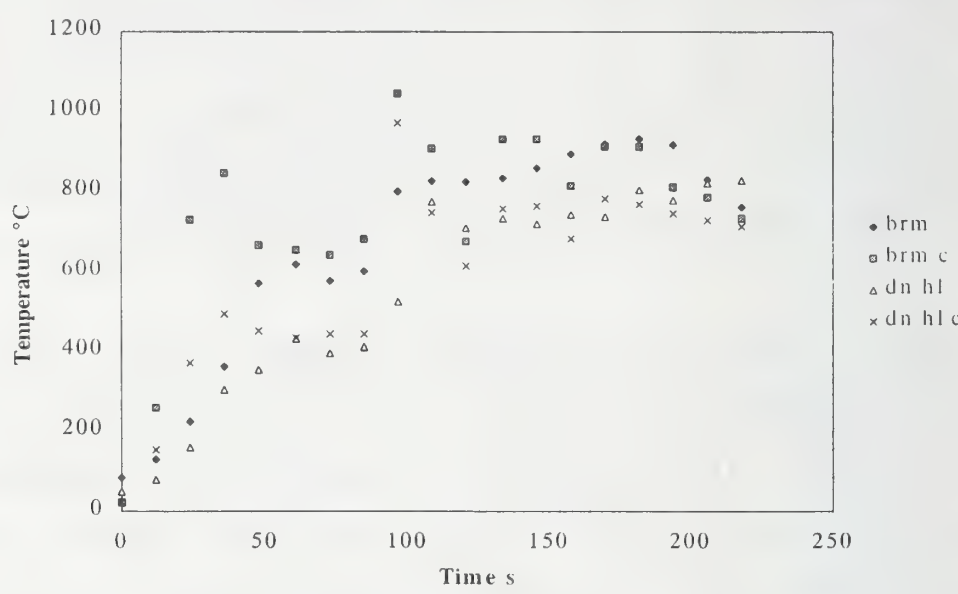


Figure 4 Sharon 2 Townhouse Plan View

To simulate the Sharon 2 test, the seven-room townhouse was divided into eight spaces and thermocouple data was used to provide ceiling jet temperatures in six of



**Figure 5 Upper layer temperature comparison for the burn room (brn) and the lower level hallway (dn hl). The “c” indicates the calculation.**

the eight spaces. A plan view of the townhouse, showing locations of the instrumentation, is shown in figure 4. In the simulation, room 2 was partitioned into a hallway and a room with the thermocouple tree, TC6, providing the temperatures for the hallway. Thermocouple trees TC1, TC2, and TC3 were used to provide data for the upstairs spaces while TC8 and TC4 were used for the other downstairs spaces. The partitioned room 2 on the first floor and the stairway were modeled spaces with no thermocouple measurements. Only the thermocouple near the ceiling was used for the input data from each tree.

The first 231 seconds of the fire was modeled for the Sharon 2 fire since, in the experiment the wood pallets in the fire room began to fall off the load cell after this time. Figures 5 and 6 provide a comparison of a representative layer temperature as



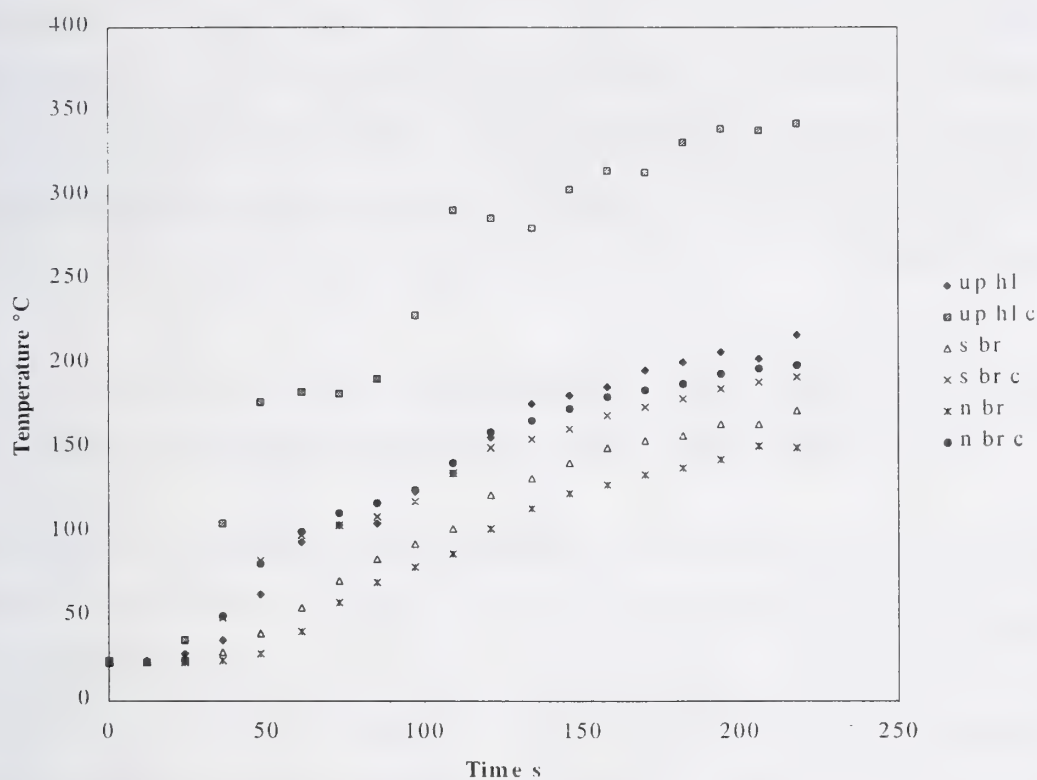


**Figure 6 Upper layer temperature comparisons for the upper hallway (up hl), south bedroom (s br), and north bedroom (n br). The “c” indicates the calculation.**

measured by the thermocouple trees with the layer temperature calculated by the model for each room. Agreement between the calculations and the measurements is quite good for all rooms although the model tends to overpredict the temperature.

The experimental layer height was determined by estimating the location of the midpoint of the temperature transition between the lower layer temperature and the upper layer temperature. The location of the midpoint above the floor was taken as the upper layer height. The calculated layer heights agree well with the estimated layer heights for most of the comparison interval. Only at the last time intervals for the second floor bedrooms do the calculated upper layer heights drop significantly below the estimated layer heights.

The predicted fire threats correlated well with the estimated occurrence of these threats for the lower level rooms using the data shown in table 2 below. The layer

heights were predicted to be lower for the upper level rooms than measured which accounts for most of the differences shown in the table for these rooms. For the bedrooms, the smoke in the room may become well mixed with a two-layer structure beginning to disappear. The cycle time for the calculations and measurements was 12 s, meaning those two or three calculations or measurement times produced several of the time differences.

Room	Burn EX	Burn SD	LL EX	LL SD	UL EX	UL SD	N EX	N SD	S EX	S SD
Visibility Limited	24	12	49	12	88	24	78	49	80	36
Toxic Gas - Thermal Hazard	24	12	49	24	99	36	103	61	94	49
Flashover	48	24	97	97	nr	nr	nr	nr	nr	nr

**Table 2** The table presents a comparison of the times in seconds between the experiment (EX) and the SDFM (SD) for the hazard conditions in the burn room (Burn), the lower level (LL) hall, the upper level (UL) hall and the two upper level bedrooms labeled N (north) and S (south). The symbol “nr” indicates that this condition was not reached.

## 5. Summary

The goal for the SDFM is to provide adequate warning of fire threats within a structure using the building sensors as detectors. For comparisons with two fire experiments, fire warnings were given that were in reasonable agreement with measurements. This agreement was obtained using data from only one sensor per room. Additional sensors in each room would permit the fire source to be more accurately located and as a result better predictive capabilities would be expected. The present results, using only single detectors in each room, provide information that would be of value to fire fighters.

The smoke detector algorithms have not yet been tested experimentally and the model needs to be tested in buildings that contain real detectors and HVAC systems. There are additional algorithms that need to be added or expanded in the model. These algorithms include but are not limited to improving the multiple detector algorithm for a single room, adding lag time algorithms for detectors, expanding the false alarm algorithm in the model, and adding a wall heating algorithm.

Version 1.1 of the SDFM has demonstrated that this type of fire model can give useful results in both simple fire conditions and in fire conditions where flashover occurs.

- 
- [1] Nelson, H. E. Functional Programming/Research Planning for High Technology Federal Office buildings. National Institute of Standards and Technology 1984; NBSIR 84-2828: 28.
  - [2] Davis, W. D. The Zone Fire Model Jet: A Model for the Prediction of Detector Activation and Gas Temperature in the Presence of a Smoke Layer. National Institute of Standards and Technology 1999; NISTIR 6324: 1-51.
  - [3] Evans, D. D. Calculating Sprinkler Actuation Time in Compartments. Fire Safety Journal 1985; 9: 147-155.
  - [4] Davis, W., D. and Reneke, P. Predicting Smoke Concentration in the Ceiling Jet. National Institute of Standards and Technology 2000; NISTIR 6480:1-12.
  - [5] Peacock, R. D., Forney, G. P., Reneke, P., Portier, R., and Jones, W. W. CFAST, the Consolidated Model of Fire Growth and Smoke Transport. National Institute of Standards and Technology 1993; NISTTN 1299: 1-235.
  - [6] McGrattan, K. B. and Forney, G. P. Fire Dynamics Simulator – User's Manual. National Institute of Standards and Technology 2000; NISTIR 6469: 1-49.
  - [7] Peacock, R. D., Davis, S., and Lee, B. T. An Experimental Data Set for the Accuracy Assessment of Room Fire Models. National Institute of Standards and Technology, 1988; NBSIR 88-3752: 1-111.
  - [8] Levine, R. S. and Nelson, H. E. Full Scale Simulation of a Fatal Fire and Comparison of Results with Two Multiroom Models Volume II – DATA. National Institute of Standards and Technology 1990; NISTIR 90-4268: 1-125.



O. Keski-Rahkonen

VTT Building and Transport, P.O. Box 1803, FIN-02044 VTT, Finland

Olavi.Keski-Rahkonen@vtt.fi

## **Revisiting modelling of fluid penetration into smoke detectors for low speed ceiling jets**

### **1. Introduction**

A smoke detector is in principle a container, which has partially permeable walls separating the gas volume in the detector from the volume around it. Walls delay fire detection as compared to a fully open detector. Heskestad [1] drafted a theory using dimensional analysis arguments for the time lag  $\Delta t$  of a products-of-combustion fire detector

$$\Delta t = \gamma l / \bar{v} \quad (1)$$

where  $\bar{v}$  is the mean convective flow velocity around the point detector,  $l$  the characteristic length scale, and  $\gamma$  a non-dimensional coefficient characteristic for the geometry. According to [1] Eq. (1) is valid presuming 'viscosity effects are not considered important'.

Brozovsky [2] observed the simple relationship of Eq. (1) did not hold for low ceiling jet velocities. In Fig. 1 his observations (dots) are plotted as a function of velocity  $\bar{v}$ . Thin solid lines represent exponential fits by Brozovsky [2] on his limited set of data. Further data manipulation showed, an equation of the form

$$\Delta t = \gamma l / (\bar{v} - \bar{v}_0) \quad (1')$$

is also a plausible fit on the data. The numerical values of the parameters were:  $\gamma l = 0.8$  m and  $\bar{v}_0 = 0.075$  m/s, which Brozovsky called a critical velocity. Fitting Heskestad's correlations on these data according to Eq. (1)

would yield curves similar to # 1 and # 2 in Fig. 1. These predictions are in contrast with experiments. No value of  $\gamma l$  would fit experimental data.

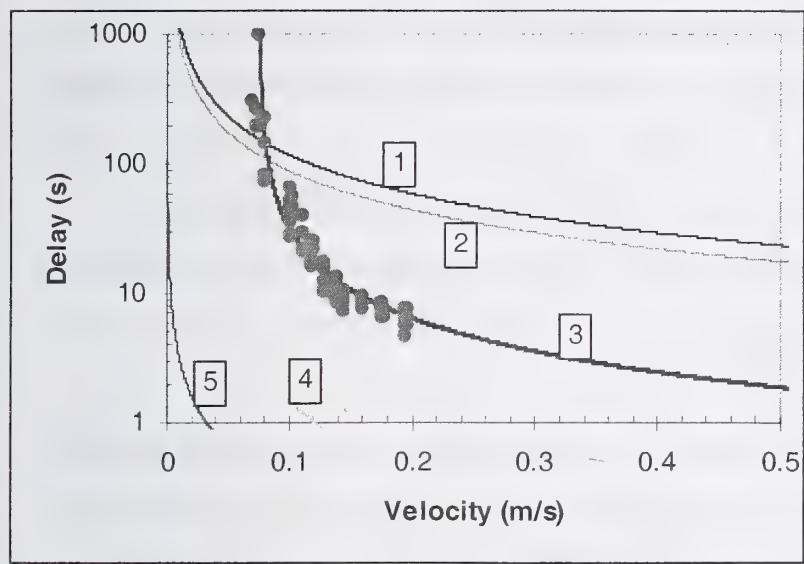


Fig. 1. Entry lag time dependence on flow velocity past a detector. Dots (experimental data). (1) and (2): The delay time according to Eq. (1) as explained in text. (3): Fit according to Eq. (1'),  $\bar{v}_0 = 0.075 \text{ m/s}$ . (4) and (5) Calculated models explained in text.

## 2. Flow and pressure fields around solid bodies

### 2.1 Principles of calculation

There is a wealth of literature on flow around solid objects in a flow field using different techniques at different level of approximation [6 - 10]. No general analytical solutions are available for all flow velocities. Furthermore, in the whole body of this literature only some references were given on works, where the body is partially transparent [7 - 8]. For these reasons here general techniques of flow modelling are attempted in the regions, where analytical solutions are available. Flow through the detector

is treated as perturbation. To grasp the salient physics of the flow we first calculate the pressure field around a totally solid body for a constant velocity, and use that information to calculate flow through the mesh in and out of the fire detector. The validity of perturbation approach is not granted. Failure of it demonstrated by related drag problem. Despite that, analytical approaches are so simple, it was decided to try them first. For calculating the flow around the detector Reynolds numbers are typically 100 ... 1000. For flow through the mesh Reynolds numbers are in the range 0.1 ... 10. Therefore, the calculation can be made in two stages, and requires different approximations in both ranges.

A smoke detector can be modelled as a solid object in a flow field, which is partially permeable. For modelling we set the center of the detector in origin, and arrange a flow along the negative x-axis with a velocity  $v_\infty$  far from the origin towards positive x. The point on the detector, where negative x-axis penetrates the outer surface is a stagnation point. On the opposite lee side, there is a point, where the dynamic pressure is the lowest. For the smoke flow through the detector the insect mesh provides the biggest flow resistance. Without quantitative calculations, only through visual inspection of some detector constructions all other channels of the flow have much bigger cross sections, and relative to the mesh penetration pressure drop can be considered only as small.

Therefore we concentrate here only on the ultimately simplified geometrical model of the detector: (i) a cylindrical or hemispherical outer mesh, (ii) small channels through the mesh into (iii) the interior of the detector of total volume  $V$ . Due to additional light scattering barriers and flow channeling guides inside the detector the volume  $V$  is considered a well stirred reactor, which communicates with the space outside the insect mesh through the holes on it. The other alternative in the inner space is to use laminar plug flow, and calculate time of smoke front moving from the



mesh the center point. For a smoke detector two geometrical, highly idealized models are used: (a) a two dimensional, infinitely long circular cylinder neglecting the presense of the ceiling, and (b) a three dimensional hemisphere setting the frictionless ceiling in the equatorial plane. First, potential flow is applied to both problems to account for the disturbance the detector causes on the free flow field.

For calculation we set the coordinate system as shown in Fig. 2. The origin  $O$  is set to the center of the detector in the plane of the ceiling. Perpendicular to the plane of the ceiling and along the center axis of the detector points the  $z$ -axis downwards. The detector screen is cylindrical or spherical showing as circle in the  $x$ - $y$ -plane of Fig. 2. The screen is partially permeable for the flow, and idealized to a surface of zero thickness. The ceiling jet is assumed to be a free constant velocity flow approaching the detector parallel to the  $x$ -axis far left. The detector screen divides the space into two regions: (1) inside, and (2) outside. For modelling flow equations are written for both regions, and boundary conditions along the surface presenting the screen bound the regions together.

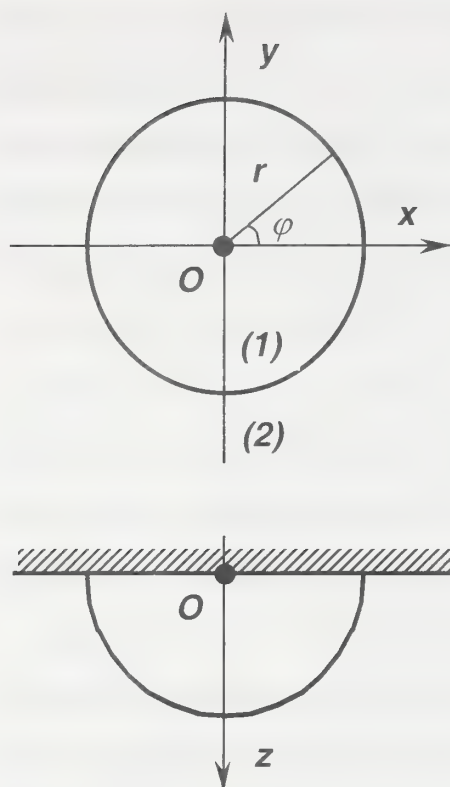


Figure 2. Coordinate system used for detector modelling.

## 2.2 Inviscid potential flow

Experimenting with different combinations of boundary conditions between the inside and outside regions showed, that no extra effects were obtainable. Therefore, potential flow a free stream of velocity  $v_\infty$  is superposed with a two (cylinder) or three (sphere) dimensional doublet [8]. For solid bodies the radial velocity component  $v_r$  disappears on the surface. For a permeable body the first order perturbation theory is attempted, which would as mismatch yield to radial velocity distribution

$$v_r = \varepsilon \cos \varphi \quad (2)$$

where the numerical value of  $\varepsilon$  is determined using experimental pressure distribution around the body slightly simplified [7]. For laminar flow from

the stagnation point to the separation angle the  $\varphi_k$  the velocity obeys Eq. (2), after which it has a constant value reached at separation point. The experimental pressure amplitude for laminar flow is

$$p_s - p_k = q\rho v_\infty^2 \quad (3)$$

where  $q \approx 1$  for a cylinder and 0.75 for a sphere. For turbulent flow the pattern is similar, but numerical values of  $q$  differ slightly. The flow was not yet turbulent around the detector, and thus this combination is not discussed further.

### 2.3 Laminar viscous flow

A creeping laminar flow past a cylinder results in a logarithmic singularity (Stokes paradox) but past a sphere (Stokes's first problem) the pressure distribution is

symmetric, given on the surface by [10]

$$p = p_\infty - \frac{3\mu v_\infty}{2a} \cos \varphi \quad (4)$$

By coupling to that field an additional radial flow velocity component into the sphere in the form of Eq. (2), it can be shown to be of the higher order in perturbation expansion than the second term in the pressure distribution of Eq. (4). Therefore, two-stage calculation is plausible. The flow inside the sphere satisfying Navier-Stokes equations to the same degree of approximation as for the outer flow takes place at constant velocity parallel to the flow far from the detector. Oseen has extended the calculation of Stokes as a power series of Reynolds number [11]. The second term of



pressure averages to zero over the sphere. Therefore, it is not taken here as a separate case.

### 3 Flow through small openings

Calculating the smoke density inside the detector for a flow, where particles do not separate from the fluid, the time constant  $\tau_w$  of well stirred volume  $V$  is given asymptotically by

$$\tau_w = V / \dot{V} \quad (5)$$

where  $\dot{V}$  volume flow in the detector. For a plug flow a similar time constant  $\tau_p$  is obtained by dividing the radius of the detector by the average velocity inside the detector. Both concepts are used here.

When the flow is laminar inviscid through the mesh volume flow is proportional to the square root of pressure difference [7].

For viscid creeping fluid the flow through the holes takes place in a layer attached onto the surface of the mesh. For an order of magnitude estimate we look fully developed viscous flow, which can be solved accurately in a closed form for rectangular channels (Poiseuille flow) [7] or for circular tubes (Hagen-Poiseuille flow) [6 - 7]. Taking the circular variation volume flow  $\dot{V}$  through a hole of radius  $a$  is given by

$$\dot{V} = -\frac{\pi r_0^4}{8 \eta} \frac{dp}{ds} \quad (6)$$

where  $\eta$  is the dynamic viscosity of air,  $dp/ds$  the pressure drop along the channel, and the radius of the circular hole  $r_0$ . In Table 1 calculation forms are given for the lag time  $\tau_w$  (s) for different reasonable combinations of ambient and grid flow conditions. The formulas are preceded by numerical factors  $c_i$ . Radius of the detector is  $a$ , ratio of combined hole areas to total grid surface area  $\kappa$ , and effective length of pressure drop through mesh  $\delta$ . In

Fig. 1 these time lags are plotted as a function of velocity  $v_\infty$  for all calculated cases using rough estimations of the numerical coefficients  $c_i$  in those cases they were not direct results from the derivation of the formulas. This is plausible for an order of magntude calculations.

Curve # 2 is viscid-viscid combination, and curve # 1 plug flow model for the same case. Curve # 5 is laminar-laminar combination with a very big difference between theory and observations. Curve # 3 presents laminar ambient causing viscid grid flow, which is still rather far from measured data.

Table 1. Lag time  $\tau_w$  (s) calculation formulas.

	Ambient laminar inviscid	Ambient creeping viscid
Grid laminar inviscid	$c_1 \frac{a}{\kappa v_\infty}$	NA
Grid creeping viscid	$c_2 \frac{\nu a \delta}{\kappa r_0^2 v_\infty^2}$	$c_3 \frac{a^2 \delta}{\kappa r_0^2 v_\infty}$

#### 4. Conclusions

Order of magnitude calculation formulas were derived for the lag time of fire detectors using two different scales of flow: (i) ceiling jet flow around the fire detector, and (ii) flow through the mesh. At different jet velocities different flow approximations apply. The experimental data do not support any of the proposed theoretical models since both the magnitudes of calculated lag times differ considerably from the observations, and

asymptotically the theoretical curves do not have a pole at a finite velocity. As for the flow through the mesh, viscosity effects cannot be neglected.

The reason for the negative result is not known for sure. Some guesses could be made to guide further research. Perturbation approach may not be valid, because the disturbance might be finite even for a very small flow through the detector. There is an analogy with the drag problem of a sphere [10]. The flow through the grid is never fully developed. This was not taken into account, because of difficulty of modelling.

No apparent experimental errors were found in [2]. Therefore, the behaviour described by Eq. (1') seems to indicate the flow might have a 'non-newtonian' character plugging the flow at velocities lower than  $\bar{v}_0$ . Qualitatively, such a flow occurs, if the fluid, which here is an aerosol, behaves collectively like a non-newtonian continuum fluid of Bingham plastic [3]. The analytical theories of such fluids would in principle allow calculation of the flow in and out of the detector [4, 5]. However, there seemed not be available experimental data of rheological properties of smoke. The tacit assumption has always been, smoke behaves like air, an almost perfect newtonian fluid. 'Non-newtonian' behaviour might also be caused by electric rather than fluid phenomena. Most of the smoke particles are charged. They might stick on the grid at low velocities. However, without further detailed experimental observations, if not yet readily available, these questions cannot be settled.

### **Acknowledgements**

This study has been partially financed by the Finnish Centre for Radiation and Nuclear Safety, the Ministry of Trade and Industry, Fortum Engineering Ltd, Teollisuuden Voima Oy, and the Finnish Fire Research



Board. I am indebted to E.L. Brozovsky for sending me the original experimental data.

## References

- [1] Heskestad, G. Generalized Characterization of Smoke Entry and Responce for Products-of-Combustion Detectors, Fire Detection of Life Safety, Proceedings of a Symposium, March 31 and April 1, 1975, National Academy of Sciences, Washington , D.C., (1977), p. 93 - 127.
- [2] Brozovsky, E.L. A Preliminary Approach to Siting Smoke Detectors Based on Design Fire Size and Detector Aerosol Entry Lag Time, Master's Thesis, Worcester Polytechnic Institute, Worcester, MA, 1991, 96 p.
- [3] Irvine, T.F., Jr., & Capobianchi, M., 1998. Non-Newtonian Flows, in R.W. Johnson (Ed.) The Handbook of Fluid Dynamics, CRC Press, Boca Raton, Chapter 22.
- [4] Kawase, Y. & Moo-Young, M., 1992. Flow and Heat Transfer in Turbulent Slurries, International Communications in Heat and Mass Transfer 19, 485 - 498.
- Bukowski, R.W. & Mulholland, G.W. 1978. Smoke Detector Design and Smoke Properties, NBS Technical Note 973, National Burea of Standards, Washington, D.C., 51 p.
- [5] Patel, N. & Ingham, D.B., 1994. Flow and Heat Transfer in Turbulent Slurries, International Communications in Heat and Mass Transfer 21, 75 - 84.
- [6] Frank, P. & von Mises, R. 1943. Die Differential- und Integralgleichungen der Mechanik und Physik, Mary S. Rosenberg, New York, 2. Auflage, 1106 p.
- [7] Truckenbrodt, E., 1980. Fluidmechanik, Springer, Berlin, Band 1, 371 p., Band 2, 426 p.
- [8] Katz, J. & Potkin, A. 1991. Low Speed Aerodynamics, McGraw-Hill, New York, 632 p.
- [9] Kirchhoff, R. H. 1998. Inviscid Incompressible Flow - Potential Flow, in R.W. Johnson (Ed.) The Handbook of Fluid Dynamics, CRC Press, Boca Raton, Chapter 7.
- [10] Gursul, I. 1998. Incompressible Laminar Viscous Flows, in R.W. Johnson (Ed.) The Handbook of Fluid Dynamics, CRC Press, Boca Raton, Chapter 9.

[11] Clift, R., Grace, J.R. & Weber, M.E. 1978. Bubbles, Drops, and Particles, Academic, New York, 380 p.

## A General Approach for Simulating Signals of Scattering Light Detectors

### 1 Introduction

The simulation of fire signals is an important tool in automatic fire detection. It is useful for developing new detection algorithms or for testing existent algorithms. Simulations make it possible to develop algorithms for fire detection without expensive measurements in fire detection laboratories. This article introduces a first approach of a general method of simulation. The basis of such a simulation is a statistical model of the measured signal which describes the fire. In this article the point of view lies on the signal processing and decision making part of the automatic fire detection [1], where we concentrate on scattering light detectors. Those signals (figure 1) often include impulsive parts, which have been seen as noise in earlier approaches [2, 3]. There, the impulsive noise has been

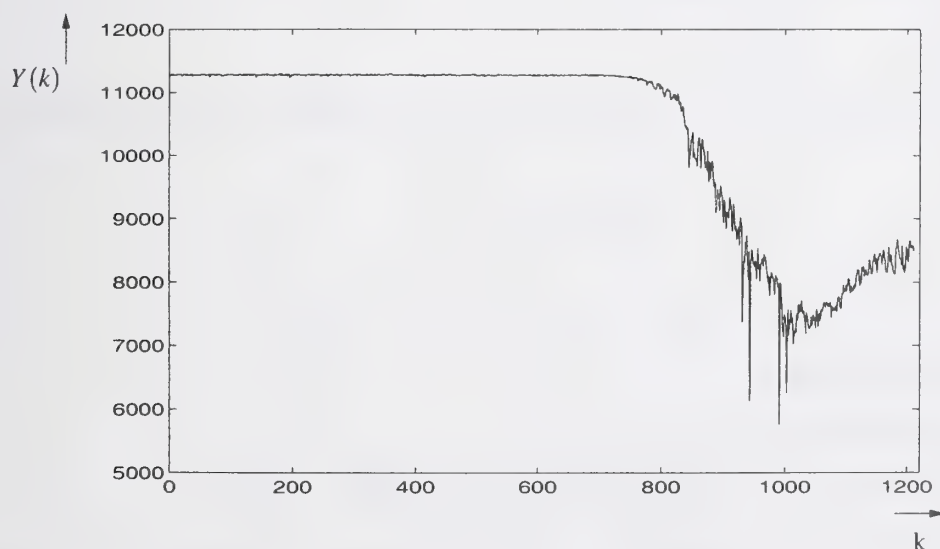


Figure 1: Signal of scattering light detector (sampling rate 1hz)



suppressed in a first step of data processing and has been added in a further step as additive noise signal. Here, in our general approach the impulses are seen as a part of the signal and will be simultaneously considered by simulating the signal to circumvent the inefficient and maybe unprecise two-step approach.

## 2 Motivation

One advantage of simulating fire signals is the possibility of testing detection algorithms with a few number of measured fire signals. Fire signals which were measured by testfires can be used to simulate new fire signals. So after changing the parameters of an algorithm or developing a new algorithm, these simulated signals can be used to test the algorithm. This test can be done on a PC without implementing the algorithm on any hardware. To achieve comparable testresults a large number of tests with different data are necessary. With simulating fire signals it is possible to generate a large number of data *without* measuring a lot of test fires. This means saving time and costs. Difficulties with simulating the signals of a scattering light detector are described in the next section.

## 3 Model of the Signal

The basis of the simulation is an additive model of the signal, that can be described as follows:

$$Y(k) = X_d(k) + X(k)$$

with

$Y(k)$ : measured signal

$X_d(k)$ : deterministic part of the fire signal

$X(k)$ : statistic part of the fire signal including noise

The figures 2 and 3 show the deterministic and the statistical part of the signal shown in figure 1. The deterministic part is suppressed in the first step of processing the signal simply by highpassfiltering, only the statistical part will be simulated. The figure 3

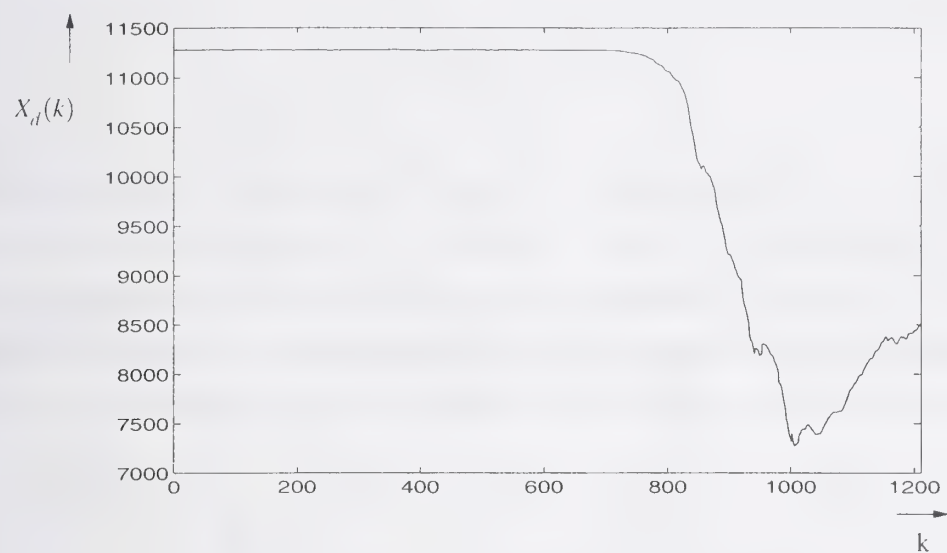


Figure 2: deterministic part of the fire signal

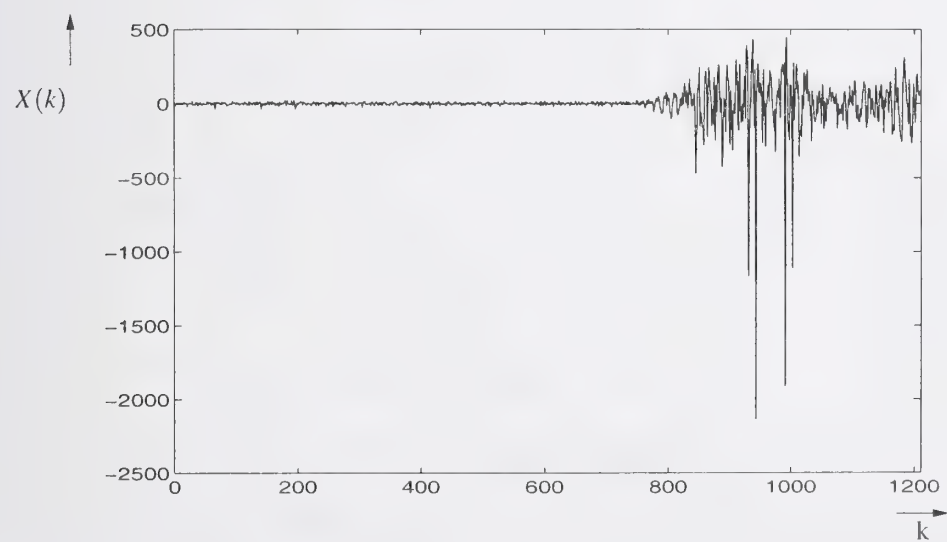


Figure 3: statistical part of the fire signal

shows that the fire signal is not stationary, the statistic properties change with time. But the signal can be separated into stationary segments of different length. This is done after filtering the deterministic part of the signal. Therefore the signal power of the signal is evaluated. It is obvious that the signal energy of the signal in figure 3 for  $0 < k < 700$  is

less than the energy for  $k > 700$ . The stationary segments of the fire signal are described by an autoregressive (AR) process  $X(k)$  of the order  $p$ , which looks as follows

$$X(k) = \sum_{i=1}^p a_i X(k-i) + N(k),$$

where  $X(k-i)$  are former samples of the signal  $X(k)$  and  $N(k)$  is a so-called stable distributed random process. So  $X(k)$  at the discrete time  $k$  is the sum of former values of the signal  $X(k-i)$  which are weighted with the coefficients  $a_i$  and the noise signal  $N(k)$  at the same point of time. For simulating the signal the coefficients  $a_i$  have to be estimated by the given measured signal  $X(k)$ . Figure 4 shows such an AR model, where  $z^{-1}$  is a time

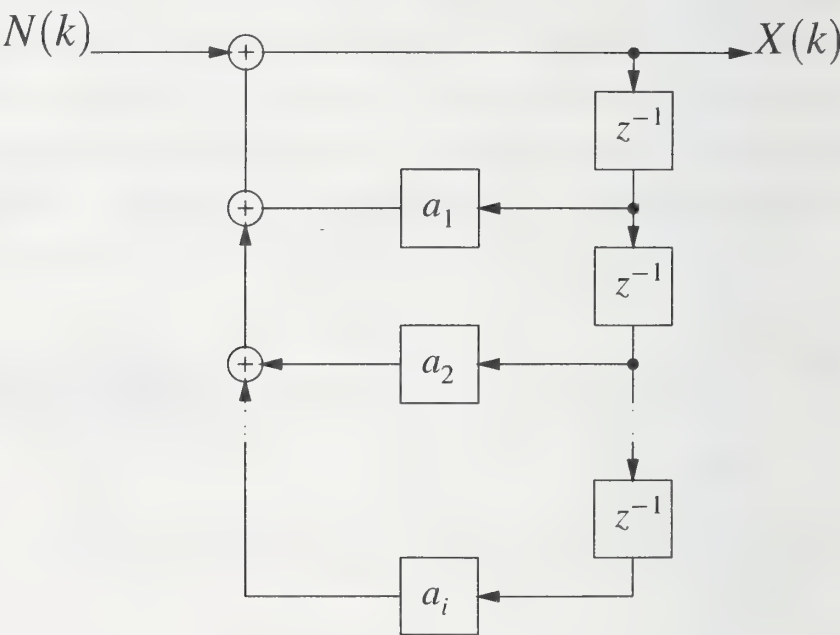


Figure 4: autoregressive (AR) model

delay of one sample.

#### 4 Symetric $\alpha$ -Stable ( $S\alpha S$ Noise)

In this general approach symmetric  $\alpha$ -stable ( $S\alpha S$ ) noise with zero mean is used as input signal for the AR model to simulate the fire signal. A random variable is called  $\alpha$ -stable,



if its characteristic function (the Fourier transformation of the probability density function) can be described as follows [6]

$$\varphi(z) = e^{\gamma|z|^\alpha}$$

with

$0 < \alpha \leq 2$ : characteristic exponent

$\gamma > 0$ : dispersion

Figure 5 shows an example for a  $S\alpha S$  stable random signal  $N_{S\alpha S}(k)$  with  $\alpha = 1.5$ . A special case of the symmetric  $\alpha$ -stable distribution is the gaussian distribution which is described by  $\alpha = 2$ . Figure 6 shows the probability density function  $p_{N_{S\alpha S}}(n)$  of  $S\alpha S$

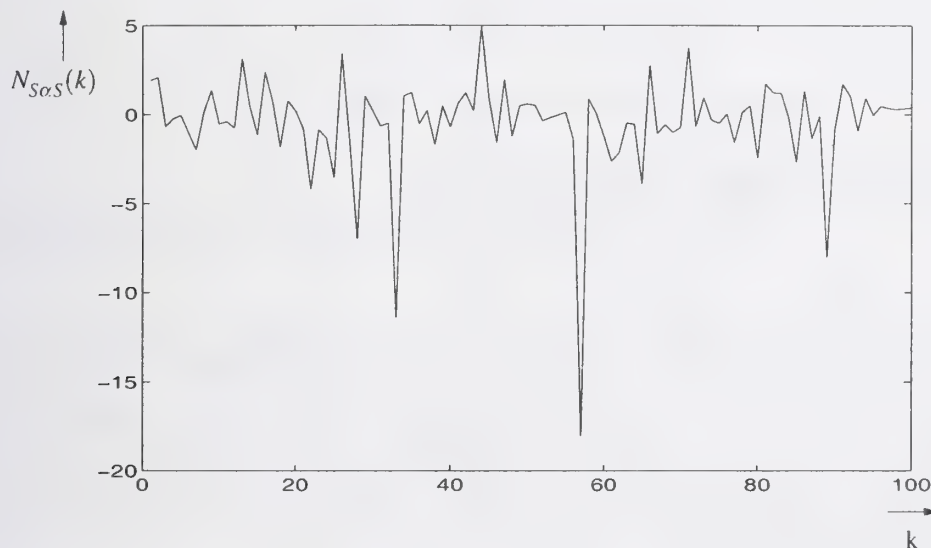


Figure 5:  $\alpha$ -stable distribution with  $\alpha = 1.5$

signals with different characteristic exponents  $\alpha$ . The diagram shows that with decreasing  $\alpha$  the tails of the function becomes heavier. For  $\alpha = 2$ , the gaussian case, the tails are the smallest. Because of the heavy tails there is one problem with processing signals with  $\alpha$ -stable distribution. The moments with a order of  $\alpha$  or higher *do not exist* except for the special case of the gaussian distribution. For this reason estimation procedures which use second or higher order moments can not be used in the case of  $\alpha$ -stable distribution with  $\alpha < 2$  as the popular least squares (LS) method for example. In this case other methods have to be used. In the literature there are different solutions for this problem [6, 4]. Some of these solutions are modified LS methods or use lower order ( $p < 2$ ) moments.

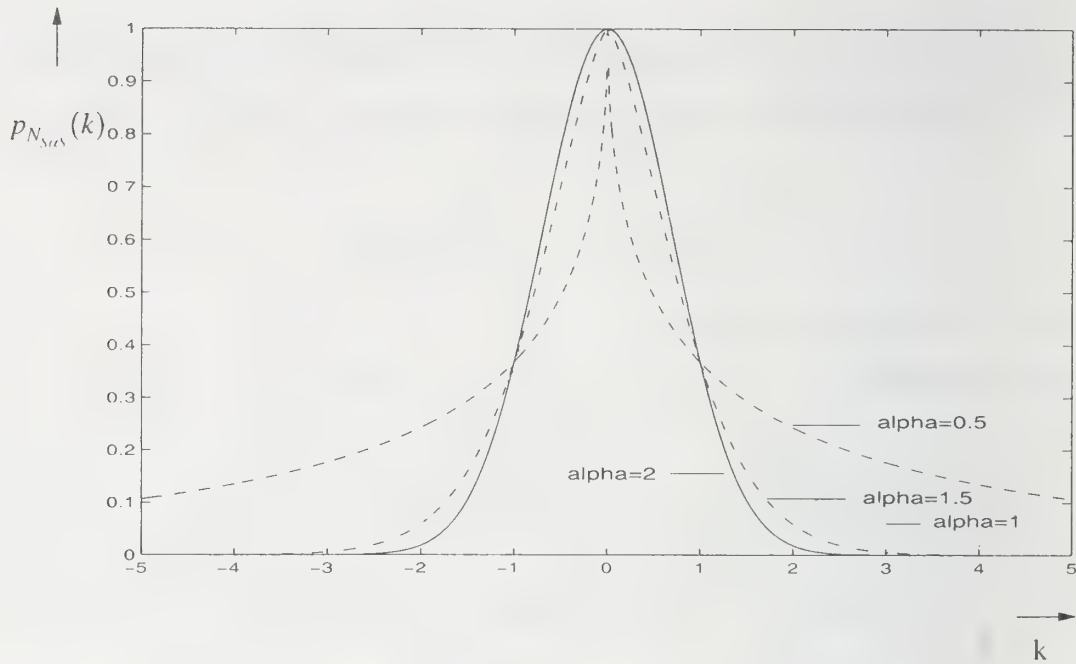


Figure 6:  $\alpha$ -stable distribution with  $\alpha = 1.5$

## 5 Simulation with gaussian Noise

The object of this approach [2] is the estimation of the parameters of the AR process which describes the signal. As described before the signal  $X(k)$  has to be separated in stationary segments. The segmentation is done with the Maximum-Likelihood method where the energie of the prediction errors of different signal segments are compared. The prediction error is calculated in the following way

$$\hat{n}(k) = \sum_{i=1}^p \hat{a}_i x(k-i) + x(k),$$

where  $\hat{n}(k)$  and  $\hat{a}_i$  are estimated values. The AR parameters  $\hat{a}_i$  are estimated by minimizing this prediction error. During this segmentation algorithm the impulsive part of the signal is suppressed. If the energy of the prediction error exceed a threshold the signal is extrapolated at this point of time. The extrapolated value of the signal is calculated by an AR process using former values of the signal as input in the following way

$$\hat{x}(k) = \sum_{i=1}^p \hat{a}_i(k) x(k-i),$$

where the AR parameter change with every step of iteration. After finding the steady segments their AR parameters are estimated by using the least squares methods for each

of the segments. With this AR parameters and the limits of the segments the stationary segments of the fire signal can be simulated. After the simulation a random signal is generated which contains the impulses. This signal is added to the simulated signal. Figure 7 shows a schematic diagram for this classical approach.

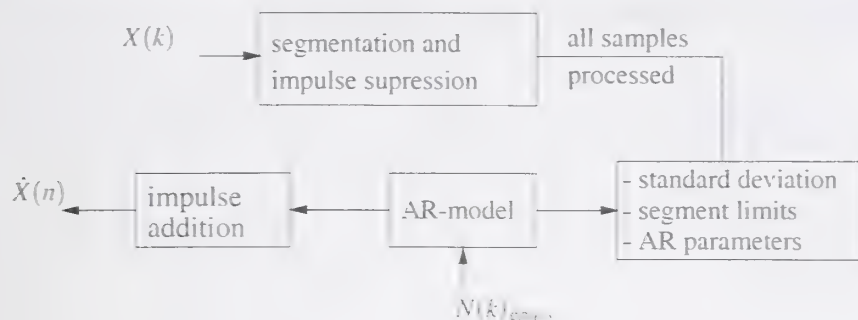


Figure 7: Structure of classical simulation approach

## 6 Simulation with $\alpha$ -stable Noise

In our approach of simulating a fire signal, the impulses are not interpreted as noise but as a part of the signal. Contrary to the algorithm described in the in section before the impulses are not suppressed but considered at the estimation of the AR parameter. There are different methods described in the literature to estimate AR parameter for models with impulsive noise as input signal [6, 4]. In this work a method is used which minimizes the p-th order moment. The minimizing problem of this  $l_p$ -norm looks as follows:

$$\operatorname{argmin}_{\hat{a}} \sum_{k=1}^K |x(k) - \sum_{n=1}^N \hat{a}_n x(k-n)|^p$$

where

$\hat{a} = [a_1, a_2, \dots, a_N]^T$ : estimated AR coefficients

$x(k) = 0$  for  $k \leq 0$

$1 < p < \alpha$

$K$ : single length of  $x(k)$

$N$ : order of AR model



This  $l_p$  norm is a generalization of the least squares deviation where  $p$  is equal to 2. In this work the iteratively reweighted least squares (IRLS) algorithm is used to solve the minimization problem [4, 8]. The algorithm starts with the LS solution and in every step it solves a weighted LS solution whereby the weights are the iteratively calculated residuals of the signal. The algorithm looks as follows [4, 5]

1.  $\mathbf{a}(0) = (\chi^T \chi)^{-1} \chi^T \mathbf{s}$
2.  $r_k(i) = [\mathbf{s} - \chi \mathbf{a}(i)]_k$
3.  $W_{kk}(i) = p|r_k(i)|^{p-2}$
4.  $\mathbf{a}(\mathbf{i} + \mathbf{1}) = (\chi^T \mathbf{W}(i) \chi)^{-1} \chi^T \mathbf{W}(i) \mathbf{s}$
5. IF  $\frac{\|\mathbf{r}(i+1)\|_{(p)} - \|\mathbf{r}(i)\|_{(p)}}{\|\mathbf{r}(i)\|_{(p)}} < \varepsilon$  then stop  
 else go to step 2)

where

- $\mathbf{a}(i)$ : the parameters of the AR model at the  $i$ -th iteration
- $\mathbf{s}$ : one value shifted version of the data vector  $x = [x(k - 1), x(k - 2), \dots]$
- $\mathbf{r}$ : residual vector
- $\mathbf{W}$ : diagonal matrix of the residuals (weight matrix)  $W_{i,j} = 0$  if  $i \neq j$
- $\|_{(p)}$  =: the  $p$ -th norm  $\|\mathbf{r}(i)\|_{(p)} = \sqrt[p]{\sum_k |r_k(i)|^p}$
- $\chi$ : matrix of the data

$$\chi = \begin{pmatrix} x(1) & 0 & \dots & 0 \\ x(2) & x(1) & \dots & 0 \\ \vdots & \vdots & & \vdots \\ x(P) & x(P - 1) & \dots & x(1) \\ \vdots & \vdots & & \vdots \\ x(L) & x(L - 1) & \dots & x(L - P + 1) \end{pmatrix}$$

$P$ : order of the AR model

$L$ : length of the signal

The structure of the algorithm is shown in figure 8. This algorithm has been implemented

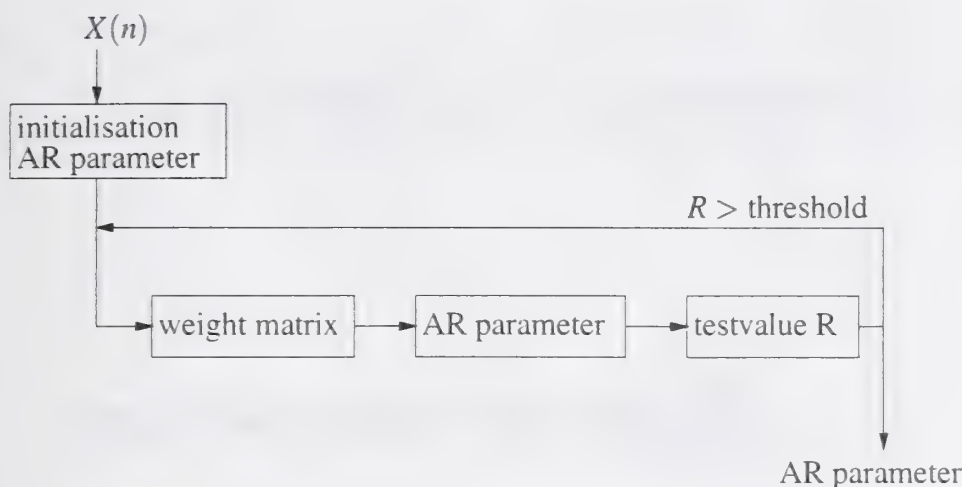


Figure 8: Structur of the IRLS algorithm

to estimate the AR parameter for *simulating the signal of a scattering light detector*. The structure of simulating a signal with the IRLS algorithm is similar to the one shown in figure 7 except that the impulse supression is not necessary and the input of the AR filter is  $S\alpha S$  noise.

## 6.1 Simulation of Fire Signals

After estimating the AR parameter the stationary segments of the measured fire signal can be simulated by using an AR model with the estimated parameters. This leads to another signal which exhibits the same *statistical* properties as the measured signal. Of course it does not look the same. The input of this filter is  $\alpha$ -stable noise with the same standard deviation as the fire signal.  $\alpha$  can be estimated from the signal. There are different approaches for the estimation of  $\alpha$ . In this work the  $\log|S\alpha S|$  [6. 7] estimator is used. With the  $\log|S\alpha S|$  estimator a new random variable  $Y$  is evaluated where  $Y(k)$  is

$$Y(k) = \log|X(k)|,$$

$X(k)$  is a  $S\alpha S$  random variable. For the estimation of  $\alpha$  exists the following equation:

$$\text{Var}(Y(k)) = \frac{\pi^2}{6} \left( \frac{1}{\alpha^2} + \frac{1}{2} \right)$$

which only depends on  $\alpha$ . The variance of  $Y(k)$  exists and can be estimated from the samples of the known signal  $Y(k)$  and the mean value. This estimation gives very good

results for a large number of samples ( e.g. 10000 samples) for signals with few samples ( e.g. 100 samples) the simulated value of  $\alpha$  deviates from the real value. Figure 9

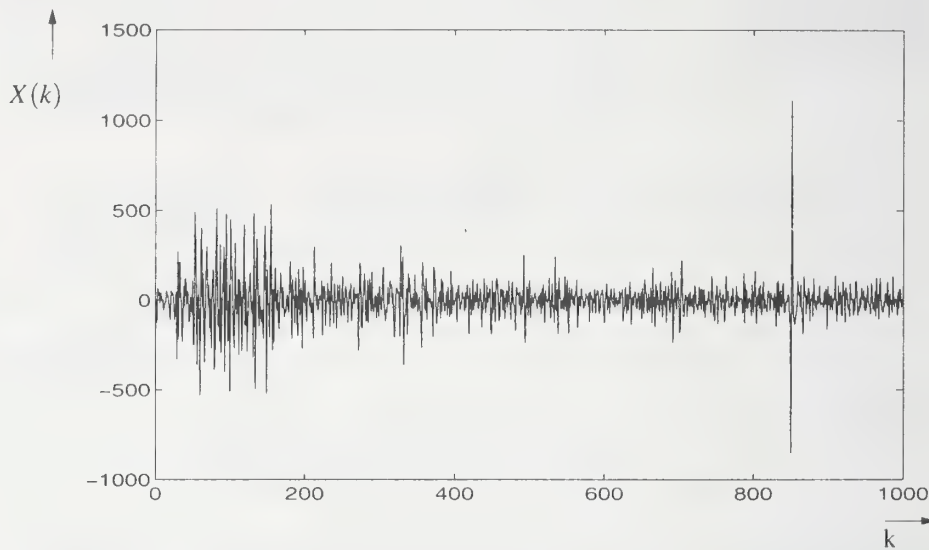


Figure 9: Measured and highpass-filtered fire signal part

shows the high frequency part of the signal of a testfire measured with a scattering light detector, figure 10 shows a simulation of this fire signal with stable noise with the characteristic exponent  $\alpha = 1.8$ . It can clearly be seen that both signal have the same statistical properties.

## 7 First Conclusion

Both the model using gaussian noise as well as the one which uses general stable noise have advantages and disadvantages. In the first algorithm not all the impulses of the signal are suppressed and after the simulation not all the found impulses are added to the signal again. The correlation of the impulses gets lost by fitting the impulses into the simulated signal in a brutal manner. One benefit of the estimation of AR model parameters by using least squares is that it is a well known procedure and the algorithm converges fast. By using the IRLS algorithm the suppression of the impulses is not necessary. On the other hand using an AR model with impulsive noise to simulate the fire signal exceeds the following problem. The number and the amplitude of the impulses depends on the value  $\alpha$ . If  $\alpha$  decreases the number of impulses and the amplitude increases. It is not



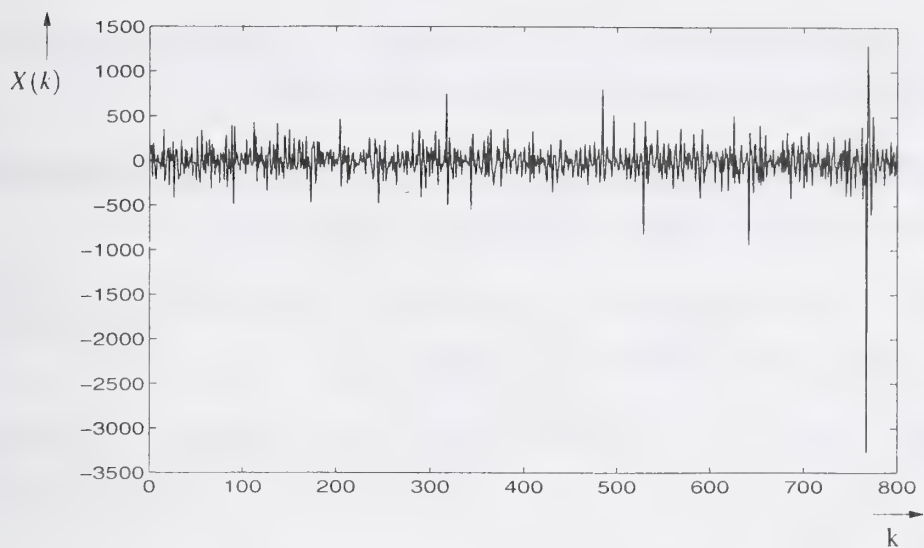


Figure 10: Simulated fire signal part

possible to generate noise with less impulses but with a high amplitude by using  $\alpha$ -stable noise. In the signals of scattering light detectors there are few impulses with a high amplitude compared to the signal. So it may be necessary to choose another input signal than  $\alpha$ -stable noise. The figures 9 and 10 show an example where the simulated signal corresponds very good to the measured signal, but this must not be. One advantage of the algorithm using stable noise is that the correlation of the impulses is still contained in the simulated signal.

Actually a combination of both described algorithms is already realised. The segmentation is done with the algorithms using the LS method, then the AR parameters for the model are estimated with the IRLS algorithm for every found segment. In the literature exist fast evaluation techniques for the IRLS algorithm which are based on FFT [9], so that the implemented IRLS algorithm become faster.

## References

- [1] Luck, H.O. Does an Over-All Modelling Make Sense in Automatic Fire Detection. Proceedings AUBE'99, Duisburg, Germany, 1999
- [2] Klose J. Ermittlung der Eigenschaften von Signaldetektoren durch Analyse und Sim-

ulation von Zufallsprozessen mit einer Anwendung in der automatischen Brandentdeckung. PhD Thesis, Universität Duisburg, Germany, 1992

- [3] Fischer A. Ein nichtlineares Signalmodell für Zufallsprozesse auf der Basis der Multilayer Perzeptrons. PhD Thesis, Universität Duisburg, Germany, 1995
- [4] Kuruoglu E.E. Signal processing in  $\alpha$ -stable noise environments: a least  $l_p$ -norm approach. PhD Thesis, University of Cambridge, 1998
- [5] Kuruoglu E.E., Ray P.J.W., Fitzgerald W.J. Least  $L_p$ -norm estimation of autoregressive model coefficients of symmetric  $\alpha$ -stable process. IEEE signal Processing Letters, July 1997, Vol.4 7:210-203
- [6] Nikias C.L., Shao M. Signal processing with alpha-stable distributions and applications. John Wiley & Sons, 1995
- [7] Ma X., Nikias, C.L. Parameter estimation and blind channel identification in impulsive signal environments. IEEE Trans. on Signal Processing, Dec 1995, Vol.43, 12:2884-2897
- [8] Burrus C.S., Barreto J.A., Selesnik I.W. Iterative reweighted least-squares design of FIR filters. IEEE Trans. on Signal Processing, Nov 1995, Vol.42, 11:2926-2936
- [9] Yarlagadda M.D., Bednar J.B., Watt T.L. Fast algorithm for  $l_p$  deconvolution. IEEE Trans. on Acoustics, Speech, Signal Processing, Feb. 1995, Vol.ASSP-33 1:174-182

**Fire Detection Modeling – The Research-Application Gap**

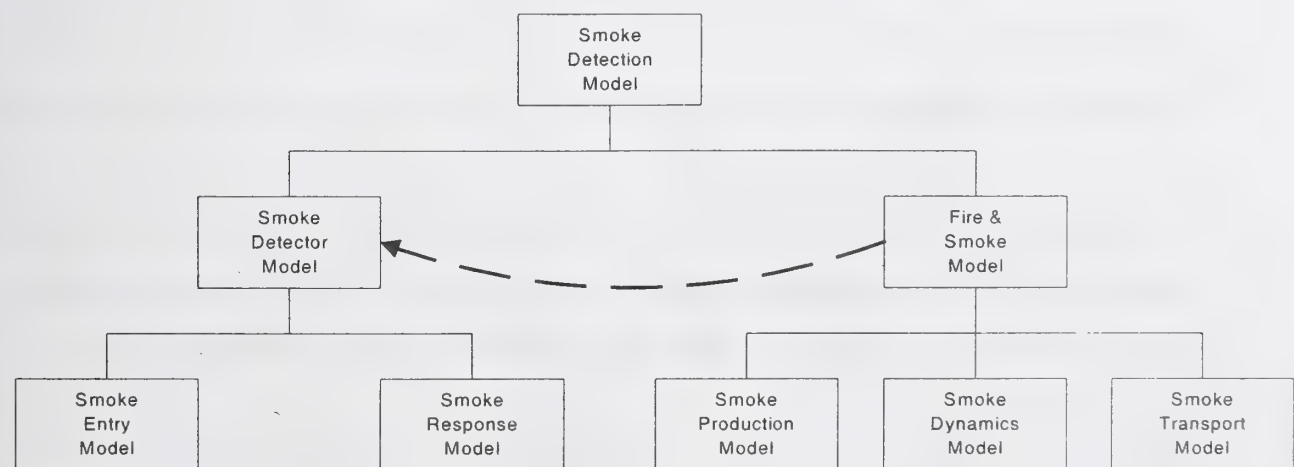
**1. ABSTRACT**

Fire detection is a rapidly evolving discipline. New sensor technologies and sampling algorithms are being developed to monitor traditional parameters of smoke and heat as well as new parameters involving gas and radiation. However, the engineering application of fire detection has lagged behind and has remained essentially unchanged for the past 20 years. In fact, there are very few engineering tools for fire detection applications. Also, the few tools that do exist do not have a known degree of accuracy. This paper uses smoke detection as a catalyst to discuss the widening gap between the fire researcher, the sensor designer, and the application engineer.

**2. INTRODUCTION**

In order to model *smoke detection*, the application engineers need a *fire model* or *fire data* and a *detector/sensor model*. The relationships between these models are shown in Figure 1. The fire model or fire data must be in a form suitable for use by the sensor model.

**Figure 1 Smoke Detection Model**





For example, fire researchers most often measure and report data on heat release rate, temperature and velocity of fire gases, and the optical density or obscuration per unit distance of the smoke at various locations. Of these, only optical density or obscuration relates directly to smoke. Although called obscuration, it is more accurately called attenuation since the light beam may be absorbed, reflected or refracted by the smoke.

Optical density and obscuration are useful data for evaluating visibility. However, the only commercially available smoke detector that operates by sensing the attenuation of a light beam is the projected beam type smoke detector. Further, these measurements are sensitive to the wavelength of light used. Thus, to be valuable for estimating the response of a projected beam smoke detector, the data must be measured and reported using the same wavelength as the light source used by the detector. Alternatively, the error introduced by modeling or using data generated at a different wavelength needs to be incorporated into the results. The two most common types of smoke detectors are ionization type and photoelectric type. Neither type operates using light attenuation. Without a correlation between the optical density data and the response characteristics of a particular detector, accurate modeling is not possible.

Examining Figure 1 it is seen that when data is presented for smoke measurements at a detector location, it is only valid for use in modeling situations where the *Production*, *Dynamics* and *Transport* are substantially the same as in the test that generated the data.

In addition, detectors often use complex response algorithms rather than simple threshold or rate-of-change response levels. These algorithms vary from detector to detector and are generally not published by the

manufacturers. Thus, even if correlations between optical density and the response of scattering and ionization type smoke detectors were available, the signal-sampling algorithm affects the actual response of each model.

In order to determine whether or not a smoke detector will respond at a given time after ignition or at some threshold heat release rate, a large number of factors must be evaluated. These include: smoke aerosol production and characteristics, aerosol transport, including dynamic changes during transport, detector aerodynamics, and sensor response.

Smoke aerosol characteristics at the point of production or generation are a function of the fuel composition, the combustion state (smoldering or flaming), and the degree of vitiation of the combustion air. The characteristics considered include particle size and distribution, particle number or concentration at various sizes, composition, color, and refractive index. Given the dynamic nature of fire growth, fire spread and fuels involved, ventilation conditions will change over time, thus affecting the characteristics of the smoke produced.

Smoke dynamics during transport changes to the aerosol characteristics that occur with time and distance from the source. For instance, do particles agglomerate or coagulate? How does the size and number concentration vary? How do the optical properties change?

Smoke transport considerations include transport time and velocity as well as soot deposition causing changes in airborne concentrations. Transport time is a function of the characteristics of the travel path from the source to the detector, and includes ceiling height and configuration (sloped, beamed,

etc.), intervening barriers such as doors, and buoyancy effects such as layering and thermal inversions.

Once smoke reaches the detector, other factors become important, namely the aerodynamic characteristics of the detector and the type of sensor. The aerodynamics of the detector relate to the ease with which smoke can pass through the detector housing and enter the sensor. In addition, the location of the entry portion of the housing relative to the velocity profile of the detector normal to the plane of the ceiling is also a factor. Finally, different sensing modes (e.g., ionization or photoelectric) will respond differently, depending on the characteristics of the transported aerosol. Within the family of photoelectric devices, there will be variations depending upon the wavelengths of light and the scattering angles employed. Also, algorithms used to sample and weight the sensor's response are introduced by the manufacturer and affect the detector's response.

Standard practice for the design of smoke detection systems is much the same as that for heat detection systems. Recommended spacing criteria are established based on detector response to a specific parameter, such as the optical density within an enclosure. A variety of smoke tests are used to verify that the detector responds between defined upper and lower activation thresholds and within required response times to a range of different types of smoke. This information translates into recommended spacing criteria that are intended to ensure that the detector responds within defined parameters. In some cases, the recommended spacing can be increased, or must be decreased, depending on factors such as compartment configuration and airflow velocity.<sup>1</sup>



In applications where estimating the response of a detector is not critical, the recommended spacing criteria provides sufficient information for design of a basic smoke detection system. If the design requires detector response within a certain time frame, optical density, specified heat release rate, or temperature rise, additional analysis may be required. In this case, information concerning the expected fuel, fire growth, sensor, and compartment characteristics is required.

### **3. MODELING SMOKE DETECTOR RESPONSE - GENERAL**

The response of smoke detectors to fire conditions is not easily modeled. The response characteristics of smoke detectors vary widely compared with thermal detectors. In addition, less is known about the production and transport of smoke in the early stages of a fire. Natural and forced air currents have a larger effect on the movement of smoke at the time of interest (very early in the fire) than they do on the stronger thermal currents required to alarm heat detectors.

A comparison of how smoke detectors operate with the smoke measurement methods most often employed and reported by researchers shows that smoke measurements do not generally include the factors that we need to model smoke detector response<sup>2</sup>. Thus, there is a gap between the data generated by fire researchers and the data needed to model smoke detector response.

Researchers most often use optical density or obscuration as a measurement of smoke. These are calculated as follows:

Percent obscuration, %Ob.:

$$\%Ob. = 100 \left( 1 - \frac{I}{I_0} \right)$$

Percent obscuration per unit distance, %O<sub>u</sub>:

$$\%O_u = 100 \left[ 1 - \left( \frac{I}{I_0} \right)^{1/l} \right]$$

Optical density, D:

$$D = \log_{10} \left( \frac{I_0}{I} \right) = -\log_{10} \left( \frac{I}{I_0} \right)$$

Optical density per unit distance, D<sub>u</sub> (m<sup>-1</sup>):

$$D_u = \frac{D}{l} = \frac{1}{l} \log_{10} \left( \frac{I_0}{I} \right) = -\frac{1}{l} \log_{10} \left( \frac{I}{I_0} \right) \quad \text{m}^{-1}$$

Where I<sub>0</sub> is the initial intensity of a light beam reaching a photocell and I is the intensity of the light beam in the presence of smoke.

Optical density and obscuration are useful data for evaluating visibility. However, the only commercially available smoke detector that operates by sensing the attenuation of a light beam is the projected beam type smoke detector. Further, these measurements are sensitive to the wavelength of light used. Thus, to be valuable for estimating the response of a projected beam smoke detector, the data must be measured and reported using the same wavelength as the light source used by the detector.

The two most common types of smoke detectors are ionization type and photoelectric type. Neither type operates using light attenuation. Without a correlation between the optical density data and the response characteristics of a particular detector, accurate modeling is not possible.

In addition, detectors often use complex response algorithms rather than simple threshold or rate-of-change response levels. The algorithms are used to reduce false and nuisance alarms and to enhance fire signature matching. These algorithms vary from detector to detector and are generally not published by the manufacturers. Thus, even if correlations between optical density and the response of scattering and ionization type smoke detectors were available, the signal-sampling algorithm affects the actual response of each model.

Nevertheless, there are methods that can be used to grossly estimate smoke detector response. These estimation methods may not provide accurate prediction of time to detector response because the potential errors in the estimation methods are not generally known and because the response algorithms for a particular detector are not known. Without knowledge of the accuracy of the models and the potential errors, these estimation methods should not be used to compare detector response to other model calculations such as egress time calculations or time to untenability. Estimation methods are best used to compare changes in the response of a particular detector as a result of changes in spacing or location, while holding all other variables constant.

In addition to these estimation methods, actual fire tests with detectors present may provide information to compare smoke detector response to other factors such as egress time, structural response, heat release rate, etc.



Product performance tests may be sources of data. Although, the actual response may not be reported in manufacturer's literature, the minimum and maximum permissible performance imposed by the test standard provides ranges of possible response.

#### **4. MODELING SMOKE DETECTOR RESPONSE - LIGHT OBSCURATION SMOKE DETECTORS**

For projected beam type detectors, fire or smoke models that calculate the optical density per unit length,  $D_u$ , in a space or the total optical density in the path of the detector,  $D$ , may be used to determine when the detector would respond. Manufacturer specifications will typically indicate at what levels of total obscuration or total optical density the detectors respond. Projected beam smoke detectors generally have adjustable response thresholds.

Many fire models estimate the unit optical density,  $D_u$ , in a uniform upper layer or volume. This is referred to as zone modeling. The optical density over the entire length of the beam is then determined by multiplying  $D_u$  by the path length,  $l$ . The path length is the distance between the source and receiver or the projected beam smoke detector. This method assumes homogenous distribution of smoke throughout the path, an assumption that may not be valid.

Another method to model the response of projected beam obscuration type detectors is to calculate the unit optical density,  $D_u$ , at several discrete points or in several discrete segments between the source and the receiver of the projected beam smoke detector. This is a form of field modeling. The

optical density per unit length is then multiplied by the length of that particular segment. The total optical density of the path is then the sum of all of the densities for the individual segments.

## **5. MODELING SMOKE DETECTOR RESPONSE - LIGHT SCATTERING (PHOTOELECTRIC) SMOKE DETECTORS**

The amount of light scattered by smoke is very complex and is related to factors such as the particle number density and size distribution, refractive index, the wavelength of the light source, and the angle between the source and the receiver. The manufacturer for a particular detector can describe some of these variables. Some require information about the smoke produced by the fuel and its transport to the detector location.

Information about smoke properties related to light scattering is presently limited to a few types of fuels and is not readily available to practicing fire protection engineers. In addition, the data may not be in a useable format. For instance, the data must match the wavelength of the light source used in the detector being modeled. Scattering data at other wavelengths introduces errors and uncertainties.

Meacham has shown that it is possible to model the response of light scattering detectors using information about smoke properties obtained by small scale testing of various fuels.<sup>3, 4</sup> However, the recommended test methods have not been further developed, tested and incorporated into fire test programs.

At the present time, there are no practical methods available to directly model the response of light scattering type detectors. However, obscuration

or optical density modeling, as was discussed above for obscuration type detectors, can be used in a limited way to estimate scattering type smoke detector response.

A scattering type detector will respond at different optical densities for different types of smoke. For example, a scattering type smoke detector that responds at an optical density of  $.029 \text{ m}^{-1}$  (2.0%/ft obscuration) to smoke produced by a smoldering gray cotton lamp wick may not respond until an optical density of  $0.15 \text{ m}^{-1}$  (10%/ft) is reached for smoke from a kerosene fire. At the response threshold, both types of smoke are scattering the same amount of light to the receiver of the scattering photoelectric smoke detector. There are many factors involved in this effect. One is that the darker smoke from the kerosene fire does not reflect as much light as the lighter colored smoke from the lamp wick.

Another way to understand the differing response of a scattering type detector to two types of smoke is to consider the amount of light being scattered when both smoke samples have the same optical density. Both samples of smoke equally block our vision of the light reflected by an object. One type of smoke may be composed of large, highly reflective smoke particles that cause the incident light to scatter in many directions. Thus, it reduces the amount of light in the forward direction. The other type of smoke may consist of a smaller number of larger particles that absorb light more readily than they reflect it. Though they have equal optical densities, one is more likely to scatter light and set off a scattering type detector.

In order to model the response of a scattering type detector using obscuration or optical density, it is necessary to know the optical density required for a particular type of smoke to alarm a particular model detector.



For example, many manufacturers label their smoke detectors with a unit optical density,  $D_u$ , or unit obscuration,  $\%O_u$  based on a calibration test that is part of UL standard number 268.<sup>5</sup> That number indicates the unit optical density required for that detector to respond to smoke having very specific characteristics. The optical density required to alarm a particular detector as quoted by the manufacturer is just one value for a given particle size distribution, concentration, color, etc. used in the laboratory calibration test of that model detector. If the smoke and conditions are similar to that used in the test of the detector, the specified alarm threshold can be used in calculations.

It is not sufficient to have data for a particular fuel and detector combination. It is known that smoke changes as it moves away from a fire.<sup>6</sup> There may be changes in the number of particles, their size, shape and velocity. The optical density at response to any smoke signature other than the laboratory calibration test will be different and will vary with different fuels and burning modes.

Threshold response data to various fuels for a particular detector are not readily available. Some manufacturers may provide data if available and when requested. Product performance and safety tests as well as fire tests with detectors present are useful sources of limiting performance data. Product standards typically test detectors in rooms with specified fuels and smoke build-up rates and velocities. The detectors must respond at certain levels or within certain time limits. While the exact performance data may not be made available, the test limits are useful for estimating the range of possible detector response.

## 6. MODELING SMOKE DETECTOR RESPONSE - IONIZATION SMOKE DETECTORS

The signal produced by the chamber of an ionization detector has been shown to be proportional to the product of the number of particles and their diameter.<sup>7, 8, 9, 10</sup> The exact signal produced by an ionization smoke detector is given by a more complex equation in the literature and requires an additional number called the chamber constant. The chamber constant varies with each different model of detector.

Given the quantity and size distribution of smoke particles and the chamber constant (from the manufacturer), it is possible to model the ionization smoke detector. Unfortunately, there are no fire models that provide the required detector model input. In addition, manufacturer specifications do not presently include chamber constants.

Newman modified the chamber theory to account for ionization detector sensitivity to the small electrical charge carried by some fire aerosols.<sup>11</sup> Newman also developed a method to model ionization smoke detector sensitivity as a function of the soot yielded by a particular fuel. Using his method, the change in a detector's signal,  $\Delta I$ , can be related to the optical density of smoke measured at a particular wavelength,  $D_{u\lambda}$ .

To use the method proposed by Newman it is necessary to know what change in detector chamber signal,  $\Delta I$ , will cause a detector or system to alarm. Although manufacturers do not presently provide this data they may be persuaded to do so in the future.

Newman's work was done using a small-scale apparatus and three ionization smoke detectors. A wider range of tests, including some full scale testing is needed to verify this method.

Presently, the only way to model ionization detector response is to use the optical density estimations as discussed for obscuration type detectors.

## **7. MODELING SMOKE DETECTOR RESPONSE - ENTRY RESISTANCE**

In addition to smoke characteristics and the detector's operating mechanism, the ability to get the smoke into the chamber effects the response of the unit. For spot type photoelectric and ionization type smoke detectors, bug screens, chamber design and the detector's aerodynamic characteristics cause entry resistance.

In a scenario where the optical density at the detector location is increasing with time, the optical density inside the detector chamber will always be less than that outside the detector chamber. Similarly, if a detector is placed in a smoke stream having a constant optical density, there will be a time delay before the optical density inside the chamber approaches that outside the detector. As with heat transfer to heat detectors, smoke entry resistance can be characterized by a detector time constant,  $\tau$ :

$$\frac{dD_{ui}}{dt} = \frac{1}{\tau} (D_u - D_{ui}) \quad \text{s}^{-1} \text{m}^{-1} \quad (5)$$



Where  $D_{ui}$  ( $m^{-1}$ ) is the optical density per unit length inside the detector chamber,  $D_u$  ( $m^{-1}$ ) is the optical density per unit length outside the detector and  $\tau$  (s) is the detector time constant.

If the time constant and the rate of change of optical density outside the detector are constant, then this equation can be solved. Further, substituting  $D_{ur}$  for the optical density outside the detector at response and  $D_{uo}$  for the optical density required inside the detector to produce response yields the following<sup>12, 13</sup>:

$$D_{ur} = D_{uo} + \tau \left( \frac{dD_u}{dt} \right) \left\{ 1 - \exp \left[ -D_{ur} \frac{1}{\tau} \left( \frac{dD_u}{dt} \right) \right] \right\} \quad m^{-1}$$

Heskestad proposed that the time constant could be represented by the following:

$$\tau = \frac{L}{u} \quad \text{seconds}$$

Where  $L$  is the detector's characteristic length and  $u$  is the velocity of the ceiling jet flowing past the detector.

The characteristic length is thought to be a property of the detector that is independent of the smoke and ceiling jet properties. It is interpreted as the distance the smoke would travel at the velocity  $u$  before the optical density inside the detector reaches the value outside of the detector. Combining the equations:

$$D_{ur} = D_{uo} + \frac{L}{u} \left( \frac{dD_u}{dt} \right) \left\{ 1 - \exp \left[ -D_{ur} \frac{u}{L} \left( \frac{dD_u}{dt} \right) \right] \right\} \quad \text{m}^{-1} \quad (8)$$

The exponential term is small compared to the rest of the equation, allowing the equation to be simplified.<sup>12</sup> Simplification of the equation is not necessary when calculations are made using a computer. However, the simplified form clearly shows the effect of entry resistance.

$$D_{ur} = D_{uo} + \tau \left( \frac{dD_u}{dt} \right) \quad \text{or} \quad D_{ur} = D_{uo} + \frac{L}{u} \left( \frac{dD_u}{dt} \right) \quad \text{m}^{-1} \quad (9)$$

This form of the entry resistance equation clearly shows that when the optical density outside a detector is increasing with time, the optical density inside the detector will lag behind if there is any entry resistance.

Heskestad and later Bjorkman et al. have plotted test data to determine the L number for a variety of smoke detectors. Additional work has been done by Marrion and by Oldweiler to study the effects of detector position and gas velocity on the L number.<sup>14, 15</sup>

Bjorkman et al., Marrion and Oldweiler all observed variations in L that may be attributed to a dependence on velocity. Marrion and Oldweiler's data also imply that there may also be a dependence on the characteristics of the smoke. Table 1 below summarizes the results from the works cited above.

**Table 1– Range of Characteristic Length (L) Numbers**

Researcher	Ionization Detector L (m)	Scattering Detector L (m)
Heskestad	1.8	15 (a)
Bjorkman et al.	3.2 +/- 0.2 (b)	5.3 +/- 2.7 (c)
Marrion	Not tested	7.2 (d), 11.0 - 13.0 (e), 18.4 (f)
Oldweiler	4.0 - 9.5 (g), 4.3 - 14.2 (h)	Not tested

Notes:

- a) Older style detector with more elaborate labyrinth.
- b) L determined by best fit for three test velocities.
- c) L based on a single test velocity & a limited number of tests (complete equation used).
- d) Low L number at low test velocity.
- e) Range of L for several fuels and detector positions.
- f) L increased by adding “fence” to further restrict smoke entry.
- g) Range of L for a variety of velocities using simplified equation for entry resistance
- h) Range of L for a variety of velocities using complete equation for entry resistance

Examination of the data and analysis work cited above shows that more work needs to be done to study the effects of low velocities and the effects of smoke characteristics on detector entry characteristics. The sharp increase in L at lower velocities appears to indicate that entry resistance may be related to smoke particle size. It is also possible that L is a function of the smoke momentum at low velocities. Thus, the time lag would be inversely proportional to the velocity squared.



Engineers can use  $L$  as a measure of entry resistance and the resulting time lag. However, in scenarios where the ceiling jet velocity is low, there will be greater uncertainty in the results.

Without validation of  $L$  as a measure of lag time, manufacturers and test laboratories are not measuring or reporting  $L$  in their literature. Nevertheless, the range of  $L$  numbers reported in Table 1 can be used to estimate possible errors in detector response time.

## **8. MODELING SMOKE DETECTOR RESPONSE – SMOKE DILUTION AND THE EFFECTS OF FORCED AIRFLOW**

Smoke dilution refers to a reduction in the quantity of solid and liquid aerosols (smoke) available for detection. Dilution can occur through natural convection (entrainment in the plume or the ceiling jet) or through the effects of by forced ventilation systems.

Air flow effects become less as fire size increases. Conversely, when detection is desired at smaller fire sizes, air flow effects may become a dominant factor in the response of the smoke detector. Velocity profiles of the air movement within a room or smoke tests under various conditions may assist in determining optimum smoke detector placement.

Computational fluid dynamics (CFD) modeling has been used to show the effects of ducted air supply and air return on smoke spread.<sup>16, 17, 18</sup> That work used three dimensional color graphics plots to show areas of non-activation for given scenarios and assumptions. That research effort verified a long standing rule that smoke detectors should not be located within

approximately one meter of conventional air supply diffusers and air return grills due to the high level of dilution. However, because air dilution and smoke movement in a compartment is such a complex problem with a large number of variables, the research program was not able to create simplified engineering relations or tools for use in design of smoke detection systems.

CFD modeling can be a useful tool for complex scenarios involving airflow. However, potential sources of error exist. For example, CFD models generally do not model fires. Instead, they model the transport of the mass and energy “injected” or “produced” at the fire location. Thus, many of the same discussions above concerning mass optical density, soot deposition, smoke particle characteristics, optical density vs. temperature correlations are also applicable to this type of modeling.

## **9. TEMPERATURE APPROXIMATION METHOD FOR MODELING SMOKE DETECTION**

The temperature approximation theory is a method used to estimate the optical density produced by flaming fires. The theory hypothesizes that the mass concentration of smoke particles at a point is proportional to the change in temperature due to the fire (at that point).<sup>19</sup> The following assumptions are necessary:

- Particle size distribution is constant in space and time
- Mass generation rate is proportional to mass burning rate
- There is no heat transfer between particles or between the particles and the confining surfaces
- The smoke does not continue to react as it travels

Heskestad then hypothesized that the ratio of optical density to temperature rise would be a constant for a particular fuel and burning mode (flaming, smoldering, vertical combustion, horizontal combustion, etc.). There are actually three parts to this hypothesis.

The first is that each fuel and burning mode results in a unique optical density required to alarm a particular model and type of detector. This was discussed previously regarding photoelectric, ionization and projected beam smoke detectors. This phenomenon is regularly observed, explained by theory, and accepted by the scientific and engineering community.

The second part of the hypothesis is that for each fuel and burning mode the optical density at a point is proportional to the mass concentration of particles.

$$D_u \propto C \quad (10)$$

The final part of the hypothesis is that for each fuel and burning mode the mass concentration of particles is proportional to the change in temperature at a point.

$$C \propto \Delta T \quad (11)$$

Combining these proportionalities, optical density is proportional to the change in gas temperature for a given fuel and combustion mode:

$$D_u \propto \Delta T \quad (12)$$



Therefore, the ratio of optical density to temperature rise is constant for a given fuel.

$$\frac{D_u}{\Delta T_g} = CONSTANT$$

This hypothesis assumes that the only way to move the smoke particles from the source to the detector at the ceiling is by buoyant forces.

Heskestad and Delichatsios examined experimental data for obscuration and temperature rise at various locations on a ceiling for different fuels. They concluded that while the data showed some variation in time at different radial positions relative to the fire source, the ratio could be approximated as a constant. Table 2 lists the ratios recommended by Heskestad and Delichatsios for various fuels.<sup>19</sup>

**Table 2**

Material	$\frac{10^2 D_u}{\Delta T} \left( \frac{1}{ft^0F} \right)$	Range of Values
Wood	0.02	0.015 - 0.055
Cotton	0.01/0.02	0.005 - 0.03
Paper	0.03	Data not available
Polyurethane	0.4	0.2 - 0.55
Polyester	0.3	Data not available
PVC	0.5/1.0	0.1 - 1.0

Foam rubber PU	1.3	Data not available
Average	0.4	0.005 - 1.3

Examining the original data, the last column has been added to show the range of values for each fuel. Averages have also been calculated and listed in the last row of the table for reference.

Others experiments have resulted in data that differ from that of Heskestad and Delichatsios. Bjorkman et.al. reported values for polyurethane that are approximately one half that reported by Heskestad and Delichatsios.<sup>20</sup>

The data produced by Heskestad and Delichatsios show the ratio of optical density to temperature rise was not constant. The authors concluded that the variation was the result of slowly changing characteristics of the smoke particles as they left the flaming source and traveled in the plume and ceiling jet. Nevertheless, they concluded that a constant value could be used as a rough approximation to allow engineers to model optical density produced by a fire. Although it has not yet been done, it is possible to examine their original data and place error bars on the values recommended in the above table. With today's availability of desktop computers to perform modeling calculations, it may be possible to develop and use a functional relationship for the ratio of optical density to temperature rise in lieu of a constant.

A fire model can be used to calculate the temperature rise at a smoke detector location or in a layer. Then, using the ratios reported by

researchers, the optical density at that location as a function of time can be approximated.

## 10. MASS OPTICAL DENSITY METHOD FOR MODELING SMOKE DETECTION

The fuel characteristics of primary concern for smoke detection are: (1) material and (2) mode of combustion. These two parameters are important for determining pertinent features of expected products of combustion, such as particle size, distribution, concentration, and refractive index. Assuming a well-mixed smoke-filled volume, data on smoke characteristics for given fuels can provide an estimation of detector response. Some fire models calculate the optical density of smoke in a space using the following relationship for the optical density per unit length,  $D_u$ :

$$D_u = \frac{D}{l} = D_m \frac{\Delta m}{V_c} \quad (\text{m}^{-1})$$

$l$  is the path length (m)

$D_m$  is the mass optical density ( $\text{m}^2/\text{g}$ )

$\Delta m$  is the mass of the fuel burned (g)

$V_c$  is the volume that the smoke is dissipated in ( $\text{m}^3$ )

This method will be referred to as the mass optical density method.  $D_m$  varies depending on the fuel, and is determined experimentally. Tables of  $D_m$  can be found in the SFPE Handbook of Fire Protection Engineering.<sup>6, 21</sup>

The mass optical density method for estimating the optical density of smoke produced by a fire requires that the variable  $D_m$  be selected for the particular fuel and burning mode. The most complete set of data available



are in the SFPE Handbook of Fire Protection Engineering. However, not all fuels and burning modes have been tested and reported. Also, more complex fuel packages, such as upholstered chairs, require that  $D_m$  be chosen for one fuel even though more than one may be burning at the same time. When a model using this method is employed, users should check to see if the model selects an appropriate value of  $D_m$  for the fuel being studied. Some models may use a single value of  $D_m$  regardless of the fuel. In that case, answers can be modified by dividing the calculated  $D_u$  by the  $D_m$  used in the program, then multiplying by the appropriate value of  $D_m$  selected from the available data.

$$D_{u(new)} = D_{u(calc)} \frac{D_{m(new)}}{D_{m(calc)}} \quad m^{-1} \tag{15}$$

Mass optical density can be derived by burning a sample in a closed chamber and measuring the optical density in the chamber. The following equation is used to calculate  $D_m$ :

$$D_m = \frac{DV_c}{l\Delta m} \quad \frac{m^2}{g} \tag{16}$$

Where

- D is the optical density measured in the test
- l is the path length over which D was measured (m)
- $V_c$  is the volume of the test chamber ( $m^3$ )
- $\Delta m$  is the mass of the fuel sample consumed in the test (g)

A different equation is used for open test arrangements that involve a flow of air and combustion products through a test chamber.

$D_m$  data are often measured in small scale tests due to the need for accurate measurements of mass loss and optical density. The use of  $D_m$  from small

scale tests to calculate the resulting  $D_u$  in a large scale scenario introduces error. Some comparisons show qualitative correlation. However, it has been reported that the correlation breaks down with complex fires.<sup>6</sup>

The value of optical density,  $D$ , measured in the test depends on the wavelength of the light used. For a given set of test conditions, if the wavelength of the measuring light beam is reduced, the measured optical density will increase. This occurs because particles must have a diameter on the same order of magnitude or larger than the light wavelength in order to obscure the light. Shorter wavelength lights will be obscured by the smaller particles not seen by the longer wavelength light. Also, most light sources produce a range of different wavelengths, usually having some specific distribution and some nominal peak. The exception is when a precise laser light source is used. Finally, the receiver that senses the light and produces a corresponding output also has a response distribution curve for various wavelengths.

Examination of test data reported by Tewarson show that  $D_m$  found using a nominal wavelength of  $1.06 \mu$  (microns) might be as much as 5 times less than  $D_m$  found with a  $0.458 \mu$  light source.<sup>21</sup> Unfortunately, the tables of data for various fuels in the SFPE Handbook do not all list the wavelength used to determine  $D_m$ . If the wavelength (and distribution) of the light used to determine  $D_m$  is the same as the wavelength of light used to test a smoke detector and report its sensitivity, then no error is introduced. For these data to be useful in modeling smoke detector response, they should be determined using a light source and receiver having characteristics similar to most commercially available smoke detectors. Commercially available detectors use light sources having peak wavelengths in the infrared band.

Meacham has reported that two manufacturers use LED sources having peak wavelengths on the order of 880 to 950 nm (0.880 to 0.950  $\mu\text{m}$ ).<sup>3</sup>

Another method for determining  $D_m$  involves a calculation using the yield of smoke for a particular fuel. Tewarson examined data from several sources and arrived at the following equations<sup>21</sup>:

$$D_m = 0.10 \ln Y_s + 0.52 \left( \frac{m^2}{g} \right) \text{ for flaming fires} \quad (17)$$

$$D_m = 0.17 \ln Y_s + 0.65 \left( \frac{m^2}{g} \right) \text{ for smoldering fires} \quad (18)$$

In these equations  $Y_s$  is the yield of smoke in grams per gram of fuel consumed. These equations provide an additional method for determining  $D_m$  when test reports include  $Y_s$ . However, the determination of  $Y_s$  may also introduce errors in the calculation of  $D_m$  and hence  $D_u$ . The nature and extent of these possible errors is beyond the scope of this paper.

Models that calculate the optical density in a space using  $D_m$  assume that the smoke produced is distributed evenly throughout a specific volume. This is called a zone model. In short, one zone is the hot upper layer which has a uniform temperature and smoke optical density throughout. The second zone is the cooler, near ambient lower layer. Some models treat the lower layer as being at the initial, ambient conditions, while others consider the amount of smoke and heat added to the layer. Since real fires tend to produce varying optical density throughout the space, the uniform zone assumption introduces error in any detector response modeling. Larger



volumes and larger horizontal distances from the fire plume increase the errors caused by the use of simplified zone modeling.

When the mass optical density method is used, all smoke produced by the fire is assumed to contribute to the optical density of the smoke in the assumed volume. However, the actual mass loss and smoke production occurs over time. Depending on the actual conditions in the space and the nature of the fuel, some amount of the smoke will have been deposited on the walls, ceilings, furnishings and other surfaces as soot. In addition, the potential for transport out of the space exists whenever vents are present. Most computer fire models do not contain a routine to account for soot deposition when calculating the resulting optical density.<sup>2</sup>

Most fire models determine the volume of the upper smoke layer by calculating the distance below the ceiling at which the temperature drops off significantly. In an actual fire, the demarcation between the two layers is not necessarily distinct, as some amount of the smoke cools and diffuses into the lower layer.

It has also been shown that smoke ages, changing its characteristics with time. Smoke aging effects include agglomeration of small particles into larger particles, possible continued oxidation of unburned fuel mass in the smoke layer and other chemical and physical changes that affect the optical density of the smoke. The effects of smoke deposition and smoke aging on smoke detector response modeling may be negligible in the early stages of a fire and when a detector is close to and in the same room as the fire. In cases where the detector is far from the fire, in another room, or where the smoke must travel an indirect path to the detector, results will be less

accurate. These phenomena have been investigated by Yamauchi<sup>22</sup> but have not yet been incorporated into available detector models.

## 11. DISCUSSION RELATED TO THE USE OF FIRE MODELS FOR HEAT AND SMOKE DETECTOR MODELING

Some computer fire models or sets of computational tools include routines for calculating heat or smoke detector response. It is important for users to understand the underlying detector models being used so that limitations and potential errors can be understood. For heat detection, most use a lumped mass model. However, for smoke detection some use a temperature rise model and some use a mass optical density or specific extinction area model. The specific extinction area,  $\sigma_f$ , is similar to the mass optical density except that it is based on calculations using the natural log,  $e$ , rather than  $\log_{10}$ . Most do not include entry resistance modeling. Some permit the use of fuel specific parameters for smoke yield and mass optical density. Others use preset values.

## 12. CONCLUSIONS

It is not possible to accurately compare smoke detector response to other fire related models such as egress time or structural response to heat. If smoke detection is to be a part of tomorrow's performance based solutions fire models and detector models must evolve and work together. The evolution of the *fire* and *detector* models must include a feedback loop to ensure that they can be integrated to form a *detection* model.

Additional research is needed to test and verify certain aspects of detector models. Most important is additional work on the entry resistance model and the scattering detector model. Additional work should also be done to further test and refine Newman's model for ionization detector response.

Detector manufacturers, product certification laboratories and application engineers need to agree on a method for cataloging specific detector response algorithms. This needs to be done in a way that protects manufacturer's patents and confidentiality rights while still providing useful engineering information. Further, it must be done in a way that is easy to measure and verify.

Fire researchers need to examine detector models and develop instrumentation and data gathering methods that match the detector models. Raw data should be made available for input to detector models. Where possible, functional models produced from data should be developed in a format suitable for incorporation into detector models.

Detector and fire models, whether modular or integrated to form a detection model, need to better report and present limitations and potential errors. Finally, application engineers must be more conscious of the limits on a model's accuracy and precision and must provide useful feedback to researchers involved in product development and fire research.

### 13. REFERENCES

---

- [<sup>1</sup>] NFPA 72, *National Fire Alarm Code*, National Fire Protection Association, Quincy, MA (1999).



- 
- [<sup>2</sup>] R.P. Schifiliti and W.E. Pucci, *Fire Detection Modeling: State of the Art*, the Fire Detection Institute, Bloomfield, CT, 1996.
- [<sup>3</sup>] Brian J. Meacham, "Characterization of Smoke from Burning Materials for the Evaluation of Light Scattering-Type Smoke Detector Response," MS Thesis, WPI Center for Firesafety Studies, Worcester, MA (1991).
- [<sup>4</sup>] B.J. Meacham and V. Motevalli, "Characterization of Smoke from Smoldering Combustion for the Evaluation of Light Scattering-Type Smoke Detector Response," *J. of Fire Protection Engineering, SFPE*, Vol. 4, No. 1 (1992).
- [<sup>5</sup>] UL 268, *Standard for Safety Smoke Detectors for Fire Protective Signaling Systems*, Underwriters Laboratories, Inc., Northbrook, IL (1989).
- [<sup>6</sup>] G. Mulholland, "Smoke Production and Properties", *SFPE Handbook of Fire Protection Engineering*, Chapter 2-15, 2<sup>nd</sup> ed. NFPA 1995.
- [<sup>7</sup>] J. Hoseman, "Uber Verfahren zur Bestimmung der Korngrossenverteilung hokkonzentrierter Polydispersionen von MiePartikeln", Ph.D. Thesis, Aachen, 1970.
- [<sup>8</sup>] C.D. Litton, "A Mathematical Model for Ionization Type Smoke Detectors and the Reduced Source Approximation," *Fire Technology*, Vol. 13, No. 4, NFPA, November 1974.
- [<sup>9</sup>] R.W. Bukowski and G.W. Mulholland, "Smoke Detector Design and Smoke Properties", US Dept. of Commerce, National Bureau of Standards, November 1978.

- 
- [<sup>10</sup>] C. Helsper, H. Fissan, J. Muggli and A. Scheidweiler, "Verification of Ionization Chamber Theory," *Fire Technology*, Vol. 19, No. 1, 1983
- [<sup>11</sup>] J. Newman, "Modified Theory for the Characterization of Ionization Smoke Detectors," *Fire Safety Science-Proceedings of the Fourth International Symposium*, 1994.
- [<sup>12</sup>] G. Heskestad, "Generalized Characteristics of Smoke Entry and Response for Products-of-Combustion Detectors," *Proceedings, 7th International Conference on Problems of Automatic Fire Detection*, Rheinisch-Westfalischen Technischen Hochschule Aachen, March 1975.
- [<sup>13</sup>] M. Kokkala et al, "Measurements of the Characteristic Lengths of Smoke Detectors," *Fire Technology*, Vol. 28, No. 2, National Fire Protection Association, Quincy, MA (1992).
- [<sup>14</sup>] C.E. Marrion, "Lag Time Modeling and Effects of Ceiling Jet Velocity on the Placement of Optical Smoke Detectors," MStHesis, WPI Center for Firesafety Studies, Worcester, MA (1989).
- [<sup>15</sup>] A. Oldweiler, "Investigation of the Smoke Detector L Number in the UL Smoke Box," MS Master's Thesis, Worcester Polytechnic Institute, Worcester, MA, 1995
- [<sup>16</sup>] Klote, J. H.; Forney, G. P.; Davis, W. D.; Bukowski, R. W. Simulating the Effects of HVAC Induced Air Flow From Slot Diffusers on Detector Response. National Institute of Standards and Technology, Gaithersburg, MD National Fire Protection Assoc., Quincy, MA NISTIR 5908; 79 p. December 1996.
- [<sup>17</sup>] Klote, J. H.; Forney, G. P.; Davis, W. D.; Bukowski, R. W. Field Modeling: Simulating the Effects of HVAC Induced Air Flow From

---

Various Diffusers and Returns on Detector Response. International Fire Detection Research Project. Technical Report. Year 3. National Institute of Standards and Technology, Gaithersburg, MD National Fire Protection Research Foundation, Quincy, MA Technical Report; Year 3; 79 p. April 1996.

[<sup>18</sup>] Klote, J. H.; Davis, W. D.; Forney, G. P.; Bukowski, R. W. Field Modeling: Simulating the Effects of HVAC Induced Air Flow From Various Diffusers and Returns on Detector Response. International Fire Detection Research Project. Year 4 Report/Data. National Institute of Standards and Technology, Gaithersburg, MD National Fire Protection Research Foundation, Quincy, MA Year 4 Report/Data; 1998.

[<sup>19</sup>] Heskestad, G. and Delichatsios, M.A., "Environments of Fire Detectors - Phase I: Effect of Fire Size, Ceiling Height and Material," Volume I - "Measurements" (NBS-GCR-77-86), May 1977, Volume II - "Analysis" (NBS-GCR-77-95), June 1977, National Technical Information Service (NTIS), Springfield, VA 221

[<sup>20</sup>] J. Bjorkman, O. Huttunen, and M. Kokkala, "Paloilmaisimien toimintaa kuvaavat laskentamallit (Calculation models for fire detector response)," Technical Research Center of Finland, Research Notes 1036, 1989.

[<sup>21</sup>] A. Tewarson, "Generation of Heat and Chemical Compounds in Fires", Chapter 1-13, in Philip J. DiNenno Ed., *SFPE Handbook of Fire Protection Engineering*, National Fire Protection Association, Quincy, MA, 1988.



---

[<sup>22</sup>] Y. Yamauchi, "Prediction of Response Time of Smoke Detectors in Enclosure Fires, US Dept. of Commerce, National Bureau of Standards, January 1988.

Z. Liu, J. Makar and A. K. Kim

Institute for Research in Construction

National Research Council of Canada, Ottawa, Canada, Email: [zhigang.liu@nrc.ca](mailto:zhigang.liu@nrc.ca)

## **Development of Fire Detection Systems in the Intelligent Building**

### **Abstract**

Fire detection and its corresponding safety systems are crucial parts of an intelligent building. This paper reviews the current state of development of fire detection and alarm systems in the intelligent building. New technologies and concepts developed in intelligent buildings, such as advanced multi-function sensors, computer vision systems and wireless sensors, real-time control via the Internet, and integrated building service systems, have also been reviewed and discussed. These new technologies and concepts will improve the capability of fire detection systems to discriminate between fire and non-fire threats and will increase the time available for property and life protection. However, much effort is still needed to remove barriers to the further development of these new technologies.

### **Introduction**

An intelligent building can be defined as one that combines the best available concepts, designs, materials, systems and technologies to provide a responsive, effective and supportive intelligent environment for achieving the occupants' objectives over the full life-span of the building [1-6]. Compared with traditional buildings, intelligent buildings should be able to reduce energy consumption, reduce maintenance and service operation costs, provide improved security services, improve ease of layout planning and re-planning, and increase the satisfaction of building occupants [4-7]. Other benefits should include its adaptability to changing uses and technology and its environmental performance in providing safer, healthier and more comfortable working conditions. Intelligent building proponents also believe that these buildings will improve worker productivity through improved work environments. Over the last two decades, the

intelligent building concept has become an important consideration in the planning of many new or upgraded office buildings [3-6]. It has also been further developed to embrace other types of living and working environments such as homes, factories and education facilities.

Fire detection and the corresponding safety systems are crucial parts of an intelligent building. Billions of dollars are spent annually to install and maintain fire detection systems in buildings to assure safety from unwanted fires [8]. Intelligent systems developed in the intelligent building offer opportunities to meet this task more effectively, efficiently and economically. New sensors will produce earlier and more reliable fire detection. Wireless systems will eliminate the need for cabling and offer opportunities for fire fighters to work out fire fighting strategies before arrival at the fire scene. Integrated building systems hold the potential for reducing false alarms, speeding building evacuation and assisting in fire fighting. These changes will create new ways to provide fire safety and new markets for fire detection, alarm and fighting systems [9]. As these technologies mature, changes to building practices may also result.

This paper reviews the current state of the art for fire detection and alarm systems in intelligent buildings. It identifies new technologies and concepts developed for intelligent buildings that could be used to improve the capability of fire safety systems. The potential effects of integrated building service systems and barriers to the development of fire detection and alarm systems in intelligent buildings are discussed. The paper concludes by examining how these new systems may be combined to provide the next generation of intelligent fire safety systems.

### **Emerging Sensor Technologies**

New sensor technologies will be key components in the next generation of intelligent buildings. Current intelligent buildings often have embedded processors and dedicated information networks. The new generation is expected to add the capability to learn about the building's circumstances and its occupants' needs and change the behaviour of its control systems accordingly [10]. The employment of a large number of sensors



within the building will allow it to operate in a responsive manner, rather than using pre-programmed control models as are employed in the first two generations of intelligent building. The information provided by sensors includes changes in both internal and external environments of a building, such as smoke, temperature and humidity, air quality, air movement, and the number of building occupants as well as a host of other properties. The system will use sensors to identify how a particular person tends to react to particular circumstances and to learn different behaviours for different people.

The number of sensors required to obtain this type of functionality is quite high, especially since one of the major goals of intelligent buildings is to allow individualized control of an environment. This need will increase the cost of intelligent buildings and make it difficult to manage the resulting large amount of data. Development of cost-effective sensors has consequently been identified as a key need for intelligent buildings [11]. Fortunately, many of the properties that need to be monitored can be used for multiple purposes. Security systems that can track the entry and exit of occupants from an office building can also be used to ensure complete evacuation of a building during a fire or even, in more advanced forms, determine where occupants may be trapped and unable to escape. Similarly, parameters such as temperature and air movement are as relevant to fire detection as the maintenance of the indoor working environment. Dual use sensors and sensor systems that are flexible enough to interpret data from different events will be key to making cost efficient intelligent buildings.

Efforts are being made to develop multi-function sensors for simultaneously detecting fire and monitoring indoor air quality (IAQ). Multi-function sensors that combine inputs from several different chemicals or physical processes would be expected to reduce the rate of false alarms and increase the speed of detection of real problems. They should therefore enhance fire safety while at the same time lowering total system costs. The chemical gas sensor has potential for this type of application. Chemical sensor techniques are now available for measuring almost any stable gaseous species emitted from materials and prior to or during combustion [12]. Chemical species can be sensed through a multitude of interactions, including catalytic, electrochemical, mechanic-chemical, and optical processes. In one square inch, several hundred individual sensors

can be placed in an array. By coating each sensor with a different semi-conducting material, several hundred different readings for gas signatures can be made by an expert system [13]. Recently, one olfactory sensor array system has been developed for environmental monitoring and for fire and smoke detection [14]. Such a system consists of an array of broadly-selective chemical sensors coupled to microprocessor-based pattern-recognition algorithms so that the changes in environmental conditions, such as CO, CO<sub>2</sub> and smoke, can be detected.

A major issue in any sensor system is differentiating between different causes of the event being detected. Higher than expected levels of CO<sub>2</sub>, for example, may be the signs of a fire, but may also be a sign of poor air circulation within a room. When separate sensors installed in the building for fire safety, thermal comfort control and environmental monitoring can be integrated, sensitivity to fires and false alarm immunity can be significantly enhanced [15]. These sensors are located in different positions in the building. Once a fire occurs, the system can take multiple fire signatures and the spatial relationship and status of adjacent detectors into account in making decisions. Separate fire sensitivity information produced by these sensors would be transmitted to a control panel where fire signal processing and alarm and fault determinations are made. The use of a powerful central processing unit (CPU) in the control panel would also allow the system to use complex algorithms and advanced signal processing for fire signature identification.

The role of the control panel in improving fire detection capability has already been recognized, with a system using control panels for decision making being one of two main versions of intelligent fire detection systems [16]. Modern control panels are much more powerful and flexible because of the widespread use of integrated circuits and digital components that allow functions to be fully computer controlled. These control panels have powerful signal processing capability and use artificial intelligent techniques, to improve fire detection system reliability, response times to incipient fires, false alarm rates and maintenance requirements. The Building and Fire Research Laboratory at NIST has recently initiated a project to further develop advanced fire detection and alarm panels [8]. This project aims to use information provided by sensors and advanced models of

fire growth and smoke spread in buildings to discriminate between fire and non-fire threats, identify the exact location of a fire in a building, and provide continuous estimates on the short and long term behavior of fire growth and smoke spread in the building. Such fire information will allow building operators and fire fighters to make a more accurate and responsive evaluation of any fire-related incident in the building, to control fires and supervise the evacuation from the building.

Computer vision systems can also be used as a type of multi-function sensor. Computer vision applications have included building security, improving response rate and energy saving for HVAC systems by identifying occupant numbers and their locations [17], monitoring electrical power switchboards and control panels [18] and lighting level sensing and control [2]. Computer vision also has strong advantages for use in sensing and monitoring a fire. Cameras and corresponding facilities required in the computer vision system are already standard features of many buildings for other applications. Additional fire detection capability can therefore be added with minimal cost through changes in software and correlating results between the computer vision system and other sensors. One such application is the machine vision fire detection system (MVFDS), which uses a combination of video cameras, computers, and artificial intelligence techniques [19-22]. It processes multiple spectral images in real time to reliably detect a small fire at large distances in a very short time. It can also identify the location of a fire, track its growth and monitor fire suppression. For some applications, the MVFDS is further combined with radiation sensors (UV and IR) to enhance its detection capabilities or a CCD camera to automatically evaluate the scene through identification of bright regions associated with the fire radiation and increase system reliability [21, 22]. The development of this computer vision system is still ongoing and is viewed as being restricted due to the need for expensive and sophisticated software and hardware components.

Wireless sensors are another important emerging technology for intelligent buildings. Wireless fire detectors are already available in the market. An alarm signal is transmitted to the control panel by radio, infra red transmission, ultra sonic and microwaves when smoke or rapid temperature changes are detected. Their significance comes not from



their ability to measure new parameters, but because they do not require a hardwired connection to the data acquisition system that will record their readings. This capability not only allows wireless sensors to be located anywhere inside a room, but also means that they can be installed in the exterior envelope or other locations that would be too expensive or physically impossible to monitor in any other way [2]. Wireless technology may also be a necessity for retrofitting intelligent building technology in older buildings, where the difficulty and cost of installation is a significant barrier. In many cases installing intelligent building systems in older buildings requires major renovations. It can rarely, if ever, be done without damage to existing walls, floors and ceilings. It is likely that wireless networks will need to be developed to retrofit older buildings. Without such techniques, these older buildings will gradually become uncompetitive with new construction, reducing the value of the existing built environment.

In large buildings, wireless sensors communicate with other building systems through wireless networks in the building. Intra-office data networks based on 10 GHz wireless networks are already becoming widely available [23]. Wireless networks are expected to become the dominant media for low to medium bit rates for many intelligent building network applications. However, significant further development will be necessary for them to reach their full potential, and to overcome attenuation problems, such as absorption by office partitioning and reflection from wall, windows and other surfaces. Other major problems include the need to significantly lower the cost of wireless sensors, and the requirement for the development of suitable power supply systems that will allow the long-term operation of these sensors.

### **Development of Remote Monitoring and Control Techniques**

There is increasing interest in remotely monitoring building service systems. Intelligent remote monitoring can significantly increase efficiency and reduce costs for building management operations. They may be especially important for small facilities where skilled technical supervision would otherwise be too expensive to consider. These systems could let a single person supervise a number of buildings.

Most commercial monitoring systems use a modem and remote dial-up to access the building's operating system. Alarm messages from the building systems can also be directly sent to the equipment's manufacturer without intervention from the building's operator. More recently, studies have been carried out using the Internet for real-time control of a building automation system [24, 25]. Compared to "voice/touch-tone" interface, the Internet is able to provide more information (text, images and sound clips). Researchers at the University of Essex in the United Kingdom are developing an embedded-internet within a building that will allow building users or manufacturers to directly communicate with the building service systems [24]. The City University of Hong Kong has carried out an initial research project to use the Internet for real-time control of building automation systems [25]. Their studies have shown that the Internet has the potential to extend the monitoring and control of a typical building automation system out of the building so that users can gain access to it at anytime and from anywhere. Their work also shows that one central 24-hour management office is able to manage a real estate portfolio with hundreds of buildings.

Remote monitoring and control also has the potential to improve fire safety. It is estimated that 67 percent of all fires occur outside of office hours [26]. Remote monitoring of fire detection and alarm systems can reduce response time and improve response effectiveness by providing adequate fire information to the building supervisor, activating fire suppression systems and immediately summoning the appropriate fire brigade.

Some current advanced fire control panels have already incorporated a modem for remote access control. With the development of real-time control via the Internet, fire detection systems will perform automatic fault detection and diagnosis with early warning of sensor contamination before the overall integrity of the system is affected. Human intervention at the first sign of a warning should permit more efficient discrimination between fire and non-fire threats. When a fire occurs, detailed and adequate local fire information could be directly sent to the appropriate fire department. Firefighters could also access information from the Internet to identify the locations of potentially hazardous materials or occupants who will need special assistance to leave the fire location. Fully integrated remote access

systems will allow planning for fighting fires to take place enroute to the fire, rather than at the building's fire panel. Remote access systems should therefore provide valuable additional time for property and life protection.

However, real-time control via the Internet, is still in its infancy [25]. Development of the advanced, Internet based remote access fire protection systems described above has not yet begun. In addition, significant issues, such as real-time control of security and safety, still need to be considered. Internet access to fire safety systems also creates its own unique fire safety issues concerning computer and network security. The full implementation of Internet based monitoring systems will require strong assurances of data integrity and resistance to computer hacking. Without these protections, fire fighters may receive false information about the existence, location or size of fires.

### **Integrated Building Service Systems**

Today's fire detection and alarm systems have been partially integrated with other building systems. Once a fire occurs in a building, fire detection and alarm systems in some buildings activate various fire safety systems, such as smoke control, and various pressurization and smoke exhaust system. They also activate elevator recall, the door release system, flashing exit signs and fire suppression systems [27]. Currently, however, the level of integration of all the disparate building systems is still limited. Even though building service systems that have similar functionality, such as fire safety systems and security systems, or HVAC systems and lighting systems, have been integrated together [5, 6], there is a limited level of information-sharing among the systems. Systems on the same cabling backbone are all provided by the same manufacturer. Various building service systems involving HVAC, lighting, fire safety and security monitoring in the building are not integrated together on the basis of a common communication protocol. This is mainly due to fragmentation of the building and communication industries, a reluctance to change established practices as well as the lack of standardized, broadly-based communication protocols that allow different types of building service systems to communicate with each other. Many tenants and developers also prefer to have a lesser degree of systems' integration due to fears of



excessive complexity, potential total system failure and possible slowdown of the central control [28, 29].

Various methods and concepts have been developed to enhance integration of building systems and to increase reliability of the integrated systems [5, 6, 30]. Efforts are also being made to develop communication protocols that enable different manufacturers to “interoperate” together and allow the building systems to communicate with each other over a network [8]. These protocols include BACnet, LonWorks, CAN, NEST, EHSA and CAB [10]. They prescribe a detailed set of rules and procedures that govern all aspects of communicating information from one cooperating machine to another. BACnet prefers a hierarchical model in which the whole system is divided into a number of subsystems, each with a separate central processing unit [31]. The coordination of the subsystems is achieved by hardwired interconnection or software interconnection. This method simplifies installation and maintenance and the damage caused by the failure of the CPU to EMCS and the fire safety systems is only limited to the local level, instead of to the whole integrated system. BACnet is most suitable to the traditional processing and communications models used by current HVAC hardware. However, BACnet does not support dynamically structured networks, nor does it emphasize distributed processing. Efforts are being made to expand BACnet beyond the HVAC realm. The first commercial BACnet fire system products will be introduced within the next two years, and new features are also being added to the protocol that will enhance the use of BACnet in life-safety systems [8].

Other communication protocols, such as LonWorks, on the other hand, prefer “networking integration” in which there is no central processing unit, just intelligent field cabinets. Each intelligent field cabinet is a “node” on the network and has equal status to the other nodes. Each cabinet controls local or zoned all energy management functions, all fire alarm functions and smoke control functions. It does not depend on any remote central processing unit or another intelligent field cabinet. The microprocessors in the field cabinet can support advanced diagnostics and manage all the local building functions. The nodes in the network can communicate with each other and can be approached and managed through a central station or by a personal computer. This type

of network further simplifies installation and maintenance, and increases the reliability of the system. Once a fire damage or a fault occurs, only the immediate area is affected, and the fire command station or any other man/machine interface location could maintain communication with any other field cabinet on the network loop by transmission of data in two directions. Response of this type of network to a fire threat is very fast, because there is no need for a CPU to scan and process whole building systems. The intelligent field cabinet recognizes the fire alarm within its own area and acts upon that event within the cabinet.

## **Conclusion**

New intelligent building technologies have strong potential to improve fire safety. Multi-function sensors (i.e., chemical gas sensors, integrated sensor systems and computer vision systems) and wireless sensors will not only reduce expenditure on sensors, but also reduce false alarms, speed response times and reduce fire-related losses. Real-time control via the Internet will extend the monitoring and control of building service systems and fire safety systems out of the building, which will increase the efficiency and reduce costs for building management operations, more efficiently discriminate between fire and non-fire threats, and increase the time available for property and life protection. The integration of fire detection and alarm systems with other building systems should also increase fire safety in the building.

However, the application of intelligent building technology may also create completely new risks. Sensor technologies will need to be robust enough to prevent false alarms, accurately discriminate between fire and non-fire threats, and ensure that vital information such as the location of occupants is not lost due to data overload during a fire. Internet based monitoring and control of building service systems will need to be completely secure to prevent false fire information being provided to building owners and fire brigades. Integrated building systems will need to be designed not only to give fire safety priority over other building activities but also that fire emergencies do not crash the building service system. A close examination of the concept of system integration will need to be conducted as intelligent building systems become more prevalent in order to

determine whether a full integrated building system has sufficient redundancy to provide adequate fire safety.

In addition to the need for further research in developing new fire safety systems and ensuring that intelligent building systems do not hinder fire safety, additional work is needed to overcome the problems that are common to all parts of the intelligent building industry. Fragmentation of the building and communication industries, a reluctance to change established practices, the complexity of intelligent building systems, and the lack of universal communication standards have all slowed intelligent building progress. Much effort is needed to remove these barriers.

## References

1. McClelland, S., "Intelligent Building," An IFS Executive Briefing, IFS Publication/Springer Verlag, Blenheim Online, England, 1985.
2. So, A. T. and Chan, W. L., "Intelligent Building Systems," Kluwer Academic Publishers, Norwell, USA, 1999
3. Lafontaine, J., "Intelligent Building Concept," Public Works and Government Services Canada, January, 1999
4. DEGW/Teknibank, "The Intelligent Building in Europe," DEGW/Teknibank, 1992
5. Harrison, A, Loe, E. and Read, J., "Intelligent Buildings in South East Asia," E & FN SPON, 1998
6. DEGW, Ove Arup & Partners and Northcroft, "Intelligent Buildings in Latin America," DEGW, Ove Arup & Partners and Northcroft, 1999
7. Read, J., "Today's Intelligent Buildings –What can they really offer," Conference Proceedings: Intelligent Buildings Realising the Benefits, Oct. 1998, Watford, UK
8. Chapman, R. E., "Benefits and Costs of Research: A Case Study of Cybernetic Building Systems," NIST report, NISTIR 6303, 1999
9. Ennals, B., "Integrated Systems – An Evolution in Building Control," Fire Safety, April, 1999



10. Sharples, S., Callaghan, V. and Clarke, G., "A Multi-Agent Architecture for Intelligent Building Sensing and Control," *Sensor Review*, Volume 19, No. 2, pp.135-140, 1999.
11. "Commercial Whole Building Road Map," Commercial Whole Buildings Workshop, San Francisco, California, USA, 1999.
12. Grosshangler, W. L., "An Assessment of Technologies for Advanced Fire Detection," *Heat and Mass Transfer in Fire and Combustion Systems*, HTD-vol. 223, pp. 1-10, ASME, December 1992
13. McAvoy, T. J., "Using Multivariate Statistical Methods to Detect Fires," *Fire Technology*, No.1, 1996
14. Byfield, M. P. and May, I. P., "Olfactory Sensor Array System: The Electronic Nose," *GEC J. of Research*, Vol. 13, No.1, 1996
15. Grosshangler, W. L., "1995 Workshop on Fire Detection Research," NISTIR 5700, June 1995
16. Tice, L., "Options within Intelligent Fire Detection Systems," *Fire Safety*, June 1999
17. So, A. T. P., Chan, W. L. and Chow, T. T., "A Computer Vision Based HVAC Control Systems," *ASHRAE Transactions*, Vol. 102, Pt. 1, p. 661, 1996.
18. So, A. T. P. and Chan, W. L., "A Computer Vision Based Power Plant Monitoring System," *Proc. IEE Int. Conf. Adv. In Power System Control, Operation and Management*, Hong Kong, November, 1991.
19. So, A. T. P. and Chan, W. L., "A Computer Vision Based Fuzzy Logic Aided Security and Fire Detection System," *Fire Technology*, Vol. 30, No. 3, 1994.
20. Lloyd, D., "Video Smoke Detection (VSD-8)," *Fire Safety*, p. 26, Jan. 2000.
21. Meacham, B. J., "International Developments in Fire Sensor Technology," *J. of Fire Protection Engineering*, 6 (2), 1994, pp 89-98.
22. Jacobson, E., "Finding Novel Fire Detection Technologies for the Offshore Industry," *Fire*, March 2000, p.26
23. Smith, S., "The Integration of Communications Networks in the Intelligent Building," *Automation in Construction*, Vol. 6, 1997
24. Deng, K., "Embedded-Internet," *Univeristy of Essex*, 1999

25. So, A. T. P., Chan W. L. and Tse W. L., "Building Automation on the Information Superhighway," ASHRAE Transactions, p176, 1998
26. Winter, J., "When Every Second Counts," Fire Safety Engineering, August 2000
27. Buckley, J. B., "High-Rise Office Building Fire Safety Systems - It Isn't Just the Integration of the EMCS with the Fire Alarm System -or Is It?," ASHRAE Transactions, p657, 1985
28. Dillon, M. E., "Some Reasons not to Integrate," ASHRAE Journal, April, 1985.
29. Ivanovich, M., "The Future of Intelligent Buildings Is Now," HPAC Heating/Piping/AirConditioning, May, 1999
30. Zivney, R. C., "Integration: Not a Matter of Debate," ASHRAE J., April, 1985
31. Bushby, S. T. "BACnet's<sup>TM</sup>: a Standard Communication Infrastructure for Intelligent Buildings," Automation in Construction 6, pp.529-540, 1997.

Walter W. Jones and Richard W. Bukowski

Building and Fire Research Laboratory

National Institute of Standards and Technology, Gaithersburg, MD 20899

## **Using High Reliability Detection for Fire Service Response in Buildings**

### **1 Introduction**

Reliable fire detection is an essential aspect of fire protection in all constructed facilities, first for the safe evacuation of occupants and second as a means to initiate manual suppression to for control and extinguishment of unwanted fires.

Firefighting in buildings is complicated by lack of information about the environment inside the building. Even residential buildings (one and two family dwellings) are equipped with detection and alarm devices, that provide early warning for occupant evacuation. As technology for device interconnection, such as embodied in the the IEEE 802.11b standard, becomes more wide spread, the capability for communication even within residences increases and reporting such signals over a residential network will provide increased reliability.

Most commercial and industrial buildings have fire detection systems that supply limited information from detectors in the building to fire alarm panels, generally located in a designated area of the of the building. The information available today, and likely to be available in the future in new buildings with advanced sensors, can be used to improve the fire service effectiveness and improve safety of the firefighting effort.



In order to enhance the safety and effectiveness of fire fighting operations in buildings containing modern fire alarm systems, we need to improve the type of information that is made available to the fire service, the means by which it is presented, the channels through which it is distributed. More timely information on the state of the fire and the building environment will lead to better tactical decisions by the fire service.

The range of uses for modern transducers covers building management and indoor air quality, as well as 1<sup>st</sup> responders. While building management information display will be available on high resolution monitors, 1<sup>st</sup> responders need a much wider range of devices from laptops for vehicles use to handheld devices such as "pagers." The delivery of information must scale across this wide range of input and output devices, obviously with the detail available on small footprint displays being much less than on the high resolution devices.

The National Fire Alarm Code (NFPA 72-1996) requires that,

*"The primary purpose of fire alarm system annunciation is to enable responding personnel to identify the location of a fire quickly and accurately and to indicate the status of emergency equipment or fire safety functions that might affect the safety of occupants in a fire situation."*

In light of this requirement it is surprising that many fire departments report they seldom use the features provided by alarm panels. The root cause appears to stem from inconsistent interfaces, displays and controls. This paper describes an improvement in the type of information that is made available from buildings, describes a means to achieve that end and proposes an interface protocol that meets the diverse range of the needs of the fire service.

## **2 Background**

As transducers become more commonplace in the built environment, it is desirable to utilize this information in a more complete way to assure safety. There are two facets to doing this, incorporating our knowledge of fires and other extreme events into the measuring and reporting capability, and insuring that all systems are functioning the way in which they were intended. The former is commonly referred to as smart sensing, while the latter deals with fault detection and redundancy. Combining the two is an information delivery infrastructure. These are the prime components of a system which will allow reliable real-time prediction of the environment in a building.

To accomplish this objective, it is important to have access to information about the building and its environment. The shortcoming in understanding what the information implies is transcended by providing sufficient computing and memory capacity to allow reasonable algorithms a chance to work in real time.

Taken together, we are trying to understand what transducers actually tell us about the environment in a building. In order to predict the environment, we must first understand the meaning of the data that is delivered. Then we can use the information in a system which is sufficiently faster than real time that the predicted information is useful. What is needed is an understanding of the measure that the sensor itself takes and effect that the surrounding environment has on the data. Essentially this means understanding entry characteristics of the sensing element, and the response of the transducers themselves, such as the thermal lag of

thermocouples, accumulation of dust on optics, and similar instrument functions.

Given the sensor information, the second part of the problem is being able to modify an environmental model "on the fly" to change the parameters being used as the initial conditions. CFAST has been able to do this since its inception (using the restart function) but the process 1) assumes a well defined consistent state, and 2) is not fast enough for this application. We have developed a method to start (in the real sense of *ab initio*) the model with (almost) arbitrary values. The results do not (and should not ) track exactly, but asymptotically converge as they should.

The third is information delivery. The majority of the effort is in developing consistent controls and icons which convey the critical information and allow meaningful response. It is generally accepted that suitable graphics convey a great deal more information than simple text messages<sup>1</sup>.

This information should be available whenever and where ever it is needed, and to whomever will benefit from the knowledge. The stakeholders range from the building owner, to the maintenance service contractor for the fire systems, to the firemen responding to emergencies. The means by which it is provided should provide for multiple transmission media, from low band wireless to broadband wired lines. In the former, alarm prioritizing must occur and in the latter, video can be provided. The amount of information delivered must be commensurate with the delivery capability.

### **3 Fire Service Needs**

The immediate focus of this project is information delivery for those who respond to emergencies. The fundamental questions that must be asked are



1) what information is needed, 2) when is the information needed, and 3) how can it best be presented to be most useful?

The first two are closely linked. Though the fire service information needs differ with time, most relate to the most effective allocation of resources. There are three distinct operation times, dispatch, arrival and deployment and incident management.

Initially, the most important item is to provide some metric for the likelihood that the alarm is genuine – particularly when it derives from a single device. Perhaps a three level metric of low, moderate and high confidence would be enough. The basis for assessing confidence is currently unclear but may involve heuristic algorithms based on sensors keeping history data and reacting to excursions from that history. There is significant concern among the fire service over liability for damage they cause by forced entry when an incident turns out to be false. They would also like information they could use to decide what resources are required. For small fires growing slowly a single unit may be enough. For a fast growing major incident, additional units dispatched early can be of great help in minimizing losses and assuring firefighter safety.

At arrival, the most important information is (1) the location and size of the fire within the building, (2) the location of occupants, (3) how to get to the fire, (4) a safe location to stage, location of standpipes, and other points of interest (hazardous materials, locked areas), and (5) how fast is the fire growing. In addition, there are specific bits of information that are needed to make good choices about resource deployment, including temperature, carbon dioxide and monoxide concentrations, and whether conditions are conducive to full room involvement. The initial decisions about tactics and

resource deployment for search and rescue, ventilation and suppression can have a significant impact on the effectiveness of the attack.

Finally, during the incident, information on (1) location and rate of spread of smoke/gas and of fire, (2) measures of operational effectiveness and safety of crews, and (3) potential benefits or dangers of ventilation.

These ideas extend to the less extreme environment found during normal conditions. Improved information gathering and processing could provide building owners and managers with more cost effective ways to maintain conditions which are acceptable for the occupants. The primary difference is the range of sensor input, and their concomitant calibration.

#### **4 What needs to be done**

In order to extract information from both current and the next generation of transducers, it is crucial to calibrate these sensor(s). There are two regimes of sensing: low level which is appropriate to ignition and early fire growth, and high level which occurs during the later phases of a fire, perhaps extending to full room involvement and complete (visual) obscuration.

NIST has developed the fire emulator and detector evaluation (FE/DE)<sup>2</sup> test chamber to calibrate sensors at extremely low signal levels. The FE/DE has been designed to evaluate fire detection technologies such as new sensors, multi-element detectors, and detectors that employ complex algorithms.

The FE/DE is useful for calibrating transducers at low levels. These are important in early detection. However, in order to provide information and tactical aids during an entire incident, the calibration of the sensors to more extreme conditions must be accomplished.

There is a cost/benefit tradeoff in asking for such extensions. For example, with current sensors, there is a limit to how well they can be expected to perform without hardening. While use of current technology for hardened sensors is more expensive, as the new technologies come online, this cost disadvantage will disappear. And as the expectation for reliability grows, there will be a greater demand for such transducers.

## **5 Why we need to do it**

From residential housing to complex office buildings, active technology is playing a greater and greater role in assuring the well being of their occupants. In the residential end, refrigerators which “know” about their contents as well as maintenance needs are the bases for using technology to improve the living conditions of the occupants. In the complex office building, eliminating “sick building” syndrome is a desirable end. All of these advances are fueled by monitoring and sensing of the environment and providing this information at the appropriate place in a timely manner.

In the specific case of firefighting, the availability of tactically significant information across a wide range of media facilitates the delivery of this information to the hands where it can be used to best advantage. For example, information on the current location and intensity of the fire delivered wireless to pagers or PDAs could prove lifesaving to truck companies doing ventilation on a roof, or search and rescue teams already inside a building. Detailed information on the fire monitored at dispatch could indicate the need for special units or additional resources before it becomes critical to the “on scene” commanders. Critical information could even be shared with Fire Wardens in high rise buildings undergoing partial phased evacuation.



## **6 How it can be done**

The best scheme is to examine the sensor input from a building in the normal (operating) state and look for deviations from this baseline. An anomaly at this level should trigger a closer examination. The closer examination would be to initiate a model of the environment using data from the transducers. In algorithmic terms, one would need an initial guess, followed by a prediction, followed by a comparison of the ongoing measurements with the output from the model.

Since we are interested in the full range of environmental conditions, sensing from very low levels is needed to extreme conditions is needed. While current sensor implementation, hardness and calibration, is suitable for the low level signals, decision aids for sustained fire fighting will require a much broader range of detection and robustness.

Generally, it is not feasible to run a predictive model continuously. Indeed, most of the time such computing power could better be used for other purposes. The requirement is to filter signals including a means to detect any deviations. This would provide a starting point for a prediction of the environment. Even at this point, long term predictions are not useful. However, the reliability of confirming trouble or alarm signals through modeling is of great use. Even if a building cannot be specified completely, a calibration of nominal and expected conditions can be done as an empirical technique, much as a ventilation system is balance prior to occupancy. Such calibration and spot checking of sensor systems can be done relatively cheaply in terms of computer resources.

A typical building with a modern alarm system and environmental monitoring will have in excess of 10 000 transducers. This argues for using relatively simplistic filtering techniques to extract significant deviation, and utilizing the readings from a dozen nearby sensors as initial conditions for a predictive model. We have demonstrated that such filtering can be done on a real-time basis with current microprocessor technology<sup>3</sup>. A decision to model the environment can be a relatively frequent occurrence, perhaps one per second per zone in an occupied building. An example of appropriate filtering would be the exceeding a nuisance alarm threshold for smoke detectors. At this point in time, an quick estimate of the heat release rate or carbon monoxide buildup could be extracted as an initial fire signature and posed as the initial conditions for estimating the time to a notable event.

The level of detail available is closely related to the resolution of the display devices. This also affects the possible interaction. At the "high" end of technology, one would expect high resolution screens. Pointing devices such as touch screens or trackballs would complement this technology. At the laptop ("in truck") level, the amount of information which can be conveyed becomes constrained. The need to accommodate a wide range of lighting conditions renders fine detail found in graphic display unsuitable. Similarly, the freedom to point is constrained by vibration, distractions and possibly inclement weather which necessitates gloves. Further reductions in information availability and interactivity occur at the personal level, exemplified by beepers and PDAs.

In all cases, touch screens or similar "point and click" devices are available; toggles and similar switches are not scalable. Scaling both paradigms argues for layers of information. At the highest level of resolution, one can show building graphics and video signals to confirm alarms. Pointing at

rooms would bring up additional information such as text showing temperature, geometry and other suitable data. At the laptop level, the channel bandwidth will nominally be lower and video confirmation is probably not feasible. At the level of a PDA, only a single text line will be available. The information on alarm size and location can be conveyed with such constraints, but details of the number of devices in alarm is beyond its capability. And interactivity with a stylus and total display size 1"x3" lends itself only to acknowledgment and requests for status information.

The browser paradigm, shown in figure (1), is an example of an implementation. It would include the basic panel information as elements. We would propose three layers, corresponding to three resolutions of devices: layer 1 for palm pilot, beeper, cell phones; layer 2 for basic panels and fire service interaction; and layer 3 for building management, dispatch and similar protected displays. In the example, layer 1 is represented by the "Elevation" information, layer 2 by the "Fire Service Controls," and layer 3 by the building schematic, "Plan view, 3rd Floor."

## **7 Display requirements**

In order to achieve the goal of "information anywhere, anytime," it is important that display of building conditions be possible across a wide range of technologies, and through a wide range of conduits.

At the "high" end, for example in a building management or security center, one would expect the luxury of high resolution displays with detailed drawings and schematics of building components. In these cases, fragility of the hardware, and ambient lighting conditions can be controlled. However, as one takes even this same display capability to remote locations, prioritizing of signals is necessary.



A similar push comes from lower resolution and ruggedized requirements, such as would be imposed on information centers which might be carried in command vehicles or even on-scene. In these cases, ruggedness must be considered, as must the lack of control of ambient lighting.

In the extreme case of portable systems, i.e., Palm Pilots, beepers and hand-held browsers, it will only be possible to convey a very limited amount of information. Not only must the most important information be display first, there will be only limited capability of interaction so in general the information shown must be relevant to immediate needs, i.e., announcement, location and so on.

One might envision four levels of display to be in 1) a building management office, 2) a command vehicle, 3) a small building annunciator panel, and 4) a personal information manager. In each case, it is crucial to provide information about the location and size of the *fire*. As the display capability improves, additional layers of information can be accommodated. In the realm of simple annunciator panels, the capability to access other systems, such as the status of the elevators, would be possible. At the highest end, devices such as CCTV would be available.

One of the basic concepts deals with the actual display of information. Graphical displays are recognized as being a compact and efficient way to transfer information from electronic signals to humans. It would seem to be natural to use a set of icons to represent the information that can be delivered which will be generally meaningful. Although we are not intending for this to be "intuitive," the closer the symbols are to commonly accepted notions of signals that are of interest the more reliable the information transfer to the user.

An initial set of icons was developed for this purpose from icons used for similar purposes in Japan and from standard symbols for engineering drawings from NFPA170. An example of a set of icons is shown in figure (2). The set and style chosen were dictated by scalability and the desire to allow information to be displayed in monochrome.

## **8 Modeling the building in a hostile environment**

Over the past decade we have developed a model of fire growth and smoke spread (CFAST<sup>4</sup>) which has seen a wide variety of uses. This model is used by specifying the geometry of the building, characteristics of the fire and the venting available for combustion. It is based on solving a set of equations that predict state variables (pressure, temperature and so on) based on the enthalpy and mass flux over small increments of time. These equations are derived from the conservation equations for energy mass, and momentum, and the ideal gas law. The perspective has been understanding the environment for a specified building. In this context the overall computation time is paramount.

If we can presume sufficient information to make a prediction with sufficiently small error bounds, an example of an approach that might be taken would be the following: use transducer data to start a simulation of a building; predict the environment for the next 10 seconds (30 seconds, ...); gather the actual conditions for this period of time, then compare the curves. If these curves are close and the imputed heat release rate is indicative of a fire, then an alarm is sounded. There are several other possibilities. One is that the prediction and measurements do not agree. This would indicate that some assumption in the building model is incorrect, or that a transducer is giving an incorrect reading. Another is that

the cause of the discrepancy is from some cause other than a fire. Either scenario would trigger an alarm. Another is, of course, that prediction and measurement are in agreement and no untoward event is happening. The latter is, hopefully, the case the majority of the time. An implied acceptance criterion is that there be no false positives (false alarms) or false negatives (missed fires). Actually, any extreme event is a candidate for an alarm, and some thought will need to be given to the various conditions that warrant intervention.

In order to implement such a paradigm, there are three areas in which we need to make improvements: a real-time environmental response model of fire growth and smoke transport, we must be able to make a very quick assessment of how good a comparison there is between a prediction such a model makes, and the actual data which are subsequently measured and we need a way to interpret sensor signals to know what the environment being detected is. There are several component to such an endeavor. The natural evolution, at least for a first try, is to improve upon our current framework of models, verification and sensor modeling.

We started with the framework provided by CFAST and have modified it to read a sensor suite as might be delivered from an alarm panel, and compare this curve with an actual data set. Figure (3) shows an example of modifying a pair of time-velocity curves to bring them into the "best" agreement, which would then provide the basis for a restart at the "correct" time. This is only a first step, and provides a match based only on making the curves agree in shape and minimum difference between the curves. In this example, the fire in the prediction was started too soon, that is the fire was thought to have started earlier than the measurement data indicates. The procedure was done for a single sensor, using 120 data points in time. The time for this computation was 0.8 seconds. In order to make this



practical, we need to be able to apply the technique to ~5000 transducers using ~20 data points (in time), and the total computation time must be under one second. So the matching algorithm must be improved and the time to do the comparison must be reduced.

A related issue is the ability to say how close two curves are, that is whether a value extrapolated from a model of the process agrees with the actual progression of events. In the alarm industry, this is manifested in the Underwriters' Laboratory Test Standards for smoke detector suitability, UL 268. The assumption is that if the time series sensed by smoke detectors were found in habited compartments, this would indicate that there is a high likelihood that dangerous conditions would exist, absent corrective action. This is an implicit statement of reliability, indicating a high level of confidence that this series of fires is indicative of conditions which will become extreme.

The paper by Forney<sup>5</sup> has examined the mathematical robustness of fire models using the CFAST model as an example. While the ability to compare a fire model with experimental data is the thesis of the paper, the issues are the same for comparing real time measurements from multiple sensors, and making an assessment of parameter extraction. Key to both sensitivity analysis and fire model comparisons is the ability to quantify the difference between two time series<sup>6</sup>.

Functional analysis is a generalization of linear algebra, analysis, and geometry. It is a field of study that arose around 1900 from the work of Hilbert and others. Functional analysis is becoming of increasing importance in a number of fields including theoretical physics, economics, and engineering to answer questions on differential equations, numerical methods, approximation theory, and applied mathematical techniques.

Functional analysis allows problems to be described in vector notation and defines appropriate operations on these vectors to allow quantitative analysis of the properties of the underlying physical system.

Figure (4) shows another simple example of fictitious experimental data compared with three model predictions. Model 1 is simply the experimental data multiplied by 0.9. Model 2 has the same peak value as model 1, but with the peak shifted -25 s. Model 3 has the same peak as Model 1 and Model 2, but with a 20 s plateau centered around the peak of the experimental data. Weighted area comparisons would show that these three models are essential identical. Clearly this comparison fails to capture the differences. If such an algorithm were used, there would not be a high degree of confidence that an alarm would be justified.

These examples are based on single point measurements and predictions. The mathematics can be extended to multiple sensors, multiple compartments and more than one sensible variable (temperature as well as smoke, for example). Then the data fusion implied by the national fire alarm code, chapter 2, section 3.4.5.1.1 would be rigorously defined. The implication is that more detectors mean higher reliability of the ability to detect and report fires. While the emphasis in existing codes and standards are for single compartments, the ideas can be extended to different types of transducers, placed in non-contiguous compartments and systems.

## **9 Emerging technologies**

Current technology for sensors covers quite a wide range of measurement capability. The commonly used measures are sensors for carbon monoxide sensors, temperature (thermocouple) or thermister, opacity (photo

detectors), smoke particle counters (ionization current), beam (laser), carbon dioxide sensors, oxygen concentration, and water vapor (moisture).

These are the types of measurements needed to understand the environment from normal operating conditions to the extreme environments found in hazardous situations. Much of the future development of sensors for additional gases will be in the arena called "electronic noses." These are sensors which detect small amounts of polymeric substances. The particular focus today is on detecting bombs and the vapors from organic materials (foods), but the principle should apply to any odor or volatile hydrocarbon.

## **10 Recent Results**

There are three separate thrusts: display of information, preprocessing to provide more understanding of the sensors data, and tactical tools. For the first, a proposal has been submitted to NFPA as a new appendix for the Fire Alarm Code. This will incorporate the display paradigm discussed earlier. We have demonstrated a prototype with new icon based display and reported on an assessment of techniques and technologies to the International Association of Fire Chiefs. The proposal is for the 2002 Edition of NFPA 72. To implement the second part, we have developed a consortium with NEMA and the major fire alarm companies to acquire in-situ data from current buildings. The third will depend on the experience of use of these systems in actual responses to emergencies.

## **11 Conclusion**

We are using our knowledge and practical experience in developing predictive models of fire growth and smoke transport to develop the capability for making real time predictions in buildings using existing



transducers. There are three research threads involved: developing a computer model which can make predictions in real time; understanding the instrument function in order to use data from building transducers; and finding a metric for the "goodness of fit" between two time varying curves. These avenues are being explored and there is progress in all three areas. This should allow for a prototype of such a tool in the near future. At present we are pursuing these concepts using tools we have developed, but if they are not suitable, or sufficiently robust, then we will develop ones that are.

This will provide a higher level of information to the building industry for monitoring the environment in buildings. The endpoint is to provide appropriate information whenever and where-ever it is needed. This includes early warning of system malfunctions, hazardous environments, in-situ monitoring and prediction for building managers as well as real-time assessment of fire fighter conditions.

The immediate application is to provide environment measurement and prediction for "first responders," those who have to know very quickly where a fire is and how large it has become and what is likely to occur in the near future. A possible future development would be to use data reported from PASS devices to indicate to scene commanders when a fire fighter is likely to be in conditions in which it is not possible to operate safely, even with appropriate gear.

## 12 References

---

- [1] Shneiderman, B., *Designing the User Interface, Strategies for Effective Human-Computer Interaction*, Addison-Wesley Publishing Company, 1987.
  
- [2] Cleary, T. G.; Grosshandler, W. L.; Chernovsky, A., Smoke Detector Response to Nuisance Alarms, International Conference on Automatic Fire Detection '99", 11th. Proceedings. University of Duisburg.
  
- [3] Using Sensor Data to Predict the Environment in a Building, WW. Jones, RD Peacock, GP Forney and PA Reneke, FPRF Suppression and Detection Application Symposium, Orlando (1998).
  
- [4] A Technical Reference for CFAST: Engineering Tools for Estimating Fire Growth and Smoke Transport, Walter W. Jones, Richard. D. Peacock, Glenn P. Forney, and Paul A. Reneke, NIST Technical Note 1431 (2000).
  
- [5] Forney, G. P., and Moss, W. F., " Analyzing and Exploiting Numerical Characteristics of Zone Fire Models," *Fire Science and Technology*, 14, No. 1/2, 4960, 1994.
  
- [6] Peacock, RD, Reneke, P A, Davis, W D, Jones, WW, Quantifying Fire Model Evaluation Using Functional Analysis, *Fire Safety Journal*, 33, 167 (1999).

## **AN OPEN DISTRIBUTED FIRE DETECTION SYSTEM**

**Abstract:** This paper introduces an open distributed fire detection system. This system consists of three layers: base layer, middle layer and upper layer. The base layer connecting the detectors to control unit uses a special digitized bus. In order to have reliable and effective data transport, the digital bus protocol should make requirements to the physical layer, the link layer, the network layer and the transport layer. The middle layer which links the control units to one another adopts LONWORKS as its internal bus, implementing real distributed control between the control units. The upper layer, providing the interfaces between the fire detection system and other control systems, adopts standard network variables conformed to LONMARK protocol completely. The characteristic of the open system makes the integration between the fire alarm system and other control systems come true.

### **1 Epigraph**

The devices of fire alarm system can be divided into three types according to topological structure. The first one concerns the field devices including various fire detectors, manual call points, special indicators and execution units of fire fighting system. The second one is usually composed of the control units, which are connected with the field devices, providing the interface of man-machine conversation for monitoring and testing. The third one is the center of the whole system, monitoring the alarms, sending off control signals, providing interfaces to security systems, building automation systems and city fire alarm network systems.

With the developing of microelectronics and network communication technology, the fire alarm system demands more adoption of these technologies.



Many new methods are adopted in fire detection in consequence of the progressing of sensor technology. The fire detectors become more stable because of multi fire detection technology. More information can be transmitted through the internal network with high speed.

Because of the advanced network technology, the large-scale and super large-scale fire alarm systems have been widely used. In order to insure the stability of the systems, the control units must have the characteristic of independence in case of failure of the internal network.

Now integration is a tendency of the control systems within buildings. So a fire alarm system needs the open characteristic to fit the demand.

## **2 Introduction**

The fire alarm system introduced by this paper is a kind of new and distributed monitoring system developed by GST. The system is a typical one composed of three layers. The first layer is the base layer using special digitized bus protocol and being connected to the control unit and field devices. The network topological structure can be ring type, 'T' type, or mixed type of both. The second layer is the control layer conforming to LON bus protocol and being connected to various units of the system, such as display unit, control unit, communication unit and printer unit etc. The third layer is the interconnection layer satisfied by the requirement of LonTalk protocol, accomplishing the integration with other control systems.

## **3 Network Formation**

### **3.1 Special Digitized Bus**

The special digitized bus uses the self-defining bus protocol to suit the data transporting between control unit and field devices. In order to have reliable and effective data transport, the digital bus protocol should make requirements to the physical layer, the

link layer, the network layer and the transport layer, which can be introduced respectively as follows:

- I. The physical layer: An ordinary twisted pair or an optical fiber link is used for the electric connection. If a twisted pair is used, a direct connection is all right. If an optical fiber is used, a fiber-optic transceiver is needed. The fiber-optic transceiver is specially designed for data conversion purpose.
- II. The link layer: The balance code is used with CRC calibration and sum calibration. The signal bus supplies power to detectors when it transports signals. The transmission rate is 16 kbps. Fig 3-1 shows the basic structure of the balance coding. The coding is symmetrical and self-calibrating. It has no special requirement to the wave-shaped edge and has the features of high resistance to disturbance, long transporting time and high reliability.

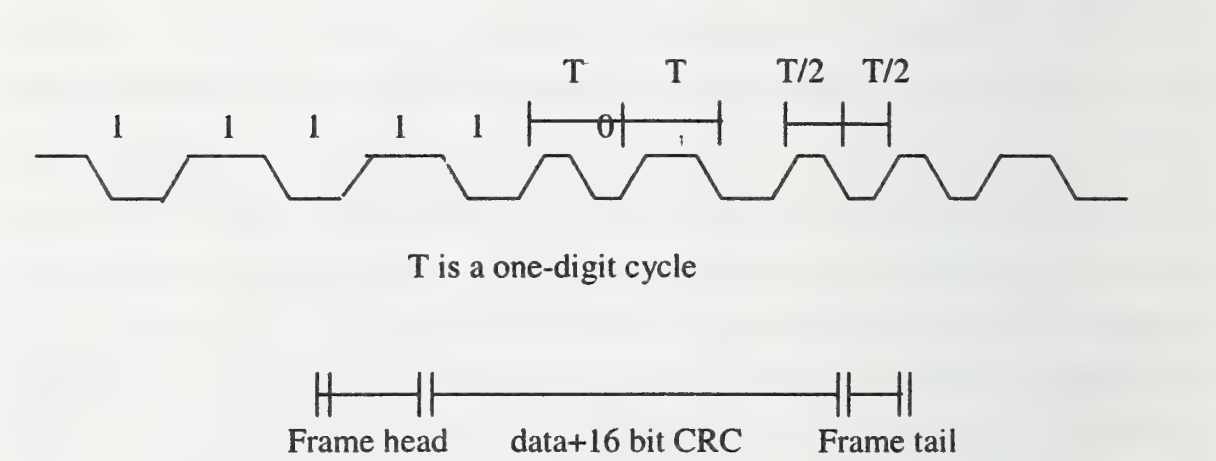


Fig3-1 Coding structure of special digital bus

- III. The network layer: An independent addressing is used and the node coding is not restricted by the protocol.
- IV. The transport layer: It provides acknowledged messages, and the calibration can be CRC calibration or sum calibration according to the degree of data importance and the spectrum of transport so that the communication is more reliable and effective.

The network between control units and detectors is a kind of master-slave, low speed, ring-type network. It has a characteristic of collision detection. Using twisted pair to transit signals and power, each control unit can be connected with 128 field devices. The network uses a kind of special digitized protocol, which includes network management, field device static signal transmission, and fire data pre-treatment.

Network management protocol regulates the manner of automatic distribution about logical addresses of the field devices. Each field device has only one number. During the period of network installation, the number is the only identifier of a detector by means of which the system can do double addresses tests and the logical addresses re-distribution.

Field devices static signal transmission protocol regulates the static signals exchange mode between control units and detectors. The static signals include production date, batch number, history and fire sensitivity etc.

Fire data pre-treatment protocol regulates the dynamic data exchange mode between control units and detectors. The protocol of the data transmission mode is based on interrupt, insuring that the signals can be transmitted rapidly and efficiently when needed. The data can be fire alarm signals or field signals pretreated by detectors.

ASIC with the firmware of special digitized bus protocol will be used in field devices. The matched circuits are also used in control unit. The data exchange is accomplished by coordination of the firmware. The custom design insures the stability and speed of the data transfer.

The protocol conforms to the requirement of the network in this layer and is also applicable for various security systems.



### **3.2 Control Unit Management Network**

Fire alarm systems are usually composed of several kinds of units, such as central management unit, field devices control unit, repeater control unit, remote communication control unit, and remote printer unit etc. Various units have separate functions. More than one identical unit might be in the same fire alarm system. The network interconnects the units to accomplish a complete task.

The internal network of the system is LonWorks, a kind of field bus network based on LonTalk protocol promoted by ECHELON USA in 1993. LonTalk protocol follows ISO OSI reference model for network protocol and operates as national standard of ANSI/EIA709.1. The protocol has been integrated in the Neuron Chip named Neuron 3120, 3150 Chip. The nodes using Neuron Chip for controlling can communicate with the other nodes on the same network via the network variables. For the integrality of the network protocol, the internal network communication is simplified.

The structure of the fire alarm system is very flexible. The topological structure of the network can be changed according to the structure of protected area. The network structure can be compacted mode, distributed mode, or mixed mode of both.

The control units in the system can be connected directly with twisted pair when the compacted mode is adopted, and the transmission rate is 78kbps. Network communication can be realized using various transceivers through various media, such as twisted pair, power line, optical fiber, when the distributed mode is adopted. A router is necessary in order to connect the compacted part with the distributed part when the mixed mode is adopted.

Many management units might be in the same network when the distributed mode is adopted. The functions of the management units can be set by software. Users can get custom designs for their fire alarm systems.

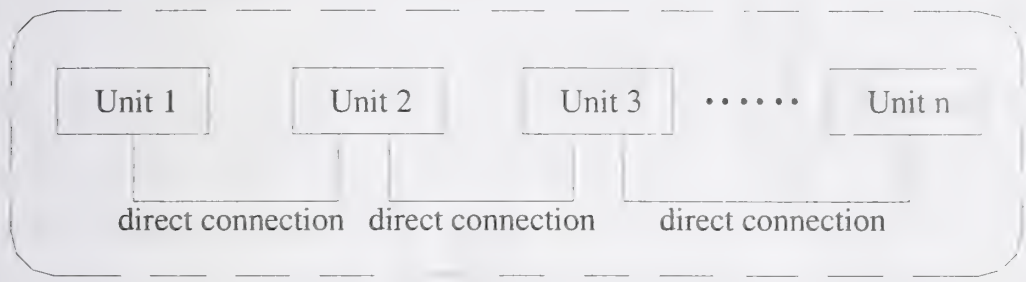


Fig3-2(a) The second layer network topological structure-the compacted mode

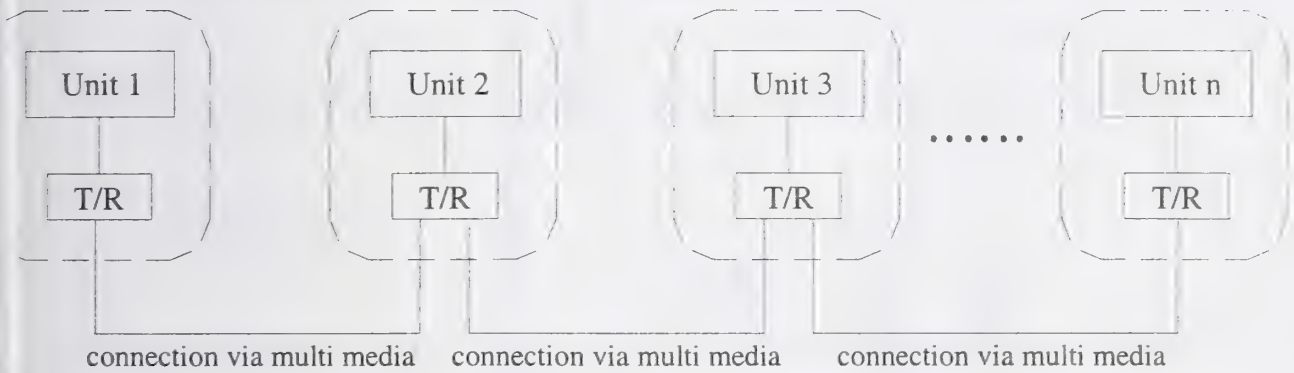


Fig3-2(b) The second layer network topological structure-the distributed mode

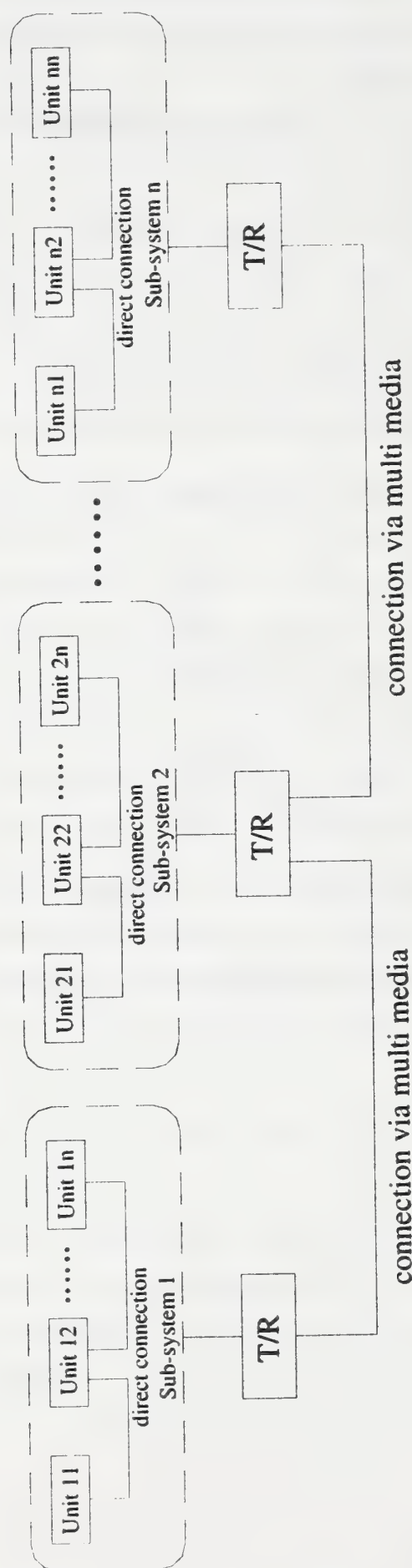


Fig3-2(c) The second layer network topological structure-the mixed mode



### **3.3 Open Data Interface**

The diversity and open characteristic of LonWorks makes this system be widely used in the area of building automation and industry control.

The signals of the fire alarm system can be divided into private type and shared type. The shared type signals are presented by network variables meeting LONMARK standard. The standard network variables are approved and managed by LONMARK organization specially. Because LONMARK standard is an open standard, the systems approved by LONMARK organization can communicate with each other directly.

The interfaces have been designed for various media, such as twisted pair, optical fiber to fulfill the needs of users. The fire alarm system can directly connect to the other control systems meeting LONMARK standard via these interfaces.

## **4 Application Sample**

We have designed an application system for Guangzhou subway using this fire alarm system. The subway system has 20 stations, 2 transformer stations, 1 vehicle center, and 1 control center.

The network system consists of two LonWorks ring-type networks, one is a twisted pair ring type network connected with the main control computer, standby control computer and a fire alarm control unit. The other is a fiber-optic ring type network connected with fire alarm control units of the stations. These two parts are connected with a router.

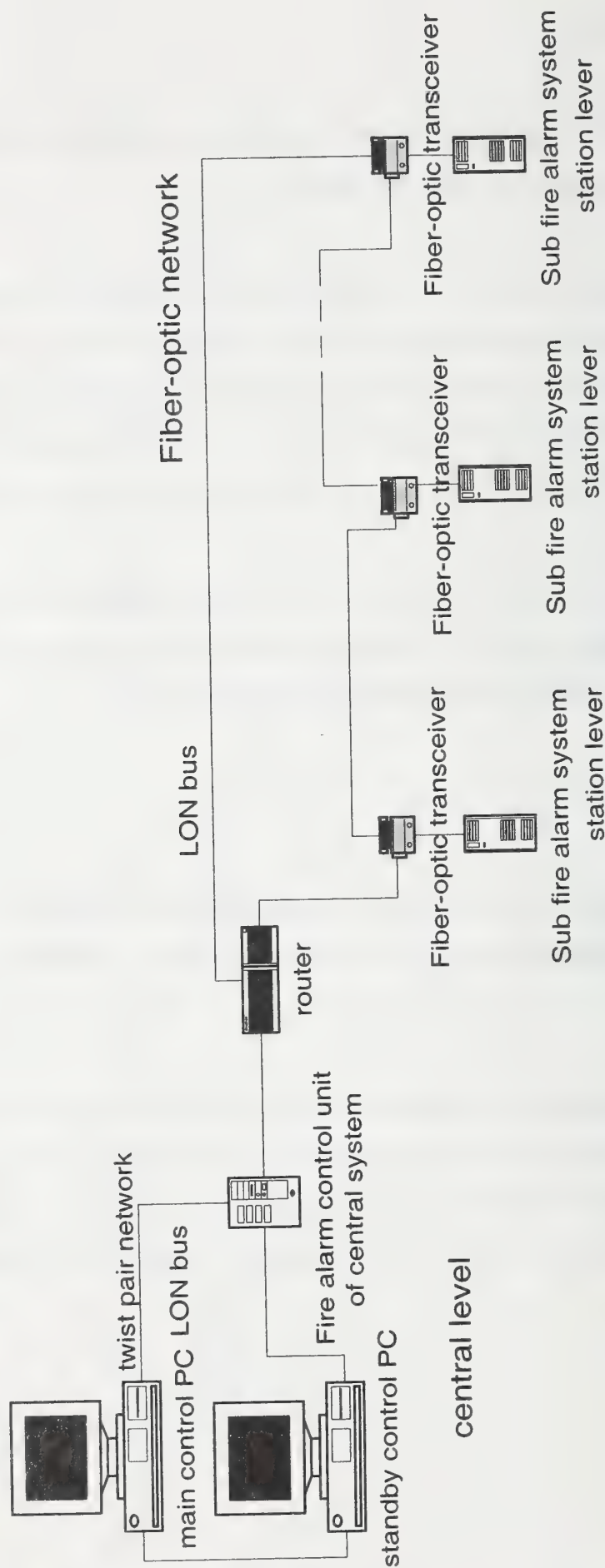


Fig4-1 Chart of the fire alarm system

The system is a distributed network system. The control unit of the station is a compacted mode fire alarm system. Each control unit is composed of a central management unit, field devices control unit and a repeater control unit. The control units are interconnected by the fiber-optic transceiver. Each node of the system can communicate with other nodes by peer to peer mode. The control center can get all the information within the network and save it to the system database and sends commands to the control units. The fire alarm control unit can work in network mode, performing the orders of the control center, and it also can work independently when the network failed. With the authorization the control units can also upgrade to a control center of part of the network or the whole network when needed.

## **5 Review**

This paper introduces a new kind of fire alarm control system. The flexibility of the system makes it suitable for all kinds of fire alarm systems, especially the large distributed fire alarm control systems.

## **6 References**

- [1] Yuhong YANG, "LON network control technology and application," XiAn University of Electronics Technology press.
- [2] Kuanming WU, "CAN bus theory and application system design," Beijing University of aeronautics & astronautics press.
- [3] Echelon Corporation, "Neuron Chip Data Book," Echelon Corporation press.
- [4] LONMARK Interoperability Association, "LONMARK Layer 1-6 Interoperability Guidelines," LONMARK Interoperability Association press.
- [5] LONMARK Interoperability Association, "LONMARK Application Layer Interoperability Guidelines," LONMARK Interoperability Association press.



CHEN Tao, WU Longbiao, FAN Weicheng, SONG Weiguo

(State Key Laboratory of Fire Science, University of Science and Technology of China, Hefei 230026, P.R.China)

## **ANALYSIS ON DATA STREAM MODEL OF NETWORK IMAGE FIRE DETECTION SYSTEM**

### **ABSTRACT**

Along with the scale of IFD (Image Fire Detection) system continuously enlarging in the field of fire detection, the capturing, transfer, and processing of a large quantity of image information inevitably result in the longer response time for fire, which contradicts the early alarm requirement of fire detection. In this paper, mathematics model of data acquisition and data processing of IFD system is constructed with the guidance of queuing theory. After the calculation and analysis of the result of emulating program, appropriate scale of IFD system is determined under certain speed of data processing and transferring.

**Key words:** Image fire detection, Queuing theory, Model analysis, Emulator

### **INTRODUCTION**

Typical development procedure of compartment fire characterized by the average gas temperature can be described in four stages, growth period, flashover, fully developed fire, decay period [1]. Flashover is disastrous and has been an increasing problem because of the use of new material in buildings [2]. So the alarm of fire must be sent out in the early stage of fire, or in the early growth period. Grosshandler outlined advances in sensor technology along with intelligence that could be implemented to improve detection time while limiting the frequency of unnecessary alarms [3] so that there is enough time for people to escape or for fire-extinguishing system to put out of the fire.

Make use of the temperature measurement methods based on primary colors [4] and the technology of infrared imaging and digital image processing, the IFD system is a vigorous developing intellectualized system that includes the technology of fire

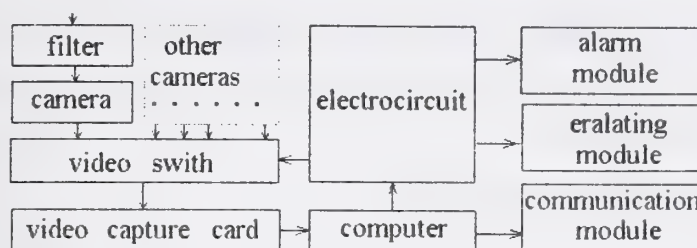


Figure 1. Hardware of IFD system

detection, recognition, alarm and control. Figure 1 gives hardware used in IFD system.

The infrared images from CCD are transferred into the central processing unit (CPU) through video cable and video card [6]. The CPU extracts the characteristic figure of the early fire flame which is distinguished from the environment, and judges whether the fire has taken place by computing the criterion of fire, then sends the command codes through I/O card to control the alert function of IFD system. If the CPU is assimilated to the brain of human, then CCD just acts as eyes.

In recent years, along with the fast development of Chinese economy, large buildings with complicated circumstance such as large spaces appear continuously, bringing forward higher demand to the field of fire detection. Traditional fire detectors such as smoke detector, temperature detector can't be competent for the large and complicated circumstance. For its high sensitivity, high reliability and high applicability, IFD system is quickly accepted by society. Now IFD system becomes one of the development trends of fire detection and control, and has broad application prospect..

However, modern buildings tend to larger-scale, which results in the increasing of fire detection area. So the number of sub-area of fire protection becomes more and more. To meet with this requirement, the scale of IFD system must be enlarged through increasing of CCD number. Consequently, in a certain interval, the number of infrared images transferred to CPU for processing increases greatly. The speed of image processing relies on frequency of CPU and time complexity of image processing algorithm. Therefore, the increase of image number conduces to overtime of image

processing, which will affect the early alarm of fire detection. so as to limit the scale of IFD system.. Given the speed of image capturing, data transferring and data processing, the mathematics model is be constructed with the guidance of queuing theory in this paper. Appropriate scale of IFD system is then gained through analyzing of model.

## BASIC QUEUING THEORY

### 2.1 Model and key points of queuing system [7]

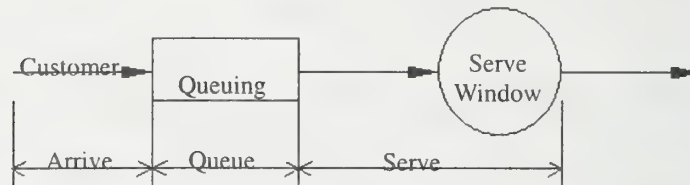


Figure 2. Simple model of queuing system

Figure 2 gives the simple model of queuing system □ Key points of queuing system:

1.  $\lambda$  □ Average arrival rate of customer (average arrival number per second);

The arrival interval between two contiguous customers  $t_i$  is a random variable, and the statistical mean of  $t_i$  is called average arrival interval, expressed as  $\bar{t} = E(t_i)$ . The average arrival rate is given by

$$\lambda = \frac{1}{\bar{t}} \quad \square 2 \square$$

2.  $\mu$  □ Service rate of system, which is a parameter to express the number of customer served by system every second. Define

$$\mu = \frac{1}{\bar{\tau}} \quad \square 3 \square$$

here  $\bar{\tau}$  is called average service time. It is the statistical mean of service time per custom,  $\tau_i$ . And  $w_i$  is the queuing time of every customer.

3.  $m$  □ It is named number of window or server, showing the number of system resource.

It is called single window queuing system when  $m=1$ , and called multi-window queuing system when  $m>1$ .

### 2.2 Service and queuing principle

1. Service principle:



The service principle is classified as FCFS (First Come, First Served), LCFS (Last Come, First Served), SIRO (Stochastic Served) and PRI (Priority)

## 2. Queuing principle:

It is defined as waiting mode and cut-off mode. Waiting mode means arrival will queue in turn until being served, while cut-off mode means arrival will be refused to serve if necessary.

### 2.3 Primary parameter of queuing system

#### 1. Queue length $k$

It points out the number of customers who are held up in system at a certain time, which includes the one who is being served. The average queue length is given by  $\bar{i} = E(t_i)$ .

#### 2. Queuing time $w$

It means the time length from arrival to beginning to be served, with average queuing time marked as  $\bar{w}$ .

#### 3. Service time $\tau$

It is the time while a customer is being served, and  $\bar{\tau}$  is called average service time.

#### 4. Standing time $T$

The whole interval, from the time when customer arrives to the time when he leaves the system, is known as standing time. And it is given by  $\bar{T} = \bar{w} + \bar{\tau}$ .

#### 5. Little formula

For a queuing system with average arrival rate of customer  $\lambda$ , the equation

$$\bar{k} = \lambda \cdot \bar{T} \quad \square 4 \square$$

presented in the meaning of average, and it is called Little formula.

#### 6. System efficiency

For multi-window queuing system with  $m$  windows, the acquisition probability is  $r/m$  when  $r$  windows are engrossed. The system efficiency can be expressed as

$$\eta = E(r/m) \quad \square 5 \square$$

#### 7. Stability

The expression  $\rho = \lambda / \mu$   $\square 6 \square$  is

entitled system strength. For waiting mode system, the system is stable when  $\rho < m$ , and it is unstable when  $\rho \geq m$ .

### 8. Sign for queuing system: $A/B/m (N, n)$

where  $A$  signifies arrival principle of customer,  $B$  signifies service principle,  $m$  is the number of windows,  $N$  indicates the number of potential customer (It can be omitted when  $N \rightarrow \infty$ ) and  $n$  means queue length of cut-off system (It indicates waiting mode when  $n \rightarrow \infty$ , and here  $n$  can be omitted).

## MATHEMATICS MODEL

### 3.1 Two common characteristic distribution

#### 1. Poisson distribution

Poisson distribution can describe the probability that there are  $k$  customers arriving in  $t$  seconds, which is expressed as

$$P_k(t) = \frac{(\lambda t)^k}{k!} e^{-\lambda t}, \quad k = 0, 1, 2, \dots \quad (t > 0) \quad \square 7 \square$$

And this distribution must satisfy three characteristics mentioned as follows:

- Stationarity: The probability  $P_k(t)$  only depends on the time interval  $t$ , while it is independent on start point of this time interval.
- No hereditary characteristic: The number of customers who appear in the two mutually disjoint interval  $(t_1 \square t_2)$  is mutually independent.
- Sparse characteristic: The maximum number of customer should be 1 in an infinitesimal interval  $\Delta t$ .

#### 2. Negative exponential distribution

When the arrival of customer satisfies Poisson distribution, it can be proved that the arrival interval between two contiguous customers  $t$  submits negative exponential distribution. The procedure is described as following.

Prove: The probability that there is no arrival ( $k=0$ ) in time interval  $t$  can get from equation (7)

$$P_0(t) = e^{-\lambda t}$$

The probability that there is arrival in  $t$  is given by

$$P(t) = 1 - P_0(t) = 1 - e^{-\lambda t}$$

The density function probability of  $t$  is negative exponential distribution

$$f(t) = \frac{dP(t)}{dt} = \lambda e^{-\lambda t} \quad \square 8 \square$$

The same result can be got from the analysis of service procedure.

### 3.2 Construction of mathematics model

In IFD system, the frame number of image that transfers from CCD to central processing unit is affected by distance of data transfer, delay of video switchover and other delay caused by hardware. So, the frame number of image isn't a simple direct ratio of time. Instead, it has a certain characteristic distribution. On the other hand, the time for image data processing varies along with the change of circumstance. For example, the quantity of characteristic information drawn from image varies as the background light intensity changes, and the area of the fire can't always be the same. Thereby, the time for digital image processing based on certain time complexity of algorithm is fluctuant. In another word, the frame number of image data which is processed in a given interval submits a certain distribution character.

According to the queuing theory, the frames of image can be considered as customers while the recourse such as video card and CPU can be regarded as window. Studying the distribution characteristic of arrival frame number of image and that of processing procedure in a given interval, it can be concluded that the two distributions are provided with the three characteristics of Poisson distribution. Therefore, the negative exponential distribution can be expressed as the model of arrival interval of image frame and the processing interval.

#### 3.2.1 Mathematics model about arrival of image frame

The time of fire growth period can defined by

$$t_{in} = \frac{1}{4\sqrt{2b(1-\varepsilon_K)}} \left[ \ln \frac{1+b^4\theta_i^4}{(1+b^2\theta_i^2+\sqrt{2b}\theta_i)^2} + 2\pi - 2 \tan^{-1} \frac{\sqrt{2b}\theta_i}{1-b^2\theta_i^2} \right]$$

where  $\varepsilon_K$  is a dimensionless characteristic of the radiation heat flux from the zone to the upper fire bed,  $\theta_i$  is dimensionless temperature, and  $b$  is given by

$$b = [\varepsilon_K / (1 - \varepsilon_K)]^{1/4}$$

It is easy to conclude that  $\varepsilon_K$  is different as for different circumstance and fuel, which result in different growth period of fire. The destination goal of fire detection and



alarm is to reduce loss as can as possible, then if fire occurs, enough time should be provided for human to escape and for fire-extinguishing system to work. So fire detection and alarm should give alarm as early as possible.

In IFD system, the image data acquisition is finished by circulation detection. To satisfy the require of early fire detection, all CCD in the system should be circulation detected in a relative short time. In the same time, a single CCD should capture several continuous frames of image to implement the image comparison, which will extract the dynamic characteristic to detect the fire.

Suppose that there are  $n$  CCD cameras for detecting in one system, every circulation detection time is 1 minute, and every CCD camera will continuously shoot 6 frames image, then, the average arrival interval between two contiguous frames image is given by

$$\bar{t}_A = 60/6n = 10/n(s)$$

It can be concluded from formula (2) that the arrival interval between two contiguous frames of image submits the negative exponential distribution

$$f(t_A) = \lambda_A e^{-\lambda_A t_A} = \frac{n}{10} e^{-\frac{n}{10} t_A} \quad \square 9 \square$$

where  $\lambda_A = 1/\bar{t}_A = n/10$  means average arrival rate of image.

### 3.2.2 Mathematics model about processing procedure

In my IFD system, the basic frequency of CPU is 300MHz, and high-velocity colorized video card DH-VRT-CG200 is used. Based on PCI bus, video card can control the speed of image data transferring without the help of CPU, and the highest picking rate is 40MB/s. The image resolution ratio picked by video card is 640×480×24bit in NTSC standard[9], so the date size of one frame of image is  $q_0 = 0.88MB$ .

The digital image processing time of CPU should consider the factors such as the speed of data transferring of video card, CPU clock period and time complexity of digital image processing algorithm. All the factors mentioned here will be regarded as

parts of service procedure, in which digital image processing algorithm mainly includes write-read process of memory, extracting the infrared image characteristic of early fire. The extracting procedure are made up by threshold comparison, flame area calculating and comparing and series of fire pattern recognition such as development of flames' edge, orderliness of flames' twinkle, that of flames' layers and that of flames' movement [5]. It is quite complex to determine the processing time for every frame of image from the analysis of time complexity of algorithm. Therefore, in this paper, it is provided by the mean of computer processing time from the results of multiple tests, which is about 0.347s. Then the average service time of service model is given by

$$\bar{\tau}_s = \frac{q_0}{40} + 0.347 = \frac{0.88}{40} + 0.347 = 0.369s$$

It can be concluded from formula (3) that the service interval time for one frame of image submits the negative exponential distribution

$$f(\tau_s) = \lambda_s e^{-\lambda_s \tau_s} = 2.710 e^{-2.710 \tau_s} \quad \square 10 \square$$

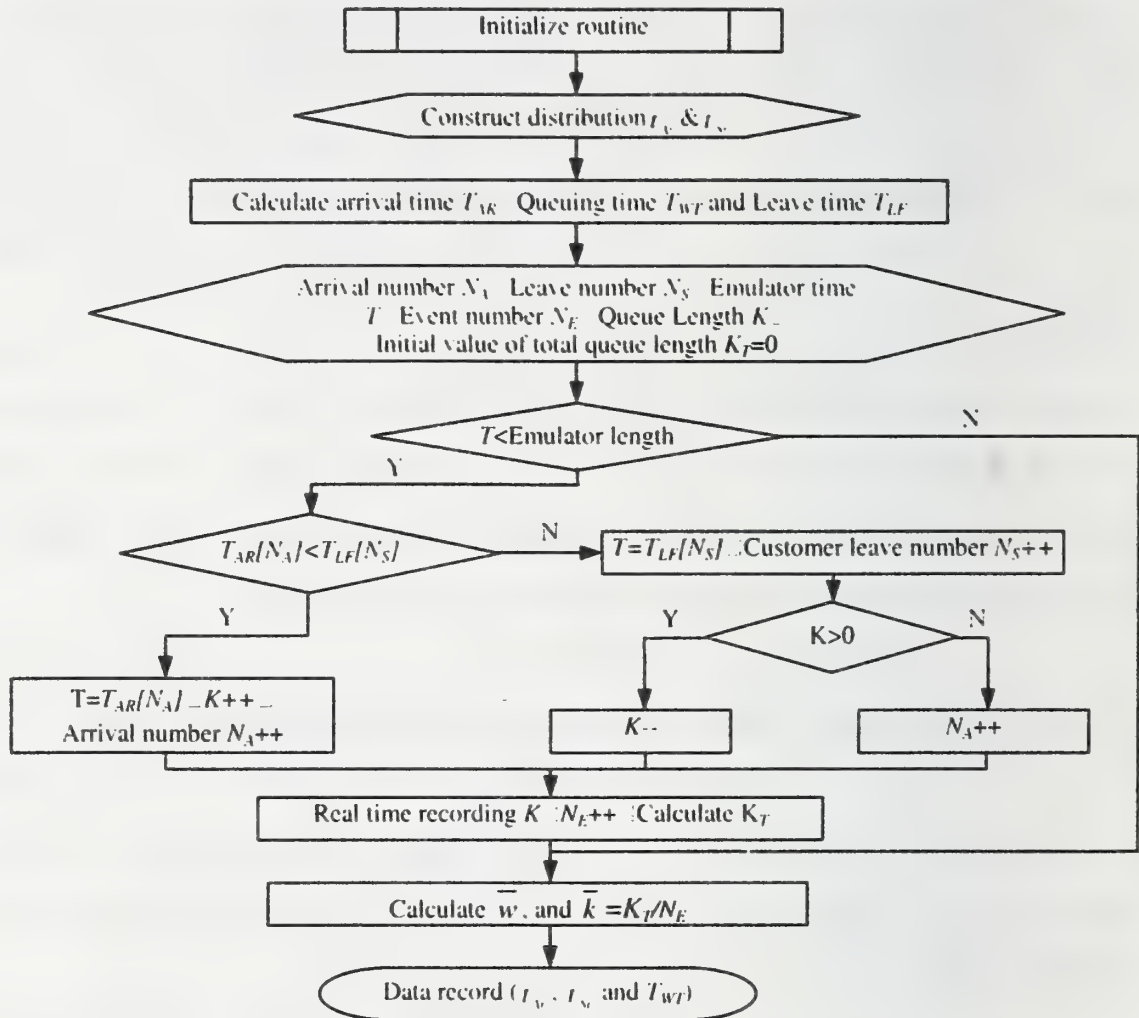
where  $\lambda_s = 1/\bar{\tau}_s = 2.710$  means average arrival rate of image.

From the analysis described above, it can be concluded that the IFD system can be simply modeled as ideal  $M/M/1$  queuing system with single queue, whose service principle is FIFO.

## STUDYING AND ANALYZING

### 4.1 Emulator program

In order to study the relation between the average queuing time for each image and the scale of IFD system, emulator program for data stream of IFD system is



designed based on queuing theory. Figure 3 shows the program flow diagram.

Figure 3. Queuing model emulation flow process chart of IFD system

### 4.2 Analyzing of result

According to the queuing theory, the average queuing time  $\bar{w}$  can be theoretically deduced.

$$\rho = \frac{\lambda_s}{\lambda_s} = \frac{\bar{t}_s}{\bar{t}_s} = \frac{0.369}{10/n} = 0.0369n \quad (11)$$

$$\bar{k} = \frac{\rho}{1-\rho} = \frac{0.0369n}{1-0.0369n} \quad (12)$$

$$\bar{w} = \frac{\rho \bar{t}_s}{1-\rho} = 0.369 \times \frac{0.0369n}{1-0.0369n} = \frac{0.0136n}{1-0.0369n} \quad (13)$$



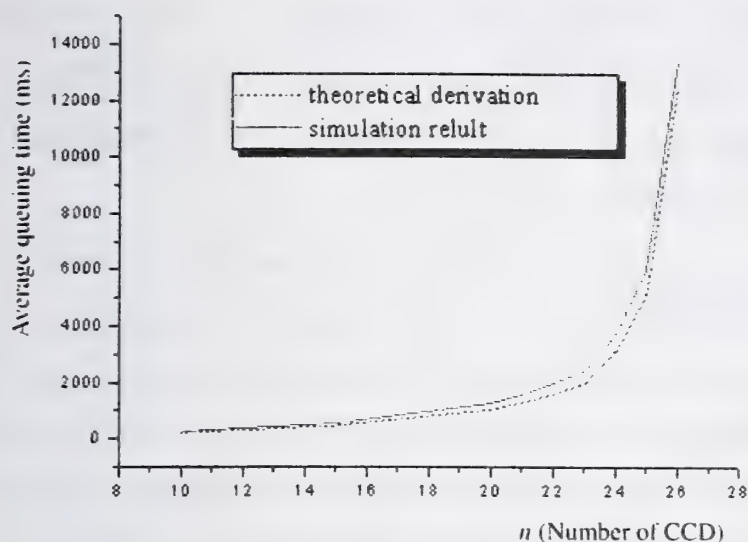


Figure 4. Comparison of theoretical derivation and simulation result

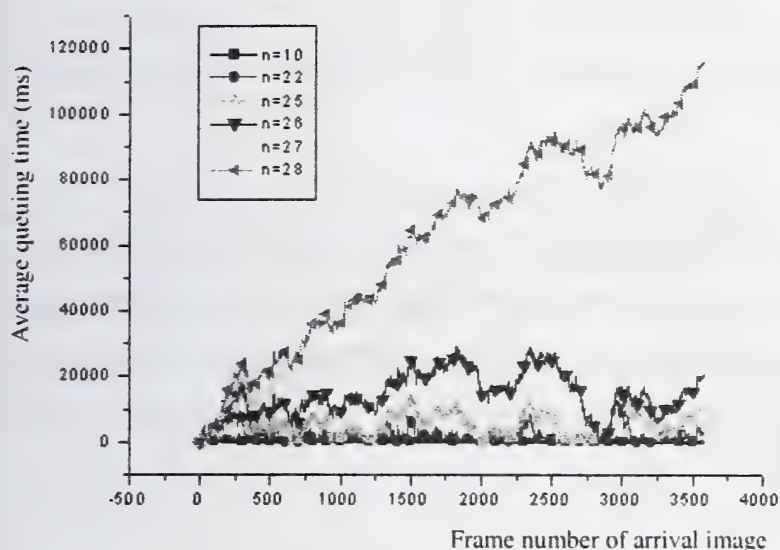


Figure 5. Average queuing time tendency against different  $n$

Therefore  $\bar{w}$  can individual gained from theoretical derivation or emulator program. The comparison of these two results is showed by figure 4. It can be concluded that the two comparison curves are both indicate the relation between  $\bar{w}$  and  $n$ , and the different calculation methods can get almost the same tendency. So, the result of emulator program can be considered right. That's to say, emulator program can be used to study the problem of data stream of IFD system.

Figure 5 clearly shows the different tendency of  $\bar{w}$  relative to variant  $n$ . If  $n = 28 \square \rho = 1.259 > 1$  is got from equation (11). So the mathematics model is unstable, the curve  $n = 28$  visibly expresses the instability of the model. The curve  $n = 27$  in the figure seems unstable while it is theoretical stable for  $\rho = 0.997 < 1$  got from equation (11). And  $\bar{w} = 122508(ms)$  can be calculated from equation (13). The reason is that the emulator time is not long enough to reflect the stability in the end. It can be predicted that this curve will be stable where  $\bar{w} = 122508(ms)$ .

However, what should be paid more attention is that it is not inevitable to reach the request if the model is stable. For example, the result of model analysis trends stable when  $n < 28$ . But considering the early alarm require of fire detection, it is not

permitted if the queuing time is too long. Suppose that the IFD system does not confirm to early alarm require for fire detection if the queuing time is more than 10 second. Then the suitable scale is  $n < 22$ , for there are some frames of image whose queuing times are more than 10 second if  $n \geq 22$ .

## DISCUSSION AND CONCLUSION

The data stream of IFD system is simulated using the emulator program based queuing theory, which is more progressive than traditional analysis method in that only the mean image processing time and that of image frame arrival interval. In traditional opinion, the scale of the IFD system is appropriate as long as the mean time of image processing is shorter than that of image frame arrival interval. However, it is not always right from the opinion of queuing theory, which has been analyzed clearly hereinbefore.

One second thoughts, it will be found that the simple theoretical analysis based on queuing theory can get nothing but the average data. Obviously, this is still not enough. However, the emulator program will solve this problem easily. The queuing time of each frame of image can be obtained through the simulation process. More dynamic curves could be achieved if necessary, which express queue length  $k$ , service time  $\tau$ , standing time  $T$  and so on.

In a word, the analysis method introduced in this paper can exactly guide the scale of IFD system.

## EXPECTATION

From the analysis result described above, the conclusion is that the IFD system based on a single CPU can not meet the requirement put forward by larger and larger buildings.

The usage of distributed processing system (DPS) may be a feasible way to solve this problem. That is to say, every sub-area of fire protection will be collocated a

distributed processor. So the digital image processing task could be decentralized into each distributed processor. Every distributed processor will send information to central processing unit after the digital image processing has finished. Of course, the quantity of information here is much fewer than image data.

With the development of fire detection technology, micro-treatment technology, the point intelligentized image detector based on digital image processing will come into being, which is an integrated module of data acquisition components and distributed processor components. This kind of detector can realize the communication with central processing unit usage 2-bus mode. The advantage is that it thoroughly solves the overtime problem that comes with the enlarging of IFD system. And based on the existing integration technology [10], it can completely integrated with the traditional detectors such as smoke detector, temperature detector that is widely used in fire detection.

The signal of temperature, smoke and acoustic signal can be introduced into fire image recognition technology. The compound detector will be formed in the future, which holds the sensor of sight, feeling, taste, and hearing, just as human being. It also holds "brain" (processor) for processing and recognizing. It can be predicted that the new detection detector will greatly improve the accuracy and early-stage of fire detection.

## REFERENCES

- [1] Drysdale, D. D., *An Introduction to Fire Dynamics*. Wiley, Chichester, UK, 1985
- [2] Rasbash, D. J., *Major Disasters Involving Flashover*. Fire Safety Journal, 17(1991)
- [3] Grosshandler, W.L., *A Review of Measurement and Candidate Signatures for Early Fire Detection*, NISTIR 5555, Gaithersburg, MD, National Institute of Standard and Technology, 1995
- [4] Cheng Xiaofang, Zhou Zhou *Principle Study of Temperature Measurement Based On Primary Colors*, Science In China (Series E), October, 1997, Vol. 40 No. 5
- [5] Song Weiguo, Wu Longbiao, Lu Jiecheng, Song Xiaowu, *Study of the Image Fire*



- [6] Song Weiguo, Wu Longbiao
- [7] Wang Shuhe, *Basic Mathematics Model*, The University of Science and Technology of China Press (in Chinese) May, 1996
- [8] T. L. Graham, G. M. Makhviladze, J. P. Robers, *On the Theory of Flashover Development*, Fire Safety Journal 25(1995)
- [9]
- [10] Chen Tao, Wu Longbiao, Fan Weicheng, *Integration of Image Fire Detection System And Fire Auto-Alert System*, Progerss in Safety Science And Technology, Vol. II (700~704)

David Blake

Federal Aviation Administration Technical Center, Atlantic City, NJ, USA

Stefan Domino, Walt Gill, Louis Gritz, Jill Williams

Sandia National Laboratories, Albuquerque, NM, USA

## **Initial Development of Improved Aircraft Cargo Compartment Fire Detection Certification Criteria.**

### **Abstract**

Most of the cargo compartments on passenger carrying aircraft are required to have fire detection systems that provide a visible indication to the flight crew within one minute from the start of a fire. Flight tests are required to demonstrate compliance with these regulations. The fire detectors in use today are either photoelectric or ionization smoke detectors. While these detectors are effective at detecting actual fires they are also prone to alarm from airborne particles not associated with fires. The use of multiple sensors and appropriate alarm algorithms have the potential to better discriminate between actual fires and nuisance alarm sources. Certification guidelines for using these types of fire detectors on aircraft do not currently exist.

Testing is being conducted to define the types of fires that should be detected and the production of smoke, heat and gases from these fires. The tests will be conducted in various sized cargo compartments to determine if the threshold fire size for detection should vary with compartment size and shape or if the fire size should remain constant and the time to detection should be varied.

Concurrent with the initial fire testing, a transient computational fluid dynamics simulation tool for the prediction of smoke transport in cargo compartments is being developed. This simulation tool will couple heat, mass, and momentum transfer in a body fitted coordinate system in order to

handle a variety of cargo bay shapes and sizes. Comparing the predicted results with the results obtained from the full-scale fire tests will validate the CFD model. Ideally, such a physics based CFD simulation tool can be used during the certification process to identify worst case locations for fires, optimum placement of detector sensors within the cargo compartment and sensor alarm levels needed to achieve detection within the required time.

Testing is being conducted at the FAA Technical Center. The code is being developed by Sandia National Laboratories. Additional partners in the project include the National Institute of Standards and Technology (NIST) and the National Aeronautics and Space Administration (NASA) Glenn Research Center.

## **1. Introduction**

Incidents of aircraft cargo compartment inflight fires are very rare events but as with all fires the consequences can be severe. Reliable detection and effective suppression or fire containment within the cargo compartment is perhaps more critical than in other occupied areas due to the inability to quickly land the aircraft and perform a rapid evacuation. Aircraft operate on some routes that could be in excess of three hours flight time from a suitable airport. Even on domestic flights, 15 to 20 minutes is often needed to descend from cruise altitude and land before an evacuation can be initiated.

The number of incidents of false alarms from aircraft cargo compartment detection system has been steadily increasing as the number of aircraft in the US fleet increases [1]. In addition, the ratio of false alarms to the detection of actual fires in cargo compartments is also increasing. For the period 1995-1999, the ratio was approximately 200:1. Because the majority of cargo compartments on passenger carrying aircraft are inaccessible



during flight, the required procedure in the event of a cargo fire alarm is to discharge fire suppression agent if available and divert and land at the nearest suitable airport. Not only are the direct costs of unnecessary diversions due to false alarms significant but they also raise safety concerns. Some of those concerns include passenger and crew injuries in the event of an emergency evacuation and the possible increased risk of an accident due to landing at unfamiliar airports, changes to air traffic patterns, shorter runways, and inferior navigation aids.

## **2 Certification of Fire Detectors**

The FAA, along with other regulatory agencies throughout the world, require that aircraft cargo compartment fire detection systems provide a visible indication to the flight crew within one minute after the start of a fire [2]. A flight test is required to demonstrate compliance with the regulation. The flight test is conducted during the certification process for a new aircraft type or when there has been a significant change in the fire detection system. The fire detectors that have been exclusively used in aircraft cargo compartments have been photoelectric or ionization smoke detectors. They are either spot detectors or in aspirated systems. A wide variety of smoke sources have been used during the required flight tests to demonstrate the functioning of the detection system. Some examples include burning tobacco, rope and chemicals and a variety of theatrical smoke generators. The methods for generating smoke and the quantities permitted in different size cargo compartments have evolved within the different certification offices over the years based on individual preferences. The FAA has issued guidance material on smoke sources and a visual representation of the appropriate quantity of smoke. However, the precise quantity of smoke is still subjective and there is currently a lack of standardization regarding exactly what the detection system is supposed to detect within one minute. Multi sensor detectors have not previously been used in aircraft cargo compartments but would seem to have the capability to reduce the

current rate of false alarms. However, there are infinite combinations of threshold alarm levels, rate of rise values, and number of sensors that can be used to trigger or suppress an alarm. There is currently very little information available for the FAA to determine what are appropriate alarm levels and algorithms for cargo fires. The environment inside a cargo compartment is subjected to fairly rapid changes in temperature, pressure and humidity as well as exposure to the exhaust from airplane and service vehicle engines.

In addition to the need to better define what should be detected, a parallel effort is underway to develop a transient computational fluid dynamics simulation tool for predicting the transport of smoke, heat and gases within a cargo compartment. Full-scale cargo fire tests will be used to validate the model. Due to the high cost of flight testing, extensive ground tests are typically conducted to define the best location for fire detectors, the worst location for the fire source and the alarm levels necessary to achieve detection in less than one minute. If enough confidence is developed in the model it could replace much of the current testing.

Research has been conducted by NIST in support of this joint project. The first phase of that effort has been a literature search to attempt to document all of the fire detection technologies that currently exist and assess their suitability for aircraft cargo compartments [3]. In addition, they have conducted testing in a Fire Emulator/Detector Evaluator apparatus to document the response of existing aircraft smoke detectors to three fire sources and three nuisance alarm sources.

NASA Glen Research Center is also contributing to this project through funding for the CFD model development and research into miniature gas sensors that could be used in multi sensor fire detectors.



### **3. Fire Sources**

The FAA Technical Center has undertaken an effort to standardize the fires to be detected and develop data for selecting appropriate alarm levels and algorithms. It is desirable for the standardized fires to be both repeatable and realistic. Anything imaginable can be carried in an aircraft cargo compartment and there is no typical cargo fire. The standardized fires described in EN 54 and UL 217 were initially considered but it was felt that those fires did not produce a realistic enough mix of the kinds of gases that would reasonably be expected from a cargo fire involving typical luggage material. Two new fire sources were developed and have undergone initial testing with promising results. Both fire sources use a mix of six plastic resins in pellet form that are heated and pressed into a 4" by 4" by 3/8" molded resin block. A length of nichrome wire is embedded within the resin block and is used as a heat source. A smoldering fire source can be produced by energizing the nichrome wire alone. The same resin block is used to produce a flaming fire source by pouring 2 ml of heptane onto the resin block and simultaneously igniting the heptane and energizing the nichrome wire. The resins used are: Nylon, Polyethylene, Polyvinyl Chloride, Polystyrene, Polybutylene Terephthalate, and Polyurethane. In the Cone Calorimeter tests, it was shown that the burning behavior of both fire sources and the production of combustion gases is very repeatable [4].

### **4. Test Results**

The FAA Technical Center has conducted tests in a below floor cargo compartment of a Boeing 707 test article. The compartment is instrumented with smoke meters, thermocouples and gas analyzers. It also simulates typical ventilation flow in the form of leakage around the perimeter of the cargo door. Figure 1 shows the 707 test article.



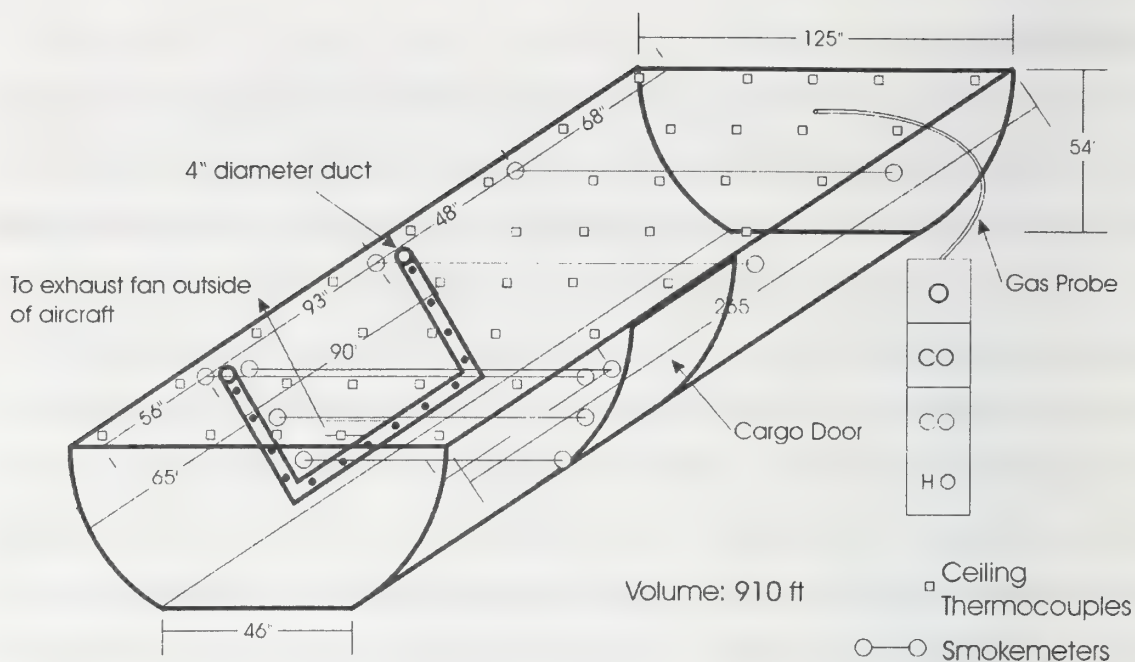


Figure 1. 707 Forward Cargo Compartment

The initial testing attempted to quantify the smoke output from a smoldering suitcase. Identical suitcases were purchased and filled with a mix of cotton and synthetic rags. A coil of nichrome wire, wrapped around several paper towels and connected to a 110 VAC supply was used as the ignition source. Figure 2 shows the smoke levels measured by the mid ceiling smoke meter during six smoldering suitcase tests. As expected, there was considerable variation in the quantity of smoke produced despite a relatively uniform fire load. Time zero on the chart is the time when smoke was first observed. That time was fairly subjective because of the different behavior from tests to test. An easily discernible smoke plume would start for some tests while for others very light wisps of smoke could be seen intermittently before a steady plume was observed. The rectangular outline on the graph shows the desired target for the quantity of smoke produced. The width of the box is the 60 second window in which detection is currently required. The height of the box represents the range of alarm levels required by Technical Standard Order (TSO) C1C which applies to aircraft cargo compartment fire detectors. It would obviously not be practical to expect a detector to alarm in the required time and at the required alarm

level if the quantity of smoke it was exposed to did not fall within that range. The smoldering suitcase did not consistently produce the desired smoke quantity.

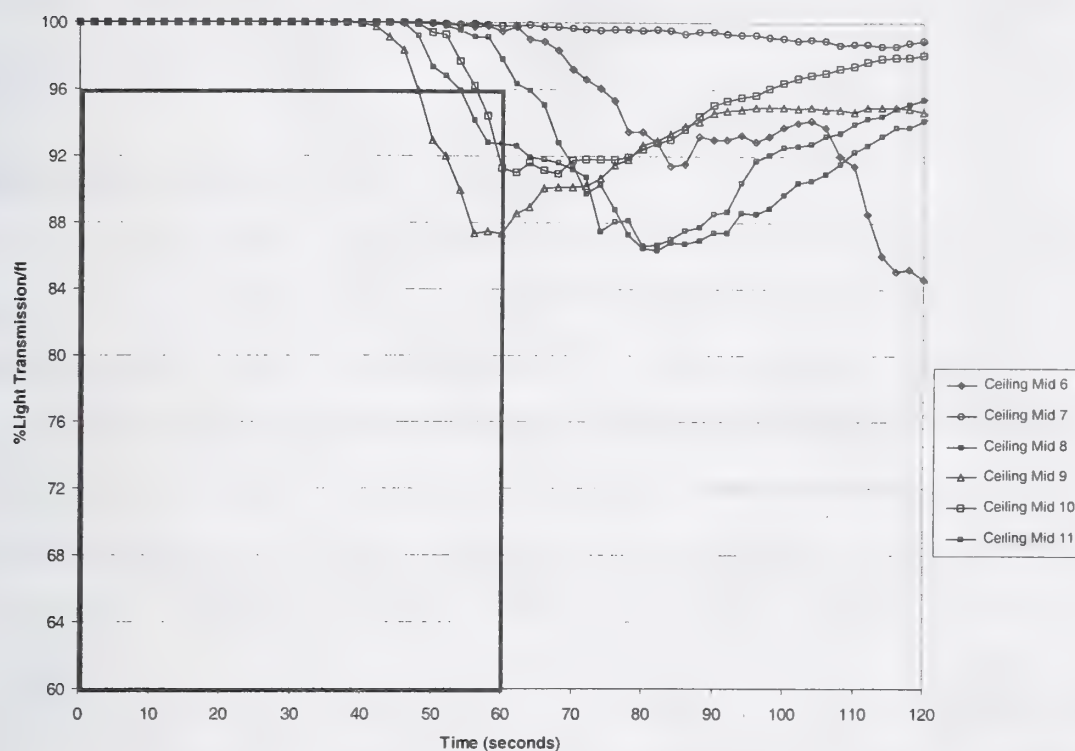


Figure 2. Smoke levels from a smoldering suitcase.

The results of initial testing using the molded resin block in a smoldering state is shown in Figure 3. The results show better repeatability and the smoke that is produced falls within the desired quantity and allotted time for this particular volume cargo compartment. The flaming fire scenario also produces the desired smoke quantity.

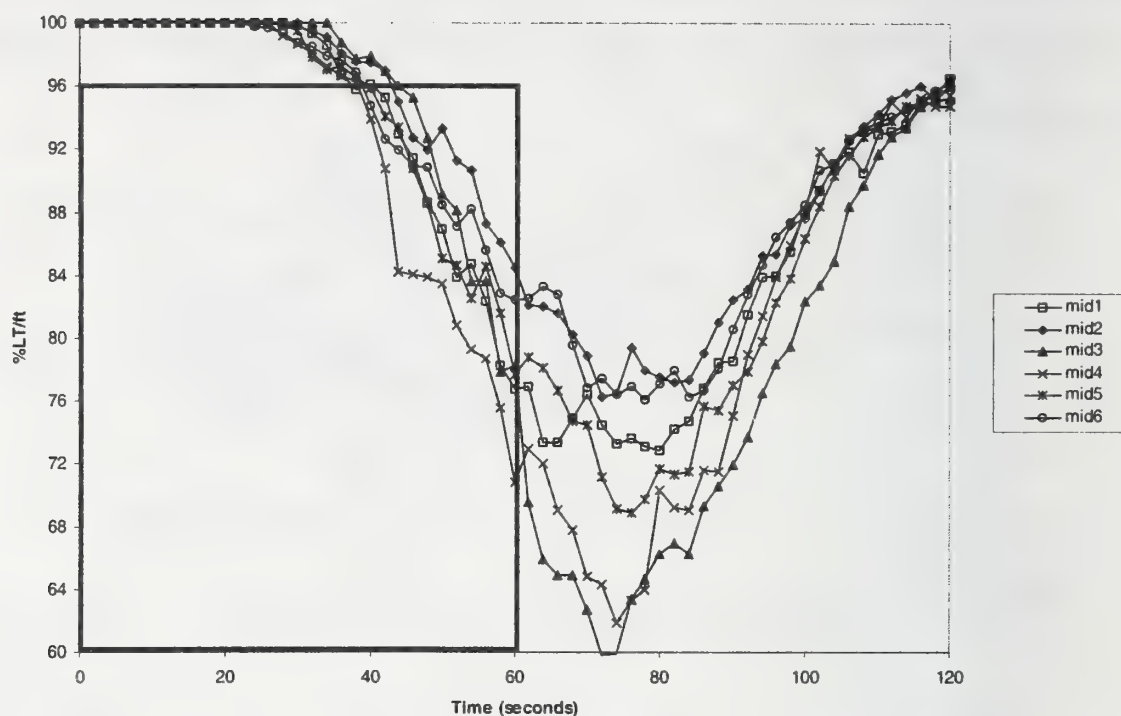


Figure 3. Smoke levels from smoldering resin block

The testing of both the smoldering and flaming resin blocks in the Cone Calorimeter employed a FTIR mass spectrometer for gas analysis. The data from those tests will be used to provide the source terms for heat release rates and smoke and gas production in the CFD model. Additional testing is also planned in the 707 cargo compartment as well as larger cargo compartments to measure the concentrations of various gases. The sample probes and the smoldering and flaming fire sources will be placed in various locations. The data will be used to validate the CFD model and to provide some guidelines for selecting appropriate alarm algorithms for multi sensor fire detectors.

## 5. Computational Fluid Dynamics Model

A computational fluid dynamics simulator is currently being developed at Sandia National Laboratories to predict the transport of smoke in cargo compartment fires. The targeted platform is a midline personal computer,



i.e., 128 MEG of memory with a 750 MHz Intel® Pentium® III processor. The simulation tool is to run quickly and efficiently at modest computational grid sizes (10-30K) in an effort to provide a convenient platform on which to identify worst case fire location scenarios for use during the certification process. It is anticipated that the total "time to detection" simulation will be on the order of one minute, whereas the total computational run time will be on the order of hours.

### **5.1 Turbulent Flow Simulation Background**

Accurately modeling the complex physical phenomena associated with heterogeneous combustion often requires physical models that couple turbulent fluid flow, heat and mass transfer, radiant energy transfer, and chemical reaction. The appropriate physical governing transport equations are discretized and solved on a computational mesh. Unfortunately, the computational expense of solving the turbulent reacting system directly for all appropriate time and length scales frequently exceeds both the computational resources of the user and the desired cost-to-accuracy ratio. Therefore, models that are largely guided by reasonable engineering assumptions have been developed to decrease the associated computational expense in solving these types of problems while attempting to preserve all controlling physical phenomena.

The description of the conservation of mass and momentum for a continuum fluid are described by the Navier-Stokes Equations [5]. These equations are equally valid for turbulent flows since the molecular mean free path is much smaller than the length scale associated with a typical eddy. Therefore, solving the instantaneous Navier-Stokes equations in a turbulent system would yield an instantaneous velocity field that, over time, would fluctuate about some mean value. In most engineering numerical implementations of turbulent flows, however, the instantaneous equations of motions are not solved due to the excessive computer memory requirements associated with

resolving the small length and time scales. Rather, the time-averaged equations are solved. This time-smoothing procedure is accomplished by separation of each independent variable into a time-mean and fluctuating part within the equations of motion and time averaging the result.

The technique of Reynolds averaging the equations of motion leads to cross terms known as Reynolds stresses [5]. These newly created cross fluctuation terms are an artifact of the Reynolds averaging procedure and must be adequately modeled. The proper modeling of these terms represents the classic closure problem of turbulent fluid mechanics.

In variable density flows, the density must also be decomposed and its inclusion within the time-smoothing technique augments the total number of Reynolds stress terms by introducing cross terms involving a fluctuating density component. In such variable density cases, it is convenient to utilize the technique of Favre-averaging [6], which eliminates this complication, by weighting the fluctuating quantities by the instantaneous density before the time averaging step. Upon Favre averaging the variable density equations of motion, triple correlation terms involving variable density terms are, therefore, eliminated. Therefore, the Favre-averaged equations appear to be exactly of the same form as the Reynolds averaged Navier-Stokes (RANS) equations when density fluctuations are neglected.

Most engineering turbulence closure CFD codes employ a form of the Boussinesq [5] hypothesis to model the Reynolds stresses that arise during the time-smoothing procedure. In this formulation, the Reynolds stresses are assumed to act analogously to molecular viscous stresses, i.e., in a gradient-type diffusion relationship. Therefore, the Reynolds stress terms are assumed to be proportional to the mean velocity gradient multiplied by a proportionality constant known as the turbulent eddy viscosity [7]. The closure problem reduces to calculating an appropriate turbulent eddy



viscosity by the utilization of models such as the two-equation  $k$ - $\epsilon$  model [7] that relates the turbulent energy production and dissipation to the turbulent eddy viscosity via the Prandtl-Kolmogorov relationship [7].

## 5.2 Current CFD formulation

The unsteady, Favre-averaged, three-dimensional incompressible Navier-Stokes equations are solved using a finite-volume method whereby the body-fitted partial differential equations are discretized. The use of a structured body-fitted coordinate system within the CFD simulator is desired in order to adequately represent the curvature of the cargo compartment walls while maintaining a low amount of total required mesh points.

In addition to the time-mean equations describing the transport of momentum, equations describing the turbulent time-mean transport of germane species, e.g., CO, CO<sub>2</sub>, soot, etc. can be computed and used for the calculation of point wise mixture properties such as molecular weight and heat capacity. A sensible enthalpy transport equation, including convection heat loss to the cargo walls, is solved to determine the temperature field using the mixture average heat capacity. Radiation effects within the code are currently neglected.

The transient partial differential equation set, in strongly conserved form, is solved for the primitive variables on a collocated grid. A fully implicit scheme, which is first order in time, is used to solve the transient equation set. Face values for the convective terms are determined by the hybrid scheme [8] that results in second order spatial accuracy for Peclet numbers less than 2.0<sup>1</sup> and first order upwind differencing for Peclet numbers greater than 2.0. To overcome the well-known pressure-velocity decoupling that can occur when using a collocated grid, a convective flux interpolation method based on the

---

<sup>1</sup> Second order spatial accuracy is formally true for only purely orthogonal grids.



work of Parameswaran, et al [9] is used. A modified version of the SIMPLE formulation [8] as described within Parameswaran et al. [9] is implemented. In cases where pressurization can occur, the Extended SIMPLE algorithm is used to include low speed compressibility effects [8]. The Boussinesq hypothesis is assumed and the turbulent eddy viscosity is determined by the standard  $k$ - $\epsilon$  equation [7].

## **6. Physical fire model formulation**

Although it is possible to include physical models that adequately describe the detailed chemical reactions germane to the fire process, such a simulation would likely exceed both the targeted simulation run-time and platform constraints. In fact, detailed multiple step kinetic devolatilization models for the materials common in airplane cargo compartments are not available. Therefore, the CFD simulator will not attempt to model the complex physical process of species devolatilization, chemical dependent heat release, and the chemical reaction interaction between high temperature free radicals. Rather, the CFD simulator utilizes experimentally time-resolved species and heat release data in lieu of simulating the complex physical phenomena associated with physical objects burning.

The CFD simulator, therefore, numerically models the fire by the placement of mass and heat source terms within the right hand side of the appropriate transport equation. The overall volumetric mass source term appears on the right hand side of the following equations: 1) continuity equation, 2) species transport equation (multiplied by the appropriate mass fraction of that particular species), and 3) the momentum equations in the form of a momentum sink. The placement of volumetric heat releases on the computational grid will model the buoyantly induced flow rather than the associated heat release due to both homogeneous and heterogeneous chemical reaction. Although the technique of prescribing source terms is certainly not the preferred method for an entirely predictive CFD code, in this particular

application where source terms are available through a detailed time-resolved experiment, it is the preferred method.

## **7. Mathematical formulation**

The partial differential equations describing momentum, species, turbulent energy, turbulent dissipation, and sensible enthalpy transport are linearized and discretized using the finite volume method [8]. The method of finite volume discretization is a conservative approach even at low discretization resolution. The discrete continuity equation, which includes the appropriate discrete volumetric mass source term, is used to form the pressure correction equation [8]. The governing equations are solved iteratively using a segregated approach. Updating the matrix coefficients through each sweep captures the non-linearity inherent to the original PDE equation set. The linear system of equations for the momentum field, species, turbulent dissipation and production, and sensible enthalpy are solved using the strongly implicit method of Stone [10] while the pressure correction equation is solved via a preconditioned conjugate gradient method. A particular time iteration is considered converged when the maximum residual of all individual linear equations is below a user-defined value that corresponds to the desired reduction in the normalized L2 norm.

## **8. Code Validation and Preliminary Simulation Results**

A concerted effort between the FAA and Sandia National Laboratories is underway to validate the CFD model by comparing the simulation results to detailed experiments that measure species and smoke concentrations at various locations within the cargo compartment. Figure 4 illustrates a preliminary simulated temperature profile ten seconds into a simulation. This initial CFD simulation utilized a heat and mass release rate of 2.25 KJ and 0.05 g/s, respectively. These boundary values correspond to a single instance of time-resolved experimental data for a flaming resin from a FAA

cone calorimeter experiment. The total number of grid points represented in this simulation is 10,000.

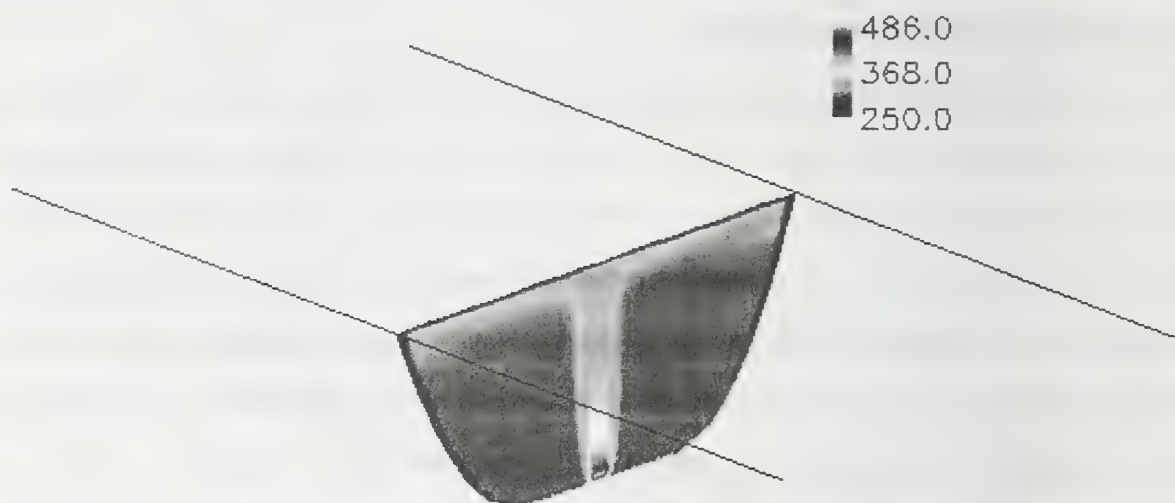


Figure 4. Simulated temperature profile, K, at 10 seconds.

Sandia is a multi-program laboratory operated by Sandia Corporation, a Lockheed Martin Company, for the United States Department of Energy under Contract DE-AC04-94AL85000.

## References

- [1] Blake, D. Aircraft Cargo Compartment Smoke Detector Alarm Incidents on U.S.-Registered Aircraft, 1974-1999, DOT/FAA/AR-TN00/29, June 2000.
- [2] Code of Federal Regulations 14 CFR Part 25.858
- [3] Cleary, T. and Grosshandler, W. Survey of Fire Detection Technologies and System Evaluation/Certification Methodologies and Their Suitability for Aircraft Cargo Compartments, NISTIR 6356, July, 1999.



- [4] Filipczak, R., Blake, D., Speitel, L., Lyon, R., Williams, J. Development and Characterization of a Smoldering Combustion Source. Fire and Materials 2001 Conference, January 22-24, 2001
- [5] Bird, R. B., Stewart, W. E. and Lightfoot, E. N. Transport Phenomena. John Wiley and Sons, New York 1960.
- [6] Favre, A. Problems of Hydrodynamics and Continuum Mechanics. Society for Industrial and Applied Mathematics, Philadelphia 1969.
- [7] Launder, B. E. and Spalding, D. B., The Numerical Computation of Turbulent Flows. Computer Methods in Applied Mechanics and Engineering. 1974; 3:269-289, 1974.
- [8] Patankar, S. Numerical Heat Transfer and Fluid Flow. McGraw-Hill, New York 1980.
- [9] Parameswaran, S., Srinivasan, A. B., and Sun, R. L. Numerical Aerodynamic Simulation of Steady and Transient Flows around Two-Dimensional Bluff Bodies Using the Non-Staggered Grid System. Numerical Heat Transfer, Part A 1992; 21:443-461.
- [10] Stone, H. Iterative Solution of Implicit Approximations of Multidimensional Partial Differential Equations. SIAM Journal of Numerical Analysis 1968; 5(3):530-557.

**Aircraft Fire Detection: Requirements, Qualification and Certification Aspects**

**1. Abstract**

For aircraft applications other or additional qualification requirements need to be fulfilled by the automatic fire detection instrument compared to those applicable to buildings. It is important to distinguish between pressurized zones and non pressurized zones due to their completely different environments (e.g. inside/outside temperature and pressure/altitude). This paper will concentrate on fire detection aspects applicable to pressurized areas of transport aircraft where passengers and cargo are located.

**2. Introduction**

For some aircraft compartments a fire/smoke detection system is required by the regulations JAR[1].and/or FAA[2]. For example:

- JAR/FAR 25.854 requires the installation of a smoke detector system or equivalent for each lavatory
- JAR/FAR 25.857 requires the installation of a separate approved smoke detector or fire detector system for some cargo compartments.
- JAR/FAR 25.858 defines details for cargo compt fire detection systems.

In addition, aircraft manufacturers install supplementary fire/smoke detection systems to increase the level of safety. These systems must comply e.g. with subsequent regulations

JAR/FAR 25.1301	Function	and	Installation:
	Each item	of	equipment must
	(a) Be of a kind and design appropriate to its intended function		
	(d) Function properly if installed		

Additional systems are installed in Airbus aircrafts to monitor areas which are not permanently occupied or monitored by crew members or passengers like

- Main avionics compartment (computer room / electrical energy center)
- Customized electronics equipment bays (e.g. In - Flight Entertainment)
- Crew rest compartments / lower deck facilities

The urgency of the corrective action subsequent to a fire/smoke warning depends directly on the risk and is reflected in the procedure to be applied by cockpit or cabin crew.

For example, a cargo compartment smoke warning will be indicated to the flight deck crew as a red warning, this means the crew has to perform the action immediately.

In this case the

- air ventilation system, if any, needs to be turned off and associated compartment isolation valves have to be closed
- fire extinguishing system needs to be activated
- crew has to land the aircraft as soon as possible, etc

As long as the crew is unable to differentiate between a true and a false warning, it has to follow the certified procedure.

The impact of a false fire/smoke warning in non accessible compartments is extensive and might include: flight diversion, declaration of emergency situation, eventually passenger evacuation, compartment inspection, fire extinguisher replacement, customer/passenger disappointment, loss of confidence in the warning system etc.

To minimize the risk, an early detection of an in-flight fire/smoke situation is mandatory to initiate the corrective action at an appropriate time. On the other hand, false/unconfirmed warnings could be critical as well.

With the 60 seconds detection time requirement as addressed in JAR/FAR 25.858 (a), the system design is always a compromise between fast detection and warning signal reliability.

This time was originally assigned to cargo compartment applications and has often been required/applied by airworthiness authorities [3] and/or system designers to in flight inaccessible compartments or remote located crew rest rooms



### **3. Fire Detection Requirement (JAR/FAR 25.858)**

If certification with cargo compartment fire detection provisions is requested, the following must be met for each cargo compartment with those provisions:

- (a) The detection system must provide a visual indication to the flight crew within one minute after the start of the fire.
- (b) The system must be capable of detecting a fire of a temperature significantly below that at which the structural integrity of the aeroplane is substantially decreased.
- (c) There must be means to allow the crew to check, in flight, the functioning of each fire detection circuit.
- (d) The effectiveness of the detection system must be shown for all approved configurations and conditions.

### **4. Experience**

An analysis of false warning scenarios identified the following main problem areas:

- sensitivity to aircraft environmental condition changes (temperature, pressure / altitude, humidity, power transients, electromagnetic interference, exhaust fumes from ground loading equipment etc)
- insufficient knowledge of either sensor/detector functions by aircraft manufacturers or specific to type aircraft environmental conditions by fire/smoke detector instrument manufacturers
- detector/sensor stability
- sensitivity to cargo/load transported in the compartment
- sensitivity to sprays used in lavatories
- insufficient detector cleaning (operator and/or interval)
- penetration of unexpected particles (contaminated/unfiltered air) into the measurement measurement chamber(s)
- detectors evaluation (open-area /point type or flow-through /duct type)
- single detector alarm dependence

From the a.m. items we can identify the two main areas of possible improvements. The fire/smoke detector itself, and the associated integration into the aircraft. The integration in

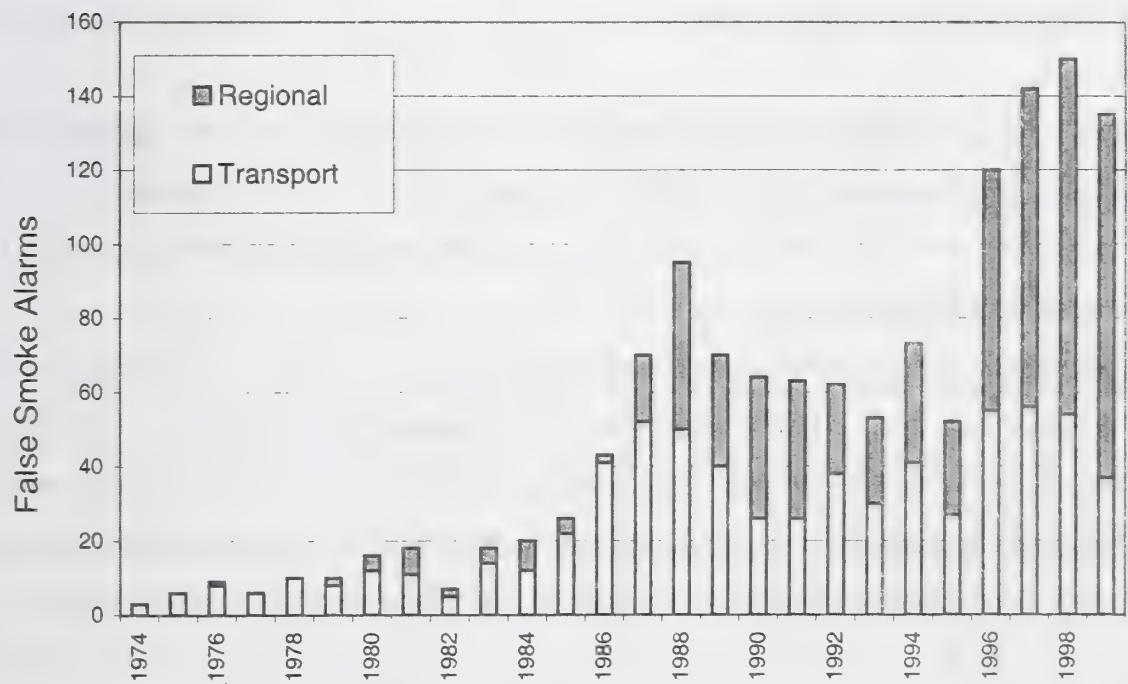
the aircraft specific environment and the need to customize specific to type solutions is a real issue which makes it difficult to standardize detectors for the various aircrafts and applications.

We, at Airbus Industries consider the minimum requirements for fire/smoke detection instruments as defined in standard JTSO/TSO-C1c [4] as not sufficient as far as fire/smoke detection performances and warning reliability is concerned.

In consideration of this, EADS-Airbus uses aircraft specific integration guidelines and purchases smoke detectors/systems according to own detailed technical specifications. In addition new detection technologies are closely monitored by system design office [5]

The following graphic shows the occurrences of false smoke warnings in cargo compartments of US-registered aircrafts within the last 25 years [6]. Of course air traffic increased and the requirements to install smoke detection systems have been amended. Therefore the general increase of false warnings per year could be explained.

False Cargo Smoke Alarms on Regional Aircraft vs. Transport Aircraft (US-registered aircrafts)



Source: David Blake, FAA Technical Center, Fire Safety Section

If we investigate in the a.m. graphic the share between regional aircrafts and transport aircrafts, we can conclude that the efforts spent by transport aircraft manufactures in the last years to reduce the rate of false warnings were efficient considering that the number of installations increased whereas the occurrence of false cargo smoke warnings maintained nearly the same level or decreased.

We are convinced that the main reasons for false smoke warnings are due to the insufficient signal processing/confirmation applied in some types of smoke detectors and/or the maximum allowed detection time of 60 seconds. If the maximum allowed detection time could be changed to e.g. 120 seconds then a significant step in false smoke alarm reduction could be made. [7]

## **5. Smoke Detector Requirements**

The function of the equipment is to detect emerging smoke and thus to detect an arising fire. Any compensation/filtering process shall not degrade the equipment's ability to detect smoke.

### **5.1 Smoke Detection Performance**

With reference to EN54-9 [8]"Methods of test of sensitivity to fire", the equipment shall at least detect the test fires TF2 to TF5 within the range given in that document

Normal operating conditions

Temperature range    -40 to 86 degree Celsius

Pressure range        1089 mbar abs to 571.8 mbar abs

Depending on the sensor's measurement principle it may be necessary to justify the ability of the equipment to detect smoke/fire in the a.m. temperature and pressure ranges. For further environmental conditions refer to the chapter Qualification Test

The equipment shall be tested by application of an appropriate test stimulus, e. g. air containing smoke having a light obscuration value of 3% per meter. For equipment in



which the sensitivity and/ or response time is affected by any factors which may be varied from one installation to another tests shall be conducted with the least sensitive and longest response time condition to be used.

Open-area/Point type smoke detector (e.g. cargo/lavatory): The equipment shall be tested with an air sample as defined above which is introduced into the equipment under standard atmospheric conditions. The equipment shall then actuate a smoke alarm within a maximum time period of 30 seconds.

Flow-through/Duct type smoke detector (e.g. avionics): The equipment shall be operated continuously by varying the pressure differential from 25% below to 25% above the rated. This pressure variation shall have no influence on the smoke detection performance.

Development smoke tests shall be carried out by the supplier to define a good compromise between adjustment of the electrical alarm threshold and the housing layout to get an acceptable response time (target within 20 seconds) if the equipment is exposed to a fire. The final sensitivity adjustment shall be recommended by the supplier and agreed with the aircraft manufacturer.

The equipment shall not revert to „no smoke“ signal condition following an alarm indication when held immersed in smoke levels at least 25% greater than the „Smoke-“ response level for the equipment for a period of ten hours.

The equipment shall revert to a „no smoke“ signal condition when the smoke level is reduced to approximately 50% of the „Smoke-“ response level.

The equipment shall include means to avoid/compensate effects caused by environmental condition changes such as e.g. temperature, altitude, acceleration and possible combinations of those parameters

The sensitivity drift due to temperature/pressure changes and component tolerances shall

not exceed +/- 15% of the corresponding thresholds. The measurement of the response threshold value shall be carried out in a manner as described in EN54-7 annex B.

With reduced tolerances (see above) following EN54-7 tests are applicable:

Repeatability	Refer	to	EN54-7	clause	6.
Directional dependence	Refer	to	EN54-7	clause	7
Reproducibility	Refer	to	EN54-7	clause	8.
Air movement	Refer	to	EN54-7	clause	10
Ambient Light	Refer to EN54-7 clause 12				

Hermeticity of Flow-through/ Duct detector:

The leakage rate shall not produce a pressure variation inside the smoke detector more than typically 5 mbar (max. 7 mbar) after 60 sec. With the equipment being exposed to an internal pressure equal to the external pressure minus 20 mbar at the beginning of the test. This test has to be applied on each unit.

Fire Resistance of open-area/ point type smoke detector

The equipment shall be able to withstand the effect of an open fire at 232,2 degrees C (450 degrees F) for 1 min. Smoke shall be indicated during test for at least 20 sec. Installation in designated fire zones is not permitted.

5.2 Fatigue Test

Detector forced to smoke / standby conditions

The purpose of this test is to demonstrate that the item of equipment will retain its proper characteristics when subjected to repeated tests.

A minimum of 120000 cycles shall be performed. Each cycle shall last one minute and consists of:

- 20 seconds alarm
- 40 seconds standby

The test shall be carried out under ambient temperature and pressure conditions. For the purpose of test runtime reduction up to 10 smoke detectors may be interfaced.

Detector-power-up-test (Reason: System may not be energized if the aircraft is parked)  
 The purpose of this test is to demonstrate that the item of equipment will retain its proper characteristic when subjected to power up.

Cycle type 1	Cycle type 2
Power-on time of 2 minutes or more	Power-on time of 2 minutes or more
Power-off time of 2 to 3 seconds	Power-off time of 5 minutes

- A minimum of 30000 cycles (type 1 and type 2) shall be performed.
- The number of each cycle applied shall be equal.
- Cycle type 2 sequence shall follow cycle type 1 sequence

It shall be verified during each test cycle that the smoke detector does neither emit a detector “Fault“, “Alarm“, nor any other failure.  
 The test shall be carried out under ambient temperature and pressure conditions.

**6. Environmental Conditions and Test Requirements Associated to Qualification**

The environmental conditions applicable to airborne equipment are largely different compared to industrial or maritime applications [9]. It is of great importance to qualify the detection performances of a fire/smoke detection instrument in an approved laboratory prior to it is release to qualification tests.

The Airborne smoke detectors to be used in Airbus shall comply with the environmental conditions and test procedures as defined in document RTCA/DO-160 [10], and ABD0100. [11], completed by the requirements contained in EN54-7 [12].

During the environmental tests, the tested smoke detector shall not:

- generate a smoke warning signal
- become inoperative
- generate a fault signal



The applicable tests and their category are defined in the technical specification to be issued by the aircraft manufacturer for each equipment/system.

## **7. Equipment Specific Software Requirements**

Software shall be produced in accordance with the definition contained in RTCA /DO-178 [13]. The software level will be identified by the System Safety Process [14]. For example Level B could be assigned to cargo compt application and Level C for lavatory application. Software partitioning is required whenever different software levels are used within an equipment..

## **8. Certification Aspects**

The smoke detection equipment/systems will be certified together with the certification of the aircraft following the aircraft type certification process or supplementary type certification procedures when applied after type certification.

To achieve certification the suppliers have to provide the aircraft manufacturer with all product relevant justifications to demonstrate compliance with the applicable airworthiness regulations. The fire/smoke detection performances of the fire/smoke detection instrument must be proven by the supplier during equipment qualification phase. These justifications will be added to those ones which have to be established by the aircraft manufacturer.

The purpose of the smoke detection test in the aircraft is only to verify that smoke generated at the most unfavourable place in a compartment will reach the approved fire/smoke detection instrument and actuate an alarm within the required time frame. Thus to demonstrate compliance with JAR/FAR 25.858 (a) for example in case of a cargo compartment.

## **9. Summary**

An early detection of an in-flight fire/smoke situation is mandatory to initiate the corrective action at an appropriate time, but false warnings could be critical as well.

Investigations showed that the problem to safely detect a fire/smoke situation and to

distinguish this from all non-fire/smoke situations is not yet fully solved in the pressurized areas of transport aircraft.

Further improvements are very limited as long as the 60 seconds detection time requirement (ref. JAR/FAR 25.858) must be fulfilled to certify fire/smoke detection systems.

## 10. References

- [1] Joint Aviation Requirements, JAR-25, Large Aeroplanes, Change 14, 27May 1994, JAA, Hoofddorp, The Netherlands
- [2] Federal Aviation Requirements, FAR part 25 incl. Amendments 1-98
- [3] Federal Aviation Administration, Advisory Circular 25-9A, Smoke Detection, Penetration and Evacuation Tests and related Flight Manual Emergency Procedures, 1/6/94, Federal Aviation Administration, Washington DC, USA
- [4] Joint/Technical Standard Order JTSO/TSO-C1c, Cargo Compartment Fire Detection Instruments", 10.June 1991
- [5] Freiling, A, New Approaches to Aircraft Fire Protection, see this book of conference
- [6] Blake, D. FAA Technical Centre, Fire Safety Section, Report No DOT/FAA/AR-TN0029, June 2000
- [7] Schmoetzer, K. "Improvement of Smoke Warning Reliability in Aircraft Application", International Aircraft Systems Fire Protection Working Group Meeting, May 2000, Atlantic Hotel, Bremen, Germany
- [8] EN 54-9 Components of automatic fire detection systems Part 9 Methods of test of sensitivity to fire",
- [9] Alroe, H., "Environmental Test Requirements for Fire Alarm Equipment Used for Marine Applications "AUBE '99", 11th, March 16-18, 1999, Gerhard Mercator University, Duisburg, Germany, Luck, H., Editor, pp. 567-575, 1999.
- [10] Radio Technical Commission for Aeronautics (RTCA) Washington D.C., RTCA/Do-160D Environmental Conditions and Test Procedures for Airborne Equipment
- [11] Airbus Directives (ABD) and Procedures, ABD0100-Equipment-Design, General Requirements For Suppliers, Issue C, December 1998.

- [12] EN 54-7 Components of automatic fire detection systems  
Part 7 Specification for point-type smoke detectors
- [13] Radio Technical Commission for Aeronautics (RTCA) Washington D.C.,  
RTCA/Do-178B Software Considerations in Airborne Systems and Equipment  
Certification
- [14] Airbus Directives (ABD) and Procedures, ABD0200-Requirements and  
Guidelines for the System Designer, Issue C, December 1998.



A. FREILING

European Aeronautic Space and Defense Company EADS Airbus GmbH, Bremen,  
Germany

## **New Approaches to Aircraft Fire Protection**

### **1. Abstract**

Currently, new fire detection technologies are under evaluation for aircraft application. The goal is to reduce the false alarm rate drastically and to improve safety and reliability figures. Gas sensor technologies, visualization devices and other multisensor/multicriteria are under discussion. In this paper, an overview of currently fire protected areas in Airbus aircraft is given. The potential to introduce specific fire protection by the means of new technologies in dedicated aircraft areas is discussed. If new fire detection technologies are used, there is the need to have modified integration tests. A comparison of a commonly used aircraft integration test to a real fire scenario is given by the example of a gas sensor based fire detector.

### **2. Introduction**

A fire protection system in an aircraft includes passive and active fire protection means [1]. Passive fire protection is realized by using fire proof or inflammable materials in all areas of the aircraft including lining, cables, interior etc. In this paper, the active fire protection system will be regarded which consists of scattering light smoke detectors managed by a central control unit and a halon extinguishing system. Several aircraft areas are equipped with fire detection instruments. These are the cargo compartments, the electronic compartments and the lavatories. The most important and critical area is the cargo compartment, which is inaccessible during flight.

For ground based applications, which includes building fire protection, new kinds of fire detectors like multisensor/multicriteria- or gas sensor based fire detectors have currently been developed or are under discussion [2, 3, 4, 5]. The main goal of using these kinds of sensors is to reduce the false alarm rate. Also the aircraft fire false alarm rate and the correlated consequences have to be reduced drastically [6, 7]. There are several

restrictions and additional requirements that come along with the airborne application [8]. For new fire detection technology to be used in aircraft, there is the necessity to revise the integration / validation test.

At EADS Airbus, new fire detection technologies are examined for aircraft application to improve the alarm reliability and to provide additional means for monitoring fire or smoke in dedicated aircraft areas.

**3. Fire protected aircraft areas – state-of-the-art**

Lavatories

The fire protection of aircraft lavatories is realized by a scattering light smoke detector near the air extraction and an automatic fire extinguisher in the receptacle. In case of a fire alarm, the lavatory door can be opened and a crew member can extinguish the fire with a handheld fire extinguisher. Figure 1 shows a drawing of a lavatory and installation points of smoke detectors.

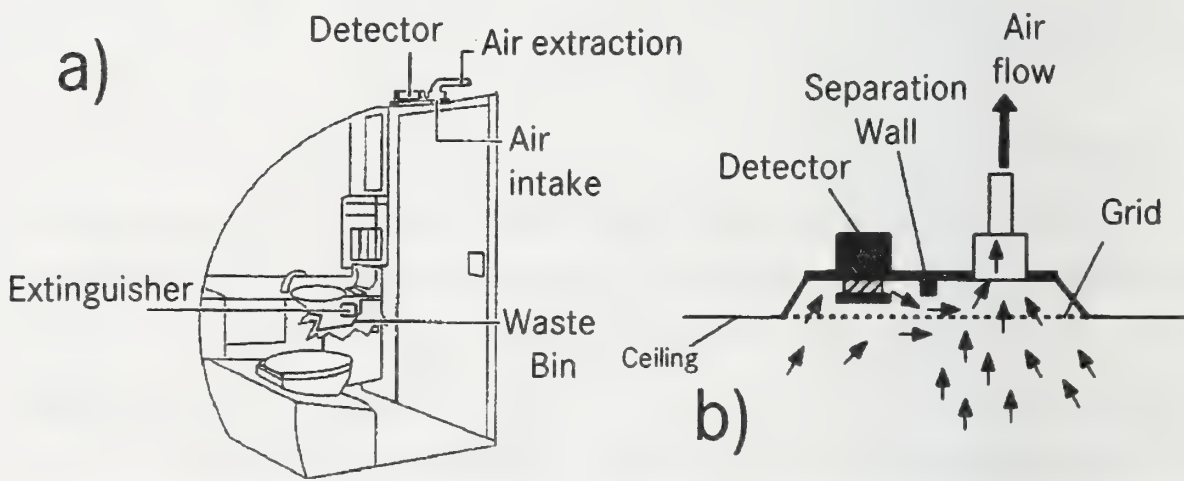


Fig. 1: a) Sketch of an aircraft lavatory  
b) Installation of a lavatory smoke detector in Airbus

### Avionics Compartment

In the avionics compartment, nearly all the electronics necessary to fly the aircraft is located. Commonly, the compartment is positioned under the cockpit, in the front part of the aircraft. In most aircraft, the avionics compartment is not accessible during flight. Only in larger Airbus aircraft, there is a small access hatch. The compartment is ventilated, with the extracted air passing through a common air extraction duct which is monitored for the presence of smoke.

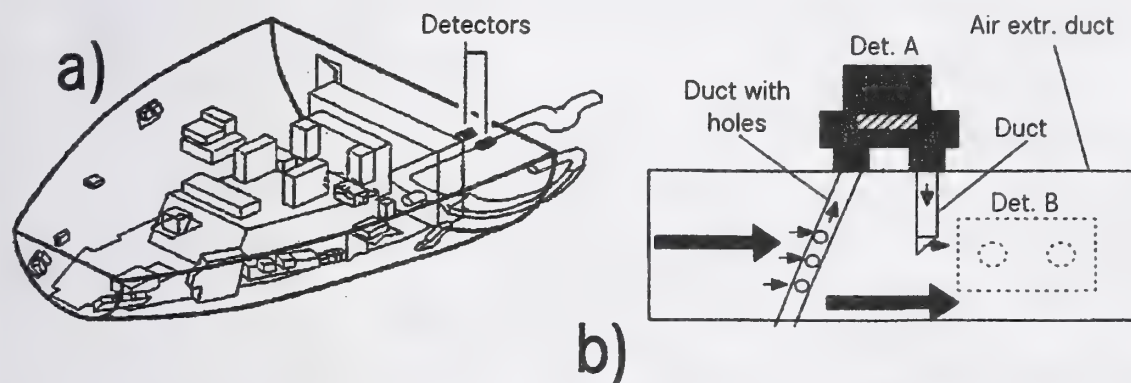


Fig. 2: a) Sketch of an aircraft avionics compartment  
b) Installation of a duct type smoke detector in Airbus

### Cargo Compartments

More critical areas in the aircraft in which smoke detectors are installed, are the cargo compartments. In transport aircraft, these compartments are normally located under the actual passenger cabin, the forward (FWD) compartment in front and the aft compartment behind the wing box. During flight, the cargo compartments are inaccessible. That means that in case of a fire warning, the pilot has got no possibility to verify if it is a real or a false alarm. The action the pilot has to take after a fire warning is to activate the extinguishing system and to land as soon as possible, eventually on an unsuitable airport [9].

A further reason for a high risk within the cargo compartment is that the freight cannot be controlled by the aircraft manufacturer. Although there are restrictions on what is allowed to be transported, there is still the possibility that dangerous ignition sources get into the aircraft.

Concerning fire extinguishing, there are fire extinguishing bottles installed in transport aircraft. As extinguishing agent, halon is used. Although halon is generally banned by the



Montreal Protocol, there is a time limited exceptional regulation and it can still be used for aircraft application. This regulation expires in 2003. Until then, alternatives have to be found.

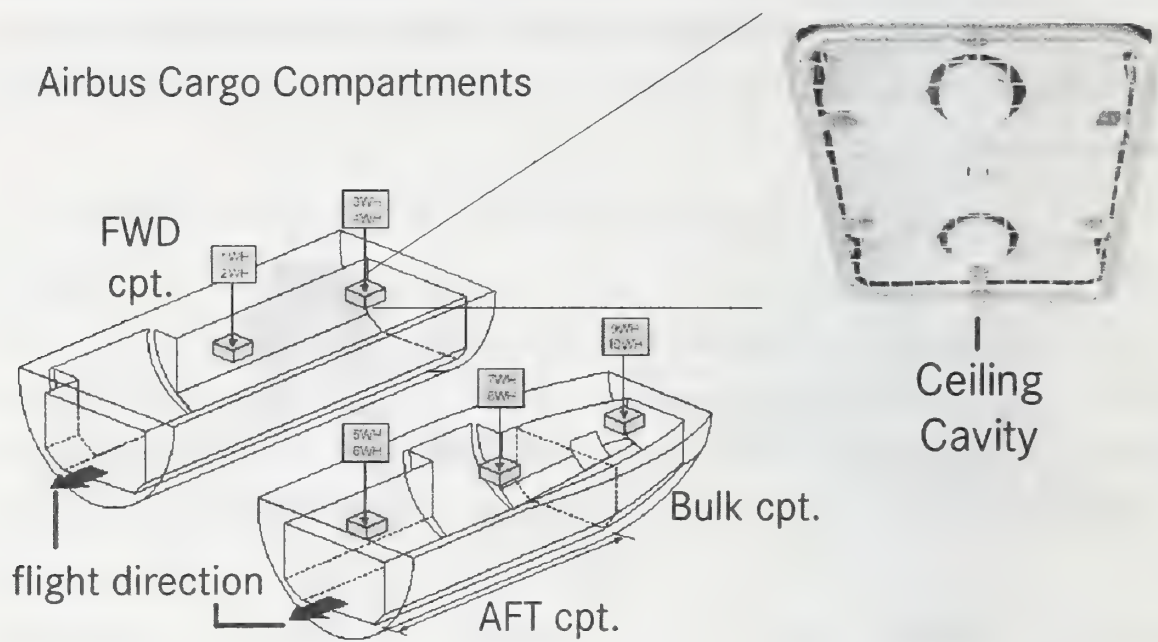


Fig. 3: Airbus Cargo Compartment Smoke Detector Positions and installation

Lower Deck Facilities

With the development and construction of larger aircraft, there comes the wish to use additional space gained in the lower deck. In order to accommodate more passengers in the main deck area, certain facilities will be located in the lower deck area of the aircraft. These are galleys, toilets, crew rest areas (with beds for the passengers/crew to sleep), etc. Along with the installation of such facilities, there comes the necessity to install fire detection.

**4. State-of-the-art aircraft fire detection technology**

The signal processing of the scattering light type smoke detectors currently applied in the Airbus aircraft series uses specifically developed smoke discrimination algorithms. Using specific light frequencies, modulations and correlation in the time domain with a database allows to differentiate between typical smoke patterns.

The overall aircraft smoke detection system consists of the smoke detectors at several locations (see section 2) and the so-called Smoke Detection Control Unit (SDCU) which

controls and reads out the detectors. A block diagram of the system architecture is given in Fig. 4. For redundancy reasons, the smoke detectors in the cargo compartment and in the avionics compartment are installed in pairs. Each pair of detectors is supplied with power by a dual redundant power supply (see Fig. 4). One detector in the pair is installed on the Smoke Detection Control Unit (SDCU) loop A, the other on loop B. The SDCU tests each loop to check whether it is functioning before it acts on a smoke alarm from a single smoke detector. When a smoke alarm is generated by the SDCU the ventilation and heating systems (if installed) will be closed automatically.

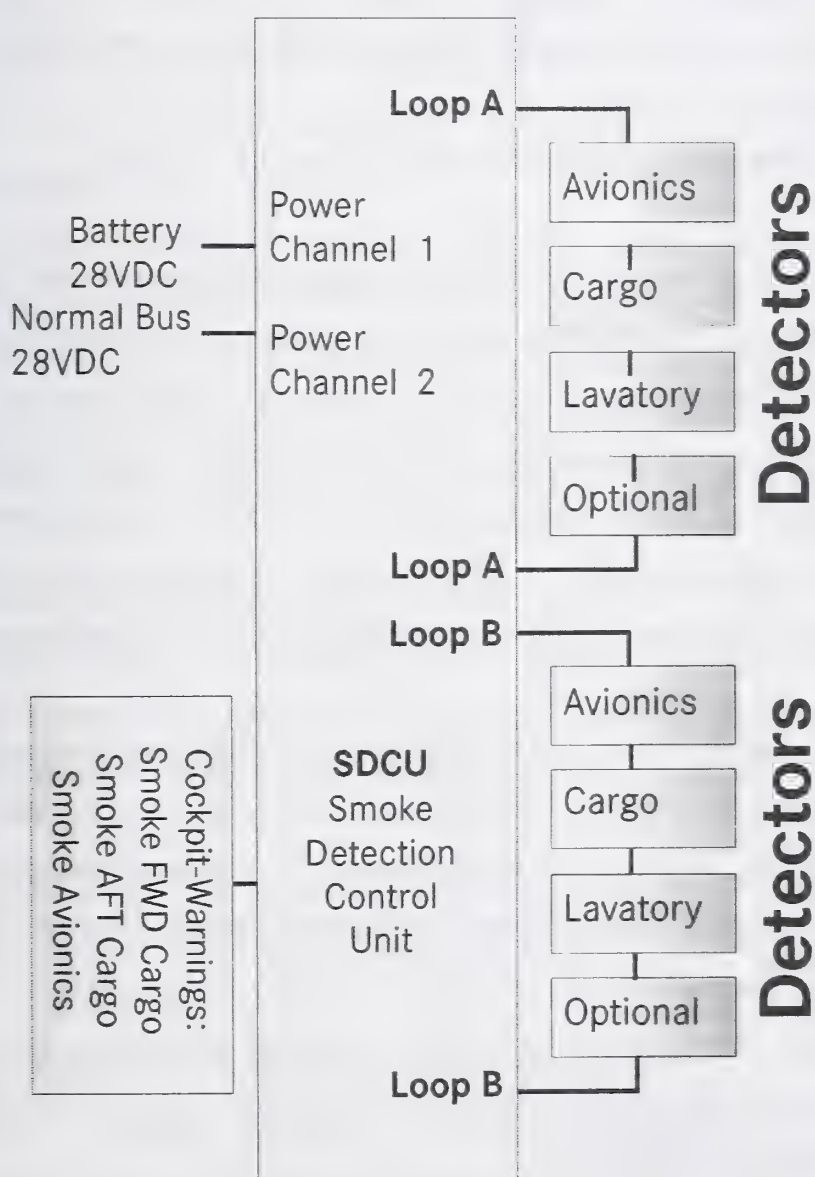


Fig. 4. Smoke Detection Loop Schematic for A340

## 5. Approaches to new kinds of fire detection

Currently under investigation are advanced fire detection technologies with the aim to identify the proper fire signatures (gas, smoke, heat etc.) as they may develop in a crucial, inaccessible area of the aircraft and develop the algorithms which allow to link these fire parameters to non-fire events that may be present in the aircraft. Technology under consideration to reach adequate detection properties includes [10]:

- Gas sensing with semiconducting metal oxide sensors in thick- or thin-film technology or/and electrochemical cells
- Optical smoke sensing with light attenuation or back-scattering devices
- Near infra-red (NIR, wavelengths  $< 1.2\mu\text{m}$ ) and visible light sensing with CCD (Charge Coupled Device) and/or CMOS (Complementary Metal Oxide Semiconductor) technology
- Infra-red sensing with thermopiles (for wavelengths  $> 1.2\mu\text{m}$ )

It is possible to subdivide several aircraft areas to dedicated fire sectors with dedicated fire protection systems. One example for that can be a special fire protection of avionics compartments where the materials that can burn are relatively well defined. So, may be the possibility to develop a system based on gas sensors that detects smouldering cable fires or overheated equipment. A certain spatial resolution in fire detection would give the pilot a decision means of what measures to take if an area of the electronics compartment becomes overheated. If the heat source is an uncritical item, then this equipment can easily be switched off.

In the Cargo compartment, where the kind of material that might burn is unpredictable, the approach is different. Here, there is the necessity to know the non-fire case in order to reduce false warnings. So far, it has never happened in Airbus aircraft that a fire was undetected when a smoke detection system was installed. The problems are false alarms caused by cargo. To improve the false alarm rate, knowledge about environmental conditions in false alarm cases is necessary. Therefore, database studies have been conducted in order to get as much information as possible about these conditions. The results are presented elsewhere [11].



## **6. Approaches to new fire extinguishing methods and dedicated fire detection**

Water mist as halon replacement in combination with nitrogen inerting is regarded as a promising alternative to the today's extinguishing system. The use of a water mist system however implies several physico-chemical aspects which could have been neglected with gaseous systems but now have to be checked and solved. Agent freezing, short circuit prevention, weight, maintenance or smoke generation are points which have to be considered.

For weight and efficiency reasons, the water mist suppression system must be associated to a smart detection/activation system which is able to accurately detect and locate the fire and activate the suppression in adequate on/off sequences. There are several requirements for the detection system that are derived from a water mist based extinguishing system.

In order to carry only a minimum amount of water in the aircraft due to weight reasons, the extinguishing process has to be optimised. An extinguishing shall only be performed where the fire is located. This implies that the fire detection system must be able to provide a certain spatial resolution. At the moment, there is no need for such a zonal detection system because the halon extinguishing system is based on a total flood philosophy.

Furthermore, the detection system has to be waterproof because it has to monitor the fire criticality status for the total remaining flight. The extinguishing efficiency of water, even in combination with an inert gas is not comparable to the properties of halon and there is a remaining risk that the fire will light up again. So, a fire monitoring function is necessary.

The research concerning these items is being funded by the European Commission within the 5th Framework Programme FireDetEx.

## **7. Aircraft integration of new fire detection technologies**

After qualifying fire/smoke detectors for aircraft application, they have to be implemented/integrated into the aircraft environment. Current integration tests for smoke detectors are defined in the FAA Advisory Circular 25-9A [12]. The integration tests mentioned herein can be performed with appropriate smoke generators, being selected out

of the following list, depending on the actual installation point of the sensor:

- paper towel burn box
- Rosco Theatrical smoke generator
- Helium-injected Rosco Theatrical smoke generator
- A pipe or cigar
- A Woodsman Bee Smoker
- Any other acceptable smoke generator

The smoke emerging from one of those sources must be detected within one minute after the start of the fire [13]. This time includes all the necessary signal processing and transduction to display an alarm message in the cockpit.

### Consequences for new technologies

The existing authority requirements concerning integration of smoke detectors restrict the development of new approaches. An example are multicriteria/multisensor devices. Such a system needs a certain time to process a certain internal signal evaluation out of the various parameters that are recorded to come to an alarm decision. This alarm decision will be of a higher reliability, but might take a little more time.

Furthermore, the event “start of a fire” is not clearly defined. The amount of smoke produced for example by a smoke generator might be equal to the smoke emitted in a rather advanced state of a real fire. Although other parameters that represent a real fire are not reflected by an artificial smoke generator. This includes heat release in terms of radiation and convection as well as gas development.

Current developments show that gas sensing technologies have a potential to be new or additional fire detectors. At the moment, there is no integration test that is could be used for certification of such a system. A real fire test as described in AC 25-9A cannot be conducted during flight. But only a real fire has the gas constitution that is detected by gas sensors.

Fig. 5 shows a test that has been conducted to compare the response of gas sensors to a currently used smoke generator in Airbus (AX1000) and a real fire of Kleenex tissue towels. The test was carried out in a standard-layout lavatory. As sensing device a GSME smouldering fire detector as it is used for lignite power plants was examined [14]. This device comprises 3 semiconducting metal oxide gas sensors with optimized selectivity for

H<sub>2</sub>, CO and NO<sub>x</sub>. The GSME detector and its signal processing algorithm had not been modified for this test. First, the smoke generator was switched on, producing an amount of smoke labeled equal to 5 kleenex tissue paper towels. It can be seen that the gas sensor device responds very poorly with all its 3 sensors and shows a slightly decreasing signal. The aircraft optical smoke detector which was also installed, reacted after 35 seconds. The GSME was positioned near the basin, which means it was not installed where the current detector is installed. By burning 3 Kleenex, the detector showed a significant signal and the internal processing algorithm predicted a certain "fire probability" which can be used for defining an alarm threshold. Not being on its proper position yet and burning 5 Kleenex resulted in a higher signal but a similar fire probability. Afterwards, the sensor was installed into the position of the current detector and again, 5 Kleenex were burned. This time, the signal shape looked different due to changed airflow conditions the sensor was exposed to and the fire probability had a higher value. The final two peaks are two cycles of cigarette smoke, the first just normally smoking and the second smoking and blowing at the detector. Cigarette smoke shows a different signal shape than Kleenex towels and it can be seen that cigarette smoke does not result in any value for the fire probability.

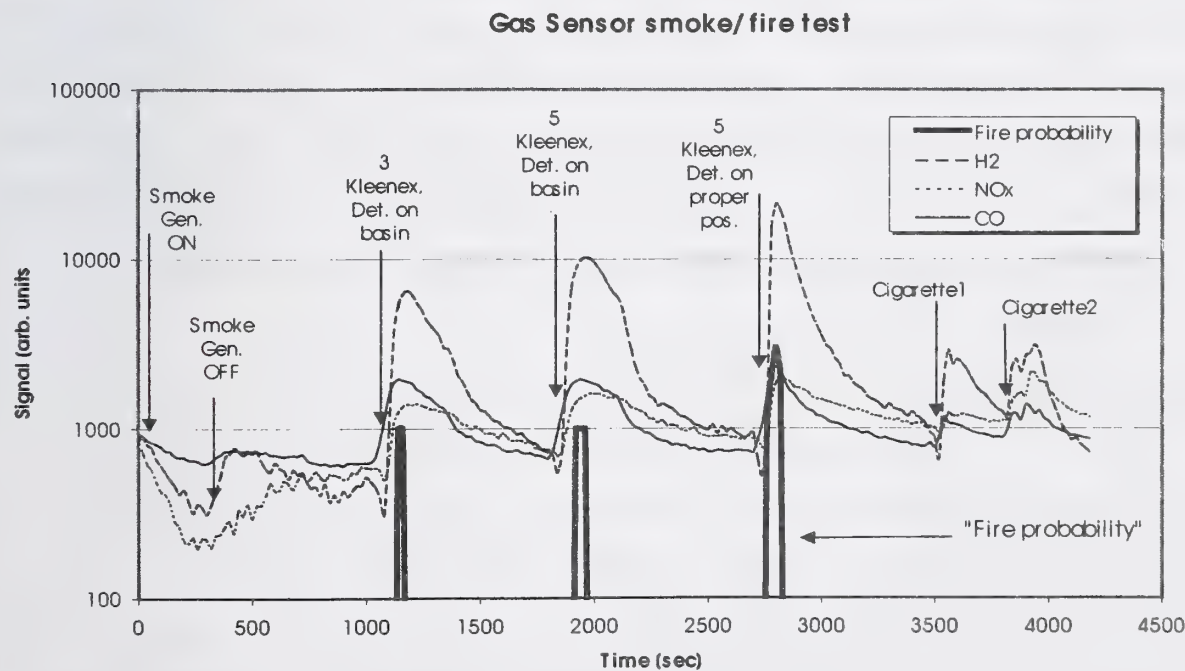


*Fig. 5: Comparison of a smoke detector test with a real fire for a gas sensor based fire detection system*



This example shows that the common smoke generator integration test is not suitable for this kind of fire detector because these types of gas sensors will never respond to this specific kind of smoke.

Only if the gas constitution of a characteristic fire is known, a gas generator might be constructed for assuring a correct integration. But in this case, all the other fire parameters will not be regarded. In this context it becomes clear, that new detection technologies need dedicated specific-to-type aircraft integration flight tests after they have proven their fire detection properties in ground tests.

## **8. Summary**

New fire detection technologies bear the potential to improve the safety of aircraft by making a fire warning more reliable and by reducing the false alarm rate. The risk of unnecessary passenger evacuations and undue emergency landings can be minimized that way. Approaches are the use of gas sensors or other multisensor/multicriteria devices as well as visualisation tools like specific cameras with associated image processing. However, the way to an aircraft integration coincides with the fulfillment of stringent environmental and many other aircraft specific requirements.

The technology that is used for fire detection instruments strongly influences the kind of testing that is necessary to validate a proper integration. For this reason the user of new fire detection instruments, in this case the aircraft manufacturing industry, has to know exactly what technology is used inside a fire detector in order to perform the right verification for demonstration of compliance with the certification requirements.

## 9. Literature

- [1] Freiling, A. Brandschutz in Airbus-Flugzeugen, S&S Report, April 2000
- [2] Gottuk, D.T., Peatross, M.J., Roby, R.J., and Beyler, C.L., "Advanced Fire Detection Using Multi-signature Alarm Algorithms," International Conference on Automatic Fire Detection "AUBE '99", 11th, March 16-18, 1999, Gerhard Mercator University, Duisburg, Germany, Luck, H., Editor, pp. 237-246, 1999.
- [3] Petig, H et al. History of Development Steps in Gas Sensor Fire Detection in RWE Powerplants for Lignite and Waste Combustion, International Conference on Automatic Fire Detection "AUBE '99", 11th, March 16-18, 1999, Gerhard Mercator University, Duisburg, Germany, Luck, H., Editor, pp. 284-294, 1999.
- [4] Müller, H.C. Rule based Detection Algorithms, Proceedings of the VdS Conference "Gas Sensors for Fire Detection", Nov. 15<sup>th</sup> and 16<sup>th</sup> 2000, Cologne, Germany, Chairing: Michael Schnell, VdS Schadenverhütung
- [5] Siebel, R. Strategies for the development of detection algorithms, Proceedings of the VdS Conference "Gas Sensors for Fire Detection", Nov. 15<sup>th</sup> and 16<sup>th</sup> 2000, Cologne, Germany, Chairing: Michael Schnell, VdS Schadenverhütung
- [6] Blake, D. Aircraft Cargo Compartment Fire Detection, International Halon Replacement Working Group Meeting, May 2000, Atlantic Hotel, Bremen, Germany, hosted by EADS Airbus GmbH
- [7] Grosshandler, W.L. (Editor), Nuisance Alarms in Aircraft Cargo Areas and Critical Telecommunication Systems: Proceedings of the Third NIST Fire Detector Workshop, December 4-5, 1997, NISTIR 6146, National Institute of Standards and Technology, Gaithersburg, MD, March 1998
- [8] Freiling, A. Requirements for Fire Detection in Civil Aviation, Proceedings of the VdS Conference "Gas Sensors for Fire Detection", Nov. 15<sup>th</sup> and 16<sup>th</sup> 2000, Cologne, Germany, Chairing: Michael Schnell, VdS Schadenverhütung
- [9] Schmötzer, K, Aircraft Fire Detection Requirements, see see this book of conference

- [10] Freiling, A, Improving Safety for Aircraft, Proceedings of the Deutscher Luft- und Raumfahrtkongress 2000, ref. DGLR-JT2000-156, Sept. 16-20 2000, Leipzig, Germany, Deutsche Gesellschaft für Luft- und Raumfahrt
- [11] Mangon, P. Fire Detection for aircraft cargo compartments, reduction of false alarms, see this book of conference
- [12] Federal Aviation Administration, Advisory Circular 25-9A, Smoke Detection, Penetration and Evacuation Tests and related Flight Manual Emergency Procedures, 1/6/94, Federal Aviation Administration, Washington DC, USA
- [13] Joint Aviation Requirements, JAR-25, Large Aeroplanes, Change 14, 27May 1994, JAA, Hoofddorp, The Netherlands
- [14] Kohl, D, Kelleter, J. Gassensor-Melder für Schwelbrände, in: Sicherstellung der Schutzfunktion von Gassensoren, A. Freiling, R. Fromm, Edts. pp. 154-165, Beuth-Verlag, Berlin, ISBN 3-410-79234-1, Dec. 1997



Philippe MANGON

CERBERUS S.A, BUC, France

## **FIRE DETECTION FOR AIRCRAFT CARGO COMPARTMENTS ,** **REDUCTION OF FALSE ALARMS**

### **Abstract**

In order to better understand the reasons for the current high false fire alarm ratio in Aeronautic Applications, an analysis of actual fire and false alarm events has been conducted using different database.

This research (funded by the European Commission within the 5th Framework Programme FireDetEx) included the following analysis :

#### **1. Analysis of false alarm cases**

A review of false fire alarm cases extracted from different data bases will be presented, For some typical cases, it will be analysed whether the alarm was triggered by a system malfunction, particular environmental conditions or by the detection of aerosol particles.

#### **2. Analysis of fire alarm cases**

Real fire alarm cases will also be considered, it will be determined what was the probable fire source, which phenomena has likely caused the ignition and what should have been the best fire sensor under these conditions.

#### **3. Definition of fire and non-fire scenario**

The fire detection system can only be improved on the basis of clear performance objectives, fire and non-fire scenario will be presented against which the performance of new fire detection concept can be measured and evaluated.

## **Introduction**

Among the various aircraft zones for which a fire protection is required, the cargo compartments are specific in this sense that their characteristics are very variable in terms of dimensions and topologies as well as environmental conditions and fire threats.

Fire sources and their combustion mechanisms and products are diversified, therefore there is no single physical parameter that would allow the detection of this wide fire spectrum with an evenly distributed sensitivity.

Under these conditions, in the currently used systems, the smoke detectors have to be adjusted so as to early detect the fire type for which their sensitivity is basically the worst (and to meet the certification requirements [1]); making them also more sensitive to environmental conditions.

Basically, a combination of several criteria to trigger a fire alarm would bring a significant benefit in terms of discrimination capabilities, provided of course that the fire and non-fire situations are well known.

Therefore in order to improve significantly the fire detection reliability, it is necessary to better understand, under this environment, the physical parameters that distinguish the start of a fire from those that are due to non-dangerous phenomenon.

# Analysis principle

Fire and false alarm events in operation were extracted from different data base [2] [3] and compiled as shown below:

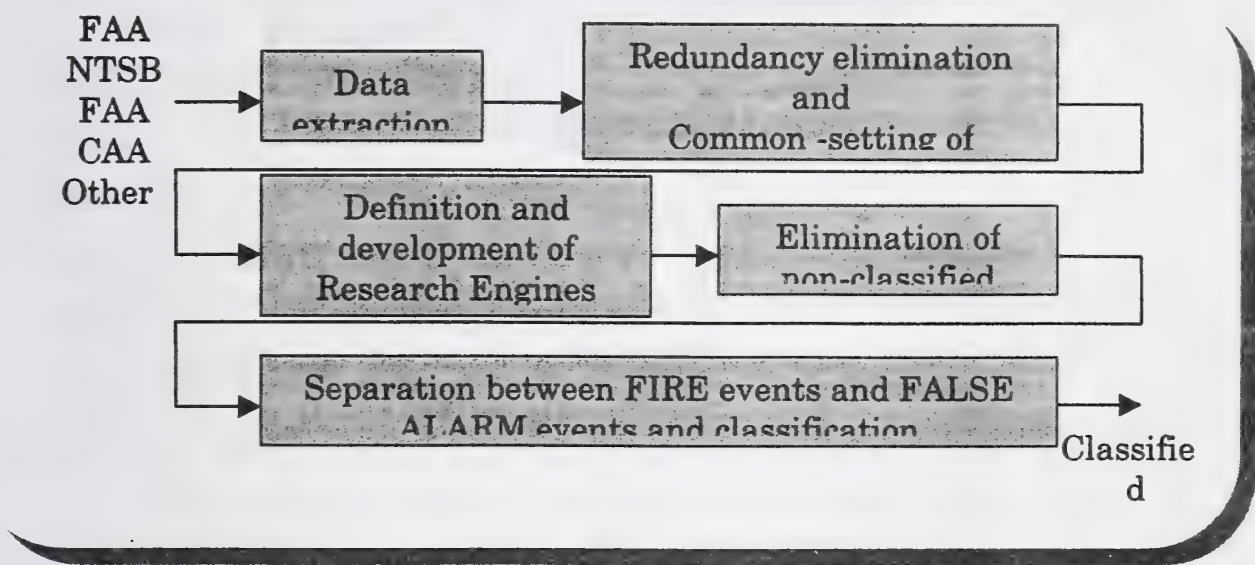


Figure 1 : Fire and false alarm events analysis

The following classification logic was applied :

FIRE FALSE ALARM	ARM	
Aircraft Flight Phase Specification Environment Conditions Atmospheric Conditions Airline Place Date Hazards Probable Cause Freight Ventilation	<div> <div>→</div> <div>Source</div> </div> <div> <div>→</div> <div>Ignition</div> </div> <div> <div>→</div> <div>Propagation</div> </div> <div> <div>→</div> <div>Non-classified</div> </div>	<div> <div>→</div> <div>System misbehaviour</div> </div> <div> <div>→</div> <div>Aerosol presence</div> </div> <div> <div>→</div> <div>Human error</div> </div> <div> <div>→</div> <div>Non-classified</div> </div> <div> <div>→</div> <div>Environment =&gt; Physical parameters</div> </div>

Figure 2 : Events classification logic

It is to be noted that at the time of the event, most of the here-above information was not recorded (and practically impossible to retrieve after).



General outcomes

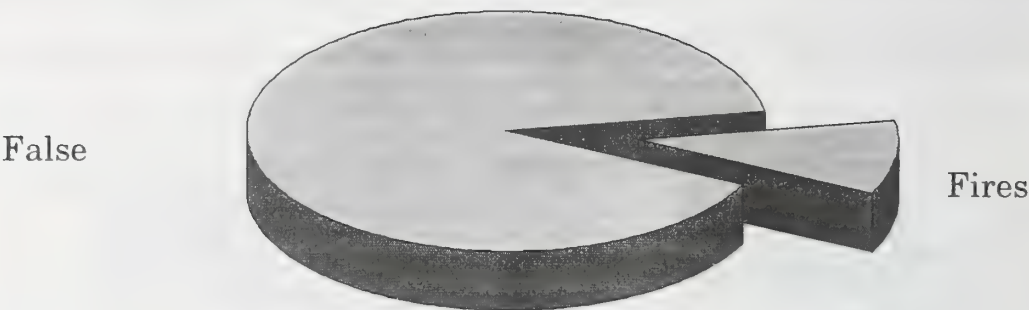


Figure 3 : Ratio fire/false alarm

In this graphic, regional aircraft are very few represented, the overall ratio (90% of false fire warnings) would be higher if this aircraft category was totally included [4].

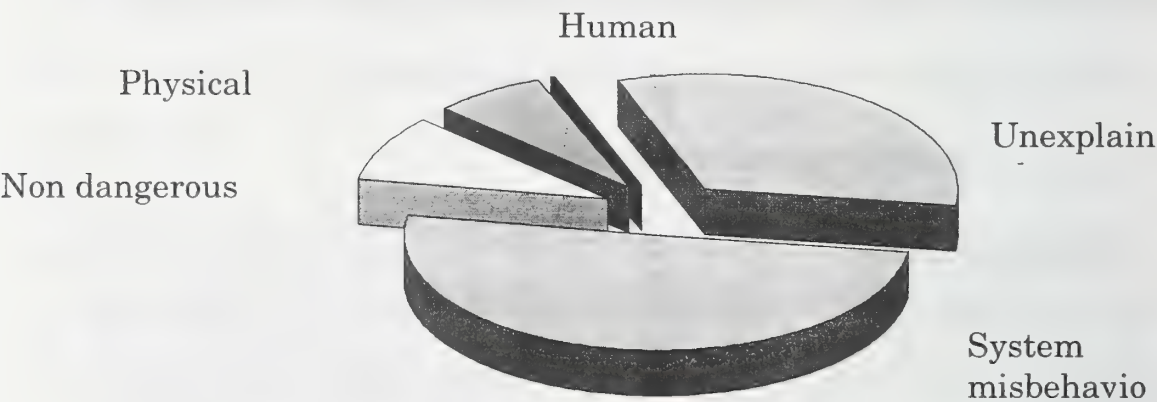


Figure 4 : False alarm analysis

In most of the cases, the conditions in the cargo compartment at the time of the alarm were not exactly known by the pilots or the crew, therefore false alarm events were often considered unexplainable or attributed to a system malfunction whereas a better knowledge of these conditions would have led to a different classification.

However, system misbehaviours under degraded situations (wiring failures, power supply failures, management of redundancies in case of

internal failures, ..) take probably a significant part in the overall ratio and have to be considered as an improvement axis.

**Analysis of typical false alarm cases**

Event 1: Description

**Date :** 21/11/1985  
**Source :** CAA (extract)  
**Aircraft Make :** BOEING B-747  
**Carrier :** NOT REPORTED  
**Phase Flight :** CRUISE

*Narrative :* Lower aft cargo hold fire warning. A/c diverted emergency evacuation. False fire warning. Following a lower aft cargo hold fire warning a/c diverted to lajes where an emergency evacuation was effected. Some difficulty due to excessive force needed to open fully doors 2 & 4 l & 2 & 5 r. Several passengers sustained minor injuries. The cause of the fire warning was attributed to condensation emanating from a considerable quantity of 'warm' fruit. The two detectors were slightly oversensitive but this is considered a very minor contributory factor. A mod has been initiated to fit a dual loop smoke detector system.

Probable environmental conditions at the time of event 1

Physical parameter	Temp	Humid/ Condens s	Radiat	Combu st Aerosol s	Other Aerosol s	Comb gases	Other gases
Probable level	Low	High	Low	Low	Mediu m	Low	High

## Event 2: Description

**Date :** 23/10/1998  
**Source :** AIRBUS (extract)  
**Aircraft Make :** AIRBUS A-340  
**Carrier :** SABENA  
**Phase Flight :** TAKE OFF

*Narrative :* At 4000 ft with configuration 1 forward cargo smoke red alarm came on. According to ec procedures the fwd cargo cooling was switched off. The switch was pre in max. One minute later the alarm went out. Visual check performed and confirmed neither smoke nor fire in the fwd compartment. Flight was continued. During cruise at flight level 290 lavatory sm warning came on. Toilet g1 triggered this alarm a lot of times. Visual confirmed nobody inside the toilet and no smoke evidence. Action: maintenance inspected fwd cargo and lavatory and did not find any indi of fire or smoke. Investigation related to oil smell in cabin revealed 3 oil quantity lower than on other engines. Suspected oil suction to air system. Deactivated engine 3 bleed system switch SDCU and smoke detector test were satisfactory. The next flights were also performed with engine 3 bleed off and oil consumption was monitored and found within limits. On ground in bru when switching APU bleed on smoke appeared in cabin cockpit. Smoke disappeared after switching off pack 2. Smoke did not with pack 2 on afterwards. Problems suspected to come from APU pneumatic duct. Maintenance found oil leak on filter bowl. O'ring replaced and leak check performed. Engine 3 bleed system was reactivated.



Probable environmental conditions at the time of event 2

Physical parameter	Temp	Humid/ Conden s	Radiat	Combu st Aerosol s	Other Aerosol s	Comb gases	Other gases
Probable level	Low	Low	Low	Mediu m or High	Low	Low or mediu m	Low

**Analysis of fire alarm cases**

Event 3: Description

**Date :** 20/03/1991

**Source :** FAA INCIDENT DATA SYSTEM

**Aircraft Make :** LKHEED L-188-C

**Carrier :** REEVE ALEUTIAN AIRWAYS INC

**Phase Flight :** FCD/PREC LDG FROM CRUISE

**Narrative :** Dense fumes in cargo compartment. Diverted and landed.

Smoke from box marked fish that contained batteries.

Probable environmental conditions at the time of event 3

Physical parameter	Temp	Humid/ Conden s	Radiat	Combu st Aerosol s	Other Aerosol s	Comb gases	Other gases
Probable level	Low	Low	Low or Mediu m	Mediu m	Mediu m or High	Mediu m	Mediu m or High

#### Event 4: Description

**Date :** 05/09/1996

**Source :** NTSB AVIATION ACCIDENT/INCIDENT DATABASE

**Aircraft Make :** DOUG DC10-10F

**Carrier :** NOT REPORTED

**Phase Flight :** CRUISE

*Narrative :* The airplane was at fl 330 when the flight crew determined that there was smoke in the cabin cargo compartment. An emergency was declared and the flight diverted to newburgh/stewart international airport and landed. The airplane was destroyed by fire after landing. The fire had burned for about 4 hours after smoke was first detected. Investigation revealed that the deepest and most severe heat and fire damage occurred in and around container 6r which contained a dna synthesiser containing flammable liquids. More of 6r's structure was consumed than of any other container and it was the only container that exhibited severe floor damage. Further 6r was the only container to exhibit heat damage on its bottom surface and the area below container 6r showed the most extensive evidence of scorching of the composite flooring material. However there was insufficient reliable evidence to reach a conclusion as to where the fire originated. The presence of flammable chemicals in the dna synthesiser was wholly unintended and unknown to the prepared of the package and shipper. The captain did not adequately manage his crew resources when he failed to call for checklists or to monitor and facilitate the accomplishment of required checklist items. The department of transportation hazardous materials regulations do not adequately address the need for hazardous materials information on file at a

carrier to be quickly retrievable in a format useful to emergency responders.

Probable environmental conditions at the time of event 4

Physical parameter	Temp	Humid/ Condens s	Radiat	Combu st Aerosol s	Other Aerosol s	Comb gases	Other gases
Probable level	High	Low	Mediu m or High	High	Low or Mediu m	High	Low

**Definition of fire and non-fire scenario**

Some fire and non fire scenario are presented here-below as possible development tests for fire detection systems.



<b>Fire cases</b>	
<ul style="list-style-type: none"> <li>• Open cellulosic fire (wood) : EN 54 - TF1 [5]</li> <li>• Smouldering pyrolysis fire (wood) : : EN 54 - TF2</li> <li>• Glowing smouldering fire (cotton) : : EN 54 - TF3</li> <li>• Open plastics fire (polyurethane) : : EN 54 - TF4</li> <li>• Liquid fire (n-heptane) : : EN 54 - TF5</li> <li>• Liquid fire (methylated spirits) : : EN 54 - TF6</li> <li>• Paper (UL268) : -Paper towels (open) -Scheduled newspapers (open) -Normal newspapers (open) -Normal newspapers (smouldering)</li> </ul>	<ul style="list-style-type: none"> <li>• Cardboard boxes : -Open cardboard fire -Smouldering cardboard fire</li> <li>• Textile : -60 % Wool / 40 % Acrylic (open) -60 % Wool / 40 % Acrylic (smouldering) -100 % cotton (open) -100 % cotton (smouldering) -100 % polyester (open) -100 % polyester (smouldering) -100 % wool (open) -100 % wool (smouldering)</li> <li>• Jet A fuel fire</li> <li>• Diesel fire</li> <li>• Oil fire</li> <li>• Cable fire</li> </ul>
<b>Non fire cases :</b>	
<ul style="list-style-type: none"> <li>• Moisture</li> <li>• Condensation</li> <li>• Fog</li> <li>• Sand and Dust</li> </ul>	<ul style="list-style-type: none"> <li>• Fruit / Animals / Vegetables</li> <li>• Oil</li> <li>• Exhaust gas</li> </ul>

Tableau 1 : Fire and non - fire scenario

## Summary

The exploitation of actual fire alarm events is tricky because most of the time, the parameters recorded at the time of the event do not allow to determine the condition for which the alarms were triggered and can even lead to wrong conclusions.

However this analysis has allowed us to clarify some typical fire and non-fire situations and to outline performance tests accordingly.

Fire sources are extremely diversified and, in particular the materials involved are most of the time unexpected or even normally forbidden as cargo loads. As well their combustion products or effects are variable with, according to the event, predominance of different physical parameters.

False alarm sources are also diversified, in some cases the corresponding single physical parameters are very close to those that characterise the start of a fire.

Under these conditions, the adjunction of several detection criterion can increase considerably the discriminatory capabilities of the fire detection systems.

The dynamic of the various signals has to be taken into account in the fire alarm decision as an additional discriminatory factor, for this a minimum analysis duration is necessary which is very often not compatible with the current certification criteria (considering in particular the propagation time of the combustion products).

Performance development or qualification tests must be on one hand feasible under well controlled metrological conditions and on the other

hand representative of a large range of realistic fire and non – fire situations.

## **References**

- [1] Schmoetzer, K . Aircraft Fire Detection: Requirements, Qualification and Certification Aspects, see this book of conference.
- [2] FAA In service events Data Base.
- [3] NTSB In service events Data Base.
- [4] Blake, D. FAA Technical Center, Fire Safety Section, Report No DOT/FAA/AR-TN0029, June 2000.
- [5] EN 54-9 Components of automatic fire detection systems Part 9 Methods of test of sensitivity to fire“.



## **The Cargo Fire Monitoring system (CFMS) for the visualisation of fire events in aircraft cargo holds**

### **1 Introduction**

Fire on board of an aircraft represents one of the most dangerous in-flight situations. Following a fire alarm from the freight compartment, the pilot is obliged to immediately activate the fire suppression system before proceeding with an emergency landing.

Up to now, detection of fire has most always meant the detection of smoke by threshold devices like photoelectric or ionisation smoke detectors. These devices are trouble-prone and lead to a reported rate of up to 200:1 false to genuine alarms [1]. Blake surveys fire alarms in aircraft cargo compartments from the last 25 years and finds that both the number of false alarms and the ratio of false to real alarms is steadily increasing [1]. This is also due to the conversion of class D to class C compartments, resulting in an increased overall number of fire detection units. This high rate of false alarms is unacceptable, as an alarm, followed by a diverting and landing at nearest suitable airport, causes high costs of approximately \$50,000 [1] and is possibly connected with a higher safety risk due to a variety of factors such as unfamiliar airports, less effective navigational aids, shorter runways, inferior fire fighting and the loss of the cargo load. Fire alarm may entice the pilot to an inadequately riskily landing, for example ditching on water during an over-water flight, and generally limits the credibility of fire alarm systems. Nevertheless, an unnecessary use of the fire suppression system often results, for the moment, still in an unwanted release of Halon 1301, which is identified as one of the substances contributing to stratospheric ozone depletion.

Additionally, with common threshold detectors used in "air tight" cargo areas, the smoke alarm equipment will continue to report an alarm condition, even if the fire has been extinguished by the suppression system. Thus, the pilot has no chance to know, if a fire has been extinguished or if it is even continuing to grow. This situation is found to

be unsatisfying and it is stated, that the pilot should have better and more reliable information about the cargo compartment status, especially about the fire growth and the effectiveness of fire suppression actions [2].

Cleary and Grosshandler [3] provide a broad survey on fire detection in aircraft cargo compartments, especially concentrating on the more common fire detection methodologies.

Digital imaging more and more becomes a means for the detection of fires [4-8]. Very early, Goedeke et al. [5] describe a detection system which is capable to detect open fire sources. Ultraviolet and infrared detectors produce event signals, an image processor then evaluates images from a colour video camera to determine bright area objects to confirm the fire event. In a detailed approach, Foo [6] applies a rule-based machine vision approach to detect and categorize hydrocarbon fires in aircraft dry bays and engine compartments. A set of heuristics based on statistical measures derived from the histogram and image subtraction analyses of successive image frames is used to differentiate between the fire and the non-fire status. Cheng et al. [7] propose a new video fire detection system and examine the underlying principles of a video based fire detection system in a more general way. They mainly conclude that fire detection could be carried out with the same video unit as the regular video observation and that is well suited for the fire detection in large spaces like warehouses. Another approach uses a colour video camera to monitor temperature and species sensitive sensors which change colour at a prescribed temperature or carbon monoxide concentration [8].

Fire detection by digital imaging is fast, can cover wide areas of observation and additionally allows visual inspection, e.g. in the case of an alarm. Most often, only the visible or infra-red radiation of a fire is monitored, which limits the detection to open fire sources. This is unsatisfactorily, because smouldering fires might remain undetected for long periods of time, containing a high risk of a sudden turning to a large open fire.

To partly overcome these restrictions, a new fire detection system based on digital imaging (CFMS) is introduced which creates the basis for an in-flight cockpit video sur-

veillance system, combined with fire detection capabilities. It allows the fast detection of both open and smouldering fires and additionally the verification of fire alarms given by other, standard fire detection systems and the monitoring e.g. of fire growth and fire suppression actions in closed spaces like in aircraft cargo compartments. Deviating from most approaches, a fire can be detected and monitored even when the flame itself is not visible. This is done by a combination of a special illumination technique and a digital imaging algorithm which is capable to clearly emphasise the relevant fire signatures. These signatures include smoke and its characteristic properties, the visible light emitted from the fire and reflected from the walls and characteristic periodic phenomena like fire flickering.

The underlying concepts of this novel video-based fire detection system are described in detail and the advantages and limitations are discussed. To evaluate its efficiency, results are presented from experiments that were conducted in a mock-up of a typical aircraft cargo compartment.

If a fire is detected, it is very useful to have the opportunity to visually inspect the compartment. Unfortunately, it is almost not possible to perceive relatively small amounts of smoke. This is especially true if the scene is observed through a small gap as it is the case with containers loaded into the compartment (Fig. 8a) or the smoke develops slowly because human vision adapts on the slowly changing scene. Therefore, an algorithm is presented to drastically enhance the visibility of smoke or fire respectively and is discussed.

## **2 Experimental**

Experiments are performed in a compartment as figured in Fig. 1. Various configurations, varying in the test fires used and the underlying set-up of lamps, cameras and the fire places were implemented from which a small selection is presented here (Table 1). The cargo compartment is monitored with a camera and the video stream is captured both real-time with a computer device and on tape.



### 2.1 Test location

The tests are performed in a mock-up of an Airbus A340 cargo compartment (Fig. 1), both in an empty (unloaded) cargo room and with two containers loaded into the compartment which confine the camera's field of view to a narrow band of 7 cm height. The difference between the two implementations is that in the case of the unloaded cargo freight, the fire, which is located on the floor, lies within the camera's field of view. In the other case, the camera peers through the gap between the compartment ceiling and the container's top, which makes the proper detection of fire more complicated because the fire can only be observed indirectly by the ascending smoke and the reflections of the fire glow.

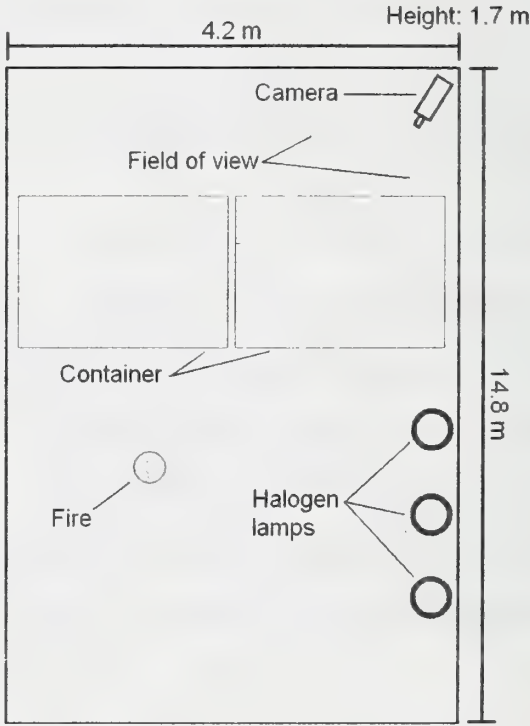


Fig. 1: Cargo bay mock-up (Airbus A340) as used within the framework of the fire tests

2.2 Test fires

Three test cases are defined in Table 1. The two mentioned test fires are described below.

2.2.1 Smouldering wood fire

About 25 pieces of birch wood (Dimensions 3.5 x 1 x 2 cm<sup>3</sup>) are placed on a heating plate which is provided with concentric ribs. Smoke of bright colour is produced after approx.. 3-5 min of heating

2.2.2 Open polyurethane foam fire

Two layers of polyurethane foam (Dimensions 25 x 25 x 2 cm<sup>3</sup>) are stacked one above the other and are ignited. A bright flame develops which produces large amounts of dark smoke.

Test case	Test fire, according to EN-54 [9]	Fire-type	Material	Container
1	TF4	open plastic fire	polyurethane foam	no
2	TF4	open plastic fire	polyurethane foam	yes
3	TF2	smouldering pyrolysis	wood	yes

Table 1: Definition of test cases 1-3

2.3 Imaging system, cameras and illumination

Regular BAS-video cameras in combination with a computer are used to record the scenes in digital form. Halogen lamps illuminate the scene. The set-up is shown in Fig. 1. It is noticeable that the lamps illuminate the scene indirectly in the sense of a dark-field illumination. This permits the visualisation not only of the open fire but of the smoke too, which would be invisible without lighting.

## 2.4 Image processing

Foo [6] describes the basis for a fire detection system based on digital imaging and statistical analysis of the frames.

Among other, the mean  $\bar{g}$  and the standard deviation  $\sigma$  of the pixel values of one image are identified as parameters that determine whether a fire is likely or is not.

The mean  $\bar{g}$  is defined as follows:

$$\bar{g} = \frac{\sum_{i=1}^n g_i}{n} \quad (1)$$

The standard deviation is defined as:

$$\sigma = \sqrt{\frac{\sum_{i=1}^n (g_i - \bar{g})^2}{n - 1}} \quad (2)$$

A fire is likely if the mean  $\bar{g}$  of the image pixels is high, according to a very well lit room. A large standard deviation  $\sigma$ , which means that there are bright spots on dark background, then verifies the fire.

A fire is unlikely if the mean  $\bar{g}$  and the standard deviation are both low. Thus, to detect a fire, the time-dependent mean and the standard variation is monitored and a fire alarm is released if the change exceeds the pre-determined thresholds.

For the enhancement of smoke visibility, it is necessary to have a reference image. This can be calculated as the mean of the time series of undisturbed images, recorded in the non-fire-case. The actual image is first smoothed and then subtracted from the reference image, yielding after suitable thresholding the smoky areas as bright regions, which can be superimposed with the actual image to result in an image which can be easily interpreted (Fig. 8).



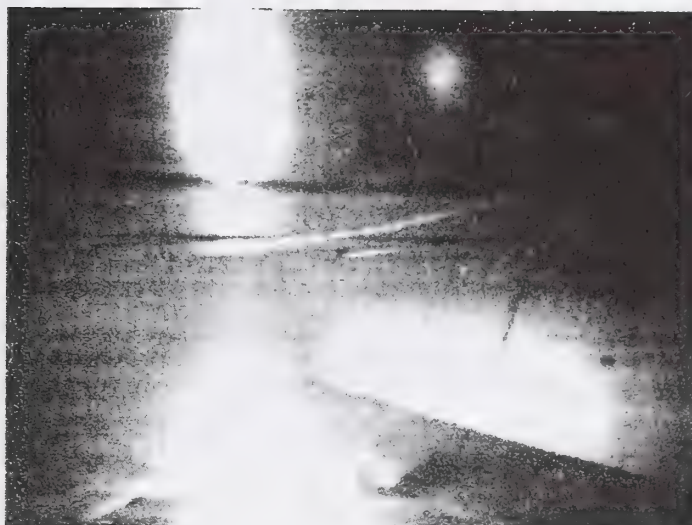


*Fig. 2: Fire according to Test-case 1, 180 s after beginning of experiment*

*a)*



*b)*



*Fig. 3: Fire according to Test-case 2, viewed through the gap between container and ceiling. The fire itself is hidden.*

*a) Before fire is ignited.*

*b) 100 s after beginning of experiment, fire is fully developed.*

### **3 Results and Discussion**

For various test cases (cf. Table 1), time-dependent sets of the mean  $\bar{g}$  and the standard deviation  $\sigma$  are computed. The results are shown in Fig. 4-Fig. 6.

For test case 1 (polyurethane fire without container, Fig. 2), there is a good response of both the mean  $\bar{g}$  and the standard deviation  $\sigma$  (Fig. 4) to the fire. The mean approximately doubles and the standard variation rises by a factor of 3.

For test case 2 (polyurethane foam fire with container, Fig. 3), the response is much smaller, what could be expected due to the smaller relative image region where the fire itself or its luminosity is visible (Fig. 5).

In test case 3, the mean is approximately constant while the standard variation rises about 20% (Fig. 6). This is quite small compared with the test cases 1 and 2 but significant in relation to the statistical fluctuations of the values  $\sigma(t)$ . Nevertheless, it has to be considered the relatively small amount of smoke produced in that experiment.

The response function can be improved if the image region is divided into separate, non-overlapping windows and the calculation of the mean and the standard variation is done for each individual window. To demonstrate, for test case 3 the image is divided into 4 sub-windows, 2 in the horizontal direction and 2 in vertical direction and statistical data is calculated for each sub-window. In Fig. 7, the calculated mean for the 4 single windows is presented.

It can be recognized, that the mean of the windows in the image's upper half (window (1,1) and (2,1)) remain constant because the regions mapped by two windows are not affected by changes induced by the developing fire. The mean in the lower left window (1,2) grows around 4% and the mean in the lower right window (2,2) lowers about 3%, which is significant compared to the variation range of the undisturbed values  $\bar{g}(t)$ . The increase is due to the illumination of the smoke by the halogen lamps which are located on the left hand side of the image. The decrease in the lower right window can be explained with the light attenuation from the left to the right.

In Fig. 8 a comparison between a source image and the processed image is presented, where the smoke is emphasized to improve its visibility. From this example it is obvious that this emphasis leads to a better observability of the fire situation, allowing a better estimation whether a fire alarm is real or is not and, if the alarm is real whether there's a large open fire or a less dangerous smouldering fire.

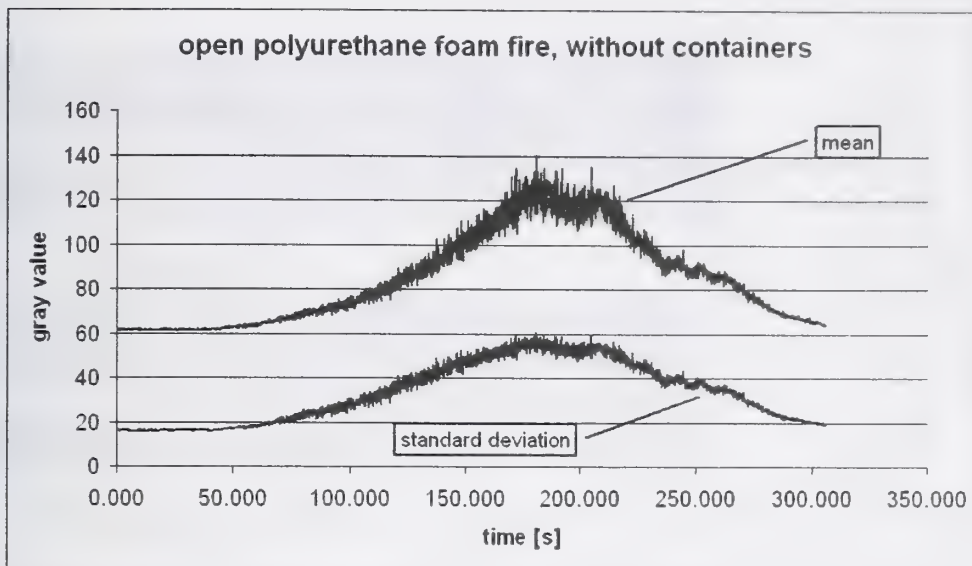


Fig. 4: Time-dependent mean and standard deviation for an open polyurethane foam fire, without containers (Test case 1).

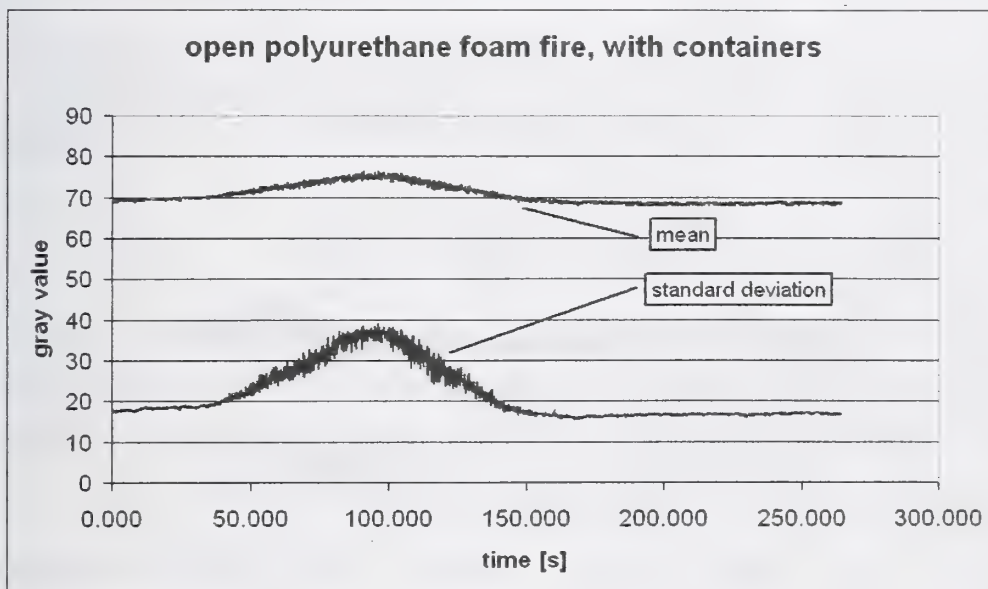


Fig. 5: Time-dependent mean and standard deviation for an open polyurethane foam fire, with containers (Test case 2).



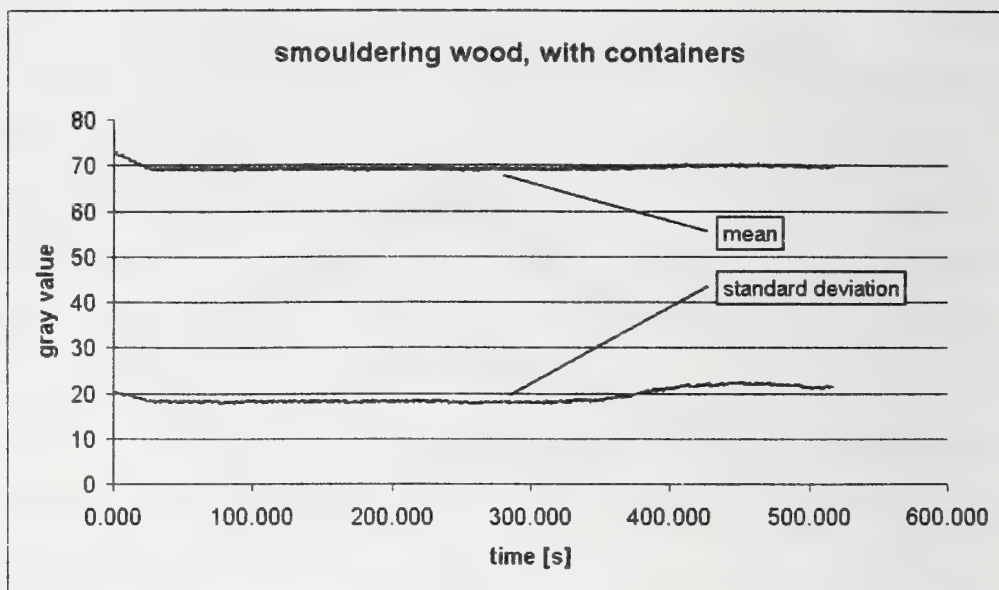


Fig. 6: Time-dependent mean and standard deviation for a smouldering wood fire, with containers (Test case 3).

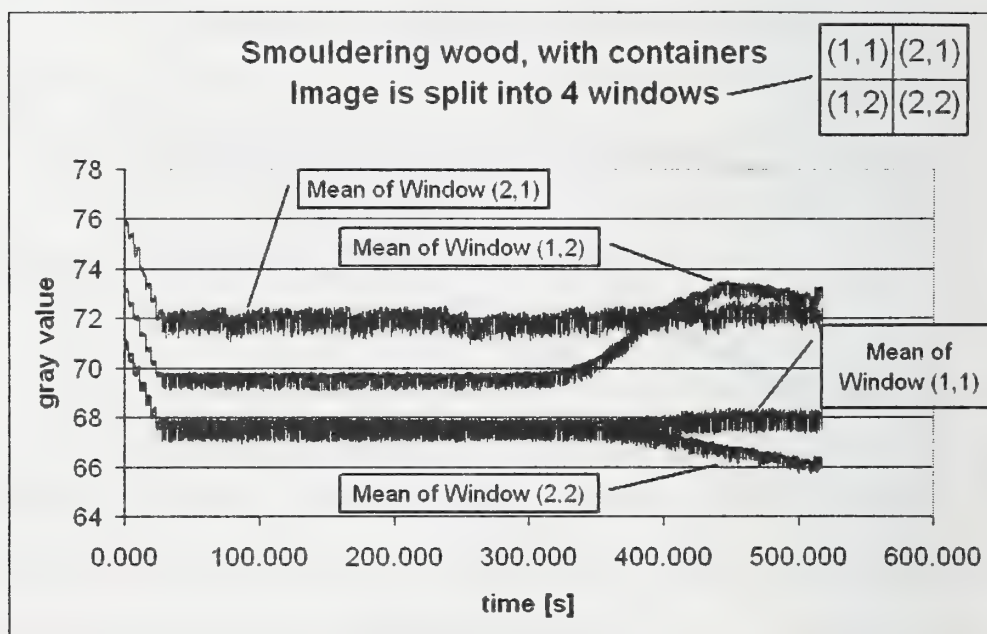
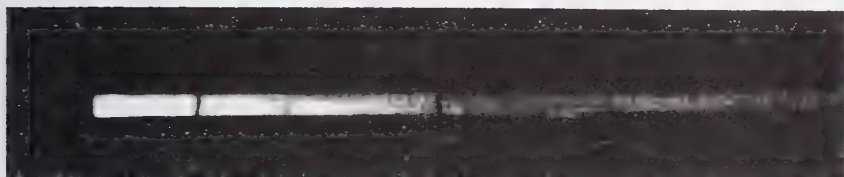
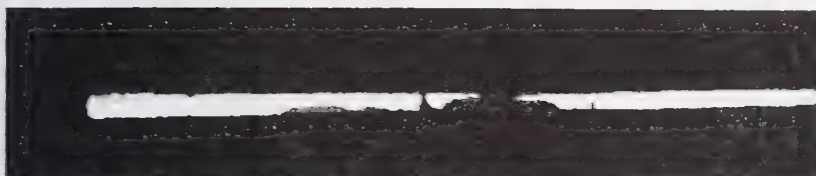


Fig. 7: Time-dependent mean for a smouldering wood fire, with containers (Test case 3). The image is split into 4 Window, each covering one quadrant of the image region. Thus, Window (1,1) is the upper left, Window (2,2) the lower right.

a)



b)



*Fig. 8: Fire according to test-case 3 (smouldering wood fire,  $t = 400$  s after start of the experiment), seen through the gap between the container's top edge and the ceiling.*

*a) Original image.*

*b) The produced smoke is reliably detected and is masked bright white.*

## 4 Summary and Outlook

The novel CFMS concept is capable to detect fires by means of a computer-based imaging system. It is able to detect both smouldering and open fire sources, even when the fire source is hidden, e.g. behind containers and if the fire produces only small amounts of smoke. From these first experiments it can be expected that the CFMS system can become a reliable fire detection tool, which provides the possibility to visually inspect the monitored compartment as an add-on, both to verify a fire alarm or, in the non-fire-case, to serve e.g. as monitoring equipment. The conducted experiments clearly demonstrate that a "naked eye" detection of fire signatures, e.g. smoke, from the captured sequences is very failure prone.

This new concept will lead to a significant improvement in the detection and observation of cargo compartment fires and the results encourage further studies.

## 5 Symbols

$\bar{g}$	Mean of pixel values
$g_i$	Pixel value
$n$	Number of pixels in an image
$\sigma$	Standard deviation

## 6 References

- [1] Blake,D., Aircraft Cargo Compartment Smoke Detector Alarm Incidents on U.S.-Registered Aircraft, 1974-1999, DOT/FAA/AR-TN00/29, Federal Aviation Administration, Atlantic City, NJ
- [2] Phillips,T., Cabin & Fire Safety: A Perspective From the Cockpit, International Aircraft Fire and Cabin Safety Research Conference, Atlantic City, NJ (1998)
- [3] Cleary,T., Grosshandler,W., Survey of Fire Detection Technologies and System Evaluation/Certification Methodologies and Their Suitability for Aircraft Cargo Compartments, NISTIR 6356, NIST, Gaithersburg, MD (1999)
- [4] Audoin,L., Kolb,G., Torero,J.L., Most,J.M., Fire Safety Journal 1995; 24:167-187
- [5] Goedeke,A.D., Droa,B., Viglione,S., Gross,H.G., Fire detection systems, US-Patent 5'153'722 (1992)
- [6] Foo,S.Y., Knowledge-based systems 1996, 9:531-540
- [7] Cheng,X., Wu,J., Yuan,X., Zhou,H., Fire Safety Journal 1999; 33:57-69
- [8] Plumb,O.A., Richards,R.F., Development of an Economical Video Based Fire Detection and Location System, NIST GCR 96-695, NIST, Gaithersburg, MD (1996)
- [9] EN54: Components of Automatic Fire Detection Systems, European Comitee for Standardisation, July 1982



G.BOUCOURT

LATECOERE 135 rue de Périole 31079 Toulouse Cedex

05/France gerard.boucourt@latecoere.fr

### **Two dimensional multi detection fire sensor, system architecture & performances**

The problem of today's fire sensor systems in aircraft is the fact that false alarms occur, and that there is no possibility to monitor the efficiency of fire extinguishing nor the cargo compartment itself.

Today, in most cases one dimensional or spot-type smoke detectors are used. The only fire parameter that is detected by these sensors is smoke. A fire can be seen as a hot point (smoldering fire), a flame or smoke. In some cases, depending on the kind of fire, smoke comes later than a certain degree of radiation. One dimensional smoke detectors need to be exposed to high energetic phenomenon to reach the sensor. In other cases detection comes later again.

False fire alarms in aircraft cargo compartments can be caused by interferences detected as a fire like mist, dust, environmental conditions, particles.

Time to detection could be too long due to the fact that the technology applied covers only some aspects of a fire and the detector covers a small area of the cargo bay and not a volume.

A real status of the cargo after or while extinguishing is not yet available to the pilot. Only a binary information correlated with a remaining probability of uncertainty is transmitted to the cockpit.

In order to improve overall fire detection system efficiency in a/c while decreasing pilot stress during fire alarms procedures, we propose a new sensor technology, associated to measurement and detection signal processing to be part of a confirmation system.

Part of the research has been funded by the European Commission within the 5th Framework Programme FireDetEx.

## **1. Sensor technology & architecture**

The purpose of the sensor is to identify all of the phases of a fire and therefore, consequentially, hot spots, flames and smoke.

The different phases of a fire are as follow:

Smoldering fire: period during which heating begins and gasification occurs.

Start of chemical reaction: period during which complete development of pyrolysis occurs. The ignition point sets off the beginning of combustion. Smoke emission and moderate convection are observed.

Flame: fast exothermic reaction covering the beginning of the flame and the completely developed fire:

- radiant energy generated around the flame,
- thermal convective energy,
- smoke emission (important for hydrocarbons).

For the detection of hot spots and measurement of radiant energy emitted by the flame, the use of infrared detectors is required. In addition, fire resistance of materials used in bays (lining) is 850°C over 15s. The device must therefore be capable of detecting temperatures well below the resistance of the materials.

Space coverage for detection must be close to 100%. This necessitates the use of two-dimensional sensors providing coverage of a significant solid angle.

The detector chosen will therefore be a 2D sensor.

The entire principle of thermo graphic cameras is based on the emission of the black body emission. The spectral response of the black body has been determined by Planck and is expressed in the following equation:

Eq.1 
$$E_{\lambda,b}(\lambda,T) = \frac{C1}{\lambda^5 [\exp(C2 / \lambda.T) - 1]}$$

$C1=3.742 \times 10^8 \text{ W } \mu\text{m}^4/\text{m}^2$

$C2=1.439 \times 10^4 \text{ } \mu\text{m.K}$

The response of the thermo graphic camera is the superposition of the spectral response of the black body with the spectral response of its sensor.

Transmission through particles:

Monochromatic transmission through spherical particles can be expressed by the following equation:

Hypothesis:

- Monodisperse distribution (the particles are all the same size).
- the particles are nonabsorbent (ex: water).

Eq.2 
$$\tau=e^{-(\pi N.a^2.Q).X}$$

with:

- N number of particles
- a particle rays

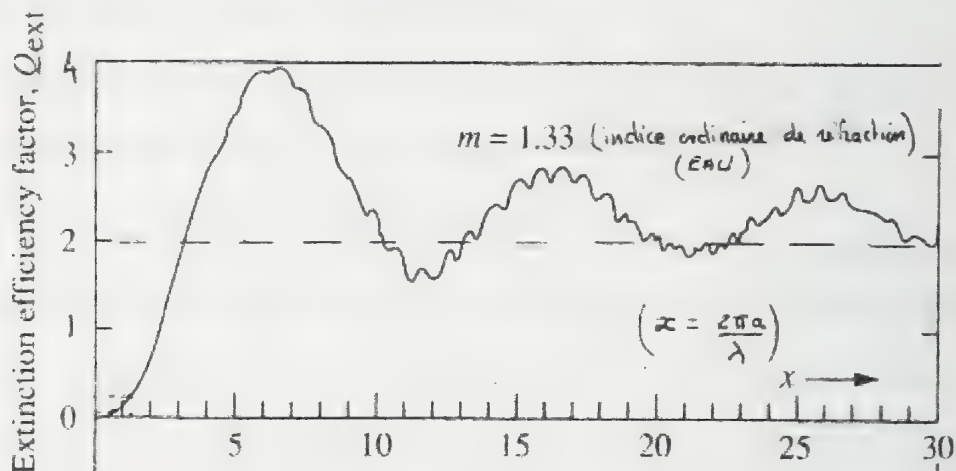


- Q effectiveness factor
- X path
- x size indicator

Eq.3  $x = \frac{2\pi a}{\lambda}$

The effectiveness factor is determined in the graph below.

Fig.3



For particles of this size, transmission is significantly degraded with the wavelength. Attenuation will be increasingly greater as particles are bigger, keeping in mind that particle sizes are from 0.01 to 100 $\mu$ m.

Selection of a technology for the FDVS program:

The choice of a technology is influenced by:

- The environment : On-board 2D sensors, due to the necessity of protecting them from the outside environment (moisture, pressure, temperature), look through a window (the 2D sensor is placed in a heated, pressurized zone or in a watertight case fitted with a viewing window).

- The precision of measurement at temperature : For measurements of temperatures in range of fire , 2D sensor working in VSW (Very Short Wave 0.4-2.7  $\mu\text{m}$ ) spectrum yield more precise results than do traditional infrared cameras. The uncertainty on the emissivity affects results of VSW 2D sensor measurements less.

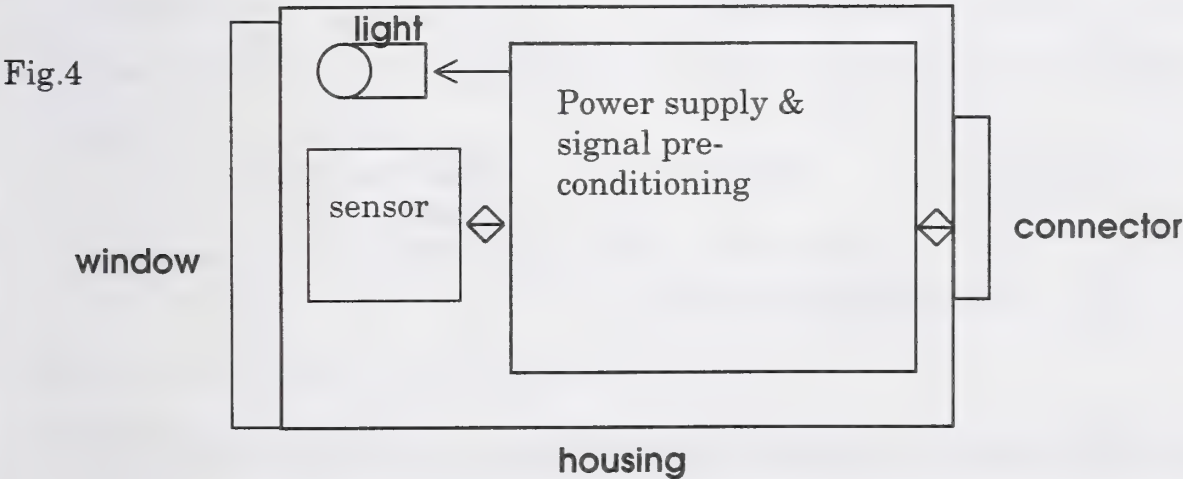
In addition, given that the emissivity of metallic materials tends to increase as wavelength decreases, this brings yet another advantage to measuring the temperatures of these materials with VSW 2D sensor when they are operating at temperatures greater than 500°C.

- The transmission (taking the size of smoke or fog particles into account), which is better in the VSW band and which therefore provides a better smoke detection.

- The cost: the cost ratio between the three sub-bands is approximately the following:

$$\text{VSW} = \text{x1}, \text{SW} = \text{x50}, \text{LW} = \text{x150}$$

CVSU architecture



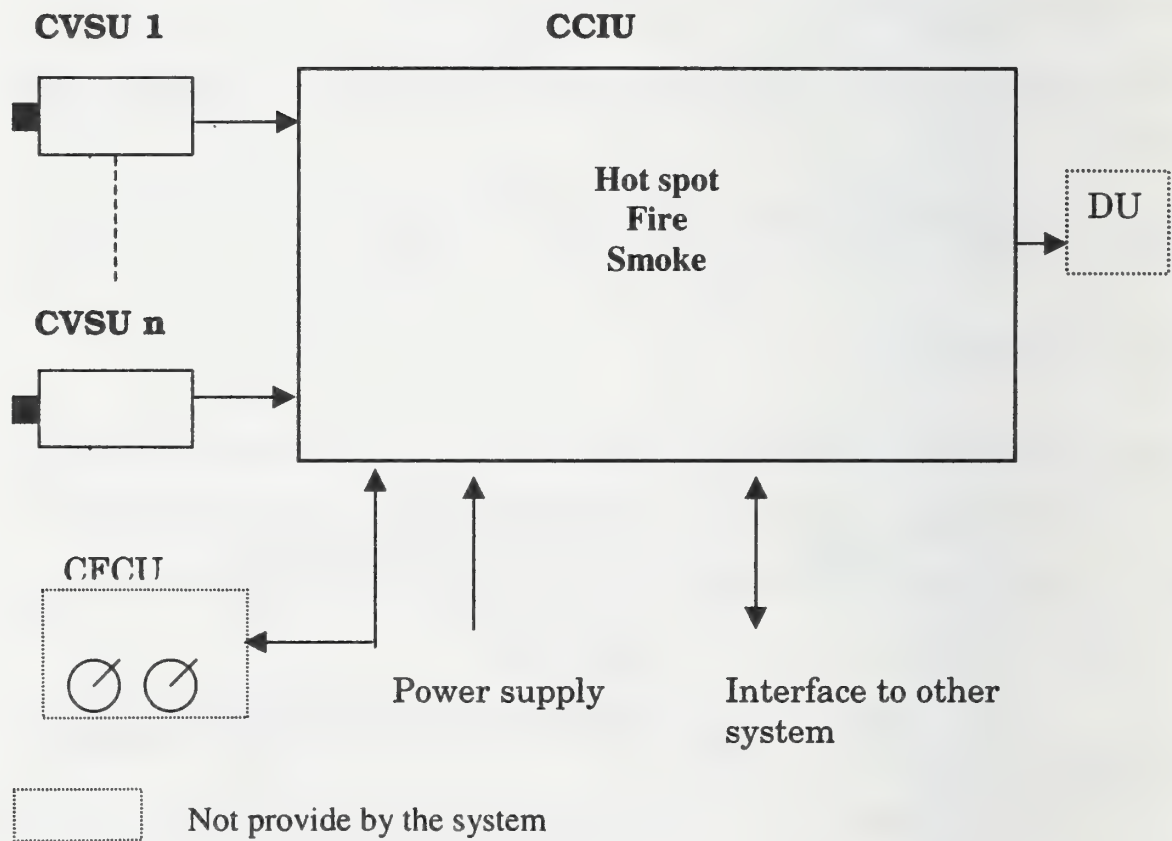
The sensor is composed of :

- 1 two dimensional sensor and its lens,
- 1 power supply, signal pre-conditioning
- 1 sealed housing with front window & connector

2- System architecture

Schematic diagram of the system.

Fig.5



The FDVS system is composed of two different equipment, CVSU& CCIU:

- Cargo Viewer & Sensor Unit (CVSU) is the hot spot, fire & smoke sensor but also provide images for the visualisation in the cockpit. The CVSU



makes detection, visualises the cargo (image capture), lights the cargo. The CVSU includes a power supply, a 2D sensor and its signal pre-conditioning, a viewing window. The CVSU has an electrical interface to the CCIU. The CVSU is interfaced to the power supply of the a/c and mechanically with the lining of the cargo compartment & structure.

- Cargo Camera Interface Unit (CCIU) is the computation of the system. It controls and interfaces with sensors and processes all signals delivered from the sensors. It interfaces to other systems: primary fire/smoke detection system, a/c flight warning system, power supply, maintenance system, extinguishing system. The CCIU processes information's (visualisation mode, detection mode), acquires information from sensors, switches the sensors, processes hot spot, smoke & fire information's, realises self control and reporting to maintenance system (BITE), processes warning, exchange data with other systems ( primary smoke/fire system, power supply, maintenance system, ventilation system, flight warning system, extinguishing system).The CCIU realises the Man Machine Interface, controls the image on relevant display unit, controls the lights on its front panel. The CCIU is interfaced to the power supply of the a/c and mechanically to electronic bay.

In case of warning from the primary system the FDVS system provides automatically to the cockpit display, a cargo compartment view including computation information.

Display Unit (DU) located in the cockpit performances

Maximum time response to hot spot event < 10 s

Maximum time response to smoke event < 10 s

Maximum time response to fire event < 60 s

## AIRCRAFT INSTALLATION

An example of the aircraft installation could be:

Fig.6

top view

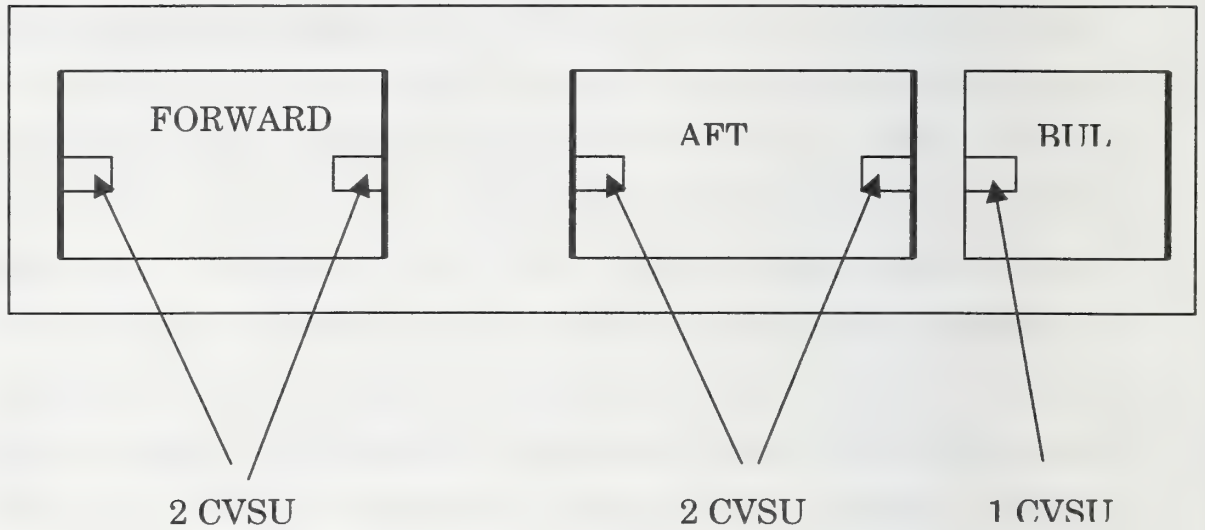
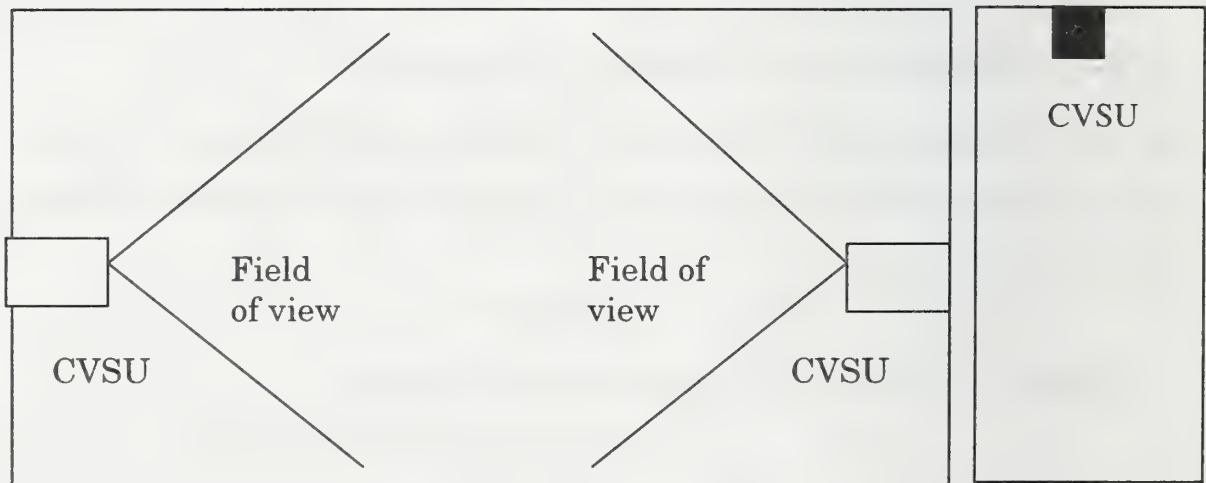


Fig.7

CARGO COMPARTMENT

Top view

Side view



The position of the cargo compartment visualisation sensors within the cargo compartment is optimised:

- Any phenomenon in the field of view of the two sensors is automatically detected and the detection coverage is 100%,
- Time of detection is always the same and it is very short (no need to reach the sensor).

This configuration allows monitoring phenomenon between containers & between containers and lining (ceiling).

### **3- Measurement & detection signal processing**

**HOT SPOT Principle:**

The principle is that of a thermographic camera and not that of a simple pyrometer. The camera provides a heat image associated to a temperature scale, and the result obtained yields a thermogram.

Hot spot detection is based on analysis of the hot spot's luminance (energy) in the dark.

**FIRE Principle:**

Fire detection is based on analysis of the fluctuation of the flame (energy, frequency) in the dark

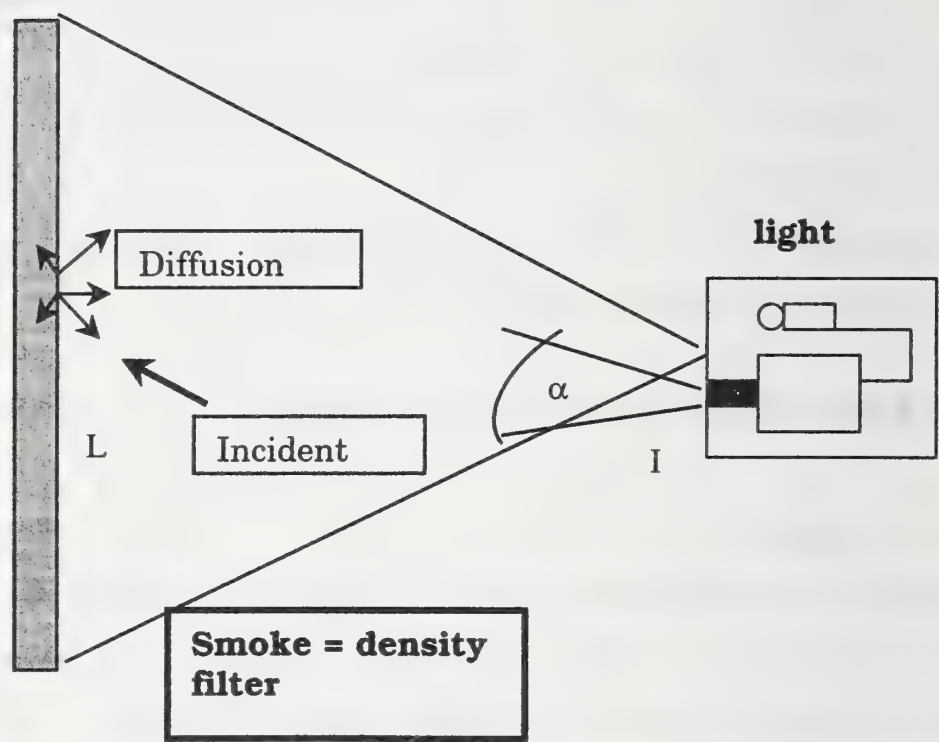
**SMOKE Principle:**

Smoke detection is based on reflection-transmission of a reflecting body.

The principle is the following:



Fig.8



The relation of the transmission is the following:

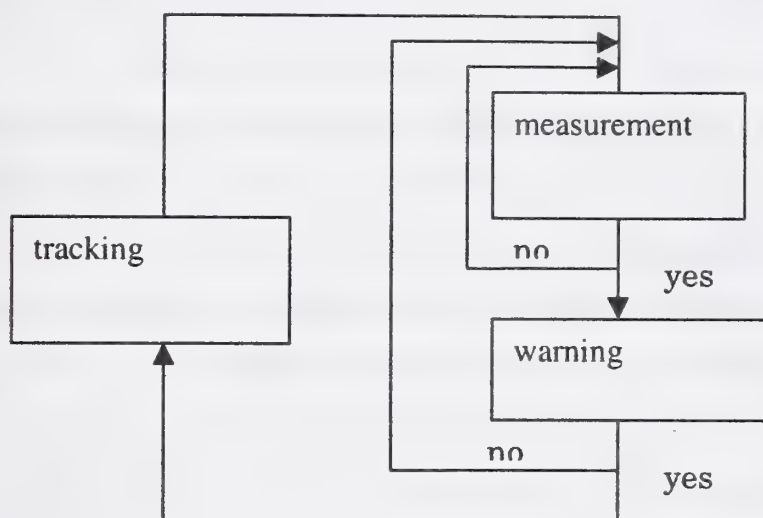
Eq.3  $\xi = \frac{I}{I_0} = 10^{-Att \times 10}$

$I_0$  reference signal (no smoke)

$I$  signal received

## Detection & tracking principle:

Fig.9



### 4- Lab test

The fire detection & visualisation system is able to recognize the fire tests TF1 through TF6 following EN 54 part 9.

Interferences like sun, rising sun, sun with chopper, do not affect (no warning) the fire detection & visualisation system.

These tests are successful in :

- a certified EN54 test chamber.
- a downscaled cargo compartment volume in an empty cargo compartment.
- a downscaled cargo compartment volume in a partially loaded cargo compartment.
- a full scale cargo compartment fully loaded.

Fog or condensation interferences do not produce a warning.

Environmental not correlated with a real fire conditions has no effect on processed images.

### Other trial

One trial was made on AIRBUS A330 a/c with 120g FAA powder and full cargo compartment loaded: FDVS sensor detection time was 5s and optical smoke did not detect. The test was stopped after 15mn.

Trials were made on AIRBUS A330 a/c with 240g FAA powder and full cargo compartment loaded: FDVS sensor detection time was 3s and optical smoke detector time was 2mn & 5s.

Trial were made on AIRBUS A300/600ST to monitor the upper and lower cargo compartment in un-pressurised conditions.

### Environment tests

Trial will be made in 2001 to mix temperature variation & pressure variation with a real fire to make sure that technology has the same potential on real environment.



Thomas Cleary and Michelle Donnelly

Building and Fire Research Laboratory, National Institute of Standards and Technology  
Gaithersburg, MD, 20899 U.S.A.

## **Aircraft Cargo Compartment Fire and Nuisance Source Tests in the FE/DE**

### **1. Introduction**

Commercial transport aircraft cargo compartments require both fire detection and suppression capabilities in order to meet regulatory requirements. Historically, while there have been few fires reported in cargo compartments, false alarms are a much more frequent event. A recent study places the false alarm to smoke detection ratio at 200:1 over the last five years [1]. A significant fraction of false alarms is thought to be due to nuisance sources such as condensed water vapor, and other aerosol sources [2]. The Federal Aviation Administration requires that detectors meet standards in SAE AS 8036 (wherein UL smoke box testing is referenced as appropriate to check alarm sensitivity) which specifies that the alarm must fall between 60 %/ft to 96 %/ft light transmission (extinction coefficients between  $3.0 \text{ m}^{-1}$  to  $0.13 \text{ m}^{-1}$ ) [3]. Each new cargo compartment design must pass a system test on the ground and in-flight using "smoke" which may be produced from aerosol generators, tobacco smoldering or other non-fire sources. An alarm must be recorded within 60 s of the start of the aerosol source. The FAA is developing standard flaming fire and smoldering fire sources that will be more repeatable than the range of aerosol sources currently in use, and that will allow other types of detectors besides smoke detectors to be qualified. In a recent survey of fire detection technologies, gas and thermal sensing were identified as plausible additions to particulate sensing in cargo compartments to improve detection [4]. Here, fire and nuisance scenarios were emulated in the fire emulator/detector evaluator (FE/DE), and gas, thermal and particulate sensor signals were gathered to determine potential sensor combinations that would overcome various nuisance alarm events in cargo compartments. The selection of the flaming, smoldering, and nuisance alarm scenarios was guided by a desire to cover a range of potential fire and nuisance alarm scenarios that would each progress to a point where current aircraft detectors would alarm; there

was no basis for these scenarios from statistical analysis of fire data, nor service difficulty reports addressing false alarms.

## 2. Fire and Nuisance Alarm Scenarios

Two separate flaming, smoldering, and nuisance scenarios tailored for aircraft cargo compartments were emulated in the FE/DE and are described here. Additional scenarios are described in a NIST report [5]. The FE/DE is a 0.3 m high by 0.6 m wide cross-section flow tunnel designed to reproduce the time-varying speed, temperature and concentration (gas and particulate) expected at detector locations in the early stages of the fire (Figure 1). The FE/DE employs a variable speed blower and resistance heaters to control velocity and temperature (ambient and higher) over ranges of 0.02 m/s to greater than 1 m/s and 20 °C to 80 °C, respectively.

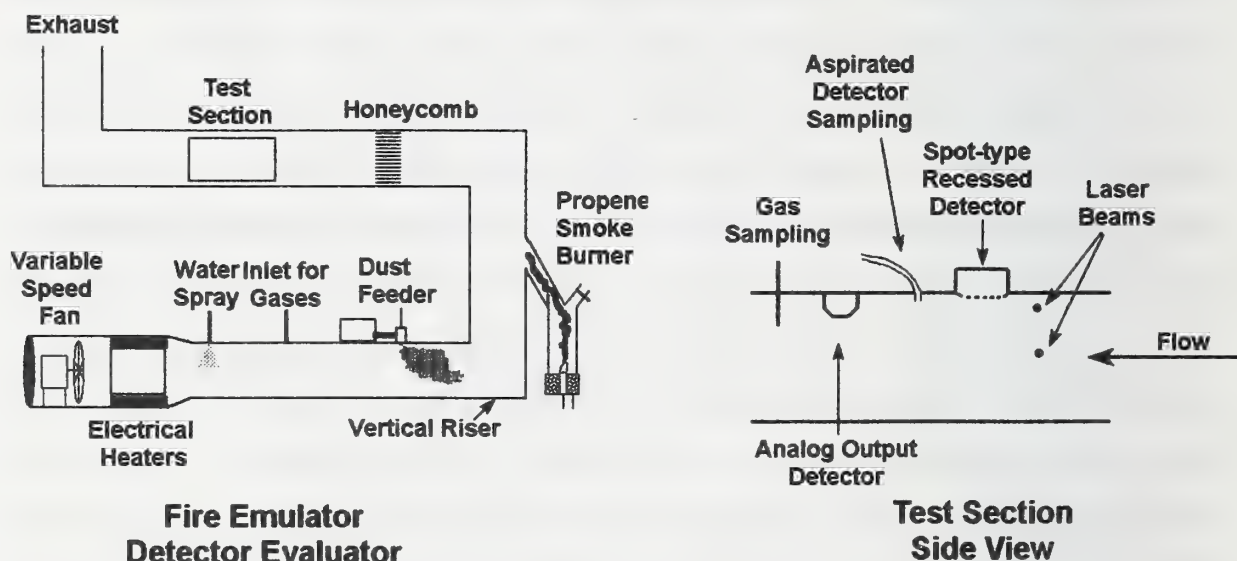


Figure 1. Schematic of fire emulator/detector evaluator.

The fire sources chosen for this study cover a wide range of fire phenomena. They consist of the following: (1) a flaming fire indicative of a plastic or liquid hydrocarbon pool fire, (2) a "low-smoke" flaming fire that consists of ethanol-soaked cotton-polyester blend fabric, (3) a smoldering cotton wick fire, and (4) a pyrolyzing mixed plastics plaque obtained from the FAA Technical Center. Two nuisance sources chosen to represent potential source of false alarms due to environmental conditions in aircraft cargo compartments were emulated. They consist of the following: (1) dust exposure,



and (2) an oil mist aerosol.

Measurements of laser light extinction, temperature, gas concentration and analog output detectors at the test section were made to characterize the fire and nuisance sources. These measurements are indicative of sensor outputs that could be part of a multi-sensor detector. Light extinction measurements are made across the tunnel duct at the test section. The light transmission path across the 0.60 m wide duct is extended to 1.50 m by reflecting the laser beam off two mirrors placed inside the duct. The beam is split outside the tunnel resulting in two parallel beams, one at 4 cm and one at 15 cm (mid-height) below the top of the duct. Photodetectors are positioned on the opposite side of the duct to record the transmitted light intensity. In smoke-free air, the photodetector output fluctuates randomly  $\pm 0.1\%$  about the mean intensity. The extinction coefficient,  $k$  ( $\text{m}^{-1}$ ) is obtained from the following equation:

$$\frac{I}{I_0} = \exp^{-kL} \quad [1]$$

$I_0$  is the smoke-free light intensity, while  $I$  is the intensity when smoke is present, and  $L$  is the path length (m). Process gas analyzers recorded CO, CO<sub>2</sub>, and water content in the air from samples drawn from the test section. The instrument ranges are 0 to  $5 \times 10^{-4}$  volume fraction CO and 0 to 0.04 volume fraction CO<sub>2</sub>. The uncertainty of the measurements are stated as  $2.5 \times 10^{-6}$  volume fraction CO and  $2 \times 10^{-5}$  volume fraction CO<sub>2</sub>. The water analyzer range is 0 to 0.05 volume fraction with an expanded uncertainty of 10 % of the measurement. The response time for these analyzers (90% of ultimate response to a step change) is 15 s. An electrochemical CO sensor was placed in the tunnel and its output recorded, then converted to CO volume fraction. Air temperature was recorded by a type-K thermocouple constructed from 0.08 mm bare wire located 5 cm from the ceiling of the duct, and approximately 15 cm downstream from the laser beam. An analog output photoelectric, ionization, and thermal detector was located on the ceiling of the test section 30 cm downstream from the laser beam. The output of this detector was previously "calibrated" against propene soot, dust and nebulized oil aerosol [6]. Two different aircraft smoke detectors were installed to indicate the smoke or nuisance source conditions that would cause existing detectors to alarm. The alarm conditions are suggestive of existing performance, however, these



tests should not be considered detector performance tests. One detector {D1} was a spot-type photoelectric unit designed to be mounted on the ceiling of the cargo compartment. It has a low profile housing and is covered by a large-opening protective metal grate. It was installed at the ceiling location in the FE/DE test section, mounted as it would be in a cargo compartment. The alarm point for this detector was set at an extinction coefficient of approximately  $0.13 \text{ m}^{-1}$  (4 %/ft, the most sensitive allowed by SAE AS8036). The other detector {D2} was a draw-through type detector that is designed to sample cargo compartment air through tubing with openings at the ceiling. The alarm point for this detector was set at an extinction coefficient of approximately  $0.31 \text{ m}^{-1}$  (9 %/ft). This detector was installed outside the test section with a 15 cm long 6 mm I.D. plastic tube extending 2.5 cm below the duct ceiling as the sample point. The flow through the detector was set at approximately 4 L/min.

### 3. Experimental Results

Test fire 1, the flaming fire, emulates conditions developed as the result of a burgeoning hydrocarbon pool or burning plastics fire. The FE/DE reproduced the flow conditions by control of the fan speed to achieve the expected ceiling jet velocity. The heater set point was controlled to provide the increasing temperature at the detector location. Smoke was provided from the propene smoke generator attached to the FE/DE. The smoke generator is an annular co-flowing, air/propene diffusion burner contained in a steel duct with damper-controlled bypass and tunnel connections. The fan speed was set at 10 Hz which yielded a mean core flow of 0.25 m/s at the test section. The damper was opened at time = 0 to let smoke flow into the duct. Figures 2-4 show representative values of smoke extinction, combustion gases and air temperature for this scenario. The alarm time for the spot-type aircraft detector is marked on the extinction graph; the draw-through detector did not record an alarm. In Figure 2, the extinction coefficient began to rise at 30 s, (this delay represents the transport of the smoke from the smoke generator to the test section). At about 40 s, both the photoelectric and ionization analog signals began to rise. The photoelectric signal reached its maximum output at 60 s while the ionization signal continued to climb until leveling off at 120 s. The ionization signal lagged the extinction value due to the smoke entry lag of the detector. Figure 3 shows CO, CO<sub>2</sub>, and water volume fractions with background values subtracted.

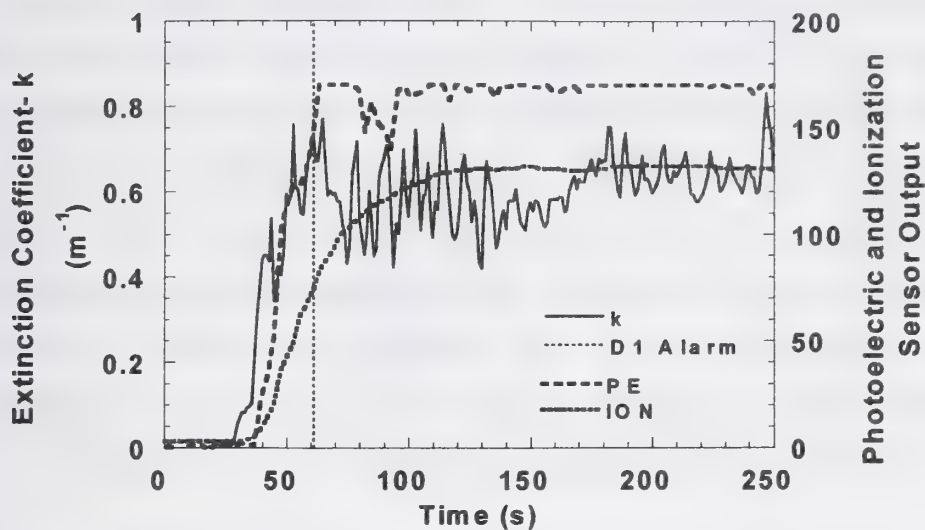


Figure 2. Smoke level for test fire 1: flaming fire.

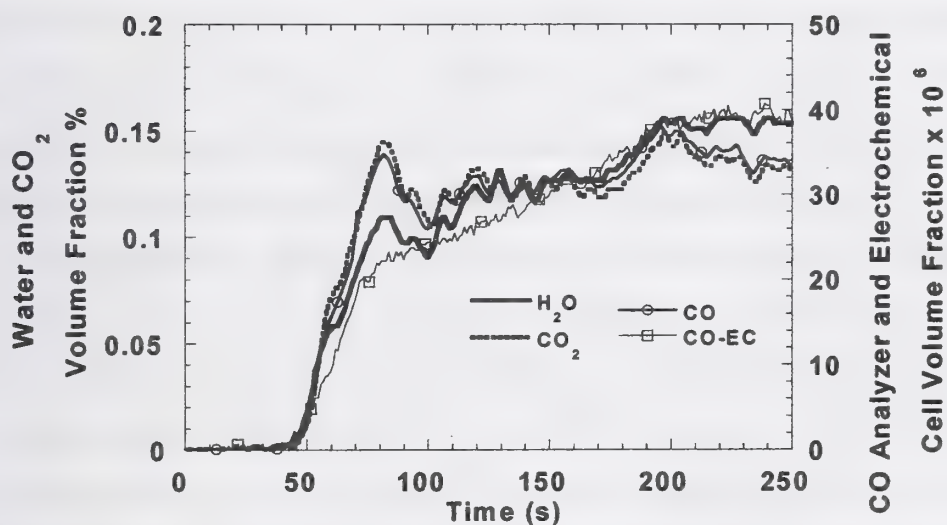


Figure 3. Gas signatures for test fire 1, flaming fire.

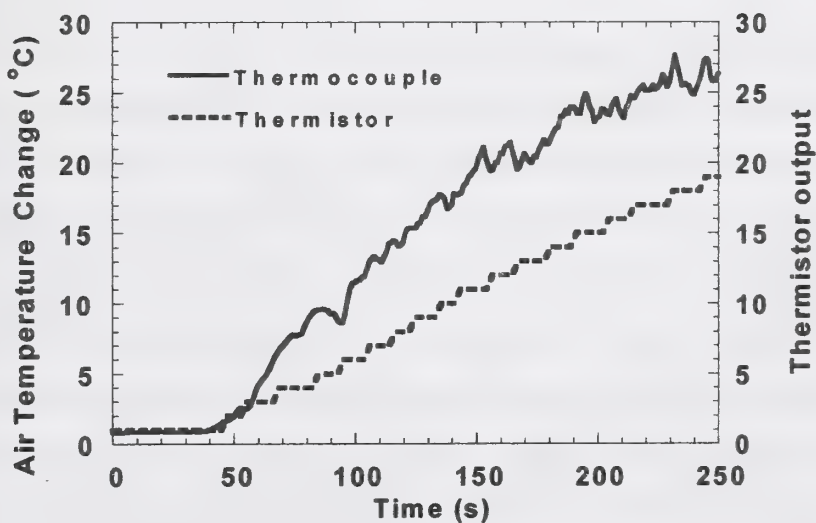


Figure 4. Temperature rise for test fire 1, flaming fire.



All gas concentrations began to rise at 45 s (time to transport gases to analyzers  $\approx$  15 s). The delayed response of the electrochemical cell is most likely due to diffusional transport delay of CO into the cell itself. The CO<sub>2</sub> and water volume fractions are nearly identical which would be expected from nearly complete combustion of propene. The CO/CO<sub>2</sub> volume ratio is about 0.025, which is reasonable for the over-ventilated diffusion flame in the smoke generator. The temperature rate of rise averaged 0.13 °C/s from 40 s to 250 s (Figure 4). The thermistor output lagged the fast-response thermocouple. This is a constant occurrence due to the relatively sluggish response characteristics of the thermistor compared to the fast-response thermocouple.

Test fire 2, the low-smoke flaming fire, was designed to emulate conditions from a cargo compartment fire that begins by ignition of alcohol-soaked baggage where the initial effluent is very low smoke until the alcohol burns out and the fabric starts to burn. The result is a temperature rise and gas signature that precedes the measurable smoke at the test section. The fuel consisted of six 7 cm diameter cotton/polyester (50/50 blend by weight) fabric circles stacked and held together with 3 staples, and wetted with 5 mL of ethanol. The wetted fabric was placed over a 10 cm glass dish and supported by two crisscrossed nichrome wires, then placed at the bottom of the vertical riser section of the FE/DE prior to ignition. The fan speed was set to 10 Hz (mean flow velocity of 0.25 m/s), then the alcohol was ignited at time = 0. At first, only the alcohol burned as it was wicked through the fabric or burned from excess in the dish below. During this phase, no appreciable smoke was produced. As the alcohol burned out, the fabric circles caught fire and burned with considerable smoke production, then burned out. Figures 5-7 show representative smoke, combustion gas production and temperature rise from this scenario. In Figure 5, the ionization signal started to rise at 20 s while the extinction and photoelectric signal started to rise at 60 s. The initial combustion produced an aerosol that was not scattering much light, but was being sensed by the ionization detector. As the fabric circles caught fire, the extinction coefficient and photoelectric signals began to rise. The extinction coefficient decayed much faster than the photoelectric or ionization signal due to hold-up of the heated smoke in the detector sensing volume. Figure 6 shows CO, CO<sub>2</sub>, and water volume fraction with background values subtracted. At 25 s water and CO<sub>2</sub> started to rise; initially, water was higher than the CO<sub>2</sub> which is expected



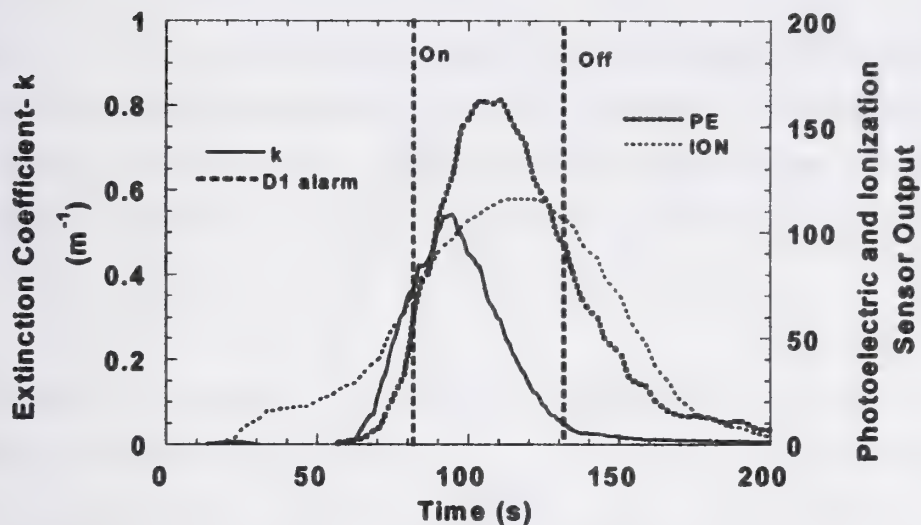


Figure 5. Smoke level for test fire 2, alcohol-soaked fabric fire.

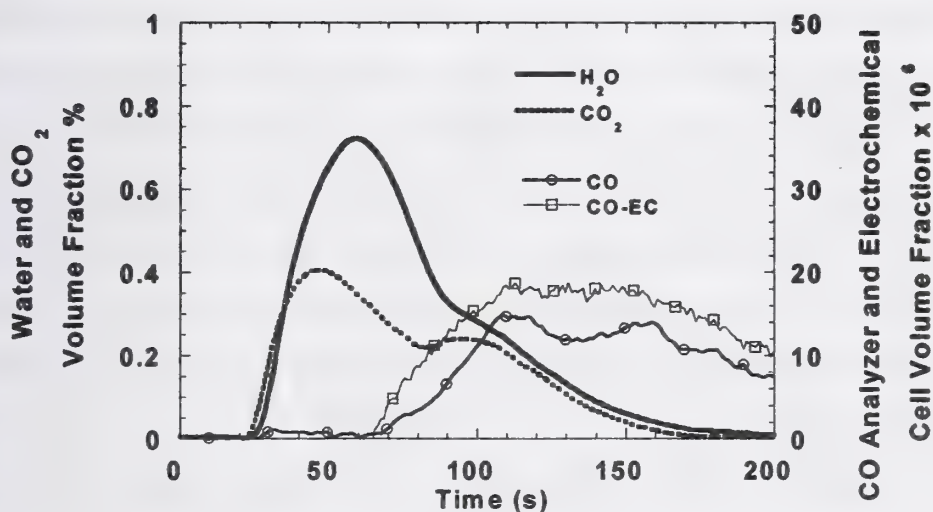


Figure 6. Gas signatures for test fire 2, alcohol-soaked fabric fire.

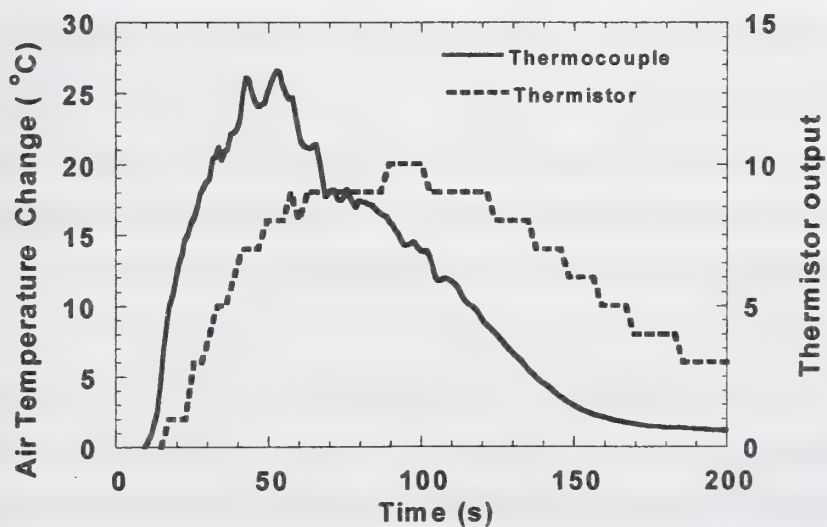


Figure 7. Temperature rise for test fire 2, alcohol-soaked fabric fire.

as the ethanol was burning. The CO concentration began to rise as the fabric started to burn and remained elevated even as the extinction decreased to near zero. The output of the electrochemical cell deviated from the CO analyzer and was most likely due to temperature and humidity effects of the cell output. Air temperature rose at a rate of nearly 1 °C/s, peaking at 27 °C above ambient ( $\approx 20$  °C) 30 s after the initial rise (Figure 7).

Test fire 3, the smoldering cotton fire source, is a variant of a standard detector sensitivity test fire EN 54 part 9 test fire 3. A staged-wick-ignition test fixture developed for use in the FE/DE holds 32 cotton wicks 6 mm in diameter (typically 15 cm long) in a vertical orientation around a circular frame. Unique to the test fixture developed here is that each wick pair is spaced so that it is 5 cm away from adjacent pairs and the bottom of each wick passes through a wound nichrome ignition wire. Opposing pairs are wired in series producing a maximum of 8 independently ignited sets of 4 wicks. For the tests here, the objective was to produce a steadily increasing smoke concentration at the test section for 120 s. This was accomplished by igniting 8 sets of 4 wicks with a 12 s delay between each set. The fan was set to 10 Hz, yielding a mean velocity of 0.25 m/s at the test section, and the ignition sequence was started at time = 0. Figures 8 and 9 show representative smoke and combustion gas production for this source. In Figure 8, the extinction started to rise at 50 s followed by the ionization signal at 60 s and the photoelectric signal at 70 s. The photoelectric signal reached its maximum output at 115 s and both of the aircraft detectors alarmed between 130 s and 135 s. The extinction coefficient peaked at 140 s. In Figure 9, the gas concentrations began to rise between 60 s and 70 s, and peaked at about 170 s. The CO/CO<sub>2</sub> volume ratio is about 1:2.6, similar to the 1:3 ratio obtained in room tests with the same cotton smolder source [7]. The CO<sub>2</sub>/water volume ratio is approximately 1:3. Air temperature rise peaked at 3.5 °C which is not uncharacteristic for low-energy-output smolder plumes

Test fire 4, pyrolyzing mixed plastics, uses the same smolder source being developed at the FAA Technical Center. It consisted of a 10 cm by 10 cm by 0.5 cm plaque of compressed plastic pellets, 2 mm to 5 mm in size with a nichrome wire embedded in it. The pellets were a mix of various plastics. The plaque was placed at the bottom of the

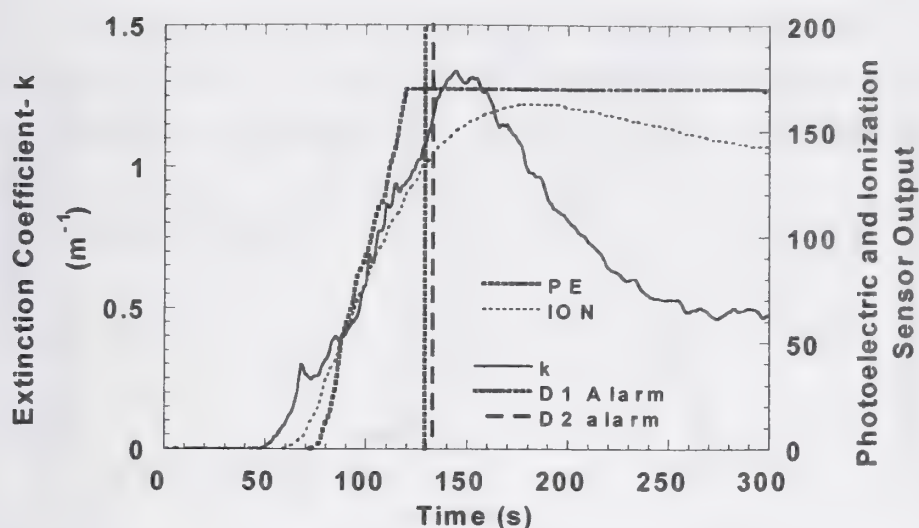


Figure 8. Smoke level for test fire 3, smoldering cotton wicks.

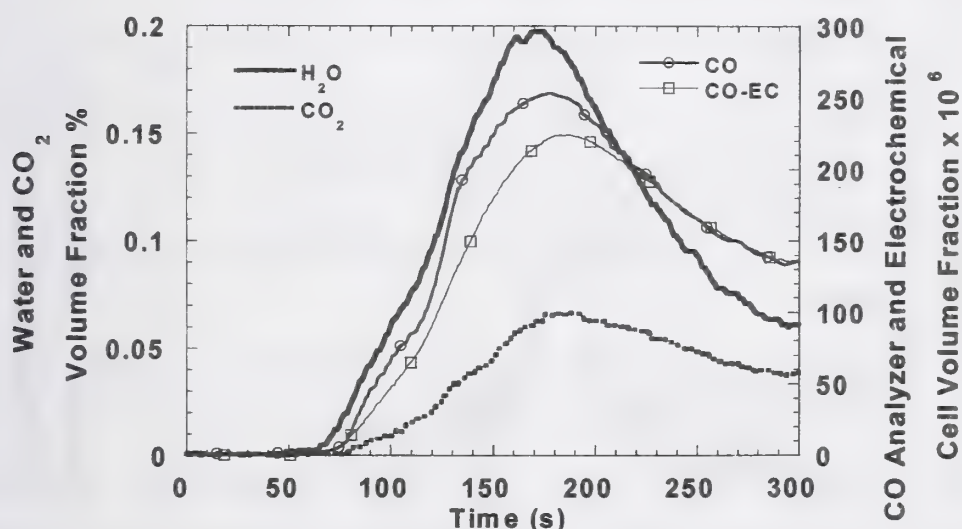


Figure 9. Gas signatures for test fire 3, smoldering cotton wicks.

vertical riser. The fan speed was set to 10 Hz yielding a mean flow velocity of 0.25 m/s at the test section. At time = 0, 40 volts AC power was applied to the nichrome wire which was sufficient to start the plastics to pyrolyze and emit smoke and gases. The power was removed at 80 s and the pyrolyzing eventually stopped. Figures 10 and 11 show representative smoke and combustion gas production for this source. The photoelectric, ionization signal, and extinction coefficient all began to rise at 30 s. The photoelectric signal reached its maximum output at 50 s while the extinction coefficient and ionization signal continued to rise peaking at 90 s and 105 s respectively. The spot-type aircraft detector alarmed at 66 s, while the draw-through detector alarmed at 88 s. The combustion gas production levels were low compared to the other smolder sources.



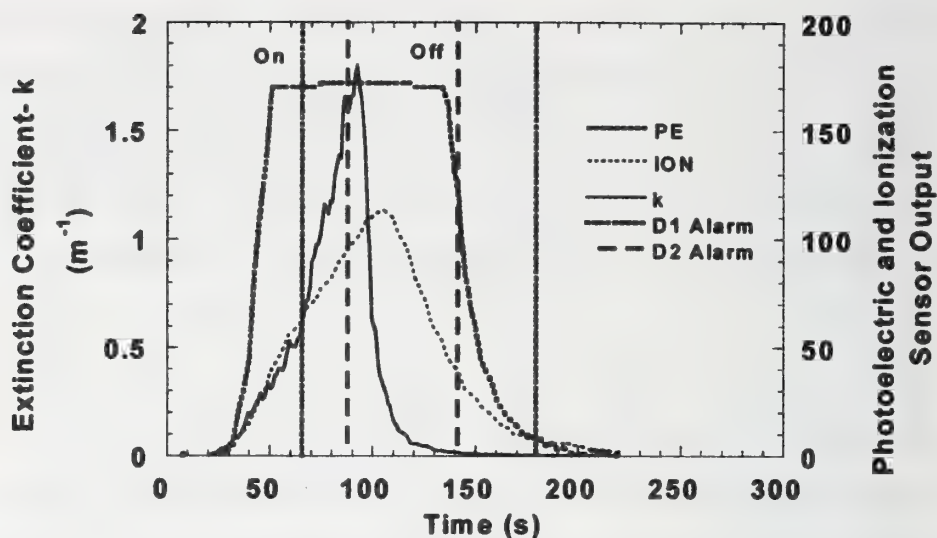


Figure 10. Smoke level for test fire 4, pyrolyzing plastics.

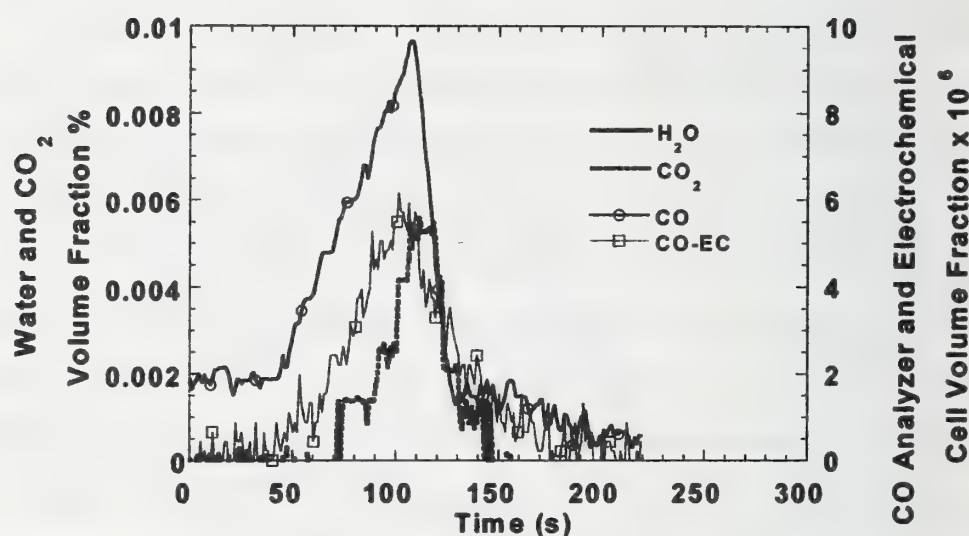


Figure 11. Gas signatures for test fire 4, pyrolyzing plastics.

The CO volume fraction peaked at  $6 \times 10^{-6}$ , while the CO<sub>2</sub> volume fraction peaked at  $5.0 \times 10^{-3}$  % above the background level. No rise in the water concentration was observed. Air temperature rise was about 1 °C above ambient temperature.

The dust aerosol was generated by injecting ISO 12103-1 fine grade Arizona test dust at a constant rate from a powder screw feeder. With the fan speed set at 10 Hz, the dust was fed into the duct at time = 0. Figure 12 shows the extinction coefficient and detector output for this source. The extinction coefficient started to rise at about 12 s followed by the photoelectric and ionization signals 10 s later. The extinction was above  $2 \text{ m}^{-1}$  at 30 s and stayed between  $2 \text{ m}^{-1}$  and  $2.5 \text{ m}^{-1}$  until the dust flow was stopped at

100s and the remaining dust blown out of the duct. The photoelectric signal reached its maximum output at about 25 s, while the ionization continued to rise until the dust flow was stopped. The spot-type aircraft detector alarmed at 59 s, while the draw-through detector alarmed at 100 s.

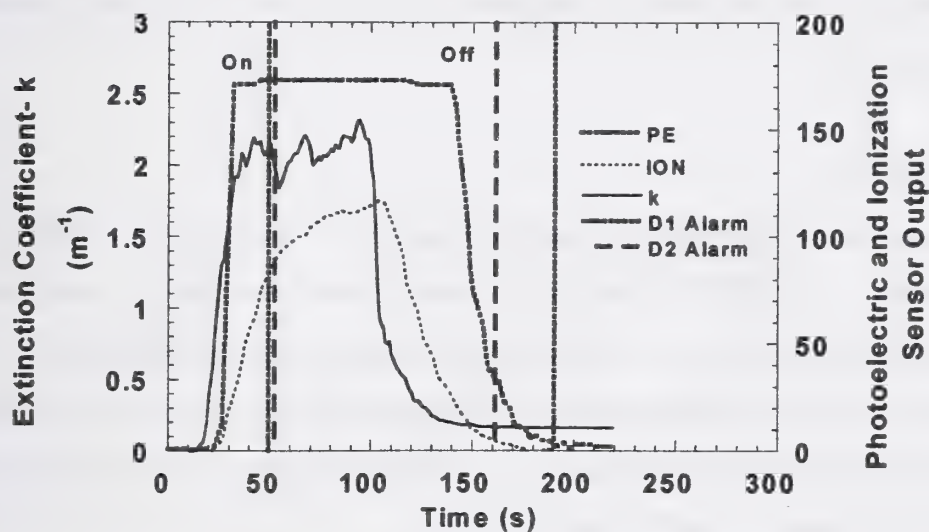


Figure 12. Particulate level for nuisance source 1, dust exposure.

The oil mist aerosol was generated by nebulizing cooking oil from a bank of 10 medical inhalent nebulizers located at the bottom of the vertical riser of the FE/DE. This aerosol is a surrogate for hydraulic oil or non-volatile mists introduced in a cargo compartment intentionally (cargo treatment) or unintentionally. The fan speed was set at 7 Hz yielding at mean flow velocity of 0.15 m/s at the test section, and the nebulizers were

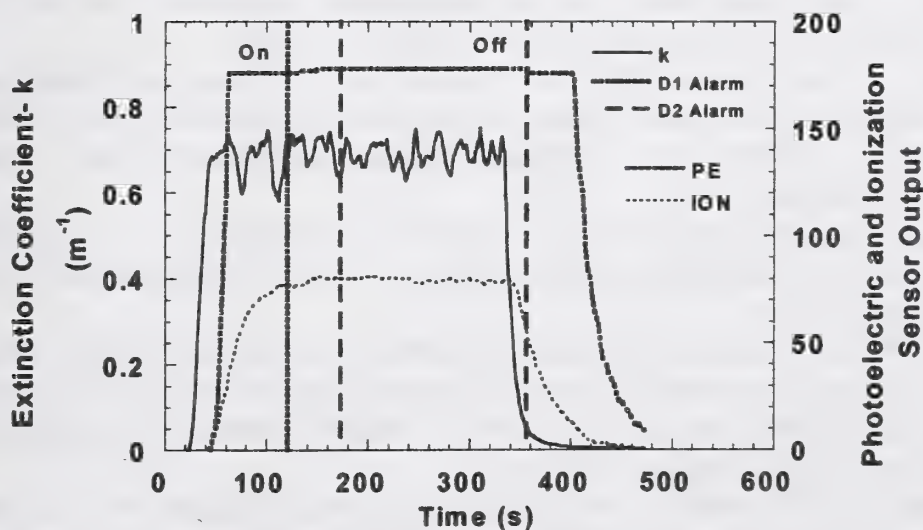


Figure 13. Particulate level for nuisance source 2, oil mist exposure.

started at time = 0. Figure 13 shows the extinction coefficient and detector outputs for this source. The extinction coefficient started to rise at 20 s and reached nearly steady values between  $0.6 \text{ m}^{-1}$  and  $0.7 \text{ m}^{-1}$  within 10 s. The photoelectric and ionization signals began to rise at 40 s with the photoelectric signal saturating at about 60 s while the ionization signal continued to rise until reaching a steady value at approximately 120 s. The spot-type aircraft detector alarmed at 120 s, while the draw-through detector alarmed at 173 s.

#### 4. Conclusions

Six plausible fire and nuisance alarm scenarios for aircraft cargo compartments were reproduced in the FE/DE. The data gathered contains particulate, combustion gas and temperature rise values that may be used to identify sensor combinations to discriminate between fire and non-fire conditions. Background levels of particulate, combustion gas and temperature fluctuations need to be included in any analysis leading to sensor selection and alarm algorithm design.

#### 5. References

- [1] D., "Aircraft Cargo Compartment Smoke Detector Alarm Incidents on U.S.-Registered Aircraft, 1974-1999," DOT/FAA/AR-TN00/29, U.S. Dept. of Trans., Federal Aviation Administration, 2000.
- [2] Grosshandler, W., (editor), "Nuisance Alarms in Aircraft Cargo Areas and Critical Telecommunications Systems: Proceedings of the 3rd NIST Fire Detector Workshop," December 4-5, 1997, NISTIR 6146, National Institute of Standards and Technology, Gaithersburg, MD, March 1998.
- [3] "Cargo Compartment Fire Detection Instruments," Aerospace Standard, AS 8036, Society of Automotive Engineers, Inc., Warrendale, PA, 1985.
- [4] Cleary, T., and Grosshandler, W., "Survey of Fire Detection Technologies and System Evaluation/Certification Methodologies and their Suitability for Aircraft Cargo Compartments," NISTIR 6356, National Institute of Standards and Technology, Gaithersburg, MD, July 1999.
- [5] Cleary, T., and Donnelly, M., "Improved Fire Detection in Aircraft Cargo Compartments," NISTIR in preparation, National Institute of Standards and Technology, Gaithersburg, MD, 2001.
- [6] Cleary, T., Grosshandler, W., and Chernovsky, A., "Smoke Detector Response to Nuisance Aerosols," Proceeding of the 11th International Conference on Automatic Fire Detection "AUBE '99," March 16-18, 1999, Gerhard Mercator University, Duisburg, Germany, Luck, H., Ed., pp 32-41, 1999.
- [7] Cleary, T., Grosshandler, W., Nyden, M., and Rinkinen, W., "Signatures of Smoldering/Pyrolyzing Fires for Multi-element Detector Evaluations," Proc. of the 7th Inter. Conf. on Fire Science and Eng., Interflam '96, Cambridge, England, March 1996.



NOT OPEN INFORMATION 702

100-1001

U.S. DEPARTMENT OF COMMERCE

Division of Economic Development

Division of Research and Technology

Room 3100, Building 3000

Division of Research and Technology, Special Projects 702

Room 3100, Building 3000, 100-1001 (February 1961)

100-1001

U.S. GOVERNMENT PRINTING OFFICE

WASHINGTON 20540

This document contains information, equipment, or material which may be identified as information in a technical or experimental procedure or design. It is not to be distributed outside the Department of Commerce, and is not to be used for any purpose other than the official business of the Department of Commerce, and is not to be reproduced, stored, or transmitted in any form or by any means, electronic, mechanical, or otherwise, without the prior written permission of the Department of Commerce.



**NIST Special Publication 965**

**February 2001**

**U.S. DEPARTMENT OF COMMERCE**

**Donald L. Evans, Secretary**

**National Institute of Standards and Technology**

**Karen H. Brown, Acting Director**

**National Institute of Standards and Technology Special Publication 965**

**Natl. Inst. Stand. Technol. Spec. Publ. 965, 707pages (February 2001)**

**CODEN: NSPUE2**

**U.S. GOVERNMENT PRINTING OFFICE**

**WASHINGTON: 2001**

Certain commercial entities, equipment, or materials may be identified in this document in order to describe an experimental procedure or concept adequately. Such identification is not intended to imply recommendation or endorsement by the National Institute of Standards and Technology, nor is it intended to imply that the entities, materials, or equipment are necessarily the best available for the purpose.







